Modelling and Simulation of Complex Biological Systems

Lead Guest Editor: Tongqian Zhang
Guest Editors: Tonghua Zhang, Xinzhu Meng, and Songbai Guo

Modelling and Simulation of Complex Biological Systems

Modelling and Simulation of Complex Biological Systems

Lead Guest Editor: Tongqian Zhang
Guest Editors: Tonghua Zhang, Xinzhu Meng, and Songbai Guo

Contents

Contents

WILEY | Hindawi

Research Article

Stability and Coexistence of a Diffusive Predator-Prey System with Nonmonotonic Functional Response and Fear Effect

Xiaozhou Feng ,[1] **Hao Sun,**[1] **Yangfan Xiao,**[1] **and Feng Xiao** [2]

^{1}College of Science, Xi'an Technological University, Xi'an 710032, China
^{2}College of Computer Science and Engineering, Xi'an Technological University, Xi'an 710032, China

Correspondence should be addressed to Xiaozhou Feng; flxzfxz8@163.com and Feng Xiao; xffriends@163.com

This paper investigates the diffusive predator-prey system with nonmonotonic functional response and fear effect. Firstly, we discussed the stability of the equilibrium solution for a corresponding ODE system. Secondly, we established a priori positive upper and lower bounds for the positive solutions of the PDE system. Thirdly, sufficient conditions for the local asymptotical stability of two positive equilibrium solutions of the system are given by using the method of eigenvalue spectrum analysis of linearization operator. Finally, the existence and nonexistence of nonconstant positive steady states of this reaction-diffusion system are established by the Leray–Schauder degree theory and Poincaré inequality.

1. Introduction

In order to describe the evolution of biological populations in the ecosystem, some mathematical theories and methods have been used to establish the corresponding biological mathematical model, which has become a research hotspot. In recent years, the research on biological models such as the predator-prey model has aroused the attention of many scientists and biologists. The predator-prey model of PDE forms is an important branch of reaction-diffusion equations. The dynamic relationship between predator and their prey is one of the dominant themes in ecology and mathematical ecology. During these thirty years, the investigation on the prey-predator models has been developed, and more realistic models are derived in view of laboratory experiments. Moreover, the research on the prey-predator models has been studied from various views and obtained many good results (see [1–22] and the references therein).

However, many studies have shown that only the presence of predators in front of the prey can affect the size of the prey population, and the effect is even greater than the effect of direct predation. Although some biologists have realized that the relationship between the prey and the predator cannot be simply described as direct killing, we should take the fear of the prey population into account. At present, there are few research studies on establishing corresponding mathematical models to explain this phenomenon.

For every specific prey-predator system, we know that the functional response of the predator to the prey density is very important, which represents the specific transformation rule of the two organisms. In [8], Pang and Wang considered a predator-prey model incorporating a nonmonotonic functional response which is called the Monod–Haldane or Holling type IV function:

$$
\begin{cases}
u_t - d_1 \Delta u = ru\left(1 - \dfrac{u}{k}\right) - \dfrac{puv}{d + u^2}, & x \in \Omega, t > 0, \\[2mm]
v_t - d_2 \Delta v = -mv + \dfrac{cpuv}{d + u^2}, & x \in \Omega, t > 0, \\[2mm]
\partial_n u = \partial_n v = 0, & x \in \partial\Omega, t > 0,
\end{cases}
\tag{1}
$$

where ∂_n is the outward directional derivative normal to $\partial\Omega$. Model (1) describes a prey population u which serves as food for a predator with population v. The parameters $r, d, m, p, c,$ and k are assumed to be only positive values: the

positive constant k is the carrying capacity of the prey and the positive constant m is the death rate of the predator; r is the growth rate of prey u; and the positive constants d_1 and d_2 are the diffusion coefficients.

In this paper, based on the above model, in order to describe the evolution law of the population in the ecosystem more specifically, we will consider the natural mortality and fear effect of the prey population and establish the corresponding PDE model within a fixed bounded domain $\Omega \subset R^N$ with smooth boundary at any given time and the natural tendency of each species to diffuse to areas of smaller population concentration [7–10]. Hence, we will investigate the following reaction-diffusion system under the homogeneous Neumann boundary conditions as follows:

$$
\begin{cases}
u_t - d_1 \Delta u = \dfrac{ru}{1+kv} - au - bu^2 - \dfrac{puv}{d+u^2}, & x \in \Omega, t > 0, \\[3mm]
v_t - d_2 \Delta v = -mv + \dfrac{cpuv}{d+u^2}, & x \in \Omega, t > 0, \\[3mm]
\dfrac{\partial u}{\partial n} = \dfrac{\partial u}{\partial n} = 0, & x \in \partial\Omega, t > 0, \\[3mm]
u(x,0) = u_0(x) \geq 0, v(x,0) = v_0(x) \geq 0, & x \in \Omega,
\end{cases}
\tag{2}
$$

where u_0 and v_0 are continuous functions of x. u and v stand for the densities of prey and predators, respectively. The parameters $a, b, c, d, r, k, p,$ and m are assumed to be only positive constants. a and m denote the intrinsic death rate of prey u and predator v, respectively. k stands for the fear factor of prey to predator. The remaining parameters refer to (1). Here, $f(u,v) = (uv/d + u^2)$ stands for Monod–Haldane functional response.

The main aim of this paper is to study the nonconstant positive steady states of (2), that is, the existence and nonexistence of nonconstant positive classical solutions of the following elliptic system:

$$
\begin{cases}
-d_1 \Delta u = \dfrac{ru}{1+kv} - au - bu^2 - \dfrac{puv}{d+u^2}, & x \in \Omega, \\[3mm]
-d_2 \Delta v = -mv + \dfrac{cpuv}{d+u^2}, & x \in \Omega, \\[3mm]
\dfrac{\partial u}{\partial n} = \dfrac{\partial u}{\partial n} = 0, & x \in \partial\Omega.
\end{cases}
\tag{3}
$$

The rest of this paper is arranged as follows. In Section 2, we discuss the stability of the equilibrium of the ODE system which corresponds to system (2). In Section 3, we establish a priori positive upper and lower bounds for the positive solutions of the PDE system. In Section 4, sufficient conditions for the local asymptotical stability of two positive equilibrium solutions of the system are established

by using the method of eigenvalue spectrum analysis of linearization operator. In Section 5, the existence and nonexistence of nonconstant positive steady states of this reaction-diffusion system are established by using the Leray–Schauder degree theory, which demonstrates the effect of large diffusivity.

2. Stability of the ODE Model

The goal of this section is to discuss the stability of the ODE model; we give the ordinary differential equation of system (3) as follows:

$$
\begin{cases}
\dfrac{du}{dt} = \dfrac{ru}{1+kv} - au - bu^2 - \dfrac{puv}{d+u^2}, \\[3mm]
\dfrac{dv}{dt} = -mv + \dfrac{cpuv}{d+u^2}, \\[3mm]
u(0) = u_0, \\[3mm]
v(0) = v_0.
\end{cases}
\tag{4}
$$

By the similar method to [7], for (4), we can get the following result.

Lemma 1. *Under initial conditions $u_0 > 0$ and $v_0 > 0$, the solution of system (4) is nonnegative and ultimately bounded which implies*

$$
\limsup_{t \to \infty} L(t) \leq \max\left\{\frac{c(r-a+m)}{4bm}, c_0 u + v_0\right\}, \text{ here } L \doteq cu + v.
\tag{5}
$$

Next, we will calculate the equilibrium point of system (4), and the result is given as follows.

Theorem 1. *System (4) always has an extinction equilibrium point $E_0 = (0,0)$. If $r > a$, then system (4) has only the equilibrium point $E_1 = (r-a/b, 0)$. If $r > a$, $cp - 2m\sqrt{d} > 0$, and $\tilde{u}_i < r - a/b$, then system (4) has two positive constant equilibrium points $E_{2,i} = (\tilde{u}_i, \tilde{v}_i)$, $i = 1$ and 2.*

Proof. It is easy to see that all equilibrium points of system (4) satisfy the following equations:

$$
\begin{cases}
\dfrac{ru}{1+kv} - au - bu^2 - \dfrac{puv}{d+u^2} = 0, \\[3mm]
-mv + \dfrac{cpuv}{d+u^2} = 0.
\end{cases}
\tag{6}
$$

It follows that system (4) obviously has equilibrium points $E_0 = (0,0)$ and $E_1 = (r-a/b, 0)$ with $r > a$. Next, we consider the existence of positive constant equilibrium point $E_{2,i}$. By calculating the second equation of (6), we directly get

$$\tilde{u}_1 = \frac{cp + \sqrt{c^2 p^2 - 4m^2 d}}{2m},$$

$$\tilde{u}_2 = \frac{cp - \sqrt{c^2 p^2 - 4m^2 d}}{2m}, \tag{7}$$

where $(cp - 2m\sqrt{d}) > 0$ ensures that $\tilde{u}_i > 0$ $(i = 1, 2)$. Substituting $\tilde{u}_i > 0$ $(i = 1, 2)$ into (6) and combining the two equations of system (6), we can obtain the following equation:

$$\frac{r\tilde{u}_i}{1 + k\tilde{v}} - a\tilde{u}_i - b\tilde{u}_i^2 - \frac{p\tilde{u}_i\tilde{v}}{d + \tilde{u}_i^2} = 0, \quad i = 1, 2. \tag{8}$$

Through the same solution deformation calculation, we can get

$$h(v) \doteq a_2\tilde{v}^2 - a_1\tilde{v} + a_0 = 0, \quad i = 1, 2, \tag{9}$$

where $a_0 = c\tilde{u}_i(r - a - b\tilde{u}_i); a_1 = -(ca\tilde{u}_i k + cb\tilde{u}_i^2 k + m);$ $a_2 = -mk$. According to the Vieta theorem, we get

$$\tilde{v}_1 + \tilde{v}_2 = -\frac{a_1}{a_2} < 0,$$

$$\tilde{v}_1\tilde{v}_2 = \frac{a_0}{a_2}. \tag{10}$$

Obviously, if $a_0 \leq 0$, then $f(v) = 0$ has no positive constant solution; if $a_0 > 0$, then $f(v) = 0$ has only one positive constant solution. Thanks to the same sign a_0 and $r - a - b\tilde{u}_i$, $a_0 > 0$ implies $r - a - b\tilde{u}_i > 0$, which ensures that $f(v) = 0$ has only one positive constant solution denoted by v_i. Thus, system (4) has two positive constant equilibrium points $E_{2,i} = (\tilde{u}_i, \tilde{v}_i)$, $i = 1$ and 2. The proof is complete. □

Theorem 2. *If $r \leq a$, then $E_0 = (0, 0)$ is globally asymptotically stable. If $r > a$, then $E_0 = (0, 0)$ is unstable.*

Proof. The proof of Theorem 2 is similar to that of Theorem 2 of [9]; hence, we omit it. □

Theorem 3. *Assume $r > a$. If $(r - a)(cpb + ma - mr) - mb^2 d < 0$, then $E_1 = (r - a/b, 0)$ is locally asymptotically stable. If $(r - a)(cpb + ma - mr) - mb^2 d > 0$, then $E_1 = (r - a/b, 0)$ is unstable.*

Proof. Through mathematical calculation, we obtain the Jacobian matrix of system (5) at the equilibrium point $E_1 = (r - a/b, 0)$ as follows:

$$J_{E_1} = \begin{pmatrix} a - r & -kru_i - \dfrac{pu_i}{d + u_i^2} \\ 0 & \dfrac{(r - a)(cpb - mr + ma) - mb^2 d}{b^2 d + (r - a)^2} \end{pmatrix}. \tag{11}$$

Obviously, when $(r - a)(cpb + ma - mr) - mb^2 d < 0$ and both eigenvalues of J_{E_1} have negative real parts, then $E_1 = (r - a/b, 0)$ is locally asymptotically stable; when

$(r - a)(cpb + ma - mr) - mb^2 d > 0$ and J_{E_1} has a positive eigenvalue, then $E_1 = (r - a/b, 0)$ is unstable. The proof is complete. □

Theorem 4. *Assume $r > a$. If $(2m^2 v_i/c^2 pb) < u_i < \sqrt{(c^2 p^2/2m^2) - d}$ $(i = 1$ and 2), then $E_{2,i} = (\tilde{u}_i, \tilde{v}_i)$ $(i = 1$ and 2) is locally asymptotically stable. If $u_i < (2m^2 v_i /c^2 pb)$ $(i = 1$ and 2), then $E_{2,i}$ is unstable.*

Proof. For $E_{2,i} = (\tilde{u}_i, \tilde{v}_i) \doteq (u_i, v_i)$, the corresponding Jacobian matrix is given by

$$J_{E_{2,i}} = \begin{pmatrix} -bu_i + \dfrac{2pu_i^2 v_i}{\left(d + u_i^2\right)^2} & \dfrac{kru_i}{(1 + kv_i)^2} - \dfrac{pu_i}{d + u_i^2} \\ \dfrac{cpv_i}{d + u_i^2} - \dfrac{2cpu_i^2 v_i}{\left(d + u_i^2\right)^2} & 0 \doteq \dfrac{cpu_i}{d + u_i^2} - m \end{pmatrix}, \quad (i = 1, 2). \tag{12}$$

By simplifying, we can get

$$J_{E_{2,i}} = \begin{pmatrix} -bu_i + \dfrac{2m^2 v_i}{c^2 p} & -\dfrac{kru_i}{(1 + kv_i)^2} - \dfrac{m}{c} \\ \dfrac{cpv_i}{d + u_i^2} - \dfrac{2m^2 v_i}{cp} & 0 \end{pmatrix}, \quad (i = 1, 2),$$

$$\det\left(\mu I - J_{E_{2,i}}\right) = \mu^2 - \mu \cdot \text{trac}\left(J_{E_{2,i}}\right) + \det J_{E_{2,i}}, \tag{13}$$

where

$$\det J_{E_{2,i}} = \left(\frac{kru_i}{(1 + kv_i)^2} + \frac{m}{c}\right) \cdot \left(\frac{cpv_i}{d + u_i^2} - \frac{2m^2 v_i}{cp}\right), \tag{14}$$

$$\text{trac}\left(J_{E_{2,i}}\right) = -bu_i + \frac{2m^2 v_i}{c^2 p}.$$

It is easy to get that $\det J_{E_{2,i}} > 0$ and $\text{trac}(J_{E_{2,i}}) < 0$ under these conditions $(2m^2 v_i/c^2 pb) < u_i < \sqrt{(c^2 p^2/2m^2) - d}$. Then, two eigenvalues of the matrix $J_{E_{2,i}}$ have negative real parts. Therefore, the equilibrium $E_{2,i} = (\tilde{u}_i, \tilde{v}_i)$ is locally asymptotically stable. If $u_i < (2m^2 v_i/c^2 pb)$ and the matrix $J_{E_{2,i}}$ has one positive eigenvalue, then $E_{2,i}$ is unstable. □

3. A Priori Estimates on Equation (3)

The main purpose of this section is to give a priori upper and lower bounds for the positive solutions. To this aim, we first recall the following maximum principle due to [23, 24].

Lemma 2. *Suppose $g(x, \omega) \in C(\Omega \times R^1)$.*
If $\omega(x) \in C^2(\Omega) \times C^1(\overline{\Omega})$ satisfies

$$\Delta\omega(x) + g(x,\omega(x)) \geq 0 \,(\leq 0), \quad x \in \Omega,$$

$$\frac{\partial\omega}{\partial n} \leq 0 \,(\geq 0), \quad x \in \partial\Omega, \tag{15}$$

and $\omega(x_0) = \max_{\overline{\Omega}}\omega$, then $g(x_0,\omega(x_0)) \geq 0 \,(\leq 0)$.

Theorem 5. *If $r > a$ and $ack\,d_1 < bd_2$, $(u,v) = (u(x),v(x))$ is a positive solution of (3). Then, the solution $(u(x),v(x))$ of (3) yields*

$$0 < u < \frac{r-a}{b}, \quad 0 < v < \aleph, \quad \max_{x\in\overline{\Omega}}v > \delta > 0, \tag{16}$$

where $\delta \doteq (r-a)((1/ak) - (cd_1/b))$ and $\aleph \doteq [cd_1 + (cd_2(r-a)/m)](r-a/b)$.

Proof. By Lemma 2, if u reaches its maximum at $\overline{x} \in \overline{\Omega}$, it follows from the first equation of (3) that

$$r - a - bu(\overline{x}) \geq \frac{r}{1+kv(\overline{x})} - a - bu(\overline{x}) - \frac{pv(\overline{x})}{d+u^2(\overline{x})} \geq 0. \tag{17}$$

Hence, $0 < u \leq (r-a/b)$. Setting $\omega = cd_1u + d_2v$ and combining two equations of system (3), we obtain

$$-\Delta\omega = -cd_1\Delta u - d_2\Delta v = \frac{cru}{1+kv} - acu - bcu^2 - mv, \tag{18}$$

that is,

$$\Delta\omega + \frac{cru}{1+kv} - acu - bcu^2 - mv = 0. \tag{19}$$

If ω reaches its maximum at $x_0 \in \overline{\Omega}$, then

$$\frac{cru(x_0)}{1+kv(x_0)} - acu(x_0) - bcu^2(x_0) - mv(x_0) \geq 0, \tag{20}$$

which results in

$$mv(x_0) \leq \frac{cru(x_0)}{1+kv(x_0)} - acu(x_0) - bcu^2(x_0),$$

$$< cru(x_0) - acu(x_0) - bcu^2(x_0), \tag{21}$$

$$< cru(x_0) - acu(x_0).$$

Thus,

$$v(x_0) < \frac{c(r-a)}{m}u(x_0) \leq \frac{c(r-a)^2}{mb}. \tag{22}$$

Thanks to $\omega = cd_1u + d_2v$, we know that

$$d_2\max_{\overline{\Omega}}v < \max_{\overline{\Omega}}\omega = \omega(x_0) = cd_1u(x_0) + d_2v(x_0)$$

$$\leq \left[cd_1 + \frac{cd_2(r-a)}{m}\right]\frac{r-a}{b}. \tag{23}$$

Let $\varphi = -cd_1u + d_2v$, then,

$$-\Delta\varphi = cd_1\Delta u - d_2\Delta v = \frac{2cpuv}{d+u^2} - \frac{cru}{1+kv} + acu + bcu^2 - mv, \tag{24}$$

that is,

$$\Delta\varphi + \frac{2cpuv}{d+u^2} - \frac{cru}{1+kv} + acu + bcu^2 - mv = 0. \tag{25}$$

If φ reaches its maximum at $x_1 \in \overline{\Omega}$, then

$$\frac{cru(x_1)}{1+kv(x_1)} - acu(x_1) - bcu^2(x_1) \leq \frac{2cpu(x_1)v(x_1)}{d+u^2(x_1)} - mv(x_1),$$

$$< \frac{2cpu(x_1)v(x_1)}{d}$$

$$- mv(x_1) < N, \tag{26}$$

where $N = (2cp(r-a)/b\,d)\aleph$, which means that

$$1 + kv(x_1) > \frac{cru(x_1)}{acu(x_1) + bcu^2(x_1) + N}. \tag{27}$$

Letting $h(u) = cru/acu + bcu^2 + N$, it is easy to get the maximum of $h(u)$, that is, $h(u) < r/a$. Thus, $v(x_1) > (r-a/ak)$:

$$d_2\max_{\overline{\Omega}}v < \max_{\overline{\Omega}}\varphi = \omega(x_1) = -cd_1u(x_1) + d_2v(x_1)$$

$$\geq (r-a)\left(\frac{d_2}{ak} - \frac{cd_1}{b}\right). \tag{28}$$

By (23) and (28), we have proved Theorem 5.

According to Theorems 5 and 1, we can easily get the following conclusion. $\qquad\square$

Theorem 6. *If $r > a$, $(r-a)(cp - 2m\sqrt{d}) > 0$, and $u < (r-a/b)$, then system (3) has two positive constant solutions $E_{2,i} = (\widetilde{u}_i, \widetilde{v}_i)$, $i = 1$ and 2.*

Theorem 7. *Suppose that (u,v) is a nonnegative classical solution of (3). If $r \leq a$, then (u,v) is always zero solution.*

Proof. Integrating the equation for u in (3) over Ω by parts, we get

$$0 = -d_1\int_\Omega \frac{\partial u}{\partial n}\,dx = -\int_\Omega d_1\Delta u\,dx$$

$$= \int_\Omega u\left(\frac{r}{1+kv} - a - bu - \frac{pv}{d+u^2}\right)dx. \tag{29}$$

Thus,

$$0 \leq \int_\Omega bu^2 \mathrm{d}x = \int_\Omega u\left(\frac{r}{1+kv} - a - \frac{pv}{d+u^2}\right)\mathrm{d}x$$

$$\leq \int_\Omega (r-a)u\mathrm{d}x \leq 0. \tag{30}$$

Hence, $u \equiv 0$. Substituting $u = 0$ into the second equation of (3), we get

$$0 = -\int_\Omega d_2\Delta v\mathrm{d}x = -m\int_\Omega v\mathrm{d}x, \tag{31}$$

and then, $v \equiv 0$. The proof is complete. $\qquad\square$

4. Stability of the Equilibrium of Equation (3)

The goal of this section is to investigate the local and global stability of the positive constant steady state $(\tilde{u}_i, \tilde{v}_i) = \tilde{U}$. We first discuss the local stability of $\tilde{U}_i$. To this end, we need to introduce some notations for developing our result.

Let

$$f(u,v) = \frac{ru}{1+kv} - au - bu^2 - \frac{puv}{d+u^2},$$

$$g(u,v) = -mv + \frac{cpuv}{d+u^2}. \tag{32}$$

Therefore, system (3) becomes the following forms:

$$u_t = d_1\Delta u + f(u,v),$$
$$v_t = d_1\Delta v + g(u,v). \tag{33}$$

It follows that two positive solutions $(\tilde{u}_i, \tilde{v}_i)$ ($i = 1$ and 2) satisfy

$$f(\tilde{u}_i, \tilde{v}_i) = g(\tilde{u}_i, \tilde{v}_i) = 0,$$

$$(\tilde{u}_1, \tilde{v}_1) = \left(\frac{cp + \sqrt{c^2p^2 - 4m^2d}}{2m}, \tilde{v}_1\right),$$

$$(\tilde{u}_2, \tilde{v}_2) = \left(\frac{cp - \sqrt{c^2p^2 - 4m^2d}}{2m}, \tilde{v}_2\right), \tag{34}$$

where $\tilde{v}_i$ ($i = 1, 2$) satisfies

$$\frac{r}{1+kv} - a - b\tilde{u}_i - \frac{pv}{d+\tilde{u}_i^2} = 0, \quad i = 1, 2. \tag{35}$$

In order to get the linearization operator of (3) at the positive constant solution $(\tilde{u}_i, \tilde{v}_i)$, for (33), we calculate the partial derivatives with respect to u and v, respectively, at the equilibrium point $(\tilde{u}_i, \tilde{v}_i)$, as follows:

$$f_u(\tilde{u}_i, \tilde{v}_i) = -b\tilde{u}_i + \frac{2p\tilde{u}_i^2\tilde{v}_i}{\left(d+\tilde{u}_i^2\right)^2} \doteq f_1,$$

$$f_v(\tilde{u}_i, \tilde{v}_i) = -\frac{kr\tilde{u}_i}{\left(1+k\tilde{v}_i\right)^2}\frac{p\tilde{u}_i}{d+\tilde{u}_i^2} \doteq f_2 < 0, \tag{36}$$

$$g_u(\tilde{u}_i, \tilde{v}_i) = \frac{cp\tilde{v}_i\left(d - \tilde{u}_i^2\right)}{\left(d+\tilde{u}_i^2\right)^2} \doteq g_1 < 0 \text{ as } i = 1; g_1 > 0 \text{ as } i = 2,$$

$$g_u(\tilde{u}_i, \tilde{v}_i) = \frac{cp\tilde{u}_i}{d+\tilde{u}_i^2} - m \doteq g_2 = 0. \tag{37}$$

Next, give some results as follows:

(i) $0 = \mu_0 < \mu_1 < \mu_2 < \mu_3 < \cdots < \mu_i \cdots < \infty$ are the eigenvalues of $-\Delta$ on Ω under homogeneous Neumann boundary condition, and m_i is the algebraic multiplicity of eigenvalue μ_i.

(ii) $\phi_{ij}, 1 \leq j \leq m_i$, are the normalized eigenfunctions corresponding to μ_i, and then $\{\phi_{ij}\}$ ($i \geq 0, 1 \leq j \leq m_i$) are the orthonormal basis of $L^2(\Omega)$.

If $d_1\mu_1 < f_1$, then there exists $i_\alpha \doteq i_\alpha(\alpha, \Omega)$ satisfying

$$d_1\mu_i < f_1, \, i < i_\alpha, \, 1 \leq i_\alpha < +\infty. \tag{38}$$

Defining

$$\tilde{d}_2^{(i)} = \tilde{d}_2^{(i)}(\alpha, \Omega) \doteq \min_{1 \leq i \leq i_\alpha} d_2^{(i)},$$

$$d_2^{(i)} = \frac{f_2 g_1}{(d_1\mu_i - f_1)\mu_i}. \tag{39}$$

Theorem 8

(1) If $f_1 < 0$ and $d_2 > (f_2g_1/(d_1\mu_i - f_1)\mu_i)$, then the positive constant steady state $(\tilde{u}_1, \tilde{v}_1)$ of (3) is locally asymptotically stable. If $f_1 < 0$ and $d_2 < (f_2g_1/(d_1\mu_i - f_1)\mu_i)$, then the positive constant steady state $(\tilde{u}_1, \tilde{v}_1)$ of (3) is unstable. If $f_1 > d_1\mu_1$, then the positive constant steady state $(\tilde{u}_1, \tilde{v}_1)$ of (3) is unstable.

(2) If $f_1 < 0$, then the positive constant steady state $(\tilde{u}_2, \tilde{v}_2)$ of (3) is locally asymptotically stable; if $f_1 > 0$, then the positive constant steady state $(\tilde{u}_2, \tilde{v}_2)$ of (3) is unstable.

Proof. The linearization operator of (3) at the positive constant solution $(\tilde{u}_i, \tilde{v}_i)$ ($i = 1$ and 2) can be written as

$$L_\sigma = \begin{pmatrix} d_1\Delta + f_1 & f_2 \\ g_1 & d_2\Delta + g_2 \end{pmatrix}, \tag{40}$$

where f_1, f_2, g_1, and g_2 are defined in (36)-(37). According to the linear stability theory, if the real parts of all eigenvalues of L_σ are negative, then $(\tilde{u}_i, \tilde{v}_i)$ is locally asymptotically stable; if there exists the positive real part of the eigenvalue of L_σ, then $(\tilde{u}_i, \tilde{v}_i)$ is unstable.

Let $(\phi(x)$ and $\psi(x))$ be the eigenfunctions corresponding to the eigenvalue λ. Then,

$$L_\sigma(\phi(x), \psi(x)) = \lambda(\phi(x), \psi(x)), \tag{41}$$

that is,

$$\begin{aligned}(d_1\Delta\phi(x) + (f_1 - \lambda)\phi(x) + f_2\psi(x), \\ d_2\Delta\psi(x) + (g_2 - \lambda)\psi(x) + g_1\phi(x)) = (0, 0).\end{aligned} \tag{42}$$

Let

$$\begin{aligned}\phi &= \sum_{0 \leq i < \infty, 1 \leq j \leq m_i} (a_{i,j}\phi_{ij}), \\ \psi &= \sum_{0 \leq i < \infty, 1 \leq j \leq m_i} (b_{i,j}\phi_{ij}), \\ B_i &= \begin{pmatrix} f_1 - d_1\mu_i - \lambda & f_2 \\ g_1 & g_2 - \lambda - d_2 u_i \end{pmatrix}.\end{aligned} \tag{43}$$

Thus, the eigenvalue equation of system (3) is equivalent to

$$\sum_{0 \leq i < \infty, 1 \leq j \leq m_i} B_i(a_{ij}, b_{ij})^T \phi_{ij} = 0. \tag{44}$$

λ is an eigenvalue of L_σ if and only if there exists $i \geq 0$ such as $\det(B_i) = 0$, which is equivalent to

$$\lambda^2 + \tilde{P}_i\lambda + \tilde{Q}_i = 0, \tag{45}$$

where

$$\begin{aligned}\tilde{P}_i &= (d_1 + d_2)\mu_i - f_1, \\ \tilde{Q}_i &= -d_2\mu_i(f_1 - d_1\mu_i) - f_2 g_1.\end{aligned} \tag{46}$$

Next, we check the stability of $(\tilde{u}_1, \tilde{v}_1)$ and $(\tilde{u}_2, \tilde{v}_2)$, respectively.

(1) For the case $(\tilde{u}_1, \tilde{v}_1)$. If $f_1 > d_1\mu_1$, then $\tilde{Q}_0 < 0$ with $i < i_\alpha$. Hence, $(\tilde{u}_1, \tilde{v}_1)$ are unstable. If $f_1 < 0$ and $d_2 > (f_2 g_1/(d_1\mu_i - f_1)\mu_i)$, then $\tilde{P}_i, \tilde{Q}_i > 0$. Thus, $\mathrm{Re}\lambda < 0$ and $(\tilde{u}_1, \tilde{v}_1)$ are locally asymptotically stable. If $f_1 < 0$ and $d_2 < (f_2 g_1/(d_1\mu_i - f_1)\mu_i)$, then $\tilde{Q}_i < 0$. Thus, $\mathrm{Re}\,\lambda > 0$ and $(\tilde{u}_1, \tilde{v}_1)$ are unstable.

(2) For the case $(\tilde{u}_2, \tilde{v}_2)$, if $f_1 < 0$, then $\tilde{P}_i$ and $\tilde{Q}_i > 0$. Thus, $\mathrm{Re}\,\lambda < 0$ and $(\tilde{u}_2, \tilde{v}_2)$ are locally asymptotically stable. If $f_1 > 0$, then $\tilde{P}_0 = -f_1 < 0$ and $\tilde{Q}_0 > 0$. Thus, there exists some unstable $\mathrm{Re}\,\lambda > 0$ and $(\tilde{u}_2, \tilde{v}_2)$. The proof is complete. □

5. Nonconstant Positive Steady States of Equation (3)

The main purpose of this section is to provide some sufficient conditions for the existence and nonexistence of a nonconstant positive solution of (3) by using the Leray–Schauder degree theory [12, 24, 25]. Next, we will establish these results by dividing into two sections.

5.1. Nonexistence. The goal of this part is to establish some sufficient conditions for the nonexistence of nonconstant positive solutions of (3) by the energy norm method. Some related research studies can refer to [8–10]. For the ease of notation, we set

$$\begin{aligned}\bar{u} &= \frac{1}{|\Omega|}\int_\Omega u\,dx, \\ \bar{v} &= \frac{1}{|\Omega|}\int_\Omega v\,dx,\end{aligned} \tag{47}$$

where (u, v) is a positive solution of (3).

Theorem 9. *If $d_1 > (r - a/\mu_1)$ and $cp < 2m\sqrt{d}$, then system (3) has no nonconstant positive classical solution.*

Proof. Let $\omega = u - \bar{u}$ and $\chi = v - \bar{v}$, then $\int_\Omega \omega\,dx = \int_\Omega \chi\,dx = 0$.

Multiplying the second equation of v by χ and integrating over Ω by parts, we obtain

$$\begin{aligned}d_2\int_\Omega |\nabla\chi|^2\,dx &= \int_\Omega\left(-mv + \frac{cpuv}{d + u^2}\right)\chi\,dx, \\ &= \int_\Omega\left[\frac{cpuv}{d + u^2} - \frac{cpu\bar{v}}{d + u^2}\right]\chi\,dx \\ &\quad + \int_\Omega\left[\frac{cpu\bar{v}}{d + u^2} - \frac{cp\bar{u}\bar{v}}{d + \bar{u}^2}\right]\chi\,dx + m\int_\Omega\bar{v}\chi\,dx \\ &\quad - m\int_\Omega v\chi\,dx, \\ &= \int_\Omega\frac{cpu}{d + u^2}\chi^2\,dx + \int_\Omega\frac{cp\bar{v}(d - u\bar{u})}{(d + u^2)(d + \bar{u}^2)}\omega\chi\,dx \\ &\quad - m\int_\Omega\chi^2\,dx, \\ &= \int_\Omega\frac{cp\bar{v}(d - u\bar{u})}{(d + u^2)(d + \bar{u}^2)}\omega\chi\,dx \\ &\quad - \int_\Omega\left(m - \frac{cpu}{d + u^2}\right)\chi^2\,dx.\end{aligned} \tag{48}$$

Thanks to the boundary of u and v (see in Theorem 5), we get

$$d_2 \int_\Omega |\nabla \chi|^2 \mathrm{d}x \le C_1 \int_\Omega |\omega \chi| \mathrm{d}x - C_2 \int_\Omega \chi^2 \mathrm{d}x, \qquad (49)$$

where $C_1 = cp\, d\aleph > 0$ and $C_2 = m - cp/2\sqrt{d}$. Applying Cauchy inequality, we obtain

$$|\omega \chi| \le \frac{\omega^2}{4C_2/C_1} + \frac{C_2}{C_1}\chi^2 = \frac{C_1 \omega^2}{4C_2} + \frac{C_2}{C_1}\chi^2. \qquad (50)$$

Substituting (50) into (49) and using Poincaré inequality, we get

$$d_2 \int_\Omega |\nabla \chi|^2 \mathrm{d}x \le \frac{C_1^2}{4C_2} \int_\Omega \omega^2 \mathrm{d}x \le \frac{C_1^2}{4C_2 \mu_1} \int_\Omega |\nabla \omega|^2 \mathrm{d}x. \qquad (51)$$

Because u and v are nonnegative, we obtain

$$-d_1 \Delta u \le u(r-a). \qquad (52)$$

Multiplying the above equation of u by ω and integrating over Ω by parts, using Poincaré inequality again, we obtain

$$d_1 \int_\Omega |\nabla \omega|^2 \mathrm{d}x \le (r-a) \int_\Omega |\omega^2| \mathrm{d}x \le \frac{r-a}{\mu_1} \int_\Omega |\nabla \omega|^2 \mathrm{d}x, \qquad (53)$$

that is,

$$\int_\Omega |\nabla \omega|^2 \mathrm{d}x \le \frac{r-a}{d_1 \mu_1} \int_\Omega |\nabla \omega|^2 \mathrm{d}x. \qquad (54)$$

If $d_1 > (r-a/\mu_1)$, then $\int_\Omega |\nabla \omega| \mathrm{d}x \equiv 0$. Substituting $\int_\Omega |\nabla \omega| \mathrm{d}x \equiv 0$ into (51), we get

$$\int_\Omega |\nabla \omega| \mathrm{d}x = \int_\Omega \nabla \chi \mathrm{d}x \equiv 0, \qquad (55)$$

which implies that ω and χ are always constant. The proof is complete. $\qquad\square$

5.2. Global Existence.

The goal of this section is to establish the global existence of nonconstant positive classical solutions to (3) when the diffusion coefficients d_1 and d_2 vary while the parameters r, a, b, c, d, m, p, and k are fixed.

For simplicity, we only consider the existence of nonconstant positive classical solutions near $(\tilde{u}_2, \tilde{v}_2)$ which are denoted by $(\tilde{u}, t\tilde{v})$. Letting $\hat{u} = u - \tilde{u}, \hat{v} = v - \tilde{v}$, system (3) can be written as follows:

$$\begin{cases} -d_1 \Delta u = f_1 \hat{u} + f_2 \hat{v} + f_3, \\ -d_2 \Delta v = g_1 \hat{u} + g_3, \end{cases} \qquad (56)$$

where $f_3 \doteq o(|\hat{u}|, |\hat{v}|)$ and $g_3 \doteq o(|\hat{u}|, |\hat{v}|)$.

Define the space S and E as follows:

$$S = \left\{ (\hat{u}, t\hat{v}) : -\hat{u} < \hat{u} < \frac{r-a}{b} - \hat{u}, \quad -\tilde{v} < \hat{v} < \aleph - \tilde{v} \right\},$$

$$E = \left\{ (u, v) : u, v \in C^{1+\beta}(\Omega), \frac{\partial u}{\partial n} = \frac{\partial v}{\partial n} = 0, \quad x \in \partial \Omega \right\}. \qquad (57)$$

Set $U = (\hat{u}, t\hat{v})$, and then, (56) becomes

$$U = \mathrm{KU} + \mathrm{HU}, \qquad (58)$$

where

$$\begin{aligned} \mathrm{KU} &= \left(2f_1 G_{d_1}(\hat{u}) + f_2 G_{d_1}(\hat{v}), g_1 G_{d_2}(\hat{u}) + g_1 G_{d_2}(\hat{v}) \right), \\ \mathrm{HU} &= \left(G_{d_1}(f_3), G_{d_2}(g_3) \right) = o(|U|), \\ G_{d_1} &= (-d_1 \Delta + f_1)^{-1}, \\ G_{d_2} &= (-d_2 \Delta + g_1)^{-1}. \end{aligned} \qquad (59)$$

Theorem 10. *Suppose $cp < 2m\sqrt{d}$ and $d_1\mu_1 < f_1 < \min\{-(f_2/2), d_1\mu_2\}$. If the principal eigenvalue μ_1 has an odd multiple eigenfunction and $d_2 > d_2^{(1)}$, then system (3) has at least one nonconstant positive solution.*

Proof. It is easy to see that system (3) has no solution on the boundary of the space S. According to Homotopy invariance of degree theory, for all $d_1 > 0$, $\deg(I - K - H, E \cap S, 0)$ is well defined and constant. Next, we will prove

$$\deg(I - K - H, E \cap S, 0) = 1. \qquad (60)$$

Assume that $(0, 0)$ is an isolated fixed point of $I - K - H$, then

$$\deg(I - K - H, E, 0) = \mathrm{index}\left(I - K(d_1), (0, 0)\right) = (-1)^\tau, \qquad (61)$$

where τ is the sum of algebraic multiplicity of all eigenvalues greater than 0. Assume that λ is the eigenvalue of $K - I$ and the corresponding eigenfunction is denoted by (ξ, η), then

$$\begin{aligned} -d_1(\lambda+1)\Delta \xi &= (1-\lambda)f_1 \xi + f_2 \eta, \\ -d_2(\lambda+1)\Delta \eta &= g_1 \xi + \lambda g_1 \eta. \end{aligned} \qquad (62)$$

Let

$$\begin{aligned} \xi &= \sum_{0 \le i < \infty, 1 \le j \le m_i} a_{ij} \phi_{ij}, \\ \eta &= \sum_{0 \le i < \infty, 1 \le j \le m_i} b_{ij} \phi_{ij}. \end{aligned} \qquad (63)$$

Thus, the eigenvalue equation of system (3) is equivalent to

$$\sum_{0 \le i < \infty, 1 \le j \le m_i} B_i (a_{ij}, b_{ij})^T \phi_{ij} = 0, \qquad (64)$$

where

$$B_i = \begin{pmatrix} (1-\lambda)f_1 - d_1(1+\lambda)\mu_i & f_2 \\ g_1 & -\lambda g_1 - d_2(1+\lambda)\mu_i \end{pmatrix}. \qquad (65)$$

Thus, all eigenvalues of $K - I$ satisfy

$$\begin{aligned} &\left(f_1 g_1 + d_1 \mu_i g_1 + d_1 d_2 \mu_i^2 + d_2 \mu_i f_1 \right)\lambda^2 \\ &+ \left(2d_1 d_2 \mu_i^2 + d_1 \mu_i g_1 - f_1 g_1 \right)\lambda + d_1 d_2 \mu_i^2 - d_2 f_1 \mu_i - f_2 g_1 = 0. \end{aligned} \qquad (66)$$

Set

$$P_i = 2d_1 d_2 \mu_i^2 + d_1 \mu_i g_1 - f_1 g_1 \text{ and}$$
$$Q_i = d_1 d_2 \mu_i^2 - d_2 f_1 \mu_i - f_2 g_1. \tag{67}$$

Notice that $f_2 < 0, g_1 > 0$, and $f_1 > 0$ are defined in (36)-(37), and it follows that L_σ and $K(d_1) - I$ have the same number of eigenvalues. Thanks to Theorem 9, let $d_1 = \max\{r - a/\mu_1, f_1/\mu_1\} + 1$, then

$$\deg(I - K - H, E \cap S, 0) = \text{index}(I - K(d_1), (0, 0)) = 1. \tag{68}$$

Next, we will calculate the sum of algebraic multiplicity of all eigenvalues of $K - I$ greater than 0.

Owing to $d_1 \mu_1 < f_1$ and $d_2 > d_2^{(1)}$, it is easy to see that

$$Q_i = -d_2 \mu_1 (f_1 - d_1 \mu_1) - f_2 g_1 < -d_2^{(1)} \mu_1 (f_1 - d_1 \mu_1)$$
$$- f_2 g_1 = 0, \quad P_0 < 0, Q_0 > 0. \tag{69}$$

Since $d_1 \mu_2 > f_1$, then

$$Q_i > 0,$$
$$P_i = 2d_1 d_2 \mu_i^2 + d_1 \mu_i g_1 - f_1 g_1 > 0, \quad i \geq 2. \tag{70}$$

Hence, $K - I$ has positive eigenvalues such as λ_1, λ_2, and λ_3, where λ_1 satisfies

$$(f_1 g_1 + d_1 \mu_1 g_1 + d_1 d_2 \mu_1^2 + d_2 \mu_1 f_1)\lambda^2$$
$$+ (2d_1 d_2 \mu_1^2 + d_1 \mu_1 g_1 - f_1 g_1)\lambda + d_1 d_2 \mu_1^2 - d_2 f_1 \mu_1 - f_2 g_1 = 0, \tag{71}$$

and λ_2 and λ_3 satisfy

$$(f_1 g_1 + d_1 \mu_0 g_1 + d_1 d_2 \mu_0^2 + d_2 \mu_0 f_1)\lambda^2$$
$$+ (2d_1 d_2 \mu_0^2 + d_1 \mu_0 g_1 - f_1 g_1)\lambda + d_1 d_2 \mu_0^2 - d_2 f_1 \mu_0 - f_2 g_1 = 0. \tag{72}$$

Therefore, we denote the algebraic multiplicity of λ_j by τ_j with $d_2 > d_2^{(1)}$, and then

$$\tau = \bigcup_{i=1}^{3} \tau_i,$$
$$\tau_j = \dim \bigcup_{i=1}^{\infty} \ker A_j^i, \tag{73}$$
$$A_j = K - (\lambda_j + 1)I, \quad j = 1, 2, 3.$$

We notice that $\tau_1 = m_1$ if and only if $\ker(A_1) \cap R(A_1) = 0$. It is easy to see that

$$\ker(A_1) = \{(f_2, d_1 \mu_1 (1 + \lambda_1) + f_1 (\lambda_1 - 1))^T \phi_{1j}, \quad 1 \leq j \leq m_1\}. \tag{74}$$

Thanks to $R(A_1) = [\ker(A_1^*)]^\perp$, suppose $(\xi, \eta) = \ker(A_1^*)$, then

$$K^*(\xi, \eta)^\perp = (\lambda_1 + 1)(\xi, \eta)^\perp,$$
$$K^*(\xi, \eta)^\perp = (2f_1 G_{d_1}(\xi) + g_1 G_{d_2}(\eta), f_2 G_{d_1}(\xi) + g_1 G_{d_2}(\eta)), \tag{75}$$

that is,

$$2f_1 G_{d_1}(\xi) + g_1 G_{d_2}(\eta) = (\lambda_1 + 1)\xi,$$
$$f_2 G_{d_1}(\xi) + g_1 G_{d_2}(\eta) = (\lambda_1 + 1)\eta. \tag{76}$$

According to the definition of G_{d_1} and G_{d_2}, we obtain

$$d_1 d_2 (f_2 - 2f_1)(\lambda_1 + 1)\Delta\xi = f_\xi \xi - f_\eta \eta,$$
$$d_1 d_2 (f_2 - 2f_1)(\lambda_1 + 1)\Delta\eta = g_\xi \xi - g_\eta \eta, \tag{77}$$

where

$$f_\xi = 2d_2 f_1 [(1 - \lambda_1)f_1 - f_2] + d_1 g_1 f_2 (\lambda_1 + 1),$$
$$f_\eta = 2d_2 f_1^2 (1 + \lambda_1) - d_1 g_1 (f_2 + 2\lambda_1 f_1),$$
$$g_\xi = d_2 f_2 [(1 - \lambda_1)f_1 - f_2] + d_1 g_1 f_2 (\lambda_1 + 1),$$
$$g_\eta = d_2 f_1 f_2 (1 + \lambda_1) - g_1 (f_2 + 2\lambda_1 f_1). \tag{78}$$

By calculating, it follows that

$$B_i^* = \begin{pmatrix} (f_\xi + d_1 d_2 (f_2 - 2f_1)(1 + \lambda_1)\mu_1 & -f_\eta \\ g_\xi & -g_\eta + d_1 d_2 (f_2 - 2f_1)(1 + \lambda_1)\mu_1 \end{pmatrix},$$
$$\ker(A_1^*) = \{((1 + \lambda_1)(f_1 + d_1 \mu_1), f_2 + (\lambda_1 - 1)f_1 + (\lambda_1 + 1)d_1 \mu_1)^T \phi_{1j}, \quad 1 \leq j \leq m_1\}. \tag{79}$$

Next, we will prove that

$$f_2 (1 + \lambda_1)(f_1 + d_1 \mu_1) + [d_1 \mu_1 (1 + \lambda_1) + (\lambda_1 - 1)f_1]$$
$$\times [f_2 + (\lambda_1 - 1)f_1 + (\lambda_1 + 1)d_1 \mu_1] \neq 0. \tag{80}$$

Because λ_1 satisfies

$$(f_1 g_1 + d_1 \mu_i g_1 + d_1 d_2 \mu_i^2 + d_2 \mu_i f_1)\lambda^2$$
$$+ (2d_1 d_2 \mu_i^2 + d_1 \mu_i g_1 - f_1 g_1)\lambda + d_1 d_2 \mu_i^2 - d_2 f_1 \mu_i - f_2 g_1 = 0, \tag{81}$$

define the function $H(\lambda)$ as follows:

$$
\begin{aligned}
H(\lambda) = & \left(f_1 g_1 + d_1 \mu_i g_1 + d_1 d_2 \mu_i^2 + d_2 \mu_i f_1\right)\lambda^2 \\
& + \left(2d_1 d_2 \mu_i^2 + d_1 \mu_i g_1 - f_1 g_1\right)\lambda + d_1 d_2 \mu_i^2 \\
& - d_2 f_1 \mu_i - f_2 g_1.
\end{aligned} \tag{82}
$$

It is easy to see that $H(1) > 0$, so $\lambda_1 < 1$. Notice that

$$
\begin{aligned}
& f_2(1 + \lambda_1)(f_1 + d_1\mu_1) + \left[d_1\mu_1(1 + \lambda_1) + (\lambda_1 - 1)f_1\right] \\
& \quad \times \left[f_2 + (\lambda_1 - 1)f_1 + (\lambda_1 + 1)d_1\mu_1\right] \\
& < f_2(1 + \lambda_1)(f_1 + d_1\mu_1) + 2d_1\mu_1(f_2 + 2d_1\mu_1) \\
& < f_2(1 + \lambda_1)(f_1 + d_1\mu_1) + 2d_1\mu_1(f_2 + 2f_1) < , \neq 0.
\end{aligned} \tag{83}
$$

It follows that $\ker(A_1) \cap (\ker(A_1^*))^\perp = 0$, so $\tau_1 = m_1$. Because λ_0 is a simple eigenvalue, by the similar method, we can get the following result:

$$
\begin{aligned}
\ker(A_2) &= \left\{(f_2, f_1(\lambda_1 - 1))^T \phi_{11}\right\}, \\
\ker(A_2^*) &= \left\{((\lambda_1 - 1)(f_1 + d_1\mu_1), f_2 + (\lambda_1 - 1)f_1)^T \phi_{11}\right\}.
\end{aligned} \tag{84}
$$

It is easy to get

$$
f_2(\lambda_1 + 1)(f_1 + d_1\mu_1) + f_1(\lambda_1 - 1)\left[f_2 + (\lambda_1 - 1)f_1\right] < 0. \tag{85}
$$

Then $\ker(A_2) \cap (\ker(A_2^*))^\perp = 0$, and it follows that $\tau_2 = 1$. Similarly, we can get $\tau_3 = 1$. Combining the above results, we get

$$
\tau = \tau_1 + \tau_2 + \tau_3 = m_1 + 1 + 1. \tag{86}
$$

So τ is an odd number, and we get

$$
\deg(I - K - H, E \cap S, 0) = (-1)^\tau = -1. \tag{87}
$$

The proof is complete. □

6. Conclusion

This paper investigates the diffusive predator-prey system with nonmonotonic functional response and fear effect under homogeneous Neumann boundary conditions. Firstly, we discussed the stability of the equilibrium of the ODE system which corresponds to system (2). Secondly, we established a priori positive upper and lower bounds for the positive solutions of the PDE system by maximum principle (see Theorems 5–7), which means that the density of the two organisms must be in a bounded range if they can coexist in the system. Thirdly, sufficient conditions for the local asymptotical stability of two positive equilibrium solutions of the system are proved by using the method of eigenvalue spectrum analysis of linearization operator (see Theorem 8), which shows that the density values of the two organisms are locally stable at the positive equilibrium point when the model parameters meet certain conditions. Finally, the existence and nonexistence of nonconstant positive steady states of this reaction-diffusion system are established by

using the Leray–Schauder degree theory (see Theorems 9-10). The results of Theorem 9 show that the two organisms cannot coexist in the biological system when the diffusion rate of the prey satisfies some specific conditions. However, the results of Theorem 10 show that two species can coexist in a biological system if their diffusivity satisfies certain conditions at the same time. In fact, we have used different methods to study the similar dynamic behavior of the solution on another predator-prey model in reference [26], and one can refer to it for more detailed results.

Data Availability

No data were used to support this study.

Conflicts of Interest

The authors declare that there are no conflicts of interest regarding the publication of this paper.

Acknowledgments

References

[1] A. J. Lotka, *Elements of Physical Biology*, Williams and Wilkins Co., Baltimore, MD, USA, 1925.

[2] V. Volterra, R. N. Chapman, Variations and fluctuations of the number of individuals in animal species living together," in *Animal Ecology*, pp. 409–448, McGraw-Hill, New York, NY, USA, 1931.

[3] H. Nie and J. Wu, "Multiplicity and stability of a predator-prey model with non-monotonic conversion rate," *Nonlinear Analysis: Real World Applications*, vol. 10, no. 1, pp. 154–171, 2009.

[4] X. Wang, L. Zanette, and X. Zou, "Modelling the fear effect in predator-prey interactions," *Journal of Mathematical Biology*, vol. 73, no. 5, pp. 1179–1204, 2016.

[5] J. Blat and K. J. Brown, "Bifurcation of steady-state solutions in predator-prey and competition systems," *Proceedings of the Royal Society of Edinburgh: Section A Mathematics*, vol. 97, pp. 21–34, 1984.

[6] W.-M. Ni and M. Tang, "Turing patterns in the Lengyel-Epstein system for the CIMA reaction," *Transactions of the American Mathematical Society*, vol. 357, no. 10, pp. 3953–3969, 2005.

[7] R. Wang, W. B. Yang, and L. Y. Li, "Qualitative annlysis of a class of predator-prey model with fear effect," *Chinese Journal of Engineering Mathematics*, vol. 36, no. 4, pp. 439–450, 2019.

[8] P. Y. H. Pang and M. X. Wang, "Non-constant postive steady states of a predator-prey system with non-monotonic functional response and diffusion," *Proceedings of the London Mathematical Society*, vol. 88, no. 3, pp. 135–157, 2004.

[9] J. Yan and X. Liu, "A predator-prey system with Beddington-DeAngelis functional response and fear effect," *Journal of Southwest University*, vol. 46, no. 6, pp. 109–114, 2018.

[10] W. Yang, "Existence and asymptotic behavior of solutions for a predator-prey system with a nonlinear growth rate," *Acta Applicandae Mathematicae*, vol. 152, no. 1, pp. 57–72, 2017.

[11] Y. Du and Y. Lou, "Qualitative behaviour of positive solutions of a predator-prey model: effects of saturation," *Proceedings of the Royal Society of Edinburgh: Section A Mathematics*, vol. 131, no. 2, pp. 321–349, 2001.

[12] E. N. Dancer, "On the indices of fixed points of mappings in cones and applications," *Journal of Mathematical Analysis and Applications*, vol. 91, no. 1, pp. 131–151, 1983.

[13] E. N. Dancer, "On uniqueness and stability for solutions of singularly perturbed predator-prey type equations with diffusion," *Journal of Differential Equations*, vol. 102, no. 1, pp. 1–32, 1993.

[14] W. Yang, X. Feng, S. Liang, and X. Wang, "Asymptotic behavior analysis of a fractional-order tumor-immune interaction model with immunotherapy," *Complexity*, vol. 2020, Article ID 7062957, 2020.

[15] T. Huang, H. Zhang, X. Cong, G. Pan, X. Zhang, and Z. Liu, "Exploring spatiotemporal complexity of a predator-prey system with migration and diffusion by a three-chain coupled map lattice," *Complexity*, vol. 2019, Article ID 3148323, 2019.

[16] S. Li, C. Huang, and X. Song, "Bifurcation based-delay feedback control strategy for a fractional-order two-prey one-predator system," *Complexity*, vol. 2019, Article ID 9673070, 2019.

[17] K. Wonlyul and R. Kimun, "Coexistence states of a predator-prey system with non-monotonic functional response," *Nonlinear Analysis*, vol. 8, pp. 769–786, 2007.

[18] G. Liu, X. Wang, X. Meng, and S. Gao, "Extinction and persistence in mean of a novel delay impulsive stochastic infected predator-prey system with jumps," *Complexity*, vol. 2017, Article ID 1950970, 2017.

[19] F. Dai, X. Z. Feng, and C. T. Li, "Existence of coexistent solution and its stability of predator-prey with Monod-Haldane functional response," *Journal of Xi'an Technological University*, vol. 34, no. 11, pp. 861–865, 2014.

[20] Z. Feng and Y. Zhou, "Long time behavior of solutions for predator-prey system with saturated competition and Leslie-Gower functional response," *Computer Engineering and Applications*, vol. 55, no. 2, pp. 50–53, 2019.

[21] H. Zhu, S. Campbell, and G. Wolkowicz, "Bifurcation analysis of a predator-prey system with nonmonotonic functional reponse," *SIAM Journal on Applied Mathematics*, vol. 63, no. 2, pp. 636–682, 2003.

[22] S. Ruan and D. Xiao, "Global analysis in a predator-prey system with nonmonotonic functional reponse," *SIAM Journal on Applied Mathematics*, vol. 61, no. 4, pp. 1445–1472, 2000.

[23] C. V. Pao, *Nonlinear Parabolic and Elliptic Equations*, Plenum Press, New York, NY, USA, 1992.

[24] Q. Ye, Z. Li, M. Wang, and Y. Wu, "Introduction to reaction-diffusion equations," *Foundations of Modern Mathematics Series*, Science Press, Beijing, China, 2011, in Chinese.

[25] J. Smoller, *Shock Waves and Reaction-Diffusion Equations*, Springer, New York, NY, USA, 1983.

[26] X. Feng, Y. Song, J. Liu, and G. Wang, "Permanence, stability, and coexistence of a diffusive predator-prey model with modified Leslie-Gower and BCD functional response," *Advances in Difference Equations*, vol. 2018, p. 314, 2018.

WILEY | Hindawi

Research Article

The Adjustment of Covariates in Cox's Model under Case-Cohort Design

Guocai Rong,[1] **Luwei Tang,**[2] **Wenting Luo,**[2] **Qing Li,**[1] **and Lifeng Deng** ⓘ[1]

[1]*College of Mathematics and Systems Science, Shandong University of Science and Technology, Qingdao 266590, Shandong, China*
[2]*School of Mathematics and Statistics, Nanning Normal University, Nanning 530001, Guangxi, China*

Correspondence should be addressed to Lifeng Deng; laiji1234@163.com

Case-cohort design is a biased sampling method. Due to its cost-effective and theoretical significance, this design has extensive application value in many large cohort studies. The case-cohort data includes a subcohort sampled randomly from the entire cohort and all the failed subjects outside the subcohort. In this paper, the adjustment for the distorted covariates is considered to case-cohort data in Cox's model. According to the existing adjustable methods of distorted covariates for linear and nonlinear models, we propose estimating the distorting functions by nonparametrically regressing the distorted covariates on the distorting factors; then, the estimators for the parameters are obtained using the estimated covariates. The proof of consistency and being asymptotically normal is completed. For calculating the maximum likelihood estimates of the regression coefficients subject in Cox's model, a minorization-maximization (MM) algorithm is developed. Simulation studies are performed to compare the estimations with the covariates undistorted, distorted, and adjusted to illustrate the proposed methods.

1. Introduction

Many survival data have the characteristics of large sample size and high censoring rate. The cost is very high when all variables of each individual in the data are measured. To reduce the cost and improve the efficiency of cohort studies, Prentice [1] firstly proposed the case-cohort design and gave a pseudolikelihood method to estimate regression parameters. Since the publication of the landmark article [1], case-cohort design has been applied more and more, especially with the development of big data in recent years. For example, some scholars have applied this design to Life Science [2–5] and natural disasters [6], and some other scholars have further improved this design [7, 8], respectively.

In practice, some subjects may be interfered by other factors due to their characteristics, so their corresponding real covariates cannot be observed; only the distorted covariates and the distorting factors can be observed. For example, for the Modification of Diet in Renal Disease (MDRD) study [9, 10], glomerular filtration rate (GFR) and serum creatinine (SCr) data are distorted by the body surface area (BSA). To show the relationship of the two covariates, we need to adjust them by correcting the distorting effect of BSA. The covariate-adjusted regression was introduced for situations where both predictors and response in a regression model are not directly observable, but are contaminated with a multiplicative factor that is determined by the value of an observable factor [11]. For the nonlinear regression model, how to estimate the distorting functions was proposed by nonparametric regression the predictors and response on the distorting covariates [12]. Then, the covariate-adjusted method was extended to other models [13–15]. The data studied in these documents is all complete data. In this paper, the studied data is survival data with right censored data, in which only distorted covariates and distorting factors are included, and the nonparametric method [12] to

estimate the distorting functions to obtain the adjusted value of the distorted covariates on the distorting factors, where the nonparametric method is a kernel smoothing method.

In this article, inspired by the idea of Ding et al. [16] and Deng et al. [17], we construct a surrogate function with a diagonal Hessian matrix by using the convexity of the exponential function and the negative logarithm function and then maximize this surrogate function with a diagonal Hessian matrix. This algorithm is minorization-maximization (MM) algorithm. That is, the first M is to construct a mi-surrogate function and the second M is to maximize the function.

The rest of the article is organized as follows. In Section 2, we firstly fit data from case-cohort design to Cox's model with distorting factors and secondly adjust the distorted covariates by using the kernel function. In Section 3, the convergence of the adjusted covariates and the asymptotic properties for the proposed estimators is completed. In Section 4, we propose a MM algorithm for implementation of the estimation and present a cross-validation (CV) to obtain the optimal bandwidth and a nonparametric boot-strap approach to get the standard error estimation. Several simulation studies are conducted to compare the estimations without distorting factors, with distorting factors, and adjusted with distorting factors in Section 5. Real data analysis of heart failure data is in Section 6. Discussion is stated in Section 7. All proofs are given in Appendix.

2. Design and Estimation

2.1. Model and Design.
Suppose that there are n independent subjects in the studies cohort, where $\widetilde{T}_i$ is the failure time, C_i is the censoring time, $T_i = \min(\widetilde{T}_i, C_i)$ is the observe time for the ith subject, $\Delta_i = I(\widetilde{T}_i \leq C_i)$ is the right-censoring indicator for failure, $Y_i(t) = I(T_i \geq t)$ is the at risk process, and $N_i(t) = \Delta_i I(T_i \leq t)$ is the counting process, where $I(\cdot)$ is an indicator function, τ is the end of study time, and Z_i is a pth covariate for subject i; we focus on the time-independent covariate.

Let $\beta = (\beta_1, \beta_2, \ldots, \beta_p)$ be the unknown p-dimensional vector of regression coefficients. $\widetilde{T}_i$ arises from Cox's model as the following form:

$$\lambda(t|Z) = \lambda_0(t)\exp\{\beta^\top \mathbf{Z}_i(t)\}, \tag{1}$$

where $\lambda_0(t)$ is an unspecified baseline hazard function. The corresponding partial likelihood function is widely used for the inference of β [18] as the following form:

$$L_F(\beta) = \prod_{i=1}^{n} \left[\frac{\exp\{\mathbf{Z}_i(T_i)\beta^\top\}}{\sum_{l=1}^{n} Y_l(T_i)\exp\{\mathbf{Z}_i(T_i)\beta^\top\}}\right]^{\Delta_i}. \tag{2}$$

Under the case-cohort design, let $\widetilde{A}$ denote the sub-cohort, which is selected from the full cohort by simple random sampling, and ξ_i be an indicator, equaling 1 if the ith subject is selected into the subcohort and 0 otherwise. Let A denote the case-cohort sample which contained the subjects

from the subcohort $\widetilde{A}$ and the case outside the subcohort. Therefore, the observed data structure can be summarized as follows: $\{T_i, \Delta_i, (\xi_i + \Delta_i(1 - \xi_i))\mathbf{Z}_i(t), 0 \leq T_i\}$.

The pseudolikelihood function [1] was proposed, and the corresponding pseudolikelihood function takes the following form:

$$L_p(\beta) = \sum_{i=1}^{n} \omega_i \Delta_i \left[\beta^\top \mathbf{Z}_i(T_i) - \log \sum_{i=1}^{n} Y_l(T_i)\omega_l \exp\{\beta^\top \mathbf{Z}_l(T_i)\}\right], \tag{3}$$

where $\omega_i = \Delta_i + (1 - \Delta_i)\xi_i$.

2.2. The Adjustment of Covariates.
We now study that the covariates are distorted by some distorting factors. The distorted observed data structure is

$$\left\{T_i, \Delta_i, (\xi_i + \Delta_i(1 - \xi_i))\widetilde{Z}_i(t), U_i, 0 \leq t \leq T_i\right\}, \tag{4}$$

where U_i is the ith distorting factor and $\widetilde{Z}_i(t)$ is the ith distorted covariate. Here, $Z_i(t)$ is unobservable, and $\phi(U)$ is denoted as the unknown distorting functions of observable factor U.

Firstly, we give some basic assumptions [12] as follows:

(i) $\widetilde{Z}_r = \phi_r(U)\mathbf{Z}_r$

(ii) $E[\phi_r(U)] = 1, r = 1, 2, \ldots, p$

(iii) $(\mathbf{Z}_r, U)$ are independent of each other, $r = 1, 2, \ldots, p$

Under these assumptions, the working-likelihood function (3) can be rewritten as the following form:

$$\begin{cases} \widetilde{l}_p(\beta) = \sum_{i=1}^{n} \omega_i \Delta_i \left[\beta^\top \widetilde{Z}_i(T_i) - \log \sum_{l=1}^{n} Y_l(T_i)\omega_i \exp\{\beta^\top \widetilde{Z}_l(T_i)\}\right], \\ \widetilde{Z}_{ri} = \phi_r(U_i)Z_{ri}. \end{cases} \tag{5}$$

Now, our object is to estimate the unknown coefficients β based on observation (4) and function (5). From condition (A3), we have

$$\phi_r(U) = \frac{E[\widetilde{Z}_r|U]}{E[\mathbf{Z}_r]}, \quad 1 \leq r \leq p. \tag{6}$$

Many scholars have exposed some methods to estimate $\phi_r(U)$ [19]. So, we construct the function $\phi_r(U)$ by using the classic kernel method, for $1 \leq r \leq p$:

$$\widehat{\phi}_r(U) = \frac{1/(nh)\sum_{i=1}^{n} K((u - U_i)/h)\widetilde{Z}_{ir}}{1/(nh)\sum_{i=1}^{n} K((u - \omega_i)/h)} \times \frac{1}{\overline{\widetilde{Z}}_r}, \tag{7}$$

where $\overline{\widetilde{Z}}_r = 1/n\sum_{i=1}^{n} \widetilde{Z}_{ri}$, $K(\cdot)$ is a kernel function, and h is bandwidth.

Let $\widehat{Z}_{ri} = \widetilde{Z}_{ri}/\widehat{\phi}_r(U_i)$ denote the adjusted covariate. That is, we obtain the adjusted covariates by removing the distorting factors from the distorted covariates. Then, function (4) can be abbreviated as

$$\widehat{l}_p(\beta) = \sum_{i=1}^{n} \omega_i \Delta_i \left[\widehat{Z}_i(T_i)\beta^\top - \log \sum_{l=1}^{n} Y_l(T_i)\omega_l \exp\{\widehat{Z}_l(T_i)\beta^\top\} \right]. \tag{8}$$

Under the case-cohort design, the estimate $\widehat{\beta}$ about the adjustment of covariates is defined as follows:

$$\widehat{\beta} = \arg\max_{\beta} \widehat{l}_p(\beta). \tag{9}$$

3. Consistency and Asymptotic Normality

To present the asymptotic results, we will introduce some notations. Let β_0 denote the true value of β. For $d = 0, 1, 2$, define

$$S^d(\beta, t) = \frac{1}{n} \sum_{i \in A} Y_i(t) \exp\{\mathbf{Z}_i^T \beta\} \mathbf{Z}_i^{\otimes d},$$

$$\widetilde{S}^d(\beta, t) = \frac{1}{\widetilde{n}} \sum_{i \in \widetilde{A}} Y_i(t) \exp\{\mathbf{Z}_i^\top \beta\} \mathbf{Z}_i^{\otimes d},$$

$$Q^d(\beta, t, \omega) = \frac{1}{n} \sum_{i \in A} Y_i(t) Y_i(\omega) \exp\{2\mathbf{Z}_i^\top \beta\} \mathbf{Z}_i^{\otimes d}, \tag{10}$$

$$\widetilde{Q}^d(\beta, t, \omega) = \frac{1}{\widetilde{n}} \sum_{i \in \widetilde{A}} Y_i(t) Y_i(\omega) \exp\{2\mathbf{Z}_i^\top \beta\} \mathbf{Z}_i^{\otimes d},$$

where $\mathbf{a}^{\otimes 0} = 1$, $\mathbf{a}^{\otimes 1} = \mathbf{a}$, and $\mathbf{a}^{\otimes 2} = \mathbf{a}\mathbf{a}^\top$ for a vector $\mathbf{a}$.

Define

$$E(\beta, t) = \frac{S^{(1)}(\beta, t)}{S^{(0)}(\beta, t)},$$

$$\widetilde{E}(\beta, t) = \frac{\widetilde{S}^{(1)}(\beta, t)}{\widetilde{S}^{(0)}(\beta, t)}. \tag{11}$$

We impose the following conditions throughout the paper. Note that convergence properties involve $n \longrightarrow \infty$ and $\| \cdot \|$ refers to the Euclidean norm in these conditions:

(A1) $\int_0^\tau \lambda_0(t) \mathrm{d}t < \infty$.

(A2) There exists some $\delta > 0$ such that $n^{-1/2} \sup_{i, t \in [0, \tau]} Y_i(t) |\mathbf{Z}_i| I\{\mathbf{Z}_i^T \beta_0 > -\delta |\mathbf{Z}_i|\} \overset{P}{\longrightarrow} 0$.

(A3) There exists a neighborhood β of β_0, and functions $s^d(\beta, t)$, $d = 0, 1, 2$, defined on $\beta \times [0, \tau]$, which satisfy

  (i) $\sup_{\beta \in \mathscr{B}, t \in [0, \tau]} \|S^d(\beta, t) - s^d(\beta, t)\| \overset{P}{\longrightarrow} 0$, $d = 0, 1, 2$.

(ii) $s^d(\beta, t)$, $d = 0, 1, 2$, are continuous of β on $\mathscr{B}$ uniformly in $t \in [0, \tau]$; $s^d(\beta, t)$, $d = 0, 1, 2$, are bounded on $\mathscr{B} \times [0, \tau]$, and $s^{(0)}(\beta, t)$ is bounded away from zero; and $s^{(1)}(\beta, t) = \nabla_\beta s^{(0)}(\beta, t)$ and $s^{(2)}(\beta, t) = \nabla_\beta^2 s^{(0)}(\beta, t)$ for all $\beta \in \mathscr{B}$, $t \in [0, \tau]$.

(iii) The matrix

$$\Sigma(\beta_0) = \int_0^\tau \nu(\beta_0, t) s^{(0)}(\beta, t) \lambda_0(t) \mathrm{d}t \tag{12}$$

is positive definite, where $\nu(\beta_0, t) = ((s^{(2)}(\beta_0, t))/(s^{(0)}(\beta_0, t))) - \{(s^{(1)}(\beta_0, t))/(s^{(0)}(\beta_0, t))\}^{\otimes 2}$.

(B1) $\widetilde{n}/n \longrightarrow \alpha$ for some $\alpha \in (0, 1)$.

(B2) The sequence of distributions of $n^{1/2}\{\widetilde{E}(\beta_0, t)t - nEq(\beta_0, t)\}$ is tight on $\mathscr{B} \times [0, \tau]$ of left-continuous functions with right-hand limits equipped with the product Skorohod topology.

(B3) The existing functions $q^d(\beta, t, \omega)$, $d = 0, 1, 2$, defined on $\mathscr{B} \times [0, \tau]^2$ which satisfy

  (i) $\sup_{\beta \in \mathscr{B}, (t, w) \in [0, \tau]^2} \|Q^{(d)}(\beta, t, \omega) - q^{(d)}(\beta, t, \omega)\| \overset{P}{\longrightarrow} 0$, $d = 0, 1, 2$.

  (ii) $q^{(d)}(\beta, t, \omega)$, $d = 0, 1, 2$, are continuous of β on $\mathscr{B}$ uniformly in $(t, w) \in [0, \tau]^2$, and $q^{(d)}(\beta, t, \omega)$, $d = 0, 1, 2$, are bounded on $\mathscr{B} \times [0, \tau]^2$.

  (iii) $\sup_{n \geq 1} E\{Q^{(d)}(\beta, t, \omega)\}$, $d = 0, 1, 2$, are bounded sequences.

(B4) For $d = 0, 1, 2$,

$$\sup_{\beta \in \mathscr{B}, t \in [0, \tau]} \left\| \widetilde{S}^{(d)}(\beta, t) - s^{(d)}(\beta, t) \right\| \overset{P}{\longrightarrow} 0,$$

$$\sup_{\beta \in \mathscr{B}, (t, w) \in [0, \tau]^2} \left\| \widetilde{Q}^{(d)}(\beta, t, \omega) - q^{(d)}(\beta, t, \omega) \right\| \overset{P}{\longrightarrow} 0. \tag{13}$$

(C) All $g_r(U) = \phi_r(U)p(U)$, $1 \leq r \leq p$, and $\phi_r(U)$ and $p(U)$ are greater than a positive constant. They are differential and their derivatives satisfy the condition that there exists a neighborhood of the origin. For example, Δ and a constant $c > 0$ such that, for any $\xi \in \Delta |g_r^3(U + \xi) - g_r^3(U)| \leq c|\xi|$, $1 \leq r \leq p$, $|p^3(U + \xi) - p^3(U)| \leq c|\xi|$.

(D1) The continuous kernel function $K(\cdot)$ satisfies the following properties:

  (i) The support of $K(\cdot)$ is the interval $[-1, 1]$.
  (ii) $K(\cdot)$ is symmetric about zero.
  (iii) $\int_{-1}^{1} K(U)\mathrm{d}U = 1$ and $\int_{-1}^{1} U^d k(U)\mathrm{d}U = 0$, $d = 1, 2, 3$.

(D2) As $n \longrightarrow \infty$, the bandwidth h is in the range from $O(n^{-1/4}\log(n))$ to $O(n^{-1/8})$.

(E) $E[\mathbf{Z}_r]$ is bounded away from 0, $E[\mathbf{Z}_r]^2 < \infty$. These conditions are mild and can be satisfied in most circumstances.

Conditions (A1)–(A3) are the regularity conditions for the asymptotic results of Cox's model [20]. Conditions (B1)–(B4) are the regular conditions under the case-cohort design [21]. Conditions (C) are related to smoothness of the function $g_r(\cdot)$ and the density function $p(\cdot)$ of U. Conditions (D1)-(D2) are commonly assumed for the root n consistency of kernel-based estimation [22, 23]. Condition (E) is special for this problem [12, 22].

Under these conditions, we have the following result with detailed proofs given in Appendix.

Theorem 1. *(asymptotic properties of $\widehat{\beta}$). Under conditions (A1)–(A3), (B1)–(B4), (C), (D1)-(D2), and (E), $\widehat{\beta}$ converges in probability to β_0, and*

$$\sqrt{n}\left(\widehat{\beta} - t\beta_0\right) \xrightarrow{d} N\left(0, \Omega(\beta_0)\right), \tag{14}$$

where the asymptotic variance matrix $\Omega(\beta_0) = \Sigma_0(\beta_0) + \Sigma_1(\beta_0)$, where

$$\Sigma_1(\beta_0) = \int_0^\tau \int_0^\tau \Psi(\beta_0, t, \omega)s^{(0)}(\beta_0, t)s^{(0)}(\beta_0, \omega)\lambda_0(t)\lambda_0(\omega)\mathrm{d}t\mathrm{d}\omega,$$

$$\Psi(\beta_0, t, w) = (1 - \alpha)\alpha^{-1}\left\{s^{(0)}(\beta_0, t)s^{(0)}(\beta_0, w)\right\}^{-1}$$

$$\cdot \left\{q^{(2)}(\beta_0, t, w) - q^{(1)}(\beta_0, w, t)e(\beta_0, w)' - e(\beta_0, t)q^{(1)}(\beta_0, t, w)'\right.$$

$$\left. + q^{(0)}(\beta_0, t, w)e(\beta_0, t)e(\beta_0, w)'\right\}, \tag{15}$$

$$e(\beta_0, t) = \frac{s^{(1)}(\beta_0, t)}{s^{(0)}(\beta_0, t)},$$

$$e(\beta_0, \omega) = \frac{s^{(1)}(\beta_0, \omega)}{s^{(0)}(\beta_0, \omega)}.$$

4. The Implementation of Algorithm

In Section 3, we have finished the asymptotic properties for the adjusted estimation $\widehat{\beta}$. To obtain $\widehat{\beta}$ by solution of function (9), we can use the Newton–Raphson algorithm. However, in the process of calculation, we find that its Hessian matrix is complicated and easily irreversible. So, we proposed the MM algorithm [16] to get $\widehat{\beta}$ for the adjustment of distorted covariates under case-cohort design.

4.1. Construct Surrogate. The key of the MM algorithm to construct surrogate function: combine the ideas of [16]; we expose the surrogate function $\widehat{Q}(\beta|\beta^{(m)})$ for $\widehat{l}_p(\beta)$ by using the convexity of the exponential function e^x and the negative logarithm function $-\log(x)$:

$$\widehat{Q}\left(\beta|\beta^{(m)}\right) = \widehat{c}_0 + \sum_{i=1}^n \omega_i \Delta_i \left[\beta^\top \widehat{Z}_i(T_i) - \frac{\sum_{l=1}^n \sum_{r=1}^p Y_l(T_i)\omega_l \widehat{\lambda}_{lr}\widehat{g}_{lr}\left(\beta_r|\beta^{(m)}\right)}{\sum_{l=1}^n Y_l(T_i)\omega_l \exp\left\{\widehat{Z}_l^\top(T_i)\beta^{(m)}\right\}}\right], \tag{16}$$

where $\beta^{(m)}$ is the mth approximate of the adjusted maximum likelihood estimation $\widehat{\beta}$ defined in (9), and

$$\widehat{c}_0 = \sum_{i=1}^{n} \omega_i \Delta_i \left\{ 1 - \log\left[\sum_{l=1}^{n} Y_l(T_i)\omega_l \exp\left\{ \widehat{Z}_l(T_i)^\top \beta^{(m)} \right\} \right] \right\},$$

$$\widehat{g}_{lr}\left(\beta_r | \beta^{(m)} \right) = \exp\left[\widehat{\lambda}_{lr}^{-1} \widehat{Z}_{lr}(T_i)\left(\beta_r - \beta_r^{(m)} \right) + \widehat{Z}_l^\top(T_i)\beta^{(m)} \right], \tag{17}$$

$$\widehat{\lambda}_{lr} = \frac{\left| \widehat{Z}_{lr}(T_i) \right|}{\sum_{r=1}^{p} \left| \widehat{Z}_{lr}(T_i) \right|},$$

with $\widehat{\lambda}_{lr}^{-1} = 0$ if $\widehat{Z}_l^\top(T_i) = 0$, where β_r, $\beta_r^{(m)}$, and $\widehat{Z}_{lr}$ are the rth components of β, $\beta^{(m)}$, and $\widehat{Z}_l$, respectively.

With the surrogate function (16), we can transfer the optimization problem (9) into the problem as follows:

$$\beta^{(m+1)} = \arg\max_{\beta} \widehat{Q}\left(\beta | \beta^{(m)} \right). \tag{18}$$

Following the construction process of the surrogate function (16), we can immediately conclude that

$$\widehat{l}_p(\beta) \geq \widehat{Q}\left(\beta | \beta^{(m)} \right), \tag{19}$$

where $\widehat{l}_p(\beta) = \widehat{Q}(\beta | \beta^{(m)})$ if and only if $\beta = \beta^{(m)}$.

Then, with $\widehat{Q}(\beta^{(m+1)} | \beta^{(m)}) \geq \widehat{Q}(\beta^{(m)} | \beta^{(m)})$, we have

$$\begin{aligned} \widehat{l}_p\left(\beta^{(m+1)} \right) &= \widehat{l}_p\left(\beta^{(m+1)} \right) - \widehat{Q}\left(\beta^{(m+1)} | \beta^{(m)} \right) + \widehat{Q}\left(\beta^{(m+1)} | \beta^{(m)} \right) \\ &\geq \widehat{l}_p\left(\beta^{(m)} \right) - \widehat{Q}\left(\beta^{(m)} | \beta^{(m)} \right) + \widehat{Q}\left(\beta^{(m)} | \beta^{(m)} \right) \\ &= \widehat{l}_p\left(\beta^{(m)} \right), \end{aligned} \tag{20}$$

where $\widehat{l}_p(\beta)$ is strictly ascending when $\beta^{(m+1)} \neq \beta^{(m)}$.

With the surrogate function (16), we obtain the derivatives with respect to β if $\beta = \beta^{(m)}$ as follows.

The score vector:

$$\frac{\partial \widehat{Q}\left(\beta^{(m)} | \beta^{(m)} \right)}{\partial \beta} = \sum_{i=1}^{n} \Delta_i \left[\widehat{Z}(T_i) - \frac{\sum_{l=1}^{n} Y_l(T_i)\omega_l \widehat{Z}_l(T_i) \exp\left\{ \widehat{Z}_l^\top(T_i)\beta^{(m)} \right\}}{\sum_{l=1}^{n} Y_l(T_I)\omega_l \exp\left\{ \widehat{Z}_l^\top(T_i)\beta^{(m)} \right\}} \right]. \tag{21}$$

The negative Hessian matrix:

$$-\frac{\partial^2 \widehat{Q}\left(\beta^{(m)} | \beta^{(m)} \right)}{\partial\beta\,\partial\beta^\top} = \operatorname{diag}\left\{ -\frac{\partial^2 \widehat{Q}\left(\beta^{(m)} | \beta^{(m)} \right)}{\partial^2 \beta_1}, \ldots, \right.$$
$$\left. -\frac{\partial^2 \widehat{Q}\left(\beta^{(m)} | \beta^{(m)} \right)}{\partial^2 \beta_p} \right\}, \tag{22}$$

where

$$-\frac{\partial^2 \widehat{Q}\left(\beta^{(m)} | \beta^{(m)} \right)}{\partial \beta_r^2}$$
$$= \sum_{i=1}^{n} \Delta_i \omega_i \frac{\sum_{l=1}^{n} Y_l(T_i)\omega_l \widehat{Z}_{lr}^2 / \widehat{\lambda}_{lr} \exp\left\{ \widehat{Z}_l(T_i)\beta^{(m)} \right\}}{\sum_{l=1}^{n} Y_l(T_i)\omega_l \exp\left\{ \widehat{Z}_l(T_i)\beta^{(m)} \right\}}, \tag{23}$$

$$r = 1, 2, \ldots, p.$$

Here, the Hessian matrix is diagonal, the process of calculation changes simply and is reversible by using Newton–Raphson algorithm.

4.2. Cross-Validation and Bootstrap

4.2.1. Cross-Validation.
In the process of the adjustment for the distorted covariates, we use the cross-validation (CV) method to obtain the optimal bandwidth h to construct the kernel smoothing methods. The idea of the CV method is to calculate the coverage of error between some naive responses and the estimated responses obtained from the model fitted by the other predictors. The specific expression of the function in this article is given as follows:

$$CV(h) = \sum_{j=1}^{n} \left[\frac{1}{nh} \sum_{i=1}^{n} K\left(\frac{u_j - u_i}{h} \right) \right]^2 \Delta u$$
$$-\frac{2}{n} \sum_{j=1}^{n} \left[\frac{2}{nh} \sum_{j \neq i} K\left(\frac{u_j - u_{-i}}{h} \right) \right], \tag{24}$$

where u_{-i} is the set of removed ith element, $\Delta u = u_j - u_{j-1}$.

Then, the optimal bandwidth is defined as follows:

$$\widehat{h} = \arg\min_{h} CV(h). \tag{25}$$

4.2.2. Bootstrap.
Bootstrap has been widely used since it was first proposed [24–26]. We adopt this method to calculate the standard error of $\widehat{\beta}$; the basic idea of the nonparametric approach is to construct an empirical distribution function by repeatedly sampling from the observed data. The steps are summarized as follows:

Step 1: $\left\{ \widehat{X}_1, \widehat{X}_2, \ldots, \widehat{X}_n \right\}$ are the adjusted observations under the case-cohort design, where $\widehat{X}_i = \{ (T_i, \Delta_i, U_i, (\xi_i + (1 - \xi_i)\Delta_i)\widehat{Z}_i, 1 \leq i \leq n \}$. We use the samples

with $\Delta_i = 1$ as the failure cases and the samples with $\Delta_i = 0$ as the censoring objects to constitute the bootstrap case-cohort sample $\{\widehat{X}_1^*, \widehat{X}_2^*, \ldots, \widehat{X}_n^*\}$.

Step 2: a bootstrap replication $\widehat{\beta}^*$ can be obtained based on $\{\widehat{X}_1^*, \widehat{X}_2^*, \ldots, \widehat{X}_n^*\}$.

Step 3: repeating step 1 and step 2 B times, we can obtain B bootstrap estimate $\{\widehat{\beta}_1^*, \ldots, \widehat{\beta}_B^*\}$. Therefore, the standard error of the rth component of $\widehat{\beta}$ can be estimated by the following form:

$$\widehat{Se}(\widehat{\beta}_r) = \sqrt{\frac{1}{B-1} \sum_{b=1}^{B} \left[\widehat{\beta}_r^*(b) - \frac{1}{B} \sum_{b=1}^{B} \widehat{\beta}_r^*(b) \right]^2}, \tag{26}$$

$$r = 1, 2, \ldots, p.$$

5. Simulation

As we mentioned before, if the distorting factors on covariates were ignored, the result of inference may be misled [11, 12]. In this article, we will construct several simulation studies to compare the three estimators of regression coefficient $\widehat{\beta}$ for the covariates without distorting factors, with distorting factors, and adjusted with distorting factors in Cox's model. Under the case-cohort design, where $\widehat{\beta}_W$ denotes the estimator calculated based on the covariates without distorting factors, $\widehat{\beta}_C$ denotes the estimator calculated based on the covariates with distorting factors, and $\widehat{\beta}_A$ denotes the estimator calculate based on the adjusted covariates with distorting factors, given $(\mathbf{Z}_1, \mathbf{Z}_2)$, we consider the hazard function of the failure time $\widetilde{T}_i$ as follows:

$$\lambda(t|\mathbf{Z}_1, \mathbf{Z}_2) = \lambda_0(t) \exp(\beta_1 \mathbf{Z}_1 + \beta_2 \mathbf{Z}_2). \tag{27}$$

We set the true values of the parameters β to $(-0.25, 0.5)$, $(-0.25, 0.693)$, and $(0, 0.5)$. $\mathbf{Z}_1$ is generated from a normal distribution with mean $\mathbf{Z}$ and variance 1.44. $\mathbf{Z}_2$ is generated from a uniform distribution $U((7/3) - (\sqrt{19}/2), (7/3) + (\sqrt{19}/2))$. The distorting factor U is generated from a uniform distribution $U(4 - \sqrt{7}, 4 + \sqrt{7})$. The baseline hazard function $\lambda_0(t)$ is set to be 1 and $2t$. Thus, the failure time $\widetilde{T}$ satisfies an exponential distribution with failure rate $\exp(\beta_1 Z_1 + \beta_2 Z_2)$ and scale parameter $[\exp(\beta_1 Z_1 + \beta_2 Z_2)]^{-1/2}$, respectively. The censoring time C is generated from a uniform distribution $U(0, c)$ with c being chosen to desire the censoring rate $\rho = 80\%$, 85%, and 90%.

Under the case-cohort design, 1000 full cohort samples are generated from function (27), and the corresponding distorting factor is generated. The two parts are merged to constitute the observed sample. Then, we randomly selected $\widetilde{n} = 150$, 200, and 300 subcohort from the full cohort.

We compare the sample bias (Bias), the sample MSE (SMSE), the sample standard deviations of estimates (SD), the means of estimated standard errors (SE), and the coverage probabilities of 95% nominal confidence intervals (CP) of the three estimators to $\widehat{\beta}_C, \widehat{\beta}_W$, and $\widehat{\beta}_A$ based on 1000

independent simulated datasets and especially apply the nonparametric bootstrap approach in Section 4.2.2 with $B = 500$. We set only the covariate Z_2 to be distorted and adjusted. The distribution of the distorting factor U is set to be $\Phi(u) = ((u + 10)^2/194.9160)$. The kernel function is set to be an Epanechnikov kernel [27] $K(t) = (15/32)(3 - 7t^2)(1 - t^2)(|t| \le 1)$. The optimal bandwidth h is selected by the CV method in Section 4.2.1. The criteria are stopped with $\varepsilon = 0.0001$. The simulation results are summarized in Table 1 with $\beta = (-0.25, 0.5)$, Table 2 with $\beta = (-0.25, 0.693)$, and Table 3 with $\beta = (0, 0.5)$, respectively.

According to the simulation results, the estimators $\widehat{\beta}_W$ and $\widehat{\beta}_A$ for β_2 are all unbiased, the three values of SMSE, SD, and SE are all closed, and the CP values are reasonable. However, the estimators $\widehat{\beta}_C$ for β_2 are all biased, the difference between the two values of SMSE and SD is large, and the CP value is low. These facts confirm that ignoring the distorting factors may lead to the wrong results and conclusion and also explain that the proposed method about the adjustment of covariates is effective. For example, the estimator $\widehat{\beta}_C$ and $\widehat{\beta}_A$ for $\beta = (-0.25, 0.5)$, $\rho = 80\%$, $\widetilde{n} = 150$, for β_2, the bias is -0.1178, SMSE are 0.1521 and 0.1095, and CP are 0.735 and 0.947, respectively. Furthermore, we can conclude that the estimators for β_1 are all reasonable.

6. Real Data Analysis

The dataset is about the medical records of heart failure patients, from "Machine Learning Repository" (http://archive.ics.uci.edu/ml/datasets/Heart+failure+clinical+records). The original dataset version was collected by Tanvir Ahmad et al. (Government College University, Faisalabad, Pakistan) and made available by them on FigShare under the Attribution 4.0 International copyright in July 2017. The current version of the dataset was elaborated by Davide Chicco et al. and donated to the University of California Irvine Machine Learning Repository under the same Attribution 4.0 International copyright in January 2020.

This dataset contains the medical records of 299 patients who had heart failure, collected during their follow-up period, where each patient profile has 13 clinical features, including age, anaemia, creatinine phosphokinase, diabetes, ejection fraction, high blood pressure, platelets, serum creatinine, serum sodium, sex, smoking, time, and death event. The goal is to assess the association between clinical features and heart failure and its happened time. This real data is survival data which meets the requirements of the article. Death event and time are regarded as heart failure and its happened time, respectively. For the remaining 11 clinical features, through pairwise correlation analysis, we conclude that ejection fraction and serum sodium and anaemia and Creatinine phosphokinase are significantly related. Referring to relevant medical knowledge, we know that ejection fraction may distort serum sodium. And in the same way, anaemia may distort creatinine phosphokinase. The main purpose of our research is to evaluate the

TABLE 1: $\beta = (-0.25, 0.5)$, $Z_1 \sim N(2, 1.44)$, $Z_2 \sim U((7/3) - (\sqrt{19}/2), (7/3) + (\sqrt{19}/2))$, $u \sim U(4 - \sqrt{7}, 4 + \sqrt{7})$.

$\tilde{n}$	ρ (%)	Type	$\beta_1 = -0.25$					$\beta_2 = 0.5$				
			Bias	SMSE	SD	SE	CP	Bias	SMSE	SD	SE	CP
							$\lambda_0(t) = 1$					
150	80	$\widehat{\beta}_W$	−0.0102	0.0965	0.0960	0.0992	0.965	0.0146	0.1094	0.1085	0.1118	0.961
		$\widehat{\beta}_C$	−0.0074	0.0961	0.0958	0.0978	0.959	−0.1158	0.1499	0.0951	0.0975	0.742
		$\widehat{\beta}_A$	−0.0100	0.0960	0.0955	0.0990	0.964	0.0050	0.1105	0.1104	0.1126	0.955
	85	$\widehat{\beta}_W$	−0.0145	0.1051	0.1042	0.1053	0.950	0.0115	0.1167	0.1162	0.1189	0.960
		$\widehat{\beta}_C$	−0.0003	0.0968	0.0968	0.1030	0.956	−0.1199	0.1575	0.1022	0.1024	0.724
		$\widehat{\beta}_A$	−0.0014	0.0971	0.0971	0.1041	0.964	−0.0046	0.1201	0.1201	0.1197	0.950
	90	$\widehat{\beta}_W$	−0.0098	0.1114	0.1110	0.1153	0.961	0.0237	0.1306	0.1285	0.1328	0.957
		$\widehat{\beta}_C$	−0.0094	0.1096	0.1093	0.1141	0.962	−0.1129	0.1563	0.1081	0.1116	0.802
		$\widehat{\beta}_A$	−0.0096	0.1113	0.1109	0.1152	0.963	0.0106	0.1292	0.1288	0.1326	0.954
200	80	$\widehat{\beta}_W$	−0.0090	0.0815	0.0810	0.0878	0.969	0.0084	0.0991	0.0988	0.0992	0.943
		$\widehat{\beta}_C$	−0.0051	0.0807	0.0806	0.0868	0.971	−0.1227	0.1497	0.0858	0.0852	0.669
		$\widehat{\beta}_A$	−0.0091	0.0818	0.0814	0.0877	0.968	0.0006	0.1012	0.1013	0.0994	0.944
	85	$\widehat{\beta}_W$	−0.0049	0.0899	0.0898	0.0926	0.951	0.0005	0.1007	0.1008	0.1055	0.963
		$\widehat{\beta}_C$	−0.0027	0.0928	0.0928	0.0914	0.940	−0.1274	0.1560	0.0900	0.0897	0.666
		$\widehat{\beta}_A$	−0.0048	0.0950	0.0949	0.0923	0.941	−0.0026	0.1063	0.1063	0.1061	0.949
	90	$\widehat{\beta}_W$	−0.0094	0.1035	0.1031	0.1036	0.954	0.0117	0.1174	0.1169	0.1196	0.962
		$\widehat{\beta}_C$	−0.0089	0.1038	0.1035	0.1027	0.949	−0.1229	0.1563	0.0965	0.0986	0.720
		$\widehat{\beta}_A$	−0.0085	0.1034	0.1031	0.1034	0.953	−0.0005	0.1151	0.1152	0.1188	0.960
300	80	$\widehat{\beta}_W$	−0.0029	0.0732	0.0732	0.0737	0.951	0.0060	0.0848	0.0847	0.0850	0.954
		$\widehat{\beta}_C$	−0.0008	0.0725	0.0726	0.0730	0.941	−0.1241	0.1432	0.0714	0.0712	0.561
		$\widehat{\beta}_A$	−0.0023	0.0727	0.0727	0.0736	0.950	−0.0046	0.0844	0.0843	0.0848	0.952
	85	$\widehat{\beta}_W$	−0.0054	0.0804	0.0803	0.0795	0.948	0.0069	0.0902	0.0900	0.0929	0.959
		$\widehat{\beta}_C$	−0.0025	0.0768	0.0768	0.0792	0.953	−0.1325	0.1532	0.0768	0.0761	0.568
		$\widehat{\beta}_A$	−0.0036	0.0764	0.0763	0.0798	0.954	−0.0114	0.0927	0.0921	0.0921	0.947
	90	$\widehat{\beta}_W$	−0.0034	0.0912	0.0912	0.0910	0.958	0.0062	0.1105	0.1103	0.1078	0.950
		$\widehat{\beta}_C$	−0.0023	0.0902	0.0902	0.0904	0.961	−0.1308	0.1575	0.0877	0.0861	0.632
		$\widehat{\beta}_A$	−0.0037	0.0908	0.0907	0.0909	0.957	−0.0069	0.1093	0.1091	0.1063	0.947
							$\lambda_0(t) = 2t$					
150	80	$\widehat{\beta}_W$	−0.0067	0.1107	0.1105	0.1092	0.948	0.0103	0.1205	0.1201	0.1230	0.958
		$\widehat{\beta}_C$	−0.0037	0.1110	0.1110	0.1078	0.943	−0.1170	0.1571	0.1049	0.1082	0.773
		$\widehat{\beta}_A$	−0.0060	0.1098	0.1097	0.1091	0.948	0.0001	0.1198	0.1199	0.1238	0.958
	85	$\widehat{\beta}_W$	−0.0040	0.1111	0.1111	0.1143	0.966	0.0161	0.1316	0.1306	0.1307	0.952
		$\widehat{\beta}_C$	−0.0001	0.1104	0.1105	0.1127	0.958	−0.1183	0.1606	0.1087	0.1139	0.798
		$\widehat{\beta}_A$	−0.0036	0.1109	0.1109	0.1141	0.964	0.0069	0.1303	0.1302	0.1314	0.951
	90	$\widehat{\beta}_W$	−0.0075	0.1242	0.1240	0.1254	0.954	0.0102	0.1445	0.1442	0.1433	0.954
		$\widehat{\beta}_C$	−0.0062	0.1228	0.1227	0.1238	0.954	−0.1259	0.1737	0.1197	0.1216	0.784
		$\widehat{\beta}_A$	−0.0066	0.1234	0.1233	0.1251	0.952	−0.0037	0.1434	0.1434	0.1433	0.947
200	80	$\widehat{\beta}_W$	0.0016	0.0911	0.0911	0.0944	0.951	0.0076	0.1022	0.1020	0.1074	0.957
		$\widehat{\beta}_C$	0.0056	0.0916	0.0915	0.0932	0.952	−0.1213	0.1521	0.0917	0.0934	0.710
		$\widehat{\beta}_A$	0.0021	0.0918	0.0918	0.0943	0.954	−0.0018	0.1024	0.1025	0.1078	0.959
	85	$\widehat{\beta}_W$	−0.0062	0.0971	0.0970	0.1011	0.965	0.0116	0.1139	0.1133	0.1160	0.956
		$\widehat{\beta}_C$	−0.0033	0.0973	0.0973	0.1000	0.959	−0.1198	0.1542	0.0971	0.0997	0.747
		$\widehat{\beta}_A$	−0.0060	0.0970	0.0969	0.1010	0.964	0.0001	0.1141	0.1142	0.1164	0.946
	90	$\widehat{\beta}_W$	−0.0063	0.1060	0.1059	0.1124	0.956	0.0117	0.1278	0.1273	0.1297	0.958
		$\widehat{\beta}_C$	−0.0050	0.1061	0.1060	0.1113	0.957	−0.1212	0.1608	0.1056	0.1085	0.746
		$\widehat{\beta}_A$	−0.0069	0.1064	0.1062	0.1123	0.959	−0.0007	0.1253	0.1254	0.1296	0.956
300	80	$\widehat{\beta}_W$	−0.0008	0.0763	0.0764	0.0790	0.964	0.0036	0.0880	0.0879	0.0909	0.963
		$\widehat{\beta}_C$	0.0024	0.0758	0.0758	0.0783	0.961	−0.1238	0.1458	0.0770	0.0774	0.604
		$\widehat{\beta}_A$	−0.0003	0.0766	0.0767	0.0789	0.963	−0.0048	0.0886	0.0886	0.0909	0.959
	85	$\widehat{\beta}_W$	−0.0033	0.0871	0.0871	0.0854	0.948	0.0120	0.0991	0.0985	0.0989	0.951
		$\widehat{\beta}_C$	0.0002	0.0862	0.0862	0.0847	0.949	−0.1227	0.1479	0.0827	0.0825	0.660
		$\widehat{\beta}_A$	−0.0028	0.0870	0.0870	0.0853	0.948	0.0018	0.0979	0.0979	0.0987	0.942
	90	$\widehat{\beta}_W$	−0.0127	0.0935	0.0927	0.0978	0.969	0.0117	0.1149	0.1144	0.1141	0.945
		$\widehat{\beta}_C$	−0.0110	0.0933	0.0927	0.0970	0.961	−0.1272	0.1575	0.0929	0.0930	0.676
		$\widehat{\beta}_A$	−0.0119	0.0929	0.0922	0.0977	0.967	−0.0014	0.1125	0.1126	0.1131	0.946

Note: $\widehat{\beta}_W$ denotes the estimator calculated based on the covariates without distorting factors, $\widehat{\beta}_C$ denotes the estimator calculated based on the covariates with distorting factors, and $\widehat{\beta}_A$ denotes the estimator calculated based on the adjusted covariates with distorting factors. Algorithm: MM algorithm.

TABLE 2: $\beta = (-0.25, 0.693)$, $Z_1 \sim N(2, 1.44)$, $Z_2 \sim U((7/3) - (\sqrt{19}/2), (7/3) + (\sqrt{19}/2))$, $u \sim U(4 - \sqrt{7}, 4 + \sqrt{7})$.

$\tilde{n}$	ρ (%)	Type	$\beta_1 = -0.25$					$\beta_2 = 0.693$				
			Bias	SMSE	SD	$\hat{\beta}_A$SE	CP	Bias	SMSE	SD	SE	CP
							$\lambda_0(t) = 1$					
	80	$\hat{\beta}_W$	−0.0048	0.0998	0.0998	0.1038	0.965	0.0147	0.1190	0.1181	0.1228	0.968
		$\hat{\beta}_C$	0.0005	0.0987	0.0988	0.1016	0.969	−0.1921	0.2170	0.1009	0.1042	0.513
		$\hat{\beta}_A$	−0.0038	0.1005	0.1005	0.1038	0.963	−0.0010	0.1237	0.1237	0.1236	0.944
150	85	$\hat{\beta}_W$	−0.0141	0.1082	0.1074	0.1108	0.959	0.0110	0.1320	0.1316	0.1318	0.955
		$\hat{\beta}_C$	−0.0091	0.1042	0.1038	0.1087	0.964	−0.1980	0.2258	0.1086	0.1088	0.517
		$\hat{\beta}_A$	−0.0137	0.1078	0.1070	0.1106	0.959	−0.0058	0.1351	0.1351	0.1322	0.947
	90	$\hat{\beta}_W$	−0.0060	0.1127	0.1126	0.1207	0.974	0.0110	0.1462	0.1459	0.1446	0.953
		$\hat{\beta}_C$	−0.0038	0.1100	0.1100	0.1185	0.975	−0.2056	0.2363	0.1165	0.1160	0.537
		$\hat{\beta}_A$	−0.0057	0.1139	0.1138	0.1204	0.967	−0.0159	0.1453	0.1445	0.1443	0.946
	80	$\hat{\beta}_W$	−0.0105	0.0941	0.0936	0.0914	0.949	0.0105	0.1089	0.1085	0.1092	0.953
		$\hat{\beta}_C$	−0.0017	0.0929	0.0929	0.0897	0.954	−0.1969	0.2150	0.0863	0.0906	0.382
		$\hat{\beta}_A$	−0.0095	0.0937	0.0933	0.0913	0.948	−0.0072	0.1111	0.1109	0.1097	0.949
200	85	$\hat{\beta}_W$	−0.0083	0.0973	0.0970	0.0979	0.958	0.0115	0.1088	0.1083	0.1177	0.964
		$\hat{\beta}_C$	−0.0035	0.0955	0.0955	0.0960	0.954	−0.1990	0.2178	0.0886	0.0949	0.446
		$\hat{\beta}_A$	−0.0079	0.0979	0.0977	0.0977	0.956	−0.0087	0.1125	0.1122	0.1172	0.953
	90	$\hat{\beta}_W$	−0.0046	0.1064	0.1064	0.1084	0.956	0.0122	0.1264	0.1259	0.1326	0.971
		$\hat{\beta}_C$	−0.0022	0.1056	0.1057	0.1067	0.953	−0.2018	0.2278	0.1057	0.1040	0.461
		$\hat{\beta}_A$	−0.0036	0.1060	0.1060	0.1082	0.957	−0.0140	0.1281	0.1273	0.1312	0.959
	80	$\hat{\beta}_W$	−0.0025	0.0776	0.0776	0.0765	0.953	0.0088	0.0932	0.0928	0.0928	0.955
		$\hat{\beta}_C$	0.0038	0.0766	0.0766	0.0752	0.955	−0.2000	0.2139	0.0758	0.0745	0.260
		$\hat{\beta}_A$	−0.0011	0.0773	0.0774	0.0763	0.958	−0.0090	0.0957	0.0953	0.0923	0.945
300	85	$\hat{\beta}_W$	−0.0037	0.0833	0.0833	0.0832	0.947	0.0084	0.1041	0.1038	0.1024	0.947
		$\hat{\beta}_C$	0.0011	0.0822	0.0822	0.0819	0.945	−0.2078	0.2223	0.0791	0.0791	0.257
		$\hat{\beta}_A$	−0.0027	0.0838	0.0838	0.0831	0.951	−0.0145	0.1051	0.1042	0.1011	0.934
	90	$\hat{\beta}_W$	−0.0035	0.0959	0.0959	0.0951	0.954	0.0026	0.1153	0.1153	0.1181	0.949
		$\hat{\beta}_C$	0.0001	0.0961	0.0961	0.0940	0.949	−0.2135	0.2302	0.0861	0.0885	0.326
		$\hat{\beta}_A$	−0.0021	0.0956	0.0957	0.0950	0.953	−0.0195	0.1186	0.1170	0.1160	0.936
							$\lambda_0(t) = 2t$					
	80	$\hat{\beta}_W$	−0.0090	0.1123	0.1120	0.1137	0.952	0.0131	0.1275	0.1269	0.1338	0.954
		$\hat{\beta}_C$	0.0006	0.1110	0.1111	0.1115	0.951	−0.1890	0.2209	0.1144	0.1151	0.579
		$\hat{\beta}_A$	−0.0073	0.1111	0.1109	0.1135	0.953	−0.0032	0.1302	0.1303	0.1350	0.951
150	85	$\hat{\beta}_W$	−0.0109	0.1207	0.1203	0.1208	0.949	0.0177	0.1396	0.1386	0.1434	0.962
		$\hat{\beta}_C$	−0.0085	0.1191	0.1188	0.1180	0.953	−0.1864	0.2225	0.1216	0.1205	0.589
		$\hat{\beta}_A$	−0.0106	0.1198	0.1194	0.1205	0.946	−0.0012	0.1387	0.1388	0.1439	0.950
	90	$\hat{\beta}_W$	−0.0124	0.1287	0.1281	0.1323	0.961	0.0158	0.1631	0.1624	0.1565	0.949
		$\hat{\beta}_C$	−0.0138	0.1277	0.1270	0.1296	0.955	−0.1939	0.2305	0.1248	0.1292	0.621
		$\hat{\beta}_A$	−0.0151	0.1294	0.1286	0.1317	0.956	−0.0072	0.1557	0.1556	0.1572	0.955
	80	$\hat{\beta}_W$	−0.0115	0.0994	0.0988	0.0986	0.951	0.0162	0.1203	0.1193	0.1184	0.959
		$\hat{\beta}_C$	−0.0025	0.0941	0.0941	0.0963	0.956	−0.1909	0.2154	0.0999	0.0991	0.492
		$\hat{\beta}_A$	−0.0109	0.0988	0.0983	0.0983	0.953	−0.0011	0.1214	0.1215	0.1188	0.939
200	85	$\hat{\beta}_W$	−0.0007	0.1009	0.1010	0.1050	0.960	0.0091	0.1260	0.1258	0.1269	0.954
		$\hat{\beta}_C$	0.0036	0.1008	0.1008	0.1031	0.957	−0.1955	0.2218	0.1048	0.1042	0.489
		$\hat{\beta}_A$	−0.0009	0.1012	0.1012	0.1050	0.955	−0.0081	0.1280	0.1278	0.1272	0.949
	90	$\hat{\beta}_W$	−0.0051	0.1105	0.1105	0.1176	0.962	0.0157	0.1484	0.1477	0.1429	0.943
		$\hat{\beta}_C$	−0.0011	0.1082	0.1082	0.1155	0.970	−0.1996	0.2300	0.1144	0.1142	0.540
		$\hat{\beta}_A$	−0.0045	0.1103	0.1103	0.1173	0.961	−0.0111	0.1434	0.1430	0.1416	0.941
	80	$\hat{\beta}_W$	−0.0067	0.0799	0.0797	0.0818	0.952	0.0056	0.0934	0.0933	0.0989	0.962
		$\hat{\beta}_C$	0.0008	0.0789	0.0790	0.0805	0.948	−0.1969	0.2114	0.0769	0.0807	0.322
		$\hat{\beta}_A$	−0.0058	0.0800	0.0798	0.0817	0.947	−0.0112	0.0962	0.0956	0.0988	0.952
300	85	$\hat{\beta}_W$	−0.0083	0.0860	0.0857	0.0894	0.957	0.0081	0.1063	0.1061	0.1082	0.961
		$\hat{\beta}_C$	−0.0004	0.0854	0.0855	0.0879	0.965	−0.2018	0.2194	0.0861	0.0864	0.352
		$\hat{\beta}_A$	−0.0072	0.0867	0.0864	0.0893	0.959	−0.0115	0.1079	0.1073	0.1078	0.950
	90	$\hat{\beta}_W$	−0.0082	0.0966	0.0963	0.1007	0.961	0.0125	0.1223	0.1217	0.1259	0.963
		$\hat{\beta}_C$	−0.0034	0.0948	0.0948	0.0991	0.951	−0.2012	0.2219	0.0935	0.0964	0.428
		$\hat{\beta}_A$	−0.0060	0.0964	0.0963	0.1006	0.955	−0.0112	0.1206	0.1201	0.1239	0.954

Note: $\hat{\beta}_W$ denotes the estimator calculated based on the covariates without distorting factors, $\hat{\beta}_C$ denotes the estimator calculated based on the covariates with distorting factors, and $\hat{\beta}_A$ denotes the estimator calculate based on the adjusted covariates with distorting factors. Algorithm: MM algorithm.

Table 3: $\beta = (0, 0.5)$, $Z_1 \sim N(2, 1.44)$, $Z_2 \sim U((7/3) - (\sqrt{19}/2), (7/3) + (\sqrt{19}/2))$, $u \sim U(4 - \sqrt{7}, 4 + \sqrt{7})$.

$\tilde{n}$	ρ (%)	Type	$\beta_1 = 0$					$\beta_2 = 0.5$				
			Bias	SMSE	SD	SE	CP	Bias	SMSE	SD	SE	CP
						$\lambda_0(t) = 1$						
150	80	$\widehat{\beta}_W$	0.0016	0.0899	0.0899	0.0930	0.961	0.0106	0.1032	0.1027	0.1084	0.968
		$\widehat{\beta}_C$	0.0016	0.0900	0.0901	0.0920	0.963	−0.1184	0.1490	0.0906	0.0954	0.759
		$\widehat{\beta}_A$	0.0017	0.0903	0.0903	0.0929	0.957	0.0014	0.1058	0.1058	0.1091	0.962
	85	$\widehat{\beta}_W$	−0.0013	0.1010	0.1010	0.0999	0.959	0.0079	0.1107	0.1104	0.1151	0.964
		$\widehat{\beta}_C$	−0.0007	0.0991	0.0991	0.0989	0.961	−0.1191	0.1532	0.0964	0.0998	0.728
		$\widehat{\beta}_A$	−0.0011	0.1012	0.1012	0.0997	0.958	−0.0052	0.1114	0.1113	0.1154	0.952
	90	$\widehat{\beta}_W$	−0.0003	0.1078	0.1079	0.1083	0.954	0.0123	0.1242	0.1236	0.1282	0.965
		$\widehat{\beta}_C$	−0.0004	0.1083	0.1084	0.1074	0.946	−0.1218	0.1576	0.1000	0.1076	0.772
		$\widehat{\beta}_A$	−0.0003	0.1078	0.1079	0.1082	0.956	−0.0002	0.1225	0.1225	0.1282	0.965
200	80	$\widehat{\beta}_W$	0.0016	0.0807	0.0807	0.0823	0.963	0.0073	0.0973	0.0971	0.0963	0.951
		$\widehat{\beta}_C$	0.0029	0.0797	0.0796	0.0813	0.962	−0.1239	0.1488	0.0824	0.0827	0.633
		$\widehat{\beta}_A$	0.0017	0.0803	0.0804	0.0822	0.966	−0.0018	0.0984	0.0985	0.0965	0.943
	85	$\widehat{\beta}_W$	0.0007	0.0862	0.0863	0.0881	0.962	0.0071	0.1024	0.1022	0.1036	0.953
		$\widehat{\beta}_C$	0.0010	0.0845	0.0846	0.0873	0.960	−0.1230	0.1515	0.0884	0.0878	0.672
		$\widehat{\beta}_A$	0.0005	0.0865	0.0865	0.0881	0.965	−0.0048	0.1032	0.1031	0.1037	0.948
	90	$\widehat{\beta}_W$	0.0037	0.0940	0.0940	0.0986	0.954	0.0091	0.1148	0.1145	0.1168	0.959
		$\widehat{\beta}_C$	0.0044	0.0945	0.0944	0.0977	0.958	−0.1270	0.1580	0.0941	0.0960	0.688
		$\widehat{\beta}_A$	0.0034	0.0945	0.0945	0.0985	0.956	−0.0036	0.1158	0.1158	0.1163	0.953
300	80	$\widehat{\beta}_W$	0.0016	0.0706	0.0706	0.0703	0.951	0.0012	0.0803	0.0804	0.0827	0.964
		$\widehat{\beta}_C$	0.0010	0.0705	0.0706	0.0696	0.942	−0.1294	0.1461	0.0679	0.0692	0.526
		$\widehat{\beta}_A$	0.0019	0.0706	0.0706	0.0702	0.945	−0.0081	0.0816	0.0813	0.0826	0.955
	85	$\widehat{\beta}_W$	−0.0003	0.0767	0.0767	0.0761	0.947	−0.0006	0.0868	0.0868	0.0908	0.960
		$\widehat{\beta}_C$	0.0001	0.0765	0.0765	0.0756	0.947	−0.1321	0.1504	0.0719	0.0745	0.545
		$\widehat{\beta}_A$	−0.0002	0.0767	0.0767	0.0761	0.946	−0.0111	0.0884	0.0878	0.0904	0.950
	90	$\widehat{\beta}_W$	0.0007	0.0855	0.0855	0.0865	0.960	0.0095	0.1046	0.1042	0.1054	0.954
		$\widehat{\beta}_C$	0.0013	0.0845	0.0845	0.0861	0.969	−0.1274	0.1521	0.0831	0.0837	0.638
		$\widehat{\beta}_A$	0.0010	0.0856	0.0857	0.0865	0.959	−0.0027	0.1038	0.1038	0.1040	0.950
						$\lambda_0(t) = 2t$						
150	80	$\widehat{\beta}_W$	0.0005	0.1012	0.1013	0.1035	0.957	0.0091	0.1144	0.1140	0.1195	0.953
		$\widehat{\beta}_C$	0.0012	0.0998	0.0998	0.1024	0.959	−0.1191	0.1570	0.1024	0.1057	0.755
		$\widehat{\beta}_A$	0.0010	0.1007	0.1007	0.1034	0.956	0.0020	0.1158	0.1158	0.1201	0.954
	85	$\widehat{\beta}_W$	−0.0020	0.1059	0.1059	0.1094	0.965	0.0132	0.1210	0.1203	0.1272	0.971
		$\widehat{\beta}_C$	−0.0031	0.1048	0.1048	0.1080	0.965	−0.1185	0.1590	0.1062	0.1109	0.798
		$\widehat{\beta}_A$	−0.0020	0.1057	0.1058	0.1091	0.965	0.0016	0.1198	0.1198	0.1279	0.966
	90	$\widehat{\beta}_W$	−0.0038	0.1157	0.1157	0.1189	0.962	0.0069	0.1376	0.1375	0.1389	0.957
		$\widehat{\beta}_C$	−0.0040	0.1134	0.1134	0.1175	0.964	−0.1269	0.1698	0.1128	0.1182	0.781
		$\widehat{\beta}_A$	−0.0034	0.1160	0.1160	0.1187	0.959	−0.0036	0.1387	0.1388	0.1393	0.955
200	80	$\widehat{\beta}_W$	0.0042	0.0906	0.0905	0.0905	0.944	0.0100	0.1057	0.1053	0.1061	0.962
		$\widehat{\beta}_C$	0.0044	0.0903	0.0902	0.0892	0.944	−0.1196	0.1509	0.0921	0.0924	0.696
		$\widehat{\beta}_A$	0.0047	0.0904	0.0903	0.0903	0.942	−0.0002	0.1050	0.1050	0.1065	0.956
	85	$\widehat{\beta}_W$	−0.0018	0.0950	0.0950	0.0954	0.962	0.0093	0.1089	0.1088	0.1124	0.962
		$\widehat{\beta}_C$	−0.0016	0.0949	0.0950	0.0942	0.952	−0.1258	0.1566	0.0933	0.0960	0.700
		$\widehat{\beta}_A$	−0.0017	0.0944	0.0945	0.0952	0.957	−0.0043	0.1092	0.1092	0.1125	0.958
	90	$\widehat{\beta}_W$	−0.0001	0.1007	0.1008	0.1065	0.972	0.0144	0.1238	0.1231	0.1263	0.965
		$\widehat{\beta}_C$	0.0009	0.0991	0.0991	0.1054	0.968	−0.1211	0.1587	0.1026	0.1055	0.763
		$\widehat{\beta}_A$	0.0000	0.1004	0.1005	0.1064	0.974	0.0026	0.1239	0.1239	0.1264	0.959
300	80	$\widehat{\beta}_W$	−0.0010	0.0732	0.0732	0.0754	0.959	0.0089	0.0877	0.0873	0.0890	0.965
		$\widehat{\beta}_C$	−0.0011	0.0726	0.0726	0.0746	0.962	−0.1216	0.1439	0.0769	0.0757	0.605
		$\widehat{\beta}_A$	−0.0011	0.0733	0.0734	0.0754	0.960	−0.0012	0.0879	0.0879	0.0891	0.965
	85	$\widehat{\beta}_W$	0.0020	0.0810	0.0810	0.0813	0.954	0.0053	0.0963	0.0962	0.0969	0.959
		$\widehat{\beta}_C$	0.0011	0.0800	0.0800	0.0808	0.952	−0.1275	0.1508	0.0807	0.0812	0.628
		$\widehat{\beta}_A$	0.0015	0.0813	0.0813	0.0812	0.952	−0.0053	0.0956	0.0955	0.0967	0.952
	90	$\widehat{\beta}_W$	0.0044	0.0926	0.0926	0.0925	0.953	0.0132	0.1092	0.1084	0.1118	0.961
		$\widehat{\beta}_C$	0.0045	0.0923	0.0923	0.0919	0.954	−0.1257	0.1530	0.0872	0.0906	0.687
		$\widehat{\beta}_A$	0.0041	0.0922	0.0922	0.0924	0.949	0.0013	0.1084	0.1085	0.1108	0.960

Note: $\widehat{\beta}_W$ denotes the estimator calculated based on the covariates without distorting factors, $\widehat{\beta}_C$ denotes the estimator calculated based on the covariates with distorting factors, and $\widehat{\beta}_A$ denotes the estimator calculate based on the adjusted covariates with distorting factors. Algorithm: MM algorithm.

association between these clinical features under smoothed serum sodium and creatinine phosphokinase by ejection fraction and anaemia.

There are 96 deaths in this data, and the censoring rate is nearby 67.9%. Due to the different dimensions of the covariates, we firstly standardize each covariate. Then, we set the standardized age as Z_1, the standardized creatinine phosphokinase as $\widehat{Z}_2$, the standardized diabetes as Z_3, the standardized high blood pressure as Z_4, the standardized platelets as Z_5, the standardized serum creatinine as Z_6, the standardized serum sodium as $\widehat{Z}_7$, the standardized sex as Z_8, the standardized smoking as Z_9, the standardized ejection fraction as a distorting factor U_1, and the standardized anaemia as a distorting factor U_2, where $\widehat{Z}_2$ and $\widehat{Z}_7$ indicate that the covariate is distorted.

The case-cohort sample is composed of the subcohort randomly selected 100 from the whole data and the dead objects in the whole data expect the subcohort. We perform regression analysis on the sample using the proportional hazard function:

$$x(t|Z) = x_0(t)\exp\left\{\sum_{i=1}^{9}\beta_i Z_i\right\}. \tag{28}$$

Because the size of this data is small, to improve the reliability of the sampling method, the sampling process is repeated 100 times. The average value of the 100 distorted estimates is $(2.7224, 14.0226, 0.1603, 0.4295, -0.2667, 3.0520, 11.0269, -0.0742, 0.1933)^\top$.

Then, for the same 100 case-cohort sample, we obtain the adjusted covariates $\widehat{Z}_2$ and $\widehat{Z}_7$ by using the proposed kernel smoothing method on $\widetilde{Z}_2$ and $\widetilde{Z}_7$ and replace $\widetilde{Z}_2$ and $\widetilde{Z}_7$ with $\widehat{Z}_2$ and $\widehat{Z}_7$, respectively. On this basis, the average of adjusted estimates is $(2.5077, 1.0344, 0.1136, 0.5474, -0.3552, 2.8577, -2.4303, 0.2115)^\top$.

The kernel and bandwidth selector chosen are the same as those in Section 5. After the covariates were adjusted, the estimator of creatinine phosphokinase is adjusted from 1.0344 to 14.0226, and the estimator of serum sodium is adjusted from −2.4303 to 11.0269; the estimators of other covariates changed little after adjustment. The result is reasonable and feasible in medicine and also shows that the proposed method is effective for real data.

In practice, the covariates are measured after the case-cohort sampling to reduce costs and improve efficiency. In this real data, the size of the data is small, and the each covariate has been measured. To reduce the error, we repeat 100 samplings and set the average value as the estimators. For example, based on the 10th case-cohort sample from the original data, the distorted estimator is $(3.5393, -0.5883, 0.1934, 0.3712, 0.4114, 6.5332, -3.9763, 0.1236, 0.3585)^\top$; then, after the adjustment of covariates in the same sample, the adjusted estimator is $(4.5125, 79.7599, 0.1690, 0.2902, 1.0486, 5.9035, 12.7945, 0.1399, 0.1720)^\top$. Therefore, the estimators based on same case-cohort sample are quite different from the average of estimators, but the trends are the same. So, for real data with a large sample size, we only need to draw a case-cohort sample and measure their covariates.

7. Conclusion

We study the estimation in Cox's model with the adjusted covariates by using the nonparametric method based on the kernel function under case-cohort design. Consistency and asymptotic normality of the proposed estimators are derived. We use MM algorithm for calculating the regression coefficients, where the surrogate function with a diagonal Hessian matrix is established to overcome the operation difficulty in the Newton–Raphson algorithm. Simulation and real data studies suggest that the case-cohort design can be used to reduce the cost for cohort studies and the development of the adjustment for distorted covariates has nice performance.

Here, the adjustment for survival data is discussed in Cox's model. The method can be extended to other models, such as an accelerated failure time model [28], an additive-multiplicative model [29], and an accelerated hazards model [30]. The cost-effective case-cohort design is mainly applied to the data with the high censoring rate. However, in the sampling process, some censoring subjects have not been measured. To improve the efficiency, our future works include developments of inference for estimation with adjusted covariates under a generalized case-cohort design [31] and an outcome-dependent sampling design.

Appendix

A. Proof of Asymptotic Properties

We start with a lemma, which is frequently used in the process of proof. Then, we proceed to the proof of Theorem 1, concerning consistency and asymptotic normality.

Lemma A.1. Let $\eta(t)$ be a continuous function, satisfying $E[\eta(T)^2] < \infty$. Assume that conditions (C), (D1)-(D2), and (E) hold. The following asymptotic representation holds:

$$\sum_{i=1}^{n}(\widehat{Z}_{ir} - \mathbf{Z}_{ir})\eta(T_{ir})$$

$$= \frac{1}{2}\sum_{i=1}^{n}(\mathbf{Z}_{ir} - E[\mathbf{Z}_r])\frac{E[\mathbf{Z}_r \eta T_r]}{E[\mathbf{Z}_r]} \tag{A.1}$$

$$+ \sum_{i=1}^{n}(\widetilde{Z}_{ir} - \mathbf{Z}_{ir})\frac{E[\mathbf{Z}_r \eta T_r]}{E[\mathbf{Z}_r]} + O_p(\sqrt{n}).$$

Proof. of Lemma A.1. Recall that $\widehat{Z}_{ir} = \widetilde{Z}_{ir}/\widehat{\phi}_r(U_i)$, which is given by Section 2. Sample calculations give the following expression:

$$\sum_{i=1}^{n}(\widehat{Z}_{ir} - \mathbf{Z}_{ir}\eta)(T_{ir}) = \sum_{i=1}^{n}\widehat{Z}_{ir}\eta(T_{ir}) - \sum_{i=1}^{n}\mathbf{Z}_{ir}\eta(T_{ir}).$$

(A.2)

$$\begin{aligned}
\sum_{i=1}^{n}\widehat{Z}_{ir}\eta(T_{ir}) &= \sum_{i=1}^{n}\widehat{z}_{ir}\eta(T_{ir})\left(\frac{\widehat{P}(U_i)}{\widehat{g}_r(U_i)}\right)\widetilde{\bar{Z}}_r \\
&= \sum_{i=1}^{n}\widetilde{Z}_{ir}\eta(T_{ir})\left(\frac{\widehat{p}(U_i)}{\widehat{g}_r}\right)(U_i)E[\mathbf{Z}_r] + \sum_{i=1}^{n}\widetilde{Z}_{ir}\eta(T_{ir})\left(\frac{\widehat{p}(U_i)}{\widehat{g}_r(U_i)}\right)\left(\widetilde{\bar{Z}}_r - E[\mathbf{Z}_r]\right) \\
&\triangleq L_1 + L_2.
\end{aligned}$$

(A.3)

First, we analyze L_1. The proof is divided into three steps. Denote by L_{11}, L_{12}, and L_{13} the quantities:

$$L_{11} = \sum_{i=1}^{n}\mathbf{Z}_{ir}\eta(T_{ir}),$$

$$L_{12} = \sum_{i=1}^{n}\mathbf{Z}_{ir}\eta(T_{ir})\frac{\widehat{g}_r(U_i)}{g_r(U_i)},$$

(A.4)

$$L_{13} = \sum_{i=1}^{n}\mathbf{Z}_{ir}\eta(T_{ir})\frac{\widehat{p}(U_i)}{p(U_i)}.$$

Thus, it suffices to deal with the equation $\sum_{i=1}^{n}\mathbf{Z}_{ir}\eta(T_{ir})$. According to the type it holds that

Step 1: show that

$$L_1 = L_{11} + L_{12} + L_{13} + o_p(\sqrt{n}).$$

(A.5)

Applying the equation $\phi_r(\cdot) = (g_r(\cdot)/p(\cdot)E(\mathbf{Z}_r))$, we have

$$\begin{aligned}
L_1 &= \sum_{i=1}^{n}\mathbf{Z}_{ir}\eta(T_{ir})\frac{g_r(U_i)}{P(U_i)}\cdot\frac{\widehat{p}(U_i)}{\widehat{g}_r(U_i)} \\
&= \sum_{i=1}^{n}\sum_{r=1}^{q}\mathbf{Z}_{ir}\eta(T_{ir})\frac{g_r(U_i)}{p(U_i)}\cdot\frac{p(U_i)}{g_r(U_i)}\left(1 - \frac{\widehat{g}_r(U_i)}{g_r(U_i)} + \frac{\widehat{p}(U_i)}{p(U_i)}\right) + L_1^{k_1} - L_1^{k_2} \\
&= \sum_{i=1}^{n}\mathbf{Z}_{ir}\eta(T_{ir}) - \sum_{i=1}^{n}\mathbf{Z}_{ir}\eta(T_{ir})\frac{\widehat{g}_r(U_i)}{g_r(U_i)} + \sum_{i=1}^{n}\mathbf{Z}_{ir}\eta(T_{ir})\frac{\widehat{p}(U_i)}{p(U_i)} + L_1^{k_1} - L_1^{k_2} \\
&= L_{11} - L_{12} + L_{13} + L_1^{k_1} - L_1^{k_2},
\end{aligned}$$

(A.6)

where

$$L_1^{k_1} = \sum_{i=1}^{n}\mathbf{Z}_{ir}\eta(T_ir)\frac{(\widehat{g}_r)(U_i) - g_r(U_i^2)}{g_r(U_i) - \widehat{g}_r(U_i)},$$

$$L_1^{k_2} = \sum_{i=1}^{n}\mathbf{Z}_{ir}\eta(T_{ir})\frac{(\widehat{g}_r)(U_i) - g_r(U_i)(\widehat{p})(U_i) - p(U_i)}{p(U_i)\widehat{g}_r(U_i)}.$$

(A.7)

Equation (A.5) can be concluded by proven

$$L_1^{k_1} = o_p(n^{1/2}), \quad 1 \le i \le 2.$$

(A.8)

According to Theorem 1 of [32], Lemma 3 of [23], condition (D2), and the Law of Large Numbers (LLN) for $(1/n)\sum_{i=1}^{n}\mathbf{Z}_{ir}\eta(T_{ir})$, we then follow the arguments used in [23] to yield the higher order term:

$$\begin{aligned}
L_1^{k_1} &= O_p(ch^4) + n^{-1/2}h^{-1}\log n^2\left\{\sum_{i=1}^{n}\mathbf{Z}_{ri}\eta(T_{ri})\right\} \\
&= o_p(n^{1/2}).
\end{aligned}$$

(A.9)

Similar argument yield (A.8) for $L_1^{k_2}$.

Step 2: show that

$$L_{12} = \frac{1}{2} \sum_{i=1}^{n} \mathbf{Z}_{ir} \eta(T_{ir}) + \frac{1}{2} \sum_{i=1}^{n} \mathbf{Z}_{ri} \frac{E[\mathbf{Z}_r \eta(T_r)]}{E[\mathbf{Z}_r]} + o_p(n^{1/2}),$$

$$L_{13} = \frac{1}{2} \sum_{i=1}^{n} \mathbf{Z}_{ir} \eta(T_{ir}) + \frac{1}{2} \sum_{i=1}^{n} E[\mathbf{Z}_r \eta(T_r)] + o_p(n^{1/2}).$$

$$\text{(A.10)}$$

To analyze L_{12}, for ease of understanding, we use $p(U)$ to express the density function of U and define as follows:

$$g_r(U) = E[\widetilde{Z}_r | U] p(U), \quad 1 \le r \le p. \quad \text{(A.11)}$$

We need to work on

$$\sum_{i=1}^{n} \mathbf{Z}_{ir} \eta(T_{ir}) \frac{\widehat{g}_r(U_i)}{g_r(U_i)}. \quad \text{(A.12)}$$

We can obtain the above sum by a U-statistic with a varying kernel with the bandwidth h by applying the similar arguments used by Davis and Fang [23] again. Then, we can have the asymptotic representation [4] as

$$\sum_{i=1}^{n} \mathbf{Z}_{ir} \eta(T_{ir}) \frac{\widehat{g}_r(U_i)}{g_r(U_i)} = \frac{1}{2} \sum_{i=1}^{n} \frac{1}{h} \int \mathbf{Z}_{ir} \eta(T_{ir}) \frac{1}{g_r(U_i)} K\left(\frac{U_i - u}{h}\right) \delta \phi_r(u) P_{r,u}(\delta, u) \mathrm{d}\delta \mathrm{d}u$$

$$\text{(A.13)}$$

$$+ \frac{1}{2} \sum_{i=1}^{n} \frac{1}{h} \int \mathbf{Z}_{ir} \eta(T_{ir}) \frac{1}{g_r(U_i)} K\left(\frac{U_i - u}{h}\right) j P_{J_r,u}(j, u) \mathrm{d}j \mathrm{d}u + o_p(n^{1/2}),$$

with $P_{r,U}(\delta, U)$ being the density function of $(\mathbf{Z}_r, U)$, $J_r = \mathbf{Z}_r \eta(T_r)$ and $P_{J_r,U}(j, U)$ the density of variable (J_r, U). Note that $\mathbf{Z}_r$ and U are independent and J_r and

U are independent. According to conditions (C), (D1)-(D2), and (E), we obtain

$$\sum_{i=1}^{n} \mathbf{Z}_{ir} \eta(T_{ir}) \frac{\widehat{g}_r(U_i)}{g_r(U_i)} = \frac{1}{2} \sum_{i=1}^{n} \mathbf{Z}_{ir} \eta(T_{ir}) \frac{E[\mathbf{Z}_r]}{g_r(U_i)} \frac{1}{h} \int K\left(\frac{U_i - u}{h}\right) \phi_r(u) P_U(u) \mathrm{d}u$$

$$+ \frac{1}{2} \sum_{i=1}^{n} \mathbf{Z}_{ir} \phi_r(U_i) E[\mathbf{Z}_r \eta(Z_r)] \frac{1}{h} \int \frac{P_U(u)}{g_r(u)} K\left(\frac{U_i - u}{h}\right) \mathrm{d}u + o_p(n^{1/2}) \quad \text{(A.14)}$$

$$= \frac{1}{2} \sum_{i=1}^{n} \mathbf{Z}_{ir} \eta(T_{ir}) + \frac{1}{2} \sum_{i=1}^{n} \mathbf{Z}_{ir} \frac{E[\mathbf{Z}_r \eta(T_r)]}{E[\mathbf{Z}_r]} + o_p(n^{1/2}),$$

L_{13} can be similarly proceeded. Combining (A.5) and (A.8), we have (7):

$$L_1 = \sum_{i=1}^{n} (\mathbf{Z}_{ir} \eta(T_{ir}) - E[\mathbf{Z}_r \eta(T_r)]) - \frac{1}{2} \sum_{i=1}^{n} (\mathbf{Z}_{ir} - E[\mathbf{Z}_r]) \frac{E[\mathbf{Z}_r \eta(T_r)]}{E[\mathbf{Z}_r]}$$

$$\text{(A.15)}$$

$$+ n E[\mathbf{Z}_r \eta(T_r)] + o_p(n^{1/2}).$$

Step 3: show that

$$L_2 = \sum_{i=1}^{n} (\widetilde{Z}_{ir} - E[\mathbf{Z}_r]) \frac{E[\mathbf{Z}_r \eta(T_r)]}{E[T]_r} + o_p(n^{1/2}). \quad \text{(A.16)}$$

From (A.16) and the definition of L_2 in (A.3), we derive that

$$
\begin{aligned}
L_2 &= \frac{\bar{\bar{Z}}_r - E[\mathbf{Z}_r]}{E[\mathbf{Z}_r]} L_1 \\
&= \sum_{i=1}^{n} \left[\mathbf{Z}_{ir} \eta(T_{ir}) - E[\mathbf{Z}_r \eta(T_r)] \right] \frac{\bar{\bar{Z}}_r - E[\mathbf{Z}_r]}{E[\mathbf{Z}_r]} \\
&\quad - \frac{1}{2} \sum_{i=1}^{n} (\mathbf{Z}_{ir} - E[\mathbf{Z}_r]) \frac{E[\mathbf{Z}_r \eta(T_r)]}{E[\mathbf{Z}_r]} \frac{\bar{\bar{Z}}_r - E[\mathbf{Z}_r]}{E[\mathbf{Z}_r]} + n E[\mathbf{Z}_r \eta(T_r)] \frac{\bar{\bar{Z}}_r - E[\mathbf{Z}_r]}{E[\mathbf{Z}_r]} + o_p(n^{1/2}),
\end{aligned}
\tag{A.17}
$$

where the last equality is obtained by applying LLN to $(1/n) \sum_{i=1}^{n} (\mathbf{Z}_{ir}) \eta(T_{ir}) - E[\mathbf{Z}_r \eta(T_r)]$ and $(1/n) \sum_{i=1}^{n} (\mathbf{Z}_{ir}) - E[\mathbf{Z}_r]$.

Finally, together with the asymptotic representation of L_1 and L_2 in (A.15) and (A.17), the desired result is easy to arrive at. $\square$

Lemma A.2. *Refine*

$$
\begin{aligned}
\widetilde{A}(\beta, t) &= \sum_{i \in C} \int_0^t \left[\mathbf{Z}_i' \beta - \log \left\{ \sum_{l \in \widetilde{C}} Y_l(U) \exp(\mathbf{Z}_i' \beta) \right\} \right] dN_i(U), \\
\widehat{\widetilde{A}}(\beta, t) &= \sum_{i \in C} \int_0^t \left[\widehat{Z}_i' \beta - \log \left\{ \sum_{i \in \widetilde{C}} Y_l(U) \exp(\widehat{Z}_i' \beta) \right\} \right] dN_i(U).
\end{aligned}
\tag{A.18}
$$

Assume that conditions (C), (D1)-(D2), and (E) hold, then $\widehat{\widetilde{A}}(\beta, t)$ converge to $\widetilde{A}(\beta, t)$ asymptotically.

Proof.

$$
\begin{aligned}
\widehat{\widetilde{A}}(\beta, t) - \widetilde{A}(\beta, t) &= \sum_{i \in C} \int_0^t \left[(\widehat{Z}_i - \mathbf{Z}_i)' \beta - \log \frac{\left\{ \sum_{l \in \widetilde{C}} Y_l(U) \exp(\widehat{Z}_l' \beta) \right\}}{\left\{ \sum_{l \in \widetilde{C}} Y_l(U) \exp(\mathbf{Z}_l' \beta) \right\}} \right] dN_i(U) \\
&= \int_0^t \left[\sum_{i \in C} (\widehat{Z}_i - \mathbf{Z}_i)' \beta - \sum_{i \in C} \log \frac{\left\{ \sum_{l \in \widetilde{C}} Y_l(U) \exp(\widehat{Z}_l' \beta) \right\}}{\left\{ \sum_{l \in \widetilde{C}} Y_l(U) \exp(\mathbf{Z}_l' \beta) \right\}} \right] dN_i(U).
\end{aligned}
\tag{A.19}
$$

For $\sum_{i \in C} (\widehat{Z}_i - \mathbf{Z}_i) \beta$, according to Lemma A.1,

$$
\begin{aligned}
\Sigma_{i \in C} (\widehat{Z}_i - \mathbf{Z}_i) \beta &= \frac{1}{2} \sum_{i \in C} (\mathbf{Z}_i - E|\mathbf{Z}|)' \frac{E[Z'\beta]}{E[Z']} \\
&\quad + \sum_{i \in C} (\widetilde{Z}_i - \mathbf{Z}_i)' \frac{E[Z'\beta]}{E[Z']} + o_p(\sqrt{n}).
\end{aligned}
\tag{A.20}
$$

According to the Law of Large Numbers, (A.20) converges to 0 in probability.

Next, we prove that

$$
\sum_{i \in C} \log \frac{\left\{ \sum_{l \in \widetilde{C}} Y_l(U) \exp(\widehat{Z}_l' \beta) \right\}}{\left\{ \sum_{l \in \widetilde{C}} Y_l(U) \exp(\mathbf{Z}_l' \beta) \right\}} \xrightarrow{P} 0.
\tag{A.21}
$$

Only

$$
\sum_{i \in \widetilde{C}} Y_l(U) \exp(\widehat{Z}_l' \beta) - \sum_{i \in \widetilde{C}} Y_l(U) \exp(\mathbf{Z}_l' \beta) \longrightarrow 0.
\tag{A.22}
$$

Let

$$
\sum_{i \in C} Y_l(U) \left[\exp(\widehat{Z}_l' \beta) - \exp(\mathbf{Z}_l' \beta) \right] \longrightarrow 0.
\tag{A.23}
$$

Because $\exp(\cdot)$ is differentiable function, the first derivative of $\exp(\cdot)$, and it is obtained from (A.17) that

$$\exp\left(\widehat{Z}_i'\beta\right) - \exp\left(Z_i'\beta\right) \xrightarrow{L} 0. \qquad (A.24)$$

By (16) and (A.21), $\widehat{\widetilde{A}}(\beta, t)$ asymptotically converges to $\widetilde{A}(\beta, t)$.

Under the case-cohort sampling design, let $\widetilde{A}$ denote the sample set of the subcolumn, $\widetilde{n}$ denote the number of samples in $\widetilde{A}$, A denotes the case-cohort sample, and the set of n represents the number of samples in A. Under the case-cohort sampling design, the covariate is not completely observed; then, its likelihood function cannot be expressed as (2). According to the pseudolikelihood function given in the article of Prentice [1], the pseudolikelihood function expression is as follows:

$$L_F(\beta) = \prod_{i \in A} \left[\frac{\exp\left(\mathbf{Z}_i\beta^\top\right)}{\sum_{l \in \widetilde{R}_{(T_i)}} \exp\left(\mathbf{Z}_i\beta^\top\right)} \right]^{\Delta_i}, \qquad (A.25)$$

where adventure set $\widetilde{R}(t) = \{i : T_i \geq t, i \in \widetilde{A} \cup B(t)\}, \{B(t) = i : N_i(t) \neq N_i(t-1), i = 1, 2, \ldots, n\}$. Note that only when the individual fails at time t, the set $B(t)$ is nonempty, and the corresponding log-likelihood function is

$$l_F(\beta) = \sum_{i \in A} \Delta_i \left[\mathbf{Z}_i\beta^\top - \log \sum_{l \in R_{(T_i)}} \exp\left(\mathbf{Z}_i\beta^\top\right) \right]. \qquad (A.26)$$

$\square$

Proof of Theorem 1. To derive the asymptotic properties of the proposed estimator $\widehat{\beta}$, we first introduce the following working likelihood function:

$$\widehat{\widetilde{l}}_F(\beta) = \Sigma_{i \in C} \int_0^\tau \left[\widehat{Z}_i'\beta - \log\left\{ \Sigma_{i \in \widetilde{C}} Y_l(t) \exp\left(\widehat{Z}_i'\beta\right) \right\} \right] dN_i(t), \qquad (A.27)$$

which differs from the pseudolikelihood function $\widehat{l}_F(\beta)$ in (A.16) by using the index set $\widetilde{C}$ instead of $\widetilde{R}(t)$. The corresponding estimator based on $\widetilde{l}_F(\beta)$ is defined as

$$\widetilde{\beta} = \arg\max_{\beta \in B} \widehat{\widetilde{l}}_F(\beta). \qquad (A.28)$$

Note the argument in [21]; we can prove that the estimator $\widetilde{\beta}$ is asymptotically equivalent to the proposed estimator $\widehat{\beta}$. That is, the asymptotic properties of $\widehat{\beta}$ can be obtained by proofing the desired asymptotic behaviors of $\widehat{\beta}$.

Note that $\widetilde{l}_F(\beta) = \widetilde{A}(\beta, t)$. Mimicking the discussions in Lemma 1 of [21], we obtain that

$$\widehat{\widetilde{D}}(\beta, t) = n^{-1} \left\{ \widehat{\widetilde{A}}(\beta, t) - \widetilde{A}(\beta_0, t) \right\}$$
$$= n^{-1} \left\{ \widehat{\widetilde{A}}(\beta, t) - \widetilde{A}(\beta, t) \right\} \qquad (A.29)$$
$$+ n^{-1} \left\{ \widetilde{A}(\beta, t) - \widetilde{A}(\beta_0, t) \right\}.$$

Define

$$\widetilde{D}(\beta, t) = n^{-1} \left\{ \widetilde{A}(\beta, t) - \widetilde{A}(\beta_0, t) \right\}, \qquad (A.30)$$

where $\widetilde{D}(\beta, t)$ converges in probability to the same limit as

$$D(\beta, t) = \int_0^t \left[(\beta - \beta_0)' S^{(1)}(\beta_0, U) - \log\left\{ \frac{S^{(0)}(\beta, U)}{S^{(0)}(\beta_0, U)} \right\} S^{(0)}(\beta_0, U) \right] \cdot \lambda_0(U) dU, \qquad (A.31)$$

for $\beta \in \beta$. Therefore, $D(\beta, \tau)$ converges uniformly to

$$d(\beta, t) = \int_0^\tau \left[(\beta - \beta_0)' s^{(1)}(\beta_0, t) - \log\left\{ \frac{s^{(0)}(\beta, t)}{s^{(0)}(\beta_0, t)} \right\} s^{(0)}(\beta_0, t) \right] \cdot \lambda_0(t) dt, \qquad (A.32)$$

$$d(\beta^*) \geq d(\beta_0), \quad \beta^* \neq \beta. \qquad (A.34)$$

This inequality is in contradiction with (A.12), so we have the convergency of $\widetilde{\beta}$ to β_0 in probability.

From the basic assumptions I, II, and III, we derive that

which is a continuous and convex function of β and has a unique maximum at β_0 [20, 21]. That is,

$$d(\beta) \leq d(\beta_0), \qquad (A.33)$$

with equality if and only if $\beta = \beta_0$.

We assume that $\widetilde{\beta}$ does not converge to β_0 by a set of positive probability. So, there exists a subsequence $\{\widetilde{\beta}_{in}\}$ of $\{\widetilde{\beta}\}$ which converges to β^* not equal to β_0. Since $\{\widetilde{\beta}_{in}\}$ is the maximum, we have $D(\widetilde{\beta}_{in}, \tau) = D(\beta_0, \tau)$. We obtain the following inequality by the uniform convergency and continuity of limit:

$$E\left[E\left(\widetilde{Z}_{ij}|U_i\right)\right] = E\left[E\left(\phi_j(U_i)Z_{ij}|U_i\right)\right]$$
$$= E\left[\phi_j(U_i)E\left(Z_{ij}|U_i\right)\right]$$
$$= E\left[\phi_j(U_i)E\left(Z_{ij}\right)\right] \qquad (A.35)$$
$$= E\left(\phi_j(U_i)\right)Z_{ij}$$
$$= Z_{ij},$$

and from the above equation, we have

$$\widehat{Z}_i = \left(\widehat{Z}_{i1}, \widehat{Z}_{i2}, \ldots, \widehat{Z}_{ip}\right)^T = \left(\frac{\widetilde{Z}_{i1}}{\widehat{\phi}_1(U_i)}, \frac{\widetilde{Z}_{i2}}{\widehat{\phi}_2(U_i)}, \ldots, \frac{\widetilde{Z}_{ip}}{\widehat{\phi}_p(U_i)}\right)^{\top}$$

$$= \begin{pmatrix} \widehat{\phi}_1^{-1}(U_i) & 0 & 0\ 0\ 0 & 0 \\ 0 & \widehat{\phi}_2^{-1}(U_i) & 0\ 0\ 0 & 0 \\ 0 & 0 & .\ 0\ 0 & 0 \\ 0 & 0 & 0\ .\ 0 & 0 \\ 0 & 0 & 0\ 0\ . & 0 \\ 0 & 0 & 0\ 0\ 0 & \widehat{\phi}_p^{-1}(U_i) \end{pmatrix} \begin{pmatrix} \widetilde{Z}_{i1} \\ \widetilde{Z}_{i2} \\ . \\ . \\ . \\ \widetilde{Z}_{ip} \end{pmatrix}.$$

$$(A.36)$$

Under conditions (A1)-(A3), (B1)-(B4), (C), (D1)-(D2), and (E) and similar arguments in Self and Prentice [21], we obtain the following results:

$$-\frac{1}{n}\nabla_\beta^2 \widehat{\tilde{l}}_F(\beta_0) \xrightarrow{L} \widehat{\Sigma}(\beta_0), \frac{1}{\sqrt{n}}\nabla_\beta^2 \widehat{\tilde{l}}_F(\beta_0) \xrightarrow{L} N(0, \widehat{\Sigma})(\beta_0) + \widehat{\Sigma}_1(\beta_0).$$

$$(A.37)$$

Because $\widetilde{\beta}$ converges to β_0 in probability, Slutsky's theorem, and (A.12), we can obtain

$$\sqrt{n}\left(\widetilde{\beta} - t\beta_0\right) \xrightarrow{L} N\left(0, \widehat{\Omega}(\beta_0)\right), \qquad (A.38)$$

where the asymptotic variance matrix

$$\widehat{\Omega}(\beta_0) = \widehat{\Sigma}(\beta_0) + \widehat{\Sigma}_1(\beta_0), \qquad (A.39)$$

where

$$\widehat{\Sigma}(\beta_0) = \int_0^\tau \phi^{-1} \nu(\beta_0, t) s^{(0)}(\beta_0, t) \lambda_0(t) \phi^{-1} dt,$$

$$\widehat{\Sigma}_1(\beta_0) = \int_0^\tau \int_0^\tau \widehat{\Psi}(\beta_0, t, \omega) s^{(0)}(\beta_0, t) s^{(0)}(\beta_0, \omega) \lambda_0(t) \lambda_0(\omega) dt d\omega,$$

$$\widehat{\Psi}(\beta_0, t, w) = (1 - \alpha)\alpha^{-1} \left\{ s^{(0)}(\beta_0, t) s^{(0)}(\beta_0, w) \right\}^{-1} \widehat{\phi}^{-1}$$

$$\cdot \left\{ q^{(2)}(\beta_0, t, w) - q^{(1)}(\beta_0, w, t) e(\beta_0, w)' - e(\beta_0, t) q^{(1)}(\beta_0, t, w)' + q^{(0)}(\beta_0, t, w) e(\beta_0, t) e(\beta_0, w)' \right\} \widehat{\phi}^{-1},$$

$$\widehat{\phi}^{-1} = \sum_{l=1}^{\widetilde{n}} \phi_l^{-1}.$$

$$(A.40)$$

□

References

[1] R. L. Prentice, "A case-cohort design for epidemiologic cohort studies and disease prevention trials," *Biometrika*, vol. 73, no. 1, pp. 1–11, 1986.

[2] F. Imamura, M. B. Schulze, S. J. Sharp et al., "Estimated substitution of tea or coffee for sugar-sweetened beverages was associated with lower type 2 Diabetes incidence in case-cohort analysis across 8 European countries in the EPIC-InterAct study," *The Journal of Nutrition*, vol. 149, no. 11, pp. 1985–1993, 2019.

[3] C. Lassale, I. Tzoulaki, K. G. M. Moons et al., "Separate and combined associations of obesity and metabolic health with coronary heart disease: a pan-European case-cohort analysis," *European Heart Journal*, vol. 39, no. 5, pp. 397–406, 2018.

[4] R. J. Serfling, "Approximation theorems of mathematical statistics," *Biometrics*, vol. 37, no. 4, 1980.

[5] S. Yao, M. L. Kwan, I. J. Ergas et al., "Association of serum level of Vitamin D at diagnosis with breast cancer survival," *JAMA Oncology*, vol. 3, no. 3, pp. 351–357, 2017.

[6] Z. Xu, D. P. Sandler, and J. A. Taylor, "Blood dna methylation and breast cancer: a prospective case-cohort analysis in the sister study," *JNCI: Journal of the National Cancer Institute*, vol. 112, no. 1, pp. 87–94, 2019.

[7] P. Andronis, L. D. A. F. Amorim, and J. Cai, "Multiplicative rates model for recurrent events in case-cohort studies," *Lifetime Data Analysis*, vol. 26, no. 1, pp. 134–157, 2020.

[8] E. T. Parner, P. K. Andersen, and M. Overgaard, "Cumulative risk regression in case-cohort studies using pseudo-observations," *Lifetime Data Analysis*, vol. 26, no. 4, pp. 639–658, 2020.

[9] J. Rosman, P. Ter Wee, S. Meijer Truus et al., "Prospective randomised trial of early dietary protein restriction in chronic

renal failure," *The Lancet*, vol. 324, no. 8415, pp. 1291–1296, 1984.

[10] S. Klahr, A. S. Levey, G. J. Beck et al., "The effffects of dietary protein restriction and blood pressure control on the progression of renal disease," *New England Journal of Medicine*, vol. 330, no. 13, pp. 877–884, 1994.

[11] D. Sentürk and H. Müller, "Covariate-adjusted regression," *Biometrika*, vol. 92, no. 1, pp. 75–89, 2005.

[12] X. Cui, W. Guo, L. Lin, and L. Zhu, "Covariate-adjusted nonlinear regression," *The Annals of Statistics*, vol. 37, no. 4, pp. 1839–1870, 2009.

[13] T. Mantopoulos, P. M. Mitchell, N. J. Welton, R. McManus, and L. Andronis, "Choice of statistical model for cost-effectiveness analysis and covariate adjustment: empirical application of prominent models and assessment of their results," *The European Journal of Health Economics*, vol. 17, no. 8, pp. 927–938, 2016.

[14] X. D. Huang, G. P. Wang, and M. M. Li, "Adjusting for high-dimensional covariates in sparse precision matrix estimation by lasso penalized D-trace loss," *Chinese Applied Probability Statistics*, vol. 35, no. 5, pp. 441–452, 2019.

[15] S. H. Zhang, J. Y. Zhu, and S. G. Zhang, "A powerful procedure for multiple outcomes comparison with covariate adjustment and its application to genomic data," *Journal of University of Chinese Academy of Sciences*, vol. 36, no. 2, pp. 155–161, 2019.

[16] J. Ding, G.-L. Tian, and K. C. Yuen, "A new MM algorithm for constrained estimation in the proportional hazards model," *Computational Statistics & Data Analysis*, vol. 84, pp. 135–151, 2015.

[17] L. Deng, J. Ding, Y. Liu, and C. Wei, "Regression analysis for the proportional hazards model with parameter constraints under case-cohort design," *Computational Statistics & Data Analysis*, vol. 117, pp. 194–206, 2018.

[18] D. R. Cox, "Regression models and life-tables," *Journal of the Royal Statistical Society: Series B (Methodological)*, vol. 34, no. 2, pp. 187–202, 1972.

[19] G. K. Eagleson and H. G. Muller, "Transformations for smooth regression models with multiplicative errors," *Journal of the Royal Statistical Society: Series B (Statistical Methodology)*, vol. 59, no. 1, pp. 173–189, 1997.

[20] P. K. Andersen and R. D. Gill, "Cox's regression model for counting processes: a large sample study," *The Annals of Statistics*, vol. 10, no. 4, pp. 1100–1120, 1982.

[21] S. G. Self and R. L. Prentice, "Asymptotic distribution theory and efficiency results for case-cohort studies," *The Annals of Statistics*, vol. 16, no. 1, pp. 64–81, 1988.

[22] D. Sentürk and H. Müller, "Inference for covariate adjusted regression via varying coefficient models," *The Annals of Statistics*, vol. 34, no. 2, pp. 654–679, 2006.

[23] L.-X. Davis and K.-T. Fang, "Asymptotics for kernel estimate of sliced inverse regression," *The Annals of Statistics*, vol. 24, no. 3, pp. 1053–1068, 1996.

[24] N. L. Hjort, "Bootstrapping cox's regression model," Technical report NSF-241, Department of Statistics, Stanford University, Stanford, CA, USA, 1985.

[25] B. Efron and R. Tibshirani, *An Introduction to the Bootstrap*, Chapman & Hall, New York, NY, USA, 1993.

[26] D. Burr, "A comparison of certain bootstrap confidence intervals in the cox model," *Journal of the American Statistical Association*, vol. 89, no. 428, pp. 1290–1302, 1994.

[27] R. L. Eubank, *Spline Smoothing and Nonparametric Regression*, Dekker, New York, NY, USA, 1988.

[28] D. Y. Lin, L. J. Wei, and Z. Ying, "Accelerated failure time models for counting processes," *Biometrika*, vol. 85, no. 3, pp. 605–618, 1998.

[29] D. Y. Lin and Z. Ying, "Semiparametric analysis of general additive-multiplicative hazard models for counting processes," *The Annals of Statistics*, vol. 23, no. 5, pp. 1712–1734, 1995.

[30] Y. Q. Chen and M.-C. Wang, "Analysis of accelerated hazards models," *Journal of the American Statistical Association*, vol. 95, no. 450, pp. 608–618, 2000.

[31] J. Cai and D. Zeng, "Power calculation for case-cohort studies with nonrare events," *Biometrics*, vol. 63, no. 4, pp. 1288–1295, 2007.

[32] C. R. Rao, *Linear Statistical Inference and its Applications*, Wiley, Hoboken, NJ, USA, 2nd edition, 1973.

WILEY | Hindawi

Research Article

Complex Dynamics of Beddington–DeAngelis-Type Predator-Prey Model with Nonlinear Impulsive Control

Changtong Li [ID], Xiaozhou Feng [ID], Yuzhen Wang [ID], and Xiaomin Wang [ID]

School of Science, Xi'an Technological University, Xi'an 710032, China

Correspondence should be addressed to Xiaozhou Feng; flxzfxz8@163.com

According to resource limitation, a more realistic pest management is that the impulsive control actions should be adjusted according to the densities of both pest and natural enemy in the field, which result in nonlinear impulsive control. Therefore, we have proposed a Beddington–DeAngelis interference predator-prey model concerning integrated pest management with both density-dependent pest and natural enemy population. We find that the pest-eradication periodic solution is globally stable if the impulsive period is less than the critical value by Floquet theorem. The condition of permanent is established, and a stable positive periodic solution appears via a supercritical bifurcation by bifurcation theorem. Finally, in order to investigate the effects of those nonlinear control strategies on the successful pest control, the bifurcation diagrams showed that the model exists with very complex dynamics. Consequently, the resource limitation may result in pest outbreak in complex ways, which means that the pest control strategies should be carefully designed.

1. Introduction

Since pest outbreak can cause serious economic loss, pest control has been becoming an increasing concern to entomologists and society all over the world. Several pest control strategies can be used for farmers. As well known, chemical pesticide can directly and rapidly kill large proportion of pest, and it is the only way to prevent economic losses in many cases. Biological control is the practice of releasing of natural enemies to control pests [1, 2], sometimes which has a highly efficacious and more active role in some pest situations. However, in order to avoid the resistance development of pests to the control tactic and to protect the environment quality, different pest control techniques should be combined together rather than against overuse of a single control strategy. In particular, integrated pest management(IPM) incorporates a variety of cultural, biological, and chemical methods to high efficiency control of the pest populations, which has been proved that it is more efficient long-term strategy for pest control than the classical one (such as biological control or chemical control) [3–5].

It is reasonable and accurate that impulsive differential equations mathematically simulate the evolution of biological behaviors and complex biological phenomena, which provide conditions for people to assist in the design of IPM strategies and understand the biological phenomena from a mathematical point of view [1, 3, 6–9]. In recent years, the impulsive differential systems with integrated pest management have been systematically studied and developed rapidly [10, 11], which enriched its basic theory and analytical techniques of impulsive differential system [12–20]. However, one of the main assumptions in previous literature is that a certain proportion of pest population is killed when the pesticide is applied. Meanwhile, a constant natural enemy is released [21–28], which means that the agricultural resources have almost no effect on IPM.

In reality, the release methods and ratios of numbers of natural enemies will inevitably be affected by the limitation of agricultural resources because of the unbalance development of agricultural, such as agricultural capital, labour forces, biological resources, and pesticides. Therefore, the release ratios of numbers of natural enemies according to current density in the field could significantly affect the effect

of pest control strategy. In order to take the resource limitation into the IPM strategy, several predator-prey models with nonlinear impulse have been proposed [29–32] and mainly focused on establishing the global stability conditions. However, the nonlinear impulsive function mentioned above is only related to the density of the natural enemy population in the field. Based on resource limitation, the densities of the pest and natural enemy should be carefully monitored before IPM measures are applied. A more realistic case is that the methods for the instantaneous releasing numbers of natural enemies should be based on the dynamic changes of pest and natural enemy densities. In other words, the higher the number of pest population or the lower the number of predator population in the field, the higher the number of predator population should be released and vice versa, which has not been studied until now.

Therefore, in order to take the resource limitation into account and to understand how the nonlinear density regulatory factor for the natural enemies affect the dynamics of predator-prey model, we propose the following predator-prey model with Beddington–DeAngelis functional response and nonlinear impulsive control:

$$
\begin{cases}
\begin{aligned}
\dfrac{dx(t)}{dt} &= rx(t)\left(1 - \dfrac{x(t)}{K}\right) - \dfrac{\alpha x(t) y(t)}{c + x(t) + b y(t)} \\[2mm]
\dfrac{dy(t)}{dt} &= \dfrac{\beta x(t) y(t)}{c + x(t) + b y(t)} - \delta y(t)
\end{aligned} \Bigg\}, \quad t \neq nT, \\[6mm]
\begin{aligned}
x(t^+) &= q_1 x(t) \\[2mm]
y(t^+) &= q_2 y(t) + \dfrac{\lambda_1 x(t)}{1 + \theta_1 x(t)} + \dfrac{\lambda_2}{1 + \theta_2 y(t)}
\end{aligned} \Bigg\}, \quad t = nT.
\end{cases}
$$
$$(1)$$

where $x(t)$ and $y(t)$ are the densities of prey and predator populations, respectively, and all parameters are positive constants. IPM strategy (the nonlinear impulse) is applied at each discrete time point nT. $0 \leq q_1, q_2 \leq 1$ present survival rate of prey and predator after harvesting or pesticides; $q_2 \geq 1$ means that the pesticides only affect the pest and an impulsive increase of the predator population density is induced by release of predators. Moreover, we choose the nonlinear saturation functions or density-dependent functions as follows:

$$
y(t^+) = q_2 y(t) + \frac{\lambda_1 x(t)}{1 + \theta_1 x(t)} + \frac{\lambda_2}{1 + \theta_2 y(t)}, \quad t = nT, \quad (2)
$$

$\lambda_1, \lambda_2 \geq 0$ is the maximal release amount of the predator according to the densities of prey and predator populations respectively, and $\theta_1, \theta_2 \geq 0$ represent the shape parameter. In particular, the system with $\lambda_1 = 0, \theta_2 = 0$ (i.e., linear impulsive perturbations) has been investigated in [27, 28]. We assume that the densities of the natural enemy populations are updated to $y(t^+) = q_2 y(t) + (\lambda_1 x(t)/1 + \theta_1 x(t))$

$+ (\lambda_2/1 + \theta_2 y(t))$ at each time point nT, which is a more reasonable control strategy than previous literature [31, 32].

The purpose of this paper proposes a Beddington–DeAngelis interference model with nonlinear impulsive control to address how the nonlinear impulsive control actions affect the successful pest control strategies. By using the Floquet theorem and small-amplitude perturbation skills, we obtain that the pest-eradication periodic solution is globally stable if the period of impulsive T is less than a critical value, and a sufficient condition for the permanence of the system is obtained. Moreover, when the trivial periodic solution loses its stability, we obtain that a nontrivial periodic solution appears via a supercritical bifurcation by employing a bifurcation theorem. By bifurcation diagrams, we show that the model presents more rich and interesting dynamic behavior including periodic doubling bifurcation, period-halving bifurcations, chaotic solutions, and multi-stability. Finally, we give some related biological implications.

2. Global Stability of the Pest-Eradication Periodic Solution

As we know, eradicating the pest population is an important purpose of IPM strategy, so the existence and global stability of the pest-eradication periodic solution play a crucial role in studying the dynamical behavior. For this, we firstly study the properties of the subsystem

$$
\begin{cases}
\dfrac{dy(t)}{dt} = -\delta y(t), & t \neq nT, \\[4mm]
y(t^+) = q_2 y(t) + \dfrac{\lambda_2}{1 + \theta_2 y(t)}, & t = nT.
\end{cases}
\tag{3}
$$

Subsystem (3) is a nonlinear growth model, by using the same methods as those in reference [32], and we can have the following result.

Lemma 1. *When* $1 - q_2 \exp(-\delta T) > 0$, *model (3) has a globally stable periodic solution:*

$$
y_p(t) y^* \exp(-\delta(t - nT)), \quad t \in (nT, (n+1)T), \quad (4)
$$

where $y^* = ((\sqrt{A+1} - 1)/(2\theta_2 \exp(-\delta T)))$ *with* $A = ((4\lambda_2 \theta_2 \exp(-\delta T))/(1 - q_2 \exp(-\delta T)))$ *is a positive constant.*

Therefore, when $q_2 \exp(-\delta T) < 1$, we have that model (1) has complete expression for pest-eradication periodic solution $(x_p(t), y_p(t)) = (0, y^* \exp(-\delta(t - nT)))$.

Next, we will present a condition which guarantees the local and global asymptotic stability of pest-eradication periodic solution $(x_p(t), y_p(t))$ of model (1).

Theorem 1. *The pest-eradication periodic solution* $(x_p(t), y_p(t))$ *is locally asymptotically stable provided that*

$$
T < \frac{1}{r} \ln \frac{1}{q_1} - \frac{\alpha}{rb\delta} \ln\left(\frac{c + b y^* \exp(-\delta T)}{c + b y^*}\right). \tag{5}
$$

Furthermore, $(x_p(t), y_p(t))$ is globally asymptotically stable provided

$$T < \frac{1}{r} \ln \frac{1}{q_1} - \frac{\alpha}{rb\delta} \ln\left(\frac{c + K + by^* \exp(-\delta T)}{c + K + by^*}\right). \quad (6)$$

Proof. The local stability of the pest-eradication solution may be determined by the behavior of small-amplitude perturbations of the solution. Defining $u(t) = x(t) - x_p(t), v(t) = y(t) - y_p(t)$, then the fundamental matrix $\Phi(t)$ of model (1) satisfies

$$\frac{d\Phi(t)}{dt} = \begin{pmatrix} r - \dfrac{\alpha y_p(t)}{c + by_p(t)} & 0 \\[3mm] \dfrac{\beta y_p(t)}{c + by_p(t)} & -\delta \end{pmatrix} \Phi(t), \quad (7)$$

$$M = B(T)\Phi(T)$$

$$= \begin{pmatrix} q_1 \exp\left(\displaystyle\int_0^T \left(r - \dfrac{\alpha y_p(t)}{c + by_p(t)}\right)dt\right) & 0 \\[5mm] * & \left(q_2 - \dfrac{\lambda_2 \theta_2}{\left(1 + \theta_2 y_p(T)\right)^2}\right)\exp(-\delta T) \end{pmatrix} \quad (9)$$

has absolute value less than one, then the solution $(x_p(t), y_p(t))$ of model (1) is locally stable, and $*$ is not needed to calculate the exact form. Note that all multipliers are

$$\mu_1 = q_1 \exp\left(\int_0^T \left(r - \frac{\alpha y_p(t)}{c + by_p(t)}\right)dt\right),$$

$$\mu_2 = \left(q_2 - \frac{\lambda_2 \theta_2}{\left(1 + \theta_2 y_p(T)\right)^2}\right)\exp(-\delta T). \quad (10)$$

It is easy to see that $\mu_2 \le q_2 \exp(-\delta T) < 1$. Furthermore,

$$\frac{\lambda_2 \theta_2 \exp(-\delta T)}{\left(1 + \theta_2 y_p(t)\right)^2} \le \frac{4\lambda_2 \theta_2 \exp(-\delta T)}{\left(\sqrt{1 + 4\lambda_2 \theta_2 \exp(-\delta T)} + 1\right)^2} < 1. \quad (11)$$

So, we obtain $\mu_2 \ge q_2 \exp(-\delta T) - 1 > -1$, which means $|\mu_2| < 1$. Since $\int_0^T (r - (\alpha y_p(t)/c + by_p(t)))dt = (1/b\delta)$, $\ln ((c + by^* \exp(-\delta T))/(c + by^*))$, according to the Floquet theory of impulsive differential equation, the pest-eradication periodic solution $(x_p(t), y_p(t))$ is locally asymptotically stable if

$$T < \frac{1}{r} \ln \frac{1}{q_1} - \frac{\alpha}{rb\delta} \ln\left(\frac{c + by^* \exp(-\delta T)}{c + by^*}\right). \quad (12)$$

and $\Phi(0) = I$ is the identity matrix. From the third and fourth equations of (1), one has that

$$\begin{pmatrix} u(nT^+) \\ v(nT^+) \end{pmatrix} = \begin{pmatrix} q_1 & 0 \\[3mm] \lambda_1 & q_2 - \dfrac{\lambda_2 \theta_2}{\left(1 + \theta_2 y_p(T)\right)^2} \end{pmatrix} \begin{pmatrix} u(nT) \\ v(nT) \end{pmatrix}$$

$$= B(T) \begin{pmatrix} u(nT) \\ v(nT) \end{pmatrix}. \quad (8)$$

Therefore, if each eigenvalues of the following matrix

Next, we will show the global attractivity provided condition (6) is satisfied. From the comparison theorem of impulsive equation, we obtain $y(t) \ge y_p(t) - \varepsilon$ for all t large enough. Also, it is easy to see that $x(t) < K + \varepsilon$ for all t large enough.

For simplicity, we may assume that $y(t) \ge y_p(t) - \varepsilon$ and $x(t) < K + \varepsilon$ for all $t \ge 0$. If condition (6) holds true, then we choose an $\varepsilon > 0$ such that

$$\eta \triangleq q_1 \exp\left(\int_0^T \left(r - \frac{\alpha(y_p(t) - \varepsilon)}{c + K + \varepsilon + b(y_p(t) - \varepsilon)}\right)dt\right) < 1. \quad (13)$$

From model (1), we obtain

$$\begin{cases} \dfrac{dx(t)}{dt} \le x(t)\left(r - \dfrac{\alpha(y_p(t) - \varepsilon)}{c + K + \varepsilon + b(y_p(t) - \varepsilon)}\right), & t \ne nT, \\[5mm] x(t^+) = q_1 x(t), & t = nT. \end{cases} \quad (14)$$

Integrating on $(nT, (n+1)T]$, one obtains

$$x((n+1)T) = q_1 x(nT)\exp\left[\int_{nT}^{(n+1)T}\left(r - \frac{\alpha\left(y_p(t) - \varepsilon\right)}{c + K + \varepsilon + b\left(y_p(t) - \varepsilon\right)}\right)dt\right]$$

$$= x(nT)\eta. \tag{15}$$

Thus, $x(nT) = x(0^+)\eta^n$ and consequently $x(nT) \longrightarrow 0$ as $n \longrightarrow \infty$. Therefore, $x(t) \longrightarrow 0$ as $n \longrightarrow \infty$, since $0 < x(t) \le q_1 x(nT)\exp(rT)$ for $t \in (nT, (n+1)T]$.

Following, we only need to prove $y(t) \longrightarrow y_p(t)$ as $t \longrightarrow \infty$. There must exist a $0 < \varepsilon_1 < (\delta c/\beta)$ and $T_1 > 0$ such that $0 < x(t) < \varepsilon_1$ for $t > T_1$. Again, for simplicity, it is assumed that $0 < x(t) < \varepsilon_1$ holds true for $t \ge 0$. Then, we deduce that $(\lambda_1 x(t)/1 + \theta_1 x(t)) < \varepsilon_1 \lambda_1$ and

$$-\delta y(t) \le \frac{dy}{dt} \le y(t)\left(\frac{\beta\varepsilon_1}{c} - \delta\right), \tag{16}$$

from which we can have the following equation:

$$\begin{cases} \dfrac{dz(t)}{dt} = \left(\dfrac{\beta\varepsilon_1}{c} - \delta\right)z(t) = -\delta_1 z(t), & t \ne nT, \\[4mm] z(t^+) = q_2 z(t) + \varepsilon_1\lambda_1 + \dfrac{\lambda_2}{1 + \theta_2 z(t)}, & t = nT. \end{cases} \tag{17}$$

By Lemma 1, model (17) has a globally asymptotically stable periodic solution $z_p(t) = z^* \exp(-\delta_1(t - nT))$, where $z^* = ((-A_1 + \sqrt{A_1^2 + 4B_1(\varepsilon_1\lambda_1 + \lambda_2)})/(2B_1))$ with $A_1 = 1 - (q_2 + \varepsilon_1\lambda_1\theta_2)\exp(-\delta_1 T), B_1 = \theta_2(1 - q_2\exp(-\delta_1 T))\exp(-\delta_1 T)$ and $t \in (nT, (n+1)T]$.

According to the comparison theorem, we get $y_p(t) \le y(t) \le z(t)$ and $z(t) \longrightarrow z_p(t), z_p(t) \longrightarrow y_p(t)$ as $t \longrightarrow \infty$. Hence, for any $\varepsilon_1 > 0$, we have

$$y_p(t) - \varepsilon_1 < y(t) < z_p(t) + \varepsilon_1, \tag{18}$$

for $T_2 \ge T_1 > 0$. Furthermore, let $\varepsilon \longrightarrow 0$, we get $y_p(t) - \varepsilon_1 < y(t) < y_p(t) + \varepsilon_1$ for t large enough. In other words, $y(t) \longrightarrow y_p(t)$ as $t \longrightarrow \infty$ for t large enough. The proof is completed.

3. Permanence

Persistence is an important property of dynamical systems for addressing the long-term survival of all components of a system. Now, we investigate the sufficient condition for the permanence of model (1).

Theorem 2. *Model (1) is permanent if $T > (1/r)\ln(1/q_1) - (\alpha/rb\delta)\ln(c + by^*\exp(-\delta T)/c + by^*)$ holds true.*

Proof. Suppose that $(x(t), y(t))$ is a solution of (1) with $x(0) > 0, y(0) > 0$. It is easy to know that $x(t) < M, y(t) < M$ for all $t > 0, M > (rc/\alpha)$. Define $m_2 = y^*\exp(-\delta T) - \varepsilon$. From Theorem 1, it is easy to see that $y(t) \ge m_2$ for t large enough.

Then, we shall find an m_1 such that $x(t) \ge m_1$ for all t that are large enough. We will do it in the following two steps.

Step 1. Let $m_3 > 0, \varepsilon_1 > 0$ be small enough such that $\delta_2 = \delta - (\beta m_3/c + m_3) > 0$ and $\eta \triangleq q_1 \exp(rT - (rm_3 T/K) - (\alpha/b\delta_2)\ln(c + bu^*\exp(-\delta_2 T)/c + b u^*) - (\alpha\varepsilon_1 T/c)) > 1$, where $u^* = ((-A_2 + \sqrt{A_2^2 + 4B_2(m_3\lambda_1 + \lambda_2)})/(2B_2))$ with $A_2 = 1 - (q_2 + m_3\lambda_1\theta_2)\exp(-\delta_2 T), B_2 = \theta_2(1 - q_2\exp(-\delta_2 T))\exp(-\delta_2 T)$. We will prove that $x(t) < m_3$ cannot hold for all $t > 0$. Otherwise,

$$\frac{dy(t)}{dt} \le -\delta_2 y(t). \tag{19}$$

From Lemma 1, we then obtain $y(t) \le u(t)$ and $u(t) \longrightarrow u_p(t), t \longrightarrow \infty$, where $u(t)$ is the solution of

$$\begin{cases} \dfrac{du(t)}{dt} = -\delta_2 u(t), & t \ne nT, \\[4mm] u(t^+) \le q_2 u(t) + \lambda_1 m_3 + \dfrac{\lambda_2}{1 + \theta_2 u(t)}, & t = nT, \end{cases} \tag{20}$$

and $u_p(t) = u^*\exp(-\delta_2(t - nT)), t \in (nT, (n+1)T]$ with $u^* = ((-A_2 + \sqrt{A_2^2 + 4B_2(m_3\lambda_1 + \lambda_2)})/(2B_2))$. Consequently, there exists a $\widehat{T} > 0$ such that $y(t) \le u(t) < u_p(t) + \varepsilon_1$ and

$$\frac{dx(t)}{dt} \ge x(t)\left(r - \frac{rm_3}{K} - \frac{\alpha y(t)}{c + by(t)}\right)$$

$$\ge x(t)\left(r - \frac{rm_3}{K} - \frac{\alpha u_p(t) + \alpha\varepsilon_1}{c + bu_p(t) + b\varepsilon_1}\right) \tag{21}$$

$$\ge x(t)\left(r - \frac{rm_3}{K} - \frac{\alpha u_p(t)}{c + bu_p(t)} - \frac{\alpha\varepsilon_1}{c}\right),$$

for $t > \widehat{T}$. Furthermore, we get

$$\begin{cases} \dfrac{dx(t)}{dt} \ge x(t)\left(r - \dfrac{rm_3}{K} - \dfrac{\alpha u_p(t)}{c + bu_p(t)} - \dfrac{\alpha\varepsilon_1}{c}\right), & t \ne nT, \\[4mm] x(t^+) = q_1 x(t), & t = nT, \end{cases} \tag{22}$$

for $t > \widehat{T}$. Integrating (22) on $(nT, (n+1)T]$, where $nT > \widehat{T}$, we obtain

$$x((n+1)T) \ge x(nT^+)\exp\left(\int_{nT}^{(n+1)T}\left(r - \frac{rm_3}{K} - \frac{\alpha u_p(t)}{c + bu_p(t)} - \frac{\alpha\varepsilon_1}{c}\right)dt\right)$$

$$= x(nT)\eta. \tag{23}$$

Then, $x((n+k)T) > x(nT)\eta^n \longrightarrow \infty$ as $k \longrightarrow \infty$, which is a contradiction. Therefore, there exists a $t_1 > 0$ such that $x(t_1) \geq m_3$.

Step 2. If $x(t) \geq m_3$ for all $t \geq t_1$, then model (1) is permanent. If not, we can define $t^* = \inf_{t>t_1}\{x(t) < m_3\}$, Then, $x(t) \geq m_3$ for $t \in [t_1, t^*]$ since the continuity of $x(t)$ and $x(t^*) = m_3$. We only need to consider two possible cases.

Case (1): $t^* = n_1 T$. For some $n_1 \in Z_+$, then we have $q_1 m_3 \leq x(t^{*+}) = q_1 x(t^*) < m_3$. Select $n_2, n_3 \in Z_+$ such that

$$q_1^{n_2}\eta^{n_3}\exp((n_2+1)\eta_1 T) > 1, \tag{24}$$

where $\rho = r - (m_3 r/K) - (\alpha/c)M < 0$. Let $T' = n_2 T + n_3 T$, we will show that there exists a $t^* < t_2 \leq t^* + T'$ such that $x(t_2) \geq m_3$. If not, by (20) with $u(t^{*+}) = y(t^{*+})$, we can see that $y(t) \leq u(t) \leq u_p(t) + \varepsilon_1$ for $t \in [t^* + n_2 T, t^* + T']$. An argument similar to Step 1 yields

$$x(t^* + T') \geq x(t^* + n_2 T)\eta^{n_3}. \tag{25}$$

Since $y(t) \leq M$, when $t \in [t^*, t^* + n_2 T]$, we get

$$\begin{cases} \dfrac{dx(t)}{dt} \geq x(t)\left(r - \dfrac{m_3 r}{K} - \dfrac{\alpha}{c}M\right), & t \neq nT, \\ x(t^+) = q_1 x(t), & t = nT. \end{cases} \tag{26}$$

Furthermore, we integrate equation (26) on $[t^*, t^* + n_2 T]$, then we know

$$x(t^* + n_2 T) \geq m_3 q_1^{n_2-1}\exp(n_2\rho T). \tag{27}$$

From above, we obtain $x(t^* + T') \geq m_3 q_1^{n_2-1}\exp(n_2\rho T)\eta^{n_3} > m_3$ which leads to a contradiction.

Now, let $\tilde{t} = \inf_{t>t^*}\{x(t) \geq m_3\}$, then $x(t) \leq m_3$ for $t \in (t^*, \tilde{t})$ and $x(\tilde{t}) = m_3$. For any $t^* < t < \tilde{t}$, let us assume that there exists $k \in Z_+$ such that $t \in (t^* + (k-1)T, t^* + kT]$ and $k \leq n_2 + n_3$, so, from (26), we obtain

$$\begin{aligned} x(t) &\geq x(t^{*+})q_1^{k-1}\exp((k-1)\rho T)\exp(\rho(t - (t^* + (k-1)T))) \\ &\geq m_3 q_1^k \exp(k\rho T) \\ &\geq m_3 q_1^{n_2+n_3}\exp((n_2+n_3)\rho T). \end{aligned} \tag{28}$$

Let $m_1' = m_3 q_1^{n_2+n_3}\exp((n_2+n_3)\eta_1 T)$, thus, for $t \in (t^*, \tilde{t})$, we get $x(t) \geq m_1'$. For $t > \tilde{t}$, we can continue the same arguments since $x(\tilde{t}) \geq m_3$.

Case (2): $t^* \neq n_1 T, n_1 \in Z_+$. We have $x(t^*) = m_3$ since $x(t)$ is continuous. Suppose $t^* \in (n_1'T, (n_1'+1)T), n_1' \in Z_+$, we consider the following two cases for $t \in (t^*, (n_1'+1)T)$.

Case (2a): $x(t) < m_3$ for $t \in (t^*, (n_1'+1)T]$. In this case, we continue this process by using step case (1), we can prove that there exists a $\hat{t} = \inf_{t>t^*}\{x(t) \geq m_3\}$ such that $x(t) < m_3, t \in (t^*, \hat{t})$, and $x(\hat{t}) = m_3$. For any $t \in (t^*, \hat{t})$, suppose $t \in (n_1'T + (l'-1)T, n_1'T + l'T], l' \leq 1 + n_2 + n_3$, we obtain

$$\begin{aligned} x(t) &\geq m_3 q_1^{l'-1}\exp(l'\eta_1 T) \\ &\geq m_3 q_1^{n_2+n_3}\exp((n_2+n_3+1)\rho T) \triangleq m_1. \end{aligned} \tag{29}$$

Since $m_1 < m_1'$, thus, for $t \in (t^*, \hat{t})$, we have $x(t) \geq m_1$.

Case (2b): there is a $t' \in (t^*, (n_1'+1)T)$ such that $x(t') \geq m_3$. In this case, a similar argument as above, there is $\bar{t} = \inf_{t>t^*}\{x(t) > m_3\}$ such that $x(t) < m_3, t \in (t^*, \bar{t})$. Therefore, integrating equation (26) on $[t^*, t)(t \leq \bar{t})$, we can get that $x(t) \geq x(t^*)\exp(\rho(t - t^*)) \geq m_1$. Thus, the similar argument can be continued for both cases since $x(t) \geq m_1$ for some $t > t_1$. This completes the proof. □

Remark 1. Define $T^* = (1/r)\ln(1/q_1) - (\alpha/rb\delta)\ln((c + by^*\exp(-\delta T))/(c + by^*))$, the pest-eradication periodic solution loses its stability if $T > T^*$. Therefore, T^* is the critical threshold value to discriminate between stability and permanence.

4. Bifurcation

Now, we will deal with the existence of nontrivial solution near the pest-eradication solution. We use the bifurcation theory in earlier publications [33].

Theorem 3. *Model (1) has a positive nontrivial periodic solution when $T = T^*$, which is supercritical if $q_2 > \theta_2\lambda_2$ and $K\alpha < 4rbc$.*

Proof. It is convenient for the computation to exchange x and y and change the period T to τ.

$$
\begin{cases}
\begin{rcases}
\dfrac{dx(t)}{dt} = \dfrac{\beta x(t)y(t)}{c + y(t) + bx(t)} - \delta x \\[4mm]
\dfrac{dy(t)}{dt} = ry\left(1 - \dfrac{y}{K}\right) - \dfrac{\alpha x(t)y(t)}{c + y(t) + bx(t)}
\end{rcases}, \quad t \neq n\tau, \\[10mm]
\begin{rcases}
x(t^+) = q_2 x(t) + \dfrac{\lambda_1 y(t)}{1 + \theta_1 y(t)} + \dfrac{\lambda_2}{1 + \theta_2 x(t)} \\[4mm]
y(t^+) = q_1 y(t)
\end{rcases}, \quad t = n\tau.
\end{cases}
$$
$$(30)$$

Let Φ be the solution of the pulse-free system associated with system (30). Also, we get $X(t) = \Phi(t, X_0)$ with $X_0 = X(0)$. We define the mapping $\Theta_1, \Theta_2: R^2 \longrightarrow R^2$ by

$$
\Theta_1(x, y) = q_2 x + \frac{\lambda_1 y}{1 + \theta_1 y} + \frac{\lambda_2}{1 + \theta_2 x},
$$
$$(31)$$

$$
\Theta_2(x, y) = q_1 y, \xi(t) = \left(y_p(t), 0\right),
$$

and the map $F_1, F_2: R^2 \longrightarrow R^2$ by

$$
F_1(x, y) = \frac{\beta x(t)y(t)}{c + y(t) + bx(t)} - \delta x,
$$
$$(32)$$

$$
F_2(x, y) = ry\left(1 - \frac{y}{K}\right) - \frac{\alpha x(t)y(t)}{c + y(t) + bx(t)}.
$$

Furthermore, to establish the nontrivial periodic solution of system (30), we employ the techniques in [33]. Then, we have

$$
\frac{\partial\Phi_1(t, X_0)}{\partial x} = \exp\left(\int_0^t \frac{\partial F_1(\xi(t))}{\partial x} dt\right),
$$

$$
\frac{\partial\Phi_1(t, X_0)}{\partial y} = \int_0^t \exp\left(\int_s^t \frac{\partial F_1(\xi(s))}{\partial y} ds\right) \frac{\partial F_1(\xi(v))}{\partial x} \exp\left(\int_0^v \frac{\partial F_2(\xi(s))}{\partial y} ds\right) dv,
$$

$$
\frac{\partial\Phi_2(t, X_0)}{\partial x} = 0,
$$

$$
\frac{\partial\Phi_2(t, X_0)}{\partial y} = \exp\left(\int_0^t \frac{\partial F_2(\xi(t))}{\partial y} dt\right) > 0.
$$
$$(33)$$

Thus, by simple calculations, we obtain

$$
\begin{aligned}
d_0' &= 1 - \left(\frac{\partial\theta_2}{\partial y} \cdot \frac{\partial\Phi_2}{\partial y}\right)_{(\tau_0, X_0)} \\
&= 1 - q_1 \exp\left(\int_0^{\tau_0}\left(r - \frac{\alpha y_p(t)}{c + by_p(t)}\right)dt\right),
\end{aligned}
$$
$$(34)$$

where τ_0 is the root of $d_0 = 0$. Actually, it is easy to see that $d_0' = 0$ is equivalent to $\tau_0 = T^*$.

Also, we obtain that

$$
a_0' = 1 - \left(\frac{\partial\theta_1}{\partial x} \cdot \frac{\partial\Phi_1}{\partial x}\right)_{(\tau_0, X_0)} = 1 - q_1 \exp(-DT) > 0,
$$

$$
\begin{aligned}
b_0' &= -\left(\frac{\partial\theta_1}{\partial x} \cdot \frac{\partial\Phi_1}{\partial y} + \frac{\partial\theta_1}{\partial y} \cdot \frac{\partial\Phi_2}{\partial y}\right)_{(\tau_0, X_0)} \\
&= -\left(q_2 - \frac{\theta_2\lambda_2}{(1 + \theta_2 y^* \exp(-DT))^2}\right)\frac{\partial\Phi_1(\tau_0, X_0)}{\partial y} - \lambda_1\frac{\partial\Phi_2(\tau_0, X_0)}{\partial y}.
\end{aligned}
$$
$$(35)$$

Note that $b_0' < 0$ if $q_2 > \theta_2\lambda_2$.

Following, we should calculate the second-order partial derivatives:

(a)

(b)
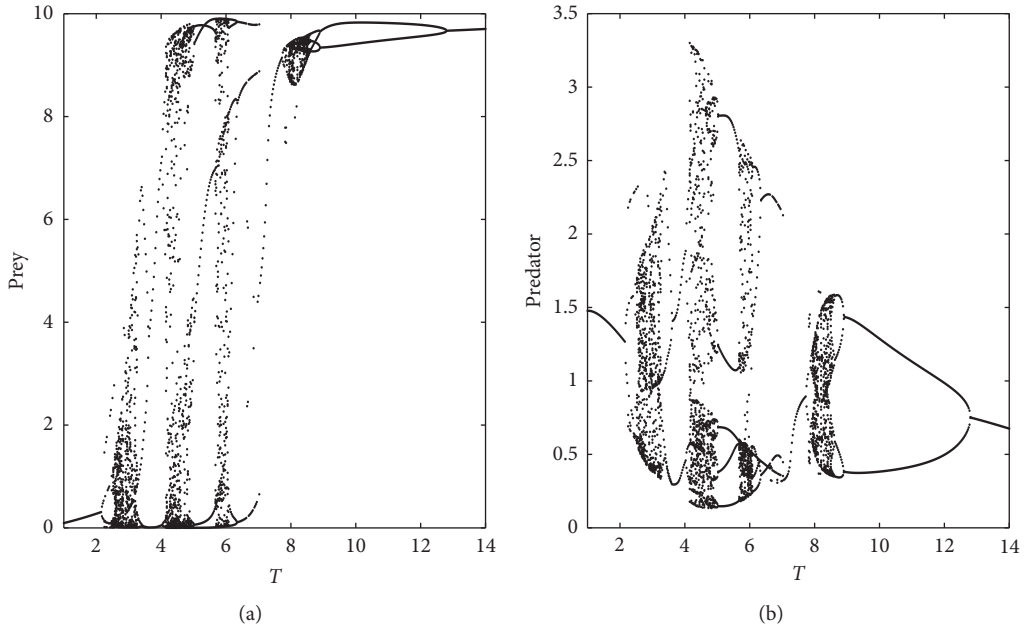
FIGURE 1: Bifurcation diagrams of model (1) with respect to T. The parameter values are as follows. $r = 2.72, K = 10, c = 1, b = 0.001, \alpha = 1.2, \beta = 0.48, \delta = 0.59, \theta_1 = 12, \theta_2 = 1, q_1 = 0.62, q_2 = 0.98, \lambda_1 = 4.4,$ and $\lambda_2 = 10.2$.

(a)

(b)

(c)

(d)
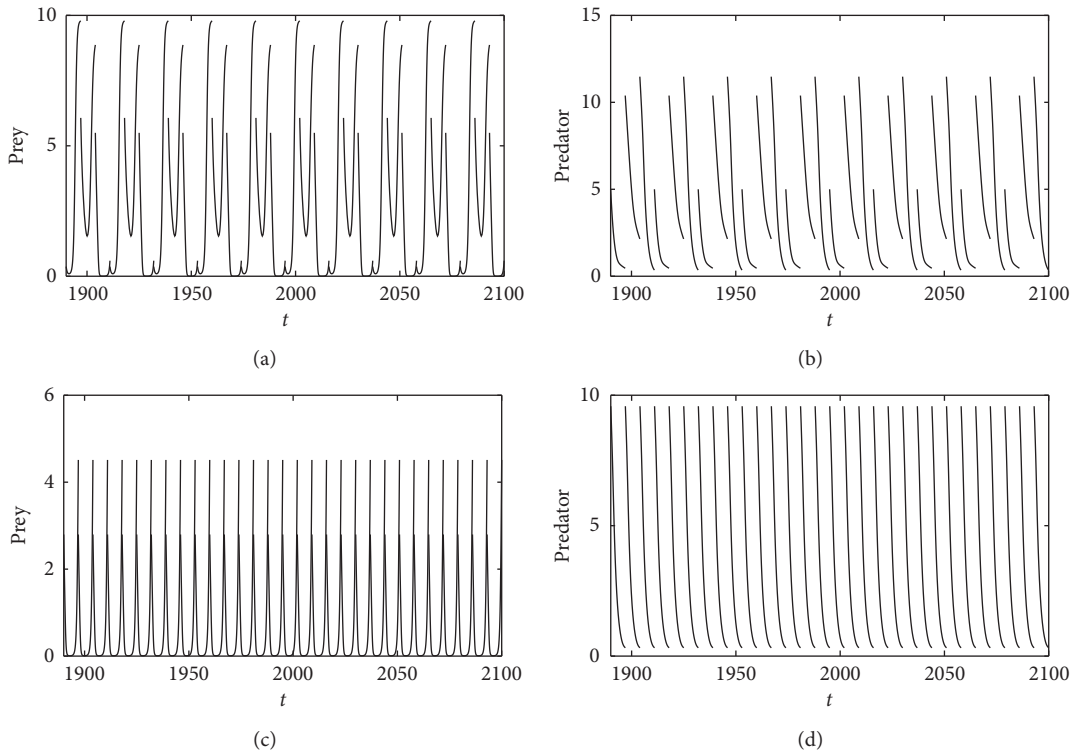
FIGURE 2: Two coexisting attractors of model (1) with $T = 7$. The other parameter values are identical to those in Figure 1. The initial conditions are as follows: $(A - B)(x_0, y_0) = (1.4, 2.1)$; $(C - D)(x_0, y_0) = (1.8, 2.6)$.

(a)   (b)
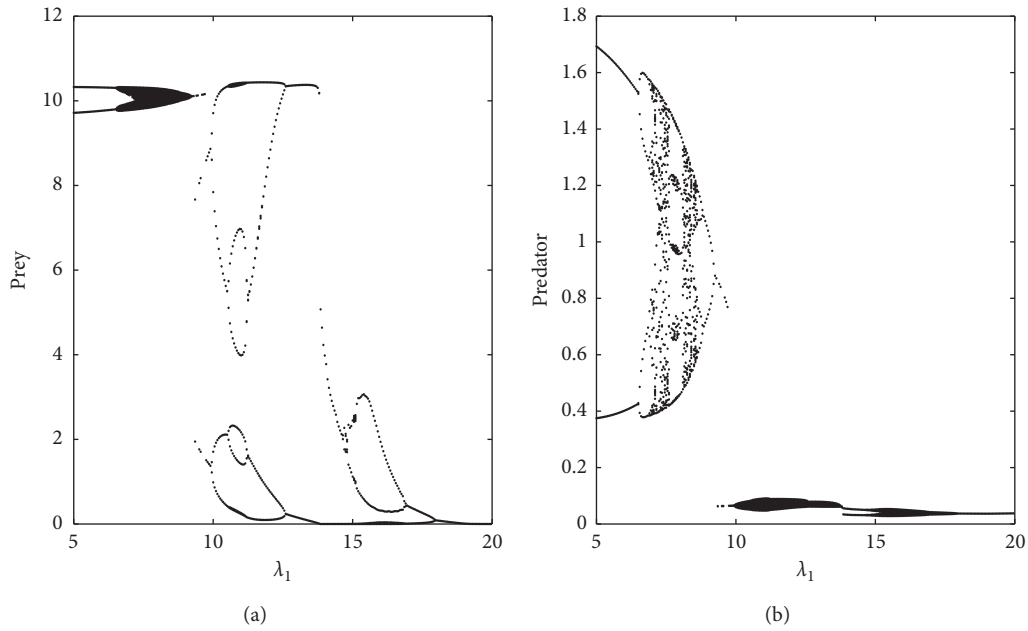
FIGURE 3: Bifurcation diagrams of model (1) with respect to λ_1. The other parameters are identical to those in Figure 1 and $K = 10.5, T = 10$.

(a)   (b)

(c)   (d)
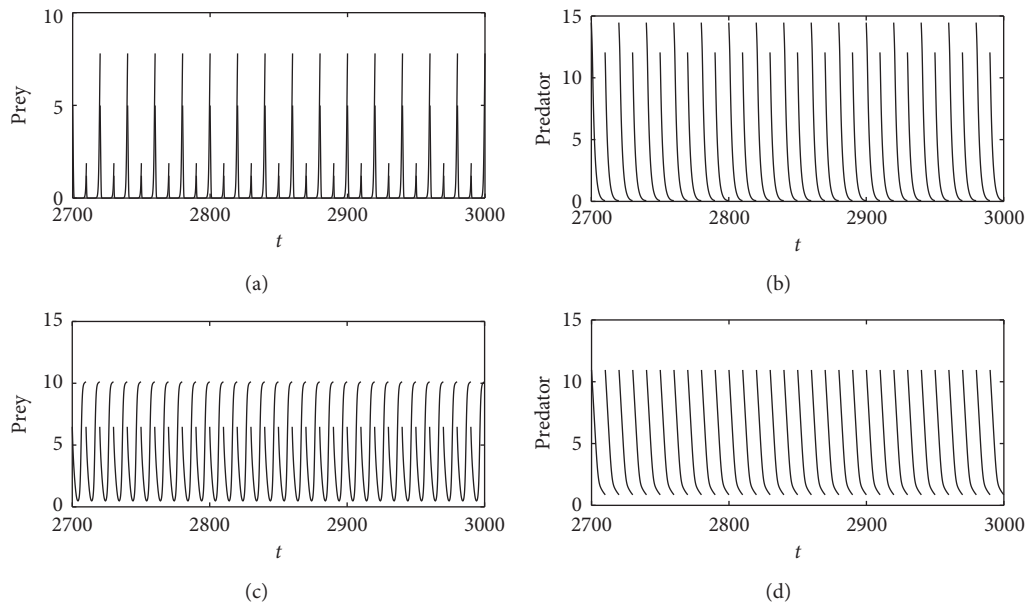
FIGURE 4: Two coexisting attractors of model (1) with $\lambda_1 = 9.4$. The other parameter values identical to those in Figure 3. The initial conditions are as follows: $(A - B)(x_0, y_0) = (1.4, 2.1); (C - D)(x_0, y_0) = (1.8, 2.6)$.

$$\frac{\partial^2 \Phi_2(\tau_0, X_0)}{\partial x \, \partial y} = \int_0^{\tau_0} \exp\left(\int_s^{\tau_0} \frac{\partial F_2(\zeta(t))}{\partial y} \, dt\right) \frac{\partial^2 F_2(\zeta(t))}{\partial x \, \partial y} \exp\left(\int_0^s \frac{\partial F_2(\zeta(t))}{\partial y} \, dt\right) ds$$

$$= -\int_0^{\tau_0} \exp\left(\int_s^t \frac{\partial F_2(\zeta(t))}{\partial y} \, dt\right) \frac{b\alpha y_p(s)}{\left(c + b y_p(s)\right)^3} \exp\left(\int_0^s \frac{\partial F_2(\zeta(t))}{\partial y} \, dt\right) ds \tag{36}$$

$$< 0.$$
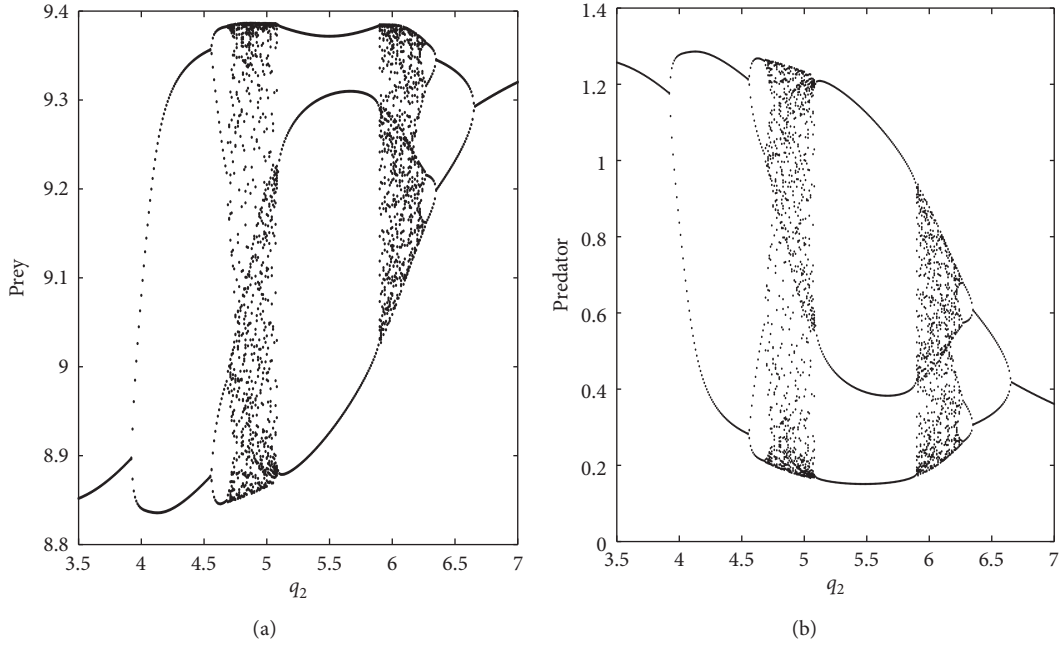
FIGURE 5: Bifurcation diagrams of model (1) with respect to q_2. Parameter values are as follows: $r = 2.12, K = 10, c = 1, b = 0.01, \alpha = 1.2, \beta = 0.48, \delta = 0.39, \theta_1 = 12.5, \theta_2 = 1.5, q_1 = 0.11, \lambda_1 = 1.5,$ and $\lambda_2 = 2$.

By the same methods as shown above, we have

$$
\begin{aligned}
\frac{\partial^2 \Phi_2(\tau_0, X_0)}{\partial y^2} &= \int_0^{\tau_0} \exp\left(\int_s^{\tau_0} \frac{\partial F_2(\zeta(t))}{\partial y} dt\right) \frac{\partial^2 F_2(\zeta(t))}{\partial y^2} \exp\left(\int_0^s \frac{\partial F_2(\zeta(t))}{\partial y} dt\right) ds \\
&\quad + \int_0^{\tau_0} \left[\exp\left(\int_s^{\tau_0} \frac{\partial F_2(\zeta(t))}{\partial y} dt\right) \frac{\partial^2 F_2(\zeta(s))}{\partial y \partial x} \cdot \int_0^s \exp\left(\int_v^s \frac{\partial F_1(\zeta(t))}{\partial x} dt\right) \frac{\partial F_1(\zeta(s))}{\partial y} \exp\left(\int_0^v \frac{\partial F_2(\zeta(t))}{\partial y} dt\right) dv\right] \\
&= \int_0^{\tau_0} \exp\left(\int_s^{\tau_0} \frac{\partial F_2(\zeta(t))}{\partial y} dt\right) \left(-\frac{2r}{K} + \frac{2\alpha y_p(s)}{(c + by_p(s))^2}\right) \exp\left(\int_0^s \frac{\partial F_2(\zeta(t))}{\partial y} dt\right) ds \\
&\quad - \int_0^{\tau_0} \left[\exp\left(\int_s^{\tau_0} \frac{\partial F_2(\zeta(t))}{\partial y} dt\right) \frac{b\alpha y_p(s)}{(c + by_p(s))^3} \cdot \int_0^s \exp\left(\int_v^s \frac{\partial F_1(\zeta(t))}{\partial x} dt\right) \frac{\alpha y_p(v)}{c + by_p(v)} \exp\left(\int_0^v \frac{\partial F_2(\zeta(t))}{\partial y} dt\right) dv\right] ds, \\
\frac{\partial^2 \Phi_2(\tau_0, X_0)}{\partial \tau \partial y} &= \frac{\partial F_2(\zeta(\tau_0))}{\partial y} \exp\left(\int_0^{\tau_0} \frac{\partial F_2(\zeta(t))}{\partial y} dt\right) \\
&= \left(r - \frac{\alpha y_p(\tau_0)}{c + by_p(\tau_0)}\right) \exp\left(\int_0^{\tau_0} \left(r - \frac{\alpha y_p(t)}{c + by_p(t)}\right) dt\right).
\end{aligned}
\tag{37}
$$

Therefore, we can deduce that

(a)

(b)

FIGURE 6: Bifurcation diagrams of model (1) with respect to q_2. Parameter values are as follows: $r = 2.18, K = 5.5, c = 1.15, b = 0.01, \alpha = 0.55, \beta = 0.87, \delta = 0.34, \theta_1 = 1.2, \theta_2 = 2, q_2 = 0.98, \lambda_1 = 1.4, \lambda_2 = 2.2$, and $T = 16.5$.

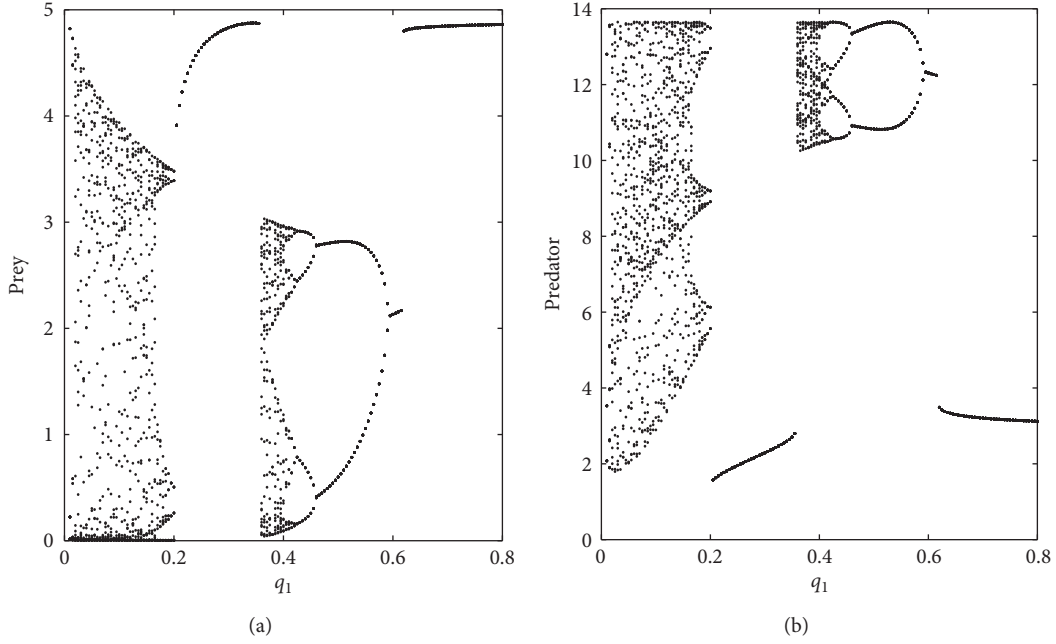$$
\begin{aligned}
B &= -\frac{\partial^2 \Theta_2}{\partial x \partial y} \left(\frac{\partial \Phi_1 (\tau_0, X_0)}{\partial \tau} + \frac{\partial \Phi_1 (\tau_0, X_0)}{\partial x} \frac{1}{a_0'} \frac{\partial \Theta_1}{\partial x} \frac{\partial \Phi_1 (\tau_0, X_0)}{\partial \tau} \right) \frac{\partial \Phi_2 (\tau_0, X_0)}{\partial y} \\
&\quad - \frac{\partial \Theta_2}{\partial y} \left(\frac{\partial^2 \Phi_2 (\tau_0, X_0)}{\partial x \partial y} \frac{1}{a_0'} \frac{\partial \Theta_1}{\partial x} \frac{\partial \Phi_1 (\tau_0, X_0)}{\partial \tau} + \frac{\partial^2 \Phi_2 (\tau_0, X_0)}{\partial \tau \partial y} \right) \\
&= -q_1 \left(\frac{\partial^2 \Phi_2 (\tau_0, X_0)}{\partial x \partial y} \frac{1}{a_0'} \left(q_2 - \frac{\theta_2 \lambda_2}{\left(1 + \theta_2 y_p (\tau_0) \right)^2} \right) y_p'(\tau_0) + \left(r - \frac{\alpha y_p (\tau_0)}{c + b y_p (\tau_0)} \right) \exp \left(\int_0^{\tau_0} \left(r - \frac{\alpha y_p (t)}{c + b y_p (t)} \right) dt \right) \right), \\
C &= -2 \frac{\partial^2 \Theta_2}{\partial x \partial y} \left(-\frac{b_0'}{a_0'} \frac{\partial \Phi_1 (\tau_0, X_0)}{\partial x} + \frac{\partial \Phi_1 (\tau_0, X_0)}{\partial y} \right) \frac{\partial \Phi_2 (\tau_0, X_0)}{\partial y} \\
&\quad - \frac{\partial^2 \Theta_2}{\partial y^2} \left(\frac{\partial \Phi_2 (\tau_0, X_0)}{\partial y} \right)^2 + 2 \frac{a_0'}{b_0'} \frac{\partial \Theta_2}{\partial y} \frac{\partial^2 \Phi_2}{\partial x \partial y} - \frac{\partial \Theta_2}{\partial y} \frac{\partial^2 \Phi_2 (\tau_0, X_0)}{\partial y^2} \\
&= 2 q_1 \frac{b_0'}{a_0'} \frac{\partial^2 \Phi_2 (\tau_0, X_0)}{\partial x \partial y} - q_1 \frac{\partial^2 \Phi_2 (\tau_0, X_0)}{\partial y^2}.
\end{aligned}
\tag{38}
$$

Now, we determine the sign of B, For this, let $g(t) = r - ((\alpha y_p(t))/(c + b y_p(t)))$, then $g'(t) = (\alpha \delta c y * \exp(-\delta t)/(c + b y_p(t))^2) > 0$, so $g(t)$ is strictly increasing. Since $\int_0^{\tau_0} g(t)dt = \ln(1/q_1) > 0$, which indicates that $g(\tau_0) > 0$, i.e. $(\partial^2 \Phi_2(\tau_0, X_0)/\partial y \partial \tau) > 0$. Therefore, $B < 0$. Defining $\varphi(t) = -(r/K) + (\alpha t/(c + bt)^2)$, it is easy to know that $-(r/K) + (\alpha t/(c + bt)^2) \leq 0$ if $K\alpha < 4rbc$, which means $\varphi(y_p(t)) = -(r/K) + (\alpha y_p(t)/(c + b y_p(t))^2) \leq 0$ for all $y_p(t) > 0$. So, we have $(\partial^2 \Phi_2(\tau_0, X_0)/\partial y^2) < 0$. From above, we have $C > 0$.

Hence, $BC < 0$; according to Theorem 2 of [33], a supercritical bifurcation occurs at $T = T^*$.

5. Numerical Simulation

To confirm our theoretical results and facilitate their interpretation, we will focus on the complex dynamics by bifurcation analysis numerically, which can obtain the properties of a dynamics system.

Firstly, we investigate the effect of pulse period T on dynamical of system. Figure 1 shows that model (1) could exist with complex and interesting dynamic behavior with increase of parameter T, such as period-doubling bifurcation, period-halving bifurcations, chaos band, and non-unique dynamics, i.e., several attractors may coexist with the

same T. For example, Figure 2 indicates that two different attractors can coexist with each other with the same $T = 7$. If we choose different initial value $(x_0, y_0) = (1.4, 2.1)$ and $(x_0, y_0) = (1.8, 2.1)$, a $3T$-periodic solution coexists with T-periodic solution, which indicates that the final stable states of pest and natural enemy population depend on their initial densities. All these results confirm that varying impulsive period T could dramatically change the dynamics of model (1).

It follows from Figure 3 that the nonlinear impulsive parameter λ_1 affects the dynamics of model (1). As parameter λ_1 increases, system (1) experiences period-doubling bifurcation, chaotic, period-halving bifurcations, and multiple stability. When $\lambda_1 = 9.4$, two attractors with different amplitudes appear, i.e., a T-periodic solution and $2T$-periodic solution coexist (see Figure 4). Therefore, the initial values of both the pest and predator populations are crucial. The above results reveal that the parameter λ_1 can dramatically change dynamics of system (1).

From the bifurcation diagrams Figure 5, we observe that a positive periodic solution appears when the pest-eradication solution loses its stability. The behavior of positive periodic solution is kept until $q_2 \approx 3.9$, and then a period-doubling bifurcation occurs, which means that a T-periodic solution disappears suddenly at this point and $2T$-periodic solution appears. With the increasing of q_2, a series of period-doubling bifurcations lead model (1) from periodicity to chaos. When $q_2 \geq 5.16$ and nearby 5.16, the chaos disappears and a $3T$-periodic solution appears. As q_2 increases further, the evidence for $3T$-periodic solution leading to chaos can be seen. Following these, the system displays a series of period-halving bifurcations.

Similarly, we investigate the effect of parameter q_1 on dynamic of system. The bifurcation diagrams with respect to parameter q_1 in the range $[0, 0.8]$ are shown in Figure 6. We can observe that model (1) also displays very complex dynamical behaviors with q_1 increasing.

6. Conclusion

Based on resource limitation, the optimal pest control strategy is that the instantaneous releasing numbers of natural enemies should be adjusted according to the densities of both pest and natural enemy in the field. A more natural understanding is that when the higher the number of pest population or the lower the number of predator population in the field, the higher the number of predator population should be released and the converse is also true. For this, we have investigated effects of nonlinear impulsive perturbations on a predator-prey model with Beddington–DeAngelis functional response. We have proven that there is a global stability of pest-eradication periodic solution if the impulsive period $T < T^*$ by using the Floquet theorem and small amplitude perturbation skills, and model (1) is permanent when the period $T > T^*$. Hence, $T = T^*$ plays a bifurcation threshold, and the system bifurcates to a positive periodic solution via supercritical bifurcation once a threshold condition is reached. By bifurcation diagrams, we can show that the system contains very rich dynamical

behavior, including period-doubling bifurcation, period-halving bifurcations, chaos, and nonunique attractors, i.e., the system could exist with two stable positive periodic solutions and even more complex dynamics (see Figures 2 and 4). Also, bifurcation analyses reveal that the final dynamics of the system depends on the initial densities, and the nonlinear impulsive may result in complexity of pest control. All those results confirm that the pest control strategy should be carefully designed once the nonlinear impulsive control measures have been taken into account.

Based on the present study, we found that the system with nonlinear impulsive control actions provides more rich results and more realistic than the previous systems with linear impulsive control, and thus nonlinear impulsive control should be taken into account when implementing integrated pest management. However, the aim of IPM should reduce pest populations to below the economic threshold rather than eradication, which can be naturally and accurately described by the state-dependent impulsive differential equations and result in more difficulty for analyzing the global dynamics. We leave for future research.

Data Availability

There were no data used to support this study.

Conflicts of Interest

The authors declare that they have no conflicts of interest.

Acknowledgments

References

[1] R. E. Stinner, "Efficacy of inundative releases," *Annual Review of Entomology*, vol. 22, no. 1, pp. 515–531, 1977.

[2] J. L. Capinera and D. R. Dent, "Integrated pest management," *The Florida Entomologist*, vol. 80, no. 2, pp. 307-308, 1997.

[3] J. C. Van Lenteren and J. Woets, "Biological and integrated pest control in greenhouses," *Annual Review of Entomology*, vol. 33, no. 1, pp. 239–269, 1988.

[4] H. I. Freedman, "Graphical stability, enrichment, and pest control by a natural enemy," *Mathematical Biosciences*, vol. 31, no. 3-4, pp. 207–225, 1976.

[5] Y. N. Xiao and F. Van Den Bosch, "The dynamics of an eco-epidemic model with biological control," *Ecological Modelling*, vol. 168, no. 1-2, pp. 203–214, 2003.

[6] W. W. Murdoch, J. Chesson, and P. L. Chesson, "Biological control in theory and practice," *The American Naturalist*, vol. 125, no. 3, pp. 344–366, 1985.

[7] S. Nundloll, L. Mailleret, and F. Grognard, "Influence of intrapredatory interferences on impulsive biological control

efficiency," *Bulletin of Mathematical Biology*, vol. 72, no. 8, pp. 2113–2138, 2010.

[8] S. Nundloll, L. Mailleret, and F. Grognard, "Two models of interfering predators in impulsive biological control," *Journal of Biological Dynamics*, vol. 4, no. 1, pp. 102–114, 2010.

[9] N. Bajeux, F. Grognard, and L. Mailleret, "Augmentative biocontrol when natural enemies are subject to Allee effects," *Journal of Mathematical Biology*, vol. 74, no. 7, pp. 1561–1587, 2017.

[10] V. Lakshmikantham, D. D. Bainov, and P. S. Simeonov, *Theory of Impulsive Differential Equations*, World Scientific, Singapore, 1989.

[11] D. D. Bainov and P. S. Simeonov, "Impulsive differential equations: periodic solutions and applications,"*PitmanMonographs and Surveys in Pure and Applied Math,* vol. 66,Longman Scientific and Technical, New York, NY, USA, 1993..

[12] X. Liu and L. Chen, "Global dynamics of the periodic logistic system with periodic impulsive perturbations," *Journal of Mathematical Analysis and Applications*, vol. 289, no. 1, pp. 279–291, 2004.

[13] B. Liu, Y. J. Zhang, L. S. Chen, and L. H. Sun, "The dynamics of a prey-dependent consumption model concerning integrated pest management," *Acta Mathematica Sinica, English Series*, vol. 21, no. 3, pp. 541–554, 2005.

[14] B. Liu, Y. Zhang, and L. Chen, "Dynamic complexities in a lotka-volterra predator-prey model concerning impulsive control strategy," *International Journal of Bifurcation and Chaos*, vol. 15, no. 02, pp. 517–531, 2005.

[15] S. Tang and R. A. Cheke, "State-dependent impulsive models of integrated pest management (IPM) strategies and their dynamic consequences," *Journal of Mathematical Biology*, vol. 50, no. 3, pp. 257–292, 2005.

[16] S. Tang and R. A. Cheke, "Models for integrated pest control and their biological implications," *Mathematical Biosciences*, vol. 215, no. 1, pp. 115–125, 2008.

[17] S. Tang, Y. Xiao, and R. A. Cheke, "Multiple attractors of host-parasitoid models with integrated pest management strategies: eradication, persistence and outbreak," *Theoretical Population Biology*, vol. 73, no. 2, pp. 181–197, 2008.

[18] Q. Xiao and B. Dai, "Periodic solutions generated by impulses for state-dependent impulsive differential equation," *Discrete Dynamics in Nature and Society*, vol. 2015, Article ID 816325, 7 pages, 2015.

[19] Z. Xiang, S. Tang, C. Xiang, and J. Wu, "On impulsive pest control using integrated intervention strategies," *Applied Mathematics and Computation*, vol. 269, pp. 930–946, 2015.

[20] S. Tang, W. Pang, R. A. Cheke, and J. Wu, "Global dynamics of a state-dependent feedback control system," *Advances in Difference Equations*, vol. 2015, no. 322, 2015.

[21] C. T. Li and S. Y. Tang, "The effects of timing of pulse spraying and releasing predator and releasing periods on dynamics of generalized predator-prey moedl," *International Jouranla of Biomathematics*, vol. 5, no. 1, pp. 1–28, 2012.

[22] W. J. Qin, S. Y. Tang, and R. A. Cheke, "The effects of resource limitation on a predator-prey model with control measures as nonlinear pulses," *Mathematical Problems in Engineering*, vol. 2014, Article ID 450935, 13 pages, 2014.

[23] G. Tang, S. Tang, and R. A. Cheke, "Global analysis of a holling type II predator-prey model with a constant prey refuge," *Nonlinear Dynamics*, vol. 76, no. 1, pp. 635–647, 2014.

[24] S. Y. Tang, B. Tang, A. L. Wang, and Y. N. Xiao, "Holling II predator-prey impulsive semi-dynamic model with complex poincare map," *Nonlinear Dynamics*, vol. 81, pp. 1579–1596, 2015.

[25] L. Dong and L. Chen, "A periodic predator-prey-chain system with impulsive perturbation," *Journal of Computational and Applied Mathematics*, vol. 223, no. 2, pp. 578–584, 2009.

[26] H. Zhang, P. Georgescu, and L. Chen, "On the impulsive controllability and bifurcation of a predator-pest model of IPM," *Biosystems*, vol. 93, no. 3, pp. 151–171, 2008.

[27] H. K. Baek, "Qualitative analysis of Beddington-DeAngelis type impulsive predator-prey models," *Nonlinear Analysis: Real World Applications*, vol. 11, no. 3, pp. 1312–1322, 2010.

[28] S. L. Sun and G. H. Guo, "Dynamics of a beddington-deangelis type predator-prey model with impulsive effect," *Journal of Mathematics*, vol. 2013, Article ID 826857, 11 pages, 2013.

[29] C. T. Li and S. Y. Tang, "Complex dynamics and coexistence of period-doubling and period-halving bifurcations in an integrated pest management model with nonlinear impulsive control," *Advances in Difference Equations*, vol. 514, pp. 1–23, 2020.

[30] I. U. Khan and S. Y. Tang, "The impulsive model with pest density and its change rate dependent feedback control," *Discrete Dynamics in Nature and Society*, vol. 2020, Article ID 1561241, 20 pages, 2020.

[31] X. Wang, Y. Tian, and S. Y. Tang, "A holling type II pest and natural enemy model with density dependent IPM strategy," *Mathematical Problems in Engineering*, vol. 2017, Article ID 8683027, 12 pages, 2017.

[32] C. Li and S. Tang, "Analyzing a generalized pest-natural enemy model with nonlinear impulsive control," *Open Mathematics*, vol. 16, no. 1, pp. 1390–1411, 2018.

[33] A. Lakmeche and O. Arino, "Bifurcation of non-trivial periodic solutions of impulsive differential equations arising chemotherapeutic treatment," *Dynamics of Continuous, Discrete and Impulsive System*, vol. 7, no. 2, pp. 265–287, 2000.

WILEY | Hindawi

Research Article

Regression Analysis for Outcome-Dependent Sampling Design under the Covariate-Adjusted Additive Hazards Model

Yingli Pan,[1] Songlin Liu [ID],[1] Yanli Zhou [ID],[2] and Guangyu Song[1]

[1]*Hubei Key Laboratory of Applied Mathematics, Faculty of Mathematics and Statistics, Hubei University, Wuhan 430062, China*
[2]*School of Finance, Zhongnan University of Economics and Law, Wuhan 430073, China*

Correspondence should be addressed to Songlin Liu; liusonglin@hubu.edu.cn and Yanli Zhou; yanli.zhou1517@zuel.edu.cn

This paper provides a new insight into an economical and effective sampling design method relying on the outcome-dependent sampling (ODS) design in large-scale cohort research. Firstly, the importance and originality of this paper is that it explores how to fit the covariate-adjusted additive Hazard model under the ODS design; secondly, this paper focused on estimating the distortion function through nonparametric regression and required observation of the covariate on the confounding factors of distortion; moreover, this paper further calibrated the contaminated covariates and proposed the estimators of the parameters by analyzing the calibrated covariates; finally, this paper established the large sample property and asymptotic normality of the proposed estimators and conducted many more simulations to evaluate the finite sample performance of the proposed method. Empirical research demonstrates that the results from both artificial and real data verified good performance and practicality of the proposed ODS method in this paper.

1. Introduction

Generally, the major cost of studying large cohort is tied up in collecting the expensive exposure variables, which casts a poor shadow over the researchers with the burden of limited budgets. Therefore, the simple random sampling design with the characteristics of cost expensive and time consuming has been risking losing ground in the long run. To achieve some certain goal, it is no wonder that many cost-effective strategies have been invoked. In the early 1980s, Prentice [1] proposed the notation of case-cohort design, and the exposure variables were measured on a simple random sample, which is called a subcohort, as well as all the cases that experienced events that we were interested in. Since then, the application of case-cohort sampling in the survival analysis has been reported by Self and Prentice [2], Tsai [3], and Kim et al. [4]. The case-cohort design is expected to be economical and effective sampling techniques for rare events. When the censoring rate is relatively low or medium, the method of generalized case-cohort design has been

developed in responding to lowering the research cost. In addition to randomly selecting a subcohort from the entire cohort, the information containing the relevant covariables is collected for only a subset of the failure individuals (e.g., Chen [5], Cai and Zeng [6], and Kang and Cai [7]).

As a matter of fact, the failure time outcome-dependent sampling (ODS) design is considered to be another economical and effective alternative to the simple random sampling design. Exposure variables are measured against samples from two components, the subcohort and additional supplementary samples (see Chatterjee et al. [8], Zhou et al. [9], and Weaver and Zhou [10]). Regarding the ODS data, massive research has been carried out and formed a wealth of literatures. For completely observed data, the studies by Zhou et al. [11, 12] and Qin and Zhou [13] offer the comprehensive analysis of the inference methods based on the partially regression linear models for data from the ODS design. The key systematic study of how to fit the generalized linear model with the data obtained from two-stage ODS design was reported by Yan et al. [14]. For

censored data, detail examination of the ODS design by Ding et al. [15] showed the estimated impact of environmental pollutants on women's subfertility. A significant discussion on estimating the equation method with an ODS sampling scheme under Cox's proportional hazards model was presented by Yu et al. [16].

In clinical trials and biomedical, instead of direct observation, the covariates are observed by multiplication of unknown functions of an observable confounder. As a result, the regression with contaminated covariates was originally derived by Şentürk and Müller [17, 18], in which the contamination information for model covariates cannot be ignored; otherwise, it will result in a biased estimator and the statistical inference may be misled. Since then, numerous extensions in various aspects have been developed by Şentürk and Müller [19], Cui et al. [20], and Li et al. [21]. For completely observed data, one study by Cui [22] proposed to use the nonparametric kernel estimation method to calibrate the contaminated variables and then conducted parameter estimation under the covariate-adjusted linear model, and further research conducted by Zhang et al. [23] extended the method to the nonlinear models with contaminated variables. A key study by Delaigle et al. [24] derived the process of several nonparametric covariate-adjusted estimators of conditional mean function. A preliminary nonparametric test for covariate-adjusted models was undertaken by Zhao and Xie [25], who found that the proposed test statistic has the same limit distribution as the response and predictors are supposed to be obtained directly. For survival data with censoring, very few studies have investigated survival models with contaminated covariates and even fewer people are ready to tackle the challenge in the ODS design we are discussing here.

We study the following covariate-adjusted additive hazards model under the ODS design in this paper:

$$\begin{cases} \lambda(t \mid Z) = \lambda_0(t) + \theta^{\mathrm{T}} H + \gamma X, \\ W = \phi(U) X, \end{cases} \tag{1}$$

where $\lambda_0(t)$ is the unknown baseline hazard function, $\beta = (\theta^{\mathrm{T}}, \gamma)^{\mathrm{T}}$ is the unknown parameter of p-dimension, θ and γ are $(p-1)$-dimensional and 1-dimensional parameter, respectively, $Z = (H^{\mathrm{T}}, X)^{\mathrm{T}}$ is the p-dimensional covariate, H is the observed $(p-1)$-dimensional covariate, X is the unobservable 1-dimensional covariate, W is the actual observed 1-dimensional covariable, and $\phi(\cdot)$ is the unknown distorting function of observable confounding variable U. We focus on the method of nonparametric kernel estimation to obtain the estimator of the distortion function and calibrate the covariate X. Meanwhile, we attempt to weigh the contributions of the subcohort and the supplemental sample differently, which resulted in a weighted estimation equation with the help of calibrated covariates. Owing to the ODS design and the covariate-adjusted process, it happens to be challengeable in the work of theoretical developments. To overcome the challenge, it will be followed by an approximation to the weighted estimation equation, which is taken as the main basis for obtaining the theory properties of our proposed estimator.

The structure of the rest of the paper is as follows. Section 2 analyzes the process that ODS sampling data is fitted to additive hazard model with covariate adjustment. Then, in Section 3, we describe the large sample properties of our proposed estimator in progress to verify the finite sample performance of the proposed method by numerical approach in Section 4. In Section 5, the empirical research shows that the method we proposed has good practicality in the practical example of datasets from a pulmonary exacerbations analysis. Finally, the conclusion and prospect are summarized in Section 6.

2. Estimation Setup

Suppose that a cohort contains N independent subjects. For the ith ($i = 1, \ldots, N$) subject, $\widetilde{T}_i$ is the failure time and C_i is the censoring time. $T_i = \min(\widetilde{T}_i, C_i)$ is the observed time and $\Delta_i = I(\widetilde{T}_i \leq C_i)$ is the indicator variable of the right censoring. Denote $Y_i(t) = I(T_i \geq t)$, $V_i(t) = \Delta_i I(T_i \leq t)$ and Z_i to be the at-risk process, the counting process, and the time-independent p-dimensional exposure variable, respectively. Denote τ to be the study end time.

The additive hazards model proposed by Lin and Ying [26] is as follows:

$$\lambda(t \mid Z_i) = \lambda_0(t) + \beta^{\mathrm{T}} Z_i, \tag{2}$$

where $\lambda_0(t)$ is the unknown baseline hazard function and β is the parameter of p-dimension. If we have access to gather information about everyone's exposure, the following estimation function is commonly used for the inference of β:

$$U(\beta) = \frac{1}{N} \sum_{i=1}^{N} \int_0^\tau \{Z_i - \overline{Z}\} \{\mathrm{d}V_i(t) - Y_i(t)\beta^{\mathrm{T}} Z_i \mathrm{d}t\}, \tag{3}$$

where $\overline{Z} = \sum_{i=1}^{N} Y(t) Z_i / \sum_{i=1}^{N} Y_i(t)$.

Under the ODS design, the scope of the failure time of the cases is divided into $\widetilde{K}$ disjoint strata $\{\widetilde{A}_l = (a_{l-1}, a_l] : l = 1, \ldots, \widetilde{K}\}$ by positive constants $\{a_l : l = 1, \ldots, \widetilde{K}\}$ satisfying $0 = a_0 < \ldots < a_{l-1} < a_l < \ldots < a_{\widetilde{K}} = \tau$. We first sample n_0 SRS individuals from the cohort, and let ξ_i be the indicator, by value 1 if the ith subject being into the SRS and 0 otherwise. Denote $\widehat{\alpha} = P(\xi_i = 1) = n_0/N$. We sample subset A_k ($K \leq \widetilde{K}$) stratum from set $\widetilde{A}_l (l = 1, \ldots, \widetilde{K})$ and then n_k ($k = 1, \ldots, K$) additional samples are drawn from the members who experience failure and not in the SRS, but in stratum A_k. Denote η_{ik} to be the indicator whether the ith individual from A_k is sampled into the additional samples. Denote $\widehat{\gamma}_k = P(\eta_{ik} = 1 \mid \Delta_i = 1, \xi_i = 0, T_i \in A_k) = n_k/(\widetilde{n}_k - n_{0,k})$, where $\widetilde{n}_k$ and $n_{0,k}$ is the number of the cohort failure individuals and the SRS failure individuals dropped into A_k. The samples of n_0 SRS sample and n_k ($k = 1, \ldots, K$) additional sample make up the ODS sample.

Denote Λ_0 to be the set of SRS individual and Λ_k ($k = 1, \ldots, K$) to be the supplemental sample from A_k. Denote $\overline{\Lambda}$ to be the set of individuals outside ODS sample. Then, we can summarize the observed datasets obtained by the design of ODS as follows:

(i) The ODS sample $\{$ The SRS sample : $\{T_i, \Delta_i, Z_i\}$, $i \in \Lambda_0$, The supplemental sample : $\{T_i, \Delta_i, Z_i \mid \Delta_i = 1, T_i \in A_k\}$, $i \in \Lambda_k$.

(ii) The nonvalidation sample: $\{T_i, \Delta_i\}$, $i \in \overline{\Lambda}$.

For the ODS design, we only observe the variable Z for the selected subjects. The regression parameters β can be derived by $U_\omega(\beta) = 0$, where

$$U_w(\beta) = \frac{1}{N} \sum_{i=1}^{N} \int_0^\tau \omega_i \{Z_i - \overline{Z}_\omega\} \{dV_i(t) - Y_i(t)\beta^T Z_i dt\},$$

$$(4)$$

and $\overline{Z}_\omega = S^{(1)}(t)/S^{(0)}(t)$, $S^{(d)}(t) = (1/N) \sum_{i=1}^{N} \omega_i Y_i(t) Z_i^{\otimes d}$, $(d = 0, 1, 2)$, with $a^{\otimes 0} = 1$, $a^{\otimes 1} = a$, and $a^{\otimes 2} = aa^T$ for a vector a; and the weight w_i is defined by

$$\omega_i = \frac{\xi_i(1 - \Delta_i)}{\widehat{\alpha}} + \frac{\xi_i \Delta_i(1 - \zeta_i)}{\widehat{\alpha}} + \xi_i \Delta_i \zeta_i + (1 - \xi_i)\Delta_i \sum_{k=1}^{K} \frac{\zeta_{ik}\eta_{ik}}{\widehat{\gamma}_k},$$

$$i = 1, 2, \ldots, N,$$

$$(5)$$

where $\zeta_i = \sum_{k=1}^{K} \zeta_{ik}$ and $\zeta_{ik} = I(\widetilde{T}_i \in A_k)$.

Note that the weight of nonvalidation samples are 0, whereas the subcohort censored individuals are $\widehat{\alpha}^{-1}$. The weight of the subcohort cases are 1 if their failure time belongs to $A_k (k = 1, \ldots, K)$ and are $\widehat{\alpha}^{-1}$, otherwise. The selected cases, not in the subcohort, are weighted by $\widehat{\gamma}_k^{-1}$, when their time of failure belongs to $A_k (k = 1, \ldots, K)$. The estimator $\widehat{\beta}$ defined by (4) takes the explicit form as follows:

$$\widehat{\beta} = G_N^{-1} F_N,$$

$$(6)$$

where

$$G_N = \int_0^\tau \left\{ S^{(2)}(t) - \frac{S^{(1)}(t)^{\otimes 2}}{S^{(0)}(t)} \right\} dt,$$

$$F_N = \frac{1}{N} \sum_{i=1}^{N} \int_0^\tau \omega_i \{Z_i - \overline{Z}_\omega\} dV_i(t).$$

$$(7)$$

In practice, some covariates may be contaminated by some distorting factors. In this paper, we assume $Z_i = (H_i^T, X_i)^T$, where H_i is the observed $(p-1)$-dimensional covariate and X_i is the unobservable 1-dimensional covariate and satisfies

$$W_i = \phi(U_i)X_i, \quad i = 1, 2, \ldots, N,$$

$$(8)$$

where W_i is the actual observable 1-dimensional variable, U_i is the known confounder covariate, and $\phi(\cdot)$ is the unknown distorting function of observable variable U_i. At this point, for the ODS design, the available data have the form:

(i) The ODS sample $\{$ The SRS sample : $\{T_i, \Delta_i, U_i, (H_i^T, W_i)^T\}$, $i \in \Lambda_0$, The supplemental sample : $\{T_i, \Delta_i, U_i, (H_i^T, W_i)^T \mid \Delta_i = 1, \quad T_i \in A_k\}$, $i \in \Lambda_k$.

(ii) The nonvalidation sample: $\{T_i, \Delta_i\}$, $i \in \overline{\Lambda}$.

Combining model (2) and equation (8), we assume $\widetilde{T}_i(i = 1, 2, \ldots, N)$ is generalized from the covariate-adjusted additive hazards model in this paper:

$$\begin{cases} \lambda(t \mid Z_i) = \lambda_0(t) + \theta^T H_i + \gamma X_i, \\ W_i = \phi(U_i) X_i, \end{cases}$$

$$(9)$$

where θ and γ are $(p-1)$-dimensional and 1-dimensional regression parameters of primary interest, respectively. According to Şentürk and Müller [18], two conditions on model (9) can be listed as follows:

(C1) $E[\phi(U)] = 1$

(C2) $\{X, U\}$ are mutually independent

Note that condition (C1) ensured that the mean distorting effect vanishes. Based on conditions (C1) and (C2), we obtain $E[W] = E[X]$. Owing to the presence of distortion, the covariate X_i is unobservable, and the estimating function (4) can be no longer used for the inference of β. If we use directly W_i instead of X_i, it might lead to inaccurate statistical inference. Therefore, we should calibrate the covariate X_i based on the known covariate W_i and confounder covariate U_i. From (8) and condition (C2), it can obtain that

$$\phi(u) = \frac{E[W \mid U = u]}{E[X]}.$$

$$(10)$$

Define $\Phi(u) = E[W \mid U = u]$, and we adopt kernel method to estimate $\Phi(u)$:

$$\widehat{\Phi}(u) = \frac{\sum_{i=1}^{n} K((u - U_i)/h) W_i}{\sum_{i=1}^{n} K(u - U_i)/h},$$

$$(11)$$

where $K(\cdot)$ is a kernel function and h is a bandwidth. It is easy to show that $\overline{W} = n^{-1} \sum_{i=1}^{n} W_i$ converges almost to $E[W]$. By $E[W] = E[X]$, equations (10) and (11), the distorting function $\phi(u)$ can be estimated by

$$\widehat{\phi}(u) = \frac{\widehat{\Phi}(u)}{\overline{W}},$$

$$(12)$$

and the covariate X_i can be calibrated by

$$\widehat{X}_i = \frac{W_i}{\widehat{\phi}(U_i)}, \quad i = 1, 2, \ldots, N.$$

$$(13)$$

Denote $\widehat{Z}_i = (H_i^T, \widehat{X}_i)^T$, and the proposed estimator $\widehat{\beta}_p$ for model (9) can be defined as the solution of the function:

$$\widehat{U}_\omega(\beta) = \frac{1}{N} \sum_{i=1}^{N} \int_0^\tau \omega_i \left\{ \widehat{Z}_i - \widehat{\overline{Z}}_\omega \right\} \{dV_i(t) - Y_i(t)\beta^T \widehat{Z}_i dt\},$$

$$(14)$$

where $\widehat{\overline{Z}}_\omega = \widehat{S}^{(1)}(t)/\widehat{S}^{(0)}(t)$ and $\widehat{S}^{(d)}(t) = (1/N) \sum_{i=1}^{N} \omega_i Y_i(t) \widehat{Z}_i^{\otimes d}$, $(d = 0, 1, 2)$. The explicit form of the proposed estimator $\widehat{\beta}_p$ can be described as follows by some simple calculation:

$$\widehat{\beta}_p = \widehat{G}_N^{-1} \widehat{F}_N, \qquad (15)$$

where

$$\widehat{G}_N = \int_0^\tau \left\{ \widehat{S}^{(2)}(t) - \frac{\widehat{S}^{(1)}(t)^{\otimes 2}}{\widehat{S}^{(0)}(t)} \right\} dt, \qquad (16)$$

$$\widehat{F}_N = \frac{1}{N} \sum_{i=1}^N \int_0^\tau w_i \left\{ \widehat{Z}_i - \widehat{\overline{Z}}_\omega \right\} dV_i(t).$$

3. Main Results

In this section, we would like to establish the asymptotic properties of $\widehat{\beta}_p$ in (15).

Firstly, we give the following definition.

Definition 1. Define

$$s^{(0)}(t) = E[Y_1(t)],$$

$$s_{HX} = E[Y_1(t)HX],$$

$$s_X^{(d)}(t) = E[Y_1(t)X^{\otimes d}],$$

$$s_H^{(d)}(t) = E[Y_1(t)H^{\otimes d}], \quad d = 1, 2,$$

$$M_i(t) = V_i(t) - \int_0^t Y_i(s)\lambda_0(s)ds - \int_0^t Y_i(s)\beta^{\mathrm{T}}Z_i ds, \qquad (17)$$

$$S_i(\beta_0) = \int_0^\tau \left\{ Z_i - \frac{E[Y_1(t)Z]}{E[Y_1(t)]} \right\} dM_i(t), \quad i = 1, 2, \ldots, N,$$

$$D_1(\beta_0) = E\left[(1 - \Delta_1)S_1(\beta_0)^{\otimes 2} \right],$$

$$D_2(\beta_0) = E\left[\Delta_1(1 - \zeta_1)S_1(\beta_0)^{\otimes 2} \right],$$

$$D_3(\beta_0) = E\left[\Delta_1 \zeta_{1k} S_1(\beta_0)^{\otimes 2} \right],$$

$$\sum(\beta_0) = E\left[\int_0^\tau \left\{ Z_1 - \frac{E[Y_1(t)Z]}{E[Y_1(t)]} \right\}^{\otimes 2} dV_1(t) \right], \qquad (18)$$

$$\sum_1(\beta_0) = \frac{1-\alpha}{\alpha} D_1(\beta_0) + \frac{1-\alpha}{\alpha} D_2(\beta_0) + \sum_{k=1}^K (1-\alpha) \frac{1-\gamma_k}{\gamma_k} D_3(\beta_0), \qquad (19)$$

$$G_1 = \int_0^\tau \left\{ s_H^{(2)}(t) - \frac{s_H^{(1)}(t)^{\otimes 2}}{s^{(0)}(t)} \right\} dt, \qquad (20)$$

$$G_2 = \int_0^\tau \left\{ s_{HX}(t) - \frac{s_H^{(1)}(t)s_X^{(1)}(t)}{s^{(0)}(t)} \right\} dt, \qquad (21)$$

$$G_3 = \int_0^\tau \left\{ s_X^{(2)}(t) - \frac{s_X^{(1)}(t)^2}{s^{(0)}(t)} \right\} dt, \qquad (22)$$

where $M_i(t)$ is a locally square integrable martingale (Lin and Ying [26]) and $\beta_0 = (\theta_0^{\mathrm{T}}, \gamma_0^{\mathrm{T}})$ is the true parameters value.

Secondly, the following additional regular conditions are concluded to illustrate the process:

(C3) $\int_0^\tau \lambda_0(t)dt < \infty.$

(C4) $P(Y_1(t) = 1, \text{ for any } t \in [0, \tau]) > 0.$

(C5) $E[\sup_{0 \le t \le \tau} |Y_1(t)Z_1^{\otimes 2}(\beta^{\mathrm{T}}Z_1^2)|] < \infty.$

(C6) The matrix $\sum(\beta_0)$ appeared in (18) is finite positive definite.

(C7) The matrix $G = \begin{bmatrix} G_1 & G_2 \\ G_2^{\mathrm{T}} & G_3 \end{bmatrix}$ is nonsingular.

(C8) As $N \longrightarrow \infty$, $\widehat{\alpha} \longrightarrow \alpha \in (0, 1)$ and $\widehat{\gamma}_k \longrightarrow \gamma_k \in (0, 1)$ for $k = 1, \ldots, K.$

(C9) $\phi(u)$, $f(u)$, and $g(u) = \phi(u)f(u)$ are differential, and the 3-order derivatives of $f(u)$ and $g(u)$ meet the following condition, and there exist $a > 0$ and a neighborhood of origin, such that, if δ fails to the neighborhood, we have $|f^{(3)}(u + \delta) - f^{(3)}(u)| \le a|\delta|$ and $|g^{(3)}(u + \delta) - g^{(3)}(u)| \le a|\delta|$, where $f(u)$ is a density function of U.

(C10) The function $K(\cdot)$ appeared in (11) meets

(i) The support of $K(\cdot)$ is the interval $[-1, 1]$.
(ii) $K(\cdot)$ is symmetric about zero.
(iii) $\int_{-1}^1 K(u)du = 1$, $\int_{-1}^1 u^i K(u)du = 0$, $i = 1, 2, 3.$

(C11) As $N \longrightarrow \infty$, the bandwidth h falls from $O(N^{-1/4}\log N)$ to $O(N^{-1/8}).$

(C12) $E[X]$ is bounded away from 0 and $E[X]^2 < \infty.$

The above conditions are mild and suitable in many circumstances. Conditions (C3)–(C8) are regular conditions of the regression parameters which are similar to Yu et al. [27]. However, the likes of conditions (C9)–(C12) can be traced to Cui et al. [20].

Theorem 1. *If conditions (C1)–(C12) hold, as $N \longrightarrow \infty$, we have $\widehat{\beta}_p \overset{P}{\longrightarrow} \beta_0.$*

Theorem 2. *If conditions (C1)–(C12) hold, as $N \longrightarrow \infty$, we have*

$$\sqrt{N}(\widehat{\beta}_p - \beta_0) \xrightarrow{d} \mathcal{N}\left(0, G^{-1}\left(\sum(\beta_0) + \sum_1(\beta_0) + \gamma_0^2 \frac{\text{Var}(W) - (3/4)\text{Var}(X)}{[\text{E}(X)]^2} LL^{\text{T}}\right)G^{-1}\right), \tag{23}$$

where $L = [G_2, G_3]^T$. In other words,

$$\sqrt{N}(\widehat{\theta}_p - \theta_0) \xrightarrow{d} \mathcal{N}\left(0, G^{-1}\left(\sum(\beta_0) + \sum_1(\beta_0)\right)G^{-1}\right), \quad \sqrt{N}(\widehat{\gamma}_p - \gamma_0) \xrightarrow{d} \mathcal{N}\left(0, \sigma + \gamma_0^2 \frac{\text{Var}(W) - 3/4\text{Var}(X)}{[\text{E}(X)]^2}\right), \tag{24}$$

where $\widehat{\beta}_p = (\widehat{\theta}_p^{\text{T}}, \widehat{\gamma}_p)^{\text{T}}$ and σ is the $(p+1, p+1)$-element of matrix $G^{-1}(\sum(\beta_0) + \sum_1(\beta_0))G^{-1}$.

To prove Theorem 1, the following definition and deformation lemmas are needed.

Definition 2. Define

$$S_H^{(d)}(t) = \frac{1}{N}\sum_{i=1}^N \omega_i Y_i(t) H_i^{\otimes d},$$

$$S_X^{(d)}(t) = \frac{1}{N}\sum_{i=1}^N \omega_i Y_i(t) X_i^{\otimes d},$$

$$S_{\widehat{X}}^{(d)}(t) = \frac{1}{N}\sum_{i=1}^N \omega_i Y_i(t) \widehat{X}_i^{\otimes d}, \quad d = 1, 2, \tag{25}$$

$$S_{HX}(t) = \frac{1}{N}\sum_{i=1}^N \omega_i Y_i(t) H_i X_i,$$

$$S_{H\widehat{X}}(t) = \frac{1}{N}\sum_{i=1}^N \omega_i Y_i(t) H_i \widehat{X}_i.$$

In order to prove conveniently the results, we define the partitioned matrices:

$$\widehat{F}_N = \begin{bmatrix} \widehat{F}_{N_1} \\ \widehat{F}_{N_2} \end{bmatrix},$$

$$F_N = \begin{bmatrix} F_{N_1} \\ F_{N_2} \end{bmatrix},$$

$$\widehat{G}_N = \begin{bmatrix} \widehat{G}_{N_1} & \widehat{G}_{N_2} \\ \widehat{G}_{N_2}^{\text{T}} & \widehat{G}_{N_3} \end{bmatrix}, \tag{26}$$

$$G_N = \begin{bmatrix} G_{N_1} & G_{N_2} \\ G_{N_2}^{\text{T}} & G_{N_3} \end{bmatrix},$$

where

$$\widehat{G}_{N_1} = G_{N_1} = \int_0^\tau \left[S_H^{(2)}(t) - \frac{S_H^{(1)}(t)^{\otimes 2}}{S^{(0)}(t)}\right]dt,$$

$$\widehat{G}_{N_2} = \int_0^\tau \left[S_{H\widehat{X}}(t) - \frac{S_H^{(1)}(t)S_{\widehat{X}}^{(1)}(t)}{S^{(0)}(t)}\right]dt,$$

$$G_{N_2} = \int_0^\tau \left[S_{HX}(t) - \frac{S_H^{(1)}(t)S_X^{(1)}(t)}{S^{(0)}(t)}\right]dt,$$

$$\widehat{G}_{N_3} = \int_0^\tau \left[S_{\widehat{X}}^{(2)}(t) - \frac{S_{\widehat{X}}^{(1)}(t)^2}{S^{(0)}(t)}\right]dt,$$

$$G_{N_3} = \int_0^\tau \left[S_X^{(2)}(t) - \frac{S_X^{(1)}(t)^2}{S^{(0)}(t)}\right]dt, \tag{27}$$

$$\widehat{F}_{N_1} = F_{N_1} = \frac{1}{N}\sum_{i=1}^N \int_0^\tau \omega_i \left[H_i - \frac{S_H^{(1)}(t)}{S^{(0)}(t)}\right]dV_i(t),$$

$$\widehat{F}_{N_2} = \frac{1}{N}\sum_{i=1}^N \int_0^\tau \omega_i \left[\widehat{X}_i - \frac{S_{\widehat{X}}^{(1)}(t)}{S^{(0)}(t)}\right]dV_i(t),$$

$$F_{N_2} = \frac{1}{N}\sum_{i=1}^N \int_0^\tau \omega_i \left[X_i - \frac{S_X^{(1)}(t)}{S^{(0)}(t)}\right]dV_i(t).$$

Lemma 1. *If conditions (C3)–(C8) hold, then*

$$\sup_{t\in[0,\tau]}\left\|S^{(d)}(t) - s^{(d)}(t)\right\| \xrightarrow{\text{P}} 0, \quad d = 0, 1, 2. \tag{28}$$

Proof. Applying Glivenko–Cantelli theorem, we obtain that

$$\sup_{t\in[0,\tau]}\left\|S^{(0)}(t) - s^{(0)}(t)\right\| \xrightarrow{\text{P}} 0, \tag{29}$$

where $s^{(0)}(t) = \text{E}[Y_1(t)]$. By corollary (III).2 from Andersen and Gill [28], the uniform convergence of $S^{(1)}(t)$ and $S^{(2)}(t)$ can be similarly shown. □

Lemma 2 (see from Cui et al. [20]). *If conditions (C1), (C2), and (C9)–(C12) hold, then*

$$\frac{1}{N}\sum_{i=1}^{N}\left(\widehat{X}_i - X_i\right)\psi(H_i, X_i, t) - Q_N E[X\psi(H, X, t)] = o_p\left(N^{-1/2}\right), \tag{30}$$

where $\psi(h, x, t)$ is a function of h, x, and t satisfying $E[\psi(H, X, t)]^2 < \infty$, and

$$Q_N = \frac{1}{NE[X]}\left[\sum_{i=1}^{N}\left(W_i - \frac{X_i}{2} - \frac{E[X]}{2}\right)\right]. \tag{31}$$

Lemma 3. *If conditions (C1)–(C12) hold, then*

$$\begin{aligned}\widehat{F}_N - F_N &= o_p(1), \\ \widehat{G}_N - G_N &= o_p(1).\end{aligned} \tag{32}$$

Proof. By Lemma 2 with $\psi(H_i, X_i, t) = \omega_i Y_i(t)$ and $E[Q_N] = 0$, we obtain

$$\begin{aligned}S_{\widehat{X}}^{(1)}(t) - S_X^{(1)}(t) &= \frac{1}{N}\sum_{i=1}^{N}\left[\omega_i Y_i(t)\left(\widehat{X}_i - X_i\right)\right] \\ &= s_X^{(1)}(t)Q_N + o_p\left(N^{-1/2}\right) = o_p(1),\end{aligned} \tag{33}$$

where $s_X^{(1)}(t) = E[Y_1(t)X]$. By Lemma 2 with $\psi(H_i, X_i, t) = \omega_i Y_i(t)H_i$, we have

$$\begin{aligned}S_{H\widehat{X}}(t) - S_{HX}(t) &= \frac{1}{N}\sum_{i=1}^{N}\omega_i Y_i(t)H_i\left(\widehat{X}_i - X_i\right) \\ &= s_{HX}(t)Q_N + o_p\left(N^{-1/2}\right) = o_p(1),\end{aligned} \tag{34}$$

where $s_{HX}(t) = E[Y_1(t)HX]$. Applying Lemma 2 with $\psi(H_i, X_i, t) = \omega_i Y_i(t)X_i$, we obtain

$$\begin{aligned}S_{\widehat{X}}^{(2)}(t) - S_X^{(2)}(t) &= \frac{1}{N}\sum_{i=1}^{N}\omega_i Y_i(t)\left(\widehat{X}_i^2 - X_i^2\right) \\ &= \frac{2}{N}\sum_{i=1}^{N}\omega_i Y_i(t)X_i\left(\widehat{X}_i - X_i\right) \\ &\quad + \frac{1}{N}\sum_{i=1}^{N}\omega_i Y_i(t)\left(\widehat{X}_i - X_i\right)^2 \\ &= 2s_X^{(2)}(t)Q_N + \frac{1}{N}\sum_{i=1}^{N}\omega_i Y_i(t)\left(\widehat{X}_i - X_i\right)^2 \\ &\quad + o_p\left(N^{-1/2}\right),\end{aligned} \tag{35}$$

where $s_X^{(2)}(t) = E[Y_1(t)X^{\otimes 2}]$. Similar to the proof of $D_2 = o_p(N^{1/2})$ in Proposition 1 from Cui et al. [20], we have

$$\sup_{0 \le t \le \tau}\sum_{i=1}^{N}\left[\omega_i Y_i(t)\left(\widehat{X}_i - X_i\right)^2\right] = o_p\left(N^{1/2}\right). \tag{36}$$

Therefore,

$$S_{\widehat{X}}^{(2)}(t) - S_X^{(2)}(t) = 2s_X^{(2)}(t)Q_N + o_p\left(N^{-1/2}\right) = o_p(1). \tag{37}$$

By equation (33) and the uniform convergence of $S_X^{(1)}(t)$ to $s_X^{(1)}(t)$, we obtain

$$\begin{aligned}S_{\widehat{X}}^{(1)}(t)^2 - S_X^{(1)}(t)^2 &= \left(S_{\widehat{X}}^{(1)}(t) - S_X^{(1)}(t)\right)\left(S_{\widehat{X}}^{(1)}(t) + S_X^{(1)}(t)\right) \\ &= \left(s_X^{(1)}(t)Q_N + o_p\left(N^{-1/2}\right)\right) \\ &\quad \cdot \left(2S_X^{(1)}(t) + o_p(1)\right) \\ &= 2s_X^{(1)}(t)^2 Q_N + o_p\left(N^{-1/2}\right).\end{aligned} \tag{38}$$

From the partitioned matrices in the above notation, we obtain that

$$\begin{aligned}\widehat{F}_N - F_N &= \begin{bmatrix} 0 \\ \widehat{F}_{N_1} - F_{N_2} \end{bmatrix}, \\ \widehat{G}_N - G_N &= \begin{bmatrix} 0 & \widehat{G}_{N_2} - G_{N_2} \\ \widehat{G}_{N_2}^{\mathrm{T}} - G_{N_2}^{\mathrm{T}} & \widehat{G}_{N_3} - G_{N_3} \end{bmatrix}.\end{aligned} \tag{39}$$

Then, by equation (33) and Lemma 2 with $\psi(H_i, X_i, t) = V_i(\tau)$, we obtain that

$$\begin{aligned}\widehat{F}_{N_2} - F_{N_2} &= \frac{1}{N}\sum_{i=1}^{N}\left[\omega_i\left(\widehat{X}_i - X_i\right)V_i(\tau)\right] \\ &\quad - \frac{1}{N}\sum_{i=1}^{N}\omega_i\int_0^\tau\left\{\frac{S_{\widehat{X}}^{(1)}(t) - S_X^{(1)}(t)}{S^{(0)}(t)}\right\}dV_i(t) \\ &= Q_N E[XV_1(\tau)] - \frac{Q_N}{N}\sum_{i=1}^{N}\omega_i\int_0^\tau\frac{s_X^{(1)}(t)}{s^{(0)}(t)}dV_i(t) \\ &\quad + o_p\left(N^{-1/2}\right) = Q_N E[XV_1(\tau)] \\ &\quad - Q_N E\left[\int_0^\tau\frac{s_X^{(1)}(t)}{s^{(0)}(t)}dV_1(t)\right] + o_p\left(N^{-1/2}\right) \\ &= Q_N E\left[\int_0^\tau\left\{X - \frac{s_X^{(1)}(t)}{s^{(0)}(t)}\right\}dV_1(t)\right] + o_p\left(N^{-1/2}\right) \\ &= o_p(1),\end{aligned} \tag{40}$$

where $s^{(0)}(t) = E[Y_1(t)]$. By equations (39) and (40), we have

$$\widehat{F}_N = F_N + o_p(1). \tag{41}$$

By equations (33) and (34), we have

$$\widehat{G}_{N_2} - G_{N_2} = \int_0^\tau \left[\left(S_{H\widehat{X}}(t) - S_{HX}(t) \right) - \frac{S_H^{(1)}(t) \left(S_{\widehat{X}}^{(1)}(t) - S_X^{(1)}(t) \right)}{S^{(0)}(t)} \right] dt$$

$$= \int_0^\tau \left[s_{HX}(t) Q_N - \frac{s_H^{(1)}(t) s_X^{(1)}(t)}{s^{(0)}(t)} Q_N \right] dt = Q_N G_2 + o_p\left(N^{-1/2}\right) = o_p(1), \tag{42}$$

where G_2 appeared in (21). By equations (37) and (38), we have

$$\widehat{G}_{N_3} - G_{N_3} = \int_0^\tau \left[S_{\widehat{X}}^{(2)}(t) - S_X^{(2)}(t) - \frac{S_{\widehat{X}}^{(1)}(t)^2 - S_X^{(1)}(t)^2}{S^{(0)}(t)} \right] dt$$

$$= \int_0^\tau \left[2 s_X^{(2)}(t) Q_N - \frac{2 s_X^{(1)}(t)^2 Q_N}{s^{(0)}(t)} \right] dt + o_p\left(N^{-1/2}\right) = 2 Q_N G_3 + o_p\left(N^{-1/2}\right) = o_p(1), \tag{43}$$

where G_3 appeared in (22). Then, by equations (39), (42), and (43), we have

$$\widehat{G}_N = G_N + o_p(1). \tag{44}$$
□

Proof of Theorem 1. Applying Lemma 3 and the definition of the notation of G_N and G, we obtain

$$\widehat{G}_N \overset{P}{\longrightarrow} G. \tag{45}$$

By equation (45), condition (C7) and Slutsky Lemma, we show that $\widehat{G}_N$ is nonsingular in probability. Thus, it obtains that

$$\begin{aligned} \widehat{\beta} &= G_N^{-1} F_N, \\ \widehat{\beta}_p &= \widehat{G}_N^{-1} \widehat{F}_N. \end{aligned} \tag{46}$$

Similar to Yu et al. [27], we get $\widehat{\beta} \overset{P}{\longrightarrow} \beta_0$; then, by equations (45) and (46), Lemma 3 and Slutsky Lemma, it holds that

$$\widehat{\beta}_p \overset{P}{\longrightarrow} \beta_0. \tag{47}$$

Therefore, Theorem 1 has been proved. □

To prove Theorem 2, the following deformation lemma is needed.

Lemma 4. *If conditions (C1)–(C12) hold, then*

$$\widehat{U}_\omega(\beta_0) = U_\omega(\beta_0) - \gamma_0 Q_N L + o_p\left(N^{-1/2}\right), \tag{48}$$

where $L = [G_2, G_3]^T$, G_2 and G_3 appeared in (21) and (22), respectively.

Proof. By equations (4) and (14), we obtain

$$\widehat{U}_\omega(\beta_0) = \widehat{F}_N - \widehat{G}_N \beta_0 = \begin{bmatrix} \widehat{F}_{N_1} - \widehat{G}_{N_1}\theta_0 - \widehat{G}_{N_2}\gamma_0 \\ \widehat{F}_{N_2} - \widehat{G}_{N_2}^T \theta_0 - \widehat{G}_{N_3}\gamma_0 \end{bmatrix},$$

$$U_\omega(\beta_0) = F_N - G_N \beta_0 = \begin{bmatrix} F_{N_1} - G_{N_1}\theta_0 - G_{N_2}\gamma_0 \\ F_{N_2} - G_{N_2}^T \theta_0 - G_{N_3}\gamma_0 \end{bmatrix}. \tag{49}$$

By equation (41), we have

$$\widehat{F}_{N_2} - F_{N_2} = Q_N E \left[\int_0^\tau \left\{ X - \frac{s_X^{(1)}(t)}{s^{(0)}(t)} \right\} dV_1(t) \right] + o_p\left(N^{-1/2}\right). \tag{50}$$

By equations (42) and (43), we have

$$\begin{aligned} \widehat{G}_{N_2} - G_{N_2} &= Q_N G_2 + o_p\left(N^{-1/2}\right), \\ \widehat{G}_{N_3} - G_{N_3} &= 2 Q_N G_3 + o_p\left(N^{-1/2}\right). \end{aligned} \tag{51}$$

Similar to Yu et al. [27], we have

$$U_\omega(\beta_0) = \frac{1}{N} \sum_{i=1}^N \int_0^\tau \omega_i \left\{ Z_i - \frac{S^{(1)}(t)}{S^{(0)}(t)} \right\} dM_i(t), \tag{52}$$

where $M_i(t)$ appeared in (17), which is a square integrable martingale. Then, performing a simple calculation, we obtain that

$$\widehat{U}_\omega(\beta_0) - U_\omega(\beta_0) = \begin{bmatrix} \left(G_{N_2} - \widehat{G}_{N_2}\right)\gamma_0 \\ \widehat{F}_{N_2} - F_{N_2} + \left(G_{N_2} - \widehat{G}_{N_2}\right)^T \theta_0 + \left(G_{N_3} - \widehat{G}_{N_3}\right)\gamma_0 \end{bmatrix}. \tag{53}$$

By $U_\omega(\beta_0) = F_N - G_N\beta_0$ and $E[U_\omega(\beta_0)] = 0$, we have

$$E[F_N - G_N\beta_0] = 0. \tag{54}$$

Then, we have $E[F_{N2}] = (E|G_{N2}|)^T\theta_0 + E[G_{N3}]\gamma_0$, that is,

$$E\left[\int_0^\tau \left\{X - \frac{s_X^{(1)}(t)}{s^{(0)}(t)}\right\}dV_1(t)\right] = G_2^T\theta_0 + G_3\gamma_0. \tag{55}$$

By equations (50) and (55), we have

$$\widehat{F}_{N_2} - F_{N_2} = Q_N\big(G_2^T\theta_0 + G_3\gamma_0\big) + o_p\big(N^{-1/2}\big). \tag{56}$$

Therefore, by equations (51), (53), and (56), we have

$$\begin{aligned}\widehat{U}_\omega(\beta_0) &= U_\omega(\beta_0) - \gamma_0 Q_N[G_2, G_3]^T + o_p\big(N^{-1/2}\big) \\ &= U_\omega(\beta_0) - \gamma_0 Q_N L + o_p\big(N^{-1/2}\big).\end{aligned} \tag{57}$$

Theorem 2 can be proven by using the properties of Lemma 4. □

Proof of Theorem 2. By Lemma 4, we have

$$\sqrt{N}\widehat{U}_\omega(\beta_0) = \sqrt{N}U_\omega(\beta_0) - \sqrt{N}\gamma_0 Q_N L + o_p(1). \tag{58}$$

Through the calculation of double expectation, we have

$$\mathrm{Cov}\big(\sqrt{N}U_\omega(\beta_0), \sqrt{N}Q_N\big) = \frac{1}{E[X]}$$

$$E\left\{U_\omega(\beta_0)\left[\sum_{i=1}^N \left(W_i - \frac{X_i}{2} - \frac{E[X]}{2}\right)\bigg| H_i, W_i, U_i\right]\right\} = 0. \tag{59}$$

By Yu et al. [27], we have

$$\mathrm{Var}\big[\sqrt{N}U_\omega(\beta_0)\big] = \sum(\beta_0) + \sum_1(\beta_0), \tag{60}$$

where $\sum(\beta_0)$ and $\sum_1(\beta_0)$ appeared in (20) and (21), respectively. By performing a simple calculation, we obtain

$$\begin{aligned}\mathrm{Var}\big(\sqrt{N}Q_N\big) &= \frac{1}{(E[X])^2}\mathrm{Var}\left(W - \frac{X}{2}\right) \\ &= \frac{1}{(E[X])^2}\left[\mathrm{Var}(W) + \frac{1}{4}\mathrm{Var}(X) - \mathrm{Cov}\left(W, \frac{X}{2}\right)\right].\end{aligned} \tag{61}$$

By conditions (C1) and (C2), we have

$$\mathrm{Cov}\left(W, \frac{X}{2}\right) = E(\phi(U))E\big(X^2\big) - E(\phi(U))E(X)^2 = \mathrm{Var}(X). \tag{62}$$

Combining equations (61) and (62), we obtain that

$$\mathrm{Var}\big(\sqrt{N}Q_N\big) = \frac{\mathrm{Var}(W) - (3/4)\mathrm{Var}(X)}{[E(X)]^2}. \tag{63}$$

Thus, by (58)–(60) and (63), we have

$$\begin{aligned}\mathrm{Var}\big(\sqrt{N}\widehat{U}_\omega(\beta_0)\big) &\overset{P}{\longrightarrow} \sum(\beta_0) + \sum_1(\beta_0) \\ &\quad + \gamma_0^2\frac{\mathrm{Var}(W) - (3/4)\mathrm{Var}(X)}{(E(X))^2}LL^T.\end{aligned} \tag{64}$$

Then, we obtain that

$$\begin{aligned}\sqrt{N}\big(\widehat{\beta}_p - \beta_0\big) &= \left[\frac{\partial\widehat{U}_\omega(\beta)}{\partial\beta}\bigg|_{\beta=\bar{\beta}_n}\right]^{-1}\big[\sqrt{N}\widehat{U}_\omega(\beta_0)\big] = -G^{-1}\big[\sqrt{N}\widehat{U}_\omega(\beta_0)\big] \\ &+ o_p(1) \overset{d}{\longrightarrow} \mathcal{N}\left(0, G^{-1}\left(\sum(\beta_0) + \sum_1(\beta_0) + \gamma_0^2\frac{\mathrm{Var}(W) - (3/4)\mathrm{Var}(X)}{[E(X)]^2}LL^T\right)G^{-1}\right),\end{aligned} \tag{65}$$

where $\bar{\beta}_n$ is a point of the line between $\widehat{\beta}_p$ and β_0, and

$$\begin{aligned}&G^{-1}\left(\sum(\beta_0) + \sum_1(\beta_0) + \gamma_0^2\frac{\mathrm{Var}(W) - (3/4)\mathrm{Var}(X)}{[E(X)]^2}LL^T\right)G^{-1} \\ &= G^{-1}\left(\sum(\beta_0) + \sum_1(\beta_0)\right)G^{-1} + \gamma_0^2\frac{\mathrm{Var}(W) - (3/4)\mathrm{Var}(X)}{[E(X)]^2}G^{-1}(G_2, G_3)^T\big(G_2^T, G_3\big)G^{-1} \\ &= G^{-1}\left(\sum(\beta_0) + \sum_1(\beta_0)\right)G^{-1} + \gamma_0^2\frac{\mathrm{Var}(W) - (3/4)\mathrm{Var}(X)}{[E(X)]^2}R,\end{aligned} \tag{66}$$

where R is a $(p+1)$-dimensional matrix with all elements being zero except for the $(p+1) \times (p+1)$-element being 1. Therefore, we conclude that

$$\sqrt{N}(\widehat{\theta}_p - \theta_0) \stackrel{d}{\longrightarrow} \mathcal{N}\left(0, G^{-1}\left(\sum(\beta_0) + \sum_1(\beta_0)\right)G^{-1}\right), \sqrt{N}(\widehat{\gamma}_p - \gamma_0) \stackrel{d}{\longrightarrow} \mathcal{N}\left(0, \sigma + \gamma_0^2 \frac{\mathrm{Var}(W) - (3/4)\mathrm{Var}(X)}{[\mathrm{E}(X)]^2}\right), \quad (67)$$

where σ is the $(p+1, p+1)$-element of matrix $G^{-1}(\sum(\beta_0) + \sum_1(\beta_0))G^{-1}$.

Here, Theorem 2 has been proven regarding the asymptotic convergence properties of normal distribution. It was from a different viewpoint compared to previous research. □

4. Numerical Approach

Strictly speaking, we carry out some simulations in the section. The underlying additive hazards model considered is as follows:

$$\lambda(t|H, X) = \lambda_0(t) + \theta H + \gamma X, \quad (68)$$

where the baseline function $\lambda_0(t)$ is set to be $3t^2 + 1$ and $e^{-t} + t$, respectively. The true parameters $\theta = 0.3$ and $\gamma = -0.2$. The covariate $H \sim \mathcal{N}(0, 1)$ and $X \sim \mathrm{E}(1)$. The censoring time $C \sim \mathrm{uniform}(0, c)$, where constant c is chosen to approximately produce three censoring rate $\rho = 30\%$, 50%, and 80%. The confounding variable $U \sim \mathrm{uniform}(4 - \sqrt{7}, 4 + \sqrt{7})$ and the distortion function $\phi(U) = (1 + U)^3/a$, where the constant a is chosen such that the distorting function satisfies the identifiability constraint $\mathrm{E}[\phi(U) = 1]$. The observed covariate $W = \phi(U)X$. We choose a high-order kernel function $K(t) = (15/32)(3 - 7t^2)(1 - t^2) I(|t| \leq 1)$ and use leave-one-out crossvalidation to select the bandwidth.

Under the design of ODS, we sample $n_0 = 400$ subcohort individuals without replacement from $N = 4000$. Then we partition the observed failure time into three strata by quantiles of observed failure time. In order to study the influence of different cutpoints, we consider 0.2 and 0.8 quantile and 0.3 and 0.7 quantile, respectively. We sample the additional individuals of size $n_1 = 25$ and $n_3 = 25$ from the first stratum and the third stratum. In addition, we compare our proposed covariate-adjusted estimator (Proposed) with two estimators, for example, oracle estimator (Oracle) which is calculated based on the true covariate X and naive estimator (Naive) which is computed based on the contaminated covariate W. Note that the oracle estimator is computed from the observations of X, which is not available in the real data. Meanwhile, the naive method is sure to exploit to regard directly the contaminated covariate W as the true covariate X. Under each configuration, the results presented in Tables 1 and 2 are obtained from 1000 independently generated datasets, including the biases of the estimates (Bias), the sample standard deviation (SD), the

estimated standard error (SE), and the 95% normal confidence interval (CP).

By comparison and analysis, the oracle estimator is considering to be the best of all three estimators. To be specific, the proposed estimators for both θ and γ are all unbiased, and the statistical performance can compete with that of the oracle estimator. Foremost, the 95% normal confidence intervals are reasonable. When it comes to the naive estimator, the result for γ is biased. However, through covariate-adjusted process, the main results in Section 3. In addition, it is a fact that the efficiency gains are higher when cutpoint is (0.2, 0.8) than when cutpoint is (0.3, 0.7).

Additionally, we conduct simulation studies to evaluate the behavior of the proposed method when the censoring time C depends on the covariate. The setup is the same as in Tables 1 and 2, except that the censoring time C is taken as $U[0, 1]I(H < 0) + U[0, 3]I(H \geq 0)$ and $\mathrm{E}(1)I(H < 0) + \mathrm{E}(1/3)I(H \geq 0)$, respectively. The results are reported in Table 3 when $\lambda_0(t) = 3t^2 + 1$ and Table 4 when $\lambda_0(t) = e^{-t} + t$, which show that the proposed method performs satisfactorily in the cases.

5. Empirical Analysis

Studies have been completed to conclude the real-world analysis. Our study data contains 641 patients. The accumulation of extracellular DNA in the lung during bacterial infection can bring out progressive deterioration of lung function and aggravation of respiratory symptoms in patients with cystic fibrosis. Therefore, the dependent variable that we are interested in is time to relapse, and the censoring rate of the dependent variable is approximately 62.4%. Under the ODS design, we sample 200 individuals as subcohort sample. We partition the dependent variable that are not in the subcohort into three strata. We choose two kinds of cutpoints similar to the simulations. The supplemental samples of size $n_1 = 10$ and $n_3 = 10$ are selected from the first stratum and the third stratum.

Two variables relevant to potential confounders have been found, such as vital capacity and patient's type of treatment (Type), divided into placebo and rhDNase. In this study, we measured forced expiratory volume twice and abbreviated FEV_1 and FEV_2 separately. Then, we regarded $\mathrm{FEV}((\mathrm{FEV}_1 + \mathrm{FEV}_2)/2)$ as a disorder index of vital capacity. It has become apparent that the confounder factor U follows a uniform distribution over $[0, 1]$ on the basis of average. A comprehensive study of the additive hazards model has been

TABLE 1: Simulation results when $\lambda_0(t) = 3t^2 + 1$.

ρ	Cutpoints	Method	$\widehat{\theta}$				$\widehat{\gamma}$			
			Bias	SD	SE	CP	Bias	SD	SE	CP
30%	(0.3, 0.7)	Oracle	−0.0034	0.1198	0.1149	0.931	0.0052	0.0991	0.0948	0.941
		Naive	−0.0032	0.1202	0.1151	0.935	0.1154	0.0697	0.0631	0.523
		Proposed	−0.0034	0.1200	0.1149	0.932	0.0014	0.1024	0.0980	0.943
	(0.2, 0.8)	Oracle	−0.0012	0.0996	0.0962	0.936	0.0014	0.0801	0.0800	0.942
		Naive	−0.0018	0.0994	0.0962	0.935	0.1119	0.0544	0.0531	0.436
		Proposed	−0.0012	0.0996	0.0962	0.937	−0.0008	0.0828	0.0830	0.945
50%	(0.3, 0.7)	Oracle	−0.0018	0.0959	0.0978	0.944	0.0030	0.0797	0.0792	0.950
		Naive	−0.0018	0.0958	0.0977	0.947	0.1138	0.0544	0.0537	0.428
		Proposed	−0.0018	0.0961	0.0978	0.942	0.0015	0.0828	0.0822	0.955
	(0.2, 0.8)	Oracle	−0.0074	0.0871	0.0880	0.953	0.0026	0.0723	0.0715	0.951
		Naive	−0.0073	0.0869	0.0880	0.956	0.1109	0.0510	0.0485	0.351
		Proposed	−0.0075	0.0869	0.0880	0.955	−0.0002	0.0753	0.0745	0.951
80%	(0.3, 0.7)	Oracle	−0.0015	0.0940	0.0951	0.952	0.0168	0.0777	0.0752	0.957
		Naive	−0.0020	0.0934	0.0951	0.950	0.1184	0.0533	0.0501	0.308
		Proposed	−0.0016	0.0939	0.0951	0.953	0.0155	0.0817	0.0783	0.959
	(0.2, 0.8)	Oracle	−0.0062	0.0941	0.0927	0.941	0.0163	0.0717	0.0725	0.949
		Naive	−0.0062	0.0934	0.0926	0.941	0.1157	0.0507	0.0486	0.304
		Proposed	−0.0063	0.0941	0.0927	0.942	0.0146	0.0750	0.0755	0.952

"Oracle" denotes the oracle estimator calculated based on the true covariate. "Naive" denotes the naive estimator calculated based on the unadjusted covariate. "Proposed" denotes the proposed estimator calculated based on the adjusted covariate.

TABLE 2: Simulation results when $\lambda_0(t) = e^{-t} + t$.

ρ	Cutpoints	Method	$\widehat{\theta}$				$\widehat{\gamma}$			
			Bias	SD	SE	CP	Bias	SD	SE	CP
30%	(0.3, 0.7)	Oracle	−0.0005	0.0774	0.0761	0.935	0.0071	0.0560	0.0544	0.945
		Naive	−0.0005	0.0770	0.0759	0.943	0.1131	0.0391	0.0369	0.155
		Proposed	−0.0006	0.0774	0.0760	0.932	0.0035	0.0591	0.0571	0.941
	(0.2, 0.8)	Oracle	−0.0027	0.0670	0.0645	0.931	0.0059	0.0480	0.0476	0.945
		Naive	−0.0037	0.0666	0.0645	0.928	0.1123	0.0344	0.0319	0.090
		Proposed	−0.0031	0.0670	0.0645	0.932	0.0028	0.0503	0.0499	0.947
50%	(0.3, 0.7)	Oracle	−0.0033	0.0694	0.0706	0.958	0.0110	0.0524	0.0527	0.950
		Naive	−0.0042	0.0696	0.0705	0.958	0.1142	0.0352	0.0357	0.118
		Proposed	−0.0034	0.0692	0.0706	0.961	0.0084	0.0550	0.0550	0.955
	(0.2, 0.8)	Oracle	−0.0083	0.0617	0.0640	0.962	0.0106	0.0478	0.0480	0.958
		Naive	−0.0093	0.0621	0.0640	0.959	0.1156	0.0339	0.0323	0.067
		Proposed	−0.0083	0.0618	0.0640	0.959	0.0074	0.0502	0.0501	0.958
80%	(0.3, 0.7)	Oracle	−0.0144	0.0862	0.0851	0.945	0.0169	0.0664	0.0655	0.951
		Naive	−0.0142	0.0864	0.0851	0.940	0.1177	0.0461	0.0443	0.224
		Proposed	−0.0144	0.0863	0.0851	0.946	0.0146	0.0695	0.0683	0.949
	(0.2, 0.8)	Oracle	−0.0064	0.0843	0.0837	0.935	0.0180	0.0663	0.0636	0.934
		Naive	−0.0070	0.0844	0.0837	0.939	0.1168	0.0453	0.0434	0.213
		Proposed	−0.0065	0.0842	0.0837	0.936	0.0160	0.0689	0.0664	0.935

"Oracle" denotes the oracle estimator calculated based on the true covariate. "Naive" denotes the naive estimator calculated based on the unadjusted covariate. "Proposed" denotes the proposed estimator calculated based on the adjusted covariate.

undertaken to see the effect of Type and FEV on the failure time as follows:

$$\lambda(t \mid \text{Type}, \text{FEV}) = \lambda_0(t) + \theta\text{Type} + \gamma\text{FEV}. \quad (69)$$

The Kaplan–Meier survival curves have been drawn with related theory taking the kinds of treatment types and the amount of FEV (adjusted FEV) of the patients into account. In the process of drawing, we view FEV (adjusted FEV) to be 1 when FEV (adjusted FEV) ≥ the median of FEV (the median of adjusted FEV), otherwise, to be 0. As shown in Figure 1, it can be seen that disturbance did affect relations between FEV and survival probability, and the patients with placebo or lower FEV (lower adjusted FEV) tend to have lower survival probabilities.

An analysis has been presented that it is available to derive the coefficients in model (69) with the proposed covariate-adjusted approach and summarize estimated

TABLE 3: Simulation results when $\lambda_0(t) = 3t^2 + 1$.

Cutpoints	Method	$\widehat{\theta}$				$\widehat{\gamma}$			
		Bias	SD	SE	CP	Bias	SD	SE	CP
		$C \sim U[0, 1]I(H < 0) + U[0, 3]I(H \geq 0)$							
	Oracle	0.0015	0.1096	0.1146	0.955	0.0032	0.2418	0.2365	0.939
(0.3, 0.7)	Naive	0.0017	0.1100	0.1145	0.955	0.1220	0.1569	0.1509	0.865
	Proposed	0.0014	0.1096	0.1146	0.956	0.0080	0.2377	0.2319	0.934
	Oracle	0.0000	0.0927	0.0983	0.959	−0.0028	0.2050	0.2024	0.940
(0.2, 0.8)	Naive	0.0002	0.0927	0.0984	0.961	0.1188	0.1275	0.1288	0.865
	Proposed	0.0001	0.0928	0.0983	0.959	0.0046	0.2001	0.1982	0.942
		$C \sim E(1)I(H < 0) + E(1/3)I(H \geq 0)$							
	Oracle	0.0044	0.1269	0.1265	0.950	−0.0078	0.2622	0.2604	0.942
(0.3, 0.7)	Naive	0.0046	0.1270	0.1268	0.949	0.1162	0.1691	0.1648	0.905
	Proposed	0.0042	0.1268	0.1265	0.949	0.0026	0.2556	0.2548	0.948
	Oracle	0.0051	0.1007	0.1064	0.957	−0.0156	0.2261	0.2170	0.944
(0.2, 0.8)	Naive	0.0046	0.1015	0.1065	0.955	0.1172	0.1394	0.1386	0.860
	Proposed	0.0050	0.1009	0.1064	0.957	−0.0077	0.2226	0.2126	0.943

"Oracle" denotes the oracle estimator calculated based on the true covariate. "Naive" denotes the naive estimator calculated based on the unadjusted covariate. "Proposed" denotes the proposed estimator calculated based on the adjusted covariate.

TABLE 4: Simulation results when $\lambda_0(t) = e^{-t} + t$.

Cutpoints	Method	$\widehat{\theta}$				$\widehat{\gamma}$			
		Bias	SD	SE	CP	Bias	SD	SE	CP
		$C \sim U[0, 1]I(H < 0) + U[0, 3]I(H \geq 0)$							
	Oracle	0.0012	0.0810	0.0894	0.971	−0.0033	0.1812	0.1762	0.955
(0.3, 0.7)	Naive	0.0009	0.0804	0.0895	0.973	0.1154	0.1151	0.1112	0.843
	Proposed	0.0011	0.0809	0.0895	0.971	0.0061	0.1784	0.1726	0.956
	Oracle	−0.0045	0.0746	0.0773	0.955	−0.0002	0.1533	0.1540	0.949
(0.2, 0.8)	Naive	−0.0049	0.0747	0.0774	0.957	0.1154	0.0995	0.0973	0.791
	Proposed	−0.0045	0.0746	0.0773	0.957	0.0055	0.1523	0.1511	0.950
		$C \sim E(1)I(H < 0) + E(1/3)I(H \geq 0)$							
	Oracle	−0.0001	0.0879	0.0870	0.943	0.0025	0.1836	0.1799	0.935
(0.3, 0.7)	Naive	−0.0002	0.0878	0.0872	0.943	0.1166	0.1126	0.1127	0.855
	Proposed	−0.0001	0.0877	0.0871	0.942	0.0099	0.1791	0.1762	0.941
	Oracle	0.0018	0.0738	0.0747	0.954	−0.0058	0.1598	0.1537	0.936
(0.2, 0.8)	Naive	0.0018	0.0743	0.0748	0.955	0.1180	0.0985	0.0960	0.771
	Proposed	0.0019	0.0739	0.0747	0.954	0.0013	0.1568	0.1505	0.936

. "Oracle" denotes the oracle estimator calculated based on the true covariate. "Naive" denotes the naive estimator calculated based on the unadjusted covariate. "Proposed" denotes the proposed estimator calculated based on the adjusted covariate.
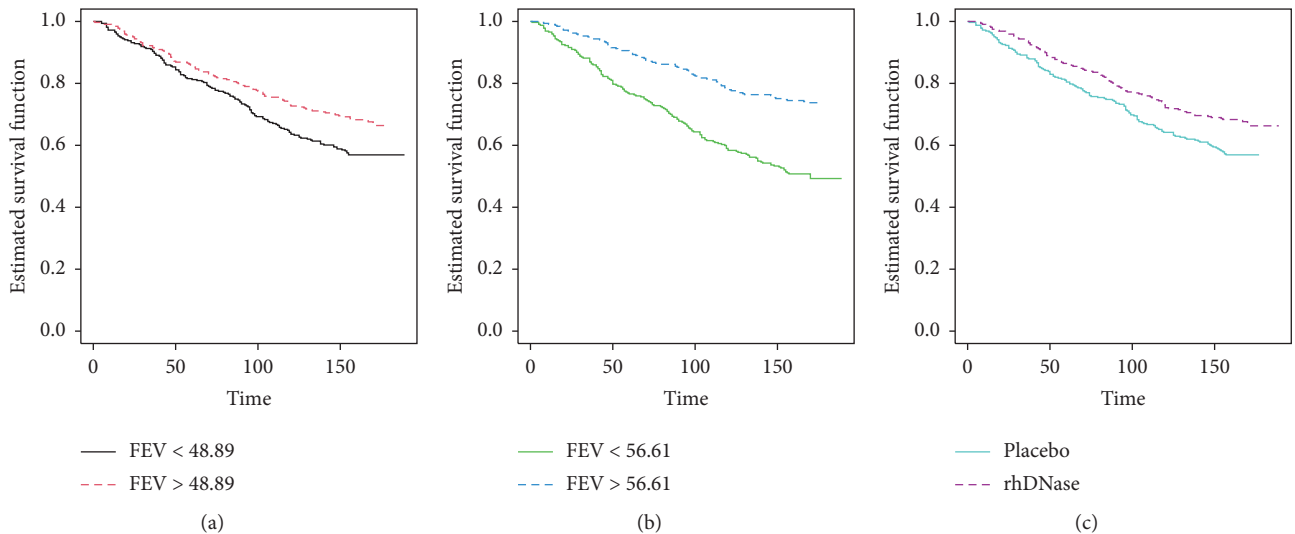

FIGURE 1: Estimated Kaplan–Meier survival curves for patients in pulmonary exacerbations study: (a) under different expiratory volumes; (b) under different adjusted expiratory volumes; (c) under different treatment types.

TABLE 5: Results for analysis of pulmonary exacerbation study data.

	Naive			Proposed		
	Est	Bias	SE	Est	Bias	SE
Cutpoints	(0.3, 0.7)					
Type	-1.1342×10^{-5}	-1.8860×10^{-6}	6.1293×10^{-6}	-3.0592×10^{-5}	-1.3562×10^{-6}	1.0596×10^{-5}
FEV	-8.6200×10^{-4}	8.9298×10^{-5}	7.1152×10^{-4}	-8.5072×10^{-4}	-3.2173×10^{-6}	7.1324×10^{-4}
Cutpoints	(0.2, 0.8)					
Type	-1.2598×10^{-5}	-6.2450×10^{-7}	6.0173×10^{-6}	-3.3581×10^{-5}	8.1670×10^{-7}	1.0456×10^{-5}
FEV	-9.5138×10^{-4}	9.9719×10^{-5}	6.9659×10^{-4}	-9.4777×10^{-4}	2.2955×10^{-6}	6.9800×10^{-4}

"Naive" denotes the naive estimator calculated based on the unadjusted covariate. "Proposed" denotes the proposed estimator calculated based on the adjusted covariate.

coefficients to be the column Est. After 1000 times artificially estimating the process, it shows the main characteristic of SE and the Bias which are calculated by the average of parameter estimates minus the corresponding Est. We also apply the contaminated covariate to calculate the estimator. The results based on our method are listed in the columns under Proposed and the results based on the contaminated covariate are put in the columns under Naive in Table 5. From the result above, we can see that, with the increase of the mount of FEV, the risk of relapse with pulmonary exacerbations will decrease. The treatment type rhDNase of pulmonary exacerbations can decrease the risk of death, which is consistent with Figure 1. Moreover, due to the covariate adjustment process, the bias of the proposed method is less than that of the Naive method. The sample standard error of the cutpoint (0.2, 0.8) is less than that of the cutpoint (0.3, 0.7), which is in accord with the simulation results.

6. Conclusion

From the point of view, the fact is that the ODS design is a benefit to lower the cost of expensive exposure variable and improve computing efficiency in large-scale cohort studies. All the results are performed for avoiding miscalculations and perfecting interpretation with adjustment on contaminated covariates. Firstly, this paper has illustrated the method of fitting covariate-adjusted additive hazard model to the data in the ODS design. Secondly, to solve the problems caused by contaminated covariates and biased-sampling schemes, this paper uses nonparametric kernel estimation method to calibrate the contaminated covariates and uses the inverse probability weighting method based on the calibration covariate to construct the weighted estimation function. In fact, this paper has carried out an extension of the theory properties of the estimator in the analysis of the proposed weighted estimation function. The numerical simulation studies have been applied to show that the estimator proposed in this paper performs well in finite sample case, and the actual data is used to show the possibility of the implement of the method.

From the perspective of research prospects, firstly, based on the methods and conclusions of this paper on the covariate adjustment problem of the additive hazard model, there has been an increasing awareness of the potential of discussing the problem of covariate adjustment of ODS studies based on some other models. For example, the accelerated failure time model discussed by Lin et al. [29], the accelerated hazard model studied by Chen and Wang [30], the nonautonomous SIRS model discussed by Lv and Meng [31], and the dynamic model of the constantor studied in [32]. Secondly, to better promote the design and keep the proposed method practical, a promising research published by Yu et al. [16] who proposed that the determination of sample sizes and the optimal sample allocation method may also be an interesting topic in the future. Furthermore, it is hoped that future research will contribute to a further development of survival models with multiple disease outcomes mentioned by Kang and Cai [7].

Data Availability

The data used to support the findings of this study are available from the corresponding author upon request.

Conflicts of Interest

The authors declare that there are no conflicts of interest regarding the publication of this paper.

Acknowledgments

References

[1] R. L. Prentice, "A case-cohort design for epidemiologic cohort studies and disease prevention trials," *Biometrika*, vol. 73, no. 1, pp. 1–11, 1986.

[2] S. G. Self and R. L. Prentice, "Asymptotic distribution theory and efficiency results for case-cohort studies," *The Annals of Statistics*, vol. 16, no. 1, pp. 64–81, 1988.

[3] W. Y. Tsai, "Pseudo-partial likelihood for proportional hazards models with biased-sampling data," *Biometrika*, vol. 96, no. 3, pp. 601–615, 2009.

[4] S. Kim, J. Cai, and W. Lu, "More efficient estimators for case-cohort studies," *Biometrika*, vol. 100, no. 3, pp. 695–708, 2013.

[5] H. Y. Chen, "Fitting semiparametric transformation regression models to data from a modified case-cohort design," *Biometrika*, vol. 88, no. 1, pp. 255–268, 2001.

[6] J. Cai and D. Zeng, "Power calculation for case-cohort studies with nonrare events," *Biometrics*, vol. 63, no. 4, pp. 1288–1295, 2007.

[7] S. Kang and J. Cai, "Marginal hazards model for case-cohort studies with multiple disease outcomes," *Biometrika*, vol. 96, no. 4, pp. 887–901, 2009.

[8] N. Chatterjee, Y. H. Chen, and N. E. Breslow, "A pseudoscore estimator for regression problems with two-phase sampling," *Journal of the American Statistical Assoctiation*, vol. 98, no. 1, pp. 158–168, 2003.

[9] H. Zhou, M. A. Weaver, J. Qin, M. P. Longnecker, and M. C. Wang, "A semiparametric empirical likelihood method for data from an outcome-dependent sampling scheme with a continuous outcome," *Biometrics*, vol. 58, no. 2, pp. 413–421, 2002.

[10] N. A. Weaver and H. Zhou, "An estimated likelihood method for continuous outcome regression models with outcome-dependent sampling," *Journal of the American Statistical Association*, vol. 100, no. 470, pp. 459–469, 2005.

[11] H. Zhou, G. Qin, and M. P. Longnecker, "A partial linear model in the outcome-dependent sampling setting to evaluate the effect of prenatal PCB exposure on cognitive function in children," *Biometrics*, vol. 67, no. 3, pp. 876–885, 2011.

[12] H. Zhou, J. You, G. Qin, and M. P. Longnecker, "A partially linear regression model for data from an outcome-dependent sampling design," *Journal of the Royal Statistical Society: Series C (Applied Statistics)*, vol. 60, no. 4, pp. 559–574, 2011.

[13] G. Qin and H. Zhou, "Partial linear inference for a 2-stage outcome-dependent sampling design with a continuous outcome," *Biostatistics*, vol. 12, no. 3, pp. 506–520, 2011.

[14] S. Yan, J. Ding, and Y. Liu, "Statistical inference methods and applications of outcome-dependent sampling designs under generalized linear models," *Science China Mathematics*, vol. 60, no. 7, pp. 1219–1238, 2017.

[15] J. H. Ding, L. Zhou, and J. Liu, "Estimating effect of environmental contaminants on women's subfecundity for the MoBa study data with an outcome-dependent sampling scheme," *Biostatistics*, vol. 15, no. 4, pp. 636–650, 2014.

[16] J. Yu, Y. Liu, J. Cai, D. P. Sandler, and H. Zhou, "Outcome-dependent sampling design and inference for Cox's proportional hazards Model," *Journal of Statistical Planning and Inference*, vol. 178, pp. 24–36, 2016.

[17] D. Şentürk and H. G. Müller, "Covariate adjusted correlation analysis via varying coefficient models," *Scandinavian Journal of Statistics*, vol. 32, no. 3, pp. 365–383, 2005.

[18] D. Şentürk and H. G. Müller, "Covariate-adjusted regression," *Biometrika*, vol. 92, no. 1, pp. 75–89, 2005.

[19] D. Şentürk and H. G. Müller, "Inference for covariate adjusted regression via varying coefficient models," *The Annals of Statistics*, vol. 34, no. 2, pp. 654–679, 2006.

[20] X. Cui, W. Guo, L. Lin, and L. Zhu, "Covariate-adjusted nonlinear regression," *The Annals of Statistics*, vol. 37, no. 4, pp. 1839–1870, 2009.

[21] F. Li, L. Lin, and X. Cui, "Covariate-adjusted partially linear regression models," *Communications in Statistics—Theory and Methods*, vol. 39, no. 6, pp. 1054–1074, 2010.

[22] X. Cui, "Statistical analysis of two types of complex data and its associated model," Ph.D. thesis, Shandong University, Shandong, China, 2008.

[23] J. Zhang, L.-P. Zhu, and L.-X. Zhu, "On a dimension reduction regression with covariate adjustment," *Journal of Multivariate Analysis*, vol. 104, no. 1, pp. 39–55, 2012.

[24] A. Delaigle, P. Hall, and W.-X. Zhou, "Nonparametric covariate-adjusted regression," *The Annals of Statistics*, vol. 44, no. 5, pp. 2190–2220, 2016.

[25] J. Zhao and C. Xie, "A nonparametric test for covariate-adjusted models," *Statistics & Probability Letters*, vol. 133, pp. 65–70, 2018.

[26] D. Y. Lin and Z. Ying, "Semiparametric analysis of the additive risk model," *Biometrika*, vol. 81, no. 1, pp. 61–71, 1994.

[27] J. Yu, Y. Liu, D. P. Sandler, and H. Zhou, "Statistical inference for the additive hazards model under outcome-dependent sampling," *Canadian Journal of Statistics*, vol. 43, no. 3, pp. 436–453, 2015.

[28] P. K. Andersen and R. D. Gill, "Cox's regression model for counting processes: a large sample study," *The Annals of Statistics*, vol. 10, no. 4, pp. 1100–1120, 1982.

[29] D. Lin, L. J. Wei, and Z. Ying, "Accelerated failure time models for counting processes," *Biometrika*, vol. 85, no. 3, pp. 605–618, 1998.

[30] Y. Chen and M. Wang, "Analysis of accelerated hazards models," *Journal of the American Statistical Association*, vol. 95, no. 450, pp. 608–618, 2000.

[31] X. Lv and X. Meng, "Analysis of dynamic behavior for a nonlinear stochastic non-autonomous SIRS model," *Mathematical Modeling and Its Applications*, vol. 7, no. 1, pp. 16–23+79, 2018.

[32] T. Zhang, N. Gao, and J. Wang, "Dynamic system of microbial culture described by impulsive differential equations," *Mathematical Modeling and Its Applications*, vol. 8, no. 1, pp. 1–13, 2019.

WILEY | Hindawi

Research Article

Calculation of Free Energy Consumption in Gene Transcription with Complex Promoter Structure

Lifang Huang,[1] Peijiang Liu,[1] Kunwen Wen,[2] and Jianshe Yu [ID][3]

[1]*School of Statistics and Mathematics, Guangdong University of Finance & Economics, Guangzhou 510320, China*
[2]*School of Mathematics, Jiaying University, Meizhou 514015, China*
[3]*Research Centre of Applied Mathematics, Guangzhou University, Guangzhou 510006, China*

Correspondence should be addressed to Jianshe Yu; jsyu@gzhu.edu.cn

From the viewpoint of thermodynamics, gene transcription necessarily consumes free energy due to nonequilibrium processes. On the other hand, regulatory molecules present on the core promoter of a gene interact often in a dynamic, highly combinatorial, and possibly energy-dependent manner, leading to a complex promoter structure. This raises the question of how gene transcription with general promoter topology consumes free energy. We propose a biophysically intuitive approach to calculate energy consumption (quantified by the production rate of entropy) of a gene transcription process. Then, we show that the numbers of the ON and OFF states of a promoter can reduce energy consumption of the gene system and the Fano factor of mRNA, and in contrast to other regulatory ways, the cooperative binding of transcription factors to DNA sites always reduces energy consumption but amplifies the mRNA noise. While our proposed approach is general, our obtained qualitative results can in turn be used to the inference of complex promoter structure.

1. Introduction

Gene expression is complex. Apart from the genetic information flow described by central dogma in biology, gene expression would involve other dynamical subprocesses such as switching between transcriptional active and inactive states [1, 2], recruitment of transcription factors (TFs) [3, 4], and feedback regulation [5, 6]. All these processes are biochemical, giving rise to stochastic fluctuations in the mRNA abundance. This stochasticity (often referred to as gene expression noise) is important for the maintenance of cellular functions and the generation of cell phenotypic diversity. Revealing gene expression mechanisms using stochastic models is a significant step toward understanding intracellular processes but is also a challenging task.

Many gene models, such as stochastic telegraph models [7–9], three-stage model [10], and gene models with feedback of various forms [11–14], have been proposed to study the stochastic mechanisms of gene expression from different viewpoints. Although these models have successfully interpreted some biological phenomena observed in experiments [12–14], they assume that the gene promoters have only one transcriptionally active (ON) state and one transcriptionally inactive (OFF) state and there are transitions between these states. This assumption is not reasonable in many situations. In fact, even for bacterial cells, the promoters that are viewed as simple can exist in a surprisingly large number of regulatory states. For example, if the PRM promoter of phage lambda in *E. coli* is regulated by two different TFs binding to two sets of three operators that can be brought together by looping out the intervening DNA, the number of regulatory states of the PRM promoter is up to 128 [15]. In contrast, eukaryotic promoters would be more complex since they involve other processes such as nucleosomes competing with or being removed by TFs [16]. Apart from the conventional regulation by TFs, the eukaryotic promoters can be also epigenetically regulated via histone modifications [17, 18]. All these may lead to complex promoter topology or complex promoter kinetics.

On the other hand, gene transcription depending on promoter structure is a nonequilibrium process from the viewpoint of thermodynamics. It has been shown that promoter kinetics regulated by TFs and/or other unspecified molecules can be expressed in terms of free energy [19–23]. This constitutes a generalization of thermodynamic methods by extending the range of systems that can be represented (i.e., including energy-consuming systems such as those of gene transcription with complex promoter structure) and the type of metrics that can be predicted (i.e., including measures of dynamic and stochastic properties) [23–25]. The usual thermodynamic formulation of cooperative and competitive association and dissociation of TFs [26] is equivalent to assigning the Gibbs-free energy to each promoter state. This representation allows one to predict equilibrium steady states (by applying a Boltzmann factor) and has been widely used to investigate the mean aspects of prokaryotic regulation [27]. However, the representation has also drawbacks; for example, it limits the analysis to energetically closed systems and forbids any investigation of the stochastic aspects of gene transcription since the representation cannot carry any kinetic information. In a word, the question of free energy consumption in gene transcription has been fully unsolved so far but has caused concerns in recent years.

In this paper, we introduce an extra set of energy values (i.e., the free energy of the activation barrier for each reaction involved in the promoter kinetics). Although difficult to access experimentally [28] and approximate to realistic cases, they can be represented in a matrix with elements being the known functions of kinetic parameters of the promoter [23, 28, 29]. Consequently, the steady-state energy consumption rate (characterizing energetic cost of promoter kinetics) can be easily calculated. In order to show the effectiveness of this method, we analyze several gene models with a representative promoter structure and derive analytical results for the corresponding energy consumption rates, which are numerically verified.

2. Models, Methods, and Theory

First, we simply introduce a biological prototype of gene expression (Figure 1(a)). To start with the expression of a gene (a DNA sequence), it is in general needed to recruit first transcription factors, histone kinases to the promoter through transcription activators, and then histone acetyltransferase complexes and other complexes to the promoter. All these histones are modified to recruit RNA polymerase II and general transcription factors to DNA, so that transcription is initialized and activated [30, 31]. This process would simultaneously accompany some repressors that inhibit transcription, until the whole part of the transcription initiation complex leaves the DNA sequence and returns to the initial state. Then, we map this biological prototype into a theoretical model of gene expression (Figure 1(b)).

We point out that Figure 1 only depicts an example for gene expression where we assume that the DNA is transcribed only when the gene is in ON state (implying the assumption that no transcription occurs in OFF state). The realistic cases of gene expression (in particular transcription) would be more complex.

In the following analysis, we will separately consider stochastic gene expression models of four kinds of promoter structures: (1) single ON and multi-OFF states, (2) single OFF and multi-ON states, (3) transcription factor dual repression, and (4) transcription factor dual promotion. We will calculate the free energy in each of these four cases and analyze the relationship between gene expression and energy dissipation.

2.1. A General Theory

2.1.1. Approximate Calculation of Probability Distribution.
Recall that, for a general chemical reaction system, if we let $P(\sigma; t)$ be the probability that the system is in state σ at time t, then the corresponding chemical master equation takes the form

$$\frac{\partial}{\partial t} P(\sigma; t) = \sum_{\sigma'} J(\sigma' \mid \sigma, t), \tag{1}$$

where $J(\sigma' \mid \sigma, t) = W(\sigma' \mid \sigma) P(\sigma'; t) - W(\sigma \mid \sigma') P(\sigma; t)$ is the probability flux with $W(\sigma' \mid \sigma)$ being the transition probability from state σ to state σ'. Now, consider a gene model at the transcription level, where the promoter structure is general; that is, the promoter may have arbitrarily many transcriptional activity (active or inactive) states and there are transitions among these states (Figure 1).

Assume that the promoter has N states in total, including K on states and $N - K$ OFF states. Let x_i represent the probability that the gene dwells in state i $(i = 1, 2, \ldots, N)$. According to the total probability principle, we apparently have the identity $\sum_{i=1}^{N} x_i \equiv 1$. Moreover, based on the promoter structure, we can directly write the following master equation for variables x_i $(1 \le i \le N)$:

$$\frac{\mathrm{d}x}{\mathrm{d}t} = \mathbf{T}x, \tag{2}$$

where $\mathbf{T} = (\lambda_{ij})$ is an $N \times N$ matrix, describing the transitions between promoter activity states and $\mathbf{x} = (x_1, \ldots, x_N)^{\mathrm{T}}$ is an n-dimensional vector. Note that $\mathbf{T}$ is actually an M-matrix (i.e., the sum of every row is equal to zero), implying that equation (2) at steady state has infinitely many solutions. But we have the conservative condition $\sum_{i=1}^{N} x_i = 1$. Therefore, all x_i can be uniquely determined if the initial conditions are given. In particular, the steady state of equation (2) can be uniquely determined. Denote by x_i^s the steady state of x_i $(i = 1, 2, \ldots, N)$.

Next, let m represent the concentration of mRNA, which is a continuous variable, and let $P_i(m; t)$ be the probability that the system is in state i. Then, the chemical master equation corresponding to the above gene model can be expressed as

$$\frac{\partial \mathbf{P}(m; t)}{\partial t} = \mathbf{T}\mathbf{P}(m; t) + \boldsymbol{\mu}(E - I)\mathbf{P}(m; t) + \boldsymbol{\delta}(E - I)[m\mathbf{P}(m; t)],$$
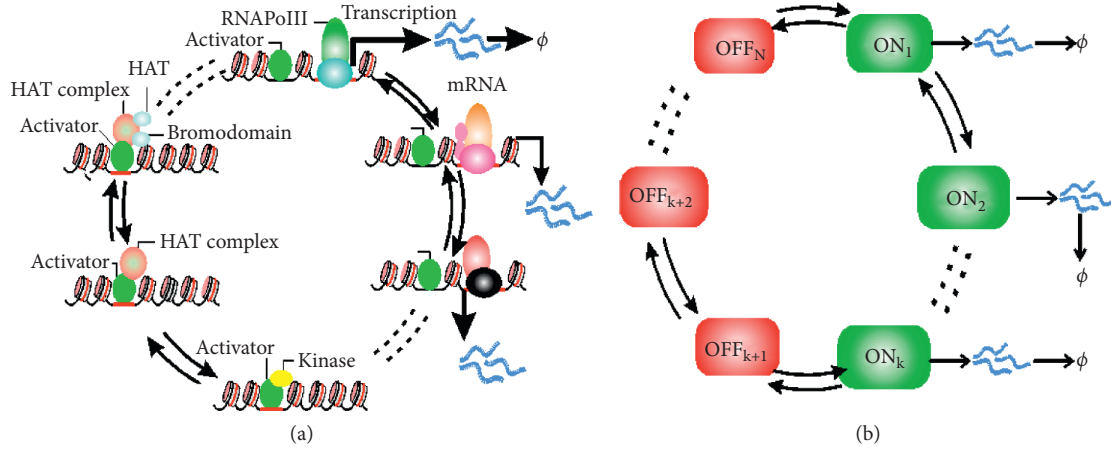
$$\tag{3}$$

FIGURE 1: (a) Schematic diagram for a biological prototype of gene expression. Both the activation and deactivation of a gene are complex processes, possibly involving recruitments of transcription factors, complexes, and histones as well as some modifications. (b) The biological prototype in (a) is mapped into a theoretical model of gene expression, where ON and OFF represent transcriptional active and inactive states. In (a) and (b), arrow represents transition direction between two distinct states.

where $\mu = \mathrm{diag}(\mu_1, \ldots, \mu_K, 0, \ldots, 0)$ is an $N \times N$ diagonal matrix describing transcription (here, we have assumed that there are K transcription exits or K ON states), $\delta = \mathrm{diag}(\delta_1, \ldots, \delta_K, 0, \ldots, 0)$ is an $N \times N$ diagonal matrix describing degradation (all δ_i will be assumed to be the same and the common degradation rate will be denoted by δ), and $\mathbf{P}(m; t) = (P_1(m; t), \ldots, P_N(m; t))^{\mathrm{T}}$ is an N-dimensional column vector. The total probability is $P(m; t) = \sum_{i=1}^{N} P_i(m; t)$. We point out that solving equation (3) and even its steady-state equation is usually difficult. Now, we give analytical approximations of factorial probabilities $P_i(m)$. In general, the switching rate of promoters is slower relative to the transcription rate in eukaryotes [27, 31], so we think that the time scale of promoter switching is slower than transcription in this paper; therefore, the probability distribution of mRNA can be obtained from the steady-state probability distribution of each state and summed with weight. So if the gene is only at OFF state l,

where $l = K + 1, \ldots, N$, then the mRNA only has degradation without production, implying that the mRNA concentration follows an exponential distribution; then $P_l(m) = x_l^s \delta e^{-\delta m}$, where x_l^s may be understood as a weight. If the gene is only at ON state i, then the mRNA has both production and degradation, implying that the mRNA concentration follows a Poisson distribution. From a mathematical viewpoint, however, the Poisson distribution can be approximated by a normal distribution. Therefore, the steady-state probability distribution in ON state i can be approximated as

$$P_k(m) = \frac{A_i}{E} \frac{1}{\sqrt{2\pi}\sigma_k} \exp\left[-\frac{(m - \Lambda_k)^2}{2\sigma_k^2}\right], \tag{4}$$

where $\Lambda_k = (\mu_k/\delta)$ is the mean, $\sigma_k^2 = (\mu_k/\delta)$ is the variance, and $k = 1, \ldots, K$. Then, the total mRNA probability distribution can be approximated as

$$P(m) = \sum_{k=1}^{K} P_k(m) + \sum_{l=K+1}^{N} P_l(m) \approx \sum_{k=1}^{K} x_k^s \frac{1}{\sqrt{2\pi}\sigma_k} \exp\left[-\frac{(m - \Lambda_k)^2}{2\sigma_k^2}\right] + \sum_{l=K+1}^{N} x_l^s \delta e^{-\delta m}. \tag{5}$$

This explicit expression is in good accordance with the one obtained by the Gillespie stochastic simulation algorithm (Figure 2), we choose two-OFF and two-ON four-state model as representatives, and these parameters are all from the experimental data [31]. This implied that the above approximation is effective. In other words, the total probability density is equal to the sum of the individual probability densities at discrete states.

2.1.2. On Free Energy Consumption.

Next, we will calculate the free energy consumption of this system; for this, we provide an effective method. First, we introduce several

definitions; we define the entropy of this system as $S(t) = -\sum_{\sigma} P(\sigma; t) \log P(\sigma; t)$ [28, 32] (i.e., the so-called Shannon entropy); then based on equation (1), the entropy generating rate (i.e., the derivative of $S(t)$ with regard to time t) can be decomposed into (see Appendix A for details):

$$\frac{\mathrm{d}S}{\mathrm{d}t} = \Pi - \Phi, \tag{6}$$

where $\Phi(t) = -\sum_{\sigma, \sigma'} J(\sigma' \mid \sigma, t) \log W(\sigma' \mid \sigma)$, that is, the so-called entropy flux rate, whereas $\Pi(t) = -\sum_{\sigma, \sigma'} J(\sigma' \mid \sigma, t) \log[W(\sigma' \mid \sigma) P(\sigma'; t)]$, that is, the so-called entropy production rate, which is an exact measurement of free energy consumption of the underlying system. $\prod(t)$ is also
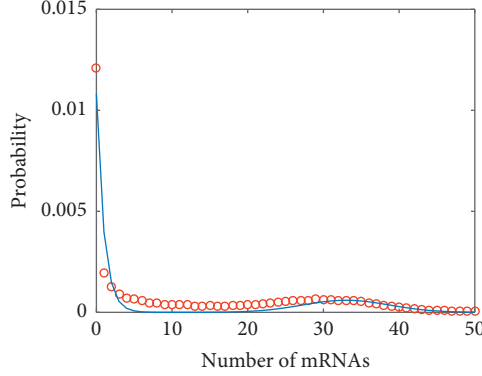
FIGURE 2: Comparison probability distributions between analytical (solid line) and numerical (empty circles) results, where parameter values are set as $(\gamma_{01} = 0.27)$, $(\gamma_{10} = 0.23)$, $(\gamma_{12} = 0.27)$, $(\gamma_{21} = 0.27 \times 0.013)$, $(\gamma_{23} = 0.23 \times 0.013)$, $(\gamma_{32} = 0.27)$, $(\gamma_{34} = 0.27)$, $(\gamma_{43} = 0.23)$, $(\mu_1 = 33)$, $(\mu_2 = 33 \times 11)$, and $(\delta = 1)$.

called the dissipation rate of free energy [23, 32–34] and will be the interest of this paper. These concepts and results are general, but the key to obtaining the free energy consumption $\prod(t)$ is how probability $P(\sigma; t)$ is obtained from equation (1) since this equation is frequently very difficult to solve. Thus, the quantity Π of our interest is also difficult to obtain. In the following, we will only consider the steady state.

In order to calculate the dissipation rate of free energy defined above, that is, Π, we define the state of the gene system as $(x_1, \ldots, x_N, m)^{\mathrm{T}}$, which is an $N + 1$ vector. Thus, every factorial probability $P_i(m)$ depends, in principle, on state $(x_1, \ldots, x_N, m)^{\mathrm{T}}$. Since the gene is only in one state at any moment, notation $P_i(m; t)$ may be rewritten as $P(x_1, \ldots \infty, x_N, m)$ where the only i component of vector $(x_1, \ldots, x_N)$ is not equal to zero. Unlike the traditional method that calculated Π directly using the expression of $P(m)$ (i.e., in one-dimensional state space), we will calculate Π in the whole state space consisting of $(x_1, \ldots, x_N, m)$. For this, we first write the dissipation rate of free energy defined above as the following form [21, 23, 28]:

$$\Pi = \sum_{A,B} (J_{AB} - J_{BA}) \ln \frac{J_{AB}}{J_{BA}}, \tag{7}$$

where A and B represent the microscopic states of the underlying gene system in the $(N + 1)$-dimensional state space and J_{AB} represents the transition probability from state A to state B. Then, we decompose Π into two parts:

$$\Pi = W + \Omega, \tag{8}$$

where W represents the free energy dissipation along the hyperplane $\sum_{i=1}^{N} x_i = 1$ in the $(N + 1)$-dimensional state space (W will be called the free energy dissipation of promoter), whereas Ω represents the free energy dissipation along the m-direction in the state space (Ω will be called the free energy dissipation of transcription). From the physical viewpoint, this decomposition seems to be reasonable and intuitive. Moreover, the decomposition has been verified by our numerical simulation (see the following sections). Therefore, we only need to calculate W and Ω separately.

Note that W can be expressed as

$$W = \sum_{A,B} \int (J_{AB} - J_{BA}) \ln \frac{J_{AB}}{J_{BA}} dm, \tag{9a}$$

where the sum is over the finite states since the promoter states are finite if the factorial probabilities $P_i(m)$ $(1 \le i \le N)$ are known. Moreover, the term $(J_{AB} - J_{BA}) \ln(J_{AB}/J_{BA})$ can be directly given based on the transition between promoter states; for example, for the transition module of the form state $i \underset{\lambda_{ij}}{\overset{\lambda_{ij}}{\rightleftarrows}}$ state j, we have $(J_{ij} - J_{ji}) \ln(J_{ij}/J_{ji}) = P_i(m; t) \lambda_{ij}$ $\ln(\lambda_{ij}/\lambda_{ji}) + P_j(m; t) \lambda_{ji} \ln(\lambda_{ji}/\lambda_{ij})$. For factorial probability $P_i(m)$, we will give a physically intuitive yet effective method to estimate $P_i(m)$.

On the other hand, Ω can be expressed as

$$\Omega = \sum_{i=1}^{N} \Omega_m^{(i)}, \tag{9b}$$

where $\Omega_m^{(i)}$ represents the free energy consumption of transcription when the gene is in state i. Since we have assumed that the promoter has only K transcription exits, the only K $\Omega_m^{(i)}$s would not be equal to zero whereas the other $\Omega_m^{(i)}$s are all equal to zero.

Before doing the calculation, we make the following preparations. For variable x_i $(i = 1, 2, \ldots, N)$, we have the master equation.

In order to calculate Ω, we first write the following differential equations for continuous variable m:

$$\frac{dm}{dt} = \sum_{k=1}^{K} \mu_k x_k - \delta m \equiv F(m). \tag{10}$$

The steady state of $m(t)$ is denoted by m^s. Then, we can write the corresponding Fokker-Planck equation as

$$\frac{\partial P(m, t)}{\partial t} = -\frac{\partial}{\partial m}(FP) + \frac{1}{2}\frac{\partial^2}{\partial m^2}(\Phi P), \tag{11}$$

where $\Phi = \sum_{k=1}^{K} \mu_{i_k} x_{i_k}^s + \delta m^s$. Recall that for the Fokker-Planck equation

$$\frac{\partial P(x;t)}{\partial t} = -\sum_{i=1}^{n} \frac{\partial}{\partial x_i} \left[\mu_i(x,t)P(x;t) \right] + \frac{1}{2}\sum_{i,j=1}^{n} \frac{\partial^2}{\partial x_i \partial x_j} \left[D_{ij}(x,t)P(x;t) \right],$$

$$(12)$$

the corresponding free energy dissipation takes the form (see Appendix B of this paper or [35, 36])

$$\Omega = \frac{1}{2}\sum_{i=1}^{n} \int \sum_{j=1}^{n} \frac{\partial}{\partial x_j} \left[D_{ij}(\mathbf{x},t)P(\mathbf{x},t) \right] \frac{\partial \ln P(\mathbf{x},t)}{\partial x_i} \, dx_i.$$
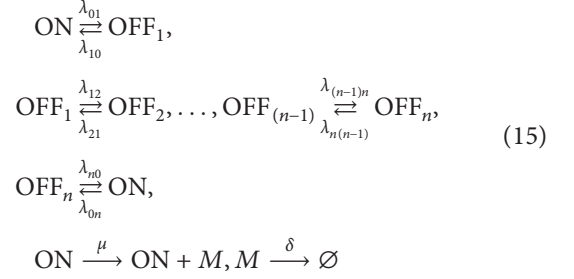
$$(13)$$

In our case, equation (12) becomes

$$\Omega = \frac{\Phi}{2}\int_0^{\infty} \frac{dP(m)}{dm}\frac{d\ln P(m)}{dm}\,dm = \frac{\Phi}{2}\int_0^{\infty} \left[\frac{dP(m)}{dm} \right]^2 \frac{1}{P(m)}\,dm.$$

$$(14)$$

From equation (9a) for the free energy dissipation of promoter W and equation (14) for the free energy dissipation of transcription Ω, we can see that the key of calculating the free energy dissipation of the whole system is that probability $P(m)$ must be known, where $P(m) = \sum_{i=1}^{N} P_i(m)$ can be approximated as equation (5).

There are many factors that affect promoter and they lead to many promoter models. Due to the limitation of space, we choose four typical models that are more concerned; there are two kinds of promoter multistate model [3, 8, 30] and two kinds of transcription factor cooperative binding model [31]. Because the complexity of the promoter can be mapped into multistate model, people want to understand the significance of the multistates of promoter and cooperation between transcription factors from different

aspects. In this paper, we want to study them from the new perspective of free energy consumption.

2.2. Case 1: One ON and Multiple OFFs.

The promoter structure is schematically shown in Figure 3(a), where we assume that the promoter has one transcriptional active (ON) state and n inactive (OFF) states, which all together form a loop. And there are transitions among these states. For convenience, we list all the reactions of the gene model as follows:

$$ON \underset{\lambda_{10}}{\overset{\lambda_{01}}{\rightleftarrows}} OFF_1,$$

$$OFF_1 \underset{\lambda_{21}}{\overset{\lambda_{12}}{\rightleftarrows}} OFF_2, \ldots, OFF_{(n-1)} \underset{\lambda_{n(n-1)}}{\overset{\lambda_{(n-1)n}}{\rightleftarrows}} OFF_n,$$

$$OFF_n \underset{\lambda_{0n}}{\overset{\lambda_{n0}}{\rightleftarrows}} ON,$$

$$ON \xrightarrow{\mu} ON + M, M \xrightarrow{\delta} \varnothing$$

$$(15)$$

where M represents mRNA, $\lambda_{01}, \lambda_{10}, \lambda_{12}, \lambda_{21}, \ldots, \lambda_{(n-1)n}$, $\lambda_{n(n-1)}, \lambda_{n0}, \lambda_{0n}$ are the transition rates between different states of the promoter, μ represents the transcription rate in ON states, and δ represents the degradation rate. These rates are assumed to be constants.

Let x_0 represent the probability that the gene dwells in ON state and x_i represent the probability that the gene dwells in OFF state i $(1 \le i \le n)$. For the promoter described in Figure 3(a), transcription matrix $\mathbf{T}$ in equation (3) of the above section takes the form

$$\mathbf{T} = \begin{pmatrix} -(\lambda_{0n}+\lambda_{01}) & \lambda_{10} & & & & \lambda_{n0} \\ \lambda_{01} & -(\lambda_{10}+\lambda_{12}) & \lambda_{21} & & & \\ & \ddots & \ddots & & \ddots & \\ & & \lambda_{(n-2)(n-1)} & -(\lambda_{(n-1)n}+\lambda_{(n-1)(n-2)}) & \lambda_{n(n-1)} & \\ \lambda_{0n} & & & \lambda_{(n-1)n} & -(\lambda_{n(n-1)}+\lambda_{n0}) \end{pmatrix},$$

$$(16)$$

where elements in the empty place are zero. The steady-state equation corresponding to equation (3) is $\mathbf{Tx} = 0$, where $\mathbf{x} = (x_0, x_1, \ldots, x_n)^T$. Solving this algebraic equation combined with the conservative condition $\sum_{i=0}^{n} x_i = 1$ yields $x_i^s = (A_i/E)$, where $A_i = \sum_{k_0,k_1,\cdots,k_n} \prod_{k \ne i} \lambda_{kk_i}$ is a constant depending on transition rates λ_{kl} $(i = 0, 1, \ldots, n)$ and $E = \sum_{i=0}^{n} A_i$. Note that there is only one ON state, implying that $K = 1$. Therefore, we have only one transcription rate, denoted by μ. Thus, from equation (9), we obtain the mean of the stationary mRNA level given by $m^s = (\mu/\delta)(A_0/E)$.

According to the general method described in the above section, we know that the probability that the gene is in ON state can be approximated as $P_0(m) = (A_0/E)(1/\sqrt{2\pi}\sigma_0)\exp[-((m-\Lambda_0)^2/2\sigma_0^2)]$, where $\Lambda_0 = (\mu/\delta)$ and $\sigma_0^2 = (\mu/\delta)$. The probabilities that the gene is in OFF states can be approximated as $P_i(m) = (A_i/E)\delta e^{-m\delta}$,

where $i = 1, 2, \ldots, n$. Therefore, the total probability $P(m)$ is given by

$$P(m) = \frac{A_0}{E}\frac{1}{\sqrt{2\pi}\sigma_0}\exp\left[-\frac{(m-\Lambda_0)^2}{2\sigma_0^2} \right] + \sum_{i=1}^{n} \frac{A_i}{E}\delta e^{-m\delta}.$$

$$(17)$$

The variance of the probability distribution is given by

$$VAR_m = \left(\frac{A_0}{E}\right)^2\frac{\mu}{\delta} + \left(\frac{A_1}{E}\right)^2\frac{1}{\delta} + \cdots + \left(\frac{A_n}{E}\right)^2\frac{1}{\delta}.$$

$$(18)$$

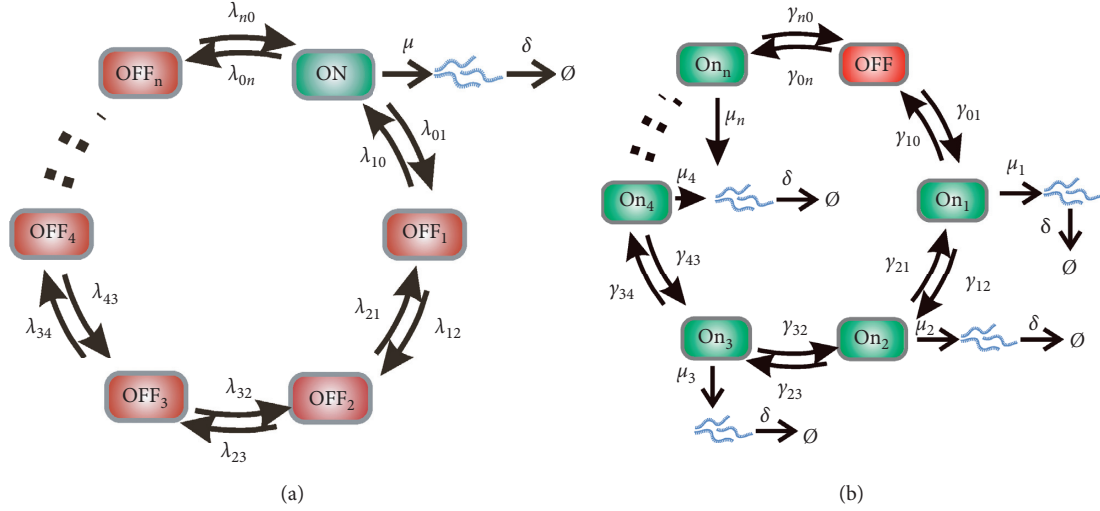Thus, the expression of the mRNA noise and Fano factor is analytically expressed as

(a)

(b)

FIGURE 3: (a) Schematic diagram for a gene model with the promoter having one ON and multiple OFFs. These chromatin states form a loop and transition from one state to its neighboring state with a constant transition rate. (b) Schematic diagram for a gene model with the promoter having one OFF and multiple ONs. These promoter states also form a loop and transition from one state to another state with a constant transition rate.

$$\eta^2 = \frac{\text{Var}_m}{(m^s)2} = \left(\frac{\delta E}{\mu A_0}\right)^2 \left[\left(\frac{A_0}{E}\right)^2 \sigma_1^2 + \left(\frac{A_1}{E}\right)^2 \frac{1}{\delta} + \cdots + \left(\frac{A_n}{E}\right)^2 \frac{1}{\delta}\right]. \tag{19a}$$

$$\text{Fano} = \frac{\text{Var}_m}{m^s} = \frac{\delta E}{\mu A_0} \left[\left(\frac{A_0}{E}\right)^2 \sigma_1^2 + \left(\frac{A_1}{E}\right)^2 \frac{1}{\delta} + \cdots + \left(\frac{A_n}{E}\right)^2 \frac{1}{\delta}\right]. \tag{19b}$$

Next, we give the analytical expression of free energy dissipation of the whole system, Π. First, consider the free energy consumption of promoter, W. Note that equation (19a) in the above section becomes

$$W = \int_0^\infty \left(P_0(m)\lambda_{01} \ln \frac{\lambda_{01}}{\lambda_{10}} + P_1(m)\lambda_{10} \ln \frac{\lambda_{10}}{\lambda_{01}}\right)$$

$$+ \left(P_1(m)\lambda_{12} \ln \frac{\lambda_{12}}{\lambda_{21}} + P_2(m)\lambda_{21} \ln \frac{\lambda_{21}}{\lambda_{12}}\right) + \cdots$$

$$+ \left(P_{n-1}(m)\lambda_{(n-1)n} \ln \frac{\lambda_{(n-1)n}}{\lambda_{n(n-1)}} + P_n(m)\lambda_{n(n-1)} \ln \frac{\lambda_{n(n-1)}}{\lambda_{(n-1)n}}\right)$$

$$+ \left(P_n(m)\lambda_{n0} \ln \frac{\lambda_{n0}}{\lambda_{0n}} + P_0(m)\lambda_{0n} \ln \frac{\lambda_{0n}}{\lambda_{n0}}\right) dm, \tag{20}$$

Using the expressions of $P_0(m)$ and $P_i(m)$ $(1 \le i \le n)$ given above, we have

$$W = \left(\frac{A_0}{E}\lambda_{01} \ln \frac{\lambda_{01}}{\lambda_{10}} + \frac{A_1}{E}\lambda_{10} \ln \frac{\lambda_{10}}{\lambda_{01}}\right)$$

$$+ \left(\frac{A_1}{E}\lambda_{12} \ln \frac{\lambda_{12}}{\lambda_{21}} + \frac{A_2}{E}\lambda_{21} \ln \frac{\lambda_{21}}{\lambda_{12}}\right) + \cdots$$

$$+ \left(\frac{A_{(n-1)}}{E}\lambda_{(n-1)n} \ln \frac{\lambda_{(n-1)n}}{\lambda_{n(n-1)}} + \frac{A_n}{E}\lambda_{n(n-1)} \ln \frac{\lambda_{n(n-1)}}{\lambda_{(n-1)n}}\right)$$

$$+ \left(\frac{A_n}{E}\lambda_{n0} \ln \frac{\lambda_{n0}}{\lambda_{0n}} + \frac{A_0}{E}\lambda_{0n} \ln \frac{\lambda_{0n}}{\lambda_{n0}}\right). \tag{21}$$
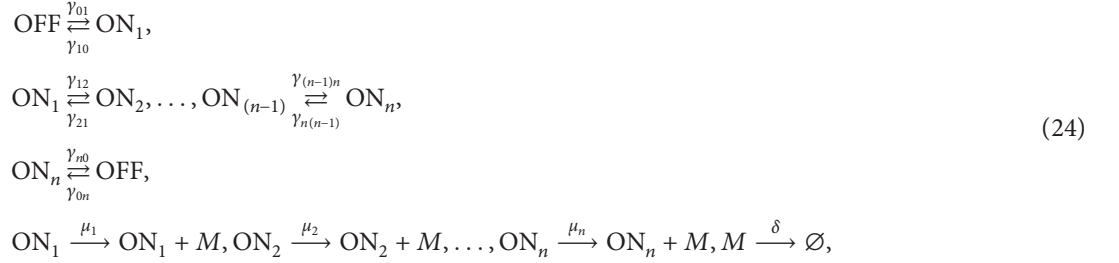
Therefore, we finally arrive at

$$W = J \ln q, \tag{22}$$

where $J = (\lambda_{01}\lambda_{12}, \ldots, \lambda_{(n-1)n}\lambda_{n0} - \lambda_{n(n-1)}\lambda_{(n-1)(n-2)}, \ldots, \lambda_{10}\lambda_{0n}/E)$ and $q = ((\lambda_{01}\lambda_{12}, \ldots, \lambda_{(n-1n}\lambda_{n0})/(\lambda_{nn-1})\lambda_{(n-1n-2)}, \ldots, \lambda_{10}\lambda_{0n}))$ are two quantities depending on transition rates between promoter states. Quantity W is exactly the heat consumption per unit time of the annular flow [28, 37] between promoter states.

Then, consider the free energy consumption of transcription, Ω. Note that Φ in equation (13) is given by $\Phi = \mu x_0^s + \delta m^s = (2\mu A_0/\delta E)$. Also, note that the probability distribution is given by equation (17). According to equation (13), we thus have

$$\Omega = \frac{\mu A_0}{\delta E} \int_0^\infty \frac{\left\{(A_0/E)\left(m - \Lambda_0/\sqrt{2\pi\sigma_0^3}\right)\exp\left[-\left((m - \Lambda_0)^2/2\sigma_0^2\right)\right] + \delta^2 \sum_{i=1}^n (A_i/E)e^{-m\delta}\right\}^2}{(A_0/E)\left(1/\sqrt{2\pi\sigma_0}\right)\exp\left[-\left((m - \Lambda_0)^2/2\sigma_0^2\right)\right] + \delta \sum_{i=1}^n (A_i/E)e^{-m\delta}} \, dm. \tag{23}$$

2.3. Case 2: One OFF and Multiple ONs.

Here, we consider another representative promoter structure, where the promoter has one OFF state and n ON states (Figure 3(b)). All the biochemical reactions are listed as follows:

$$
\begin{aligned}
&\text{OFF} \underset{\gamma_{10}}{\overset{\gamma_{01}}{\rightleftarrows}} \text{ON}_1, \\
&\text{ON}_1 \underset{\gamma_{21}}{\overset{\gamma_{12}}{\rightleftarrows}} \text{ON}_2, \ldots, \text{ON}_{(n-1)} \underset{\gamma_{n(n-1)}}{\overset{\gamma_{(n-1)n}}{\rightleftarrows}} \text{ON}_n, \\
&\text{ON}_n \underset{\gamma_{0n}}{\overset{\gamma_{n0}}{\rightleftarrows}} \text{OFF}, \\
&\text{ON}_1 \xrightarrow{\mu_1} \text{ON}_1 + M, \text{ON}_2 \xrightarrow{\mu_2} \text{ON}_2 + M, \ldots, \text{ON}_n \xrightarrow{\mu_n} \text{ON}_n + M, M \xrightarrow{\delta} \varnothing,
\end{aligned}
\tag{24}
$$

where $\gamma_{01}, \gamma_{10}, \gamma_{12}, \gamma_{21}, \cdots, \gamma_{(n-1)n}, \gamma_{n(n-1)}, \gamma_{n0}, \gamma_{0n}$ are the transition rates between different states of promoter, μ_i represents the transcription rate in ON state i, and δ represents the degradation rate.

Let x_0 represent the probability that the gene dwells in OFF state and x_i represent the probability that the gene dwells in ON state i ($1 \leq i \leq n$). For the promoter described in Figure 3(b), transcription matrix $\mathbf{T}$ in equation (3) of Section 2.1 takes the form

$$
\mathbf{T} = \begin{pmatrix}
-(\gamma_{0n} + \gamma_{01}) & \gamma_{10} & & & & \gamma_{n0} \\
\gamma_{01} & -(\gamma_{10} + \gamma_{12}) & \gamma_{21} & & & \\
& \ddots & \ddots & & \ddots & \\
& & \gamma_{(n-2)(n-1)} & -(\gamma_{(n-1)n} + \gamma_{(n-1)(n-2)}) & \gamma_{n(n-1)} & \\
\gamma_{0n} & & & \gamma\lambda_{(n-1)n} & -(\gamma_{n(n-1)} + \gamma_{n0})
\end{pmatrix},
\tag{25}
$$

where elements in the empty place are zero. The steady-state equation corresponding to equation (3) is $\mathbf{Ty} = \mathbf{0}$, where $\mathbf{y} = (y_0, y_1, \ldots, y_n)^{\mathrm{T}}$. Solving this algebraic equation combined with the conservative condition $\sum_{i=0}^{n} y_i = 1$ yields $y_i^s = (B_i/T)$, where $B_i = \sum_{k_0, k_1, \ldots, k_n} \prod_{k \neq i} \gamma_{kk_i}$ is a constant depending on transition rates γ_{kl}, $i = 0, 1, \ldots, n$, and $T = \sum_{i=0}^{n} B_i$. Note that there is only one OFF state but there are n transcription rates, denoted by μ_i ($i = 1, \ldots, n$). Thus, from equation (9), we obtain the mean of the stationary mRNA level given by $m^s = ((\mu_1 B_1 + \mu_2 B_2 + \cdots + \mu_n B_n)/\delta T)$.

According to the general method described in Section 2.1, we know that the probabilities that the gene is in ON states can be approximated as $P_i(m) = (B_i/T)(1/\sqrt{2\pi\sigma_i})\exp[-(m - \Lambda_i)^2/2\sigma_i^2]$, where $\Lambda_i = (\mu_i/\delta)$ and $\sigma_i^2 = (\mu_i/\delta)$. The probability that the gene is in OFF state can be approximated as $P_0(m) = (B_0/T)\delta e^{-m\delta}$, where $i = 1, 2, \ldots, n$. Therefore, the total probability $P(m)$ is given by

$$
P(m) = \frac{B_0}{T}\delta e^{-m\delta} + \sum_{i=1}^{n} \frac{1}{\sqrt{2\pi\sigma_i}}\exp\left[-\frac{(m - \Lambda_i)^2}{2\sigma_i^2}\right].
\tag{26}
$$

The variance of the probability distribution is given by

$$
\text{VAR}_m = \left(\frac{B_0}{T}\right)^2\frac{1}{\delta} + \left(\frac{B_1}{T}\right)^2\frac{\mu_1}{\delta} + \cdots + \left(\frac{B_n}{T}\right)^2\frac{\mu_n}{\delta}.
\tag{27}
$$

Thus, the expression of the mRNA noise and Fano factor is analytically expressed as

$$
\eta^2 = \frac{\text{Var}_m}{(m^s)^2} = \left(\frac{1}{m^s}\right)^2\left[\left(\frac{B_0}{T}\right)^2\frac{1}{\delta} + \left(\frac{B_1}{T}\right)^2\sigma_1^2 + \cdots + \left(\frac{B_n}{T}\right)^2\sigma_n^2\right],
\tag{28a}
$$

$$
\text{Fano} = \frac{\text{Var}_m}{m^s} = \frac{1}{m^s}\left[\left(\frac{B_0}{T}\right)^2\frac{1}{\delta} + \left(\frac{B_1}{T}\right)^2\sigma_1^2 + \cdots + \left(\frac{B_n}{T}\right)^2\sigma_n^2\right].
\tag{28b}
$$

Next, we give the analytical expression of free energy dissipation of the whole system, Π. First, consider the free energy consumption of promoter, W. Note that equation (19a) in the above section becomes

$$
\begin{aligned}
W = \int_0^{\infty} &\left(P_0(m)\gamma_{01}\ln\frac{\gamma_{01}}{\gamma_{10}} + P_1(m)\gamma_{10}\ln\frac{\gamma_{10}}{\gamma_{01}}\right) \\
&+ \left(P_1(m)\gamma_{12}\ln\frac{\gamma_{12}}{\gamma_{21}} + P_2(m)\lambda_{21}\ln\frac{\gamma_{21}}{\gamma_{12}}\right) + \cdots \\
&+ \left(P_{n-1}(m)\gamma_{(n-1)n}\ln\frac{\gamma_{(n-1)n}}{\gamma_{n(n-1)}} + P_n(m)\gamma_{n(n-1)}\ln\frac{\gamma_{n(n-1)}}{\gamma\lambda_{(n-1)n}}\right) \\
&+ \left(P_n(m)\gamma_{n0}\ln\frac{\gamma_{n0}}{\gamma_{0n}} + P_0(m)\lambda_{0n}\ln\frac{\gamma_{0n}}{\gamma_{n0}}\right)\mathrm{d}m.
\end{aligned}
\tag{29}
$$

Therefore, we finally arrive at

$$W = J \ln q, \tag{30}$$

where $J = ((\gamma_{01}\gamma_{12}, \ldots, \gamma_{(n-1n)}\gamma_{n0} - \gamma_{(nn-1)}\gamma_{(n-1n-2)}, \ldots, \gamma_{10}\gamma_{0n})/T)$ and $q = ((\gamma_{01}\gamma_{12}, \ldots, \gamma_{(n-1n}\gamma_{n0})/(\gamma_{nn-1)}\gamma_{(n-1n-2)}, \ldots, \gamma_{10}\gamma_{0n}))$ are two quantities depending on transition rates between promoter states. Quantity W is exactly the heat consumption per unit time of the annular flow [28, 37] between promoter states.

Then, consider the free energy consumption of transcription, Ω. Note that the probability distribution is given by equation (17). According to equation (13), we thus have

$$\Omega = m^s \int_0^\infty \frac{\left\{ (B_0/T)\delta^2 e^{-m\delta} + \sum_{i=1}^n (B_i/T)\left(m - \Lambda_i/\sqrt{2\pi\sigma_i^3}\right) \exp\left[-\left((m - \Lambda_i)^2/2\sigma_i^2\right)\right] \right\}^2}{(B_0/T)\delta e^{-m\delta} + \sum_{i=1}^n (A_i/T)\left(1/\sqrt{2\pi\sigma_i}\right)\exp\left[-\left((m - \Lambda_i)^2/2\sigma_i^2\right)\right]} \, dm. \tag{31}$$

2.4. Case 3: Dual Repression Model. Research [38–40] shows that when there are multiple binding sites in the promoter sequence, the promoter will be controlled by multiple transcription factors and multiple enzymes, and some enzymes are difficult to be separated after binding, which is called cooperative binding. Cooperative binding often occurs, so what are the benefits of cooperative binding for organisms? Why do these enzymes cooperate with each other? We will give the answer from the perspective of favorable gene expression and energy saving. In this section, we take the cooperative binding of two inhibitors (dual repression) as an example to illustrate, as shown in Figure 3(a), where k_R^{on} represents the binding rate, k_R^{off} is the dissociation rate, r is the transcription rate, and Ω is the cooperation binding degree. According to the experimental data [38, 39], $\Omega = 1$ represents independent binding and $\Omega = 0.013$ represents cooperation binding.

Figure 4(a) is the special case of Figure 3(a), so some indexes of this system, such as mean, variance, noise, Fano factor, probability distribution, and energy consumption, are just to make $n = 3$ in formulas (15)–(23). We will not go into details here, so what are the biological functions of cooperative binding of repressors? In the third part of the paper, the explanation is given based on the numerical results.

2.5. Case 4: Dual Promotion Model. Research [27] shows that the promoter will be activated by multiple transcription factors and how does the cooperation of these activators affect gene expression? We will give the answer from the perspective of favorable gene expression and energy saving. Here, we take the cooperative binding of two activators (dual promotion) as an example, as shown in Figure 4(b), where k_p^{on} is the binding rate, k_p^{off} is the dissociation rate, η_1 and η_2 are the transcription rates, where $\eta_2 = f \times \eta_1$, f is the enhancement factor, Ω is the degree of cooperative binding, according to the experimental data [31], $\Omega = 1$ represents independent binding, and $\Omega = 0.1$ represents cooperation binding.

Figure 4(b) is the special case of Figure 3(b), so some indexes of this system, such as mean, variance, noise, Fano factor, probability distribution, and energy consumption, are just to make $n = 3$ in formulas (24)–(31). We will not go into details here, so what are the biological functions of cooperative binding of activators? In the third part of the paper, the explanation is given based on the numerical results.

3. Numerical Results

In principle, the above analysis formula shows how different promoter structures affect gene expression (including mRNA distribution, average expression level, noise intensity, Fano factor, and free energy consumption), but these results are implicit and not direct. Here, we conduct numerical simulation to give intuitive results. Next, let us use the numerical value to see how the multistates of the promoter affect the free energy consumption and the significance of cooperative binding.

3.1. Free Energy Consumption of Multistate Promoters and Its Effect on Gene Expression. Promoter structure is complex. Promoter regulation involves many biochemical processes and interactions, such as splicing, chromatin remodeling, DNA methylation, nucleosome occupation, TATA box strength, transcription factor concentration, binding site number, and lncRNA regulation. We map this phenomenon into a multistate promoter model. From the perspective of evolutionism, organisms will choose the most favorable direction for their survival and development to evolve. What is the reason why the promoter structure of eukaryotes is much more complex than that of prokaryotes? We will give some explanation from the perspective of free energy consumption.

In Figure 3(a) of the multi-OFF promoter model, we set the transcription rate as $\mu = 33$, the degradation rate as $\delta = 1$, and the switching rate between promoter states as $\lambda_{01} = 0.27$, $\lambda_{10} = 0.23$, $\lambda_{12} = 0.27, \lambda_{21} = 0.23$, $\lambda_{23} = 0.27$, $\lambda_{32} = 0.23$, $\lambda_{n0} = 0.27, \lambda_{0n} = 0.23$. These parameters are all from the experimental data [31]. In Figure 3(b) of the multi-ON promoter model, we set the transcription rates as $\mu_1 = 33$, $\mu_2 = 43$, $\mu_3 = 53$, $\mu_4 = 63, \mu_5 = 73$, the degradation rate as $\delta = 1$, and the switching rate between promoter states as $\gamma_{01} = 0.27$, $\gamma_{10} = 0.23$, $\gamma_{12} = 0.27$, $\gamma_{21} = 0.23$, $\gamma_{23} = 0.27, \gamma_{32} = 0.23, \gamma_{n0} = 0.27, \gamma_{0n} = 0.23$. These parameters are all from the experimental data [31]. Note that the switching
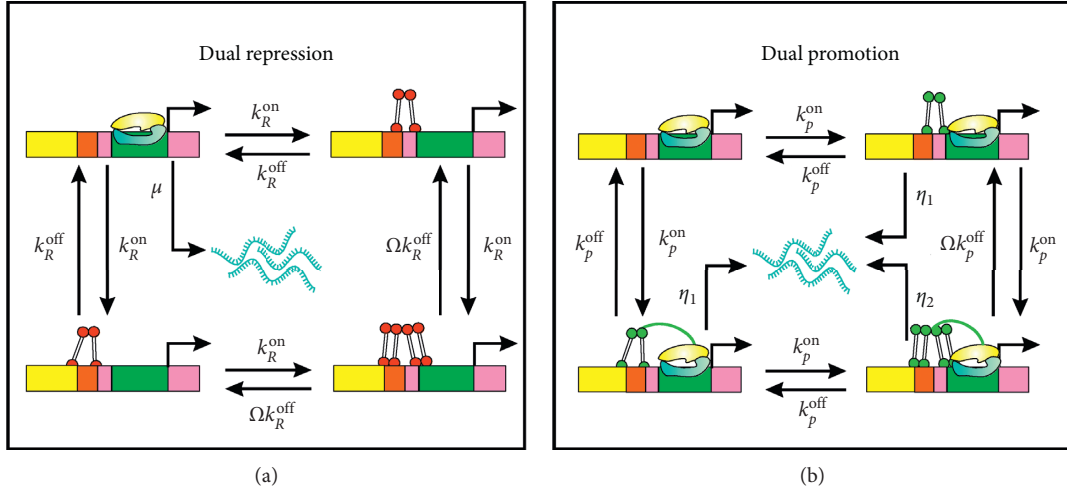
(a)

(b)

Figure 4: (a) Schematic diagram for dual repression structure. k_R^{on} represents binding rate, k_R^{off} represents dissociation rate, μ represents transcription rate, Ω represents cooperation binding degree, $\Omega = 1$ represents independent binding, and $\Omega = 0.013$ represents cooperation binding. (b) Schematic diagram for dual promotion structure. k_R^{on} represents binding rate, k_R^{off} represents dissociation rate, η_1 and η_2 represent transcription rates, where $\eta_2 = f \times \eta_1$, f is the enhancement factor, Ω represents cooperation binding degree, $\Omega = 1$ represents independent binding, and $\Omega = 0.1$ represents cooperation binding.

rates of promoters will be affected by various factors and will change at any time. In this section, we focus on the influence of multiple promoter states on gene expression, so we think that the switching rates of promoters are the same, only considering the influence of multiple states.

According to the results shown in Figure 5, if the number of ON states increases, then the mean RNA level will increase, and the noise and Fano factor decrease, while if OFF states increases, then the mean RNA level will decrease and the noise increases, but Fano factor decreases. That is, no matter multi-ON model or multi-OFF model, as long as the promoter state increases, the Fano factor will decrease accordingly. Research [31] shows that Fano factor affects the cell variability, and smaller Fano factor can reduce the variability of cells, so we think that the multipromoter states can reduce the variability of cells.

According to the results shown in Figure 5, we can see that, from the total energy of the system, no matter the multi-ON model or the multi-OFF model, the more the promoter states are, the lower the free energy consumption is. Maybe this can explain why organisms choose complex promoters from another perspective. However, for average energy consumption (defined as the total energy consumption of the system divided by the mean of mRNA, i.e., the average energy required to produce an mRNA), the multi-ON model can reduce the average energy consumption, but the multi-OFF model can increase the average energy consumption. We all know that multi-OFF promoter states can result in the bursty generation of mRNA, while bursty gene expression often leads to phenotypic diversity, which makes organisms more adaptable to the environment. In other words, multi-OFF model makes the average energy consumption of the system increase, but it is accompanied by the realization of biological functions.

3.2. Free Energy Consumption of Dual Repression or Promotion and Its Effect on Gene Expression. Researches [27, 31, 38, 39] show that the promoter will be regulated by multiple transcription factors. These transcription factors are either suppressors or activators, and many transcription factors often cooperate with each other, so what are the benefits of the cooperation of these enzymes for gene expression? In this section, we analyze its biological function through numerical results from the perspective of favorable for gene expression and free energy consumption.

In Figure 3(a) of the dual repression promoter model, we set the transcription rate as $\mu = 33$, the degradation rate as $\delta = 1$, the binding rate of transcription factors as $k_R^{\mathrm{on}} = 0.27$, and the dissociation rate of transcription factors as $k_R^{\mathrm{off}} = 0.23$; these parameters are all from the experimental data [27, 38, 39]. According to the results shown in Figure 6, the cooperative binding of dual repression ($\Omega = 0.013$ represents cooperative binding, green line) can reduce the total free energy consumption but increase the average free energy consumption compared with the independent binding ($\Omega = 1$ represents independent binding, red line). And the cooperative binding of double suppressors can significantly reduce the mean value but increase the noise and Fano factor.

In Figure 4(b) of the dual promotion model, we set the transcription rates as $\eta_1 = 33$, $\eta_2 = 33 \times f$, where $f = 11$, the degradation rate as $\delta = 1$, the binding rate of transcription factors as $k_P^{\mathrm{on}} = 0.27$, and the dissociation rate of transcription factors as $k_P^{\mathrm{off}} = 0.23$; these parameters are all from the experimental data [27, 38, 39]. From Figure 7, we observe that the cooperative binding of double activators ($\Omega = 0.1$ for cooperative binding, yellow line) can reduce the total energy consumption and increase the average energy consumption compared with the independent binding ($\Omega = 1$ for independent binding, red line). And the cooperative
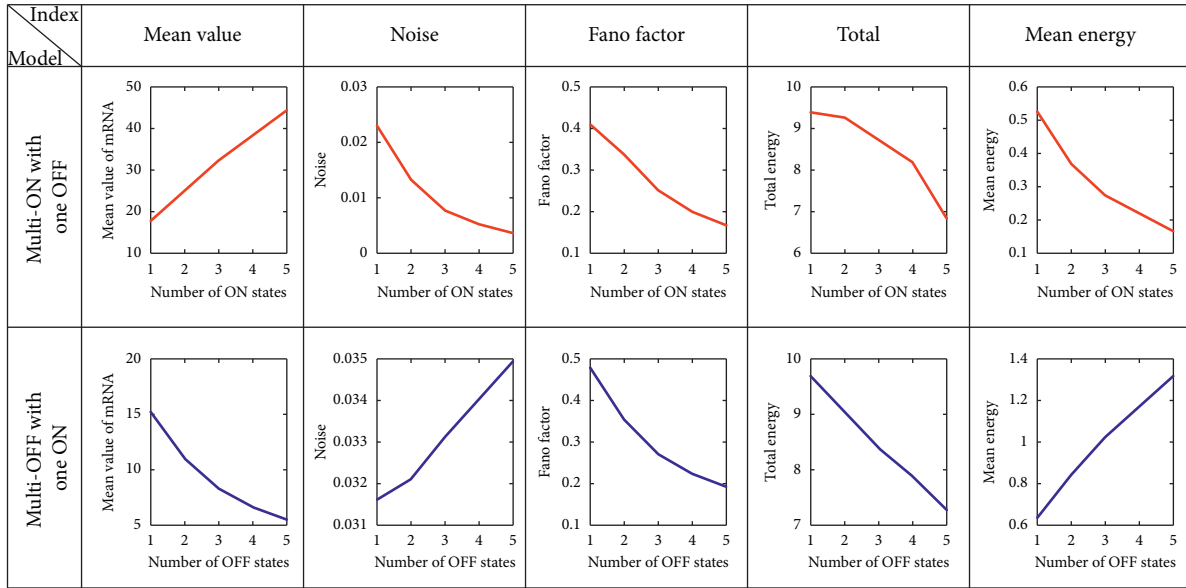
FIGURE 5: Effect of promoter's multiple states on energy consumption and gene expression (mean, noise, and Fano factor). In all the cases, the rates of activator or inhibitor association and dissociation are set as 0.27 and 0.23; that is, the switch rates of the promoter states are set as $\lambda_{01} = 0.27, \lambda_{10} = 0.23, \lambda_{12} = 0.27, \lambda_{21} = 0.23, \lambda_{23} = 0.27, \lambda_{32} = 0.23, \ldots, \lambda_{n0} = 0.27$, and $\lambda_{0n} = 0.23$, the transcription rates are set as $\mu = 33$, $\mu_1 = 33, \mu_2 = 43, \mu_3 = 53, \mu_4 = 63, \mu_5 = 73$, and degradation rate as $\delta = 1$.
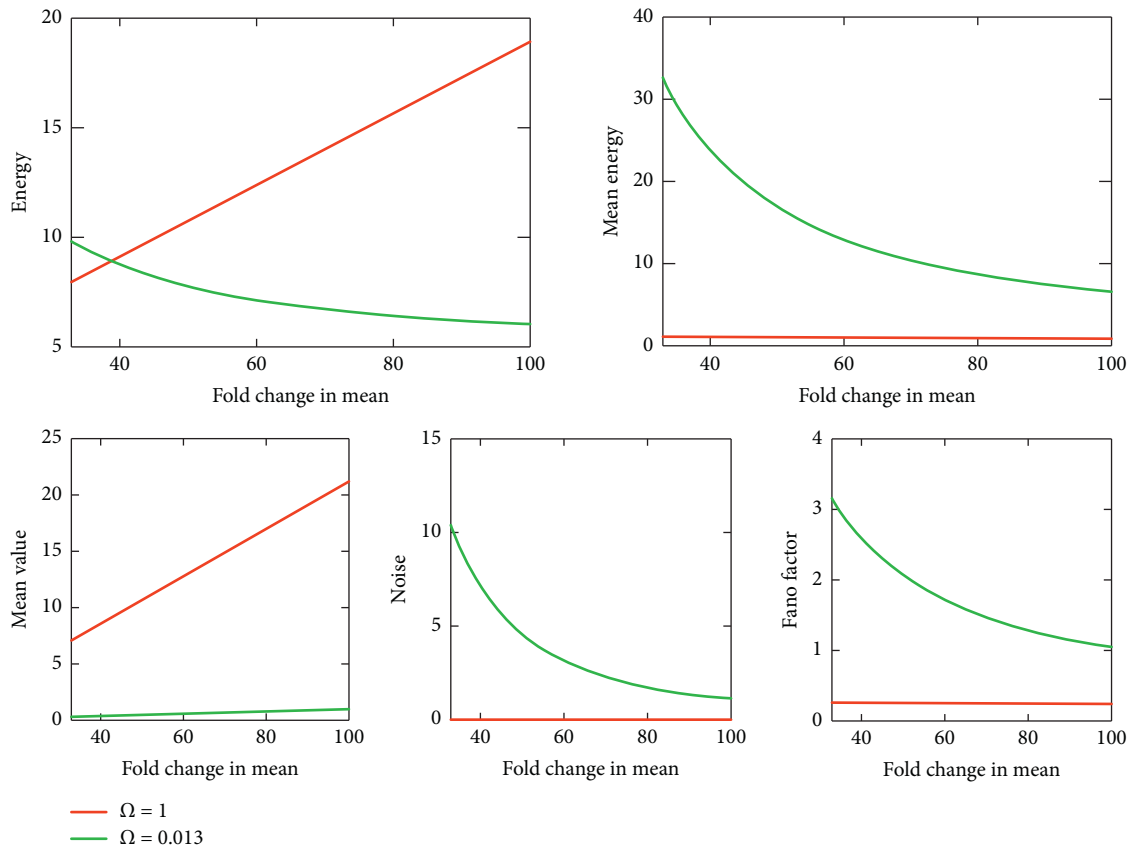
FIGURE 6: Free energy consumption of dual repression and its effect on gene expression (mean, noise, and Fano factor); parameter values are set as $k_R^{on} = 0.27, k_R^{off} = 0.23$, and $\mu = 33$.
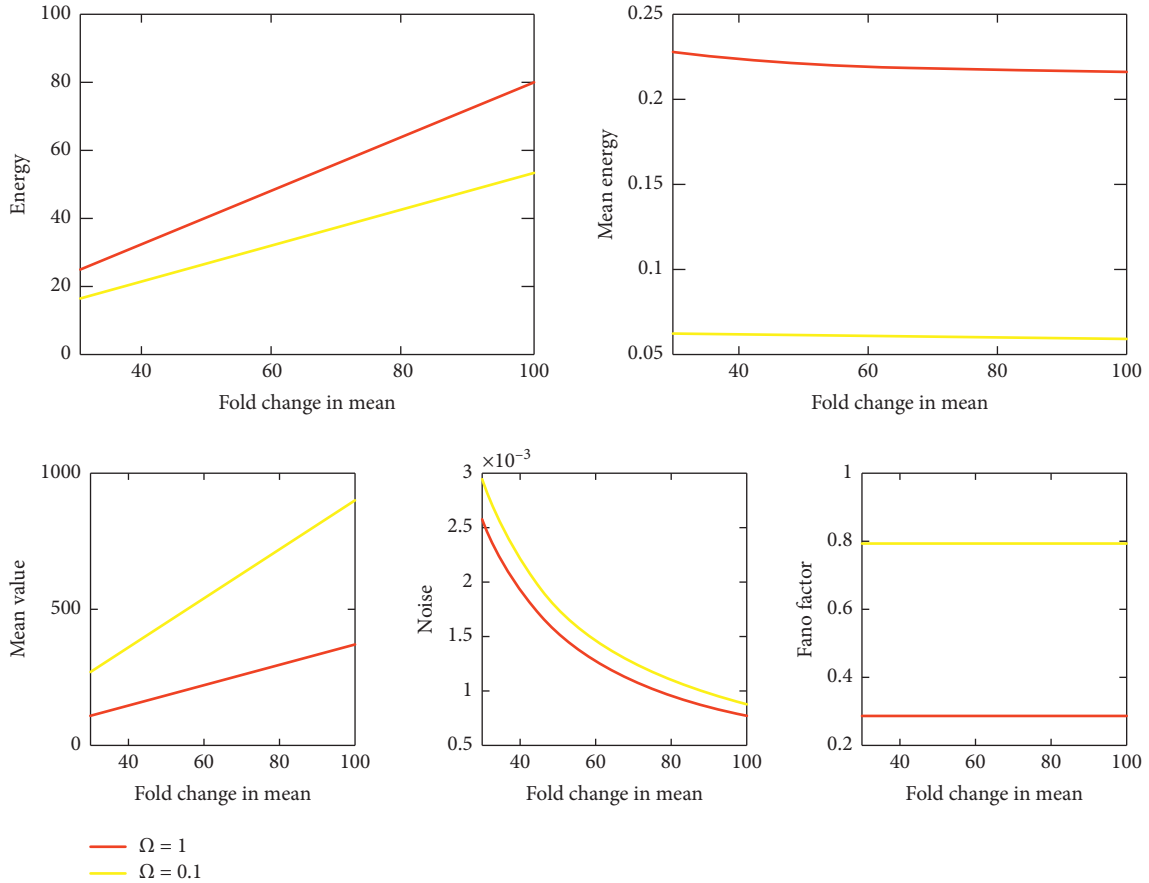
FIGURE 7: Free energy consumption of dual promotion and its effect on gene expression (including mean, noise, and Fano factor); parameter values are set as $k_A^{on} = 0.27, k_A^{off} = 0.23, \eta_1 = 33$, and $\eta_2 = 33 \times f, f = 11$.

binding of double activators can significantly increase the mean value, but the noise and Fano factor also increase.

From Figures 6 and 7, we can conclude that the cooperative binding can amplify the effect; that is to say, the cooperative binding of a double suppressor can make the inhibition effect stronger, while the cooperative binding of double activator can make the promotion effect stronger, which can be seen from the mean comparison chart. No matter the kind of cooperative binding, cooperative binding can always reduce the total free energy consumption and increase the value of noise and Fano factor; in other words, cooperative binding can reduce the free energy consumption and increase the risk of cell mutation.

4. Discussions

All living organisms not only have the ability to collect information about their environment but also adjust their internal physiological states in response to environmental changes. This common property also includes single cells' ability to respond to various possible changes in their environment by regulating their gene expression patterns. As a matter of fact, much of this regulation occurs at the transcription initiation level and is mediated by physical or chemical interactions between TFs and DNA sites, leading to many transcriptionally active and inactive states that form complex promoter structure. In addition, in prokaryotic and eukaryotic cells, the association and dissociation of most regulatory molecules (e.g., TFs) involve cooperation and competition with the other regulatory molecules bound to the DNA sites (or the promoter). Many important biological events occurring in gene expression such as DNA looping, chromatin open/closed state, and DNA methylation are also important factors impacting gene expression and are influenced by the regulatory molecules present on the promoter in a dynamic, highly combinatorial, and possibly energy-dependent manner. The combination of all these aspects also takes place in RNA polymerase recruitment and provides the promoter with various possible levels of transcriptional competency, far from the binary vision of all-or-nothing active and inactive genes.

In this paper, we have analyzed the dynamics of a single-gene promoter with an arbitrarily complex structure, focusing on the calculation of energetic cost (quantified by the energy consumption rate). Importantly, we have developed an analytical yet effective method to free energy consumed in gene transcription, which not only can greatly reduce computational complexity but also can provide an intuitive understanding of free energy dissipation in gene transcription. In particular, the derived formulas for the calculation of the energy consumption rate provide useful information on the global behavior of the underlying gene system.

Although our calculation framework is general, we do not consider the effect of feedback regulation on promoter kinetics and gene expression. However, feedback regulation is ubiquitous in gene regulatory networks. In our case, this corresponds to the case that every component of the promoter matrix describing promoter kinetics is a function of the system's state. Correspondingly, the gene promoter may exhibit more complex behavior. How free energy consumption is calculated and the mechanism of how energy consumption affects gene expression remain unexplored. It would not be difficult to extend the computational method for free energy consumption proposed in this paper to the case of feedback regulation.

Finally, modern system biology has set gene networks to the front of the stage, expecting complexity arising from the interactions among many genes. Currently, it seems that more attention should be paid to single nodes of these networks since spontaneous stochastic kinetics of the promoters are an unneglectable, considerable source of complexity. The connection between network and expression behaviors is worth further study from the viewpoint of energy consumption.

Appendixes

A. The General Theory of Entropy Generation Rate

For a Markovian biochemical reaction network, let $W(\eta' \mid \eta)$ represent the transition rate for state η to state η' in state space, and let $P(\eta, t)$ be the probability that the system is in

state η at time t. Then, the corresponding chemical master equation takes the form

$$\frac{\partial}{\partial t} P(\eta; t) = \sum_{\eta'} J(\eta' \mid \eta, t), \tag{A.1}$$

where

$$J(\eta' \mid \eta, t) = W(\eta' \mid \eta) P(\eta', t) - W(\eta \mid \eta') P(\eta, t), \tag{A.1a}$$

is the probability flow. Using this flow, if we define the entropy flux rate as

$$\Phi(t) = -\sum_{\eta, \eta'} J(\eta' \mid \eta, t) \log W(\eta' \mid \eta), \tag{A.2}$$

then the generation rate of the entropy is given by

$$\Pi(t) = -\sum_{\eta, \eta'} J(\eta' \mid \eta, t) \log\left[W(\eta' \mid \eta) P(\eta; t) \right]. \tag{A.3}$$

In fact, according to the definition of Shannon entropy, we know that the system's entropy is $S(t) = -\sum_{\eta} P(\eta; t) \log P(\eta; t)$ (which should be rewritten as the form of integral if η is a continuous variable). The derivative of $S(t)$ with regard to t yields

$$\frac{dS}{dt} = -\sum_{\eta} \left[\log P(\eta; t) + 1 \right] \frac{\partial}{\partial t} P(\eta; t). \tag{A.4}$$

Since $(\partial/\partial t) P(\eta; t) = \sum_{\eta'} J(\eta' \mid \eta, t)$, we have

$$\frac{dS}{dt} = -\sum_{\eta, \eta'} \left[\log P(\eta; t) + 1 \right] J(\eta' \mid \eta, t) = -\sum_{\eta, \eta'} J(\eta' \mid \eta, t) \log P(\eta; t) - \sum_{\eta, \eta'} J(\eta' \mid \eta, t). \tag{A.5}$$

Using $\Phi = -\sum_{\eta, \eta'} J(\eta' \mid \eta, t) \log W(\eta' \mid \eta)$, we can derive

$$\frac{dS}{dt} = -\sum_{\eta, \eta'} J(\eta' \mid \eta, t) \left\{ \log\left[P(\eta; t) W(\eta' \mid \eta) \right] + 1 \right\} - \Phi. \tag{A.6}$$

Note that

$$\sum_{\eta, \eta'} J(\eta' \mid \eta, t) = \sum_{\eta, \eta'} \left[P(\eta'; t) W(\eta \mid \eta') - P(\eta; t) W(\eta' \mid \eta) \right] = 0. \tag{A.7}$$

Since $(dS/dt) = \Pi - \Phi$, we thus prove equation (A 3).

B. Entropy Generation Rate Theory Corresponding to Fokker-Planck Equation

Consider the following Fokker-Planck equation:

$$\frac{\partial P(x; t)}{\partial t} = -\sum_{i=1}^{n} \frac{\partial}{\partial x_i} \left[\mu_i(x, t) P(x; t) \right] + \frac{1}{2} \sum_{i,j=1}^{n} \frac{\partial^2}{\partial x_i \partial x_j} \left[D_{ij}(x, t) P(x; t) \right]. \tag{B.1}$$

The entropy of the system is

$$S(t) = -\int P(x; t) \ln P(x; t) dx. \tag{B.2}$$

Differentiating both sides with regard to time t yields

$$\frac{d}{dt} S(t) = -\int \left[1 + \ln P(x; t) \right] \frac{\partial}{\partial t} P(x; t) dx. \tag{B.3}$$

Note that equation (B.1) may be rewritten as

$$\frac{\partial P(x; t)}{\partial t} = -\frac{\partial J}{\partial x}, \tag{B.4}$$

where

$$J(\mathbf{x}, t) = \sum_{i=1}^{n} \left[\mu_i(\mathbf{x}, t) P(\mathbf{x}, t) - \frac{1}{2} \sum_{j=1}^{n} \frac{\partial}{\partial x_j} \left[D_{ij}(\mathbf{x}, t) P(\mathbf{x}, t) \right] \right]. \tag{B.5}$$

Using equation (B.4), it follows from equation (B.3) that

$$\frac{\mathrm{d}}{\mathrm{d}t} S(t) = \int [1 + \ln P(x;t)] \frac{\partial J(x,t)}{\partial x} \mathrm{d}x = - \int J(x,t) \frac{\partial \ln P(x;t)}{\partial x} \mathrm{d}x. \tag{B.6}$$

Thus,

$$\frac{\mathrm{d}}{\mathrm{d}t} S(t) = -\Phi + \Pi \equiv -\sum_{i=1}^{n} \int \mu_i(\mathbf{x}, t) \frac{\partial P(\mathbf{x}, t)}{\partial x_i} \mathrm{d}x_i + \frac{1}{2} \sum_{i=1}^{n} \int \sum_{j=1}^{n} \frac{\partial}{\partial x_j} \left[D_{ij}(\mathbf{x}, t) P(\mathbf{x}, t) \right] \frac{\partial \ln P(\mathbf{x}, t)}{\partial x_i} \mathrm{d}x_i, \tag{B.7}$$

where $\Pi = 1/2 \sum_{i=1}^{n} \int \sum_{j=1}^{n} (\partial/\partial x_j) [D_{ij}(\mathbf{x}, t) P(\mathbf{x}, t)] ((\partial \ln P(\mathbf{x}, t))/\partial x_i) \mathrm{d}x_i$ represents the generation rate of the entropy and $\Phi = -\sum_{i=1}^{n} \int \mu_i(\mathbf{x}, t)(\partial P(\mathbf{x}, t)/\partial x_i) \mathrm{d}x_i$ represents the entropy flux rate.

Data Availability

The data used in the study are included in the article.

Conflicts of Interest

The authors declare that they have no conflicts of interest.

Acknowledgments

References

[1] C. Zhu, G. Han, and F. Jiao, "Dynamical regulation of mRNA distribution by cross-talking signaling pathways," *Complexity*, vol. 2020, Article ID 6402703, 11 pages, 2020.

[2] F. Jiao, "Analytical formula and dynamic profile of mRNA distribution," *Discrete & Continuous Dynamical Systems Series B*, vol. 25, no. 1, pp. 3475–3502, 2020.

[3] A. Sanchez, S. Choubey, and J. Kondev, "Regulation of noise in gene expression," *Annual Review of Biophysics*, vol. 42, no. 1, pp. 469–491, 2013.

[4] S. Rafael and d. L. Víctor, "Noise and robustness in prokaryotic regulatory networks," *Annual Review of Microbiology*, vol. 64, no. 1, pp. 257–275, 2010.

[5] L. Huang, Z. Yuan, P. Liu, and T. Zhou, "Feedback-induced counterintuitive correlations of gene expression noise with bursting kinetics," *Physical Review E*, vol. 90, no. 5, Article ID 052702, 2014.

[6] G. Hornung and N. Barkai, "Noise propagation and signaling sensitivity in biological networks: a role for positive feedback," *PloS Computational Biology*, vol. 4, no. 1, pp. 4–8, 2008.

[7] J. Peccoud and B. Ycart, "Markovian modeling of gene-product synthesis," *Theoretical Population Biology*, vol. 48, no. 2, pp. 222–234, 1995.

[8] V. Shahrezaei and P. S. Swain, "Analytical distributions for stochastic gene expression," *Proceedings of the National Academy of Sciences*, vol. 105, no. 45, pp. 17256–17261, 2008.

[9] M. Dobrzy´nski and F. J. Bruggeman, "Elongation dynamics shape bursty transcription and translation," *Proceedings of the National Academy of Sciences*, vol. 106, no. 8, pp. 2583–2588, 2009.

[10] J. Ren, F. Jiao, and J. Yu, "Nonlinear dynamics and noise actuated by the cycle of gene inactivation in stochastic transcription," *Communications in Nonlinear Science and Numerical Simulation*, vol. 91, Article ID 105398, 2020.

[11] N. Rosenfeld, M. B. Elowitz, and U. Alon, "Negative autoregulation speeds the response times of transcription networks," *Journal of Molecular Biology*, vol. 323, no. 5, pp. 785–793, 2002.

[12] A. Singh and J. P. Hespanha, "Optimal feedback strength for noise suppression in autoregulatory gene networks," *Biophysical Journal*, vol. 96, no. 10, pp. 4013–4023, 2009.

[13] D. J. Stekel and D. J. Jenkins, "Strong negative self-regulation of prokaryotic transcription factors increases the intrinsic noise of protein expression," *BMC Systems Biology*, vol. 2, no. 1, 2008.

[14] W. J. Blake, M. KÆrn, C. R. Cantor, and J. J. Collins, "Noise in eukaryotic gene expression," *Nature*, vol. 422, no. 6932, pp. 633–637, 2003.

[15] J. M. G. Vilar and amd L. Saiz, "CplexA: a mathematica package to study macromolecular-assembly control of gene expression," *Bioinformatics*, vol. 26, no. 16, pp. 2060-2061, 2010.

[16] H. Boeger, J. Griesenbeck, and R. D. Kornberg, "Nucleosome retention and the stochastic nature of promoter chromatin remodeling for transcription," *Cell*, vol. 133, no. 4, pp. 716–726, 2008.

[17] L. M. Octavio, K. Gedeon, and N. Maheshri, "Epigenetic and conventional regulation is distributed among activators of FLO11 allowing tuning of population-level heterogeneity in its expression," *PLoS Genetics*, vol. 5, no. 10, Article ID e1000673, 2009.

[18] L. Weinberger, Y. Voichek, I. Tirosh, G. Hornung, I. Amit, and N. Barkai, "Expression noise and acetylation profiles distinguish HDAC functions," *Molecular Cell*, vol. 47, no. 2, pp. 193–202, 2012.

[19] B. Schwanhäusser, D. Busse, N. Li et al., "Global quantification of mammalian gene expression control," *Nature*, vol. 473, no. 7347, pp. 337–342, 2011.

[20] A. Coulon, O. Gandrillon, and G. Beslon, "On the spontaneous stochastic dynamics of a single gene: complexity of the

molecular interplay at the promoter," *BMC Systems Biology*, vol. 4, no. 2, p. 18, 2010.

[21] Y. Cao, H. Wang, Q. Ouyang, and Y. Tu, "The free-energy cost of accurate biochemical oscillations," *Nature Physics*, vol. 11, no. 9, pp. 772–778, 2015.

[22] A. Wagner, "Energy constraints on the evolution of gene expression," *Molecular Biology and Evolution*, vol. 22, no. 6, pp. 1365–1374, 2005.

[23] P. Mehta and D. J. Schwab, "Energetic costs of cellular computation," *Proceedings of the National Academy of Sciences*, vol. 109, no. 44, pp. 17978–17982, 2012.

[24] C. Li and J. Wang, "Landscape and flux reveal a new global view and physical quantification of mammalian cell cycle," *Proceedings of the National Academy of Sciences*, vol. 111, no. 39, pp. 14130–14135, 2014.

[25] J. Wang, K. Zhang, L. Xu, and E. Wang, "Quantifying the waddington landscape and biological paths for development and differentiation," *Proceedings of the National Academy of Sciences*, vol. 108, no. 20, pp. 8257–8262, 2011.

[26] Y. J. Chen, S. Johnson, P. Mulligan, A. J. Spakowitz, and R. Phillips, "Modulation of DNA loop lifetimes by the free energy of loop formation," *Proceedings of the National Academy of Sciences*, vol. 111, no. 49, pp. 17396–17401, 2015.

[27] L. Bintu, N. E. Buchler, H. G. Garcia et al., "Transcriptional regulation by the numbers: models," *Current Opinion in Genetics & Development*, vol. 15, no. 2, pp. 116–124, 2005.

[28] H. Ge and H. Qian, "Physical origins of entropy production, free energy dissipation, and their mathematical representations," *Physical Review E*, vol. 81, Article ID 051133, 2010.

[29] L. Huang, Z. Yuan, J. Yu, and T. Zhou, "Fundamental principles of energy consumption for gene expression," *Chaos*, vol. 25, Article ID 123101, 2015.

[30] J. Zhang and T. Zhou, "Promoter-mediated transcriptional dynamics," *Biophysical Journal*, vol. 106, no. 2, pp. 479–488, 2014.

[31] A. Sanchez, H. G. Garcia, D. Jones D, R. Phillips, and J. Kondev, "Effect of promoter architecture on the cell-to-cell variability in gene expression," *PLoS Computational Biology*, vol. 7, no. 3, Article ID e1001100, 2011.

[32] J. L. Lebowitz and H. Spohn, "A Gallavotti-Cohen-type symmetry in the large deviation functional for stochastic dynamics," *Journal of Statistical Physics*, vol. 95, no. 1/2, pp. 333–365, 1999.

[33] G. Lan, P. Sartori, S. Neumann, V. Sourjik, and Y. Tu, "The energy-speed accuracy trade-off in sensory adaptation," *Nature Physics*, vol. 8, no. 2276, pp. 422–428, 2012.

[34] P. Sartori and Y. Tu, "Free energy cost of reducing noise while maintaining a high sensitivity," *Physical Review Letters*, vol. 115, no. 11, Article ID 118102, 2015.

[35] T. Tomé and M. J. de Oliveira, "Entropy production in irreversible systems described by a Fokker-Planck equation," *Physical Review E*, vol. 82, no. 2, Article ID 021120, 2010.

[36] G. A. Casas, F. D. Nobre, and E. M. F. Curado, "Entropy production and nonlinear Fokker-Planck equations," *Physical Review E*, vol. 86, no. 6, Article ID 061136, 2012.

[37] H. Qian, "Phosphorylation energy hypothesis: open chemical systems and their biological functions," *Annual Review of Physical Chemistry*, vol. 58, no. 1, pp. 113–142, 2007.

[38] N. E. Buchler, U. Gerland, and T. Hwa, "On schemes of combinatorial transcription logic," *Proceedings of the National Academy of Sciences*, vol. 100, no. 9, pp. 5135–5141, 2003.

[39] M. L. Simpson, C. D. Cox, and G. S. Sayler, "Frequency domain analysis of noise in autoregulated gene circuits," *Proceedings of the National Academy of Sciences*, vol. 100, no. 8, pp. 4551–4556, 2003.

[40] F. Jiao and C. Zhu, "Regulation of gene activation by competitive cross talking pathways," *Biophysical Journal*, vol. 119, pp. 1–11, 2020.

WILEY | Hindawi

Research Article

MTAD-TF: Multivariate Time Series Anomaly Detection Using the Combination of Temporal Pattern and Feature Pattern

Q. He [ID],[1] Y. J. Zheng [ID],[1] C.L. Zhang [ID],[1,2] and H. Y. Wang [ID][1]

[1]*School of Science, Beijing University of Civil Engineering and Architecture, Beijing 100044, China*
[2]*Beijing Advanced Innovation Center for Future Urban Design, Beijing University of Civil Engineering and Architecture, Beijing 100044, China*

Correspondence should be addressed to Q. He; heqiang@bucea.edu.cn

Currently, multivariate time series anomaly detection has made great progress in many fields and occupied an important position. The common limitation of many related studies is that there is only temporal pattern without capturing the relationship between variables and the loss of information leads to false warnings. Our article proposes an unsupervised multivariate time series anomaly detection. In the prediction part, multiscale convolution and graph attention network are mainly used to capture information in temporal pattern with feature pattern. The threshold selection part uses the root mean square error between the predicted value and the actual value to perform extreme value analysis to obtain the threshold. Finally, the model in this paper outperforms other latest models on actual datasets.

1. Introduction

Anomaly detection of time series data has always been a hot issue in academia and industry. The detection of abnormal points and the location of abnormal areas can provide important information at critical moments, so that people can intervene with abnormal events in a targeted way to prevent or eliminate abnormal events. Anomaly detection of time series data has attracted people's attention in industry, finance, military, medical treatment, insurance, robotics, multiagent, network security, IOT, complex biological systems, etc. [1, 2].

The anomaly detection of time series is to detect points with outliers, oscillations, or other abnormal conditions. In general, the proportion of anomalies in the overall time series is very low, so people hope to successfully capture the outliers by learning the distribution of original data or other characteristics through the algorithm. Univariate anomaly detection is carried out on the time series with only one feature. Since there is only one dimension of data, many traditional filtering algorithms can be used, that is, spectral residual algorithm [3]. Multivariate time series anomaly

detection refers to the anomaly detection of time series data with multiple sequences. This kind of problem is extended based on univariate time series anomaly detection. The occurrence of anomalies in multivariate time series data is often determined by multiple features, and the individual analysis of each feature cannot accurately locate the anomalies. Complex biological systems generally have this characteristic. For example, time series data from an epidemic model may include the number of patients, the number of healthy people, infection rate and the immunization rate, etc. The severity of epidemic cannot be judged by partial characteristics. Therefore, a more reasonable method is to comprehensively analyse multiple variables to identify anomalies.

At present, significant progress has been made in the study of MTAD (multivariate time series anomaly detection) in deep learning. For example, Malhotra et al. [4] proposed an encoder-decoder network based on LSTM, which modelled the reconstruction probability of "normal" time series and used reconstruction errors to detect anomalies in multiple sensors. Hundman et al. [5] used the long- and short-time memory network (LSTM) to detect the spacecraft

multivariate time series based on prediction loss. Ding et al. [6] proposed RADM, a real-time anomaly detection algorithm based on Hierarchical Temporal Memory (HTM) and Bayesian Network (BN), which improved the performance of real-time anomaly detection. However, most of the proposed methods often rely on the RNN (Recurrent Neural Network) learning properties and distribution in temporal pattern; relationship between sequences is still unutilized. Therefore, we believe that new latent dependencies can be exploited from feature pattern, which is more conductive to anomaly detection. We propose a method combination of temporal pattern and feature pattern.

Our main contribution is as follows:

(1) To the best of our knowledge, this is the first study on multivariate time series anomaly detection generally from a graph-based perspective with graph attention network in forecast

(2) We propose a new model that combines temporal with feature pattern, capturing more latent relationship between variables

(3) Experimental results show that our method outperforms the state-of-the-art methods on 3 benchmarks

The arrangement of this article is as follows. We give related work on time series anomaly detection in Section 2. In Section 3, the prerequisite knowledge of GAT and GRU in the model is introduced. In Section 4, the proposed method is introduced in detail. The fifth section conducts experiments and analysis. Finally, we summarize the full text.

2. Related Work

Anomaly detection is also known as novelty detection, outlier detection, or event detection in other related fields [7]. Time series anomaly detection is one of the most concerning problems. It can be classified into supervised, semisupervised, and unsupervised abnormal detection according to whether labels are used during training. Supervised learning method [8] requires labelled data for training and can only identify known abnormal types [9], so its application scope is limited. Semisupervised method is a kind of learning method combining supervised learning and unsupervised learning. Semisupervised method uses a large amount of untagged data as well as tagged data, rarely studied in the field of TSAD (Time Series Anomaly Detection). Therefore, research of TSAD focuses on the unsupervised problem.

According to the number of sequences in the data, the problem can be divided into univariate and multivariate time series anomaly detection. Univariate time series anomaly detection [3, 10, 11] only considers whether the variables conforms to long-term pattern; when there is a big difference between data value and the overall distribution, it is regarded as an outlier instance. The traditional method in univariate time series anomaly detection is to use mainly hand-made features to model patterns of normal and abnormal events [12]. For example, there are SVD [13], wavelet

analysis [9], ARIMA [14], and so on. Besides, Netflix released a document based on robust Principal Component Analysis [15] and received a good response. Twitter also published a method which uses the seasonal hybrid extreme study deviation test (S-H-ESD) [16]. In addition, the use of neural networks for detection has also made great progress [17]. Multivariable problems have multiple variables on each timestamp [18]. The existing multivariate time series anomaly detection methods can be divided into two categories: (1) univariate based anomaly detection [15], where each sequence is monitored separately by univariate algorithm and the results are summarized to give the final judgment, and (2) direct anomaly detection [19], where multiple features are considered at the same time for algorithm analysis. Let us focus on the second type of approach. Zong et al. [20] proposed a model which uses deep autoencoder to generate low dimensional data, represent the reconstruction errors of each input data point, and input into a Gaussian mixture model (GMM) for multivariable anomaly detection. LSTM-VAE algorithm [7] is a LSTM network based on encoder-decoder to reconstruct the error of time series and use the reconstruction error to detect the abnormal situation of some sensors. LSTM-NDT [5] is an unsupervised algorithm without parameter threshold selection. The objective of this paper is to establish an anomaly detection system to monitor the data sent back by the spacecraft which is marked by experts in related fields.

Graph neural network is very popular in recent years which have enjoyed great progress in dealing with spatial dependencies among entities in a network. Gugulothu et al. [21] combined nontime pattern reduction technology and periodic automatic encoder through the end-to-end learning framework for time series modelling. OmniAnomaly [22] proposes a stochastic recurrent neural network that captures the normal pattern of multiple variable through modelling data distribution with stochastic variables.

3. Preliminaries

3.1. Problem Statement. When analysing real-world datasets, a common requirement is to find out those instances that can be considered as outliers, which are significantly different from most other points. The goal of the anomaly detection task is to be data-driven to find abnormal of all samples. In our work, we are concerned about multivariable data $X = \{x_1, x_2, \ldots, x_N\} \in \mathbb{R}^{m*n}$; the value at time i is $x_i \in \mathbb{R}^m, i = 1, 2, \ldots, n$. m means there are m variables and n is the length of data. Our target is to determine whether x_t is an abnormal point. This is a time series problem; we have a huge amount of data; historical data is helpful for understanding the current moment x_t. To efficiently use and learn the information of X, sliding window w: $x_{t-w}, x_{t-w+1}, \ldots, x_{t-1}$ used to predict x_t which would be considered to be normal. The difference between the predicted x_t with the ground truth will be put into the threshold selection module; the larger the difference, the greater the possibility of x_t being abnormal; when such difference exceeds the threshold we set, we consider it to be an abnormality.

3.2. Basics of GAT and GRU

3.2.1. GAT (Graph Attention Network).

We know that many data are in Euclidean space. The most significant characteristic of data in Euclidean space is that it has a regular spatial structure. For example, the picture is a regular square grid, the voice data is a one-dimensional sequence, and so on. These data can be represented by a one-dimensional or two-dimensional matrix. However, many data in real life do not have a regular spatial structure, that is, data in non-Euclidean space, such as abstract graphs of electronic transactions, recommendation systems, social networks, and so on; each node in the graph is related to other nodes. The connection is not fixed. Therefore, people use graph neural networks to model data in non-Euclidean spaces. In recent years, due to the strong expressiveness of graph structure, the research of analysing graphs with machine learning methods has received more and more attention. Graph neural network (GNN) is a method of processing graph pattern information based on deep learning. Due to its better performance and interpretability, GNN has become a widely used graph analysis method. Commonly used graph neural networks include Graph convolution networks, graph attention networks, and graph autoencoder. Among them, GAT [23] proposes to utilize the attention mechanism to add weighted features of neighbouring nodes. The weight of neighbouring node features completely depends on the node, independent of the graph structure. In our model, to find the latent relationship between variables, we use GAT to calculate the correlation between nodes. The specific details are explained in Section 4.3.

3.2.2. GRU (Gated Recurrent Unit).

Recurrent neural network (RNN) is a kind of neural network that captures the dynamic information in serialized data through the periodic connection of nodes in the hidden layer. It is different from feedforward neural networks; RNN can save the state of a context and even store, learn and express relevant information in any long context window. No longer limited to the spatial boundaries of traditional neural networks, it can be extended in time series. Intuitively speaking, there is an edge between the nodes of the hidden layer of this time and the hidden layer of the next moment. But RNN's most significant drawback is that it cannot learn to preserve and exploit older information, namely, gradient vanishing and gradient explosion. Sepp Hochreiter and Jurgen Schmidhuber proposed long- and short-term memory (LSTM) in 1997 [24]. LSTM is a kind of periodic neural network, which alleviates the problem of RNN to some extent. Practice shows that this method is very suitable for processing time series data. In fact, the LSTM algorithm has evolved many variations in recent years. Rafal Jozefowicz et al. of Google conducted a comprehensive architecture search to evaluate over 10,000 different RNN/LSTM architectures [25] and as a result we could not find an architecture with better performance than the GRU, and, except for the language model, GRU works better than LSTM in other application scenarios. GRU (Gated Recurrent Unit) is a variant of LSTM, which has fewer parameters and is more efficient than LSTM. Hence, our model chooses GRU structure instead of LSTM.

Cho et al. [26] proposed a Gated Recurrent Unit (GRU) to enable each recursive unit to adaptively capture the dependencies of different time scales. Like classical recurrent neural networks, GRU are a chain of neural units too. Its structure is expressed mathematically as follows:

$$
\begin{aligned}
r_t &= \sigma\left(W_r \cdot \left[h_{t-p}, x_t\right]\right), \\
z_t &= \sigma\left(W_z \cdot \left[h_{t-p}, x_t\right]\right), \\
\widetilde{h}_t &= \tanh\left(W_{\widetilde{h}} \cdot \left[r_t * h_{t-p}, x_t\right]\right), \quad h_t = (1 - z_t) * h_{t-p} + z_t * \widetilde{h}_t, \quad y_{ts} = \sigma\left(W_o \cdot h_t\right).
\end{aligned}
\tag{1}
$$

x_t and h_{t-1} represent the input at the current time and the output $\widetilde{h}_t = \tanh(W_{\widetilde{h}} \cdot [r_t * h_{t-p}, x_t])$ at the next time. Where r_t is a set of reset gates, it is used to control how much information about previous state is forgotten. The smaller the value of reset gate, the more the past information is discarded. z_t is update gates. The update gate is used to control the degree how much information from the previous moment is brought into the current state. The larger the value is, the more the information from the current needs to remain and the less the information from the previous neuron can be retained. (,) represents two vectors concatenate, and $*$ is an element-wise multiplication.

σ is the commonly used sigmoid function which controls numbers between 0 and 1. We are accustomed to using tanh function (hyperbolic tangent function) as hidden update activation function:

$$
\begin{aligned}
\text{sigmoid: } y &= \frac{1}{\left(1 + e^{-x}\right)}, \\
\tanh: y &= \frac{\left(e^x - e^{-x}\right)}{\left(e^x + e^{-x}\right)}.
\end{aligned}
\tag{2}
$$

4. Proposed Model

4.1. Model Architecture.

As demonstrated in Figure 1, our framework consists of three core components: the temporal convolution model, the graph attention model, and threshold select model. The result obtained in the first two models is the forecasting of our MTAD-TF. The root mean square error (RMSE) between the forecasted result and the real value is input to the error threshold selection model. If the error exceeds the threshold which we set through POT, it is considered that an anomaly occurs at the moment.
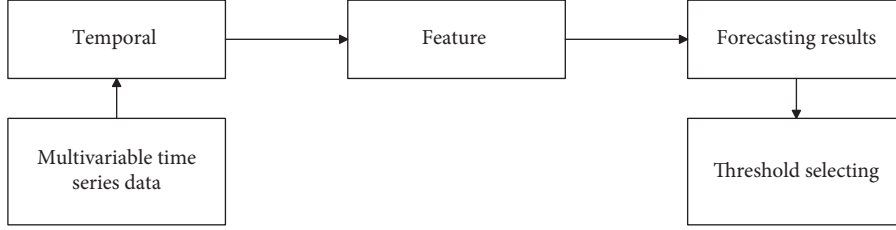
FIGURE 1: Overview of MTAD-TF.

The explanation of the forecasting model is as follows:

(i) Temporal convolution component: we propose a temporal convolution model to capture temporal patterns by multiscale 1D convolutions, which can find temporal patterns with multiple periods

(ii) Graph attention component: the graph attention network is used in the feature dimension; the interrelation between variables is beneficial to forecast the time series

4.2. Data Preprocessing.

For a multivariable time series, the dimensions of different variables are quite different. We cannot allow these differences to affect subsequent prediction and threshold selection. Therefore, we preprocess the data with the maximum-minimum normalization method in both training subsets with testing subsets:

$$\widehat{x}_t = \frac{x_t - \min X_{\text{training}}}{\max X_{\text{training}} - \min X_{\text{training}}}. \tag{3}$$

4.3. Forecasting Model.

The overview of the proposed model is shown in Figure 2. First, for the sake of alleviating the possible noise effects of the original data X, 1D convolution operation is carried out to smooth the data:

$$X_{\text{CNN}} = \text{RELU}\left(W_{\text{CNN}} * X + b_{\text{CNN}}\right),$$
$$\text{RELU} = \max\left(0, x\right). \tag{4}$$

The result of convolution X_{CNN} is then fed into three identical blocks which are shown as green box. Each block has temporal convolution component in series with graph attention networks.

4.3.1. Temporal Convolution Component.

The temporal convolution module captures sequential patterns of time series data in temporal dimension through 1D convolutional filters to come up with a temporal convolution module that is able to both discover temporal patterns with various ranges and handle long sequences, that is, using multiscale convolution filters [27]. However, how to choose the correct filter size is a challenging problem. To understand convolution in terms of communication theory and image processing, the convolution kernel size is generally set to odd [28]. The reasons are as follows: compared with even numbers, odd numbers have a center point and are more sensitive to edges and lines, which can extract edge information more effectively and avoid the

deviation of position information. In addition, the odd number can ensure that the two sides of the image are symmetrical to each other when padding, so that size of the output image is the same as size of the input. Therefore, as shown in Figure 3, we select filters sizes of 1×3, 1×5, 1×7, and 1×9 which consist of temporal inception layer. The combination of these filters of different sizes can contain some periodic temporal signals, such as data of period 12. The model can start the input layer from the first temporal convolution layer through the 1×5 and then from the second temporal convolution layer through the 1×7. The selection of small convolution kernel can not only reduce the parameters but also add more nonlinear mappings to improve the robustness. Finally, we patch the results of different convolution, respectively, to restore the previous data size. The input of temporal convolution component in block 2 is the average value of GAT's output and X_{CNN}. TC component in block 3 is the average value of block 2's input (include X_{CNN}) and block 2's output.

4.3.2. Graph Attention Network Component.

Multivariate time series anomaly detection is a challenge due to the increase of variable and data volume. However, more variable also means more information which is brought. It is actually very critical for anomaly detection. Previous models did not pay attention to feature pattern, but only focus on temporal pattern. Therefore, we combine temporal pattern and feature pattern in the model. Specially, each block has a temporal convolution component that connects to a GAT. In GAT, each node in the graph can be assigned different weights based on the characteristics of its neighbor nodes. And it does not require costly matrix operations or rely on a preconceived graph structure.

The input to the graph attention layer is a set of vectors for a node: $\{v_1, v_2, \ldots, v_n\}$, where v_i have the same dimension with x_i. The output of each node calculated by the GAT layer is shown as follows:

$$h_i = \sigma\left(\sum_{j=1}^{L} \alpha_{ij} v_j\right), \tag{5}$$

$$e_{ij} = \text{Leaky RELU}\left(W \cdot \left(v_i \oplus v_j\right)\right)^{\top}. \tag{6}$$

$$\text{Leaky RELU: } y_i = \begin{cases} x_i, & \text{if } x_i \geq 0, \\ \dfrac{x_i}{a_i}, & \text{if } x_i \leq 0, \end{cases} \quad a_i \in (1, \infty), \tag{7}$$
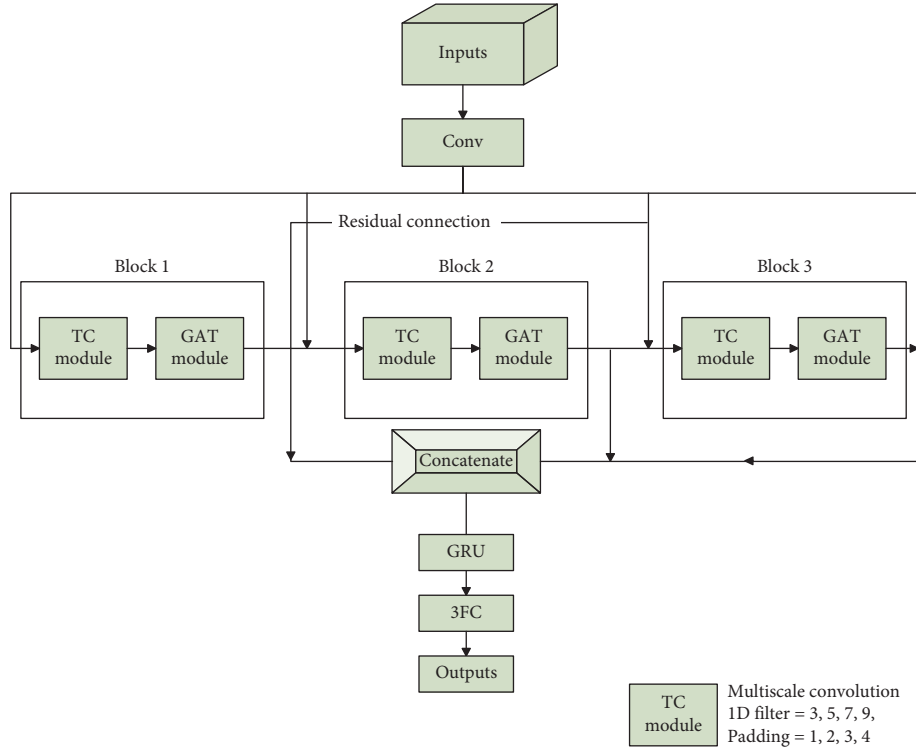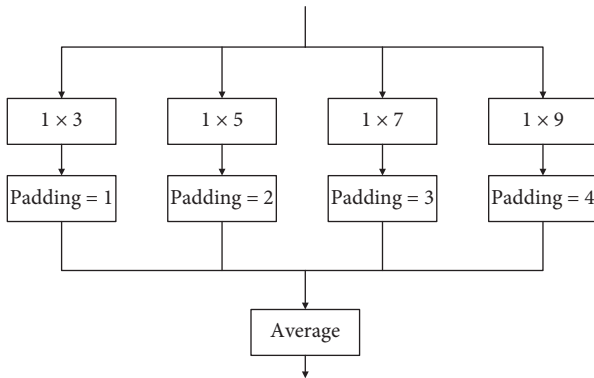
FIGURE 2: Forecasting model.

FIGURE 3: Temporal convolution component.

$$\alpha_{ij} = \frac{\exp\left(e_{ij}\right)}{\sum_{l=1}^{L} \exp\left(e_{ik}\right)}, \qquad (8)$$

where h_i is the output of node x_i with the same dimension. α_{ij} is the correlation degree between x_i and x_j like (8) is calculated: $\oplus$ is the result of concatenate of two nodes, and w is the parameters obtained by learning. Leaky RELU is a nonlinear activation function as shown in (7). L denotes the number of adjacent points to x_i.

The results of each GAT and X_{CNN} (after 1D convolution of original input X) are the data of the same dimension, which are three-dimensional tensor, and each dimension is batch size, window size, and the number of variables, respectively. The output of GAT which is in three blocks and X are concatenated in the third dimension of tensor, which

thickens the temporal information of data and is conducive to prediction from GRU. Finally, the results of the forecasting part are obtained by carrying on the three full connection layers.

4.4. Threshold Selection Model. The loss function of the prediction model selects root mean square error (RMSE) is as follows:

$$\mathrm{Loss}_{\mathrm{forecasting}}\left(t\right) = \sqrt{\sum_{i=1}^{m} \left(\widehat{y}_{t,i} - x_{t,i}\right)^2}, \qquad (9)$$

where $\widehat{y}_{t,i}$ is the prediction value of the i-th feature at time t and $x_{t,i}$ is the real value at the same time. The RMSE between them denotes loss at time t.

The test set was input to the trained forecasting model, and the RMS loss between the predicted value and the true value of each observation point in the test set was recorded as $\{l_1, l_2, \ldots, l_Q\} \in \mathbb{R}^Q$ and utilizes POT (peaks over threshold) model of EVT (extreme value theory) to select the threshold value of the subsequence.

Extreme value theory is a statistical theory to find the law of extreme values in a sequence. It is generally believed that extreme values are the outliers to be found in the problem of anomaly detection, and they are located at the tail of the distribution in most cases. The advantage of the extreme value theory is that it does not need to assume the data distribution and the threshold can be set automatically through parameter selection. The second theorem POT shows that samples larger than threshold are subject to

generalized Pareto distribution (GPD). Therefore, select the threshold th through POT:

$$\overline{F}_{th} = P(L - \text{th} > l | L > \text{th}) \sim \left(1 + \frac{\gamma l}{\beta}\right)^{1/\gamma}, \qquad (10)$$

where th is the initial threshold. γ denotes shape parameters in GPD and β is any value in scale parameters $L = \{l_1, l_2, \ldots, l_Q\}$. L-th represents the part above the threshold. th is the quantile obtained by experience. Similar to literature [10], we utilize maximum likelihood estimation (MLE) for parameter estimation of $\widehat{\gamma}$ and $\widehat{\beta}$. The threshold th_F is calculated according to the following formula:

$$\text{th}_F \simeq \text{th} - \frac{\widehat{\beta}}{\widehat{\gamma}} \left(\left(\frac{qQ}{Q_{th}}\right)^{-\widehat{\gamma}} - 1 \right). \qquad (11)$$

q is the proportion of $L > \text{th}$ and Q is the number of observed values. Q_{th} denotes the number of $L > \text{th}$. To select the threshold value of POT, the process of parameter adjustment is needed.

5. Experiment and Analysis

5.1. Benchmarks and Evaluation Metrics. Regarding datasets, we use three real-world datasets to verify the effectiveness of MTAD-TF, namely, MSL (Mars Science Laboratory) rover, SMAP (Soil Moisture Active Passive) satellite, and SMD.

MSL and SMAP are two public datasets of NASA's spacecraft [29].

SMD [22] is five weeks of server data in a large Internet company, which has been published on GitHub. SMD is divided into two parts with the same data size. The first part is the training set and the second part is the testing set. The abnormal data on the testing set has been marked by experts in related fields. Among them, the training set and the testing set contain 28 groups, which need to be trained and tested separately. That is, the model trained on the first group of data in the training set is tested by the same group of the testing set. The final score is the average of 28 groups.

The details of the three datasets are given in Table 1, including the number of variables, size of the training set and testing set, proportion of abnormal samples in the testing set, and partial variable names.

Regarding metrics, we followed the typical evaluation metrics like other anomaly detection models: precision, recall, and F1 score. They are defined as follows:

$$\text{precision}(P) = \frac{\text{TP}}{\text{TP} + \text{FP}},$$

$$\text{recall}(R) = \frac{\text{TP}}{(\text{TP} + \text{FN})}, \qquad (12)$$

$$\text{F1} = \frac{2 \times \text{precision} \times \text{recall}}{(\text{precision} + \text{recall})}.$$

Among them, TP is true positives (correctly detected anomaly), FP represents false positives (falsely detected anomaly), and FN refers to false negative (falsely detected normally). The higher the values of the above three indicators, the stronger the robustness of the model.

5.2. Baselines for Comparison. This section will show the comparison results with the other 4 baselines on 3 benchmarks. The compared models include LSTM-NDT [5], LSTM-VAE [7], DAGMM [20], and OmniAnomaly [22]:

   (i) LSTM-NDT: LSTM is used for anomaly detection of multidimensional time series which also is a dynamic and unsupervised method for determining threshold. Besides, to reduce the false positive rate and identify false positive data, a "pruning strategy" is proposed.

  (ii) LSTM-VAE: VAE's feedforward network uses LSTM replacement but does not consider the dependence between stochastic variables.

 (iii) DAGMM: combine neural network, estimation network, and Gaussian mixture model organically to do unsupervised anomaly detection.

  (iv) OmniAnomaly: the core idea of this paper is to learn latent representations to capture the normal patterns of multivariate time series while considering time dependence and stochastic.

Table 2 summarizes the evaluation results of all the baselines, which shows excellent generalization capability and achieves the best F1 score on 4 datasets.

LSTM-NDT has a high score on SMAP, but it performs poorly on MSL and SMD, reflecting that the model is very sensitive to different scenarios. Our model is stable and has excellent performance on different benchmarks.

Short-term information is also very important for multivariable time series. The reason why DAGMM's performance is not ideal is that short-term information is not considered. We utilize multiscale convolution, which can better adapt to data with different periods. This article also conducts additional ablation experiments (see Section 5.3) to compare the effectiveness of different components in our model.

OmniAnomaly applies a stochastic model, regards variables as stochastic variables, and then learns its distribution, which has high performance on the three datasets. The limitation of this model is that it does not consider the relationship between the variables.

5.3. Ablation Study. To illustrate the necessity and effectiveness of core components in the forecasting part, we conduct an ablation study on the four datasets to validate the multiscale convolution, GAT, and GRU that contribute to the improved outcomes of our proposed model. Firstly, we name the MTAD-TF without different components as follows:

TABLE 1: Dataset information.

Dataset	MSL	SMAP	SMD
No. of attributes	55	25	38
Training subset size	58317	135183	708405
Testing subset size	73729	427617	708420
Anomaly rate (%)	10.72	13.13	4.16
Variables information	Telemetry data: computational, radiation, temperature, power, activities, etc.		CPU load, network usage, memory usage, etc.

TABLE 2: Performance of our model and baselines.

Dataset	MSL			SMAP			SMD		
	Precision	Recall	F1	Precision	Recall	F1	Precision	Recall	F1
LSTM-NDT	0.5944	0.5374	0.5640	0.8965	0.8846	0.8905	0.5684	0.6438	0.6037
LSTM-VAE	0.5257	0.9546	0.6780	0.8551	0.6366	0.7298	0.7922	0.7075	0.7842
DAGMM	0.5412	0.9934	0.7007	0.5845	0.9058	0.7105	0.5835	0.9042	0.7093
OmniAnomaly	0.8867	0.9117	0.8989	0.7416	0.9776	0.8434	0.8334	0.9449	0.8857
MTAD-TF	0.9043	0.8988	0.9015	0.9779	0.8192	0.8916	0.9045	0.9048	0.8940

(i) w/o temporal: removing the multiscale convolution processing in the temporal pattern, only GAT is left in each block

(ii) w/o GAT: Removing the GAT processing in feature pattern, only temporal pattern is left in each block

(iii) w/o GRU: Removing GRU means X_{CNN} and output of three blocks are directly ingested to the FC layer

From Table 3, different components have different effect on different benchmarks. For MSL and SMD, deletion of GAT makes the F1 score drop the most, while SMAP is most affected by temporal convolution component. The score of EEG-EYE has not decreased much, but it has reduced to varying degrees.

5.4. Case Study. We will carry out case analysis of noise experiment in the EEG-EYE state data and GAT in this part.

EEG- (electroencephalogram-) EYE state is from UCI, one continuous EEG measurement with the Emotive EEG Neuroheadset, looking for the relationship between 13 EEGs in different positions of the human brain with the opening and closing of human eyes. Therefore, EEG-EYE state is a dataset that can be classified into two categories. We regard the open-eye label as the anomaly to be searched for and then perform anomaly detection on it.

5.4.1. Noise Experiment. To understand the antinoise ability of the model, we carried out case analysis of noise adding experiment. Five kinds of Gaussian white noise with mean value of 0 and variance of {0.1, 0.2, 0.3, 0.4, 0.5} were added into the training set, respectively. Then the trained model was tested with the unchanged test set, and the F1 value was obtained as shown in the blue broken line in Figure 4. As the variance of Gaussian noise increases, the data shows a downward trend, which conforms to our common sense. However, it also indicates that the model is still not robust

TABLE 3: Ablation study. F1 scores are reported.

	MSL	SMAP	SMD
MTAD-TF	0.9015	0.8916	0.8940
w/o temporal	0.7238	0.6945	0.7520
w/o GAT	0.6827	0.7089	0.6373
w/o GRU	0.8174	0.7000	0.7502

enough and the addition of noise does not play a role in data enhancement. The effect of variance 0.02 is better than that of variance 0.01. Compared with variance 0.01, the noise of variance 0.02 increases the difficulty of network training, prevents overfitting, and improves the generalization ability, which can be regarded as the effect of data enhancement.

According to the verification in literature [10], it can be known that one-dimensional convolution has the effect of smoothing data. From another perspective, we illustrate the function of 1D convolution with experimental scores, and we add a contrast experiment to the above pure noise experiment: noise with different variances is added to the model with 1D convolution removed. As shown in the orange broken line in Figure 4, compared with the score in pure noise, the score of without convolution drops significantly, indicating that the existence of convolution can reduce the impact of noise during data preprocessing.

5.4.2. GAT. We took out the correlation between abnormal and normal before the abnormality from GAT, respectively, and drew the heat map in Figure 5. The right side of Figure 5 shows the correlation between feature 1 and features 2, 3, 4, 5, 6, 16, 17, 18, 19, 20, and 21 at normal time, while the correlation was at abnormal time on the left. The darker the color block, the higher the correlation between features, and vice versa. On the same horizontal line, the large chromatic aberration between the left and right sides means that when an abnormality occurs, the correlation between features has
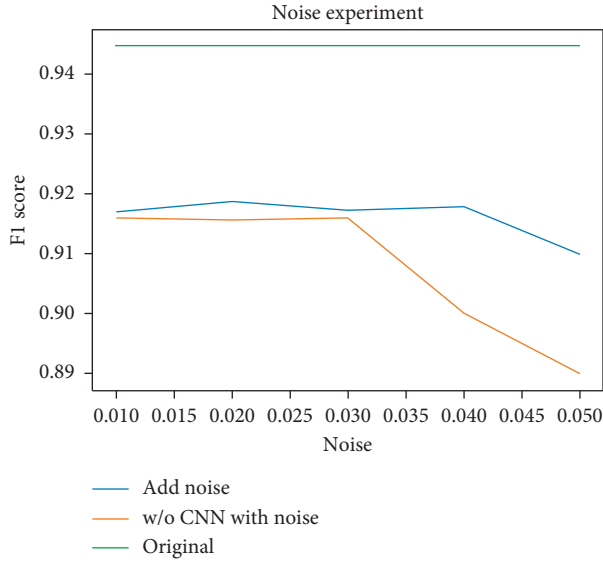
Figure 4: Noise experiment. The green line is the score of the original model without any processing; the value is as high as 0.945. The blue line is the score of the noise with different variances. The orange line is the score of the model without 1D convolution in data preprocess as well as added noises.
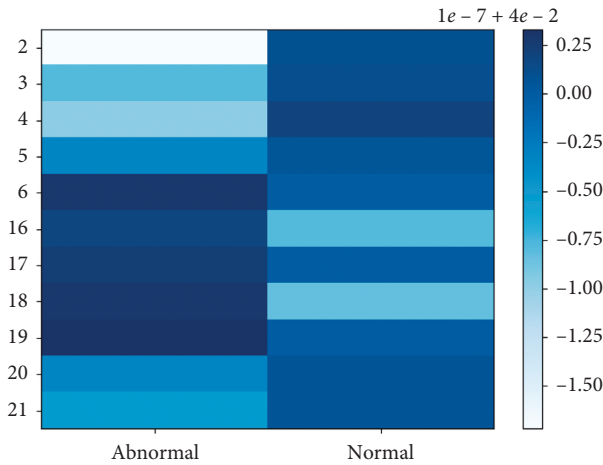

Figure 5: Heat map about correlation between variables. The number of the chromaticity bar is the chromaticity value, not the correlation between the features.

changed greatly, which can be used as a partial basis for abnormal location. Due to the lack of information about abnormal location in the dataset, further experimental verification cannot be carried out. However, it can be assumed that when an abnormality occurs, the correlation between certain features is significantly different from normal conditions.

6. Conclusions

In this paper, a new multivariate time series anomaly detection framework MTAD-TF is proposed. By using the temporal pattern and feature pattern model of multiple time series to make joint prediction, more latent information can be obtained than that of single pattern model. The method is superior to the other four baselines in the three common datasets. In addition, this model has a good antinoise ability and the GAT maybe can help with abnormal location. Future work may come from two aspects. First, attempts to combine the prediction model with the reconstruction model may further improve the accuracy of the model. Secondly, there is too little information on abnormal location and it is hoped that further abnormal location experiments can be carried out to improve the robustness of the MTAD-TF.

Appendix

A.1. Notation X

A is batch of multivariate time series input. x is an instance of X m number of variables (feature) in every instance. w is the length of X in sliding window. $\widehat{x}_i$ is an instance output after data preprocessing. v_i is input node representation for a GAT layer. v_i is input node representation for a GAT layer. h_i is output node representation for a GAT layer. α_{ij} is attention score of node j to node i in a GAT layer. k_0 is the size of filter in 1D convolution. k_1 is hidden dimension of the GRU layer in forecasting component. k_2 is hidden dimension of 3 fully connected layers in forecasting component.

A.2. Experimental Settings

We use the same sliding window $w = 100$ in SMAP and SMD. w is for MSL and EEG-EYE state is set to 120 and 50, respectively. The size of filter in 1D convolution we use in all datasets is $k_0 = 7$. $k_1 = k_2 = 150$ in all dataset except EEG-EYE state which is 100. We use the Adam optimizer to train our model for 100 epochs with an initial learning rate 0.001.

Data Availability

The data used to support the findings of this study are available from the corresponding author upon request.

Conflicts of Interest

The authors declare that there are no conflicts of interest regarding the publication of this paper.

Acknowledgments

References

[1] S. Ahmad and S. Purdy, "Real-time anomaly detection for streaming analytics," 2016, http://arXiv.org/abs/1607.02480.

[2] S. Reza and H. Javad, "Automatic support vector data description," *Soft Computing*, vol. 22, no. 1, pp. 147–158, 2018.

[3] B. Harvald, E. Schaumburg, Y. J. Wang et al., "Time-series anomaly detection service at microsoft," in *Proceedings of the 25th ACM SIGKDD International Conference on Knowledge Discovery & Data Mining*, vol. 138, no. 7, pp. 420–422, Anchorage, AK, USA, August-2019.

[4] P. Malhotra, L. Vig, G. Shroff, and P. Agarwal, "Long short term memory networks for anomaly detection in time series," *European Symposium on Artificial Neural Networks*, vol. 89, 2015.

[5] K. Hundman, V. Constantinou, C. Laporte, I. Colwell, and T. Soderstorm, "Detecting spacecraft anomalies using LSTMs and nonparametric dynamic thresholding," in *Proceedings of the 24th ACM SIGKDD International Conference on Knowledge Discovery & Data Mining*, pp. 387–395, London, UK, August 2018.

[6] N. Ding, H. Gao, H. Bu, H. Ma, and H. Si, "Multivariate-time-series-driven real-time anomaly detection based on bayesian network," *Sensors*, vol. 18, no. 10, p. 3367, 2018.

[7] P. Daehyung, H. Yuuna, and K. Charles, "A multimodal anomaly detect or for robot-assisted feeding using an LSTM-based variational autoencoder," 2017, http://arXiv.org/abs/1711.00614.

[8] A. Rodriguez, D. Bourne, M. Mason et al., "Failure detection in assembly: force signature analysis," in *Proceedings of the IEEE Conference on Automation Science & Engineering*, pp. 210–215, September 2010.

[9] W. Lu and A. A. Ghorbani, "Network anomaly detection based on wavelet analysis," *EURASIP Journal on Advances in Signal Processing*, vol. 2009, pp. 1–16, 2009.

[10] T.-Y. Kim and S.-B. Cho, "Web traffic anomaly detection using C-LSTM neural networks," *Expert Systems With Applications*, vol. 106, pp. 66–76, 2018.

[11] Y. Y. Zhan and R. C. Xu, "K-mean distance outlier factor detect for outlier pattern of time series," *Computer Engineering and Applications*, vol. 45, no. 9, pp. 141–145, 2009.

[12] M. Hossein, M. Sadegh, P. Alessandro, C. Ryad, and M. Vittorio, "Analyzing tracklets for the detection of abnormal crowd behavior," in *Proceedings of the IEEE Winter Conference on Applications of Computer Vision*, pp. 148–155, Waikoloa, HI, USA, January 2015.

[13] M. Ajay, Z. H. Ge, J. Wang et al., "Rapid detection of maintenance induced changes in service performance," in *Proceedings of the Seventh Conference on emerging Networking Experiments and Technologies*, pp. 1–12, Tokyo, Japan, December 2011.

[14] Y. Zhang, Z. H. Ge, G. Albert, and R. Matthew, "Network anomography," in *Proceedings of the 5th ACM SIGCOMM conference on Internet Measurement*, pp. 317–313, Berkeley, CA, USA, January 2005.

[15] J. Wong, C. Colburn, E. Meeks, and S. Vedaraman, "Rad—outlier detection on big data," *The Netflix Technology Blog*, vol. 19, 2015.

[16] A. Kejariwal, "Introducing practical and robust anomaly detection in a time series," Twitter Engineering Blog," *Web*, vol. 15, 2015.

[17] H. W. Xu, W. X. Chen, N. W. Zhao et al., "Unsupervised anomaly detection via variational auto-encoder for seasonal kpis in web applications," in *Proceedings of the 2018 World Wide Web Conference*, pp. 187–196, Lyon, France, April 2018.

[18] P. Malhotra, A. Ramakrishnan, G. Anand et al., "LSTM-based encoder-decoder for multi-sensor anomaly detection, ICML 2016 anomaly detection workshop," 2016, https://arxiv.org/abs/1607.00148.

[19] D. Li, D. C. Chen, L. Shi et al., "MAD-GAN: multivariate anomaly detection for time series data with generative adversarial networks," 2019, https://arxiv.org/abs/1901.04997.

[20] B. Zong, Q. Song, R. Q. Min et al., "Deep autoencoding Gaussian mixture model for unsupervised anomaly detection," in *the Proceedings of the International Conference on Learning Representations*, Vancouver, BC, Canada, February 2018.

[21] N. Gugulothu, P. Malhotra, L. Vig, and G. Shroff, "Sparse neural networks for anomaly detection in high-dimensional time series," in *AI4IOT Workshop in Conjunction with ICML*, International Joint Conference on Artificial Intelligence and European Conference on Artificial Intelligence, Stockholm, Sweden, 2018.

[22] Y. Su, Y. J. Zhao, C. H. Niu et al., "Robust anomaly detection for multivariate time series through stochastic recurrent neural network," in *Proceedings of the 25th ACM SIGKDD International Conference on Knowledge Discovery & Data Mining*, pp. 2828–2837, Anchorage, AK, USA, July 2019.

[23] P. Veličković, G. Cucurull, A. Casanova et al., "Graph attention networks," 2017, http://arXiv.org/abs/1710.10903.

[24] S. Hochreiter and J. Schmidhuber, "Long short-term memory," *Neural Computation*, vol. 9, no. 8, pp. 1735–1780, 1997.

[25] R. Jozefowicz, O. Vinyals, M. Schuster, N. Shazeer, and Y. Wu, "Exploring the limits of language modeling," 2016, http://arXiv.org/abs/1602.02410.

[26] K. Cho, B. V. Merrienboer, C. Gulcehre et al., "Learning phrase representations using RNN encoder-decoder for statistical machine translation," 2014, http://arXiv.org/abs/1406.1078v3.

[27] C. Szegedy, W. Liu, Y. Q. Jia et al., "Going deeper with convolutions," 2014, http://arXiv.org/abs/1409.4842v1.

[28] M. D. Zeiler and R. Fergus, "Visualizing and understanding convolutional networks," *In European Conference on Computer Vision*, vol. 1, pp. 818–833, 2014.

[29] P. Neill, D. Entekhabi, E. Njoku, and K. Kellogg, "The NASA soil moisture active passive (SMAP) mission: overview," in *Proceedings of the IEEE International Geoscience and Remote Sensing Symposium*, Ahmedabad, India, December 2010.

WILEY | Hindawi

Research Article

Local Similarity-Based Fuzzy Multiple Kernel One-Class Support Vector Machine

Qiang He [ID],[1] Qingshuo Zhang [ID],[2] Hengyou Wang [ID],[1] and Changlun Zhang [ID][1,3]

[1]*School of Science, Beijing University of Civil Engineering and Architecture, Beijing 100044, China*
[2]*Faculty of Information Technology, Macau University of Science and Technology, Macao 999078, China*
[3]*Beijing Advanced Innovation Center for Future Urban Design, Beijing University of Civil Engineering and Architecture, Beijing 100044, China*

Correspondence should be addressed to Qiang He; heqiang@bucea.edu.cn

One-class support vector machine (OCSVM) is one of the most popular algorithms in the one-class classification problem, but it has one obvious disadvantage: it is sensitive to noise. In order to solve this problem, the fuzzy membership degree is introduced into OCSVM, which makes the samples with different importance have different influences on the determination of classification hyperplane and enhances the robustness. In this paper, a new calculation method of membership degree is proposed and introduced into the fuzzy multiple kernel OCSVM (FMKOCSVM). The combined kernel is used to measure the local similarity between samples, and then, the importance of samples is determined based on the local similarity between training samples, so as to determine the membership degree and reduce the impact of noise. The proposed membership requires only positive data in the calculation process, which is consistent with the training set of OCSVM. In this method, the noise has a smaller membership value, which can reduce the negative impact of noise on the classification boundary. Simultaneously, this method of calculating membership has a higher efficiency. The experimental results show that FMKOCSVM based on proposed local similarity membership is efficient and more robust to outliers than the ordinary multiple kernel OCSVMs.

1. Introduction

Anomaly detection is an important aspect of data mining. It is used to find objects in a data set that are significantly different from other data to achieve the purpose of preventing abnormal events. At present, the application of anomaly detection in the field of medicine and biological systems is of great significance, and it has been successfully applied to protein detection, [1] cancer screening, [2] and health monitoring [3]. The essence of anomaly detection is a classification algorithm suitable for processing data with an extremely imbalanced class. Complex biological systems usually have this feature. For example, the data of an infectious disease model may include characteristic data of patients and characteristic data of nonpatients. But, in real life, there are far more healthy people than patients. Timely and effective detection of patients with infectious diseases is an effective way to prevent the outbreak of infectious diseases.

Support vector machine (SVM) [4, 5] is a classical classification algorithm, but its performance will deteriorate when dealing with a one-class classification problem or distribution imbalance data. Among the solutions to one-class classification problems, there are density estimation-based methods and support vector-based methods. The method based on support vector is popular because of its simplicity and high efficiency. There are two models for this method: (1) one-class support vector machine (OCSVM) [6]; (2) support vector data description (SVDD) [7]. The goal of SVDD is to find a minimum hypersphere that contains all target samples. The main idea of OCSVM is to take the origin of the feature space as a representative of the abnormal data and then separate the target sample from the origin at the maximum margin. This paper focuses on OCSVM.

Like SVM, OCSVM is also sensitive to noise, which is due to the assumption that each sample has the same importance or weight during training. Introducing fuzzy membership in SVM and constructing the fuzzy support vector machine (FSVM) [8] is one of the effective methods to solve this problem. The calculation methods of fuzzy membership are mainly focused on two kinds of classification problems [9–11]. For example, the heuristic function derived from the centered kernel alignment is used to calculate the dependency relationship between the data point and its label to calculate the fuzzy membership [9] In [10], the membership degree of each sample point is determined by the lower approximation operator of a fuzzy rough set based on Gaussian kernel. As shown in [11], entropy is used to measure the class determinacy of samples. Samples with a higher class determinacy are assigned to a larger fuzzy membership. Generally, in order to improve the robustness of OCSVM, different weights are assigned to training samples, which are called weighted one-class support vector machine (WOCSVM) [12–14]. WOCSVM reduces the impact of noise by assigning lower weights to the noise [12]. As shown in [14], using prior knowledge to assign different weights to the samples, the weight is only related to the distribution knowledge of the neighbors, which is only determined by the k-nearest neighbors of the instance. In recent years, there are many studies on calculating sample weight in one-class classification problems [15–18]. As shown in [19], membership based on fuzzy rough set theory [20, 21] is used as a weight in OCSVM.

The above method improves the robustness of OCSVM to a certain extent but has some limitations. For example, when the amount of data is too large, it [14] is too inefficient when calculating sample weights. The authors in [19] use abnormal data when calculating the membership degree of the sample. In this paper, a novel strategy is proposed to solve the problem of poor robustness of OCSVM; that is, membership degree is introduced into the model. Different from the above membership calculation method, this method only uses one category of data, which fully adapts to the characteristics of OCSVM. The membership calculation method proposed is related to the local density of the data, which is obtained by the local similarity of the training data. We take an S-type function based on local density as a membership function.

OCSVM uses kernel trick to solve the nonlinear separability problem, but it also brings the problem of kernel selection. Multiple kernel learning method [22–26] is used to solve this problem, that is, the multiple kernel one-class support vector machine (MKOCSVM) [27].

The main work of this paper is as follows:

(1) The multiple kernel learning and membership degree are introduced into OCSVM at the same time, and the fuzzy multiple kernel one-class support vector machine (FMKOCSVM) model is constructed to solve the problem of core selection and noise sensitivity.

(2) A novel method of membership calculation is proposed, which is based on local similarity.

(3) We illustrate the effectiveness of this degree of membership in the figure.

(4) According to the maximum similarity between the combination kernel and the ideal kernel, the weight coefficients of the multiple kernels are determined.

(5) It is proved by experiments that the method proposed in this paper performs better than the method of fuzzy membership and the model without membership.

The combined kernel more fully characterizes the data than the single kernel. Using multiple kernel functions at the same time can solve the difficult problem of selecting the kernel function and its parameters, and this method can be applied to different sample information.

The rest of this paper is organized as follows: Section 2 introduces the knowledge of OCSVM, MKOCSVM, and FMKOCSVM. The formulation and algorithm of our FMKOCSVM based on local similarity are detailed in Section 3; and Section 4 reports the experimental results, followed by the conclusion in Section 5.

2. Related Information

2.1. One-Class Support Vector Machine. Compared with the SVM, OCSVM is suitable for dealing with the problem of data category imbalance or one-class classification. The main idea is to first map the data from the original space to the feature space through nonlinear mapping and then take the origin of the feature space as the representative of outliers to find an optimal classification hyperplane in the feature space, in which the image of normal data can be separated from the origin by the maximum margin. A graphical illustration is shown in Figure 1. Figure 1(a) shows the description of the classification in the original space. Figure 1(b) shows the description of the classification in the feature space.

Supposed the training samples $\{\mathbf{x}_1, \mathbf{x}_2, \ldots, \mathbf{x}_l\} \in \mathfrak{R}^n$ (n is the dimension of $\mathbf{x}_i$), where l is the number of training samples. $\phi(\cdot)$ is a function that maps samples to feature spaces. Let ω, ρ denote normal vector and bias term for classification hyperplane in the feature space. The classification hyperplane is expressed as $\omega^T \phi(\mathbf{x}) - \rho = 0$.

The goal is to maximize the distance between the classification hyperplane and origin. Then, OCSVM needs to solve the following convex programming [6]:

$$\min_{\mathbf{w}, \rho, \xi} \quad \frac{1}{2}\|\boldsymbol{\omega}\|^2 + \frac{1}{\nu l} \sum_{i=1}^{l} \xi_i - \rho,$$

$$\text{s.t.} \quad \boldsymbol{\omega}^T \phi(\mathbf{x}_i) \geq \rho - \xi_i, \tag{1}$$

$$\xi_i \geq 0, \quad i = 1, 2, \ldots, l.$$

Here, ξ_i is the slack variable, which means that outliers are allowed to exist, and $\nu \in (0, 1]$ is a parameter to control the proportion of support vector and error points. Using the Lagrange multiplier method, the dual problem of the above optimization problem can be written as follows:
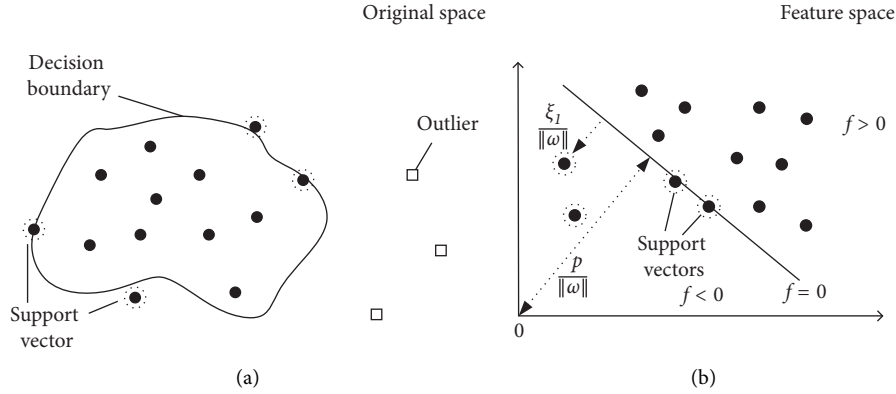
FIGURE 1: A graphical illustration of the one-class support vector machine. The black dot represents the target sample, the box represents the abnormal sample, and the black solid line represents the boundary.

$$\min_a \frac{1}{2} \sum_i^l \sum_j^l \alpha_i \alpha_j k(\mathbf{x}_i, \mathbf{x}_j),$$

$$\text{s.t.} \sum_{i=1}^l \alpha_i = 1, 0 \le \alpha_i \le \frac{1}{vl}, \quad i = 1, 2, \ldots, l. \tag{2}$$

Because the above process needs to meet the KKT (Karush–Kuhn–Tucker) condition,

$$\begin{cases} \alpha_i \ge 0, \\ \boldsymbol{\omega}^T \phi(\mathbf{x}_i) - \rho + \xi_i \ge 0, \\ \alpha_i [\boldsymbol{\omega}^T \phi(\mathbf{x}_i) - \rho + \xi_i] = 0, \\ \gamma_i \ge 0, \\ \xi_i \ge 0, \\ \gamma_i \xi_i = 0. \end{cases} \tag{3}$$

The solution of equation (3) corresponds to sample $\mathbf{x}_i$, and there is always $\alpha_i = 0$ or $\omega^T \phi(\mathbf{x}_i) = \rho - \xi_i$. When $\alpha_i = 0$, the sample $\mathbf{x}_i$ has no effect on the hyperplane. When $\alpha_i > 0$, $\omega^T \phi(\mathbf{x}_i) = \rho - \xi_i$ must be true. In this case, this sample is called a support vector. If $\alpha_i < 1/vl$, then $\gamma_i > 0$; there must be $\xi_i = 0$; that is, the sample is located on the maximum separation boundary; if $\alpha_i = 1/vl$, then $\gamma_i = 0$; in this case, when $\xi_i > 0$, the sample $\mathbf{x}_i$ is misclassified, which is called the boundary support vector. As shown in Figure 2, when different values are used, the positions of corresponding sample points are different.

Let N_{SV}, N_{BSV} represent the total number of support vectors and the total number of boundary support vectors, respectively. The maximum value of α_i is $1/vl$ and has the following constraints:

$$\sum_{i=1}^l \alpha_i = 1, 0 \le \alpha_i \le \frac{1}{vl}, \quad i = 1, 2, \ldots, l. \tag{4}$$

So we can have the following inequality:

$$N_{BSV} \frac{1}{vl} \le \sum_{i=1}^l \alpha_i \le N_{SV} \frac{1}{vl}, \quad i = 1, 2, \ldots, l. \tag{5}$$

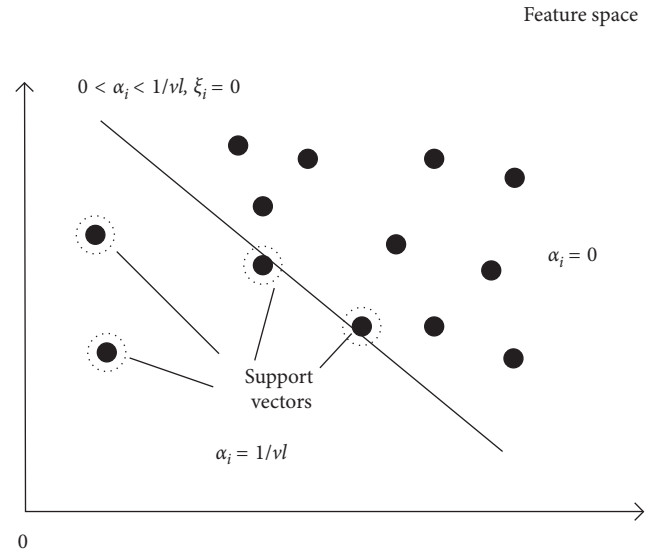Multiplying v on both sides of equation (5) gives

FIGURE 2: The definitions of support vectors. The black dot represents the target sample, and the black dot with a dotted circle represents support vector.

$$N_{BSV} \frac{1}{l} \le v \le N_{SV} \frac{1}{l}, \quad i = 1, 2, \ldots, l. \tag{6}$$

It can be known from equation (6) that the value of v determines the lower bound of the total support vector ratio and the upper bound of the boundary support vector ratio:

$$\omega = \sum_{i=1}^l \alpha_i \phi(\mathbf{x}_i). \tag{7}$$

The normal vector of the hyperplane can be obtained by using equation (7).

Let $\mathbf{x}_t^{SV}$ denote the tth support vector located on the maximum spacing plane $(0 < \alpha_t < 1/vl)$ and the bias term of the hyperplane obtained according to

$$\rho = \frac{1}{n_{sv}} \sum_{t=1}^{n_{sv}} \boldsymbol{\omega}^T \phi(\mathbf{x}_t^{SV}) = \sum_{t=1}^{n_{sv}} \alpha_i k(\mathbf{x}_i, \mathbf{x}_t^{SV}). \tag{8}$$

Thus, the decision function can be written as

$$
\begin{aligned}
f(x) &= \operatorname{sgn}\left(\boldsymbol{\omega}^T \phi(\mathbf{x}) - \rho\right) \\
&= \operatorname{sgn}\left[\sum_{i}^{l} \alpha_i k(\mathbf{x}_i, \mathbf{x}) - \rho\right].
\end{aligned} \tag{9}
$$

For a given test sample $\mathbf{x}$, after substituting $\mathbf{x}$ into equation (9), when $f(\mathbf{x})$ returns $+1$, the sample is judged as a normal point; when $f(\mathbf{x})$ returns -1, the sample is judged as an abnormal point.

2.2. Multiple Kernel One-Class Support Vector Machine.
MKOCSVM replaces the single kernel function in the conventional OCSVM with a combined kernel, which can effectively avoid the difficulty in selecting the kernel function and its parameters.

The forms of combined kernel function include linear combination and nonlinear combination, [28] expressed as

$$
k_\eta(\mathbf{x}, \mathbf{z}) = \sum_{m=1}^{P} \eta_m k_m(\mathbf{x}, \mathbf{z}), \quad \eta_m \ge 0, \tag{10}
$$

$$
k_\eta(\mathbf{x}, \mathbf{z}) = \prod_{m=1}^{P} \left[k_m(\mathbf{x}^m, \mathbf{z}^m)\right]^{\eta_m}. \tag{11}
$$

Here, η_m is the kernel weight of the mth basic kernel. The MKOCSVM model can be formulated as

$$
\min_{\boldsymbol{\omega}_\eta, \rho, \xi} \quad \frac{1}{2}\left\|\boldsymbol{\omega}_\eta\right\|^2 + \frac{1}{\nu l} \sum_{i=1}^{l} \xi_i - \rho,
$$

$$
\text{s.t.} \quad
\begin{aligned}
&\boldsymbol{\omega}_\eta^T \phi_\eta(\mathbf{x}_i) \ge \rho - \xi_i, \\
&\xi_i \ge 0, \quad i = 1, 2, \ldots, l.
\end{aligned} \tag{12}
$$

Here, $k_\eta(\mathbf{x}_i, \mathbf{x}_j) = \langle \phi_\eta(\mathbf{x}_i), \phi_\eta(\mathbf{x}_j)\rangle$. The function $f(\mathbf{x})$ can be written as

$$
\begin{aligned}
f(\mathbf{x}) &= \operatorname{sgn}\left(\boldsymbol{\omega}_\eta^T \phi(\mathbf{x}) - \rho\right) \\
&= \operatorname{sgn}\left[\sum_{i}^{l} \alpha_i k_\eta(\mathbf{x}_i, \mathbf{x}) - \rho\right].
\end{aligned} \tag{13}
$$

To seek the optimal combination weight for each basis kernel, the authors in [27] suggest optimizing the maximum kernel-target alignment value of the combination kernel and the ideal kernel, that is, solving the following objective function [29]:

$$
\begin{aligned}
\max_\eta A\left(\mathbf{K}_\eta, \mathbf{y}\mathbf{y}^T\right) &= \frac{\langle \sum_{m=1}^{P} \eta_m \mathbf{K}_m, \mathbf{y}\mathbf{y}^T \rangle_F}{\sqrt{\langle \sum_{m=1}^{P} \eta_m \mathbf{K}_m, \sum_{m=1}^{P} \eta_m \mathbf{K}_m \rangle_F \langle \mathbf{y}\mathbf{y}^T, \mathbf{y}\mathbf{y}^T \rangle_F}}, \\
&= \frac{\sum_{m=1}^{P} \sum_{i,j=1}^{l} \eta_m k_{ij}^m}{l\sqrt{\sum_{m,s=1}^{P} \eta_m \eta_s \langle \mathbf{K}_m, \mathbf{K}_s \rangle_F}},
\end{aligned} \tag{14}
$$

$$
\text{s.t.} \quad \eta_m \ge 0, \quad m = 1, 2, \ldots, P.
$$

Here, $\mathbf{K}_m$ is the kernel matrix. $\langle \mathbf{K}_1, \mathbf{K}_2 \rangle$ is the Frobenius inner product between two matrices, which is given by

$$
\langle \mathbf{K}_1, \mathbf{K}_2 \rangle_F = \sum_{i=1}^{l} \sum_{j=1}^{l} k_1(x_i, x_j) k_2(x_i, x_j). \tag{15}
$$

Only solution equation (16) is needed to obtain the optimal combination weight:

$$
\max_\eta \sum_{m=1}^{P} \sum_{i,j=1}^{l} \eta_m k_{ij}^m - \sum_{m,s=1}^{P} \eta_m \eta_s \langle \mathbf{K}_m, \mathbf{K}_s \rangle_F - \delta \sum_{m=1}^{P} \eta_m^2,
$$

$$
\text{s.t.} \quad \eta_m \ge 0, \quad m = 1, 2, \ldots, P. \tag{16}
$$

Here, δ is a regularization coefficient.

2.3. Fuzzy Multiple Kernel One-Class Support Vector Machine.
Let s_i denote membership degree of the sample $\mathbf{x}_i$, then the training set can be expressed as $\{(\mathbf{x}_1, s_1), (\mathbf{x}_2, s_2), \ldots, (\mathbf{x}_l, s_l)\} \in \Re^n$, where $s_i \in [0, 1]$. The FMKOCSVM needs to solve the following optimal programming:

$$
\min_{\boldsymbol{\omega}, \rho, \xi} \frac{1}{2}\left\|\boldsymbol{\omega}_\eta\right\|^2 + \frac{1}{\nu l} \sum_{i=1}^{l} s_i \xi_i - \rho,
$$

$$
\text{s.t.} \quad
\begin{aligned}
&\boldsymbol{\omega}_\eta^T \phi_\eta(\mathbf{x}_i) \ge \rho - \xi_i, \\
&\xi_i \ge 0, \quad i = 1, 2, \ldots, l.
\end{aligned} \tag{17}
$$

When $s_i = 1$, $i = 1, 2, \ldots, l$, the FMKOCSVM degenerates to the normal MKOCSVM.

After introducing the Lagrange multiplier $\alpha_i \ge 0, \gamma_i \ge 0$, for each inequality constraint, the Lagrange function of equation (17) is

$$L\left(\boldsymbol{\omega}_{\eta}, \boldsymbol{\xi}, \rho, \boldsymbol{\alpha}, \boldsymbol{\gamma}\right) = \frac{1}{2}\left\|\boldsymbol{\omega}_{\eta}\right\|^{2} + \frac{1}{vl}\sum_{i=1}^{l} s_{i}\xi_{i} - \rho - \sum_{i=1}^{l} \gamma_{i}\xi_{i} - \sum_{i=1}^{l} \alpha_{i}\left[\boldsymbol{\omega}_{\eta}^{T}\phi_{\eta}\left(\mathbf{x}_{i}\right) - \rho + \xi_{i}\right]. \tag{18}$$

Setting the derivatives with respect to ω_{η}, ξ, and ρ to zero, then we can obtain

$$\boldsymbol{\omega}_{\eta} = \sum_{i=1}^{l} \alpha_{i}\phi_{\eta}\left(\mathbf{x}_{i}\right),$$

$$\sum_{i=1}^{l} \alpha_{i} = 1, \tag{19}$$

$$\alpha_{i} = \frac{1}{vl}s_{i} - \gamma_{i}.$$

Substituting equation (19) into equation (18), the dual form of equation (17) can be written as

$$\min_{\boldsymbol{\alpha}} \quad \frac{1}{2}\sum_{i}^{l}\sum_{j}^{l}$$

$$\text{s.t.} \quad \sum_{i=1}^{l} \alpha_{i} \tag{20}$$

$$0 \leq \alpha_{i} \leq \frac{1}{vl}\, s_{i}, \quad i = 1, 2, \ldots, l.$$

Obviously, the only difference between the dual problems of MKOCSVM and FMKOCSVM is the upper bound of α_{i}. The upper bound of α_{i} becomes s_{i}/vl in equation (20). The function $f(\mathbf{x})$ can be written as

$$f(\mathbf{x}) = \text{sgn}\left[\sum_{i}^{l} \alpha_{i}k_{\eta}\left(\mathbf{x}_{i}, \mathbf{x}\right) - \rho\right]. \tag{21}$$

In FMKOCSVM, when the noise has a lower membership during training, the negative effect of noise on the classification hyperplane can be reduced.

3. Training FMKOCSVM with Local Similarity-Based Membership

Noise in the training set may not belong to any class at all. Therefore, if these samples with uncertainty are distributed near the edges of the target data, the model will overfit. To alleviate this phenomenon, this paper assigns membership to each training point, which makes the samples play a different role in training and reduces the negative impact of noise. In this section, we first introduce the calculation method of membership based on local similarity in detail and then propose the FMKOCSVM algorithm using membership based on local similarity.

3.1. Local Similarity-Based Memberships. Assume the target sample $\{\mathbf{x}_1, \mathbf{x}_2, \ldots, \mathbf{x}_l\} \in \mathfrak{R}^n$. Let $\mathbf{K}_{\eta}$ represent the multiple kernel matrix defined by $\mathbf{K}_{\eta} = k_{\eta}(\mathbf{x}_i, \mathbf{x}_j)_{l \times l}$, where the expression of multiple kernel function is equation (10).

Let all the elements of the upper triangle of the multiple kernel be sorted from large to small, i.e., $\mathbf{K}_{\eta} = k_{\eta}(\mathbf{x}_i, \mathbf{x}_j)_{i < j}$, and then write it as a vector $G = \{g_1, g_2, \ldots, g_t\}$, $t = l(l-1)/2$.

Next, define a constant $\varepsilon \in [0, 1]$ and let $h = [\varepsilon t]$, where $[\varepsilon t]$ is the integral part of εt. $\theta = g_h$ is a threshold. For each sample $\mathbf{x}$, let u represent the total number of $k_{ij} \geq \theta$, $j = 1, 2, \ldots, l$. In other words, u_i represents the number of samples in the target sample whose similarity with the sample $\mathbf{x}_i$ is greater than or equal to the threshold.

The kernel $k_{\eta}(\mathbf{x}_i, \mathbf{x}_j)$ measures the similarity between two target samples $\mathbf{x}_i$ and $\mathbf{x}_j$, and a large kernel indicates a large similarity. If the membership degree of the sample $\mathbf{x}_i$ to the target class is higher, it is obvious that more samples are similar to the sample $\mathbf{x}_i$ in the input sample, i.e., the greater the value of u_i. In other words, a sample with a higher value of u should have a greater contribution to the classification boundary, the penalty for misclassification of such samples is greater, and the noise will have a smaller value of u.

Therefore, we take u as a measure function, which measures the importance of the target sample to the classification hyperplane. Obviously, the value of u cannot be directly used as a membership degree of FMKOCSVM. We use an S-type function to map this measure into the membership degree in the unit interval. At the same time, this S-type function increases the difference between membership degrees of samples with different importance. The membership function is written as

$$s_{i} = \frac{1}{1 + \exp\left(-\tau\left((u_{i}/U) - (1/2)\right)\right)}, \tag{22}$$

where $U = \max\{u_i\}$. $\tau > 0$ is a constant. The value range is $(0, 1)$. Figure 3 describes the distribution of membership values by τ taking different values. According to Figure 3, when $\tau = 10$, the distribution of membership value is the best. Algorithm 1 lists the detailed calculation process of membership based on local similarity.

Since noise has a low degree of membership to the target class, there are few similar instances in the input data. In other words, the noise will get a smaller membership value. Therefore, we proposed a method that can make the noise have less influence on the classification boundary. More importantly, because the training data of OCSVM only include target samples, the traditional method of calculating membership degree is not suitable for OCSVM. However, our method of membership based on local similarity only uses the features of the target data and does not involve the information of class, which is very suitable for a one-class classification problem. Furthermore, the proposed method has obvious high efficiency.

We analyze the computational complexity of Algorithm 1 with the O notation. First, the computational
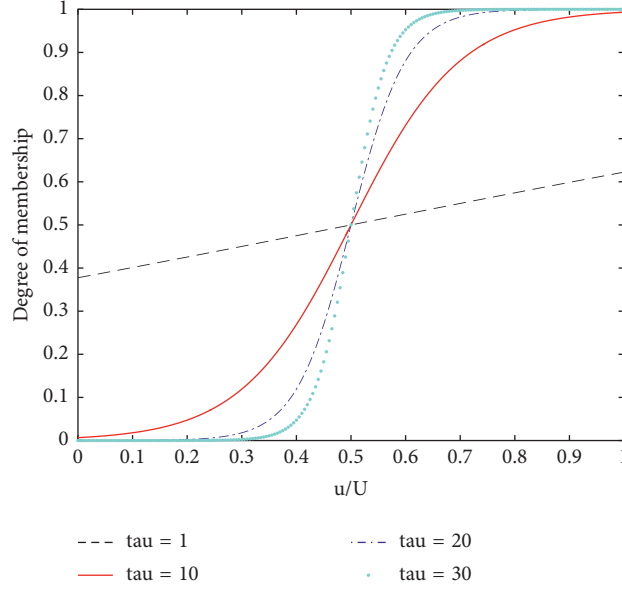
FIGURE 3: The distribution of membership with different values of τ. The horizontal axis is the values of u/U. The vertical axis is the corresponding membership value. The black dashed line is the distribution of membership when $\tau = 1$. The red solid line is the distribution of membership when $\tau = 10$. The blue dash-dotted line is the distribution of membership when $\tau = 20$. The cyan dotted line is the distribution of membership degree when $\tau = 30$.

Input: the training set $\{\mathbf{x}_1, \mathbf{x}_2, \ldots, \mathbf{x}_l\}$, the kernel function set $\{k_1, k_2, \ldots, k_P\}$,
    The kernel weight $\eta_m, m = 1, 2, \ldots, P, \varepsilon \in [0, 1]$
Output: the membership vector s_i, $i = 1, 2, \ldots, l$
(1) Preprocess the training set
(2) Calculate the combined kernel matrix $K_\eta = (k_{\eta_{ij}})_{l \times l}$ according to equation (10)
(3) Sort $K_\eta = (k_{\eta_{ij}})_{i < j}$ from large to small as $G = \{g_1, g_2, \ldots, g_t\}, t = l(l-1)/2$
(4) Calculate the constant h according to $h = [\varepsilon t]$, and fixed threshold according to $\theta = g_h$
(5) for $i = 1 : l$ do
(6)   initialize $u_i = 0$
(7)   for $j = 1 : l$ do
(8)   if $k_{ij} \geq g_h$ then
(9) $u_i = u_i + 1$
(10)   end if
(11)   end for
(12) end for
(13) Calculate $U = \max_{i}\{u_i\}$
(14) for $i = 1 : l$ do
(15) Calculate the membership degree s_i of the sample x_i according to equation (22)
(16) end for
(17) end

ALGORITHM 1: Local similarity-based memberships.

complexity of calculating the multiple kernel matrix in step 2 is $O(l^2)$. Second, the average computational complexity of multiple kernel matrix sorting in step 3 is $O(t^2)$. Third, it costs $O(l^2)$ to calculate u in steps 4 to 12. Finally, calculating the memberships in steps 13 to 16 costs $O(l)$. Hence, the total computational complexity of local similarity-based membership degree is

$$O(l^2) + O(t^2) + O(l^2) + O(l) = O(l^2) + O(l^4) + O(l^2) + O(l)$$
$$= O(l^4).$$

(23)

Compared with classification performance, $O(l^4)$ is also acceptable.

Input: the training set $\{\mathbf{x}_1, \mathbf{x}_2, \ldots, \mathbf{x}_l\}$, the kernel function set $\{k_1, k_2, \ldots, k_P\}$, the kernel parameter set $\{\sigma_1, \sigma_2, \ldots, \sigma_P\}$, the test set T

Output: the classification results of T: y

(1) Preprocess the training set

(2) for $m = 1 : P$ do

(3)   Calculate the corresponding kernel matrix $\mathbf{K}_m$ of σ_m

(4) end for

(5) Substituting the kernel matrix $\mathbf{K}_m, m = 1, 2, \ldots, P$ into equation (16)

(6) Calculate the kernel weight vector $\eta_m, m = 1, 2, \cdots, P$ according to equation (16)

(7) Calculate the combined kernel matrix $\mathbf{K}_\eta$ according to equation (10)

(8) for each $x_i \in \{\mathbf{x}_1, \mathbf{x}_2, \cdots, \mathbf{x}_l\}$ do

(9)   Calculate the membership degree s_i of the sample x_i according to equation (22)

(10) end for

(11) Train the FMKOCSVM with the fuzzy membership values.

(12) Calculate the classification results of test set according to equation (21)
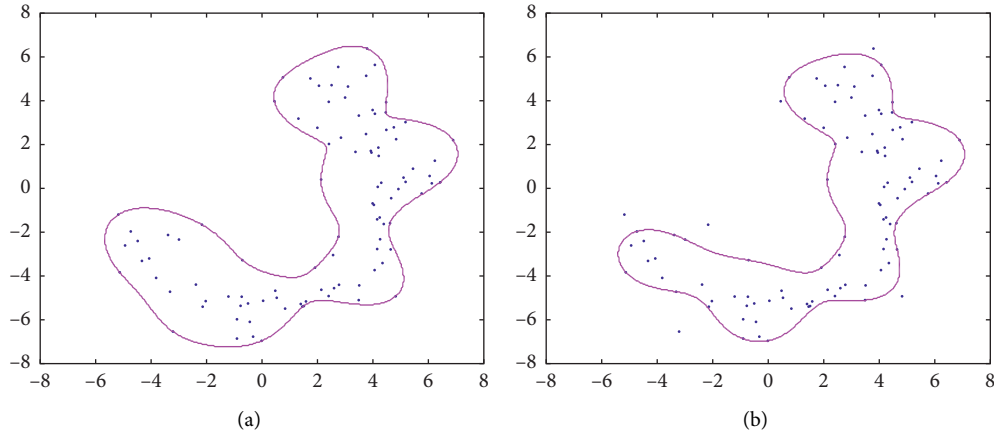
(13) end

ALGORITHM 2: FMKOCSVM_LS.

(a)

(b)

FIGURE 4: The classification performance of MKOCSVM and FMKOCSVM_LS without noises. The magenta solid line is the boundary. The blue dots are the target samples.

3.2. Overall Procedure of FMKOCSVM Based on Local Similarity.

The detailed process of FMKOCSVM based on membership degree of local similarity is listed in Algorithm 2. In the following part of this paper, we use FMKOCSVM_LS to represent the proposed algorithm.

In Figure 4, the classification performance of MKOCSVM is shown in Figure 4(a) and the classification performance of FMKOCSVM_LS proposed by us is shown in Figure 4(b). The combined kernel function is composed of seven Gaussian kernels with a width of $\{2^{-5}, 2^{-4}, 2^{-3}, 2^{-2}, 2^{-1}, 2^0, 2^1\}$. Parameter v is set to 0.02. The value of the regularization coefficient δ in equation (16) is set to 100. In order to reduce the cost of tuning extraparameter, we set ε to 0.2 and τ to 10 directly. Obviously, FMKOCSVM_LS has a tighter boundary than MKOCSVM. In Figure 4(b), some outliers are identified by FMKOCSVM_LS. However, MKOCSVM does not identify any outliers, and there are a lot of gaps inside the boundary.

After adding 10% Gaussian noise to the training set, the results are shown in Figure 5.

The parameter settings in Figure 5 are the same as in Figure 4. As we can see, when there are noises in the training set, the classification ability of FMKOCSVM_LS is much better than that of MKOCSVM. In Figure 5(a), MKOCSVM distinguishes all noises as target data, which makes the performance of MKOCSVM very bad. In Figure 5(b), we can see that most of the noises have a very small membership value, and the negative effect of noise on the boundary is weak. Therefore, FMKOCSVM_LS can improve the robustness of MKOCSVM.

In the next section, we will further prove through experiments that our proposed method of calculating membership is better than the previous method.

4. Experiments

4.1. Experiment Setup

4.1.1. Approaches.
We compared FMKOCSVM_LS with the following methods: (1) MKOCSVM: the ordinary multiple kernel one-class support vector machine [27]; (2)
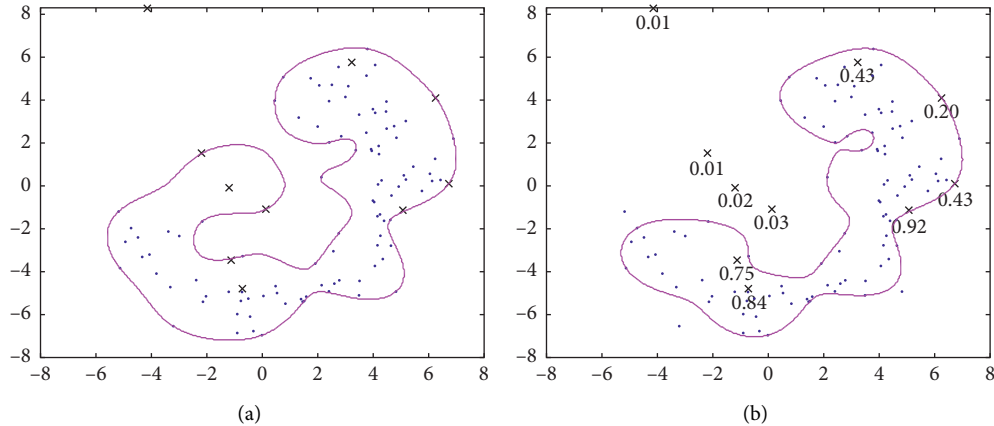
FIGURE 5: The classification performance of MKOCSVM and FMKOCSVM_LS. 10% of Gaussian noise is added. The magenta solid line is the boundary. The blue dots are the target samples. The black crosses are the noises with Gaussian distribution. The number at bottom of the noise represents its membership.

WMKOCSVM: the weighted one-class support vector machine is formed by WOCSVM [14] combined with the multiple kernel function; (3) FMKOCSVM: the fuzzy multiple kernel one-class support vector machine, in which membership is calculated based on a rough set [19]. Because two classes of samples are needed to calculate membership, the training set contains negative class samples. These negative samples are only used to calculate membership.

In MKOCSVM, the parameter v is determined by 10-fold cross validation, and the value range is $\{0.01, 0.04, 0.07, 0.10, 0.13, 0.16, 0.19\}$. The basic kernel of the multiple kernel function is seven Gauss kernel functions with kernel width $\{2^{-6}, 2^{-5}, 2^{-4}, 2^{-3}, 2^{-2}, 2^{-1}, 2^{0}\}$. The parameter δ in the multiple kernel learning algorithm is set to 100. WMKOCSVM, FMKOCSVM, and FMKOCSVM_LS also use these parameters during training. The number of nearest neighbors in WMKOCSVM is set to 10, which is the same as in [14]. In order to avoid increasing the time due to the adjustment of parameters, when calculating the membership based on local similarity in FMKOCSVM_LS, we directly set $\varepsilon = 0.5$ and $\tau = 10$.

4.1.2. Metrics. In this paper, the performance of different approaches is evaluated by three popular metrics, namely, g-mean, AUC, and training time. According to the confusion matrix in Table 1, we can get the true positive rate (TPR) and the false positive rate (FPR). In one-class classification problems, using g-mean and AUC as measures is more accurate than using accuracy:

$$TPR = \frac{TP}{TP + FN},$$

$$FPR = \frac{FP}{FP + TN},$$

$$g - mean = \sqrt{a^{+} \times a^{-}},$$

$$AUC = \frac{1 + TPR - FPR}{2}.$$

(24)

TABLE 1: Confusion matrix.

	Predicted positive	Predicted negative
Positive	TP	FN
Negative	FP	TN

4.1.3. Data Sets. In this section, we selected 14 benchmark data sets, 13 of which are from the UCI machine learning repository. There are three experiments on biological systems. The Heart data set is a data set used for heart disease diagnosis. The Breast data set is a data set used to diagnose whether a patient's breast cancer is benign or malignant. The Biomed data set is used to screen whether it is a carrier. Creditcard_cut is a part of the data set of creditcard fraud detection on Kaggle. Because the original Creditcard data set is too large, we only randomly selected 729 transaction data (483 normal transactions and 249 fraudulent transactions) for the experiment. Table 2 lists the details of these data sets.

For each data set, we use 70% of the positive data as the training set. Then, we randomly selected a part of negative data as the noise in the training set, and the proportion of noise was 10%. The rest of the data is used as the test set. The training set is normalized before training. And the test set is processed according to the standard of the training set.

4.2. Results. In order to obtain stable results, each method has done 20 independent experiments on each data set. The result used in the comparison is the average of the 20 results. Table 3 shows the optimal value of v obtained through the 10-fold cross validation. In order to get the best results of the four algorithms, v in Table 3 is used in each experiment.

Table 4 is a comparison of g-mean. Table 5 shows a comparison of AUC values. Table 6 shows the average training time of MKOCSVM, WMKOCSVM, FMKOCSVM, and FMKOCSVM_LS on each data set. Figure 6 is the total training time of 14 data sets of each method.

Table 2: Data information.

Number	Data set	Positive samples	Negative samples	Samples	Features
1	Australia	383	307	690	14
2	Balancescaleleft	288	337	625	4
3	Biomed	127	67	194	5
4	Glass	70	144	214	9
5	Heart	160	137	297	13
6	Vowel	48	480	528	10
7	Wine	48	130	178	13
8	Creditcard_cut	483	249	729	30
9	Japan	357	294	651	15
10	Iris	50	100	150	4
11	Breast	458	241	699	9
12	Wdbc	357	212	569	30
13	Pima	500	268	768	8
14	Waveform	300	600	900	21

Table 3: The optimal value of v.

Number	Data set	MKOCSVM	WMKOCSVM	FMKOCSVM	FMKOCSVM_LS
1	Australia	0.19	0.1	0.19	0.07
2	Balancescaleleft	0.19	0.1	0.07	0.04
3	Biomed	0.16	0.04	0.07	0.01
4	Glass	0.07	0.07	0.04	0.01
5	Heart	0.19	0.07	0.19	0.04
6	Vowel	0.01	0.01	0.01	0.01
7	Wine	0.01	0.01	0.01	0.01
8	Creditcard_cut	0.13	0.04	0.07	0.01
9	Japan	0.19	0.1	0.19	0.13
10	Iris	0.01	0.01	0.01	0.01
11	Breast	0.04	0.01	0.04	0.01
12	Wdbc	0.07	0.01	0.04	0.01
13	Pima	0.19	0.1	0.1	0.07
14	Waveform	0.16	0.04	0.07	0.01

Table 4: Comparison of g-mean.

Number	Data set	g-mean (mean ± std (%))			
		MKOCSVM	WMKOCSVM	FMKOCSVM	FMKOCSVM_LS
1	Australia	59.19 ± 2.22	65.08 ± 2.39	74.18 ± 2.68	74.74 ± 2.51
2	Balancescaleleft	61.38 ± 2.05	66.17 ± 2.29	66.73 ± 3.22	69.99 ± 3.09
3	Biomed	72.43 ± 5.59	76.80 ± 4.53	78.71 ± 2.98	81.07 ± 4.15
4	Glass	67.74 ± 5.41	**74.02 ± 4.38**	70.20 ± 5.34	72.51 ± 6.64
5	Heart	63.90 ± 1.79	63.76 ± 3.90	67.82 ± 5.05	**70.51 ± 3.45**
6	Vowel	79.46 ± 8.26	79.02 ± 4.79	80.42 ± 5.72	**84.88 ± 6.24**
7	Wine	81.49 ± 7.59	81.20 ± 7.17	82.87 ± 6.71	**85.68 ± 9.07**
8	Creditcard_cut	72.00 ± 3.37	74.26 ± 3.90	81.36 ± 2.18	**83.66 ± 1.91**
9	Japan	58.23 ± 4.08	64.59 ± 2.77	**73.10 ± 2.91**	68.87 ± 3.52
10	Iris	63.87 ± 15.23	69.67 ± 6.95	75.48 ± 13.65	**93.87 ± 4.76**
11	Breast	60.71 ± 4.85	65.72 ± 5.28	81.22 ± 4.54	**92.00 ± 1.93**
12	Wdbc	59.06 ± 5.03	55.31 ± 6.78	73.08 ± 4.24	**86.41 ± 1.83**
13	Pima	51.92 ± 1.91	61.03 ± 2.18	62.39 ± 2.18	**64.92 ± 2.09**
14	Waveform	68.99 ± 4.39	67.65 ± 3.49	74.13 ± 2.52	**78.23 ± 1.87**

From Tables 4 and 5, we can find that the performance of FMKOCSVM_LS is the best among the four algorithms, which proves that our membership method can improve the robustness of MKOCSVM. More importantly, WMKOCSVM and FMKOCSVM have only one best result on 14 data sets, respectively. However, our proposed method has twelve optimal performances.

On the Iris, Breast, and Wdbc data sets, FMKOCSVM_LS shows great advantages. Its g-mean is 27%~32% higher than that of MKOCSVM, 10%~18% higher

TABLE 5: Comparison of AUC value.

Number	Data set	AUC (mean ± std (%))			
		MKOCSVM	WMKOCSVM	FMKOCSVM	FMKOCSVM_LS
1	Australia	62.25 ± 1.99	65.43 ± 2.32	74.35 ± 2.62	**74.88 ± 2.49**
2	Balancescaleleft	64.21 ± 1.91	66.88 ± 2.27	68.10 ± 3.17	**70.64 ± 2.84**
3	Biomed	73.27 ± 5.17	77.10 ± 4.41	79.05 ± 2.80	**81.22 ± 4.11**
4	Glass	71.26 ± 4.31	**74.29 ± 4.13**	71.26 ± 5.33	73.63 ± 6.37
5	Heart	64.81 ± 1.66	64.08 ± 3.89	68.00 ± 5.10	**71.09 ± 2.99**
6	Vowel	80.17 ± 7.32	79.49 ± 4.65	80.78 ± 5.64	**85.32 ± 5.71**
7	Wine	82.23 ± 6.84	81.74 ± 7.02	83.62 ± 1.95	**87.04 ± 7.17**
8	Creditcard_cut	73.86 ± 2.67	75.25 ± 3.18	81.44 ± 2.20	**83.70 ± 1.90**
9	Japan	60.84 ± 3.44	64.86 ± 2.79	**73. 24 ± 2.84**	69.03 ± 3.48
10	Iris	69.90 ± 10.54	71.75 ± 6.32	78.24 ± 9.82	**94.17 ± 4.44**
11	Breast	67.87 ± 2.95	71.04 ± 3.61	82.53 ± 3.76	**92.34 ± 1.76**
12	Wdbc	65.65 ± 3.25	63.44 ± 4.02	75.17 ± 3.44	**86.50 ± 1.73**
13	Pima	57.33 ± 1.84	61.82 ± 2.07	62.75 ± 2.03	**65.09 ± 2.18**
14	Waveform	70.70 ± 3.86	69.80 ± 2.94	74.35 ± 2.53	**78.80 ± 1.82**

TABLE 6: Average training time.

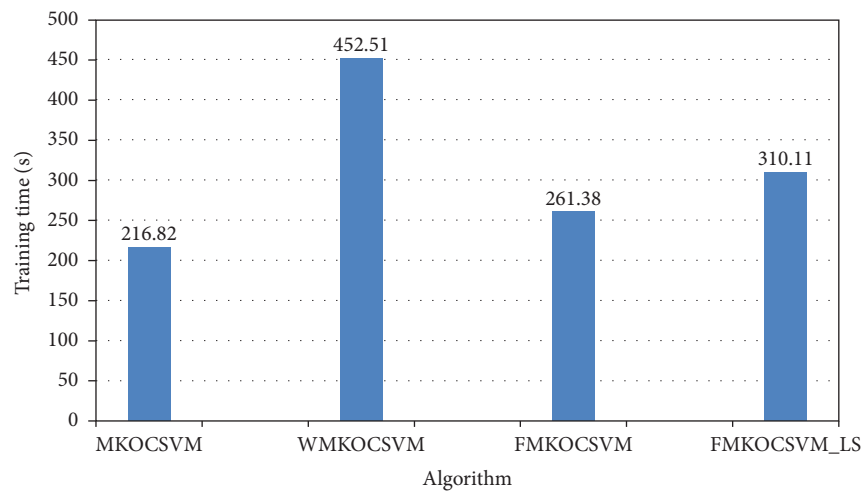| Number	Data set	Training time (s)			
		MKOCSVM	WMKOCSVM	FMKOCSVM	FMKOCSVM_LS
1	Australia	20.60	48.65	22.67	28.22
2	Balancescaleleft	13.13	30.30	16.85	19.34
3	Biomed	5.43	12.75	6.16	7.68
4	Glass	1.52	5.31	3.17	2.92
5	Heart	7.75	17.87	7.96	9.64
6	Vowel	3.57	5.11	4.58	2.95
7	Wine	1.31	4.89	1.44	3.21
8	Creditcard_cut	38.51	75.93	47.19	54.96
9	Japan	18.81	44.18	20.30	24.42
10	Iris	1.22	4.22	1.70	1.88
11	Breast	32.86	51.27	33.24	47.58
12	Wdbc	18.71	45.89	23.86	28.26
13	Pima	38.49	68.94	51.42	57.08
14	Waveform	14.91	37.20	20.84	21.97

FIGURE 6: The total training time of 14 data sets of MKOCSVM, WMKOCSVM, FMKOCSVM, and FMKOCSVM_LS.

than that of FMKOCSVM, and 23%~31% higher than that of WMKOCSVM. In the corresponding data set, the AUC value of FMKOCSVM_LS also increased significantly. On the Japan data set, although the g-mean of FMKOCSVM LS is lower than the g-mean of FMKOCSVM, it is still 10% higher than the g-mean of MKOCSVM and 4% higher than the g-mean of WMKOCSVM. AUC value is the same as g-mean. On the Glass data set, WMKOCSVM has the best result, and its result is only about 2% higher than that of FMKOCSVM_LS. However, on the Glass data set, the result of FMKOCSVM_LS is 5% higher than that of MKOCSVM, which proves that our membership calculation method can reduce the impact of noise on classification ability. In the remaining 9 data, the results of FMKOCSVM_LS are the best and have obvious advantages. For example, on the Waveform data set, the g-mean of FMKOCSVM_LS is 10% higher than that of WMKOCSVM and 4% higher than that of FMKOCSVM.

In terms of training time, although our method is not the fastest, FMKOCSVM_LS is still faster than WMKOCSVM. The training time of WMKOCSVM is 1.5 times of that of FMKOCSVM_LS on average. Compared with the training time of MKOCSVM, the increased training time of FMKOCSVM_LS is within the acceptable range.

All of the above proves that the MKOCSVM with membership is more robust. Moreover, our proposed membership based on local similarity is the best.

5. Conclusions

In order to solve the problem of poor robustness of MKOCSVM, this paper proposes a fuzzy multiple kernel one-class support vector machine based on local similarity, in which membership is based on the local similarity of the training data. Firstly, the similarity between samples is measured by combining the kernel matrix. Then, according to the selected threshold, the local similarity of each sample is determined. Finally, an S-type function is used to map the local similarity to the unit interval, and the function value is taken as the membership value. Experiments show that the membership method proposed in this paper can improve the robustness of MKOCSVM. Moreover, compared with the other two methods, our method is optimal.

The difficulty in fuzzy multiple kernel one-class support vector machine lies in how to determine the effective membership. Compared with the previous membership calculation method, only the target data are needed to calculate the membership based on the local similarity of the data, which is consistent with the OCSVM training set. In this method, the noise or outliers are assigned a small membership value, which makes the noise have the weakest impact on the classification boundary. Therefore, the membership method in this paper helps improve the robustness of MKOCSVM. In the next step, we will research the optimization method of parameters in the process of membership calculation based on local similarity.

Data Availability

The data underlying the study can be available upon request to the corresponding author.

Conflicts of Interest

The authors declare that they have no conflicts of interest.

Acknowledgments

References

[1] M. Torrisi, G. Pollastri, and Q. Le, "Deep learning methods in protein structure prediction," *Computational and Structural Biotechnology Journal*, vol. 18, pp. 1301–1310, 2020.

[2] A. Asuntha and A. Srinivasan, "Deep learning for lung cancer detection and classification," *Multimed Tools Application*, vol. 79, no. 11-12, pp. 1–32, 2020.

[3] S. Kiranyaz, M. Zabihi, A. B. Rad, T. Ince, R. Hamila, and M. Gabbouj, "Real-time phonocardiogram anomaly detection by adaptive 1D convolutional neural networks," *Neurocomputing*, vol. 411, pp. 291–301, 2020.

[4] B. E. Boser, I. M. Guyon, and V. N. Vapnik, "A training algorithm for optimal margin classifiers," in *Proceedings of the Fifth Annual Workshop on Computational Learning Theory*, pp. 144–152, Pittsburgh, PA, USA, July 1992.

[5] V. N. Vapnik, *The Nature of Statistical Learning Theory*, Springer, Berlin, Germany, 2nd edition, 1999.

[6] B. Schölkopf, R. C. Williamson, A. J. Smola et al., "Support vector method for novelty detection," in *Proceedings of the Advances in Neural Information Processing Systems in Advances 12 (NIPS)*, pp. 582–588, Denver, CO, USA, 2000.

[7] D. M. J. Tax and R. P. W. Duin, "Support vector domain description," *Pattern Recognition Letters*, vol. 20, no. 11–13, pp. 1191–1199, 1999.

[8] C. Lin and S. Wang, "Fuzzy support vector machines," *IEEE Transactions on Neural Networks*, vol. 13, no. 2, pp. 464–471, 2002.

[9] T. Wang, Y. Qiu, and J. Hua, "Centered kernel alignment inspired fuzzy support vector machine," *Fuzzy Sets and Systems*, vol. 394, pp. 110–123, 2020.

[10] Q. He and C. Wu, "Membership evaluation and feature selection for fuzzy support vector machine based on fuzzy rough sets," *Soft Computing*, vol. 15, no. 6, pp. 1105–1114, 2011.

[11] Q. Fan, Z. Wang, D. Li, D. Gao, and H. Zha, "Entropy-based fuzzy support vector machine for imbalanced datasets," *Knowledge-Based Systems*, vol. 115, pp. 87–99, 2017.

[12] M. Bicego and M. A. T. Figueiredo, "Soft clustering using weighted one-class support vector machines," *Pattern Recognition*, vol. 42, no. 1, pp. 27–32, 2009.

[13] B. Cyganek, "Image Segmentation with a hybrid ensemble of one-class support vector machines," in *Proceedings of the International Conference on Hybrid Artificial Intelligence Systems (HAIS)*, pp. 256–263, San Sebastian, Spain, 2010.

[14] F. Zhu, J. Yang, C. Gao, S. Xu, N. Ye, and T. Yin, "A weighted one-class support vector machine," *Neurocomputing*, vol. 189, pp. 1–10, 2016.

[15] M. Cha, J. S. Kim, and J. K. Baek, "Density weighted support vector data description," *Expert Systems with Applications*, vol. 41, no. 7, pp. 3343–3350, 2014.

[16] J. Yang, T. Deng, and R. Sui, "An adaptive weighted one-class SVM for robust outlier detection," in *Proceedings of the 2015 Chinese Intelligent Systems Conference*, pp. 475–484, Yangzhou, China, 2016.

[17] T. Hou, Y. Liu, K. Wang, J. Xie, and F. Liu, "A new weighted SVDD algorithm for outlier detection," in *Proceedings of the 28th Chinese Control and Decision Conference*, pp. 5456–5461, Yinchuan, China, 2016.

[18] S. Yin, X. Zhu, and C. Jing, "Fault detection based on a robust one class support vector machine," *Neurocomputing*, vol. 145, pp. 263–268, 2014.

[19] Q. Zhang, Q. He, C. Zhang, and H. Wang, "Multiple kernel one-class support vector machine," *Journal of Beijing University of Civil Engineering and Architecture*, vol. 36, no. 1, pp. 82–90, 2020, in Chinese.

[20] D. Dubois, H. Prade, and R. SŁOWIŃSKI, *Intelligent Decision Support: Handbook of Applications and Advances of the Rough Sets Theory*, Springer, Berlin, Germany, 1992.

[21] D. Chen, S. Kwong, Q. He, and H. Wang, "Geometrical interpretation and applications of membership functions with fuzzy rough sets," *Fuzzy Sets and Systems*, vol. 193, pp. 122–135, 2012.

[22] S. K. Siahroudi, P. Z. Moodi, and H. Beigy, "Detection of evolving concepts in non-stationary data streams: A multiple kernel learning approach," *Expert Systems with Applications*, vol. 91, pp. 187–197, 2018.

[23] Y. G. Zhao, Z. Song, F. Zheng, and L. Shao, "Learning a multiple kernel similarity metric for Kinship verification," *Information Sciences*, vol. 430-431, pp. 247–260, 2018.

[24] M. Gönen and E. Alpaydın, "Multiple kernel learning algorithms," *Journal of Machine Learning Research*, vol. 12, pp. 2211–2268, 2011.

[25] F. R. Bach, G. R. G. Lanckriet, and M. I. Jordan, "Multiple kernel learning, conic duality, and the SMO algorithm," in *Proceedings of the International Conference on Machine Learning*, pp. 41–48, New York, NY, USA, 2004.

[26] J. Qi, X. Liang, and R. Xu, "A multiple kernel learning model basaed on p –norm," *Computational Intelligence and Neuroscience*, vol. 2018, pp. 1–7, Article ID 1018789, 2018.

[27] Q. He, Q. Zhang, and H. Wang, "Kernel-target alignment based multiple kernel one-class support vector machine," in *Proceedings of the IEEE International Conference on Systems, Man and Cybernetics (SMC)*, pp. 2083–2088, Bari, Italy, 2019.

[28] H.-Q. Wang, F.-C. Sun, Y.-N. Cai, N. Chen, and L.-G. Ding, "Multiple kernel learning methods," *Acta Automatica Sinica*, vol. 36, no. 8, pp. 1037–1050, 2010, in Chinese.

[29] L. Chen, D. Chen, and H. Wang, "Alignment based kernel selection for multi-label learning," *Neural Processing Letters*, vol. 49, no. 3, pp. 1157–1177, 2019.

WILEY | Hindawi

Research Article

Impact of Awareness to Control Malaria Disease: A Mathematical Modeling Approach

Malik Muhammad Ibrahim [iD],[1] **Muhammad Ahmad Kamran** [iD],[2]
Malik Muhammad Naeem Mannan [iD],[3] **Sangil Kim** [iD],[1] **and Il Hyo Jung** [iD][1,4]

[1]*Department of Mathematics, Pusan National University, Busan 46241, Republic of Korea*
[2]*Department of Cogno-Mechatronics, Pusan National University, Busan 46241, Republic of Korea*
[3]*School of Allied Health Sciences, Griffith University, Gold Coast, Australia*
[4]*Finance Fishery Manufacture Industrial Mathematics Center on Big Data, Pusan National University,
 Busan 46241, Republic of Korea*

Correspondence should be addressed to Sangil Kim; sangil.kim@pusan.ac.kr and Il Hyo Jung; ilhjung@pusan.ac.kr

The mathematical modeling of malaria disease has a crucial role in understanding the insights of the transmission dynamics and corresponding appropriate prevention strategies. In this study, a novel nonlinear mathematical model for malaria disease has been proposed. To prevent the disease, we divided the infected population into two groups, unaware and aware infected individuals. The growth rate of awareness programs impacting the population is assumed to be proportional to the unaware infected individuals. It is further assumed that, due to the effect of awareness campaign, the aware infected individuals avoid contact with mosquitoes. The positivity and the boundedness of solutions have been derived through the completing differential process. Local and global stability analysis of disease-free equilibrium has been investigated via basic reproductive number R_0, if $R_0 < 1$, the system is stable otherwise unstable. The existence of the unique endemic equilibrium has been also determined under certain conditions. The solution to the proposed model is derived through an iterative numerical technique, the Runge–Kutta method. The proposed model is simulated for different numeric values of the population of humans and anopheles in each class. The results show that a significant increase in the population of susceptible humans is achieved in addition to the decrease in the population of the infected mosquitoes.

1. Introduction

Malaria is an ancient disease with challenging health issues. The tropical regions such as Africa, Asia, and America are favorable for the rapid spread of this disease [1]. In 2018, there are estimated two-hundred and twenty-eight million cases of malaria around the world. This deadly disease is the root cause of the death of four-hundred-five thousand people according to the World Health Organization (WHO) 2019 world malaria report [2]. This disease is originated by the plasmodium parasite. The transmission of this infection to human body is by the bite of a female mosquito. Medical symptoms such as a rise in the body temperature, fatigue,

pain, shivering, and sweats may occur within a few days after an infected mosquito bite. Till the time, there is no effective vaccine developed and some existing antimalarial drugs are losing their effectiveness due to the drug resistance evolved in the parasite [3].

The literature on the mathematical model for vector-borne disease likewise malaria is vast. The first published model demonstrating the life cycle of the malaria parasite was developed by Sir Ross [4]. The model proposed by Sir Ronald Ross is one of the simplest models, known as the classical Ross model in the literature. It demonstrates the crosstalk between the number of mosquitoes and the proportion of bite that produced infection in the human body.

This model was frequently used in the past due to its simplicity. However, the simplicity of the mathematical model is at the cost of limitations in the analysis. Therefore, considering the great challenge of malaria disease, several researchers have developed/modified existing models by introducing different factors/parameters in the model.

The mathematical modeling of infectious disease has proved to play an important role in understanding the insights of the transmission dynamics and appropriate control strategies [5]. In past, several mathematical models have been proposed to analyze this deadly disease. The extension of Sir Ross's model includes the modification/addition of different important factors likewise, latent period of infection [6], immunity factor [7], the heterogeneity of human and mosquito [8, 9], susceptibility to malaria in host population [10, 11], exposed human and mosquito [3, 12], and recovered human [8, 13], among others.

Macdonald has introduced the effect of exposed mosquitoes by employing a separate differential equation catering the rate of change of exposed mosquitoes [7]. Similarly, Anderson and May proposed to add the rate of change of exposed human in the model [6]. The comparison of two epidemiological models of immunity to malaria shows that different characterizations of immunity, boosted by exposure to infection, generate qualitatively different results [8]. Nagwa and Shu analyzed the deterministic differential equation model for endemic malaria in the presence of the variable host and parasite population [13]. Their results suggested that disease is persistent if the threshold parameter exceeds the barrier of magnitude unity; otherwise, a disease-free equilibrium always exists. In a similar study, Chitnis and co-authors have presented the bifurcation analysis of the reproductive number (RN) [14]. RN is the number of secondary infections that one infectious individual would create over the time course of the disease period, provided that total population except infectious is susceptible [15]. Lashari and co-authors formulated the vector-borne disease environment in the form of an optimal control problem. They have introduced three different control parameters including personal protection, disease medical treatment, and mosquito reduction strategies [3]. Ozair and co-authors have analyzed the transmission dynamics of malaria disease with a nonlinear incident rate [16]. Addawe and Lope proposed to divide the human population into two compartments: preschool (0–5 years) and over five age [17]. Their findings verify the existing results that asymptotical stability is guaranteed with RN magnitude less than unity. Mishra and co-authors, Samanta and co-authors, and Greenhalag and co-authors have proposed and analyzed a nonlinear mathematical model to assess the effect of awareness by media on the prevalence of infectious disease [18–20]. Cai et al. introduced a malaria model with an asymptomatic class in human population and exposed classes in both human and vector populations [21]. Sung Chan and co-authors have studied the vector-bias mathematical model and considered two different incidence areas: a high transmission area and a low transmission area [22]. Recently, Sung Chan and co-authors have developed a new transmission model to evaluate the rate of malaria relapse

infections in the northern part of Korea and to examine its effect at the population-level on radical cure [23].

In this article, a deterministic vector-borne disease model is proposed. Previous studies suggested that prevention is a control parameter for such infectious diseases. Thus, it shall be helpful to add awareness terms in the mathematical model of the disease. The whole infected host population is divided into two groups, aware and unaware infected individuals. We analyzed the model to study the impact of awareness programs conducted by awareness campaign through medical staff on the spread of malaria disease. In the modeling process, it is assumed that the growth rate of the cumulative density of awareness program will increase with an increase in the unaware infected individuals in the host population. We also assumed that both infected classes can spread disease when the mosquitoes contact them, but the aware class has very low chance to spread disease due to awareness campaigns. It is further assumed that due to awareness, the contact rate of infected mosquito interaction with aware humans will be reduced. The performance of the proposed model is evaluated by comparing the result with previous models. The result of the proposed model suggests that disease-free equilibrium is achieved earlier than the existing model.

The rest of the article is as follows. In section 2, the formulation of a mathematical model is presented. Section 3 describes the positivity and boundedness of solution. In section 4, the existence of disease-free equilibrium including derivation of basic reproduction number and stability analysis of the model is presented. The results of numerical simulation are illustrated in Section 5, Section 6 provides discussion, and Section 7 provides conlclusion.

2. Model Formulation

Mosquito-borne diseases, e.g., yellow fever, dengue fever, and malaria, are frequently observed in tropical and subtropical countries. These illnesses spread widely in a short period with the life-threatening impact of many human lives. Among these vector-borne diseases, malaria is one of the serious and major illnesses caused by several species of mosquito-borne parasite (*Plasmodium falciparum*, *Plasmodium malaria*, *Plasmodium ovale*, *Plasmodium vivax*, etc.) [24]. *Anopheles* female mosquito is responsible for the transmission of disease to the human body through a bite [3]. This blood meal of mosquito converts a healthy human being (susceptible) into a category called infected hosts. The human population that are not infected but under the threat that they can catch malaria infection are known as the exposed population. Individuals recovered from the infected population through medical treatment without threat to their life fall in the group of recovered ones. Figure 1 shows the schematic diagram of the proposed malaria disease model for particular population of humans and mosquitoes.

The human population is divided into five different compartments (susceptible, exposed, unaware infected, aware infected, and recovered) representing the total population at any time t. Let N_h be the total population in a region under consideration for malaria disease analysis.
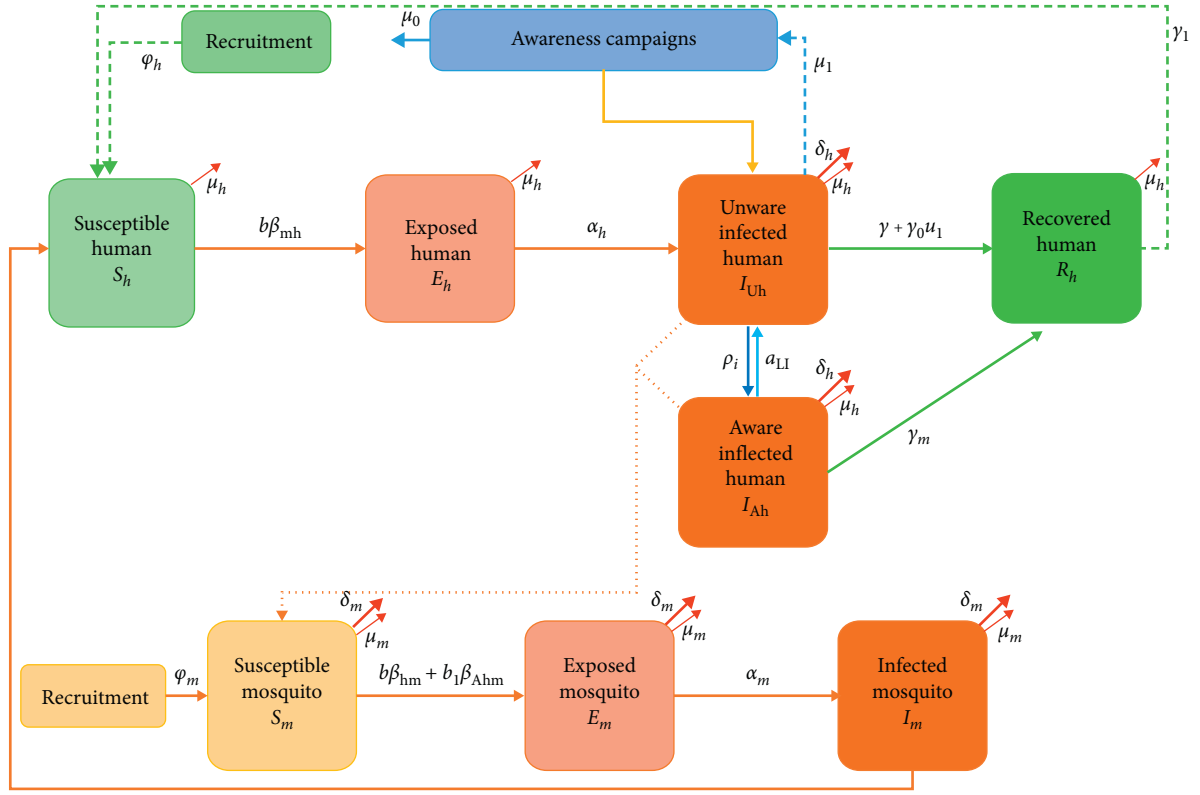
Figure 1: Schematic diagram of the proposed model algorithm.

Suppose $S_h(t)$ denotes the numbers of humans susceptible to disease, $E_h(t)$ is the count for the exposed hosts to disease, $I_{uh}(t)$ and $I_{Ah}(t)$ are showing unaware and aware infected human population, and $R_h(t)$ is the numbers of individual who have temporarily recovered from disease. Similarly, mosquito population has been grouped into three compartments. Let $S_m(t)$ is the count for susceptible mosquito population, $E_m(t)$ is the numbers for exposed mosquito population, $I_m(t)$ represents the numbers of an infected member of the mosquito population, and $N_m(t)$ is the total count of the mosquito population in a particular area of interest. Also, let $M(t)$ be the cumulative density of awareness programs driven in the region at time t. The growth rate of the density of awareness programs is assumed to be proportional to unaware infected individuals. It is assumed that the contact of infected mosquitoes with aware individuals will be reduced. The constant μ_1 represents the rate at which awareness campaigns are being implemented and μ_0 represents the depletion rate of these campaigns due to ineffectiveness, a social problem in the population.

For host population, φ_h is the recruitment rate of human population in a particular region, b is the contact rate of mosquito to human population, β_{mh} is the probability that bite of infectious mosquito result in the transmission of disease to susceptible human, γ_1 is the rate of loss of immunity in recovered human, α_h is the rate of progression from exposed to unaware infected class, γ is the treatment rate in the region, γ_0 is the recovery rate of unaware infected population with temporary immunity, u_1 represents the

successful efforts of treatment resulting recovered humans, ρ_i is the rate of awareness to unaware infected human, a_{LI} is the rate of loss of awareness of aware infected human, γ_m is the recovery rate of aware infected human (that rate is greater than the normal recovery rate due to awareness), and δ_h and μ_h are the disease and natural death rate of the human, respectively.

For mosquito population, φ_m and μ_m are the mosquito recruitment and natural death rate, δ_m represents the strategies to kill mosquito after awareness, β_{hm} is the probability that a blood meal of an infectious mosquito result in the transmission of disease to susceptible individual, β_{Ahm} is the probability of disease transmission from aware infected human to susceptible mosquitoes, b_1 is the contact rate between unaware infected human to susceptible mosquitoes, and α_m is the rate of progression from exposed mosquitoes to infected mosquitoes. The definitions of the mathematical parameters with their values are summarized in Table 1.

These definitions lead to a set of coupled nonlinear differential equations describing the proposed model, for the infectious vector-borne disease. The mathematical form of the model is described as follows:

$$\frac{dS_h(t)}{dt} = \varphi_h - b\beta_{mh}S_h(t)I_m(t) + \gamma_1 R_h(t) - \mu_h S_h(t), \quad (1)$$

$$\frac{dE_h(t)}{dt} = b\beta_{mh}S_h(t)I_m(t) - (\alpha_h + \mu_h)E_h(t), \quad (2)$$

TABLE 1: Definition and values of parameters used in the model.

Parameters	Definition	Values	References
φ_h	Recruitment rate of human	10	[3]
γ_1	Rate of loss of immunity to recovered human	1/730	[25]
μ_h	Natural death rate of human	1/60 * 365	[3]
b	Contact rate between mosquito and human	3	[3]
β_{mh}	Disease transmission rate from mosquito to human	0.001	[3]
α_h	Rate of progression from exposed to unaware infected	1/17	[3]
γ	Treatment rate in the region	0.07	[3]
γ_0	Recovery rate of unaware infected human	0.04	[3]
u_1	Successful effort of treatment (0 or 1)	1	
ρ_i	Rate of awareness to unaware infected human	0.0005	Assumed
δ_h	Disease death rate of infected human	0.01	[3]
a_{LI}	Rate of loss of awareness to uninfected human	0.02	Assumed
γ_m	Recovery rate of aware infected human	0.012	Assumed
φ_m	Recruitment rate of mosquito	50	[3]
β_{uhm}	Disease transmission rate from unaware human to mosquito	0.0001	[3]
b_1	Contact rate between mosquito and aware human	0.12	Assumed
β_{Ahm}	Disease transmission rate from aware human to mosquito	0.0001	Assumed
μ_m	Natural death rate of mosquito	1/15	[3]
δ_m	Death rate of mosquito due to human awareness	1/50	Assumed
α_m	Rate of progression from exposed mosquito to infected mosquito	1/18	[3]
μ_1	Constant rate influenced by unaware infected human	0.02	Assumed
μ_0	Depletion rate of awareness	0.01	Assumed

$$\frac{dI_{Uh}(t)}{dt} = \alpha_h E_h(t) - (\delta_h + \mu_h + \gamma + \gamma_0 u_1 + \rho_i M(t))I_{Uh}(t) + a_{LI}I_{Ah}(t), \tag{3}$$

$$\frac{dI_{Ah}(t)}{dt} = \rho_i M(t)I_{Uh}(t) - (\mu_h + \delta_h)I_{Ah}(t) - \gamma_m I_{Ah}(t) - a_{LI}I_{Ah}(t), \tag{4}$$

$$\frac{dR_h(t)}{dt} = (\gamma + \gamma_0 u_1)I_{Uh}(t) + \gamma_m I_{Ah}(t) - (\mu_h + \gamma_1)R_h(t), \tag{5}$$

$$\frac{dS_m(t)}{dt} = \varphi_m - (\mu_m + \delta_m)S_m(t) - b\beta_{hm}S_m(t)I_{Uh}(t) - b_1\beta_{Ahm}S_m(t)I_{Ah}(t), \tag{6}$$

$$\frac{dE_m(t)}{dt} = b\beta_{hm}S_m(t)I_{Uh}(t) + b_1\beta_{Ahm}S_m(t)I_{Ah}(t) - (\mu_m + \delta_m + \alpha_m)E_m(t), \tag{7}$$

$$\frac{dI_m(t)}{dt} = \alpha_m E_m(t) - (\mu_m + \delta_m)I_m(t), \tag{8}$$

$$\frac{dM(t)}{dt} = \mu_1 I_{Uh}(t) - \mu_0 M(t). \tag{9}$$

3. Positivity and Boundedness of Solutions

The mathematical model presented in the system of equations (1)–(9) describes the rate of change of different compartments of human and mosquito population. Therefore, it is important to verify that all solutions with nonnegative initial conditions shall remain nonnegative for all time. All the solutions of proposed system, which initiates inside region D, remain in region D. Mathematically,

This result can be summarized in the following theorem.

Theorem 1. *For all time $t \geq 0$, there exists a domain:*

$$D = \left\{ \begin{array}{c} (S_h(t), E_h(t), I_{Uh}(t), I_{Ah}(t), R_h(t), S_m(t), E_m(t), I_m(t)) \in R_+^8: S_h(0) > 0, E_h(0) \geq 0 \\ I_{Uh}(0) \geq 0, I_{Ah}(0) \geq 0, R_h(0) \geq 0, S_m(0) \geq 0, E_m(0) \geq 0, I_m(0) \geq 0; N_h \leq (\varphi_h/\mu_h) \\ N_m \leq (\varphi_m/\mu_m) \end{array} \right\}. \tag{10}$$

All the solutions of the system of equations (1)–(9) are bounded in domain D:

Proof. Let $(S_h(t), E_h(t), I_{Uh}(t), I_{Ah}(t), R_h(t), S_m(t), E_m(t), I_m(t))$ be any solution with positive initial conditions

$S_h(0) > 0, E_h(0) \geq 0, I_{Uh}(0) \geq 0, \quad I_{Ah}(0) \geq 0, R_h(0) \geq 0, S_m(0) \geq 0, E_m(0) \geq 0, I_m(0) \geq 0$, with $N_h(S_h(t), E_h(t), I_{Uh}(t), I_{Ah}(t), R_h(t)) = S_h(t) + E_h(t) + I_{Uh}(t) + I_{Ah}(t) + R_h(t)$ and $N_m(S_m(t), E_m(t), I_m(t)) = S_m(t) + E_m(t) + I_m(t) + E_m(t) + I_m(t)$. Notice that the sum of the first five compartments $S_h(t), E_h(t), I_{Uh}(t), I_{Ah}(t), R_h(t)$ in system of equations (1)–(9) is equal to the total human population of size N_h and the sum of compartments $(S_m(t), E_m(t), I_m(t))$ is equal to the total mosquito population of size N_m. Hence adding these equations yields the time derivative along with the solution of equations (1)–(9) given as

$$\frac{dN_h}{dt} = \varphi_h - \mu_h N_h - \delta_h(I_{Uh} + I_{Ah}) \leq \varphi_h - \mu_h N_h. \quad (11)$$

$$\frac{dN_m}{dt} = \varphi_m - \mu_m N_m - \delta_m N_m \leq \varphi_m - \mu_m N_m. \quad (12)$$

Equations (11) and (12) can be written as

$$\left(\frac{dN_h}{dt}\right) + \mu_h N_h \leq \varphi_h, \quad (13)$$

$$\left(\frac{dN_m}{dt}\right) + \mu_m N_m \leq \varphi_m. \quad (14)$$

Solving these different inequalities yields

$$N_h \leq \left(\frac{\varphi_h}{\mu_h}\right)\left(1 - e^{-\mu_h t}\right) + N_h(0)e^{-\mu_h t}, \quad (15)$$

$$N_m \leq \left(\frac{\varphi_m}{\mu_m}\right)\left(1 - e^{-\mu_m t}\right) + N_m(0)e^{-\mu_m t}. \quad (16)$$

Consequently, taking the limit as $t \longrightarrow \infty$ gives $N_h \leq (\varphi_h/\mu_h) \& N_m \leq (\varphi_m/\mu_m)$. Thus, D is positively invariant, and all the solutions are bounded in the interval $[0, \infty)$. □

4. Existence of Disease-Free Equilibrium Point

Disease-free equilibrium points are the steady-state solution, when there is no malaria infection. Thus, the disease-free equilibrium point for the system of equations (1)–(9) implies that $E_h = 0, I_{uh} = 0, I_{Ah} = 0, R_h = 0, E_m = 0$, and $I_m = 0$, and after solving the equations (1) and (6) of system yields $S_h = (\varphi_h/\mu_h)$ and $S_m = (\varphi_m/\mu_m + \delta_m)$. Thus, we obtain the disease-free equilibrium point, E_1:

$$E_1 = \left(\left(\frac{\varphi_h}{\mu_h}\right), 0, 0, 0, 0, \left(\frac{\varphi_m}{\mu_m + \delta_m}\right), 0, 0, 0\right). \quad (17)$$

4.1. Basic Reproductive Number.
The basic reproductive number R_0 measures the average number of new malaria infections generated by a single infected individual in a completely susceptible population [26].

To obtain R_0 for system of equations (1)–(9), we used the next-generation matrix technique described in [15, 25, 27, 28]. Let $x = (E_h, I_{Uh}, I_{Ah}, E_m, I_m, S_h, R_h, S_m)^T$, then the model system of equations (1)–(9) can be written as

$$\frac{dx}{dt} = F(x) - V(x), \quad (18)$$

where

$$V(x) = (V^-(x) - V^+(x)), \quad (19)$$

$$F(x) = \begin{pmatrix} b\beta_{mh}S_h I_m \\ 0 \\ 0 \\ b\beta_{hm}S_m I_{Uh} + b_1\beta_{Ahm}S_m I_{Ah} \\ 0 \\ 0 \\ 0 \\ 0 \\ 0 \end{pmatrix}, \quad (20)$$

$$V(x) = \begin{pmatrix} (\alpha_h + \mu_h)E_h \\ -\alpha_h E_h - a_{LI}I_{Ah} + (\delta_h + \mu_h + \gamma + \gamma_0 u_1 + \rho_i M)I_{Uh} \\ -\rho_i M I_{Uh} + (\mu_h + \delta_h + \gamma_m + a_{LI})I_{Ah} \\ (\mu_m + \delta_m + \alpha_m)E_m \\ -\alpha_m E_m + (\mu_m + \delta_m)I_m \\ -\varphi_h - \gamma_1 R_h + b\beta_{mh}S_h I_m + \mu_h S_h \\ -(\gamma + \gamma_0 u_1)I_{Uh} - \gamma_m I_{Ah} + (\mu_h + \gamma_1)R_h \\ -\varphi_m + (\mu_m + \delta_m)S_m + b\beta_{hm}S_m I_{Uh} + b_1\beta_{Ahm}S_m I_{Ah} \\ -\mu_1 I_{Uh} + \mu_0 M \end{pmatrix}. \quad (21)$$

Finding the partial derivative of F and V at disease-free equilibrium point E_1 gives F and V, respectively, as follows:

$$F = \begin{pmatrix} 0 & 0 & 0 & 0 & b\beta_{mh}(\varphi_h/\varphi_h) \\ 0 & 0 & 0 & 0 & 0 \\ 0 & 0 & 0 & 0 & 0 \\ 0 & b\beta_{hm}(\varphi_m/\mu_m + \delta_m) & b_1\beta_{Ahm}(\varphi_m/\mu_m + \delta_m) & 0 & 0 \\ 0 & 0 & 0 & 0 & 0 \end{pmatrix}, \quad (22)$$

$$
V = \begin{pmatrix}
\alpha_h + \mu_h & 0 & 0 & 0 & 0 \\
-\alpha_h & \delta_h + \mu_h + \gamma + \gamma_0 u_1 & -a_{\mathrm{LI}} & 0 & 0 \\
0 & 0 & \mu_h + \delta_h + \gamma_m + a_{\mathrm{LI}} & 0 & 0 \\
0 & 0 & 0 & \mu_m + \delta_m + \alpha_m & 0 \\
0 & 0 & 0 & -\alpha_m & \mu_m + \delta_m
\end{pmatrix}.
\tag{23}
$$

So that

$$
V^{-1} = \begin{pmatrix}
v_{11}^{-1} & 0 & 0 & 0 & 0 \\
v_{21}^{-1} & v_{22}^{-1} & v_{23}^{-1} & 0 & 0 \\
0 & 0 & v_{33}^{-1} & 0 & 0 \\
0 & 0 & 0 & v_{44}^{-1} & 0 \\
0 & 0 & 0 & v_{54}^{-1} & v_{55}^{-1}
\end{pmatrix},
\tag{24}
$$

where $v_{11}^{-}1 = (1/\alpha_h + \mu_h)$, $v_{21}^{-1} = (-\alpha_h/(\alpha_h + \mu_h)(\delta_h + \mu_h + \gamma + \gamma_0 u_1))$, $v_{22}^{-1} = (1/\delta_h + \mu_h + \gamma + \gamma_0 u_1)$, $v_{23}^{-1} = (-a_{\mathrm{LI}}/(\delta_h + \mu_h + \gamma + \gamma_0 u_1)(\mu_h + \delta_h + \gamma_m + a_{LI}))$, $v_{33}^{-1} = (1/\mu_h + \delta_h + \gamma_m + a_{LI})$, $v_{44}^{-1} = (1/\mu_m + \delta_m + \alpha_m)$, $v_{54}^{-1} = (-\alpha_m/(\mu_m + \delta_m + \alpha_m)(\mu_m + \delta_m))$, $v_{55}^{-1} = (1/\mu_m + \delta_m)$.

The basic reproductive number $R_0 = \rho(FV^{-1})$ is the spectral radius of the product FV^{-1}. Thus,

$$
R_0 = \rho\left(FV^{-1}\right) = \sqrt{\frac{\varphi_h \varphi_m \alpha_h \alpha_m b^2 \beta_{\mathrm{mh}} \beta_{\mathrm{hm}}}{\mu_h (\alpha_h + \mu_h)(\delta_h + \mu_h + \gamma + \gamma_0 u_1)(\mu_m + \delta_m + \alpha_m)(\mu_m + \delta_m)^2}}.
\tag{25}
$$

In equation (25), $(\alpha_h/(\alpha_h + \mu_h))$ is the probability that a human will survive the exposed state to become infectious; $(1/(\delta_h + \mu_h + \gamma + \gamma_0 u_1))$ is the average duration of the infectious period of the human; $(\alpha_m/(\mu_m + \delta_m + \alpha_m))$ is the probability that a mosquito will survive the exposed state to become infectious; and $(1/(\mu_m + \delta_m))$ is the state to become infectious. Let the basic reproductive number, R_0, be written as $R_0 = \sqrt{R_h R_m}$, where $R_h = (\varphi_h \alpha_h b \beta_{\mathrm{mh}}/\mu_h (\alpha_h + \mu_h)(\delta_h + \mu_h + \gamma + \gamma_0 u_1))$ and $R_m = (\varphi_m \alpha_m b \beta_{\mathrm{hm}}/(\mu_m + \delta_m + \alpha_m)(\mu_m + \delta_m)^2)$.

Here, R_h describes the number of humans that one infectious mosquito infects over its expected infection period in a completely susceptible human population and R_m describes the number of mosquitoes infected by one infectious human during the period of infectiousness in a completely susceptible mosquito population.

4.2. Stability Analysis of Disease-Free Equilibrium. We analyzed the stability of disease-free equilibrium of the system of equations (1)–(9) by using the basic reproductive number R_0 in the following theorem.

Theorem 2. *The disease-free equilibrium (DFE) E_1 is locally asymptotically stable if $R_0 \leq 1$ and unstable if $R_0 > 1$.*

Proof. The Jacobian of the system of equations (1)–(9) evaluated at the disease-free equilibrium point E_1 is obtained as follows:

$$
J(E_1) = \begin{bmatrix}
j_{11} & 0 & 0 & 0 & j_{15} & 0 & 0 & j_{18} & 0 \\
0 & j_{22} & 0 & 0 & 0 & 0 & 0 & j_{28} & 0 \\
0 & j_{32} & j_{33} & j_{34} & 0 & 0 & 0 & 0 & 0 \\
0 & 0 & 0 & j_{44} & 0 & 0 & 0 & 0 & 0 \\
0 & 0 & 0 & j_{54} & j_{55} & 0 & 0 & 0 & 0 \\
0 & 0 & j_{63} & j_{64} & j_{66} & j_{66} & 0 & 0 & 0 \\
0 & 0 & j_{73} & j_{74} & 0 & 0 & j_{77} & 0 & 0 \\
0 & 0 & 0 & 0 & 0 & 0 & j_{87} & j_{88} & 0 \\
0 & 0 & j_{93} & 0 & 0 & 0 & 0 & 0 & j_{99}
\end{bmatrix},
\tag{26}
$$

where $j_{11} = -\mu_h$, $j_{15} = \gamma_1$, $j_{18} = -b\beta_{\mathrm{mh}}(\varphi_h/\mu_h)$, $j_{22} = -(\alpha_h + \mu_h)$, $j_{28} = b\beta_{\mathrm{mh}}(\varphi_h/\mu_h)$, $j_{32} = \alpha_h$, $j_{33} = -(\delta_h + \mu_h + \gamma + \gamma_0 u_1)$, $j_{34} = a_{\mathrm{LI}}$, $j_{44} = -(\mu_m + \gamma_m + \delta_m + a_{LI})$, $j_{54} = \gamma_m$, $j_{55} = -(\mu_h + \gamma_1)$, $j_{63} = -b\beta_{\mathrm{hm}}(\varphi_m/\mu_m + \delta_m)$, $j_{64} = -b_1 \beta_{\mathrm{Ahm}}(\varphi_m/\mu_m + \delta_m)$, $j_{66} = -(\mu_m + \delta_m)$, $j_{73} = b\beta_{\mathrm{hm}}(\varphi_m/\mu_m + \delta_m)$, $j_{74} = b_1 \beta_{\mathrm{Ahm}}(\varphi_m/\mu_m + \delta_m)$, $j_{77} = -(\mu_m + \delta_m + \alpha_m)$, $j_{87} = \alpha_m$, $j_{88} = -(\mu_m + \delta_m)$, $j_{93} = \mu_1$, $j_{99} = -\mu_0$.

The DFE, E_1, is locally asymptotically stable (LAS) if we show that all the eigenvalues of equation (26) have negative real part. Since the first, sixth, and ninth columns of equation (26) contain only the diagonal terms, three eigenvalues $-\mu_h, -(\mu_m + \delta_m)$, and $-\mu_0$ can be obtained from these columns. Remaining eigenvalues of equation (26) can be obtained from the submatrix J_1 formed by excluding the first, sixth, and ninth rows and columns of equation (26). Hence, we have

$$J_1(E_1) = \begin{bmatrix} j_{22} & 0 & 0 & 0 & 0 & j_{28} \\ j_{32} & j_{33} & 0 & 0 & 0 & 0 \\ 0 & 0 & j_{44} & 0 & 0 & 0 \\ 0 & 0 & j_{54} & j_{55} & 0 & 0 \\ 0 & j_{73} & j_{74} & 0 & j_{77} & 0 \\ 0 & 0 & 0 & 0 & j_{87} & j_{88} \end{bmatrix}. \tag{27}$$

Similarly, the fourth column of equation (27) contains only the diagonal term which forms negative eigenvalues

$-(\mu_h + \gamma_1)$. All the remaining eigenvalues of equation (27) can be calculated by the submatrix J_2:

$$J_2(E_1) = \begin{bmatrix} j_{22} & 0 & 0 & 0 & j_{28} \\ j_{32} & j_{33} & 0 & 0 & 0 \\ 0 & 0 & j_{44} & 0 & 0 \\ 0 & j_{73} & j_{74} & j_{77} & 0 \\ 0 & 0 & 0 & j_{87} & j_{88} \end{bmatrix}. \tag{28}$$

The eigenvalues of equation (28) are the roots of the following characteristic equation:

$$(\lambda - j_{44})((\lambda - j_{22})(\lambda - j_{33})(\lambda - j_{77})(\lambda - j_{88}) - j_{28}j_{32}j_{73}j_{87}) = 0. \tag{29}$$

From equation (29), we can get five eigenvalues. One of the eigenvalues $j_{44} = -(\mu_m + \gamma_m + \delta_m + a_{LI})$ has a negative real part. The other four eigenvalues can be obtained from equation (30):

$$\left. \begin{array}{l} (\lambda - j_{22})(\lambda - j_{33})(\lambda - j_{77})(\lambda - j_{88}) - j_{28}j_{32}j_{73}j_{87} = 0 \\[2mm] (\lambda + \alpha_h + \mu_h)(\lambda + \delta_h + \mu_h + \gamma + \gamma_0 u_1)(\lambda + \mu_m + \delta_m + \alpha_m)(\lambda + \mu_m + \delta_m) \\[2mm] \left. \quad - \dfrac{b^2 \alpha_h \alpha_m \beta_{mh} \beta_{hm} \varphi_h \varphi_m}{\mu_h(\mu_m + \delta_m)} \right\} = 0 \end{array} \right\}. \tag{30}$$

If we let $b_1 = -j_{22}, b_2 = -j_{33}, b_3 = -j_{77}$, and $b_1 = -j_{88}$, then equation (30) becomes

$$a_4\lambda^4 + a_3\lambda^3 + a_2\lambda^2 + a_1\lambda + a_0 = 0, \tag{31}$$

where

$$\left. \begin{array}{l} a_4 = 1, a_3 = b_1 + b_2 + b_3 + b_4, a_2 = b_1b_2 + b_1b_3 + b_1b_4 + b_2b_3 + b_2b_4 + b_3b_4, \\[3mm] a_1 = b_1b_2b_3 + b_1b_2b_4 + b_1b_3b_4 + b_2b_3b_4, a_0 = b_1b_2b_3b_4 - \dfrac{b^2 \alpha_h \alpha_m \varphi_h \varphi_m \beta_{mh} \beta_{hm}}{\mu_h(\mu_m + \delta_m)}, \end{array} \right\} \tag{32}$$

where a_0 is in the terms of reproduction number and R_0, can be written as

$$a_0 = b_1b_2b_3b_4(1 - R_0). \tag{33}$$

We employ the Routh–Hurwitz criterion, which states that all the roots of equation (31), has negative real parts, if and only if the coefficients a_i are positive and matrices $H_i > 0$ for $i = 0, 1, 2, 3$, and 4. From equation (32), it is easy to see that $a_1 > 0, a_2 > 0, a_3 > 0$, and $a_4 > 0$ since all $b_i's > 0$. Moreover, if $R_0 < 1$, it follows from equation (33) that $a_0 > 0$. Also, the Hurwitz matrices for equation (31) are found to be positive that are given as follows:

$$\begin{aligned} H_1 &= a_1 > 0, \\[2mm] H_2 &= \det\begin{pmatrix} a_3 & a_4 \\ a_1 & a_2 \end{pmatrix} > 0, \\[2mm] H_3 &= \det\begin{pmatrix} a_3 & a_4 & a_0 \\ a_1 & a_2 & a_3 \\ 0 & a_0 & a_1 \end{pmatrix} > 0, \\[2mm] H_4 &= \det\begin{pmatrix} a_3 & a_4 & 0 & 0 \\ a_1 & a_2 & a_3 & a_4 \\ 0 & a_0 & a_1 & a_2 \\ 0 & 0 & 0 & a_0 \end{pmatrix} > 0. \end{aligned} \tag{34}$$

Therefore, all the eigenvalues of the Jacobian matrix in equation (26) have negative real parts, when $R_0 < 1$ and DFE is LAS. However, when $R_0 > 1$ we see that $a_0 < 0$ and by Descartes's rule of signs, there is exactly one sign-change in the sequence $a_4, a_3, a_2, a_1,$ and a_0 of the coefficient of equation (31). So, there is one eigenvalue with the positive real part and DFE is unstable. □

Remark 1. The case for $R_0 = 1$ is possible when $a_0 = 0$ in the characteristic equation. By considering the special case of Routh–Hurwitz stability criterion [29], and replacing this term with very small value, i.e., ε, the result could be interpreted as first case, i.e., $R_0 < 1$.

Theorem 3. *The disease-free equilibrium (DFE) of the system of equations (1)–(9) is globally asymptotically stable (GAS) on D if $R_0 < 1$.*

Proof. To prove this theorem, we adopt the method described in [30–32]. Castillo-Chavez and co-authors described this method to prove the GAS of DFE in their research article [32]. We begin the proof by defining new variables and breaking our system of equations (1)–(9) into two subsystems. With $X = (S_h, R_h, S_m)$ and $I = (E_h, I_{uh}, I_{Ah}, E_m, I_m)$, this system can be written as

$$\frac{dX}{dt} = F(X, I), \tag{35}$$

$$\frac{dI}{dt} = G(X, I) \text{ with } G(X, 0) = 0, \tag{36}$$

where $X \in R^3$ denotes the number of uninfected compartments and $I \in R^5$ denotes the number of infected compartments.

The two vector-valued functions $F(X, I)$ and $G(X, I)$ are given as

$$F(X, I) = \begin{pmatrix} \varphi_h - b\beta_{\text{muh}}S_h(t)I_m(t) + \gamma_1 R_{\text{Uh}}(t) - \mu_h S_h(t) \\ (\gamma + \gamma_0 u_1)I_{\text{Uh}}(t) - (\mu_h + \gamma_1)R_h(t) + \gamma_m I_{\text{Ah}}(t) \\ \varphi_m - (\mu_m + \delta_m)S_m(t) - b\beta_{\text{Uhm}}S_m(t)I_{\text{Uh}}(t) - b_1\beta_{\text{Ahm}}S_m(t)I_{\text{Ah}}(t) \end{pmatrix}, \tag{37}$$

$$G(X, I) = \begin{pmatrix} b\beta_{\text{mh}}S_h(t)I_m(t) - (\alpha_h + \mu_h)E_h(t) \\ \alpha_h E_h(t) - (\delta_h + \mu_h + \gamma + \gamma_0 u_1 + \rho_i M(t))I_{\text{Uh}}(t) + a_{LI} I_{\text{Ah}}(t) \\ \rho_i M(t)I_{\text{Uh}}(t) - (\mu_h + \delta_h)I_{\text{Ah}}(t) - \gamma_m I_{\text{Ah}}(t) - a_{LI} I_{\text{Ah}}(t) \\ b\beta_{\text{Uhm}}S_m(t)I_{\text{Uh}}(t) + b_1\beta_{\text{Ahm}}S_m(t)I_{\text{Ah}}(t) - (\mu_m + \delta_m + \alpha_m)E_m(t) \\ \alpha_m E_m(t) - (\mu_m + \delta_m)I_m(t) \end{pmatrix} \text{ with } G(X, 0) = 0. \tag{38}$$

$E_0 = (X^*, 0)$ denotes the disease-free equilibrium of the subsystems, where

$$X^* = \left(\left(\frac{\varphi_h}{\mu_h}\right), 0, \left(\frac{\varphi_m}{\mu_m + \delta_m}\right)\right). \tag{39}$$

The conditions (H_1) and (H_2) below must be met for the global stability:

$$(H_1): For\left(\frac{dX}{dt}\right) = F(X, 0), X^* \text{ is GAS}, \tag{40}$$

$$(H_2): G(X, I) = AI - \widehat{G}(X, I) \text{ with } \widehat{G}(X, I) \geq 0, \quad \forall(X, I) \in D, \tag{41}$$

where A is an M-matrix (the off-diagonal elements of A are nonnegative).

Now consider the reduced system $(dX/dt) = F(X, 0)$,

$$\frac{dS_h(t)}{dt} = \varphi_h + \gamma_1 R_h(t) - \mu_h S_h(t), \tag{42}$$

$$\frac{dR_h(t)}{dt} = -(\mu_h + \gamma_1)R_h(t), \tag{43}$$

$$\frac{dS_m(t)}{dt} = \varphi_m - (\mu_m + \delta_m)S_m(t). \tag{44}$$

$X^* = (S_h, R_h, S_m) = (\varphi_h/\mu_h, 0, \varphi_m/\mu_m + \delta_m)$ is the GAS equilibrium point for the reduced system $(dX/dt) = F(X, 0)$. To see this, solve equation (43) to obtain $R_h = R_h(0)e^{-(\mu_h + \gamma_1)t} \Longrightarrow R_h \longrightarrow 0$ as $t \longrightarrow \infty$. Similarly, from equation (44), we get $S_m = (\varphi_m/(\mu_m + \delta_m)) + (S_m(0) - (\varphi_m/(\mu_m + \delta_m)))e^{-(\mu_m + \delta_m)t} \Longrightarrow S_m \longrightarrow (\varphi_m/(\mu_m + \delta_m))$ as $t \longrightarrow \infty$.

Finally, equation (42) yields $S_h = (\varphi_h/\mu_h) + (S_h(0) + R_h(0) - (\varphi_h/\mu_h))e^{-\mu_h t}$ and $-R_h(0)e^{-(\mu_h + \gamma_1)t} \Longrightarrow S_h \longrightarrow (\varphi_h/\mu_h)$ as $t \longrightarrow \infty$. Hence, the convergence of solutions of equations (42)–(44) is global in D. And, $G(X, I) = [AI - \widehat{G}(X, I) \text{ with } \widehat{G}(X, I) \geq 0, \forall(X, I) \in D]$, where

$$A = \begin{bmatrix} -(\alpha_h + \mu_h) & 0 & 0 & 0 & (\varphi_h/\mu_h)b\beta_2 \\ \alpha_h & -A & a_{\text{LI}} & 0 & 0 \\ 0 & \rho_i M & -B & 0 & 0 \\ 0 & K_1 b\beta_2 & K_1 b_1\beta_3 & -C & 0 \\ 0 & 0 & 0 & \alpha_m & -D \end{bmatrix}, \tag{45}$$

where

$$\beta_1 = \beta_{\mathrm{mh}}, \beta_2 = \beta_{\mathrm{hm}}, \beta_3 = \beta_{\mathrm{Ahm}}, \qquad K_1 = (\Lambda_m/\mu_m + \delta_m),$$
$$A = \mu_h + \delta_h + \gamma + \gamma_0 u_1 + \rho_i M, \qquad B = \mu_h + \delta_h + \gamma_m + a_{\mathrm{LI}},$$
$$C = \mu_m + \delta_m + \alpha_m, \text{ and } D = \mu_m + \delta_m:$$

$$I = \begin{bmatrix} E_h \\ I_{\mathrm{Uh}} \\ I_{\mathrm{Ah}} \\ E_m \\ I_m \end{bmatrix}, \tag{46}$$

$$\widehat{G}(X, I) = \begin{bmatrix} b\beta_2 I_m\left(\left(\dfrac{\varphi_h}{\mu_h}\right) - S_h\right) \\ 0 \\ 0 \\ (b\beta_2 I_{\mathrm{Uh}} + b_1\beta_3 I_{\mathrm{Ah}})\left(\left(\dfrac{\varphi_m}{\mu_m + \delta_m}\right) - S_m\right) \\ 0 \end{bmatrix}. \tag{47}$$

This completes the proof. $\qquad\square$

4.3. Existence of Endemic Equilibrium Point.

Besides the disease-free equilibrium point, we shall show that the system of equations (1)–(9) has a unique endemic equilibrium point E_2. The endemic equilibrium point is a steady-state solution, where the disease persists in the population.

Theorem 4. *The system of equations (1)–(9) has no endemic equilibrium, when $R_0 < 1$ and a unique endemic equilibrium exists when $R_0 > 1$.*

Proof. Let $E_2 = (S_h^*, E_h^*, I_{\mathrm{Uh}}^*, I_{\mathrm{Ah}}^*, R_h^*, S_m^*, E_m^*, I_m^*, M^*)$ be a nontrivial equilibrium of system of equations (1)–(9), i.e., all components of E_2 are positive. If we set all the differential equations of system of equations (1)–(9) equal to zero, we get

$$S_h^* = \left(\frac{k_1 k_2 k_3}{kb\beta_1\varphi_m\alpha_m(\mu_h + \gamma_1)\left(kb\beta_2 I_{\mathrm{UH}}^* + b_1\beta_3\rho_i\mu_1 I_{\mathrm{UH}}^{*2}\right) + kk_2 k_3\mu_h(\mu_h + \gamma_1)}\right), \tag{48}$$

$$E_h^* = \left(\frac{k_1 b\beta_1\varphi_m\alpha_m\left(kb\beta_2 I_{\mathrm{UH}}^* + b_1\beta_3\rho_i\mu_1 I_{\mathrm{UH}}^{*2}\right)}{k(\alpha_h + \mu_h)(\mu_h + \gamma_1)\left[b\beta_1\varphi_m\alpha_m\left(kb\beta_2 I_{\mathrm{UH}}^* + b_1\beta_3\rho_i\mu_1 I_{\mathrm{UH}}^{*2}\right) + \mu_h k_2 k_3\right]}\right), \tag{49}$$

$$I_{\mathrm{Ah}}^* = \frac{\mu_1\rho_i I_{\mathrm{UH}}^{*2}}{k}, \tag{50}$$

$$R_h^* = \frac{k(\gamma + \gamma_0 u_1)I_{\mathrm{UH}}^* + \gamma_m\rho_i\mu_1 I_{\mathrm{UH}}^{*2}}{k(\mu_h + \gamma_1)}, \tag{51}$$

$$S_m^* = \frac{k\varphi_m}{k_3}, \tag{52}$$

$$E_m^* = \frac{\left(kb\varphi_m\beta_2 I_{\mathrm{UH}}^* + b_1\varphi_m\beta_3\rho_i\mu_1 I_{\mathrm{UH}}^{*2}\right)}{(\mu_m + \delta_m + \alpha_m)k_3}, \tag{53}$$

$$I_m^* = \frac{\left(Kb\varphi_m\alpha_m\beta_2 I_{\mathrm{UH}}^* + b_1\varphi_m\alpha_m\beta_3\rho_i\mu_1 I_{\mathrm{UH}}^{*2}\right)}{k_2 k_3}, \tag{54}$$

$$M^* = \frac{\mu_1 I_{\mathrm{UH}}^*}{\mu_0}, \tag{55}$$

where $\beta_1 = \beta_{\mathrm{mh}}, \beta_2 = \beta_{\mathrm{hm}}, \beta_3 = \beta_{\mathrm{Ahm}}, k = \mu_0(\mu_h + \delta_m + \gamma_m + a_{\mathrm{LI}})$, $k_1 = k\varphi_h(\mu_h + \gamma_1) + k\gamma_1(\gamma + \gamma_0 u_1)I_1 + \gamma_1\gamma_m\rho_i\mu_1 I_{\mathrm{UH}}^{*2}$, $k_2 = (\mu_m + \delta_m)(\mu_m + \delta_m + \alpha_m)$, and $k_3 = k(\mu_m + \delta_m) + kb\beta_2 I_{\mathrm{UH}}^{*} + b_1\beta_3\rho_i\mu_1 I_{\mathrm{UH}}^{*2}$. This is a positive solution of equation given by

$$A_1 I_{\mathrm{UH}}^{*3} + A_2 I_{\mathrm{UH}}^{*2} + A_3 I_{\mathrm{UH}}^{*} + A_4 = 0, \tag{56}$$

where

$$A_1 = \left\{ \frac{(b_1\beta_3\rho_i^2\mu_1^2\mu_0)\gamma_1\gamma_m}{\varphi_h\alpha_m\beta_2} \left[\frac{\varphi_h\alpha_m\beta_2(\mu_h + \gamma_1)(\mu_h + \delta_h + \gamma_m)}{\gamma_1\gamma_m(\mu_m + \delta_m)(\mu_h + \delta_h + \gamma + \gamma_0 u_1)} \right] - R_0^2 + \left(\frac{kbb_1\alpha_m\varphi_m\beta_1\beta_3\rho_i^2\mu_1^2\mu_0(\mu_h + \gamma_1)}{(\mu_h + \alpha_h)(\mu_m + \delta_m + \gamma_m)} \right) \right\},$$

$$A_1 = \left\{ \frac{(b_1\beta_3\rho_i^2\mu_1^2\mu_0)\gamma_1\gamma_m}{\varphi_h\alpha_m\beta_2} \left[\frac{\varphi_h\alpha_m\beta_2(\mu_h + \gamma_1)(\mu_h + \delta_h + \gamma_m)}{\gamma_1\gamma_m(\mu_m + \delta_m)(\mu_h + \delta_h + \gamma + \gamma_0 u_1)} \right] - R_0^2 + \left(\frac{kbb_1\alpha_m\varphi_m\beta_1\beta_3\rho_i^2\mu_1^2\mu_0(\mu_h + \gamma_1)}{(\mu_h + \alpha_h)(\mu_m + \delta_m + \gamma_m)} \right) \right\},$$

$$A_3 = \left\{ \frac{k^2\mu_0}{\varphi_h} \left[\frac{b\varphi_h\beta_1}{\gamma_1(\gamma - \gamma_0 u_1)(\mu_m + \delta_m)} - R_0^2 \right] + \frac{k(b_1\beta_3\rho_i\mu_1\mu_0)(\mu_h + \gamma_1)}{(\delta_h + \mu_h + \gamma + \gamma_0 u_1)b\beta_2} \left[\frac{Kb\beta_2}{b_1\beta_3\mu_0(\delta_h + \mu_h + \gamma + \gamma_0 u_1)} - R_0^2 \right] \right. \tag{57}$$
$$\left. + \frac{k^2\mu_0(\mu_h + \gamma_1)a}{\varphi_h\alpha_h\mu_h} \left[R_0^2 - \frac{\varphi_h\alpha_h\rho_i\mu_1 a_{LI}}{K(\delta_h + \mu_h + \gamma + \gamma_0 u_1)} \right] \right\},$$

$$A_4 = \left[k^2\mu_0(\mu_h + \gamma_1)(1 - R_0^2) \right].$$

The systems (1)–(9) have no positive solution; when $R_0 < 1$, $A_1 > 0, A_2 > 0, A_3 > 0$, and $A_4 > 0$ However, when $R_0 > 1$, $A_4 < 0$, by using Descartes's rule of sign, there is exactly one sign-change in the equation, and there exists exactly one positive root. This implies that a unique endemic equilibrium exists. This completes the proof. □

Remark 2. There are more than one endemic equilibrium existing in case, when $R_0^2 > (\varphi_h\alpha_m\beta_2(\mu_h + \gamma_1)(\mu_h + \delta_h + \gamma_m)/\gamma_1\gamma_m(\mu_m + \delta_m)(\mu_h + \delta_h + \gamma + \gamma_0 u_1))$.

5. Results

The general overview of the proposed model has been shown in Figure 1. The definitions and corresponding numeric values of the parameters/variables in the system of equations (1)–(9) have been summarized in Table 1. The definitions of the compartment variables are summarized in Table 2.

Figure 2 represents the 3D-plot for the proposed model. In this figure, the proposed models converge to the same point on different initial conditions. A comparison result of proposed model (incorporating awareness) and existing model (without awareness) has been shown in Figures 3–7 for human and mosquito populations. In each figure, reduction/growth of human and mosquito population in each class has been presented.

In Figures 3–5, the population of susceptible, unaware infected, and aware infected human population with and without awareness has been shown. We can easily see that, when there is no awareness, the population of susceptible humans is decaying rapidly (the red line) and there is a rapid increase in unaware infected human growth (the red line). But, when we give awareness to unaware infected humans,

we experienced susceptible humans are increasing and unaware infected humans are decreasing significantly. It is due to the fact that, when we provide awareness to unaware infected humans, the contact rate of infected human and infected mosquitoes has also been reduced. The result revealed that a significant reduction in the population of unaware infected humans, for different timespans, is achieved through the proposed model. It has also been shown that the corresponding growth of unaware infected human population and infected mosquitoes increases without awareness as compared with that of the proposed model. The results also revealed that a significant reduction in the population of susceptible mosquitoes and infected mosquitoes for different timespans are achieved through the proposed model. It has also been shown that the corresponding growth of infected mosquito population is higher without awareness as compared with the proposed model.

In Figures 8 and 9, we show that, when we give awareness, it also affects the contact rate between human and mosquito population.

Figures 8 and 9 describe that, when there is no awareness, the biting rate is also high in the region. And, infected human and mosquito population increases rapidly, but when we add awareness into the system, the contact rate between aware infected humans and mosquitoes has been reduced. We show the results on the different biting rates in Figures 8 and 9 with low and high awareness rates.

6. Discussion

Malaria is a mosquito vector-borne disease spread in around hundred countries worldwide. The highest mortality rates are reported in tropical countries likewise sub-Saharan Africa [33].

TABLE 2: Definition and values of variables used in the model.

Variables	Corresponding definition	I. Values	Reference
S_h	Represents the number of individuals not yet infected with the malaria parasite, at time t	100	[3]
E_h	Represents the number of individuals who are infected but not yet infectious	20	[3]
I_{uh}	Represents the individuals that are infected and are capable of transmitting the disease to susceptible mosquitoes	10	[3]
I_{Ah}	Represent the number of aware infected human in the region	0	Assumed
R_h	Represents the number of individuals who have temporarily recovered from the disease	0	[3]
S_m	Represents the number of mosquitoes not yet infected with the malaria parasite at time t	1000	[3]
E_m	Represents the number of mosquitoes who are infected but not yet infectious	30	[3]
I_m	Represents the mosquitoes that are infected and are capable of transmitting the disease to susceptible human	20	[3]
M	Represents the cumulative density of awareness programs initially	0	Assumed
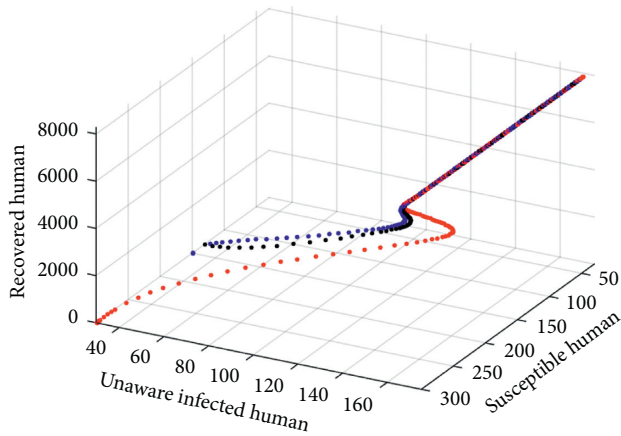
FIGURE 2: Convergence of solutions with different initial conditions.

FIGURE 4: Population of unaware infected humans with and without awareness, (without awareness (red line); with low to high awareness rate awareness (blue, green, magenta, and yellow line)).

FIGURE 3: Population of susceptible humans with and without awareness (without awareness (red line), with low to high awareness rate (blue, green, magenta, and yellow line)).
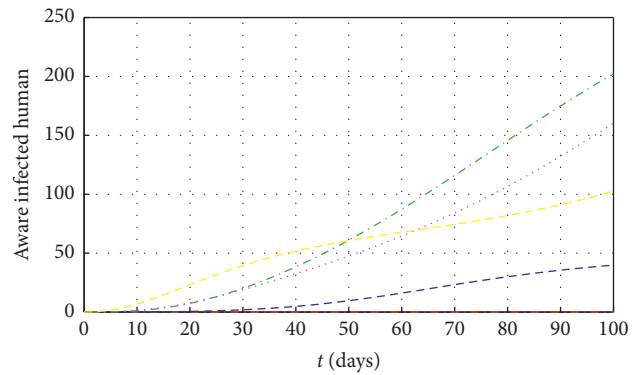
FIGURE 5: Population of aware infected humans with and without awareness (without awareness (red line); with low to high awareness rate awareness (blue, green, magenta, and yellow line)).

During the past decade, several prevention measures have been used to reduce the transmission of this deadly disease. The most frequently used measures include indoor spraying and bed nets. The vaccine of this deadly disease has not been prepared till date. The measures that can reduce the spread of this dangerous disease are preventive measures and awareness. In this paper, a mathematical model for the vector-borne disease has been proposed incorporating the awareness against this disease.

Vector-borne disease models have been proposed/modified in the past. Tumwiinw and co-authors proposed a mathematical model that tracks the dynamics of malaria in the human host and mosquito vector [34]. They incorporated infected humans recovered from infections and immune humans after the loss of immunity against this deadly disease to rejoin the susceptible class again. Addawe and Lope have modified and analyzed the mathematical model of Tumwiinw and co-authors [17]. They divided the human population into two compartments: preschool (up to five years of age) and the rest of human population (older than five years of age). Lashari and co-authors introduced three types of control
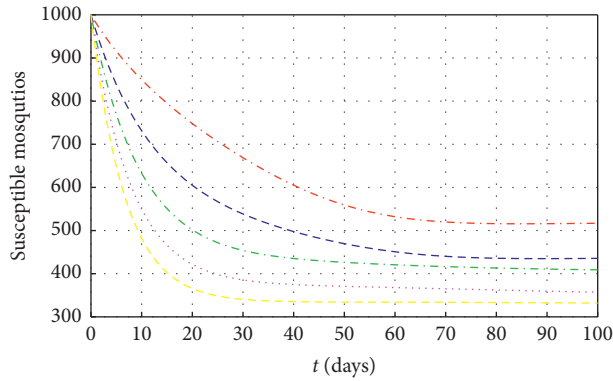
FIGURE 6: Population of susceptible mosquitoes with and without awareness (without awareness (red line); with low to high awareness rate awareness (blue, green, magenta, and yellow line)).
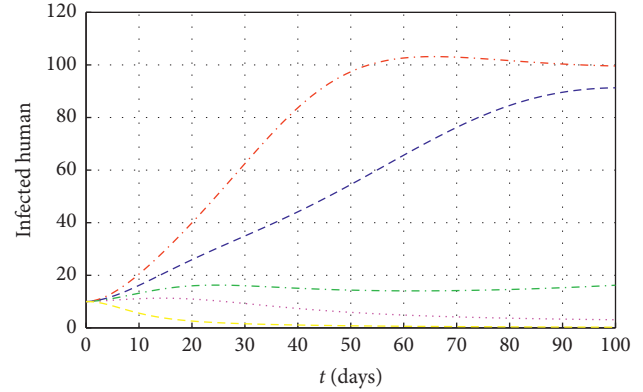

FIGURE 8: Population of unaware infected humans with different biting rates after awareness (without awareness (red line); with low to high awareness rate (blue, green, magenta, and yellow line)).
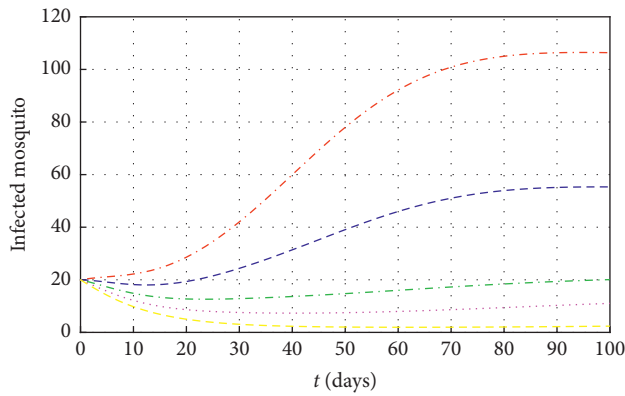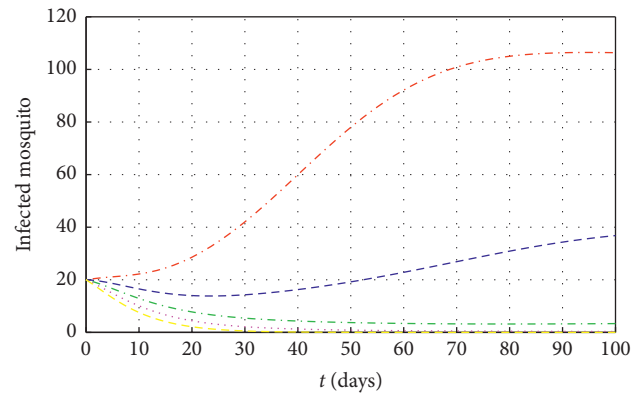

FIGURE 7: Population of infected mosquitoes with and without awareness (without awareness (red line); with low to high awareness rate awareness (blue, green, magenta, and yellow line)).

FIGURE 9: Population of infected mosquitoes with different biting rates (without awareness (red line); with low to high awareness rate (blue, green, magenta, and yellow line)).

parameters, namely, personal protection, treatment, and mosquito-reduction strategies to reduce the spread of malaria disease [3]. Thus, the previous literature suggests that the reduction of the spread of this dangerous disease could be achieved through preventive measures. Therefore, a mathematical model has been developed in this study to cater the awareness strategy as a variable in the model. The awareness could be addressed to infected humans, and the aware infected humans could reduce contact rate with mosquitoes due to awareness. The proposed model has been compared with existing model. The comparative results show that a significant improvement in the reduction of vector-borne infection could be achieved with awareness.

7. Conclusion

Malaria is a tropical infectious disease. Scientists have not succeeded till date to develop an effective vaccine to retaliate this deadly disease. Thus, the mathematical modeling of this disease has a crucial role to understand the insights of the transmission dynamics and corresponding appropriate prevention strategies. A novel mathematical model has been proposed in this study to prevent malaria disease.

The simulation results have significantly shown that awareness is an important factor to fight against this deadly disease. Thus, the spread of this illness could be prevented through effective awareness strategies in regions, where it has rapid spread.

Data Availability

No data has been used in this study.

Conflicts of Interest

The authors declare that they have no conflicts of interest.

Acknowledgments

References

[1] L. Cai, N. Tuncer, and M. Martcheva, "How does within-host dynamics affect population-level dynamics? insights from an immuno-epidemiological model of malaria," *Mathematical Methods in the Applied Sciences*, vol. 40, no. 18, pp. 6424–6450, 2017.

[2] World Health Organization, *World Malaria Report 2019*, World Health Organization, Geneva, Switzerland, 2019.

[3] A. A. Lashari, S. Aly, K. Hattaf, G. Zaman, I. H. Jung, and X.-Z. Li, "Presentation of malaria epidemics using multiple optimal controls," *Journal of Applied Mathematics*, vol. 2012, Article ID 946504, 2012.

[4] R. Ross, *The Prevention of Malaria*, John Murray.[Google Scholar], London, UK, 2nd edition, 1911.

[5] M. Ozair, A. A. Lashari, I. H. Jung, Y. I. Seo, and B. N. Kim, "Stability analysis of a vector-borne disease with variable human population," *Abstract and Applied Analysis*, vol. 2013, Article ID 293293, 2013.

[6] R. M. Anderson and R. M. May, *Infectious Diseases of Humans: Dynamics and Control*, Oxford University Press, Oxford, UK, 1992.

[7] G. Macdonald, *The Epidemiology and Control of Malaria*, Oxford University Press, London, UK, 1957.

[8] J. L. Aron, "Mathematical modeling of immunity to malaria," *Mathematical Biosciences*, vol. 90, no. 1-2, pp. 385–396, 1988.

[9] J. A. N. Filipe, E. M. Riley, C. J. Drakeley, C. J. Sutherland, and A. C. Ghani, "Determination of the processes driving the acquisition of immunity to malaria using a mathematical transmission model," *PLoS Computational Biology*, vol. 3, no. 12, p. e255, 2007.

[10] G. Hasibeder and C. Dye, "Population dynamics of mosquito-borne disease: persistence in a completely heterogeneous environment," *Theoretical Population Biology*, vol. 33, no. 1, pp. 31–53, 1988.

[11] D. Rodríguez and L. Torres-Sorando, "Models of infectious diseases in spatially heterogeneous environments," *Bulletin of Mathematical Biology*, vol. 63, no. 3, pp. 547–571, 2001.

[12] G. A. Ngwa and W. S. Shu, "A mathematical model for endemic malaria with variable human and mosquito populations," *Mathematical and Computer Modelling*, vol. 32, no. 7-8, pp. 747–764, 2000.

[13] L.-M. Cai, A. A. Lashari, I. H. Jung, K. O. Okosun, and Y. I. Seo, "Mathematical analysis of a malaria model with partial immunity to reinfection," *Abstract and Applied Analysis*, vol. 2013, Article ID 405258, 2013.

[14] N. Chitnis, J. M. Cushing, and J. M. Hyman, "Bifurcation analysis of a mathematical model for malaria transmission," *SIAM Journal on Applied Mathematics*, vol. 67, no. 1, pp. 24–45, 2006.

[15] O. Diekmann, J. A. P. Heesterbeek, and J. A. Metz, "On the definition and the computation of the basic reproduction ratio R_0 in models for infectious diseases in heterogeneous populations," *Journal of Mathematical Biology*, vol. 28, no. 4, pp. 365–382, 1990.

[16] M. Ozair, A. A. Lashari, I. H. Jung, and K. O. Okosun, "Stability analysis and optimal control of a vector-borne disease with nonlinear incidence," *Discrete Dynamics in Nature and Society*, vol. 2012, Article ID 595487, 2012.

[17] J. M. Addawe and J. E. C. Lope, "Analysis of age-structured malaria transmission model," *Philippine Science Letters*, vol. 5, no. 2, p. 169, 2012.

[18] A. Misra, A. Sharma, and J. Shukla, "Modeling and analysis of effects of awareness programs by media on the spread of infectious diseases," *Mathematical and Computer Modelling*, vol. 53, no. 5-6, pp. 1221–1228, 2011.

[19] S. Samanta, S. Rana, A. Sharma, A. K. Misra, and J. Chattopadhyay, "Effect of awareness programs by media on the epidemic outbreaks: a mathematical model," *Applied Mathematics and Computation*, vol. 219, no. 12, pp. 6965–6977, 2013.

[20] D. Greenhalgh, S. Rana, S. Samanta, T. Sardar, S. Bhattacharya, and J. Chattopadhyay, "Awareness programs control infectious disease-multiple delay induced mathematical model," *Applied Mathematics and Computation*, vol. 251, pp. 539–563, 2015.

[21] L. Cai, X. Li, N. Tuncer, M. Martcheva, and A. A. Lashari, "Optimal control of a malaria model with asymptomatic class and superinfection," *Mathematical Biosciences*, vol. 288, pp. 94–108, 2017.

[22] S. Kim, M. A. Masud, G. Cho, and I. H. Jung, "Analysis of a vector-bias effect in the spread of malaria between two different incidence areas," *Journal of Theoretical Biology*, vol. 419, pp. 66–76, 2017.

[23] S. Kim, J. H. Byun, A. Park, and I. H. Jung, "A mathematical model for assessing the effectiveness of controlling relapse in plasmodium vivax malaria endemic in the Republic of Korea," *PLoS One*, vol. 15, no. 1, Article ID e0227919, 2020.

[24] M. Ghosh, A. A. Lashari, and X.-Z. Li, "Biological control of malaria: a mathematical model," *Applied Mathematics and Computation*, vol. 219, no. 15, pp. 7923–7939, 2013.

[25] S. Olaniyi and O. Obabiyi, "Mathematical model for malaria transmission dynamics in human and mosquito populations with nonlinear forces of infection," *International Journal of Pure and Applied Mathematics*, vol. 88, no. 1, pp. 125–156, 2013.

[26] P. Van Den Driessche and J. Watmough, "Reproduction numbers and sub-threshold endemic equilibria for compartmental models of disease transmission," *Mathematical Biosciences*, vol. 180, no. 1-2, pp. 29–48, 2002.

[27] J. H. Jung, A. Park, and I. H. Jung, "Qualitative and sensitivity analysis of the effect of electronic cigarettes on smoking cessation," *Computational and Mathematical Methods in Medicine*, vol. 2018, Article ID 3738584, , 2018.

[28] K. S. Kim, M. M. Ibrahim, I. H. Jung, and S. Kim, "Mathematical analysis of the effectiveness of control strategies to prevent the autorun virus transmission propagation," *Applied Mathematics and Computation*, vol. 371, Article ID 124955, 2020.

[29] B. C. Kuo and F. Golnaraghi, *Automatic Control Systems*, Englewood Cliffs, Bergen, NJ, USA, 2003.

[30] K. Blayneh, Y. Cao, Y. Cao, and H.-D. Kwon, "Optimal control of vector-borne diseases: treatment and prevention," *Discrete & Continuous Dynamical Systems-B*, vol. 11, no. 3, pp. 587–611, 2009.

[31] J. M. Tchuenche, N. Dube, C. P. Bhunu, R. J. Smith, and C. T. Bauch, "The impact of media coverage on the transmission dynamics of human influenza," *BMC Public Health*, vol. 11, no. S1, p. S5, 2011.

[32] C. Castillo-Chavez, Z. Feng, and W. Huang, "On the computation of R_0 and its role on global stability," *Mathematical Approaches for Emerging and Reemerging Infectious Diseases: an Introduction*, vol. 1, pp. 229–250, 2002.

[33] C. N. Ngonghala, S. Y. Del Valle, R. Zhao, and J. Mohammed-Awel, "Quantifying the impact of decay in bed-net efficacy on malaria transmission," *Journal of Theoretical Biology*, vol. 363, pp. 247–261, 2014.

[34] J. Tumwiine, J. Y. T. Mugisha, and L. S. Luboobi, "A mathematical model for the dynamics of malaria in a human host and mosquito vector with temporary immunity," *Applied Mathematics and Computation*, vol. 189, no. 2, pp. 1953–1965, 2007.

Research Article

Ergodicity of a Nonlinear Stochastic SIRS Epidemic Model with Regime-Switching Diffusions

Hongxia Liu, Juan Li, Mengnan Chi, Jinlei Liu, and Wencai Zhao [ID]

College of Mathematics and Systems Science, Shandong University of Science and Technology, Qingdao 266590, China

Correspondence should be addressed to Wencai Zhao; zhaowencai@sdust.edu.cn

In this paper, taking both white noises and colored noises into consideration, a nonlinear stochastic SIRS epidemic model with regime switching is explored. The threshold parameter R_s is found, and we investigate sufficient conditions for the existence of the ergodic stationary distribution of the positive solution. Finally, some numerical simulations are also carried out to demonstrate the analytical results.

1. Introduction

It is well known that the incidence rate plays a crucial role in studying the dynamics of infectious disease models. In general, bilinear incidence βSI is considered in most infectious disease models [1, 2]. For example, Li and Ma [3] conducted the qualitative analyses of the SIS epidemic model with vaccination and varying total population size. Nakata and Kuniya [4] introduced the global dynamics of a class of SEIRS epidemic models in a periodic environment. In order to effectively investigate the rapid spread of the disease, it is rewarding to consider the behavioral changes and crowding effect of the infected individuals, as well as choose appropriate parameters to prevent the unbounded contact rate. Capasso and Serio [5] proposed the saturated incidence ($\beta SI/(1 + \alpha I)$), which is more reasonable than the bilinear incidence. For the detailed introduction of the saturated incidence, see [5].

The classical SIRS epidemic model with the saturated incidence rate is in the following form [6, 7]:

$$
\begin{cases}
\dfrac{dS(t)}{dt} = A - \dfrac{\beta S(t)I(t)}{1 + \alpha I(t)} - \mu S(t) + \omega R(t), \\[2mm]
\dfrac{dI(t)}{dt} = \dfrac{\beta S(t)I(t)}{1 + \alpha I(t)} - (\mu + \lambda + d)I(t), \\[2mm]
\dfrac{dR(t)}{dt} = \lambda I(t) - (\mu + \omega)R(t),
\end{cases}
\tag{1}
$$

where $S(t)$, $I(t)$, and $R(t)$ represent the number of susceptible, infected, and removed individuals at time t, respectively. A denotes an input of new members into the population, β stands for the transmission rate, μ is the natural mortality, d is the death rate relative to the disease, λ is the proportion of the infective class to the recovered class, and ω is the per capita rate of loss of immunity.

In nature, it is inevitable for a population to be affected by a variety of random factors [8, 9]. Consequently, it is crucial to consider the randomness which might exist during the transmission of disease [10, 11]. In general, there are two

types of random perturbations to be considered in ecosystem modeling: one is white noise which can be described as Brownian motion [12–14], and the other is colored noise (also called telegraph noise) which can be described through a finite-state Markov chain [15–17]. In [15], Liu et al. investigated the threshold behavior of a multigroup SIRS epidemic model with standard incidence rates and Markovian switching. Lin and Jin [16] considered a stochastic

SIS epidemic model with regime switching; by verifying a Foster–Lyapunov condition, the threshold condition for the ergodicity is presented. Hu et al. [17] studied a stochastic SIS epidemic model with vaccination and nonlinear incidence under regime switching.

Motivated by the above literature, we study a nonlinear stochastic SIRS epidemic model with two kinds of random interference. The model is as follows:

$$
\begin{cases}
dS(t) = \left((1 - q(\xi(t)))A(\xi(t)) - \dfrac{\beta(\xi(t))S(t)I(t)}{1 + \alpha I(t)} - \mu(\xi(t))S(t) + \omega(\xi(t))R(t) \right)dt \\
\qquad + \sigma_1(\xi(t))S(t)dB_1(t), \\
dI(t) = \left(\dfrac{\beta(\xi(t))S(t)I(t)}{1 + \alpha I(t)} - \mu(\xi(t))I(t) - \lambda(\xi(t))I(t) \right)dt + \sigma_2(\xi(t))I((t)dB_2(t), \\
dR(t) = (q(\xi(t))A(\xi(t)) + \lambda(\xi(t))I(t) - \mu(\xi(t))R(t) - \omega(\xi(t))R(t))dt + \sigma_3(\xi(t))R(t)dB_3(t),
\end{cases}
\tag{2}
$$

where q is a fraction of vaccinated individuals for newborns. The incidence rate α contains the crowding effect of the infected individuals and should not be disturbed by the noises in the environment. $B_i(t)$ $(i = 1, 2, 3)$ denotes one-dimensional standard Brownian motion, and σ_i $(i = 1, 2, 3)$ is the intensity of white noise. $\xi(t)$ is a right-continuous Markov chain taking values in $\mathcal{M} = \{1, 2, \ldots, m\}$, and the generator matrix of $\xi(t)$ is $\Gamma = (\gamma_{ij})_{1 \le i,j \le m}$. The details of the Markov chain are presented in [18], which we omit here.

In this paper, the dynamic behaviors of stochastic differential system (2) are discussed. In Section 2, we get the conditions for the extinction and persistence in mean of the infected. In Section 3, we investigate the ergodicity of system (2) by constructing a suitable Lyapunov function. Finally, numerical simulations are given in Section 4.

2. The Extinction and Persistence of the Disease

In system (2), let $N(t) = S(t) + I(t) + R(t)$; then, we have

$$
\begin{aligned}
dN(t) = {} & [A(\xi(t)) - \mu(\xi(t))N(t)]dt + \sigma_1(\xi(t))S(t)dB_1(t) \\
& + \sigma_2(\xi(t))I(t)B_2(t) \\
& + \sigma_3(\xi(t))R(t)dB_3(t).
\end{aligned}
\tag{3}
$$

From Lemma 2.1 and Lemma 2.2 of [19], we have the following.

Lemma 1. *For any initial value $(S(0), I(0), R(0), r(0)) \in R_+^3 \times \mathcal{M}$, the solution $(S(t), I(t), R(t))$ of system (2) has the following properties:*

(1) $\lim_{t \to \infty} ((S(t) + I(t) + R(t))/t) = 0$ *a.s.*
(2) $\lim_{t \to \infty} (\int_0^t S(u)dB_1(u)/t) = 0$, $\lim_{t \to \infty} (\int_0^t I(u)d B_2(u)/t) = 0$, $\lim_{t \to \infty} (\int_0^t R(u)dB_3(u)/t) = 0$ *a.s.*

Definition 1

(1) If $\lim_{t \to \infty} I(t) = 0$, then the disease tends to be extinct
(2) If $\lim_{t \to \infty} \inf (1/t)E \int_0^t I(z)dz > 0$, then the disease tends to be persistent in mean

Define a matrix

$$
M =
\begin{pmatrix}
\mu(1) - \gamma_{11} & \cdots & -\gamma_{1m} & 0 & \cdots & 0 \\
\vdots & & \vdots & \vdots & & \vdots \\
-\gamma_{m1} & \cdots & \mu(m) - \gamma_{mm} & 0 & \cdots & 0 \\
-\omega(1) & \cdots & 0 & \mu(1) + \omega(1) - \gamma_{11} & \cdots & -\gamma_{1m} \\
\vdots & & \vdots & \vdots & & \vdots \\
0 & \cdots & -\omega(m) & -\gamma_{m1} & \cdots & \mu(m) + \omega(m) - \gamma_{mm}
\end{pmatrix}.
\tag{4}
$$

Following Lemma 1 in [20], we obtain that M is a nonsingular M-matrix. By Theorem 2.10 (see Mao and Yuan [21]), for vector $\beta = (\beta(1), \beta(2), \ldots, \beta(m), 0, 0, \ldots, 0)^T \in R^{2m}$, the equation $M\eta = \beta$ has a unique solution:

$$\eta = (d_1(1), d_1(2), \ldots, d_1(m), d_2(1), d_2(2), \ldots, d_2(m))^T \in R_+^{2m}. \tag{5}$$

That is,

$$\begin{cases} \beta(k) - d_1(k)\mu(k) + \sum_{l \in \mathcal{M}} \gamma_{kl}d_1(l) = 0, & k = 1, 2, \ldots, m, \\ d_1(k)\omega(k) - d_2(k)(\mu(k) + \omega(k)) + \sum_{l \in \mathcal{M}} \gamma_{kl}d_2(l) = 0, & k = 1, 2, \ldots, m. \end{cases} \tag{6}$$

Then, we define a parameter

$$R_s = \Sigma_{k \in \mathcal{M}}\pi_k\left[d_1(k)(1 - q(k))A(k) + d_2(k)q(k)A(k) - \left(\mu(k) + \lambda(k) + \frac{\sigma_2^2(k)}{2}\right)\right]. \tag{7}$$

Theorem 1. *For any initial value* $(S(0), I(0), R(0), r(0)) \in R_+^3 \times \mathcal{M}$, *assume that* $\alpha + \widehat{d}_1 - \widehat{d}_2 > 0$; *then,*

(1) *The disease* $I(t)$ *of system* (2) *is extinct when* $R_s < 0$

(2) *The disease* $I(t)$ *of system* (2) *is persistent in mean when* $R_s > 0$

Proof. Define the function

$$U(S(t), I(t), R(t), k) = U_1(S(t), I(t), R(t), k) + U_2(I(t)), \tag{8}$$

where

$$U_1(S(t), I(t), R(t), k) = d_1(k)(S(t) + I(t)) + d_2(k)R(t),$$
$$U_2(I(t)) = \ln I(t) + \alpha I(t). \tag{9}$$

Then, applying Itô's formula, we have

$$LU_1 = d_1(k)[(1 - q(k))A(k) - \mu(k)S(t) - (\mu(k) + \lambda(k))I(t) + \omega(k)R(t)]$$

$$+ d_2(k)[q(k)A(k) + \lambda(k)I(t) - (\mu(k) + \omega(k))R(t)] + (S(t) + I(t))\sum_{l=1}^{m} \gamma_{kl}d_1(l) + R(t)\sum_{l=1}^{m} \gamma_{kl}d_2(l)$$

$$= d_1(k)(1 - q(k))A(k) + d_2(k)q(k)A(k) + \left[-d_1(k)\mu(k) + \sum_{l=1}^{m} \gamma_{kl}d_1(l)\right]S(t)$$

$$- \left[(\mu(k) + \lambda(k))d_1(k) - \lambda(k)d_2(k) - \sum_{l=1}^{m} \gamma_{kl}d_1(l)\right]I(t) \tag{10}$$

$$+ \left[d_1(k)\omega(k) - d_2(k)(\mu(k) + \omega(k)) + \sum_{l=1}^{m} \gamma_{kl}d_2(l)\right]R(t)$$

$$= d_1(k)(1 - q(k))A(k) + d_2(k)q(k)A(k) - \beta(k)S(t) - [\beta(k) + \lambda(k)d_1(k) - \lambda(k)d_2(k)]I(t),$$

$$LU_2 = \frac{\beta(k)S(t)}{1 + \alpha I(t)} - \left(\mu(k) + \lambda(k) + \frac{\sigma_2^2(k)}{2}\right) + \frac{\alpha\beta(k)S(t)I(t)}{1 + \alpha I(t)} - \alpha(\mu(k) + \lambda(k))I(t)$$

$$= \beta(k)S(t) - \alpha(\mu(k) + \lambda(k))I(t) - \left(\mu(k) + \lambda(k) + \frac{\sigma_2^2(k)}{2}\right). \tag{11}$$

By (10) and (11), one can obtain that

$$
\begin{aligned}
LU &= d_1(k)(1-q(k))A(k) + d_2(k)q(k)A(k) - \left(\mu(k) + \lambda(k) + \frac{\sigma_2^2(k)}{2}\right) \\
&\quad - [\beta(k) + \lambda(k)d_1(k) - \lambda(k)d_2(k) + \alpha\mu(k) + \alpha\lambda(k)]I(t) \\
&= d_1(k)(1-q(k))A(k) + d_2(k)q(k)A(k) - \left(\mu(k) + \lambda(k) + \frac{\sigma_2^2(k)}{2}\right) \\
&\quad - [\beta(k) + \lambda(k)(\alpha + d_1(k) - d_2(k)) + \alpha\mu(k)]I(t).
\end{aligned}
\tag{12}
$$

An application of generalized Itô's formula yields

$$
\begin{aligned}
&U(S(t), I(t), R(t), \xi(t)) \\
&= U(S(0), I(0), R(0), \xi(0)) + \int_0^t LU(S(z), I(z), R(z), \xi(z))\mathrm{d}z + \int_0^t d_1(\xi(z))\sigma_1(\xi(z))S(z)\mathrm{d}B_1(z) \\
&\quad + \int_0^t [1 + (\alpha + d_1(\xi(z)))I(z)]\sigma_2(\xi(z))\mathrm{d}B_2(z) + \int_0^t d_2(\xi(z))\sigma_3(\xi(z))R(z)\mathrm{d}B_3(z) \\
&\quad + \int_0^t \int_R (U(S(z), I(z), R(z), i_0 + \ell(\xi(z), l))) - U(S(z), I(z), R(z), \xi(z))\mu(\mathrm{d}z, \mathrm{d}l),
\end{aligned}
\tag{13}
$$

where $\mu(\mathrm{d}z, \mathrm{d}l) = \gamma(\mathrm{d}z, \mathrm{d}l) - \mu(\mathrm{d}l)\mathrm{d}z$ is a martingale measure. By using Lemma 1.9 of [21], we can get

$$
E[U(S(t), I(t), R(t), \xi(t))] = E[U(S(0), I(0), R(0), \xi(0))] + E\left[\int_0^t LU(S(z), I(z), R(z), \xi(z))\mathrm{d}z\right].
\tag{14}
$$

Then,

$$
\begin{aligned}
&E\left[\frac{U(S(t), I(t), R(t), \xi(t))}{t}\right] \\
&= E\left[\frac{U(S(0), I(0), R(0), \xi(0))}{t}\right] \\
&\quad + E\left\{\frac{1}{t}\int_0^t [d_1(\xi(z))(1-q(\xi(z)))A(\xi(z)) + d_2(\xi(z))q(\xi(z))A(\xi(z)) - \left(\mu(\xi(z)) + \lambda(\xi(z)) + \frac{\sigma_2^2(\xi(z))}{2}\right)\mathrm{d}z\right\} \\
&\quad - E\left\{\frac{1}{t}\int_0^t [\beta(\xi(z)) + \lambda(\xi(z))(\alpha + d_1(\xi(z)) - d_2(\xi(z))) + \alpha\mu(\xi(z))]I(z)\mathrm{d}z\right\}.
\end{aligned}
\tag{15}
$$

Hence,

$$\frac{R_s}{\breve{\beta} + \breve{\lambda}\left(\alpha + \breve{d}_1 - \hat{d}_2\right) + \alpha\breve{\mu}} \le \lim_{t \to \infty} \inf \frac{1}{t} E \int_0^t I(z) \mathrm{d}z$$

$$\le \lim_{t \to \infty} \sup \frac{1}{t} E \int_0^t I(z) \mathrm{d}z$$

$$\le \frac{R_s}{\hat{\beta} + \hat{\lambda}\left(\alpha + \hat{d}_1 - \breve{d}_2\right) + \alpha\hat{\mu}}. \tag{16}$$

In conclusion, based on the condition $\alpha + \hat{d}_1 - \breve{d}_2 > 0$, we have the following:

(1) If $R_s < 0$, then $\lim_{t \to \infty} I(t) = 0$, a.s.

(2) If $R_s > 0$, then $\lim_{t \to \infty} \inf (1/t) E \int_0^t I(z) \mathrm{d}z \ge (R_s/\breve{\beta} + \lambda (\alpha + \hat{d}_1 - \breve{d}_2) + \alpha\breve{\mu}) > 0$, and the disease $I(t)$ of system (2) is persistent in mean $\qquad\square$

Remark 1. According to Theorem 1, if the intensity of white noise is large enough that the condition $R_s < 0$ holds, then the disease dies out with probability 1. Conversely, if $R_s > 0$, the disease of system (2) is persistent in mean. This means that the presence of environmental noise is conducive to disease control.

3. Ergodic Stationary Distribution of System (2)

The study of the ergodicity and stationary distribution has been widely concerned by many scholars [22, 23]. In this section, in order to investigate the ergodic property of system (2), we establish a suitable Lyapunov function with Markov conversion.

Theorem 2. *For any initial value* $(S(0), I(0), R(0), \xi(0)) \in R_+^3 \times \mathcal{M}$, *if* $R_s > 0$, *stochastic process* $(S(t), I(t), R(t), \xi(t))$ *of system (2) is ergodic and has a unique stationary distribution in* $R_+^3 \times \mathcal{M}$.

Proof. Let $x(t) = \ln S(t)$, $y(t) = \ln I(t)$, and $z(t) = \ln R(t)$. System (2) can be transformed into

$$\begin{cases} \mathrm{d}x(t) = \left[\dfrac{(1 - q(\xi(t)))A(\xi(t))}{e^{x(t)}} - \dfrac{\beta(\xi(t))e^{y(t)}}{1 + \alpha e^{y(t)}} - \mu(\xi(t)) + \dfrac{\omega(\xi(t))e^{z(t)}}{e^{x(t)}} - \dfrac{1}{2}\sigma_1^2(\xi(t))\right]\mathrm{d}t + \sigma_1(\xi(t))\mathrm{d}B_1(t), \\[3mm] \mathrm{d}y(t) = \left[\dfrac{\beta(\xi(t))e^{x(t)}}{1 + \alpha e^{y(t)}} - \mu(\xi(t)) - \lambda(\xi(t)) - \dfrac{1}{2}\sigma_2^2(\xi(t))\right]\mathrm{d}t + \sigma_2(\xi(t))\mathrm{d}B_2(t), \\[3mm] \mathrm{d}z(t) = \left[\dfrac{q(\xi(t))A(\xi(t))}{e^{z(t)}} + \dfrac{\lambda(\xi(t))e^{y(t)}}{e^{z(t)}} - \mu(\xi(t)) - \omega(\xi(t)) - \dfrac{1}{2}\sigma_3^2(\xi(t))\right]\mathrm{d}t + \sigma_3(\xi(t))\mathrm{d}B_3(t). \end{cases} \tag{17}$$

The ergodic property of system (2) is the same as that of system (17). We need to prove that system (17) satisfies the three conditions of Lemma 2.2 in [18]. Obviously, conditions (1) and (2) are satisfied. Hence, we only need to prove condition (3).

Define

$$H(x, y, z, k) = \frac{1}{\vartheta + 1}\left(e^x + e^y + e^z\right)^{\vartheta+1} - a\left[d_1(k)\left(e^x + e^y\right) + d_2(k)e^z + y + \alpha e^y + \tau(k)\right] - x - z, \tag{18}$$

where $\vartheta \in (0, 1)$, $\breve{\sigma}^2 = \max_{1 \le i \le 3, k \in \mathcal{M}} \breve{\sigma}_i^2(k)$, and $a > 0$ satisfy $\hat{\mu} - (\vartheta/2)\breve{\sigma}^2 > 0$, $-aR_s + 2\breve{\mu} + \breve{\omega} + (1/2)\breve{\sigma}_1^2 + (1/2)\breve{\sigma}_3^2 \le -2$. τ_k will be determined later. There exists a unique point (x_0, y_0, z_0, k) which is the minimum value of $H(x, y, z, k)$.

Set

$$V(x, y, z, k) = H(x, y, z, k) - H(x_0, y_0, z_0, k). \tag{19}$$

Denote

$$V_1 = \frac{1}{\vartheta + 1}\left(e^x + e^y + e^z\right)^{\vartheta+1},$$

$$V_2 = -\left[d_1(k)\left(e^x + e^y\right) + d_2(k)e^z + y + \alpha e^y + \tau(k)\right],$$

$$V_3 = -x,$$

$$V_4 = -z. \tag{20}$$

An application of generalized Itô's formula yields

$$LV_1 = \left(e^x + e^y + e^z\right)^\vartheta \left(A(k) - \mu(k)e^x - \mu(k)e^y - \mu(k)e^z\right)$$

$$+ \frac{\vartheta}{2}\left(e^x + e^y + e^z\right)^{\vartheta-1}\left(\sigma_1^2(k)e^{2x} + \sigma_2^2(k)e^{2y} + \sigma_3^2(k)e^{2z}\right)$$

$$\leq 3^\vartheta A(k)\left(e^{\vartheta x} + e^{\vartheta y} + e^{\vartheta z}\right) - \mu(k)e^{(\vartheta+1)x} - \mu(k)e^{(\vartheta+1)y} - \mu(k)e^{(\vartheta+1)z}$$

$$+ \frac{\vartheta}{2}\sigma_1^2(k)e^{(\vartheta+1)x} + \frac{\vartheta}{2}\sigma_2^2(k)e^{(\vartheta+1)y} + \frac{\vartheta}{2}\sigma_3^2(k)e^{(\vartheta+1)z}$$

$$= -\left(\mu(k) - \frac{\vartheta}{2}\sigma_1^2(k)\right)e^{(\vartheta+1)x} - \left(\mu(k) - \frac{\vartheta}{2}\sigma_2^2(k)\right)e^{(\vartheta+1)y} \tag{21}$$

$$- \left(\mu(k) - \frac{\vartheta}{2}\sigma_3^2(k)\right)e^{(\vartheta+1)z} + 3^\vartheta A(k)\left(e^{\vartheta x} + e^{\vartheta y} + e^{\vartheta z}\right)$$

$$\leq -\left(\widehat{\mu} - \frac{\vartheta}{2}\widecheck{\sigma}^2\right)e^{(\vartheta+1)x} - \left(\widehat{\mu} - \frac{\vartheta}{2}\widecheck{\sigma}^2\right)e^{(\vartheta+1)y} - \left(\widehat{\mu} - \frac{\vartheta}{2}\widecheck{\sigma}^2\right)e^{(\vartheta+1)z} + 3^\vartheta \widecheck{A}\left(e^{\vartheta x} + e^{\vartheta y} + e^{\vartheta z}\right),$$

$$LV_2 = -d_1(k)(1 - q(k))A(k) - d_2(k)q(k)A(k) + \mu(k) + \lambda(k) + \frac{\sigma_2^2(k)}{2} - \sum_{l=1}^{m}\gamma_{kl}\tau(l)$$

$$+ e^x\left[d_1(k)\mu(k) - \beta(k) - \sum_{l\in\mathcal{M}}\gamma_{kl}\mathrm{d}_1(l)\right] + e^y\left[(d_1(k) + \alpha)(\mu(k) + \lambda(k)) - d_2(k)\lambda(k) - \sum_{l\in\mathcal{M}}\gamma_{kl}\mathrm{d}_1(l)\right] \tag{22}$$

$$+ e^z\left[-d_1(k)\omega(k) + d_2(k)(\mu(k) + \omega(k)) - \sum_{l\in\mathcal{M}}\gamma_{kl}\mathrm{d}_2(l)\right]$$

$$= -G_{0k} - \sum_{l=1}^{m}\gamma_{kl}\tau(l) + e^y\left[\beta(k) + (d_1(k) - d_2(k))\lambda(k) + \alpha(\mu(k) + \lambda(k))\right],$$

where we used equation (4) and

$$G_{0k} = d_1(k)(1 - q(k))A(k) + d_2(k)q(k)A(k) - \mu(k) - \lambda(k) - \frac{\sigma_2^2(k)}{2}. \tag{23}$$

Let $\tau = (\tau_1, \ldots, \tau_m)^T$ be the solution of the following Poisson system:

$$\Gamma\tau = \left(\sum_{k=1}^{m}\pi_k G_{0k}\right)\vec{1} - \begin{pmatrix} G_{01} \\ \vdots \\ G_{0m} \end{pmatrix}, \tag{24}$$

where $G = (G_{01}, G_{02}, \ldots, G_{0m})^T$.

Substituting this equality into (22), we obtain

$$LV_2 = -\sum_{k=1}^{m}\pi_k G_{0k} + e^y\left[\beta(k) + (d_1(k) - d_2(k))\lambda(k) + \alpha(\mu(k) + \lambda(k))\right], \tag{25}$$

$$LV_3 = -\left(\frac{(1 - q(k))A(k)}{e^x} - \frac{\beta(k)e^y}{1 + \alpha e^y} + \frac{\omega(k)e^z}{e^x} - \mu(k) - \frac{1}{2}\sigma_1^2(k)\right), \tag{26}$$

$$LV_4 = -\frac{q(k)A(k)}{e^z} - \frac{\lambda(k)e^y}{e^z} + \left(\mu(k) + \omega(k) + \frac{1}{2}\sigma_3^2(k)\right). \tag{27}$$
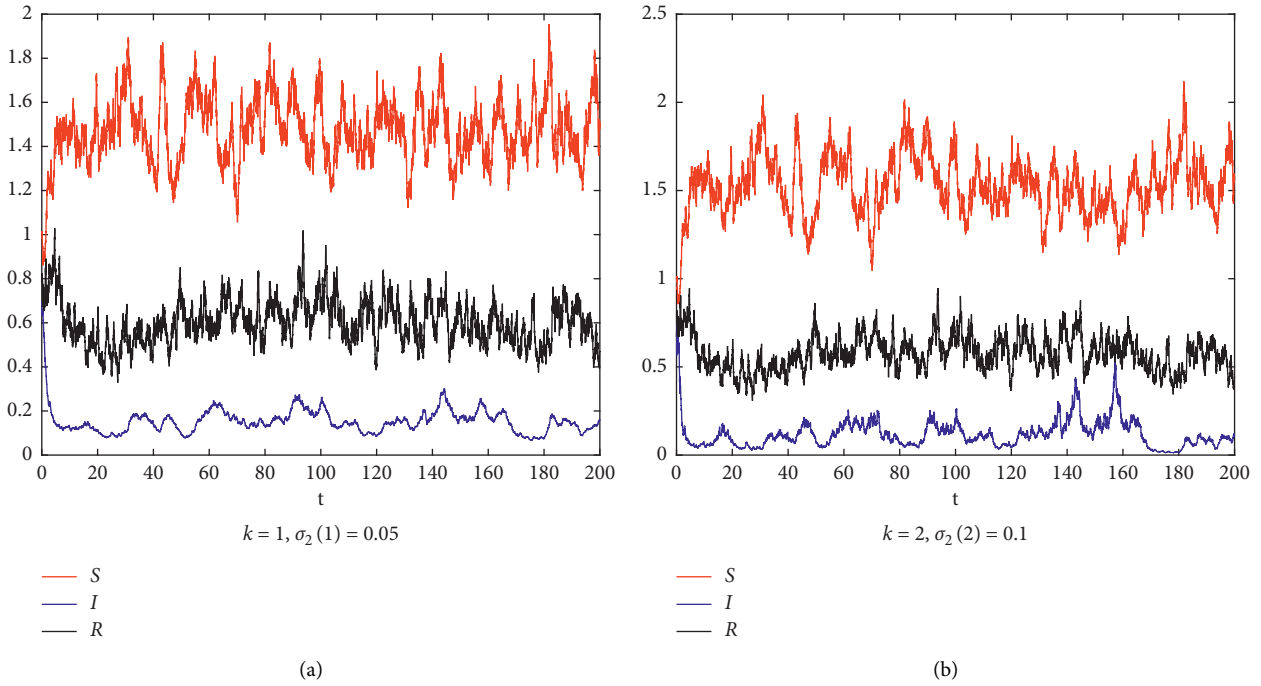
Figure 1: Simulations of the solution $(S(t), I(t), R(t))$ to stochastic model (2) with $(S(0), I(0), R(0)) = (1, 0.7, 0.8)$. (a) $k = 1, \sigma_2(1) = 0.05$. (b) $k = 2, \sigma_2(2) = 0.1$.
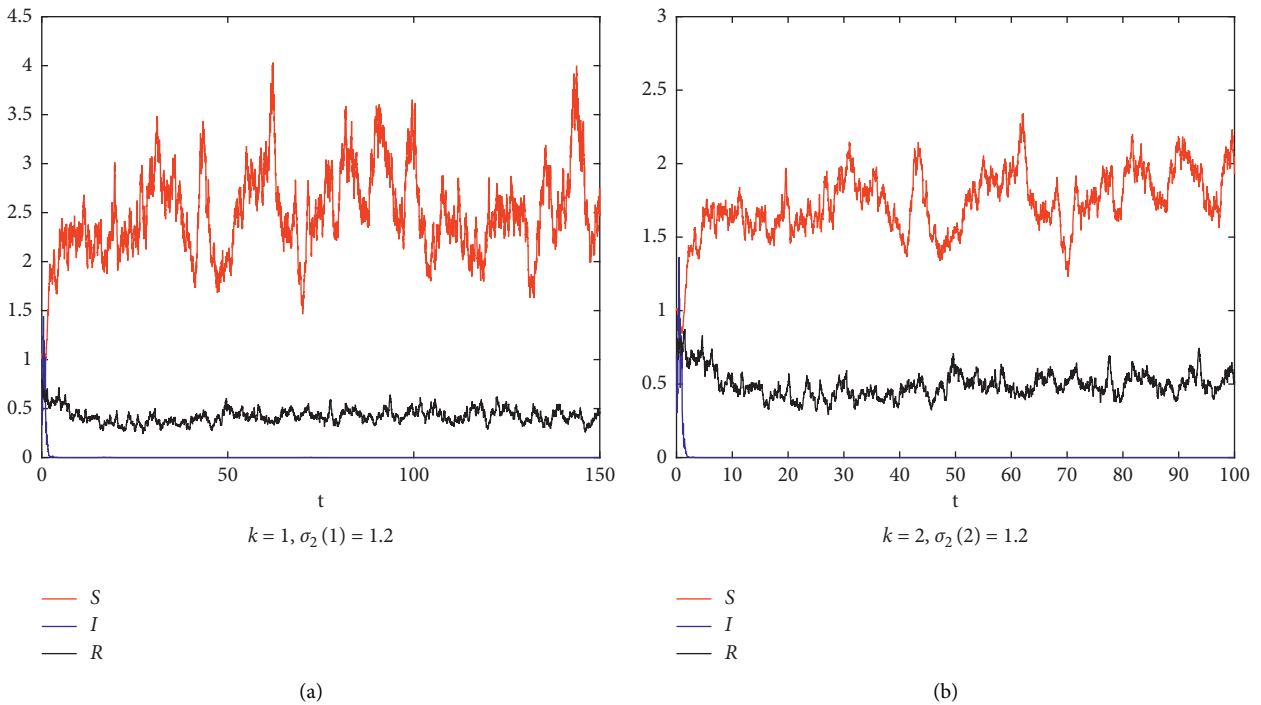

Figure 2: Simulations of the solution $(S(t), I(t), R(t))$ to stochastic model (2) with $(S(0), I(0), R(0)) = (1, 0.7, 0.8)$. (a) $k = 1, \sigma_2(1) = 1.2$. (b) $k = 2, \sigma_2(2) = 1.2$.
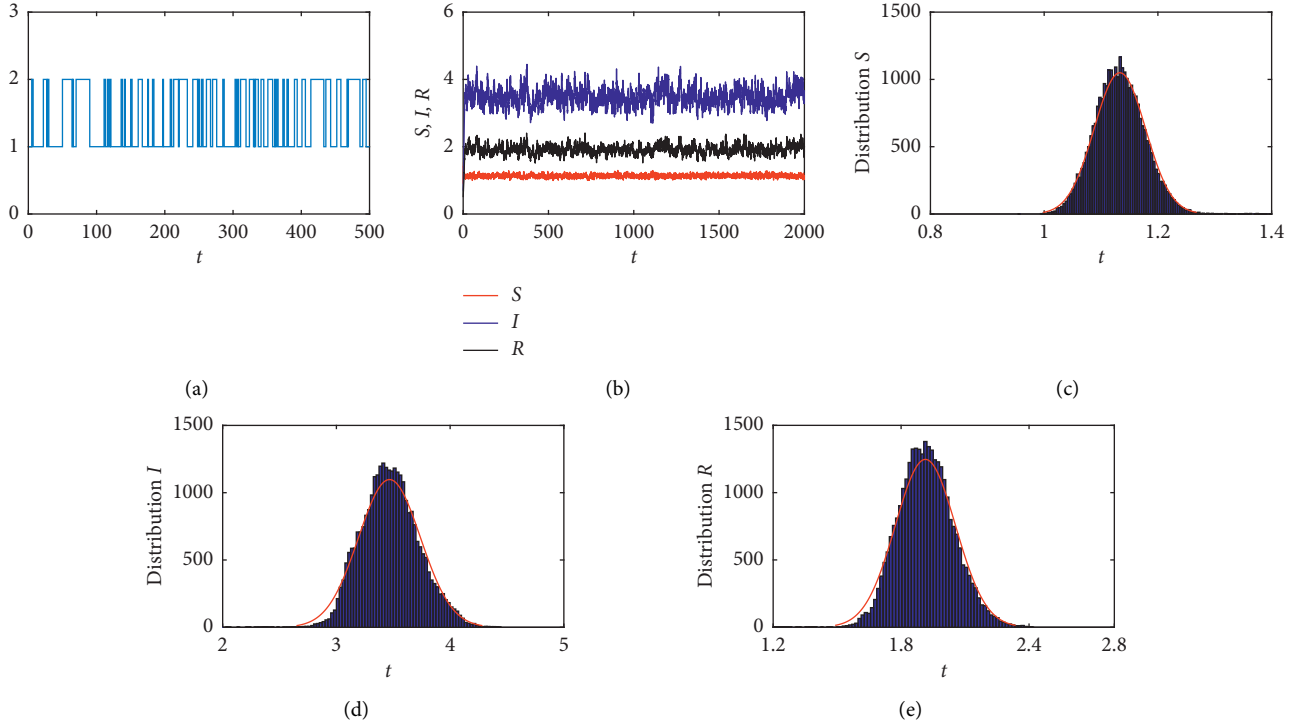
(a)

(b)

(c)

(d)

(e)

FIGURE 3: (a) Markov chain. (b), (c), (d), and (e) Distributions of $S(t), I(t)$, and $R(t)$ of model (2).

Combining (21) and (25)–(27), we have

$$LV(x, y, z, k) = LV_1 + aLV_2 + LV_3 + LV_4$$

$$\leq -\left(\widehat{\mu} - \frac{\vartheta}{2}\breve{\sigma}^2\right)e^{(\vartheta+1)x} + 3^{\vartheta}\breve{A}e^{\vartheta x} - \frac{(1 - \breve{q})\widehat{A}}{e^x} - \left(\widehat{\mu} - \frac{\vartheta}{2}\breve{\sigma}^2\right)e^{(\vartheta+1)y}$$

$$+ 3^{\vartheta}\breve{A}e^{\vartheta y} + ae^y\left[\breve{\beta} + \breve{\lambda}\left(\breve{d}_1 - \widehat{d}_2\right) + \alpha(\breve{\mu} + \breve{\lambda})\right] + \breve{\beta}e^y \tag{28}$$

$$-\left(\widehat{\mu} - \frac{\vartheta}{2}\breve{\sigma}^2\right)e^{(\vartheta+1)z} + 3^{\vartheta}\breve{A}e^{\vartheta z} - \frac{\widehat{q}\widehat{A}}{e^z}$$

$$- aR_s + 2\breve{\mu} + \breve{\omega} + \frac{1}{2}\breve{\sigma}_1^2 + \frac{1}{2}\breve{\sigma}_3^2.$$

Consequently, take ρ sufficiently large, and let $U = (-\rho, \rho) \times (-\rho, \rho) \times (-\rho, \rho)$; then, we have $LV(x, y, z, k) \leq -1$ for any $(x, y, z, k) \in U^c \times \mathcal{M}$. According to Lemma 2.2 in [18], we know that $(x(t), y(t), z(t), \xi(t))$ is ergodic and positive recurrent.

This proof is completed. □

4. Conclusions and Numerical Simulations

This paper investigated a nonlinear epidemic disease model with two kinds of noise disturbances. The threshold of extinction and persistence in mean is obtained.

(i) If $R_s < 0$, the infected individuals tend to become extinct

(ii) If $R_s > 0$, the infected individuals are persistent in mean

(iii) If $R_s > 0$, the stochastic process $(S(t), I(t), R(t), \xi(t))$ of system (2) is ergodic and has a unique stationary distribution

To verify the correctness of the theoretical analysis, numerical simulation is employed in the following example.

Example 1. In system (2), let $\xi(t)$ be a right-continuous Markov chain taking values in $\mathcal{M} = \{1, 2\}$ with the generator

$$\Gamma = \begin{pmatrix} -3 & 3 \\ 1 & -1 \end{pmatrix}. \tag{29}$$

Then, the unique stationary distribution of $\xi(t)$ is $\pi = (\pi_1, \pi_2) = (1/4, 3/4)$. Let $\alpha = 0.2$, and other coefficients in system (2) are selected as follows.

For $k = i (i = 1, 2)$, $(A(1), A(2)) = (1.3, 1.1)$, $(q(1), q(2)) = (0.2, 0.3)$, $(\beta(1), \beta(2)) = (0.6, 0.7)$, $(\mu(1), \mu(2)) = (0.45, 0.5)$, $(\lambda(1), \lambda(2)) = (0.2, 0.3)$, $(\omega(1), \omega(2)) = (0.3, 0.2)$, $(\sigma_1(1), \sigma_1(2)) = (0.2, 0.2)$, and $(\sigma_3(1), \sigma_3(2)) = (0.05, 0.2)$.

Firstly, let $(\sigma_2(1)\sigma_2(2)) = (0.05, 0.1)$. This gives $R_s = 0.52874 > 0$. According to Theorem 1, the infectious disease is permanent (Figure 1).

Then, let $(\sigma_2(1), \sigma_2(2)) = (1.2, 1.2)$. This gives $R_s = -0.1902 < 0$. Based on Theorem 1, the disease $I(t)$ goes extinct (Figure 2). It is easy to see that the disease tends to become extinct when the intensity of white noise increases.

Lastly, let $(\sigma_2(1)\sigma_2(2)) = (0.05, 0.1)$, $(\mu(1), \mu(2)) = (0.2, 0.15)$. This gives $R_s = 3.8277 > 0$. From Theorem 2, the stochastic process $(S(t), I(t), R(t), \xi(t))$ of system (2) is ergodic and has a unique stationary distribution (Figure 3). Figure 3(a) shows the Markov chain, and Figure 3(b) shows a stationary distribution of the stochastic SIRS model. From Figures 3(c)–3(e), we obtain the distributions of $S(t), I(t)$, and $R(t)$ in stochastic system (2), respectively. This means stochastic SIRS model (2) has an ergodic stationary distribution.

Data Availability

No data were used to support this study.

Conflicts of Interest

The authors declare that they have no conflicts of interest.

Acknowledgments

References

[1] H. W. Hethcote, "The mathematics of infectious diseases," *SIAM Review*, vol. 42, no. 4, pp. 599–653, 2000.

[2] M. Fan, M. Y. Li, and K. Wang, "Global stability of an SEIS epidemic model with recruitment and a varying total population size," *Mathematical Biosciences*, vol. 170, no. 2, pp. 199–208, 2001.

[3] J. Li and Z. Ma, "Qualitative analyses of SIS epidemic model with vaccination and varying total population size," *Mathematical and Computer Modelling*, vol. 35, no. 11-12, pp. 1235–1243, 2002.

[4] Y. Nakata and T. Kuniya, "Global dynamics of a class of SEIRS epidemic models in a periodic environment," *Journal of Mathematical Analysis and Applications*, vol. 363, no. 1, pp. 230–237, 2010.

[5] V. Capasso and G. Serio, "A generalization of the Kermack-McKendrick deterministic epidemic model," *Mathematical Biosciences*, vol. 42, no. 1-2, pp. 43–61, 1978.

[6] D. Greenhalgh and I. A. Moneim, "SIRS epidemic model and simulations using different types of seasonal contact rate," *Systems Analysis Modelling Simulation*, vol. 43, no. 5, pp. 573–600, 2003.

[7] C. Ji and D. Jiang, "The threshold of a non-autonomous SIRS epidemic model with stochastic perturbations," *Mathematical Methods in the Applied Sciences*, vol. 40, no. 5, pp. 1773–1782, 2017.

[8] X. Yu, S. Yuan, and T. Zhang, "Persistence and ergodicity of a stochastic single species model with Allee effect under regime switching," *Communications in Nonlinear Science and Numerical Simulation*, vol. 59, pp. 359–374, 2018.

[9] T. Feng, Z. Qiu, X. Meng, and L. Rong, "Analysis of a stochastic HIV-1 infection model with degenerate diffusion," *Applied Mathematics and Computation*, vol. 348, pp. 437–455, 2019.

[10] F. Wei and F. Chen, "Stochastic permanence of an SIQS epidemic model with saturated incidence and independent random perturbations," *Physica A: Statistical Mechanics and its Applications*, vol. 453, pp. 99–107, 2016.

[11] T. Feng, Z. Qiu, and Z. Qiu, "Global analysis of a stochastic TB model with vaccination and treatment," *Discrete & Continuous Dynamical Systems-B*, vol. 24, no. 6, pp. 2923–2939, 2019.

[12] Y. Wang, G. Liu, and G. Liu, "Dynamics analysis of a stochastic SIRS epidemic model with nonlinear incidence rate and transfer from infectious to susceptible," *Mathematical Biosciences and Engineering*, vol. 16, no. 5, pp. 6047–6070, 2019.

[13] G. Lan, Y. Huang, C. Wei, and S. Zhang, "A stochastic SIS epidemic model with saturating contact rate," *Physica A: Statistical Mechanics and Its Applications*, vol. 529, Article ID 121504, 2019.

[14] W. Guo, Q. Zhang, X. Li, and W. Wang, "Dynamic behavior of a stochastic SIRS epidemic model with media coverage," *Mathematical Methods in the Applied Sciences*, vol. 41, no. 14, pp. 5506–5525, 2018.

[15] Q. Liu, D. Jiang, D. Jiang, T. Hayat, and A. Alsaedi, "Dynamical behavior of a multigroup SIRS epidemic model with standard incidence rates and Markovian switching," *Discrete & Continuous Dynamical Systems-A*, vol. 39, no. 10, pp. 5683–5706, 2019.

[16] Y. Lin and M. Jin, "Ergodicity of a regime-switching epidemic model with degenerate diffusion," *Physica A: Statistical Mechanics and Its Applications*, vol. 526, Article ID 121134, 2019.

[17] J. Hu, Z. Teng, Z. Li, and B. Wen, "The threshold dynamics in a stochastic SIS epidemic model with vaccination and nonlinear incidence under regime switching," *Physica A: Statistical Mechanics and Its Applications*, vol. 529, Article ID 121555, 2019.

[18] Q. Liu, D. Jiang, T. Hayat, and B. Ahmad, "Periodic solution and stationary distribution of stochastic SIR epidemic models with higher order perturbation," *Physica A: Statistical Mechanics and its Applications*, vol. 482, pp. 209–217, 2017.

[19] Y. Zhao and D. Jiang, "The threshold of a stochastic SIS epidemic model with vaccination," *Applied Mathematics and Computation*, vol. 243, pp. 718–727, 2014.

[20] X. Zhang, D. Jiang, A. Alsaedi, and T. Hayat, "Stationary distribution of stochastic SIS epidemic model with vaccination under regime switching," *Applied Mathematics Letters*, vol. 59, pp. 87–93, 2016.

[21] X. Mao and C. Yuan, *Stochastic Differential Equations with Markovian Switching*, Imperial College Press, London, UK, 2006.

[22] W. Zhao, J. Li, T. Zhang, X. Meng, and T. Zhang, "Persistence and ergodicity of plant disease model with markov conversion and impulsive toxicant input," *Communications in Nonlinear Science and Numerical Simulation*, vol. 48, pp. 70–84, 2017.

[23] Y. Zhang, K. Fan, S. Gao, and S. Chen, "A remark on stationary distribution of a stochastic SIR epidemic model with double saturated rates," *Applied Mathematics Letters*, vol. 76, pp. 46–52, 2018.

WILEY | Hindawi

Research Article

A Research on Nonendangered Population Protection Facing Biological Invasion

Meng Zhang [ID],[1] **Yi Zhao,**[1] **Mingjing Shi,**[1] **and Xin Zhao** [ID][2]

[1]*School of Science, Beijing University of Civil Engineering and Architecture, Beijing, 100044, China*
[2]*Canvard College, Beijing Technology and Business University, Beijing, 101118, China*

Correspondence should be addressed to Xin Zhao; lettertozhaoxin@163.com

In nature, a biological invasion is a common phenomenon that often threatens the existence of local species. Getting rid of the invasive species is hard to achieve after its survival and reproduction. At present, killing some invasive ones and putting artificial local species are usual methods to prevent local species from extinction. An ODE model is constructed to simulate the invasive procedure, and the protection policy is depicted as a series of impulses depending on the state of the variables. Both the ODEs and the impulses form a state feedback impulsive model which describes the invasion and protection together. The existence of homoclinic cycle and bifurcation of order-1 periodic solution of the impulsive model are discussed, and the orbitally asymptotical stability of the order-1 periodic solution is certificated with a novel method. Finally, the numerical simulation result is listed to confirm the theoretical work.

1. Introduction

Biological invasion is the introduction and establishment of a species beyond its natural range where it may proliferate and spread dramatically [1]. As being predicted, the rate of biological invasion is expected to increase with the acceleration of worldwide movement of people and goods [2, 3]. Biological invasions constitute a major environmental change driver, affecting conservation, agriculture, and human health [4, 5]. Inevitably, biological invasions result in species interactions. When local community members are challenged by biological invasions, they may face novel antagonists such as predators or competitors, or they may benefit from new prey, new and underutilized host plants, or even new mutualists [6]. It is well known that some invasion cases such as the diffusion of alien invasive plants in Albania and the Mediterranean [7] and the rampant diffusion of Asian carp in America have caused great disaster in nature niche. Since biological invasions contribute a lot to rapid environmental change [8], biodiversity loss, degradation of ecosystem structure, impairment of ecosystem services [9], and significant impacts on both natural and agricultural

ecosystems [10], ecological invasion and subsequent influence are receiving increasing attention from scientists and governors. To prevent some species from extinction and destruction of niche caused by the ecological invasion, ecologists carry out some strategies such as the introduction of natural enemies, substitution of invasion species, physical prevention, and chemical prevention. These artificial controlling methods are executed periodically instead of being performed continuously. And the time point to carry out the artificial assistance is decided by the density of the species, but not the fixed period.

Recently, some mathematicians improved a lot in the state feedback impulsive dynamics. They not only set up the basic framework but also proposed and proved some useful theorems. Chen revised and improved some basic frame definitions and proposed a series of theorems which established the foundation of this area and had been widely applied in dealing with practical problems [11]. Zhang et al. improved the theory about order-1 periodic solution in the model of the Internet worm control [12]. Wei et al. dedicated a lot in the area of homoclinic cycle and heteroclinic orbit with respect to some kinds of dynamic model [13–15].

Inspired by the new results in state feedback impulsive model [16–26], and classical work in limit cycle [26] the authors propose a state feedback impulsive model, which is more suitable than the ODE model, to describe the procedure of ecological invasion and artificial control.

This paper is organized as follows. Section 2 proposes a state feedback impulsive model which describes the artificial auxiliary as an impulse relying on the state of variables and introduces some preliminaries of state feedback impulsive system. The existence of homoclinic cycle and order-1 periodic solution is proved in Section 3, and its stability is proved in Section 4. Some numerical simulations will be exhibited in Section 5.

2. State Feedback Impulsive Artificial Assistance Model and Its Preliminaries

We focus on the artificial control by releasing some artificial breeding ones and getting rid of some invasive ones to help the local species to survive from competition with invasive ones.

2.1. Free Developing Model and Analysis. We consider the model

$$
\begin{cases}
\dfrac{dx}{dt} = x\left(a - cy\right), \\[2mm]
\dfrac{dy}{dt} = y\left(d - ex\right)
\end{cases}
\tag{1}
$$

to describe the competition between the two species, where x and y are densities of local and invasive species separately, and these two species compete for the same natural resource. Considering the practical significance, we only discuss model (1) in the first quadrant. It is easy to find that model (1) has two equilibriums $O(0,0)$ and $E(d/e, a/c)$, where $O(0,0)$ is an unstable node while $E(d/e, a/c)$ is a saddle. The dynamical features of model (1) are shown in Figure 1. Since there is only one saddle in the first quadrant, we claim that there exists no limit cycle in the area $\{(x, y) \mid x > 0, y > 0\}$.

In Figure 1, unstable and stable manifolds of saddle E, shown in heavy lines, are denoted with L_1 and L_2. Then, the first quadrant is separated into four parts G_1, G_2, G_3, and G_4. The trajectories initiated from G_3 and G_4 will tend to $(\infty, 0)$ which means the local species can survive the invasion without artificial assistance. On the contrary, the trend of trajectories starting from G_1 and G_2 implies that the local species will experience a critical shrink after a certain period, and the invasion will lead to the extinction of local species sooner or later. The endangered species should have already been protected in special ways, and in this paper, we focus on the common protection of nonendangered local species during the invasion, so we only study the trajectories in G_1.

The artificial control is designed as follows. When the density of invasive species reaches a certain level which is marked with h, manual intervention will be implemented. Through some technical skills, such as spraying biocide,
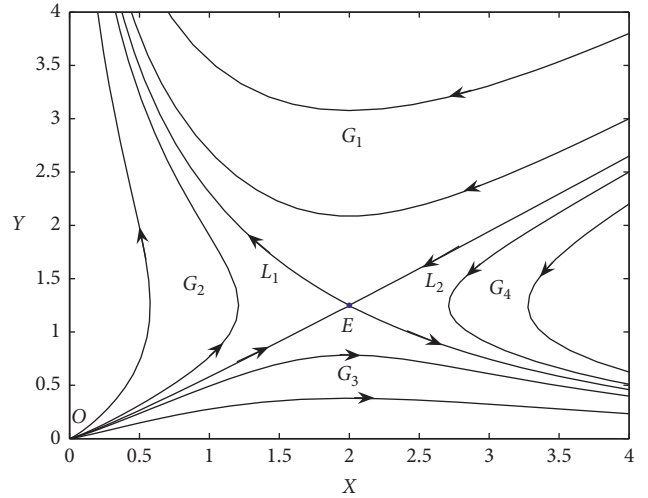

Figure 1: Trajectories of model (1) with parameter values: $a = 5, c = 4, d = 6$, and $e = 3$.

artificial killing, and releasing natural enemies, the invasive species will be partly removed. At the same time, a certain number of local species are put into circulation to replenish its density. Since the perishing of invasive species and the replenishing of local species are carried out according to the actual state of the species and all the artificial auxiliary can be finished in a relatively short period compared with the long-term struggle between the two species, the invasion and protection procedure should be described with a state feedback impulsive model. Without loss of generality, we assume the density of invasive species before mankind help is bigger than the ordinate of equilibrium E, i.e., $h > a/c$. If the mankind help is strong enough to maintain the state of the species in areas G_3 and G_4, the local system will persist. However, the power of mankind is always limited, which means the invasive species cannot be eliminated thoroughly and the local species can only be complemented with limited amount. So, we also assume that the state of two species is located in area G_1 and its boundaries after impulse.

2.2. Construction of the State Feedback Impulsive Model. The state feedback impulse control works in the following procedure. Once the density of invasive species y rises to the threshold value h, people will cull some of them at the rate of β and put in some artificial local ones at the same time. The number of artificial local ones put in the circumstance is infected by density of remainder local species. In circumstantial depiction, we put in more artificial ones to keep the local species permanence if the density of local species is lower, i.e., it is inversely proportional to the density of local species x before the impulse. To construct the model, we denote the intersection of unstable manifold L_1 and the thresh hold line $y = h$ as $A(x_A, h)$, and point $A^+(x_{A^+}, (1 - \beta)h)$ denotes the intersection of stable manifold L_2; the line consisted of the points after impulse. We also denote the intersection of thresh hold line $y = h$ and the horizontal isocline $dy/dt = 0$ as $P(x_P, y_P)$ (see Figure 2). Then, the model can be described as
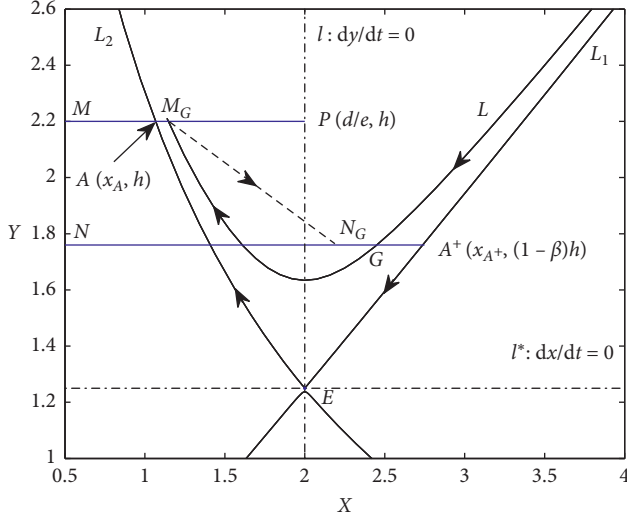
FIGURE 2: Diagram of state feedback impulsive system with parameter values: $a = 5, c = 4, d = 6, e = 3, h = 2.2$, and $\beta = 0.2$.

$$\begin{cases} \dfrac{dx}{dt} = x(a - cy), \\ \qquad\qquad\qquad y \neq h \text{ or } y = h, \, x > x_P, \\ \dfrac{dy}{dt} = y(d - ex), \\ \Delta x = \alpha(x_{A^+} - x), \\ \qquad\qquad\qquad y = h, \, x_A \leq x \leq x_P. \\ \Delta y = -\beta y, \end{cases} \qquad (2)$$

From the description above, we assume that $\alpha \leq 1$ and all the parameters in model (2) are positive. In model (2), the investment of artificial local species is monotonically decreasing with the left ones, which is in accordance with the actual situation. The less the local species left, the more the artificial ones invested.

2.3. Preliminaries.
In the following part of this section, some preliminaries about the state feedback impulsive system will be introduced.

Definition 1. A state feedback impulsive system is defined as

$$\begin{cases} \dfrac{dx}{dt} = P(x, y), \\ \qquad\qquad\qquad (x, y) \notin M\{x, y\}, \\ \dfrac{dy}{dt} = Q(x, y), \\ \Delta x = A(x, y), \\ \qquad\qquad\qquad (x, y) \in M\{x, y\}. \\ \Delta y = B(x, y), \end{cases} \qquad (3)$$

The dynamic system defined with (3) is a kind of semicontinuous dynamic system. In the system, when the variables (x, y) reach set $M\{x, y\}$, the impulse will be carried out according $\varphi: (x, y) \longrightarrow (x + \Delta x, y + \Delta y)$. Here, $M\{x, y\}$ is called impulse set and ϕ is impulsive function. Without loss of generality, the initial point P_0 of system (3)

should be restricted not in impulse set $M\{x, y\}$, i.e., $P \in \Omega = R^2 \backslash M\{x, y\}$. Define $N = \varphi(M)$, and we call it phase set. The state feedback impulsive system can be denoted with (Ω, f, φ, M), where $f(x, y) = (P(x, y), Q(x, y))$, $(x, y) \notin M\{x, y\}$. And the mapping of the state feedback impulsive system is expressed with $f \otimes \varphi(\bullet, t)$.

It is obvious that line segment $\overline{AP}$ is impulsive set of model (2), while a certain part of line $y = (1 - \beta)h$ is the corresponding phase set. While the trajectory L reaches the impulsive set AP at point M_G, the impulsive function φ maps it to the point N_G, i.e. $f \otimes \varphi(G, t) = N_G$.

Definition 2 (see [11]). Since $f \otimes \varphi(\bullet, t)$ is a mapping on itself, there exists a point G^* in phase set N and a corresponding moment t^* satisfying $f(G^*, t^*) = M_G^* \in M$; moreover, $\varphi(M_G^*) = \varphi(f(G^*, t^*)) = G^* \in N$, i.e., $f \otimes \varphi(G^*, t^*) = G^*$. Then, $f \otimes \varphi(G^*, t^*)$ is an order-1 periodic solution of model (3). And the trajectory from G^* to M_G^* controlled by f and the mapping segment line from M_G^* to G^* controlled by φ make up an order-1 limited cycle. Furthermore, if there is a saddle on the order-1 limited cycle, then they form an order-1 homoclinic cycle.

Definition 3 (see [11]). Suppose impulse set M and phase set N are straight lines (see Figure 2). To any point $G \in N$, define the absolutely value of its abscissas as its coordinate. The trajectory initiating from G intersects impulse set M at M_G; then, the impulse function φ maps M_G to N_G in phase set N, and N_G is the subsequent point of G. Then, we define the successor function of G as $F(G) = |x_{N_G}| - |x_G|$.

Remark 1. The sufficient and necessary condition of $F(G) = 0$ is that the solution from G point is an order-1 periodic solution of system (3).

Lemma 1 (see [11]). *Successor function $F(A)$ is continuous.*

Lemma 2 (see [11]). *In semicontinuous dynamic system (Ω, f, φ, M), there exist two points G_1 and G_2 in phase set N; if $F(G_1) \cdot (G_2) < 0$, then there must exist a point G^* between G_1 and G_2 in phase set N satisfying $F(G^*) = 0$, i.e., $f \otimes \varphi(G^*, t)$ is the order-1 periodic solution.*

Lemma 3. *If the impulsive condition is expressed with $\phi(x, y) = 0$, then system (3) can be rewritten as*

$$\begin{cases} \dfrac{dx}{dt} = P(x, y), \\ \qquad\qquad\qquad \phi(x, y) \neq 0, \\ \dfrac{dy}{dt} = Q(x, y), \\ \Delta x = A(x, y), \\ \qquad\qquad\qquad \phi(x, y) = 0. \\ \Delta y = B(x, y), \end{cases} \qquad (4)$$

Assume it has an order-q periodic solution $\Gamma(t) := (\xi(t), \eta(t))$, and the period is T. Then, the order-1

periodic solution is orbitally asymptotically stable if the factor μ_2 satisfies $|\mu_2| < 1$, where

$$\mu_2 = \prod_{k=1}^{q} \Delta_k \exp\left[\int_0^T \left(\frac{\partial P}{\partial x}(\xi(t), \eta(t)) + \frac{\partial Q}{\partial y}(\xi(t), \eta(t))\right)\mathrm{d}t\right],$$

$$\Delta_k = \frac{P_+ ((\partial B/\partial y)(\partial \phi/\partial x) - (\partial B/\partial x)(\partial \phi/\partial y) + (\partial \phi/\partial x)) + Q_+ ((\partial A/\partial x)(\partial \phi/\partial y) - (\partial A/\partial y)(\partial \phi/\partial x) + (\partial \phi/\partial y))}{P(\partial \phi/\partial x) + Q(\partial \phi/\partial y)}.$$

(5)

Here, P, Q, $\partial A/\partial x, \partial A/\partial y, \partial B/\partial x, \partial B/\partial y, \partial \phi/\partial x,$ and $\partial \phi/\partial y$ are the corresponding values at point $(\xi(\tau_k), \eta(\tau_k))$, and P_+ and Q_+ are calculated at $(\xi(\tau_k^+), \eta(\tau_k^+))$.

These definitions and lemmas about the state feedback impulsive system are of great significance in the following part of this paper.

3. Homoclinic Cycle and Homoclinic Bifurcation

In order to discuss the existence of homoclinic cycle and order-1 periodic solution of model (2), we choose α as a key parameter. For a certain α, the homoclinic cycle exists and then it will disappear and bifurcate an order-1 periodic solution with the changing of α.

3.1. Homoclinic Cycle of Model (2) about Parameter α. The horizontal isocline l: $\mathrm{d}y/\mathrm{d}t = 0$ of model (2) expressed as dot line in Figure 3 crosses impulsive set M: $y = h$ and phase set N: $y = (1 - \beta)h$ at P and Q (see Figure 3), and the vertical isocline l^*: $\mathrm{d}x/\mathrm{d}t = 0$ is a line passing saddle E and paralleling with x axis. From the trajectory properties of model (2), we know that the intersection point A of unstable manifold L_2 and the line $y = h$ must locate on the left side of horizontal isocline l and on the upside of vertical isocline l^*, while the intersection point A^+ of stable manifold L_1 and line $y = (1 - \beta)h$ must be on the upper right side.

According to the control of model (2), L_2, unstable manifold of saddle, E, comes out from E and reaches impulsive set M at point A. Restricting $\alpha = 1$, A will be mapped by the impulsive mapping φ of model (2), i.e.,

$$\varphi(x_A, h) = (x_{A^+}, (1 - \beta)h), \quad \varphi: A \longrightarrow A^+. \tag{6}$$

After the impulsive mapping, the trajectory moves along L_1, the stable manifold of E. So, trajectory EA, impulsive line AA^+, and trajectory A^+E form a closed cycle, and saddle E locates on it. Then, the homoclinic cycle forms (see Figure 3).

Theorem 1. *If $\alpha = 1$, then there exists an order-1 homoclinic cycle in model (2).*

3.2. Homoclinic Bifurcation about Parameter α. $\alpha > 1$ indicates that putting abundant artificial local ones can maintain the permanence of local species. But in practice, the massive release cannot be satisfied every time for the deficiency of

artificial breeding capability. Congruous with the above, we only consider the case that the phase point locates in G_1 in this paper.

In this section, we assume $\alpha < 1$, so the phase point of A which is denoted as N_A locates on the left side of A^+. Take another point B^+ $(x_{B^+}, (1 - \beta)h)$ on the left side of A^+ and assume $x_{B^+} = x_{A^+} - \varepsilon$, where $\varepsilon > 0$ is a small enough number, which means B^+ is sufficiently close to A^+. Following the fundamental theories of ordinary differential equation, there exists a unique trajectory L passing through B^+ and intersecting with the impulse set M at point $B(x_B, h)$. According to the continuous property of solution with respect to the initial value, point B locates on the right side of A and is close enough to A. Furthermore, based on the continuous characteristic of impulse function φ with respect to the independent variable, the phase point $N_B = \varphi(B)$ is also close enough to N_A, i.e., N_B is on the left side of B^+, $F(B^+) < 0$ (see Figure 4).

Then, we consider the trajectory passing Q. Following the properties of trajectories, there exists only one trajectory passing through Q denoted as L^*; it arrives the imagine set M: $y = h$ at D, then the impulsive function φ maps D to N_D. The following discussion is basedfsection, we will discuss the orbital stabi on the location of $N_D (x_{N_D}, (1 - \beta)h)$.

Case 1. $x_{N_D} = x_Q = d/e$. This condition ensures the phase points N_D and Q coincide and the successor function of Q is $F(Q) = 0$, i.e., the trajectory $\overset{\frown}{QD}$ and the impulsive mapping $\overline{DN_D}$ make up an order-1 limit cycle (see Figure 5). We denote the value of α under this situation as α^*.

Case 2. $x_{N_D} > x_Q = d/e$, i.e., $\alpha^* < \alpha < 1$. With this condition, we have that the successor function of Q is $F(Q) = x_{N_D} - x_Q > 0$. According to Lemma 2, there exists a point $C \in N$ (between Q and B^+) satisfying $F(C) = 0$. That means there exists an order-1 periodic solution of system (2) (see Figure 6).

Case 3. $x_{N_D} < x_Q = d/e$, i.e., $\alpha < \alpha^*$. Here, we can get a contrary successor function of Q, i.e., $F(Q) = x_{N_D} - x_Q < 0$. Denote the intersection of L and phase set N (L moves upside) as B^*; then, $F(B^*) > 0$. Also, from Lemma 2, there exists a point $C^* \in N$ (between B^* and Q) satisfying $F(C^*) = 0$. That means there exists an order-1 periodic solution of system (2) (see Figure 7).

From the discussion of those three cases, we have the following theorem.
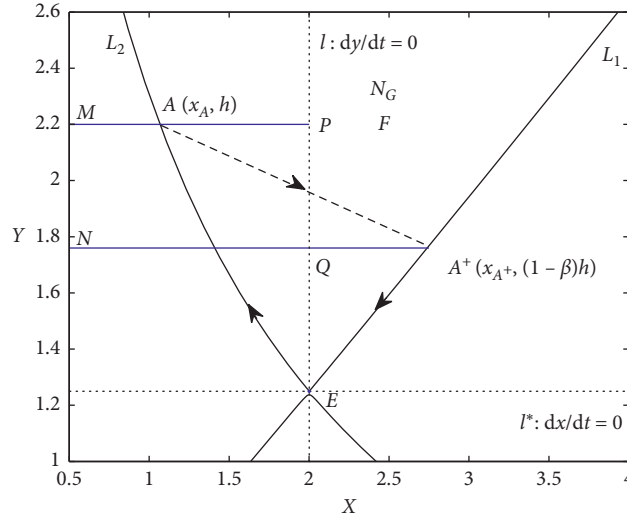
Figure 3: Homoclinic cycle of model (2) with parameter values: $a = 5, c = 4, d = 6, e = 3, h = 2.2, \beta = 0.2$, and $\alpha = 1$.
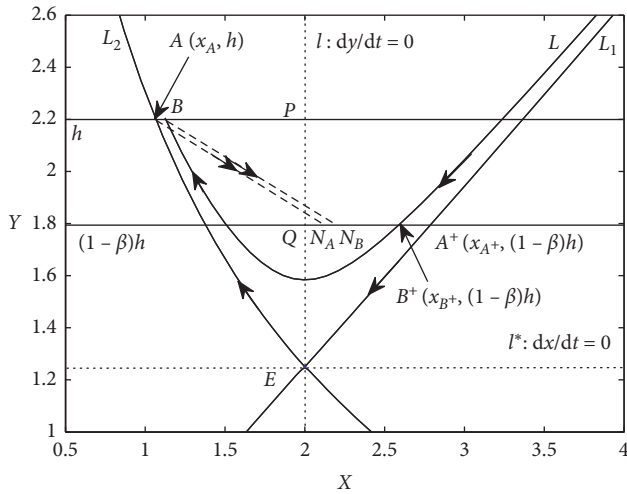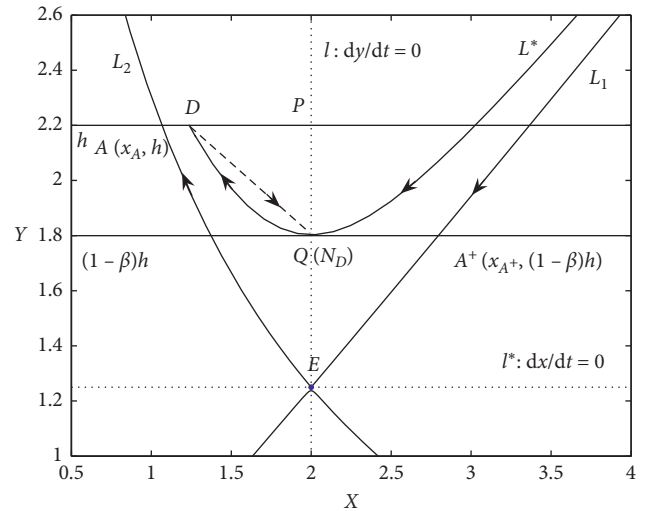

Figure 4: Trajectory L passing B^+ and impulse mapping of B with parameter values: $a = 5, c = 4, d = 6, e = 3, h = 2.2$, and $\beta = 0.2$.

Theorem 2. *If $\underline{\alpha} < \alpha < 1$ ($\underline{\alpha}$ is the threshold to make sure the phase point is located in G_1) holds, then there exists an order-1 periodic solution to system (2).*

Remark 2. From Theorems 1 and 2, we know that system (2) has an order-1 homoclinic cycle when $\alpha = 1$. For any $\underline{\alpha} < \alpha < 1$, the order-1 homoclinic cycle breaks and bifurcates an order-1 periodic solution. Then, $\alpha = 1$ is a bifurcation point for system (2).

4. Stability of the Order-1 Periodic Solution

In this section, we will discuss the orbital stability of the order-1 periodic solution.

Figure 5: Trajectory L^* passing Q and impulse mapping D of case I with parameter values: $a = 5, c = 4, d = 6, e = 3, h = 2.2$, and $\beta = 0.2$.

Theorem 3. *Suppose $(\xi(t), \eta(t))$ is an order-1 periodic solution of model (2) which initiates from $(\xi_0, \eta_0) \in N$ and it arrives the impulsive set at $(\xi_1, \eta_1) \in M$. The order-1 periodic solution $(\xi(t), \eta(t))$ is orbitally asymptotically stable if*

$$(H), \xi_0 < \frac{d}{e} \tag{7}$$

is satisfied.

Proof 1. Assume $\Gamma(t) = (\xi(t), \eta(t))$ is an order-1 periodic solution of system (2) and the period is T. Denote
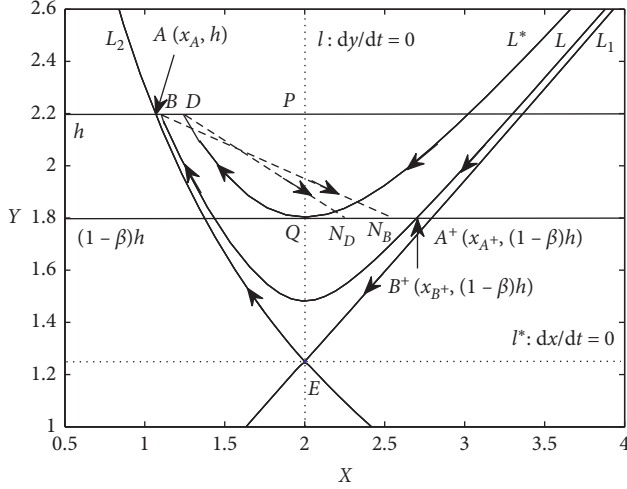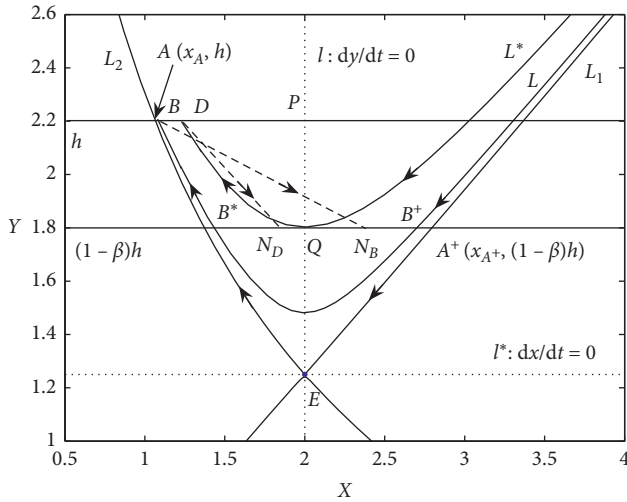
Figure 6: Trajectory L^* passing Q and impulse mapping D of case II with parameter values: $a = 5, c = 4, d = 6, e = 3, h = 2.2,$ and $\beta = 0.2$.

Figure 7: Trajectory L^* passing Q and impulse mapping D of case III with parameter values: $a = 5, c = 4, d = 6, e = 3, h = 2.2,$ and $\beta = 0.2$.

$$
\begin{aligned}
\xi_0 &= \xi(0), \\
\xi_1 &= \xi(T), \\
\eta_0 &= \eta(0) = (1 - \beta)h, \\
\eta_1 &= \eta(T) = h,
\end{aligned}
\tag{8}
$$

$$
\begin{aligned}
\xi_1^+ &= \xi(T^+) = \xi_1 + \alpha(x_{A^+} - \xi_1) = \xi_0, \\
\eta_1^+ &= \eta(T^+) = \eta_0 = (1 - \beta)h.
\end{aligned}
\tag{9}
$$

Following the expression of system (2), we have

$$
\begin{aligned}
P(x, y) &= x(a - cy), \\
Q(x, y) &= y(d - ex), \\
A(x, y) &= \alpha(x_{A^+} - x), \\
B(x, y) &= -\beta y, \\
\phi(x, y) &= y - h.
\end{aligned}
\tag{10}
$$

Then, their values can be calculated as

$$
\begin{aligned}
\frac{\partial P}{\partial x} &= a - cy, \\
\frac{\partial P}{\partial y} &= -cx, \\
\frac{\partial Q}{\partial x} &= -ey, \\
\frac{\partial Q}{\partial y} &= d - ex, \\
\frac{\partial A}{\partial x} &= -\alpha, \\
\frac{\partial A}{\partial y} &= 0, \\
\frac{\partial B}{\partial x} &= 0, \\
\frac{\partial B}{\partial y} &= -\beta, \\
\frac{\partial \phi}{\partial x} &= 0, \\
\frac{\partial \phi}{\partial y} &= 1.
\end{aligned}
\tag{11}
$$

We also have

$$
\begin{aligned}
\Delta_1 &= \frac{(1 - \alpha)Q_+}{Q} = \frac{(1 - \alpha)(d - e\xi_0)\eta_0}{(d - e\xi_1)\eta_1} \\
&= (1 - \alpha)(1 - \beta)\frac{d - e\xi_0}{d - e\xi_1},
\end{aligned}
\tag{12}
$$

$$
\begin{aligned}
&\int_0^T \left(\frac{\partial P}{\partial x}(\xi(t), \eta(t)) + \frac{\partial Q}{\partial y}(\xi(t), \eta(t)) \right) dt \\
&= \int_0^T \left(\frac{\dot{x}}{x} + \frac{\dot{y}}{y} \right) dt \\
&= \ln \frac{\xi_1}{\xi_0} \cdot \frac{\eta_1}{\eta_0}.
\end{aligned}
\tag{13}
$$

Then,

$$
\begin{aligned}
\mu_2 &= \Delta_1 \cdot \exp \int_0^T \left(\frac{\partial P}{\partial x}(\xi(t), \eta(t)) + \frac{\partial Q}{\partial y}(\xi(t), \eta(t)) \right) dt \\
&= (1 - \alpha) \cdot \frac{d - e\xi_0}{d - e\xi_1} \cdot \frac{\xi_1}{\xi_0}.
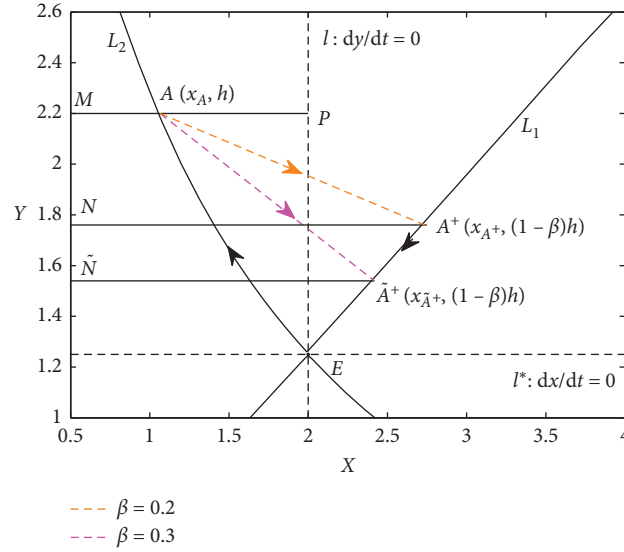\end{aligned}
\tag{14}
$$

FIGURE 8: Homoclinic cycle of model (2) when $\alpha = 1$ with parameter values: $a = 5, c = 4, d = 6, e = 3$, and $h = 2.2$. The case of $\beta = 0.2$ is shown in hazel line while that of $\beta = 0.3$ is exhibited in pink line.

In area G_1, variable x shows a continuous decrease when it is controlled by the first two equations of model (2). (ξ_0, η_0) and (ξ_1, η_1) are coordinates of the intersections of the order-1 periodic solution with phase set and impulsive set. It is obvious that the trajectories move from the intersection on phase set to the one on impulsive set, so we can draw the conclusion that $\xi_1 < \xi_0$. With these conditions, if

$$(H), \xi_0 < \frac{d}{e}, \tag{15}$$

also holds, i.e., the intersection of the order-1 periodic solution and the phase set locates on the left side of the horizontal isocline, we have $0 < (d - e\xi_0/d - e\xi_1) < 1$. Then, $|\mu_2| < 1$ is satisfied. Following Lemma 3, we can draw the conclusion that the order-1 periodic solution is orbitally asymptotically stable. This completes the proof. □

5. Numerical Simulation and Discussion

System (1) is a state feedback impulsive dynamic system whose corresponding system without impulse is model (2). In Section 3 and Section 4, we have proved that system (2) has either a homoclinic cycle or an order-1 periodic solution according to different parameter values. To verify the result, we show some results which display the conclusion more intuitively.

In the following numerical simulation of model (2), we assume $a = 5, c = 4, d = 6, e = 3$, and $h = 2.2$ while the parameters α and β which control the intensity of impulse take different values.

Figure 8 shows that homoclinic cycles exist when $\alpha = 1$ while the parameter β takes different values. It means the existence of homoclinic cycle is not influenced by the value of parameter β as long as the impulsive set is located above the saddle E.
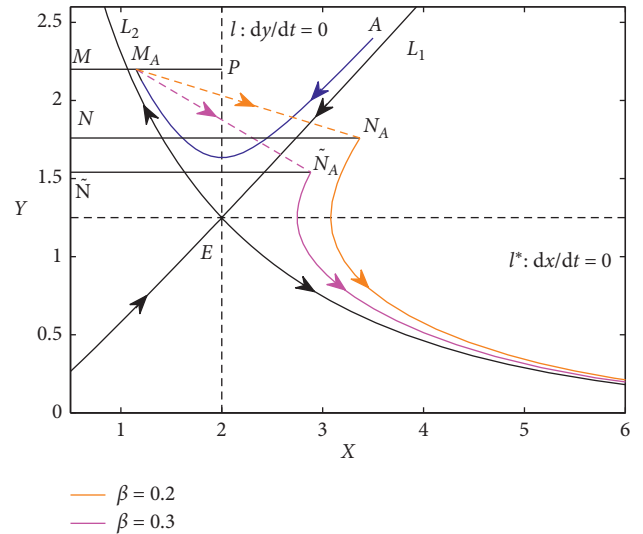

FIGURE 9: Situations of impulsive model (2) when $\alpha = 1.4$ with parameter values: $a = 5, c = 4, d = 6, e = 3$, and $h = 2.2$ and initial values $(3.5, 2.4)$. The case of $\beta = 0.2$ is shown in hazel line while that of $\beta = 0.3$ is exhibited in pink line.

Figure 9 exhibits the situation when $\alpha > 1$. When $\alpha > 1$, the phase point will drop in area G_4 which means the trajectory definitely runs to $(\infty, 0)$. In reality, if there are plenty of artificial local ones can be invested in the competition together with getting rid of a certain amount of invasive ones, then the local species will success and sustain. If artificial breeding local species is easy, impulsive replenish of enough amount of artificial local ones can help the local species hold advantage in the competition with invasive ones. So, strengthening the local species with supplying plentiful amount in single impulse is the best strategy when dealing with ecological invasion.
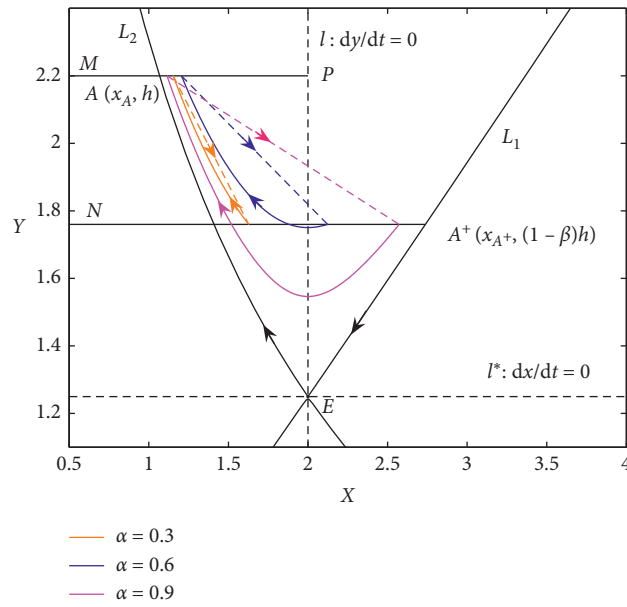
FIGURE 10: Existence of order-1 periodic solution when $\alpha < 1$ with parameter values: $a = 5, c = 4, d = 6, e = 3, h = 2.2,$ and $\beta = 0.2$ and initial values $(3.5, 2.4)$. The cases of $\alpha = 0.3$, $\alpha = 0.6$, and $\alpha = 0.9$ are shown with hazel, blue, and pink lines coordinately.
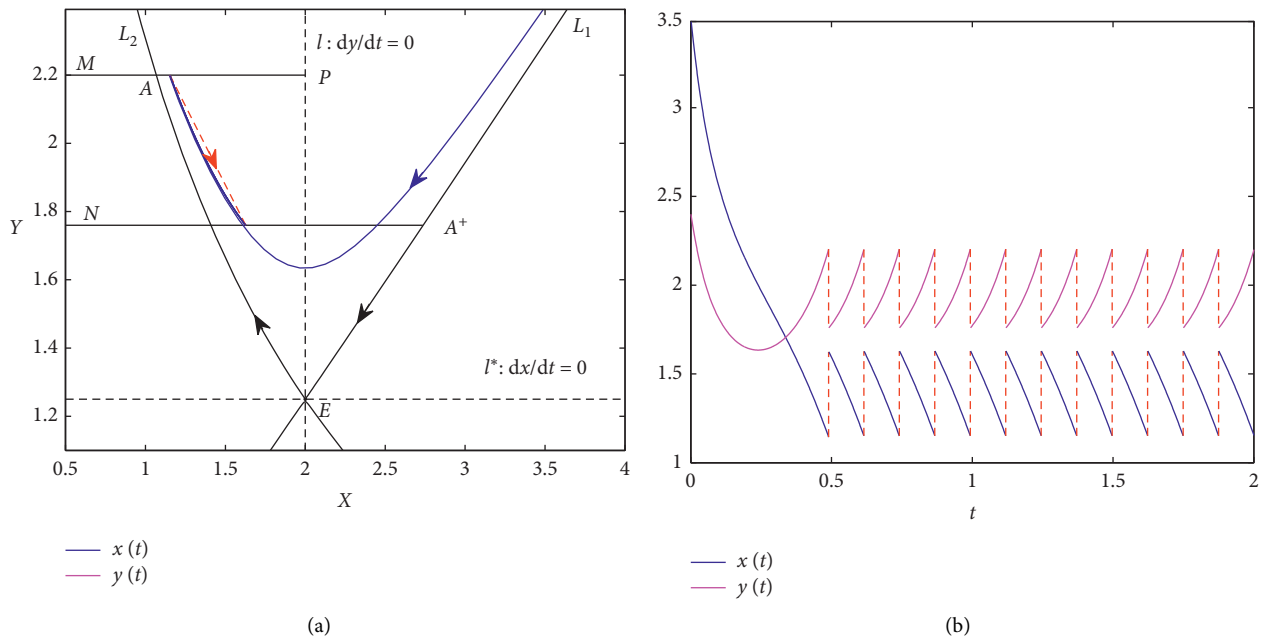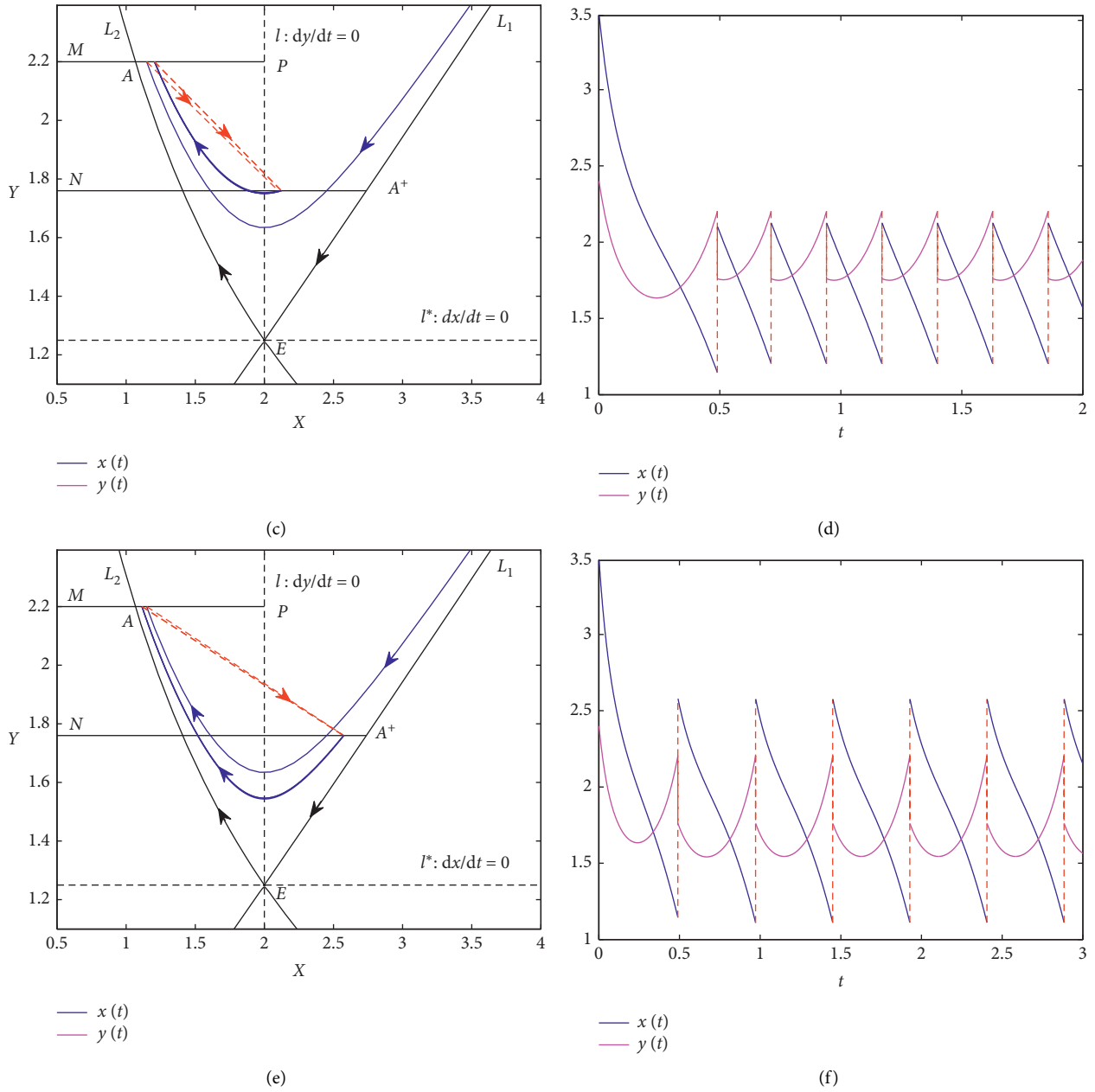

(a)

(b)

FIGURE 11: Continued.

(c)

(d)

(e)

(f)

FIGURE 11: The order-1 periodic solution of model (2) and time series of x and y with parameters $a = 5, c = 4, d = 6, e = 3, h = 2.2$, and $\beta = 0.2$ and initial values $(3.5, 2.4)$. (a, b) $\alpha = 0.3$. (c, d) $\alpha = 0.6$. (e, f) $\alpha = 0.9$. (a), (c), and (e) show the order-1 periodic solution, while (b), (d), and (f) exhibit the time series of variables x and y.

When $\overline{\alpha} < \alpha < 1$, there exists order-1 periodic solution in model (2), and Figure 10 shows the specific situation. It means that removing some invasive species and supplying a certain amount of local species can keep the local species and prevent it from extinction. In reality, when the local species is not quite easy to breed, proper amount investment of local species and removal of invasive ones will keep the two species into periodic circumstances. Both local species and invasive species will be kept, and their amounts appear to have a complex relation with each other. The single situation and the time series of local species x and invasive species y are shown in Figure 11. It is easy to find that both time

period and amplitude increase with the growing of α based on the fixed β. This means that more supplement of artificial breeding of local species can make the local species steady when facing disturbance.

To different β, model (2) has an order-1 periodic solution for $\overline{\alpha} < \alpha < 1$. Figure 12 shows the order-1 periodic solutions of model (2) when $\beta = 0.3$.

Based on the theoretical and numerical results, we can conclude that killing invasive species and investing artificial breeding local species into circumstances can help the local ones resist the ecological invasion. Investing plenty of local species in one time can even support the local species win the
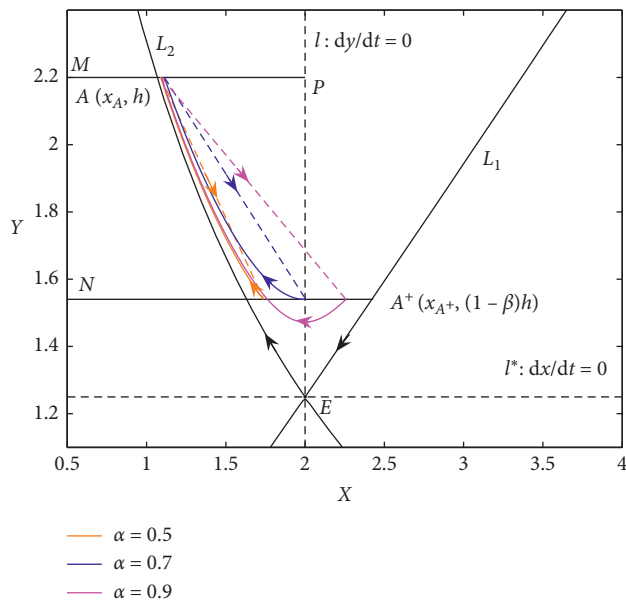
Figure 12: Existence of order-1 periodic solution when $\beta = 0.3$ with parameter values: $a = 5, c = 4, d = 6, e = 3$, and $h = 2.2$ and initial values $(3.5, 2.4)$. The cases of $\alpha = 0.5$, $\alpha = 0.7$, and $\alpha = 0.9$ are shown with hazel, blue, and pink lines coordinately.

competition. If the supplement of local species is not enough, we should also replenish it as abundant as we can, since the more we invest, the stronger the local species will be.

Data Availability

No data were used to support the study.

Conflicts of Interest

The authors declare that they have no conflicts of interest.

Acknowledgments

References

[1] D. Simberloff, *Invasive Species: What Everyone Needs to Know*, Oxford University Press, Oxford, UK, 2013.

[2] F. Essl, S. Dullinger, W. Rabitsch et al., "Socioeconomic legacy yields an invasion debt," *Proceedings of the National Academy of Sciences*, vol. 108, no. 1, pp. 203–207, 2011.

[3] H. Seebens, M. T. Gastner, and B. Blasius, "The risk of marine bioinvasion caused by global shipping," *Ecology Letters*, vol. 16, no. 6, pp. 782–790, 2013.

[4] S. L. Chown, K. A. Hodgins, P. C. Griffin, J. G. Oakeshott, M. Byrne, and A. A. Hoffmann, "Biological invasions, climate change and genomics," *Evolutionary Applications*, vol. 8, no. 1, pp. 23–46, 2015.

[5] P. Peter and D. M. Richardson, "Invasive species, environmental change and management, and ecosystem health," *Annual Review of Environment and Resources*, vol. 35, pp. 25–55, 2010.

[6] A. I. Queiroz and P. Simon, *Histories of Bioinvasions in the Mediterranean (Environmental history Series*, Springer, Cham, Switzerland, 2018.

[7] D. Simberloff, J.-L. Martin, P. Genovesi et al., "Impacts of biological invasions: what's what and the way forward," *Trends in Ecology & Evolution*, vol. 28, no. 1, pp. 58–66, 2013.

[8] N.-M. Gabriela and S. Fei, "Understanding macroscale patterns and processes of invasion. theses and dissertations available from ProQuest," 2018.

[9] C. Hui and D. M. Richardson, *Invasion dynamics*, Oxford University Press, Oxford, UK, 2017.

[10] J. A. Lau and C. P. Terhorst, "Causes and consequences of failed adaptation to biological invasions: the role of ecological constraints," *Molecular Ecology*, vol. 24, no. 9, pp. 1987–1998, 2015.

[11] L. Chen, X. Liang, and Y. Pei, "The periodic solutions of the impulsive state feedback dynamical system," *Communications in Mathematical Biology and Neuroscience*, vol. 2018, Article ID 14, 2018.

[12] M. Zhang, G. Song, and L. Chen, "A state feedback impulse model for computer worm control," *Nonlinear Dynamics*, vol. 85, no. 3, pp. 1561–1569, 2016.

[13] C. Wei and L. Chen, "Heteroclinic bifurcations of a prey-predator fishery model with impulsive harvesting," *International Journal of Biomathematics*, vol. 06, no. 05, Article ID 1350031, 2013.

[14] C. Wei and L. Chen, "Dynamic analysis of mathematical model of ethanol fermentation with gas stripping," *Nonlinear Dynamics*, vol. 57, no. 1-2, pp. 13–23, 2009.

[15] C. Wei and L. Chen, "Periodic solution of prey-predator model with beddington-DeAngelis functional response and impulsive state feedback control," *Journal of Applied Mathematics*, vol. 2012, Article ID 607105, 2012.

[16] T. Zhang, N. Gao, J. Wang et al., "Dynamic system of microbial culture described bu impulsive differential equations," *Mathematical Modelling and Its Application*, vol. 8, no. 01, pp. 1–13, 2019.

[17] S. Huang, "Modeling and solution to the problem of optimal epidemic control: a review," *Mathematical Modelling and Its Application*, vol. 8, no. 03, pp. 1–36, 2019.

[18] C. Wei and L. Chen, "Periodic solution and heteroclinic bifurcation in a predator-prey system with allee effect and impulsive harvesting," *Nonlinear Dynamics*, vol. 76, no. 2, pp. 1109–1117, 2014.

[19] H. Gritli and S. Belghith, "Walking dynamics of the passive compass-gait model under OGY-based state-feedback control: analysis of local bifurcations via the hybrid poincaré map," *Chaos, Solitons & Fractals*, vol. 98, pp. 72–87, 2017.

[20] H. Gritli and S. Belghith, "Diversity in the nonlinear dynamic behavior of a one-degree-of-freedom impact mechanical oscillator under OGY-based state-feedback control law: order, chaos and exhibition of the border-collision bifurcation," *Mechanism and Machine Theory*, vol. 124, pp. 1–41, 2018.

[21] G. Pang and L. Chen, "Periodic solution of the system with impulsive state feedback control," *Nonlinear Dynamics*, vol. 78, no. 1, pp. 743–753, 2014.

[22] M. Sun, Y. Liu, S. Liu, Z. Hu, and L. Chen, "A novel method for analyzing the stability of periodic solution of impulsive state feedback model," *Applied Mathematics and Computation*, vol. 273, pp. 425–434, 2016.

[23] H. Guo, L. Chen, and X. Song, "Qualitative analysis of impulsive state feedback control to an algae-fish system with bistable property," *Applied Mathematics and Computation*, vol. 271, pp. 905–922, 2015.

[24] B. Liu, Y. Tian, and B. Kang, "Dynamics on a holling ii predator-prey model with state-dependent impulsive control," *International Journal of Biomathematics*, vol. 05, no. 03, Article ID 1260006, 2012.

[25] Y. Tian, K. Sun, and L. Chen, "Geometric approach to the stability analysis of the periodic solution in a semi-continuous dynamic system," *International Journal of Biomathematics*, vol. 07, no. 02, Article ID 1450018, 2014.

[26] C. Wei and L. Chen, "Homoclinic bifurcation of prey-predator model with impulsive state feedback control," *Applied Mathematics and Computation*, vol. 237, pp. 282–292, 2014.

[27] Y. Ye, *Limit Cycle theory*, Shanghai Science and Technology Press, Shanghai, China, 1984, in Chinese.

Research Article

Stability Analysis and Clinic Phenomenon Simulation of a Fractional-Order HBV Infection Model

Yongmei Su ㏇,[1] Sinuo Liu,[1] Shurui Song,[1] Xiaoke Li,[2] and Yongan Ye ㏇[2]

[1]*School of Mathematics and Physics, University of Science and Technology Beijing, Beijing 100083, China*
[2]*Institute of Liver Diseases, Beijing University of Chinese Medicine,*
 Dongzhimen Hospital Affiliated to Beijing University of Chinese Medicine, Beijing 100700, China

Correspondence should be addressed to Yongmei Su; suym71@ustb.edu.cn and Yongan Ye; yeyongan@vip.163.com

In this paper, a fractional-order HBV model was set up based on standard mass action incidences and quasisteady assumption. The basic reproductive number R_0 and the cytotoxic T lymphocytes' immune-response reproductive number R_1 were derived. There were three equilibrium points of the model, and stable analysis of each equilibrium point was given with corresponding hypothesis about R_0 or R_1. Some numerical simulations were also given based on HBeAg clinical data, and the simulation showed that there existed positive logarithmic correlation between the number of infected cells and HBeAg, which was consistent with the clinical facts. The simulation also showed that the clinical individual differences should be reflected by the fractional-order model.

1. Introduction

Viral infection is a major global problem, and mathematical models are an important tool for the study of biological phenomenon [1–5] and viral infectious disease [6–9] because they can help us to understand the dynamics of some infectious diseases and some chronic viral infections.

Mathematical models were also used to interpret experimental and clinical results in the fields of (anti-) HIV, HBV, and HCV infections [10–12]. These models were all set up with ordinary differential equation. In recent years, fractional differential equation models were often used in biology because the researchers found that the biological cell membranes have electron conductivity, which could be classified as a fractional-order model [13, 14]. In addition, some biological models established by fractional differential equations have proved to be more advantageous than integers [14]. In particular, the biggest difference between the fractional-order model and the integer-order model is that the fractional-order model has the memory, while the characteristic of the immune response contains the memory [14].

So, when we discuss virus immune models, fractional mathematical models have become important tools.

Arafa et al. [14] proposed a fractional-order HIV infection model, Wang et al. [15] proposed a fractional-order HIV infection model, considering the logistic growth of the healthy CD4 cells, and Yan and Kou [16] had further proposed the following HIV model:

$$
\begin{cases}
D^\alpha x = \lambda - \mathrm{d}x + \rho x\left(1 - x + \dfrac{y}{x_{\max}}\right) - \beta x v, \\[2mm]
D^\alpha y = \beta x v - a y, \\[2mm]
D^\alpha v = k y - \gamma v.
\end{cases}
\tag{1}
$$

Within-host HBV models of fractional order were also discussed [17, 18], and the model in paper [17] was as follows:

$$
\begin{cases}
D^\alpha x = \lambda - \mathrm{d}x - \beta x v + \delta y, \\
D^\alpha y = \beta x v - (a + \delta)y, \\
D^\alpha v = k y - \gamma v,
\end{cases}
\tag{2}
$$

where x, y, and v represent the concentration of uninfected hepatocytes cells, infected cells, and viruses, the death rate of

them is d, a, and γ, reprectively, the uninfected hepatocytes are supposed to be produced at rate λ, β is the infection rate at which the uninfected cell becomes infected, and the infected hepatocytes are cured by noncytolytic processes at a constant rate δ per cell. Based on model (2), Cardoso et al. [18] also disused a fractional model of hepatitis B with drug therapy by representing β and k in model (2) with $(1 - \rho)\beta$ and $(1 - \mu)k$, in which ρ and μ represent the drug efficacy.

It should be pointed out that the bilinear incidences $\beta x v$ were used to describe the infection between uninfected cells and virus in [14–18], but Min et al. changed it to standard incidence function $(\beta x v/(x + y))$ to describe the HBV infection model, which seemed more reasonable because it is independent of the number of total cells of liver [19]. On the other hand, Bartholdy et al. and Wodarz et al. [20] found that the turnover of free virus was much faster than that of infected cells, which means quasisteady assumption could be used, that is, the amount of free virus is simply proportional to the number of infected cells, so the number of infected cells y can also be considered as a measure of virus load. Based on quasisteady assumption, Guo and Cai [21] discussed a HBV infection model by $(\beta x y/(x + y))$ instead of $(\beta x v/(x + y))$, but the model is integral order. On the other hand, model (2) does not include the immune cell, while the cytotoxic T lymphocyte (CTL) immune response after viral infection is universal and necessary to eliminate or control the disease.

Though fractional differential equations have proved to be a good choice to describe biological phenomenon, most discussions only focus on mathematic analysis and numerical simulation, and so far, almost no papers have used fractional-order models to explain clinic phenomenon about HBV. In this paper, based on the above discussion and quasisteady assumption, a HBV model was set up as follows:

$$\begin{cases} D^\alpha x = \lambda - \mathrm{d}x - \dfrac{\beta x y}{(x + y)} + \delta y, \\ \\ D^\alpha y = \dfrac{\beta x y}{(x + y)} - ay - pyz - \delta y, \\ \\ D^\alpha z = cyz - bz, \end{cases} \tag{3}$$

in which $0 < \alpha < 1$, the meanings of x and y are the same as those in model (2), z represents the number of CTL, where the immune response is assumed to get stronger at a rate cyz and decays exponentially at a rate bz, which is proportional to their current concentration, and the parameter p expresses the efficacy of the nonlytic component.

This paper is organized as follows. In Section 2, some definitions and lemmas of fractional-order differential equation are cited. In Section 3, we mainly discuss the existence and uniqueness of positive solutions. The stability analysis is given in Section 4. The simulation is given in Section 5. This paper ends with a conclusion in Section 6 and discussion in Section 7.

2. Primary Concept and Lemma

It is known that fractional derivative has a variety of definitions [17, 22]. In this paper, we used the Caputo fractional derivatives which are defined as follows.

Definition 1 (see [14]). The Caputo fractional derivatives of order $\alpha > 0, n - 1 < \alpha < n, n \in N$, are defined as

$$D^\alpha f(t) = \frac{1}{\Gamma(n - \alpha)} \int_0^t \frac{f^{(n)}(s)}{(t - s)^{\alpha + 1 - n}} \mathrm{d}s, \tag{4}$$

where $\Gamma(n - \alpha) = \int_0^\infty t^{n - \alpha} e^{-t} \mathrm{d}t$.

Definition 2 (see [20]). The discriminant $D(f)$ of a polynomial

$$f(x) = x^n + a_1 x^{n-1} + a_2 x^{n-2} + \cdots + a_n, \tag{5}$$

is defined by $D(f) = (-1)^{(n(n-1)/2)} R(f, f')$, where f' is the derivative of f. $R(f, f')$ is the determinant of the corresponding $(2n - 1) \otimes (2n - 1)$ Sylvester matrix. The Sylvester matrix is formed by filling the matrix beginning with the upper left corner with the coefficients of $f(x)$ and then shifting down one row and one column to the right and filling in the coefficients starting there until they hit the right side. The process is then repeated for the coefficients of $f'(x)$.

The following lemmas were useful to our arguments.

Lemma 1 (see [23]). *For a fractional-order system:*

$$\begin{cases} D^\alpha x(t) = f(t, x(t)), \\ x(t_0) = x_0, \end{cases} \tag{6}$$

with $0 < \alpha < 1$ and $x \in R^n$, the equilibrium point of the system is locally asymptotically stable if all eigenvalues λ_i of Jacobian matrix $J = (\partial f/\partial x)$ evaluated at the equilibrium point satisfy

$$\left|\arg(\lambda_i)\right| > \frac{\alpha\pi}{2}. \tag{7}$$

Lemma 2 (see [24]). *For the polynomial equation,*

$$P(\lambda) = \lambda^n + d_1 \lambda^{n-1} + d_2 \lambda^{n-2} + \cdots + d_n = 0. \tag{8}$$

The conditions which make all the roots of (8) satisfy (7) are displayed as follows:

  (i) For $n = 1$, the condition is $d_1 > 0$

  (ii) For $n = 2$, the conditions are either Routh–Hurwitz conditions or

$$d_1 < 0,$$

$$4d_2 > (d_1)^2,$$

$$\left|\tan^{-1}\left(\frac{\sqrt{4d_2 - (d_1)^2}}{d_1}\right)\right| > \frac{\alpha\pi}{2}. \tag{9}$$

  (iii) For $n = 3$,

    (a) If the discriminant $D(P)$ of $P(\lambda)$ is positive, then Routh–Hurwitz conditions are the

necessary and sufficient conditions, that is, $d_1 > 0, d_3 > 0, d_1 d_2 > d_3$

(b) If $D < 0, d_1 \geq 0, d_2 \geq 0$, and $d_3 > 0$, then (7) holds when $\alpha < (2/3)$

(c) If $D(P) < 0, d_1 < 0$, and $d_2 < 0$, then (7) holds when $\alpha > (2/3)$

(d) If $D(P) < 0, d_1 > 0, d_2 > 0$, and $d_1 d_2 = d_3$, then (7) holds for all $\alpha \in [0, 1)$

Lemma 3 (see [25]). *Assume that the vector function f: $R^+ \times R_3 \longrightarrow R_3$ satisfies the following conditions:*

(1) *Function $f(t, x(t))$ is Lebesgue measurable with respect to t on R^+*

(2) *Function $f(t, x(t))$ is continuous with respect to $x(t)$ on R_3*

(3) *$(\partial f(t, x(t))/\partial x)$ is continuous with respect to $x(t)$ on R_3*

(4) *$\|f(t, X)\| \leq \omega + \lambda\|x\|, \forall t \in R^+, X \in R_3$*

Here ω and λ are two positive constants; then, initial value problems $D^\alpha X(t) = f(t, x(t)), X(t_0) = x_0, \alpha \in (0, 1]$ have a unique solution.

Lemma 4 (see [26]). *Let $m(t) \in C^q[(t_0, T], R]$ and assume that $\forall t_1 \in (t_0, T], m(t_1) = 0$ and $m(t) > 0, t \in [t_0, t_1]$; then, $D^q m(t_1) < 0$.*

3. The Existence and Uniqueness of Positive Solutions

For the proof of the existence and uniqueness about the positive solution, we firstly prove that there exists a positively invariant region for system (3).

Let

$$N(t) = x + y + \frac{p}{c}z, \tag{10}$$

and we have

$$D^\alpha N(t) = \lambda - dx - ay - \frac{pb}{c}z \leq \lambda - h\left(x + y + \frac{p}{c}z\right), \tag{11}$$

in which $h = \min\{d, a, b\}$, so we have

$$N(t) \leq \left(-\frac{\lambda}{h} + N(0)\right)E_\alpha(-ht^\alpha) + \frac{\lambda}{h}. \tag{12}$$

Let $D = \{x + y + (p/c)z \leq (\lambda/h), x, y, z \geq 0\}$; it is easy to see that D is a positively invariant region for model (3).

Theorem 1. *For any initial condition in D, system (3) has a unique solution $X(t) = (x(t), y(t), z(t))^T$, and the solution will remain nonnegative for all $t \geq 0$.*

Proof 1. Firstly, we prove the existence and uniqueness of the solution. We denote

$$f(t, X) = \begin{pmatrix} \lambda - dx - \left(\dfrac{\beta xy}{(x+y)}\right) + \delta y \\ \\ \left(\dfrac{\beta xy}{x+y}\right) - ay - pyz - \delta y \\ \\ cyz - bz \end{pmatrix}. \tag{13}$$

Obviously $f(t, X)$ satisfies conditions (1)–(3) of Lemma 3, and we only prove that system (3) satisfies the last condition (4) of Lemma 3. Let

$$\eta = \begin{pmatrix} \lambda \\ 0 \\ 0 \end{pmatrix},$$

$$A_1 = \begin{pmatrix} -d & \delta & 0 \\ 0 & -a-\delta & 0 \\ 0 & 0 & -b \end{pmatrix},$$

$$A_2 = \begin{pmatrix} -\beta & 0 & 0 \\ \beta & 0 & 0 \\ 0 & 0 & 0 \end{pmatrix},$$

$$A_3 = \begin{pmatrix} 0 & 0 & 0 \\ 0 & -p & 0 \\ 0 & 0 & 0 \end{pmatrix}, \tag{14}$$

$$A_4 = \begin{pmatrix} 0 & 0 & 0 \\ 0 & 0 & 0 \\ 0 & 0 & c \end{pmatrix},$$

$$X(t) = \begin{pmatrix} x(t) \\ y(t) \\ z(t) \end{pmatrix}.$$

Hence,

$$\|f(t, X)\| = \left\| A_1 X(t) + \frac{y(t)}{x(t) + y(t)} A_2 X(t) + z(t) A_3 X(t) + y(t) A_4 X(t) + \eta \right\|,$$

$$\leq \|A_1 x(t)\| + \|A_2 X(t)\| + \frac{c}{p} m\|A_3 X(t)\| + m\|A_4 X(t)\| + \|\eta\|, \tag{15}$$

$$\leq \left(\|A_1\| + \|A_2\| + \frac{c}{p} m\|A_3\| + m\|A_4\| \right)\|X(t)\| + \|\eta\|,$$

in which $m = (\lambda/h)$. By Lemma 3, system (3) has a unique solution.

We now prove the solution is nonnegative for all $t \geq 0$. From model (3), we know

$$D^\alpha x|_{x-0} = \lambda \geq 0,$$
$$D^\alpha y|_{y=0} = 0, \quad (16)$$
$$D^\alpha y|_{z=0} = 0.$$

By Lemma 4, the solution is nonnegative. In summary, the system has a unique nonnegative solution.

4. Stable Analysis

In this section, we will discuss the stability of model (3). This system always has an infection-free equilibrium $E_0 = (x_0, 0, 0)$, where $x_0 = (\lambda/d)$.

The basic reproduction number is

$$R_0 = \frac{\beta}{(a + \delta)}. \quad (17)$$

When $R_0 > 1$, system (3) will have an immune-absence equilibrium $E_1 = (x_1, y_1, 0)$, where

$$x_1 = \frac{\lambda(a + \delta)}{(a + \delta)d + a(\beta - a - \delta)},$$
$$\quad (18)$$
$$y_1 = \frac{\lambda(\beta - a - \delta)}{(a + \delta)d + a(\beta - a - \delta)},$$

which means the uninfected cells and infected cells coexist but the immune response is not activated yet, that is, $cy_1 < b$. Further, we will give the immune-response reproductive number $R_1 = (cy_1/b)$ when $R_1 > 1$, that is, $cy_1 > b$, which means immune response is activated. So, when $R_1 > 1$, there is another immune-response equilibrium $E_2 = (x_2, y_2, z_2)$, where

$$x_2 = \frac{\Delta + \sqrt{\Delta^2 + 4d\left(\delta y_2^2 + \lambda y_2\right)}}{2dc},$$
$$y_2 = \frac{b}{c}, \quad (19)$$
$$z_2 = \frac{\beta c x_2}{p(cx_2 + b)} - \frac{(a + \delta)}{p},$$

in which $\Delta = \lambda - dy_2 - \beta y_2 + \delta y_2$. Note that x_2, y_2, and z_2 must be positive, and we can prove $z_2 > 0$ holds only when $R_1 > 1$. Hence, E_2 exists if and only if $R_1 > 1$.

Now, we introduce the main theorem.

Theorem 2. *For system (3), if $R_0 < 1$, the equilibrium E_0 is globally asymptotically stable. If $R_0 > 1$, the equilibrium E_0 is unstable.*

Proof 2. Jacobian matrix J at E_0 is

$$J = \begin{pmatrix} \lambda + d & \beta - \delta & 0 \\ 0 & \lambda + a + \delta - \beta & 0 \\ 0 & 0 & \lambda + b \end{pmatrix}. \quad (20)$$

The characteristic equation for the infection-free equilibrium E_0 is given as follows:

$$(\lambda + d)(\lambda + a + \delta - \beta)(\lambda + b) = 0. \quad (21)$$

We can see that the characteristic roots $\lambda_1 = -d < 0, \lambda_2 = -b < 0$, and when $R_0 < 1$, $\lambda_3 = \beta - a - \delta < 0$, all the characteristic roots satisfied $|\arg \lambda_i| = \pi > \alpha(\pi/2)$, which shows that E_0 is locally asymptotically stable by Lemma 1. If $R_0 > 1$, $|\arg \lambda_3| = 0 < \alpha(\pi/2)$, E_0 is unstable.

Let

$$V(x) = y + \frac{p}{c}z, \quad (22)$$

and we have

$$D^\alpha V = D^\alpha y + \frac{p}{c}D^\alpha z,$$
$$= \left(\frac{\beta x y}{(x + y)}\right) - ay - pyz - \delta y + \frac{p}{c}(cyz - bz),$$
$$\quad (23)$$
$$= \left(\frac{x}{x + y}\right) * \beta y - (a + \delta)y - \frac{pb}{c}z,$$
$$\leq \beta y - (a + \delta)y = (a + \delta)y(R_0 - 1).$$

Since $R_0 < 1$, we have $D^\alpha V \leq 0$. Let $M = \{(x, y, z) \in D, D^\alpha V = 0\}$; obviously, $M \subset \{(x, y, z) \in D, y = 0\}$. Let E be the largest positively invariant subset of M; obviously, E is nonempty since $((\lambda/d), 0, 0) \in E$. Let $(x(t), y(t), z(t))$ be the solution of system (3) with initial value $(x_0, y_0, z_0) \in E$; then, $y(t) = 0$. By the first and the third equations of (3), we have

$$\begin{cases} x(t) = \left(-\frac{\lambda}{d} + x(0)\right)E_\alpha(-dt^\alpha) + \frac{\lambda}{d}, \\ z(t) = z(0)E_\alpha(-bt^\alpha), \end{cases} \quad (24)$$

and when, $x(t) \longrightarrow (\lambda/d)$, $z(t) \longrightarrow 0$, by the invariance of E, $x(t) = (\lambda/d)$, $z(t) = 0$. By $t \longrightarrow \infty$ the Lyapunov–LaSalle theorem [26], when $t \longrightarrow \infty$, all solutions in the set D approach E_0. Noting that E_0 is locally asymptotically stable, the infection-free equilibrium E_0 is globally asymptotically stable.

Theorem 3. *For system (3), when $R_0 > 1$,*

(1) The equilibrium E_1 is locally asymptotically stable if $R_1 < 1$

(2) If $R_1 > 1$, the equilibrium E_1 is unstable

Proof 3. The characteristic equation for the equilibrium E_1 is given as

$$\det\begin{pmatrix} \lambda + d + \dfrac{\beta y_1^2}{(x_1 + y_1)^2} & \dfrac{\beta x_1^2}{(x_1 + y_1)^2} - \delta & 0 \\[3mm] -\dfrac{\beta y_1^2}{(x_1 + y_1)^2} & \lambda - \dfrac{\beta x_1^2}{(x_1 + y_1)^2} + a + \delta & p y_1 \\[3mm] 0 & 0 & \lambda - c y_1 + b \end{pmatrix} = 0, \tag{25}$$

that is,

$$(\lambda - c y_1 + b)\left[\lambda^2 + \left(a + \delta + d + \dfrac{\beta(y_1^2 - x_1^2)}{(x_1 + y_1)^2}\right)\lambda + (a + \delta)d + \dfrac{\beta(a y_1^2 - d x_1^2)}{(x_1 + y_1)^2}\right] = 0. \tag{26}$$

We can see $\lambda_1 = c y_1 - b$, and when $R_1 < 1$, λ_1 is negative and $|\arg\lambda_1| = \pi > \alpha(\pi/2)$.

Next, we consider the following equation:

$$\lambda^2 + \left(a + \delta + d + \dfrac{\beta(y_1^2 - x_1^2)}{(x_1 + y_1)^2}\right)\lambda + (a + \delta)d + \dfrac{\beta(a y_1^2 - d x_1^2)}{(x_1 + y_1)^2} = 0. \tag{27}$$

We let

$$B = a + \delta + d + \dfrac{\beta(y_1^2 - x_1^2)}{(x_1 + y_1)^2} = a + \delta + d + \beta\dfrac{(y_1 - x_1)}{(x_1 + y_1)} = (a + \delta)(R_0 - 1) + d,$$

$$C = (a + \delta)d + \dfrac{\beta(a y_1^2 - d x_1^2)}{(x_1 + y_1)^2} = \dfrac{d(a + \sigma)(a + \delta)(R_0 - 1) + a(a + \delta)^2(R_0 - 1)^2}{\beta}. \tag{28}$$

Since $R_0 > 1$, we can see $B > 0$, $C > 0$; hence, (27) has two negative real roots, and we denote them by λ_2 and λ_3 ($|\arg\lambda_2| = \pi > \alpha(\pi/2)$ and $|\arg\lambda_3| = \pi > \alpha(\pi/2)$), so when $R_1 < 1$, the equilibrium E_1 is locally asymptotically stable. When $R_1 > 1$, λ_1 is positive, and $|\arg\lambda_1| = 0 < \alpha(\pi/2)$, E_1 is unstable.

Finally, we discuss the local stability of the immune-response equilibrium state E_2, and the Jacobian matrix at E_2 is given by

$$J = \begin{pmatrix} -d - \dfrac{\beta y_2^2}{(x_2 + y_2)^2} & -\dfrac{\beta x_2^2}{(x_2 + y_2)^2} + \delta & 0 \\[3mm] \dfrac{\beta y_2^2}{(x_2 + y_2)^2} & \dfrac{\beta x_2^2}{(x_2 + y_2)^2} - a - \delta - p z_2 & -p y_2 \\[3mm] 0 & -c z_2 & c y_2 - b \end{pmatrix}. \tag{29}$$

The corresponding characteristic equation is

$$P(\lambda) = \lambda^3 + a_1\lambda^2 + a_2\lambda + a_3 = 0, \tag{30}$$

where

$$a_1 = d + a + \delta + p z_2 + \dfrac{\beta y_2^2 - x_2^2}{(x_2 + y_2)^2},$$

$$= d + \dfrac{\beta x_2}{x_2 + y_2} + \dfrac{\beta(y_2 - x_2)}{x_2 + y_2},$$

$$= d + \dfrac{\beta y_2}{x_2 + y_2} > 0,$$

$$a_2 = \dfrac{\beta y_2^2}{(x_2 + y_2)^2}(a + p z_2) + p b z_2 + d(a + \delta + p z_2) - \dfrac{\beta x_2^2 d}{(x_2 + y_2)^2},$$

$$= \dfrac{\beta y_2^2}{(x_2 + y_2)^2}(a + p z_2) + p b z_2 + d\dfrac{\beta x_2}{x_2 + y_2} - \dfrac{\beta x_2^2 d}{(x_2 + y_2)^2},$$

$$= \dfrac{\beta y_2^2}{(x_2 + y_2)^2}(a + p z_2) + p b z_2 + \beta d\dfrac{x_2 y_2}{(x_2 + y_2)^2} > 0,$$

$$a_3 = p b z_2\left(d + \dfrac{\beta y_2^2}{(x_2 + y_2)^2}\right) > 0. \tag{31}$$

It is easy to verify that

$$a_1 a_2 > pbz_2 \left(d + \frac{\beta y_2}{x_2 + y_2} \right) > pbz_2 \left(d + \frac{\beta y_2^2}{(x_2 + y_2)^2} \right) = a_3.$$
(32)

Based on Definition 2, we obtain

$$D(P) = - \begin{vmatrix} 1 & a_1 & a_2 & a_3 & 0 \\ 0 & 1 & a_1 & a_2 & a_3 \\ 3 & 2a_1 & a_2 & 0 & 0 \\ 0 & 3 & 2a_1 & a_2 & 0 \\ 0 & 0 & 3 & 2a_1 & a_2 \end{vmatrix}$$
(33)

$$= 18 a_1 a_2 a_3 + (a_1 a_2)^2 - 4a_1^3 - 4a_2^3 - 27 a_3^2.$$

By Lemma 2, we have the following theorem.

Theorem 4. *For system (3), when $R_1 > 1$,*

(1) *If the discriminant $D(P)$ of $P(\lambda)$ is positive, the equilibrium E_2 is locally asymptotically stable for $0 < \alpha < 1$*

(2) *If $D(P) < 0$, then the equilibrium E_2 is locally asymptotically stable for $0 < \alpha < (2/3)$*

5. Numerical Simulation

5.1. Simulation of the Immune-Response Equilibrium. We first simulate the stability of E_2, and the locally stable condition of E_2 is given by Theorem 4. The parameters we used are listed in Table 1 which can make $R_1 = 578.5076 > 1$, $D(P) = -0.1296 < 0$ hold. We choose $\alpha = 0.55$, $\alpha = 0.6$ and $\alpha = 0.65$, which satisfy $0 < \alpha < (2/3)$, and the simulation is shown in Figure 1. The dynamic routes of uninfected and infected cells are shown in Figures 1(a) and 1(b), and the CTL cells are shown in Figure 1(c). The simulation shows that the immune-response equilibrium E_2 is locally asymptotically stable for $0 < \alpha < (2/3)$, which is consistent with the conclusion of Theorem 4.

5.2. Simulation of Correlation between HBeAg and Infected Cells. A positive correlation was found between log-HBV DNA and log-HBeAg in [27], that is, the higher the HBeAg, the higher the HBV DNA load. Since by quasisteady assumption, the amount of free virus is simply proportional to the number of infected cells, the number of infected cell should also be positive logarithmic correlative with HBeAg. Since we could not get the specific number of infected cells from clinic, HBeAg can be quantified. In the following part, we will testify the positive correlation between the infected cell and the HBeAg based on the clinical data of HBeAg by numerical simulation. We use four CHB patients' HBeAg clinical data of 108 weeks with the treatment of entecavir from Dongzhimen Hospital; two patients were from successful-treatment group, and the other two patients were from unsuccessful-treatment group; the data are shown in Tables 2 and 3.

By Theorem 2, the infection-free equilibrium $E_0 = (x_0, 0, 0)$ is asymptotically stable if $R_0 < 1$. When simulating the successful-treatment group, the parameters we choose should make $R_0 < 1$. Considering the biological significance of the parameters, we choose the parameters in Table 4 as follows.

A human liver contains approximately 2×10^{11} hepatocytes [28], and a patient has a total of about 3000 ml plasma. Usually, clinical testing quantification is based on one millilitre. Consequently, we can assume that $(\lambda/d) \approx (2 \times 10^{11}/3000)$. Since the half-life of a hepatocyte is about half a year, we choose $d = 0.00379$ similar to [28]. The half-life of CTL is about 77 days [29], so we choose $b = 0.009$. Other parameters were chosen by simulation. The parameters in Table 4 can make $R_0 = 0.045 < 1$ hold. We give three simulation results with $\alpha = 1$, $\alpha = 0.9$, and $\alpha = 0.8$; the simulations are shown in Figure 2. The dynamic routs of uninfected cells and CTL cells are shown in Figures 2(a) and 2(b), and the HBeAg and infected cells are shown in Figure 2(c). The simulation shows that the infection-free equilibrium E_0 is asymptotically stable with different $0 < \alpha < 1$ which is consistent with the conclusion of Theorem 2, but when $\alpha = 1$, the dynamic route is obviously different. From the simulation in Figure 2(c), we can also observe the positive correlation between log-infected cells and log-HBeAg for different $\alpha < 1$, which is consistent with clinical fact. On the other hand, from the clinical data of HBeAg, we can see that the change rate was different between different patient, though they have same change trend, which shows that individual differences do exist in clinical therapy even with the same medicine and the same dose; the clinical phenomenon may be explained by our model to some extent. From the simulation, we can see that the larger the α, the slower the decrease rate of infected cells and CTL in the former stage, but the faster the decrease rate in the later stage; the individual difference may be reflected by different α, and the fractional-order model should be a good tool to describe HBV infection.

When we simulate the unsuccessful-treatment group in Table 3, the patients' ALT level was lower than normal standard, so we can think that the patient has not yet developed an immune response to the hepatitis B virus. When $R_0 > 1$, there exists the equilibrium E_1 without immune activities, so we choose the immune parameter b larger than that in Table 4 and the immune parameter c smaller than that in Table 4. The death rate of infected cells should decrease without immune activities, so we choose parameter a which is smaller than that in Figure 2. Since E_1 is asymptotically stable, if $R_1 < 1$, the parameter we choose in Table 5 can make $R_0 = 2.4253 > 1$ and $R_1 = 0.1351 < 1$ hold. We also used $\alpha = 0.9$, $\alpha = 0.85$, and $\alpha = 0.8$ to simulate, and the simulation is shown in Figure 3. The dynamic routes of uninfected cells and CTL cells are shown in Figures 3(a) and 3(b), and the HBeAg and infected cells are shown in Figure 3(c). From the simulation, the dynamic routes of uninfected cells, infected cells, and CTL cells show that the immune-absence equilibrium E_1 is asymptotically stable with different α which is consistent with the conclusion of Theorem 3. From the simulation, there still exists the same change trend but

TABLE 1: Parameters in Figure 1.

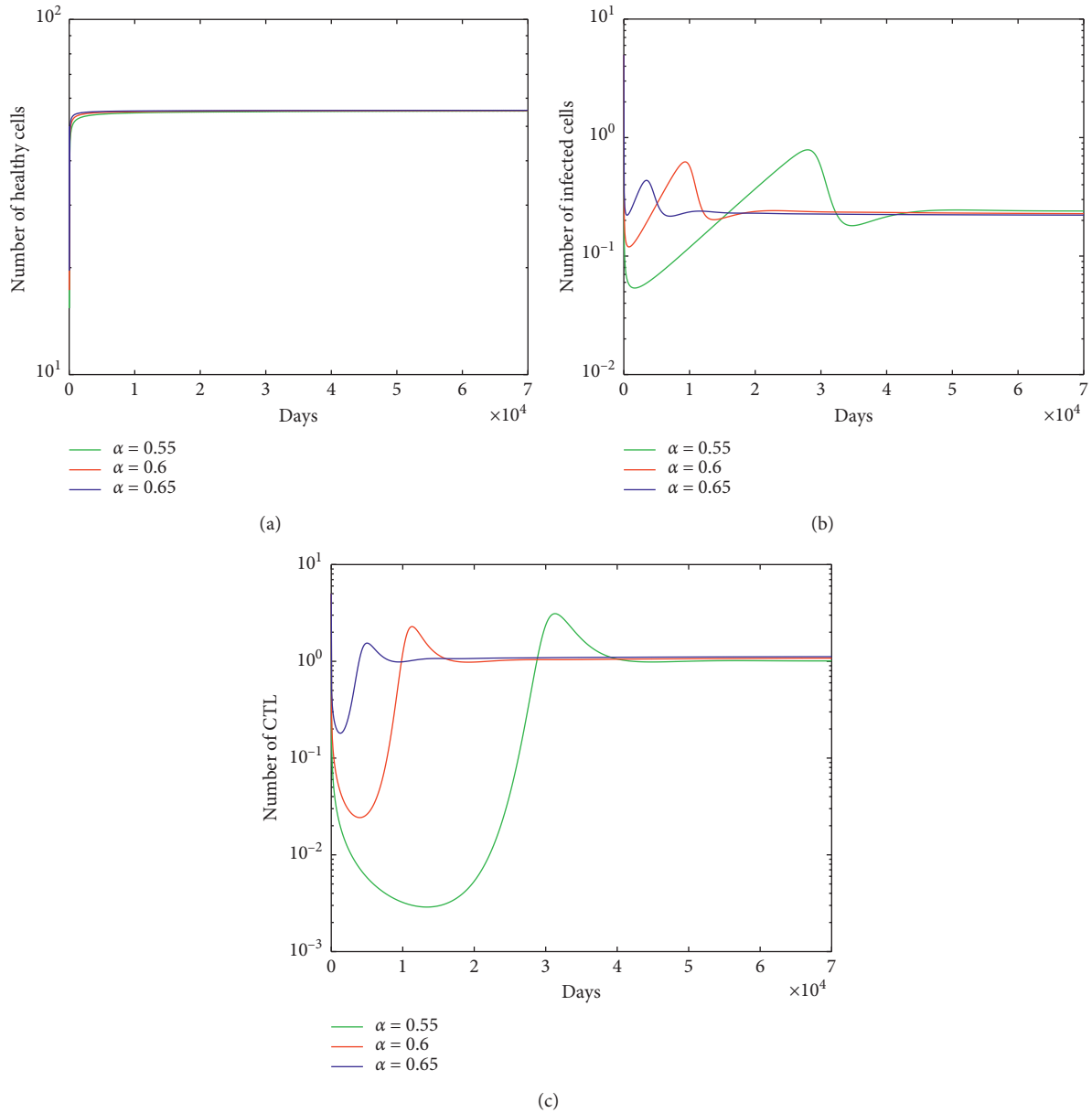| Parameter	Value	Parameter	Value
λ	10	c	0.051
β	0.01	d	0.18
a	0.003	p	0.006
b	0.011	δ	0.000000018

(a)

(b)

(c)

FIGURE 1: Simulation results of immune-response equilibrium E_2 with different α.
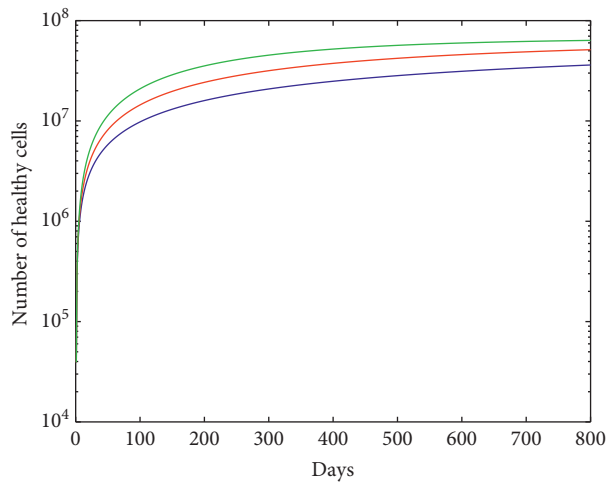
TABLE 2: HBeAg data of successful-treatment group.

	0	12	24	36	48	60	72	84	96	108 (week)
I	819.51	34.55	12.44	4.23	1.12	0.61	0.44	0.38	0.38	0.44
II	874.31	12.15	1.88	1.65	1.15	0.82	0.36	0.4	0.37	0.31

TABLE 3: HBeAg data of unsuccessful-treatment group.

	0	12	24	36	48	60	72	84	96	108 (week)
I	36.79	138.6	221.36	314.88	393.78	391.75	378.63	411.61	407.91	342.63
II	44.11	85.05	140.27	141.82	125.86	142.63	158.75	194.48	0.6	243.72

TABLE 4: Parameters in Figure 2.

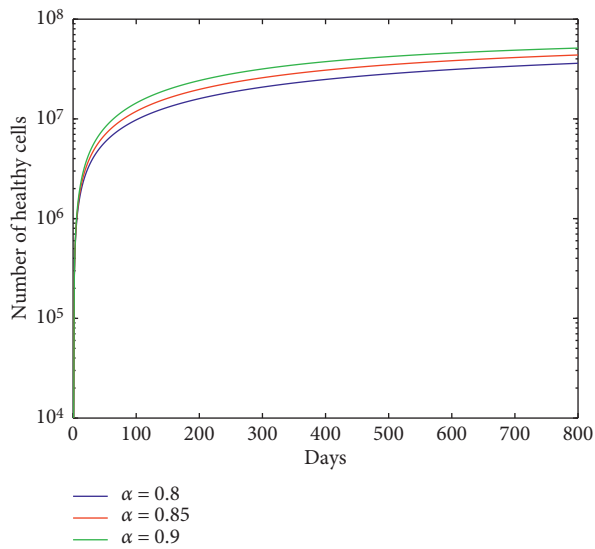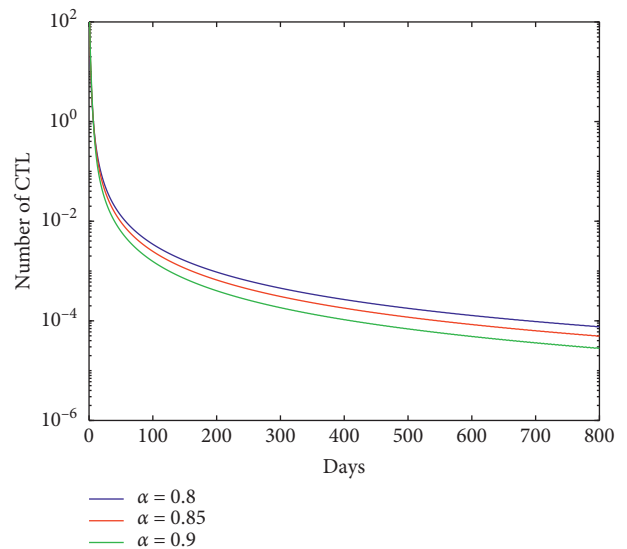| Parameter	Value	Parameter	Value
λ	$2.53e + 005$	c	$0.31e - 007$
β	$6.9e - 004$	a	$4 * 3.79e - 003$
d	$3.79e - 003$	p	$1.5e - 004$
b	$0.9e - 002$	δ	$1.9e - 004$

(a)
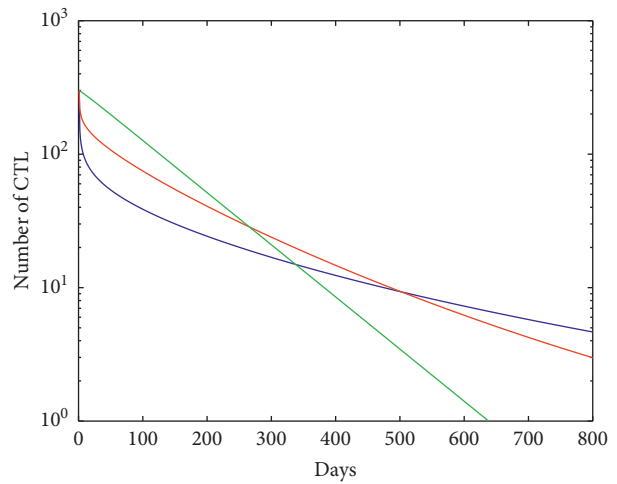
(b)

FIGURE 2: Continued.
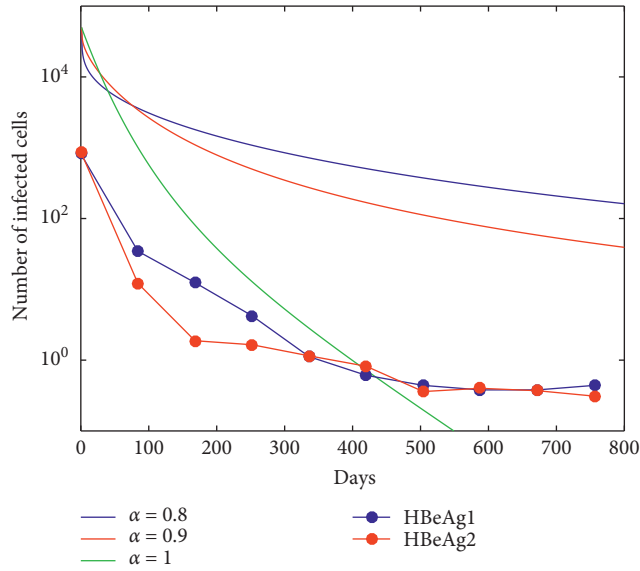
(c)

FIGURE 2: Simulation results of successful-treatment group.

TABLE 5: Parameters in Figure 3.

Parameter	Value	Parameter	Value
λ	$2.53e + 005$	c	$0.31e - 009$
β	$(6.9e - 003) * 2$	a	$3.79e - 003$
d	$3.79e - 003$	p	$1.5e - 004$
b	0.9	δ	$1.9e - 004$

(a)

(b)

FIGURE 3: Continued.

(c)
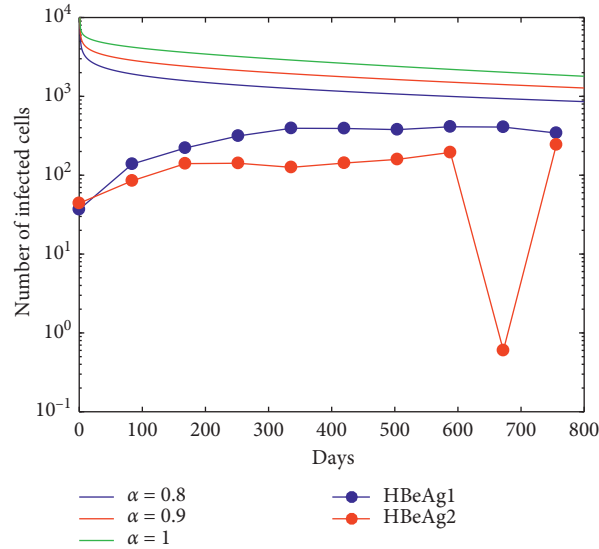
FIGURE 3: Simulation results of successful-treatment group.

different change rate with different α, and the positive correlation between log-infected cells and log-HBeAgis reflected roughly. The positive correlation is not so good for patient 2's HBeAg data, but the trend is consistent between the infected cells and HBeAg. We can see there also exists some difference with different α which may reflect the individual difference.

6. Conclusions

In this paper, based on the fact that immune response has memory, we discussed a fractional-order HBV model with standard mass action incidences, and we obtained the basic reproductive numbers R_0 and the cytotoxic T lymphocytes' immune-response reproductive number R_1. When $R_0 < 1$, we have proved that E_0 is globally asymptotically stable which meant the infected person can eventually recover automatically even when infected with a large number of HBV. When $R_0 > 1$ and $R_1 < 1$, E_1 was locally asymptotically stable which meant the one infected by HBV with no immune response would be infected persistently. When $R_1 > 1$, we also gave the local stable condition of E_2, which meant the infected person has immune response to HBV, but the persistent infection still existed. Furthermore, we gave some simulations with different α to test our theoretical results and some clinical phenomena. The simulation showed that our model can simulate the positive correlation between log-infected cells and log-HBeAg to some extent. On the other hand, even with the same initial conditions and the same parameters, we also found that there existed some difference in the dynamic routes with different order α, which may reflect the individual difference. From the analysis and simulation, we can see the fractional-order model maybe more reasonable to describe HBV immune course.

7. Discussion

In our paper, we found that the fractional-order model can reflect the characteristics of immune memory and clinical individual differences, but it should be pointed out that there are only three variables in our model; the model only described HBV infection roughly. Furthermore, we could not obtain the number of uninfected cells, infected cells, and CTL; when we performed the simulation, we only chose the parameters from biological meaning, not from real clinical data, so there are still many works to be done in the future.

Data Availability

The HBeAg data used to support the findings of this study are included within the article.

Conflicts of Interest

The authors declare that there are no conflicts of interest regarding the publication of this paper.

Acknowledgments

References

[1] Y. Xiao, X. Xu, and S. Tang, "Sliding mode control of outbreaks of emerging infectious diseases," *Bulletin of Mathematical Biology*, vol. 74, no. 10, pp. 2403–2422, 2012.

[2] Y. Zheng, L. Q. Min, Y. Ji, Y. Su, and Y. Kuang, "Global stability of endemic equilibrium point of basic virus infection

model with application to HBV infection," *Journal of Systems Science and Complexity*, vol. 23, no. 6, pp. 1221–1230, 2009.

[3] G. Huang, W. Ma, and Y. Takeuchi, "Global properties for virus dynamics model with Beddington-DeAngelis functional response," *Applied Mathematics Letters*, vol. 22, no. 11, pp. 1690–1693, 2009.

[4] G. Huang, H. Yokoi, Y. Takeuchi, T. Kajiwara, and T. Sasaki, "Impact of intracellular delay, immune activation delay and nonlinear incidence on viral dynamics," *Japan Journal of Industrial and Applied Mathematics*, vol. 28, no. 3, pp. 383–411, 2011.

[5] T. Q. Zhang, J. L. Wang, Y. Li, Z. Jiang, and X. F. Han, "Dynamics analysis of a delayed virus model with two different transmission methods and treatments," *Advances in Difference Equations*, vol. 2020, no. 1, pp. 1–17, 2020.

[6] W. Wang, W. B. Ma, and Z. S. Feng, "Dynamics of reaction–diffusion equations for modelling CD4$^+$ T cells decline with general infection mechanism and distinct dispersal rate," *Nonlinear Analysis: Real World Applications*, vol. 51, no. 2, Article ID 102976, 2020.

[7] C. Yan and W. Wang, "Modeling HIV dynamics under combination therapy with inducers and antibodies," *Bulletin of Mathematical Biology*, vol. 81, no. 7, pp. 2625–2648, 2019.

[8] R. Q. Shi, T. Lu, and C. H. Wang, "Dynamic analysis of a fractional order delayed model for hepatitis B virus with CTL immune response," *Virus Research*, vol. 277, no. 2, Article ID 197841, 2020.

[9] S. He, S. Y. Tang, S. Tang, and L. Rong, "A discrete stochastic model of the COVID-19 outbreak: forecast and control," *Mathematical Biosciences and Engineering*, vol. 17, no. 4, pp. 2792–2804, 2020.

[10] A. S. Perelson, "Modelling viral and immune system dynamics," *Nature Reviews Immunology*, vol. 2, no. 1, pp. 28–36, 2002.

[11] M. A. Nowak, S. Bonhoeffer, A. M. Hill, R. Boehme, H. C. Thomas, and H. McDade, "Viral dynamics in hepatitis B virus infection," *Proceedings of the National Academy of Sciences*, vol. 93, no. 9, pp. 4398–4402, 1996.

[12] G. K. Lau, M. Tsiang, J. Hou et al., "Combination therapy with lamivudine and famciclovir for chronic hepatitis B-infected Chinese patients: a viral dynamics study," *Hepatology*, vol. 32, no. 2, pp. 394–399, 2000.

[13] L. Zhang, G. Huang, A. Liu, and R. Fan, "Stability analysis for a fractional HIV infection model with nonlinear incidence," *Discrete Dynamics in Nature and Society*, vol. 2015, Article ID 563127, 11 pages, 2015.

[14] A. A. M. Arafa, S. Z. Rida, and M. Khalil, "A fractional-order model of HIV infection with drug therapy effect," *Journal of the Egyptian Mathematical Society*, vol. 22, no. 3, pp. 538–543, 2014.

[15] Y. Wang, L. Liu, X. Zhang, and Y. Wu, "Positive solutions of an abstract fractional semipositone differential system model for bioprocesses of HIV infection," *Applied Mathematics and Computation*, vol. 258, pp. 312–324, 2015.

[16] Y. Yan and C. Kou, "Stability analysis for a fractional differential model of HIV infection of CD4$^+$ T-cells with time delay," *Mathematics and Computers in Simulation*, vol. 82, no. 9, pp. 1572–1585, 2012.

[17] S. M. Salman and A. M. Yousef, "On a fractional-order model for HBV infection with cure of infected cells," *Journal of the Egyptian Mathematical Society*, vol. 25, no. 4, pp. 445–451, 2017.

[18] L. C. Cardoso, F. L. P. Dos Santos, and R. F. Camargo, "Analysis of fractional-order models for hepatitis B," *Computational and Applied Mathematics*, vol. 37, no. 4, pp. 4570–4586, 2018.

[19] Y. Su, L. Zhao, and L. Min, "Analysis and simulation of an adefovir anti-hepatitis B virus infection therapy immune model with alanine aminotransferase," *IET Systems Biology*, vol. 7, no. 5, pp. 205–213, 2013.

[20] K. Wang, W. Wang, H. Pang, and X. Liu, "Complex dynamic behavior in a viral model with delayed immune response," *Physica D: Nonlinear Phenomena*, vol. 226, no. 2, pp. 197–208, 2007.

[21] B. Z. Guo and L. M. Cai, "A note for the global stability of a delay differential equation of hepatitis B virus infection," *Mathematical Biosciences & Engineering*, vol. 8, no. 3, pp. 689–694, 2012.

[22] D. Tavares, R. Almeida, and D. F. M. Torres, "Caputo derivatives of fractional variable order: numerical approximations," *Communications in Nonlinear Science and Numerical Simulation*, vol. 35, pp. 69–87, 2016.

[23] Y. Emvudu, D. Bongor, and R. Koïna, "Mathematical analysis of HIV/AIDS stochastic dynamic models," *Applied Mathematical Modelling*, vol. 40, no. 21-22, pp. 9131–9151, 2016.

[24] E. Ahmed, A. M. A. El-Sayed, and H. A. A. El-Saka, "On some Routh-Hurwitz conditions for fractional order differential equations and their applications in Lorenz, Rössler, Chua and Chen systems," *Physics Letters A*, vol. 358, no. 1, pp. 1–4, 2006.

[25] J. Huo, H. Zhao, and L. Zhu, "The effect of vaccines on backward bifurcation in a fractional order HIV model," *Nonlinear Analysis: Real World Applications*, vol. 26, pp. 289–305, 2015.

[26] M. Çiçek, C. Yakar, and B. Oğur, "Stability, boundedness, and Lagrange stability of fractional differential equations with initial time difference," *The Scientific World Journal*, vol. 2014, Article ID 939027, 2014.

[27] W. J. Yin, F. Wang, L. P. Shen et al., "The positive correlation of log hepatitis B virus (HBV) deoxyribonucleic acid load and log HBeAg and log antibody to HBeAg," *Chinese Journal of Vaccines and Immunization*, vol. 18, no. 4, pp. 316–319, 2012.

[28] L. Q. Min, Y. M. Su, and Y. Kuang, "Mathematical analysis of a basic virus infection model with application to HBV infection," *Rocky Mountain Journal of Mathematics*, vol. 38, no. 5, pp. 1573–1585, 2008.

[29] M. Hellerstein, M. B. Hanley, D. Cesar et al., "Directly measured kinetics of circulating T lymphocytes in normal and HIV-1-infected humans," *Nature Medicine*, vol. 5, no. 1, pp. 83–89, 1999.

WILEY | Hindawi

Research Article

A Method for Parameters Estimation in a Dynamical Model of Ebola Virus Transmission in Sierra Leone

Li Li,[1,2] Li-Xia Du,[1] Ziheng Yan,[3] Jie Zhang,[1] and Yong-Ping Wu [4]

[1]*School of Computer and Information Technology, Shanxi University, Taiyuan 030006, Shanxi, China*
[2]*Science and Technology on Electronic Test and Measurement Laboratory, North University of China, Taiyuan 030051, China*
[3]*Chang'an University, Middle Section of Nan'er Huan Road, Xi'an, Shannxi 710064, China*
[4]*College of Physics Science and Technology, Yangzhou University, Yangzhou, Jiangsu 225002, China*

Correspondence should be addressed to Yong-Ping Wu; ypwu@yzu.edu.cn

Ebola is an infectious virus that causes Ebola hemorrhagic fever in primates and humans, which was first found in 1976. The Ebola virus outbreak in West Africa in 2014 was the largest ever. A lot of researchers use mathematical models to analyze the characteristics of infectious diseases. However, many parameters in the model cannot be estimated completely. To ease the difficulty, we proposed an approach to estimate the parameter based on genetic algorithm (GA). GA uses the natural selection method of the fittest to find the optimal solution of the model. The least residual squares sum is used as fitness function to measure the performance of GA in parameter estimation. Moreover, we used a dynamical model and the real data of Ebola in Sierra Leone to verify the validity of GA. The experimental results indicate that the GA has strong competitiveness compared with the classical method, and it is a feasible method for estimating the parameters of infectious disease models.

1. Introduction

Ebola virus belongs to the family Filoviridae and is considered a prototype pathogen of viral hemorrhagic fever [1]. The virus was first detected in the Ebola river basin in southern Sudan and Congo in 1976 [2–9]. Since the discovery of Ebola virus, only four species of this virus cause human disease, namely, *Zaire ebolavirus*, *Tai Forest ebolavirus*, *Sudan ebolavirus*, and *Bundibugyo ebolavirus* [10]. The Reston virus causes only animal disease, not human disease. Therefore, the source of the Ebola virus is unknown. Researchers found evidence of asymptomatic infection of Ebola virus in three species of the fruit bats, which suggested that the bats are most likely to be the source of the deadly virus [11]. The bats could carry Ebola virus to other animals and even humans [12–14].

Ebola virus is transmitted through the saliva, the urine, and other body fluids [15, 16]. People can cause infection by direct contact with body fluids which carry the virus, with the virus entering the body through the nose, the mouth, the eyes, and the damaged skin [17]. Humans become infected after contact with the blood, the body fluids, and the infected fruit bats, as well as through the sexual contact [18].

Since there were no good treatments and approved vaccines at the time, the management of Ebola virus was limited to the use of obstacles and palliative care to suppress transmission [19]. A large-scale Ebola outbreak occurred in West Africa in 2014, mainly in Guinea, Liberia, and Sierra Leone. The number of confirmed cases is far greater than that in the past [10]. The lack of effective preventive measures at the time resulted in more people being infected with the Ebola virus [20]. In [21], the authors investigated the effectiveness of small interfering RNAs treatments for Ebola-infected patients. RNA interference can suppress the expression of viral genes; thus it is effective in suppressing Ebola virus replication, and the authors developed monoclonal antibodies against Ebola glycoprotein for the treatment of Ebola-virus-infected people [22]. In addition, some researchers used Sierra Leone's disease data to study mathematical models of Ebola virus, predict the progress of

the epidemic, and propose preventive control measures and recommendations [5, 23–25].

Research on infectious diseases using dynamic models has become one of the important methods [26–32]. The propagation coefficient of the disease in the model affects the prediction results directly, and, consequently, it is important to estimate the propagation coefficient correctly. Classical parameter estimation methods are the Markov Chain Monte Carlo (MCMC) method, the least-squares method, and so on. The basic principle of the MCMC method is to construct a Markov chain by using the joint posterior probability distribution of the model propagation coefficients and assign any initial value to the simulation until it converges to a stable distribution. This determines the propagation coefficient [33–35]. There are many improved MCMC methods, such as using sequential Monte Carlo (SMC) filter techniques to estimate the propagation coefficients in the model [36]. However, firstly, the traditional method is limited by the calculation cost of the high-dimensional nonlinear model, which may take a lot of calculation time; it is usually not easy to obtain high-precision results, and it is not possible to get all the propagation coefficients at once [37, 38]. Secondly, the numerical estimation of the marginal probability distribution is difficult to achieve in the high-dimensional inversion model [39]. The least-squares method is performed by convolving the simulated data with the real data [40]. Although it has low calculation cost and generality, it does not consider the uncertainty of the inverse problem solution, and the initial value of the propagation coefficient will affect the efficiency of the algorithm. The least-squares method has certain flaws in determining the initial value. If it is set close to the optimal propagation coefficient, the result will be obtained quickly. If it is set far from the optimal propagation coefficient, it will increase the time of the algorithm [41].

In this paper, we present a method to solve inverse problems of differential equations based on GA. The GA is a method that is widely used in parameter estimation and other fields, and it has been proven to be a reliable method for estimating parameters based on nonlinear functions [42, 43]. It has a powerful adaptive search technology and uses the natural selection method of the fittest to simulate the evolution process, and thereby it can effectively solve the optimization problem [44]. When searching in high-dimensional models, GAs are superior to the other traditional search techniques due to their simplicity, effectiveness, versatility, and robustness [45, 46]. We have used the GA of adaptive mutation operator to estimate the parameters of differential equations. The advantage of this method is that the parameters in the high-dimensional model can be completely estimated by a small amount of data and all parameters combinations can be quickly obtained in a limited evolution process. In addition, an effective combination of multiple propagation coefficients can be obtained by GA for reference in studying the propagation dynamics.

The remainder of this paper is organized as follows. In Section 2, we introduced the transmission dynamical model of Ebola in Sierra Leone and the theories and processes of GA. In Section 3, we estimated the values of the parameters in a dynamical model based on GA. What is more, we validate the accuracy of the experiment results. Finally, we give the discussion and conclusions in Section 4.

$$
\begin{cases}
\dfrac{\mathrm{d}S}{\mathrm{d}t} = -\left(\beta_1 \dfrac{SI_S}{N} + \beta_2 \dfrac{SI_P}{N} + \beta_H \dfrac{SH}{N} + \beta_F \dfrac{SF}{N}\right) + \lambda_1 p I_S, \\[4mm]
\dfrac{\mathrm{d}E}{\mathrm{d}t} = \beta_1 \dfrac{SI_S}{N} + \beta_2 \dfrac{SI_P}{N} + \beta_H \dfrac{SH}{N} + \beta_F \dfrac{SF}{N} - m_1 \eta E - m_2(1-\eta)E, \\[4mm]
\dfrac{\mathrm{d}I_S}{\mathrm{d}t} = m_2(1-\eta)E - \lambda_1 p I_S - \lambda_2 q(1-p)I_S - \lambda_3(1-q)(1-p)I_S, \\[4mm]
\dfrac{\mathrm{d}I_P}{\mathrm{d}t} = \lambda_3(1-q)(1-p)I_S + m_1 \eta E - r_h \theta I_P - \delta_1(1-\theta)r_d I_P - r_i(1-\theta)(1-\delta_1)I_P, \\[4mm]
\dfrac{\mathrm{d}H}{\mathrm{d}t} = r_h \theta I_P - r_{dh} \delta_2 H - r_{ih}(1-\delta_2)H, \\[4mm]
\dfrac{\mathrm{d}F}{\mathrm{d}t} = \lambda_2 q(1-p)I_S + \delta_1(1-\theta)r_d I_P + r_{dh} \delta_2 H - r_f F, \\[4mm]
\dfrac{\mathrm{d}R}{\mathrm{d}t} = r_i(1-\theta)(1-\delta_1)I_P + r_{ih}(1-\delta_2)H + r_f F.
\end{cases}
\tag{1}
$$

2. Main Method

2.1. A Dynamical Model of Ebola Virus Transmission in Sierra Leone. The time series of Ebola-confirmed case reports were collected from the World Health Organization (WHO) and the Ministry of Health of Sierra Leone. The data include the Ebola outbreak in 14 regions of Sierra Leone, including the suspected cases (I_S), the probable cases (I_P), and the hospital-confirmed cases (H), which are thought to represent the best available data of the Ebola epidemic. Due to the fact that hospitalization is a result of real infections, while suspected and probable cases may not be completely converted into hospitalized cases, it is more accurate to use hospitalization cases to indicate the actual number of the Ebola infections. We collected the newly infected cases for 34 weeks from May 19th, 2014, to January 11th, 2015. More detailed data can be found in [47].

We used a GA based on adaptive mutation operator. Think of the propagation coefficient of the Ebola virus model as a genetic target. It is binary-encoded, and then the genetic operators of random selection with elitism, multipoint crossover, and gene site mutation are used to simulate evolution to find the optimal solution. Set evaluation index for parameter genetic process as fitness function which is a sum of variances of fitted data and real data. We estimated the parameters based on the dynamical model established in [6]. Record the optimal parameter set of each generation and perform comparison with the optimal parameter set of the next generation, always save the optimal set, and wait until the evolution has completed obtaining all the parameters in the model.

Based on other literature analyses, this article divides Ebola virus transmission into seven categories, namely, susceptible (S), exposed (E), suspected individuals may be misdiagnosed (I_S), probable individuals (I_P), hospital-confirmed cases (H), the individuals who may infect others at a funeral (F), and removed (R) [6]. Figure 1 depicted the transmission mechanism of the Ebola virus.

Consequently, we have used the following system of equation (1) to simulate the transmission dynamics of the Ebola virus in Sierra Leone and the biological meanings of parameters can be obtained in Table 1. We quantified the uncertainty of parameter estimates, and we give the 95% confidence intervals in Table 1.

2.2. Genetic Algorithm. GA is a method for finding solutions based on biological evolution process [42]. The process includes random selection, crossover, and mutation for an individual with the best combination of genes. GA begins with initializing the propagation coefficient in model (1) for binary encoding. The encoding length is determined by parameter range and accuracy. We used par to represent the parameters set: $\text{par} = [\beta_1, \beta_2, \beta_H, \beta_F, \lambda_1, p, m_1, \eta, m_2, \lambda_2, q, \lambda_3, r_h, \theta, \delta_1, r_d, r_i, r_{dh}, \delta_2, r_{ih}, r_f]$. Assuming that all propagation coefficients are within $[0, 1]$, the accuracy is 4 digits after decimal point, and thus the coding length can be determined by the following formula:

$$2^{13} < \frac{\text{range}_{\max} - \text{range}_{\min}}{\text{accuracy}} = \frac{1 - 0}{0.0001} = 10000 < 2^{14}. \quad (2)$$

Therefore, a parameter can be represented by 14 bits of binary, and par consisting of all parameters needs to be encoded with $14 \times 21 = 294$ bits of binary. We collected the disease status of Ebola for 34 weeks, and the detailed data are shown above, so we set the initial population of parameters to 34 parameters set. Afterwards, we need to determine the fitness function; we take the minimum residual sum of squares between the solution of the infected case in the model and the actual infected case:

$$\text{fitness} = \sum_{t=1} \left(\widetilde{I}(t) - I(t) \right)^2, \quad t = 1, 2, \ldots, 34, \quad (3)$$

where $\widetilde{I}(t)$ represents the infected cases in the model at time t and $I(t)$ represents the actual infected cases at time t. We use fitness function to evaluate the initial population and give the initial fitness value of parameters.

GA mainly includes three genetic operators: selection, crossover, and mutation. Selection is to apply the selection operator to the group. The purpose of selection is to inherit the optimized parameters directly to the next generation or to generate a new par to the next generation through pairing and crossover. Selection operations are based on the fitness evaluation of parameters in the population. Here we adopt a random selection combined with elitism, which means that we will copy the parameters with higher fitness once, replace the ones with the least fitness, and retain the best parameters of each generation. This is the elite strategy; then we randomly select parameters for crossover and mutation.

Crossover operator plays a key role in GA. It is mainly divided into single-point crossover, two-point crossover, and multiple-point crossover. The commonly used is the single-point crossover; that is, a cross point is randomly set in the parameter string, when the intersection is performed, in front of this point or partial structures of two parameters sets exchange and thus two new parameters sets are generated. An example of a single-point crossover is shown in Figure 2. Because our parameter binary is too long, single-point crossover cannot meet our needs, so we chose multiple-point crossover to increase the diversity of parameters.

The mutation operator is to change certain gene positions of parameter strings in the population; for example, 0 becomes 1, and 1 becomes 0. An example of mutation is shown in Figure 3. We adopted the gene locus mutation with adaptive mutation operator in GA; that is, each gene position was mutated with a certain mutation probability. Moreover, the mutation probability can be adaptively adjusted by the parameters set fitness. When the difference between parameters set fitness and the average fitness of the population is small, it means that parameters are close to each other, which is not conducive to the next crossover. Therefore, it is necessary to increase the mutation probability and reduce the mutation probability when the difference is large, because the mutation probability is usually between 0.001 and 0.1, and the probability of mutation is small, so that it is not easy to destroy the genes of the dominant parameters, and it can jump out when the algorithm falls into the local optimal
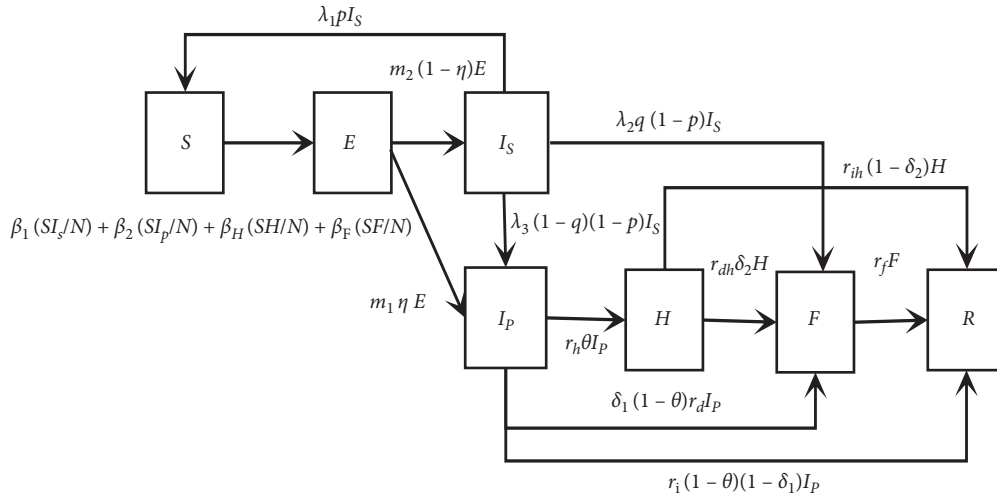
FIGURE 1: Ebola's transmission mechanism in Sierra Leone.

TABLE 1: Description of parameters in model (1).

| Parameter	Description	Value	95% confidence intervals
β_1	Transmission coefficient between communities S and I_s	0.9162	[0.1173, 1.1247]
β_2	Transmission coefficient between communities S and I_P	0.8929	[0.1341, 1.1803]
β_H	Transmission coefficient at the hospital	0.1674	[0.0623, 1.0713]
β_F	Transmission coefficient during the funerals	0.2736	[0.0887, 1.0665]
p	Misdiagnosed proportion in I_S	0.657	[0.1638, 0.6891]
q	Proportion of correctly diagnosed suspected cases that move to F	0.1447	[0.0531, 1.1805]
η	Proportion of exposed cases entering the I_P compartment	0.619	[0.1008, 1.1189]
θ	Proportion of infected and hospitalized	0.0023	[0.1476, 0.3507]
λ_1	Time from suspected to susceptible	1.59 days	[0.0641, 1.002]
λ_2	Average time from suspected to death	4.88 days	[0.0418, 1.0139]
λ_3	Time from suspected to probable	2.38 days	[0.0661, 1.0172]
m_1	Time from exposed to probable	1.0007 days	[0.0611, 1.2091]
m_2	Time from exposed to suspected	20.9 days	[0.1053, 1.2612]
r_h	Time from probable to hospitalized	3.56 days	[0.2733, 0.5884]
r_{dh}	Average time from hospitalization to death	1.2 days	[0.1109, 1.187]
r_i	Time from probable to removed	5.69 days	[0.1221, 1.1318]
r_{ih}	Time from hospitalized to removed	2.56 days	[0.0844, 1.1501]
r_f	Average time from death to burial	1.21 days	[0.1323, 0.9899]
r_d	Time from probable to death	1.11 days	[0.0099, 1.183]
δ_1	Mortality rate from probable to death	0.5141	[0.1219, 1.0691]
δ_2	Mortality rate from hospitalized to death	0.6214	[0.0455, 1.1318]
N	Size of the Sierra Leone population	6348350	[47]
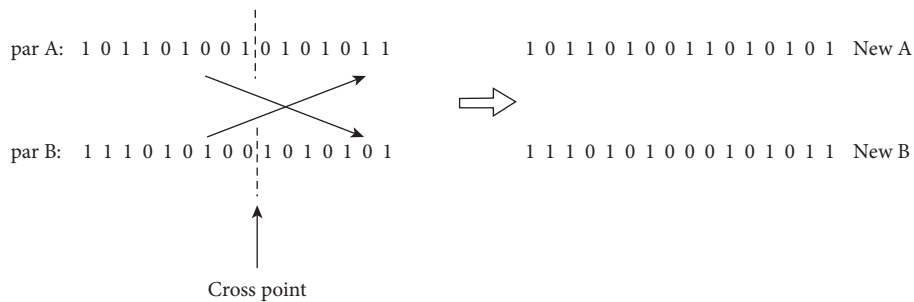
FIGURE 2: The two parameters sets A and B exchange the part after the cross point and reconstitute two new parameters sets.

par A: 1 0 1 1 0 1 0 0 1 0 1 0 1 0 1 1

⟵ Mutation point

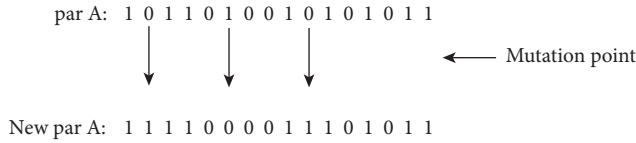New par A: 1 1 1 1 0 0 0 0 1 1 1 0 1 0 1 1

FIGURE 3: Parameters sets gene mutations generate new parameters sets.

solution. The mutation characteristic of GA can make the solution process randomly search the entire space where the solution may exist and ensure the diversity of the population, so the global optimal solution can be obtained to a certain extent.

Next, we solve model (1), decode the parameters into decimalism, and substitute them into the model solution to get the estimated value of confirmed-infection cases, that is, hospitalization cases. Fitness function (3) is used to fit the real infected cases. Then we find the parameters with the highest fitness in this generation, that is, the parameters with the least error, and keep them in the next-generation genetic process. Afterwards, we cyclically execute selection, crossover, mutation, and evaluation of new parameters set until the maximum number of iterations is reached.

The general steps of using GA to estimate parameters of Ebola model are explained as follows:

Step 1: consider the parameter to be estimated as a gene chromosome, define the parameter using binary coding, and then initialize the population.

Step 2: assign a fitness value to each parameter using equation (3). Starting from the second generation of parameters, parameters are ranked from small to large according to fitness values, and the first two parameters sets with the greatest fitness are duplicated once to replace the two parameters sets with the smallest fitness.

Step 3 (selection process): add randomly initialized parameters to the population to increase population diversity, and then two parameters sets are randomly selected as paternal parameters sets.

Step 4 (crossover): two new offspring parameters are generated by crossing the two parents at multiple points.

Step 5 (mutation): use the gene locus mutation described above in combination with adaptive mutation operator.

Step 6: solve equation (1) using the ode function.

Step 7: convert the types of parameters sets from binary to decimal, substitute it into the solution of equation (1), obtain the predicted value of the diseased cases, and use equation (3) to evaluate the fitness value of the new parameters set to obtain an optimal parameters set.

Step 8: when the fitness of the new offspring produced by genetic manipulation is higher than that of the parent, the new parameters sets replace the parents and are inserted into the parent population for the next genetic manipulation. If the optimal individual remains unchanged for 30 consecutive times, multiple-point crossover and mutation are carried out.

Step 9: save the best parameters set of this generation.

Step 10: if the number of iterations is not reached, proceed with step 2.

The above steps are executed iteratively until the termination condition is reached. Parameter estimation is finished whenever the genetic operation completed. The parameter values to be used in the model are the optimal solution of the last generation of parameters, and the specific values are shown in Table 1. We can study the propagation dynamics and preventive measures of Ebola.

3. Main Results

There are many methods for parameter estimation, including Markov Chain Monte Carlo (MCMC) method and least-squares method. It is not easy to analyze and estimate the parameters in the infectious disease model because there are many parameters in the model which cannot be estimated fully. Consequently, we propose to estimate the parameters in model (1) using GA, which are described in Section 2. Algorithm 1 shows the scheme of GA used on parameter estimation of the Ebola model. In this algorithm, par denotes a set of parameters, constants a and b represent two parameters sets randomly selected from par set and crossed according to the crossover probability p_x to get a' and b'. In mutation, a' and b' are changed to $\tilde{a}$ and $\tilde{b}$ by gene locus mutations, according to mutation probability p_m. IC denotes the initial value of each variable in equation (1) and t indicates the time of virus transmission. "count" indicates that successive generations of optimal values have not changed.

In this study, we used different genetic operators and fitness functions (3) to conduct data fitting for the real hospital-diagnosed cases. We conducted 70 experiments and selected a set of parameters which performed well. The results are listed in Table 1. After experimental verification, we chose the crossover probability p_x to be 0.8 and the initial mutation probability p_m to be 0.01. The genetic algebra Constant is 3000 times. The fitting result for the cumulative number of cases is shown in Figure 4.

Figure 5 represents the evolutionary process of the optimal value of each generation in GA. With the increase of genetic algebra, the error between the model solution and the real data is gradually decreasing, which means that the fitness of the model is increasing. Until the maximum genetic algebra is reached, a set of near-optimal parameters are obtained. Since the error persists, we can regard the sub-optimal solution as the optimal solution. The subgraph in Figure 5 is an enlarged view of early inheritance. Although this set of parameters performs well and converges quickly, we can see from the figure that it converges around 200 generations, but, because of the instability of GA, sometimes it takes a long time to converge to the optimal value. Therefore, we unified the genetic algebra to 3000 generations during the experiment. It can be seen from the figure that the

(1) Parameter length C_L is determined according to parameter range.
(2) Each parameter is represented by a chromosome of C_L length to get a complete parameters set par $= [\beta_1, \beta_2, \dots, r_f]$.
(3) Initialize all parameters set, $par_c = [\beta_1, \beta_2, \dots, r_f]$, $c = 34$.
(4) Evaluate the fitness of each par using f.
(5) for $i = 1, 2, \dots$, Constant **do**
(6)   **if** $i = 2$ **do**
(7)   Sort par allocation fitness in an ascending order.
(8) $par_{34} = [\beta_1, \beta_2, \dots, r_f] = par_1 = [\beta_1, \beta_2, \dots, r_f]$.
(9) $par_{33} = [\beta_1, \beta_2, \dots, r_f] = par_2 = [\beta_1, \beta_2, \dots, r_f]$.
(10)   **end if**
(11)   Randomly add an initialization parameter to replace one of the par
(12)   **if** max f (par) close to average f (par) **do**
(13)   Mutation probability $p_m = 0.1$.
(14)   **end if**
(15)   Randomly select $a, b \in$ par $(a \neq b)$.
(16)   Cross over a and b according to p_x, $a, b \Longrightarrow a', b'$.
(17)   Perform mutation on a' and b' according to p_m, $a', b' \Longrightarrow \tilde{a}, \tilde{b}$.
(18) $D = $ ebolaSol (par, IC, t).
(19)   Evaluate fitness $f = $ sum $(D - \text{Data})^2$.
(20)   **if** $f(\tilde{a}) < f(a)$ **do**
(21)   par $(a) = $ par $(\tilde{a})$.
(22)   **end if**
(23)   **if** count > 30 **do**
(24)   Multiple crossover and variation.
(25)   **end if**
(26)   Find the best parameters set in this generation $best_p (i)$ that satisfies $best_p (i) = \min f$ (par).
(27) **end for**
(28) Find the best parameters set par_{best} that satisfies $par_{best} = best_p$ (Constant).

ALGORITHM 1: Parameter estimation of GA.

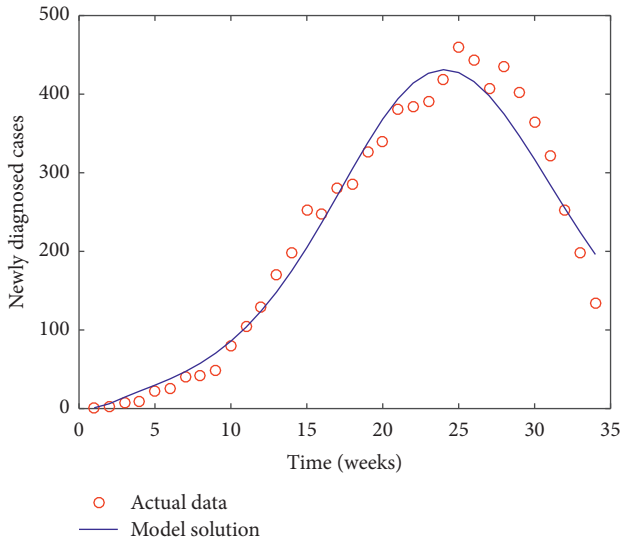FIGURE 4: The fitting result for actual data of Ebola virus disease in Sierra Leone for 34 weeks with the deterministic model (1).
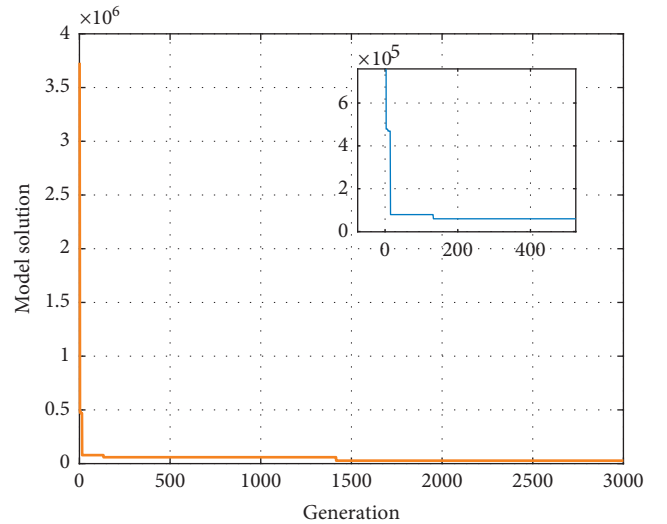

FIGURE 5: Evolutionary process of model optimal solution. Here, the yellow solid line represents the evolutionary process of the fitness values corresponding to the optimal parameters of each generation, while the blue solid line represents the early amplification part of the model solution.

GA can quickly reduce the error in the early stage, and the convergence speed is very fast, which shows the effectiveness of our algorithm.

In [5], the parameters $\beta_I = 0.0498$, $\beta_H = 0.0225$, and $\beta_F = 0.0013$ are given, and, in [23], the parameters $\beta_I = 0.128$, $\beta_H = 0.08$, $\beta_F = 0.111$, and $\delta_1 = \delta_2 = 0.75$ are given.

Meanwhile, the parameters $\beta_F = 0.489$, $\delta_1 = 0.8$, $\delta_2 = 0.4$ are given in [6]. Although some of the propagation coefficients are very different from those in other papers, because the deterministic models are different, we have that cabins are

more, and we cannot directly compare them with those in other papers. We are uncertain about patients in the exposed period, so the propagation coefficient associated with it is uncertain. We can only use GA to solve each parameter value. Thus, we only perform comparison with some important parameters. In this paper, $\delta_1 = 0.5141$, $\delta_2 = 0.6214$ are close to the above literature to some extent. We obtain the basic reproduction number of Ebola virus in Sierra Leone $R_0 \approx 1.895$ which is calculated in the same way as in Xia et al.'s work [6]; it is basically consistent with $R_0 \approx 1.7$ given in [5] and $R_0 \approx 1.78$ given in [23]. The results show that the GA can accurately estimate all the parameters in the model, and the data are fitted well. Another advantage of the GA is that you are free to set the parameters precision, but you need to consider the length of the parameters set, which is very useful for getting high-precision parameters. It can be seen that GA can be used as a feasible method for parameter estimation.

Due to the fact that we are using a certain mathematical model, we only need to use the actual diseased data as test data and apply them in model (1) to get a set of near-optimal parameters. We set each of the parameter ranges to [0, 1], randomly generate the initial parameters as the input of the model, and use the GA to obtain a set of parameters that fit the model better. We can use GA to give a variety of parameter combinations for researchers' reference. However, some parameters may have overfitting problems, so we conducted 70 experiments to select a set of parameters that are more realistic. We calculated the 95% confidence intervals for the best set of parameters in the 70 experiments, and almost all parameters are within the confidence intervals, which also shows the validity of the GA for parameter estimation. The confidence intervals for all the parameters are shown in Table 1.

4. Discussion and Conclusion

This work proposed a GA parameter estimation method based on adaptive mutation operator, which could be applied to biomathematical models and differential equations in other fields. Through GA's adaptive search parameters, the parameters in various models can be effectively found, and multiple parameter combination schemes can be given, which reduces the process of manual adjustment of parameters by researchers and provides an effective reference for scientific research. In addition, in the study of infectious diseases, due to the complexity of the model, all of the parameters are often difficult to obtain, and the basic reproduction number R_0 for evaluating whether there is an outbreak of an infectious disease needs to be obtained by calculating parameters; and the parameters can indicate the transmission dynamics of infectious diseases and the scale of transmission visually. Thus, parameter estimation is the most important, and the GA can be used to effectively find all the parameters in the model, which make up for the shortcomings of the traditional method, such as long calculation time and slow convergence speed. The method we have proposed has been evaluated in the experimental process, where the performance has reached the desired level. Finally, the GA can be applied not only to infectious disease models but also to other mathematical and physical models, and it proposes a new idea for parameter estimation.

Since the initial population of GA needs to assign values randomly, it will lead to output instability; we cannot quantify the uncertainty due to the discrete distribution of the output parameters, which is a common problem of GA and needs to be improved. On the other hand, fitness function is an important factor to determine the pros and cons of genetic evolution, so it is very important to select a suitable fitness function. Finally, a very important step in GA is to find the solution of the model, so it may not be suitable for the unsolvable equation, but it is applicable for most models. There are many improved genetic algorithms, and we can improve the existing algorithms and expand their scope of application.

The GA can solve specific problems with only a small amount of data, and the corresponding fitness function can be used for searching. Therefore, it is a general-purpose algorithm used in many fields. In function optimization, GA can estimate not only the parameters of biomathematical model but also the kinetic parameters of microorganisms. It can also solve the performance parameters of nonlinear physical problems. In addition, GA performs well in path planning, cloud computing task scheduling, communication network design, image feature extraction, and other fields. Furthermore, there are some studies that combine GA with machine learning methods such as neural network.

In this paper, we introduce the basic process of adaptive mutation genetic algorithm, introduce how to use GA to estimate the parameters of Ebola virus model in Sierra Leone, and give the data curve and genetic iterative process for fitting actual infections. In addition, we offer a new idea for parameter estimation in other research fields, such as dynamical model of disease transmission [48–50] or predator-prey interactions [51–53] with spatial effects [32, 54–56] in the form of reaction-diffusion equations.

Data Availability

The data used to support the findings of this study are included within the article.

Conflicts of Interest

The authors declare that they have no conflicts of interest.

Acknowledgments

References

[1] M. Bray and S. Mahanty, "Ebola hemorrhagic fever and septic shock," *The Journal of Infectious Diseases*, vol. 188, no. 11, pp. 1613–1617, 2003.

[2] M. Borchert, I. Mutyaba, M. D. V. Kerkhove et al., "Ebola haemorrhagic fever outbreak in Masindi district, Uganda: Outbreak description and lessons learned," *BMC Infectious Diseases*, vol. 11, p. 357, 2011.

[3] O. Reynard, B. Escudero-Perez, and V. Volchkov, "Dérégulation de l'hémostase dans les infections à filovirus," *Médecine/Sciences*, vol. 31, no. 2, pp. 143–150, 2015.

[4] A. S. Khan, "The reemergence of ebola hemorrhagic fever, democratic Republic of the Congo," *The Journal of Infectious Diseases*, vol. 179, no. 1999, pp. S76–S86, 1995.

[5] L. Li, "Transmission dynamics of ebola virus disease with human mobility in Sierra Leone," *Chaos, Solitons & Fractals*, vol. 104, pp. 575–579, 2017.

[6] Z.-Q. Xia, S.-F. Wang, S.-L. Li et al., "Modeling the transmission dynamics of Ebola virus disease in Liberia," *Scientific Reports*, vol. 5, no. 1, p. 13857, 2015.

[7] Infectious Diseases Society of America, *IDSA Ebola Guidance*, Infectious Diseases Society of America, Arlington, VA, USA, 2014.

[8] M. A. Bwaka, M. J. Bonnet, P. Calain et al., "Ebola hemorrhagic fever in Kikwit, democratic Republic of the Congo: Clinical observations in 103 patients," *The Journal of Infectious Diseases*, vol. 179, no. s1, pp. S1–S7, 1999.

[9] P. E. Rollin and T. G. Ksiazek, "Ebola haemorrhagic fever," *Lancet*, vol. 377, pp. 147-148, 2011.

[10] P. Shears and T. J. D. O'Dempsey, "Ebola virus disease in Africa: Epidemiology and nosocomial transmission," *Journal of Hospital Infection*, vol. 90, no. 1, pp. 1–9, 2015.

[11] E. M. Leroy, B. Kumulungui, X. Pourrut et al., "Fruit bats as reservoirs of Ebola virus," *Nature*, vol. 438, no. 7068, pp. 575-576, 2005.

[12] Centers for Disease Control and Prevention, Diseases and Conditions.

[13] G. Grard, R. Biek, J.-J. Muyembe Tamfum et al., "Emergence of divergent Zaire Ebola virus strains in democratic Republic of the Congo in 2007 and 2008," *Journal of Infectious Diseases*, vol. 204, no. suppl 3, pp. S776–S784, 2011.

[14] P. Rouquet, J. M. Froment, M. Bermejo et al., "Wild animal mortality monitoring and human ebola outbreaks, Gabon and Republic of Congo, 2001–2003," *Emerging Infectious Diseases*, vol. 11, pp. 283–290, 2005.

[15] E. M. Leroy, S. Baize, V. E. Volchkov et al., "Human asymptomatic Ebola infection and strong inflammatory response," *The Lancet*, vol. 355, no. 9222, pp. 2210–2215, 2000.

[16] X. Luo, N. Shao, J. Cheng, and W. Chen, "Modeling the trend of outbreak of COVID-19 in the diamond princess cruise ship based on a time-delay dynamic system," *Mathematical Modeling and its Applications*, vol. 9, pp. 15–22, 2020.

[17] A. J. Georges, E. M. Leroy, A. A. Renaut et al., "Ebola hemorrhagic fever outbreaks in Gabon, 1994–1997: Epidemiologic and health control issues," *The Journal of Infectious Diseases*, vol. 179, no. s1, pp. S65–S75, 1999.

[18] A. Mbonye, J. Wamala, W. K. V. Winyi-Kaboyo, V Tugumizemo, J. Aceng, and I. Makumbi, "Repeated outbreaks of viral hemorrhagic fevers in Uganda," *African Health Sciences*, vol. 12, no. 4, p. 579, 2012.

[19] X. Qiu, G. Wong, J. Audet et al., "Reversion of advanced Ebola virus disease in nonhuman primates with ZMapp," *Nature*, vol. 514, no. 7520, pp. 47–53, 2014.

[20] M. I. Meltzer, C. Y. Atkins, S. Santibanez et al., "Estimating the future number of cases in the Ebola epidemic-Liberia and Sierra Leone, 2014-2015," *Semantic Scholar*, vol. 63, no. suppl 3, pp. 1–14, 2014.

[21] Z. Sun, "Analysis for the process of preventing and controlling plague," *Mathematical Modeling and Its Applications*, vol. 9, pp. 9–14, 2020.

[22] J. A. Wilson, "Epitopes involved in antibody-mediated protection from Ebola virus," *Science*, vol. 287, no. 5458, pp. 1664–1666, 2000.

[23] L. Ellard, R. Katznelson, M. Wasowicz et al., "Modeling the impact of interventions on an epidemic of ebola in Sierra Leone and Liberia," *PLos Currents*, vol. 6, p. e62, 2014.

[24] S. Helleringer and A. Noymer, "Assessing the direct effects of the ebola outbreak on life expectancy in Liberia, Sierra Leone and Guinea," *PLos Currents*, vol. 7, p. e62, 2015.

[25] A. Khan, M. Naveed, M. Dur-E-Ahmad, and M. Imranet, "Estimating the basic reproductive ratio for the Ebola outbreak in Liberia and Sierra Leone," *Infectious Diseases of Poverty*, vol. 4, no. 1, p. 13, 2015.

[26] Z.-G. Guo, L.-P. Song, G.-Q. Sun, C. Li, and Z. Jin, "Pattern dynamics of an SIS epidemic model with nonlocal delay," *International Journal of Bifurcation and Chaos*, vol. 29, no. 2, Article ID 1950027, 2019.

[27] L. Li, "Patch invasion in a spatial epidemic model," *Applied Mathematics and Computation*, vol. 258, pp. 342–349, 2015.

[28] G.-Q. Sun, M. Jusup, Z. Jin, Y. Wang, and Z. Wang, "Pattern transitions in spatial epidemics: Mechanisms and emergent properties," *Physics of Life Reviews*, vol. 19, pp. 43–73, 2016.

[29] G.-Q. Sun, J.-H. Xie, S.-H. Huang, Z. Jin, M.-T. Li, and L. Liu, "Transmission dynamics of cholera: Mathematical modeling and control strategies," *Communications in Nonlinear Science and Numerical Simulation*, vol. 45, pp. 235–244, 2017.

[30] L. Li, J. Zhang, C. Liu, H.-T. Zhang, Y. Wang, and Z. Wang, "Analysis of transmission dynamics for Zika virus on networks," *Applied Mathematics and Computation*, vol. 347, pp. 566–577, 2019.

[31] Y. Xing, L. Song, G.-Q. Sun, Z. Jin, and J. Zhang, "Assessing reappearance factors of H_7N_9 avian influenza in China," *Applied Mathematics and Computation*, vol. 309, pp. 192–204, 2017.

[32] G.-Q. Sun, C.-H. Wang, and Z.-Y. Wu, "Pattern dynamics of a Gierer-Meinhardt model with spatial effects," *Nonlinear Dynamics*, vol. 88, no. 2, pp. 1385–1396, 2017.

[33] B. Rannala, "Identifiability of parameters in MCMC bayesian inference of phylogeny," *Systematic Biology*, vol. 51, no. 5, pp. 754–760, 2002.

[34] E. Mossel and E. Vigoda, "Phylogenetic MCMC algorithms are misleading on mixtures of trees," *Science*, vol. 309, no. 5744, pp. 2207–2209, 2005.

[35] C. Andrieu, N. de Freitas, A. Doucet, and M. I. Jordan, "An introduction to MCMC for machine learning," *Machine Learning*, vol. 50, pp. 5–43, 2003.

[36] N. M. Shahtori, C. Scoglio, A. Pourhabib et al., "Sequential Monte Carlo filtering estimation of Ebola progression in West Africa," in *Proceedimgs of the American Control Conference (ACC)*, pp. 1277–1282, Boston, MA, USA, July 2016.

[37] P. R. Conrad, Y. M. Marzouk, N. S. Pillai et al., "Accelerating asymptotically exact MCMC for computationally intensive models via local approximations," *Publications of the American Statistical Association*, vol. 111, pp. 1591–1607, 2014.

[38] J. D. Hadfield, "MCMC methods for multi-response generalised linear mixed models:The MCMCglmm R package," *Journal of Statistical Software*, vol. 33, no. 2, pp. 1–22, 2010.

[39] A. E. Gelfand and A. F. M. Smith, "Sampling-based approaches to calculating marginal densities," *Publications of the American Statistical Association*, vol. 85, pp. 398–409, 1990.

[40] A. Savitzky and M. J. E. Golay, "Smoothing and differentiation of data by simplified least squares procedures," *Analytical Chemistry*, vol. 36, no. 8, pp. 1627–1639, 1964.

[41] J. A. K. Suykens and J. Vandewalle, "Least squares support vector machine classifiers," *Neural Processing Letters*, vol. 9, no. 3, pp. 293–300, 1999.

[42] L. Wang, F. Tang, and H. Wu, "Hybrid genetic algorithm based on quantum computing for numerical optimization and parameter estimation," *Applied Mathematics and Computation*, vol. 171, no. 2, pp. 1141–1156, 2005.

[43] A. F. Sheta and K. De Jong, "Time-series forecasting using GA-tuned radial basis functions," *Information Sciences*, vol. 133, no. 3-4, pp. 221–228, 2001.

[44] D. E. Goldberg and J. H. Holland, "Genetic algorithms and machine learning," *Machine Learning*, vol. 3, no. 2-3, pp. 95–99, 1988.

[45] R. Wu, J. T. Painumkal, J. M. Volk et al., "Parameter estimation of nonlinear nitrate prediction model using genetic algorithm," in *Proceedings of the IEEE Congress on Evolutionary Computation*, Donostia-San Sebastian, Spain, June 2017.

[46] C. B. Lucasius and G. Kateman, "Understanding and using genetic algorithms Part 1. Concepts, properties and context," *Chemometrics and Intelligent Laboratory Systems*, vol. 19, no. 1, pp. 1–33, 1993.

[47] Data for the 2014 Ebola outbeak in West Africa, http://github.com/cmrivers/ebola, 2014.

[48] W. M. van Ballegooijen and M. C. Boerlijst, "Emergent trade-offs and selection for outbreak frequency in spatial epidemics," *Proceedings of the National Academy of Sciences*, vol. 101, no. 52, pp. 18246–18250, 2004.

[49] Z.-G. Guo, G.-Q. Sun, Z. Wang, Z. Jin, L. Li, and C. Li, "Spatial dynamics of an epidemic model with nonlocal infection," *Applied Mathematics and Computation*, vol. 377, Article ID 125158, 2020.

[50] R. Ostfeld, G. Glass, and F. Keesing, "Spatial epidemiology: An emerging (or re-emerging) discipline," *Trends in Ecology & Evolution*, vol. 20, no. 6, pp. 328–336, 2005.

[51] T. Reichenbach, M. Mobilia, and E. Frey, "Mobility promotes and jeopardizes biodiversity in rock-paper-scissors games," *Nature*, vol. 448, no. 7157, pp. 1046–1049, 2007.

[52] G.-Q. Sun, S.-L. Wang, Q. Ren, Z. Jin, and Y.-P. Wu, "Effects of time delay and space on herbivore dynamics: Linking inducible defenses of plants to herbivore outbreak," *Scientific Reports*, vol. 5, no. 1, Article ID 11246, 2015.

[53] T. Reichenbach, M. Mobilia, and E. Frey, "Noise and correlations in a spatial population model with cyclic competition," *Physical Review Letters*, vol. 99, no. 23, Article ID 238105, 2007.

[54] G.-Q. Sun, C.-H. Wang, L.-L. Chang, Y.-P. Wu, L. Li, and Z. Jin, "Effects of feedback regulation on vegetation patterns in semi-arid environments," *Applied Mathematical Modelling*, vol. 61, pp. 200–215, 2018.

[55] L. Li, Z. Jin, and J. Li, "Periodic solutions in a herbivore-plant system with time delay and spatial diffusion," *Applied Mathematical Modelling*, vol. 40, no. 7-8, pp. 4765–4777, 2016.

[56] Q. Li, Z. Liu, and S. Yuan, "Cross-diffusion induced turing instability for a competition model with saturation effect," *Applied Mathematics and Computation*, vol. 347, pp. 64–77, 2019.

WILEY | Hindawi

Research Article

Modelling and Analysis of Complex Viscous Fluid in Thin Elastic Tubes

Yufang Gao[1] and Zongguo Zhang [ID] [2]

[1]*College of Applied Meteorology, Jiangsu Key Laboratory of Agricultural Meteorology,*
 Nanjing University of Information Science and Technology, 219 Ning Liu Street, Nanjing 210044, China
[2]*School of Mathematics and Statistics, Qilu University of Technology (Shandong Academy of Sciences), Jinan 250353, China*

Correspondence should be addressed to Zongguo Zhang; zhangzongguo@qlu.edu.cn

Cardiovascular disease is a major threat to human health. The study on the pathogenesis and prevention of cardiovascular disease has received special attention. In this paper, we have contributed to the derivation of a mathematical model for the nonlinear waves in an artery. From the Navier–Stokes equations and continuity equation, the vorticity equation satisfied by the blood flow is established. And based on the multiscale analysis and perturbation method, a new model of the Boussinesq equation with viscous term is derived to describe the propagation of a viscous fluid through a thin tube. In order to be more consistent with the flow of the fluid, the time-fractional Boussinesq equation with viscous term is deduced by employing the semi-inverse method and the fractional variational principle. Moreover, the approximate analytical solution of the fractional equation is obtained, and the effect of viscosity on the amplitude and width of the wave is studied. Finally, the effects of the fractional order parameters and vessel radius on blood flow volume are discussed and analyzed.

1. Introduction

In recent years, in the field of biological rheology, the rheology which is related to the blood, blood vessels, and heart that constitute the human blood circulation has been developed rapidly. Blood circulation is a complex system that can cause great damage to the whole body when a certain organ is diseased. In order to better understand the physiological and pathological behavior of the human cardiovascular system, it is necessary to deeply study the dynamics of blood flow in the arteries and the mechanical factors of blood flow.

Soliton phenomena exist in many fields [1–3]. Organism is a completely nonlinear complex medium, and both the blood composition and the structure of blood vessels show obvious nonlinear characteristics. The nonlinearity of blood flow has long been discovered by Womersley [4, 5] and McDonald [6, 7], which also provides a new direction and

way for people to understand the law of life movement. Since then, many scholars have begun to study the field and made great progress. Ravindran et al. [8] derived the nonlinear Schödinger equation (the terms of pseudodifferential operators) governing the modulation of periodic waves. The KdV equation describing blood flow is obtained by Sigeo [9], to explain the steepness of pressure waves during propagation. Hashizume [10] analyzed the propagation of pressure waves from a theoretical perspective. Liu [11] combined arterial flow as a balanced flow with periodic small pulsatile flow and analyzed the effect of vascular elasticity on blood flow. Demiray [12, 13] considered propagation of wave through a viscous incompressible fluid contained in a prestressed thin elastic tube. Choy [14] deduced the mathematical model of nonlinear wave modulation of artery with stenosis.

Fractional derivative theory and methods [15–18] are widely used in the study of nonequilibrium systems of

various intermediate processes and critical phenomena in physics and mechanics, especially in nonlinear science [19–22]. Fractional differential equations are transformed in a standard differential equation by replacing the time derivative or the space derivative with the fractional derivative. Compared with integer-order differential equations, the most important advantage of fractional derivative equations is that it can better fit some natural physical processes and dynamic system processes. Moreover, the study of solving partial differential equations also has a new exploration, such as the extended tanh method [23], the exp-function method [24], the variational-iteration method [15, 25], the Hirota bilinear method [19], and the (G'/G)-expansion method [26].

The structure of the full article is as follows: in Section 2, the Boussinesq equation with viscous term is derived by the multiscale analysis and perturbation method and used for the first time to describe blood flow. Based on the new model, we obtain the time-fractional Boussinesq equation with viscous term in Section 3. In Section 4, the approximate analytical solution of the above fraction equation and the viscous effect is discussed. Finally, the effects of fractional order, vascular radius, and blood flow velocity on stroke volume are analyzed and studied.

2. Derivation of the Boussinesq Equation

As we all know, the cardiovascular system is a complete closed conduit system. Thus, the blood can be considered as an incompressible non-Newtonian fluid. When dynamic equilibrium of the blood is disturbed by a pressure pulse generated by the motion of the heart, a harmonic wave type of motion will be developed in the blood. Although previous researchers have done some research about this question, the viscosity of fluid is often ignored. We consider blood vessel as cylindrical shape and adopt cylindrical coordinate system to describe the motion of blood. In this paper, we set x as the central axis of a blood vessel and axial coordinate and set r as the radial coordinates. Therefore, based on Womersley theory [4], basic equations of pulsatile flow in arteries are described as follows:

$$\rho\left(\frac{\partial u}{\partial t} + u\frac{\partial u}{\partial x} + v\frac{\partial u}{\partial r}\right) - \eta\left(\frac{\partial^2 u}{\partial t^2} + \frac{1}{r}\frac{\partial u}{\partial r} + \frac{\partial^2 u}{\partial x^2}\right) = -\frac{\partial P}{\partial x},$$
(1)

$$\rho\left(\frac{\partial v}{\partial t} + u\frac{\partial v}{\partial x} + v\frac{\partial v}{\partial r}\right) - \eta\left(\frac{\partial^2 v}{\partial t^2} + \frac{1}{r}\frac{\partial v}{\partial r} + \frac{\partial^2 v}{\partial x^2} - \frac{v}{r^2}\right) = -\frac{\partial P}{\partial r},$$
(2)

$$\frac{\partial u}{\partial x} + \frac{1}{r}\frac{\partial rv}{\partial r} = 0, \quad (3)$$

where u and v are the axial and radial velocities of blood, respectively; p is the atmospheric pressure; ρ is the blood density; and η represents the viscosity coefficient of blood. From (3), we can define the flow function of blood which satisfies

$$u = \frac{1}{r}\frac{\partial \Psi}{\partial r},$$

$$v = -\frac{1}{r}\frac{\partial \Psi}{\partial x}.$$
(4)

Substituting (4) into (1) and (2), we can gain the vorticity equation of blood flow with viscosity term:

$$\rho\left(\frac{\partial}{\partial t} + \frac{1}{r}\frac{\partial \Psi}{\partial r}\frac{\partial}{\partial x} - \frac{1}{r}\frac{\partial \Psi}{\partial r} + \frac{2}{r^2}\frac{\partial \Psi}{\partial x}\right)D^2\Psi$$

$$- \eta\left(\frac{\partial^2}{\partial r^2} - \frac{1}{r}\frac{\partial}{\partial r} + \frac{\partial^2}{\partial x^2}\right)D^2\Psi = 0,$$
(5)

where $D^2 \equiv ((\partial^2/\partial r^2) - (1/r)(\partial/\partial r) + (\partial^2/\partial x^2))$. Through analysis, we assume that the basic law of blood flow can be expressed by the Poiseuille flow. Therefore, the speed of blood can be expressed as

$$\overline{u}(r) = u_{\max}\left[1 - \left(\frac{r}{R}\right)^2\right],$$
(6)

where $u_{\max} = (\Delta pR^2/4\mu\Delta L)$ is the maximum velocity of central axis of the blood vessel. ΔL represents the length of the blood fluid, and μ represents viscosity coefficient of blood. Δp is the pressure difference between two ends of blood, and R is the radius of the blood vessel. Next, when considering the viscosity of the vascular wall, we can get the revised form of the Poiseuille flow:

$$\overline{u}(r) = u_{\max}\left[\frac{2r^2}{R^2}\ln\frac{r}{R} + 1 - \left(\frac{r}{R}\right)^2\right].$$
(7)

We set basic flow function of blood as $\overline{\psi}$. Therefore, it meets

$$\overline{u} = \frac{1}{r}\frac{\partial \overline{\psi}}{\partial r},$$
(8)

where we define disturbed flow function $\varphi(r, x, t)$ which represents disturbance of blood flow. Therefore, the flow function can be expressed as

$$\Psi(r, x, t) = \overline{\psi}(r) + \varphi(r, x, t).$$
(9)

And then, from (8) and (4), we can obtain

$$u = \overline{u} + \frac{1}{r}\frac{\partial \varphi}{\partial r},$$

$$v = -\frac{1}{r}\frac{\partial \varphi}{\partial x}.$$
(10)

Substituting (9) and (10) into (5) and considering that there are other effects of dissipation which can offset $(2a\eta/\rho)$, we obtain

$$\left(\frac{\partial}{\partial t} + \frac{1}{r}\frac{\partial \varphi}{\partial r}\frac{\partial}{\partial x} - \frac{1}{r}\frac{\partial \varphi}{\partial x}\frac{\partial}{\partial r} + \frac{2}{r^2}\frac{\partial \varphi}{\partial x} + \overline{u}\frac{\partial}{\partial x}\right)D^2\varphi - a\frac{\partial \varphi}{\partial x}$$

$$= \frac{\eta}{\rho}\left(D^2 D^2\varphi\right),$$
(11)

where $a = (4u_{max}/R^2)$ and $\lim_{r \to 0} \overline{u}(r) = u_{max}$. The above equation is a vorticity equation of disturbed flow function φ which contains information about the effects on the heart when physiological or psychological condition changes dramatically.

In the previous studies, researchers have obtained the KdV equation from the Navier–Stokes equation and continuity equation of blood flow. However, with the development of nonlinear theory increasing, more equations which have stronger nonlinear properties are needed to describe problems in reality. Therefore, the Boussinesq equation model will be deduced in this paper. In order to obtain this equation, we firstly define coordinate

transformations with long wave approximation and adopt the space-time transformation as follows:

$$
\begin{aligned}
X &= \varepsilon(x - ct), \\
T &= \varepsilon^2 t, \\
r &= r,
\end{aligned}
\tag{12}
$$

and we set

$$
\frac{\eta}{\rho} = \varepsilon^3 Q,
\tag{13}
$$

where ε is a small parameter. Substituting (12) into (11) yields

$$
\begin{aligned}
&\left(\frac{\partial}{\partial T} \varepsilon^2 + \frac{1}{r} \frac{\partial \varphi}{\partial r} \frac{\partial}{\partial X} \varepsilon - \frac{1}{r} \frac{\partial \varphi}{\partial X} \frac{\partial}{\partial r} \varepsilon + \frac{2}{r^2} \frac{\partial \varphi}{\partial X} \varepsilon + (\overline{u} - c) \frac{\partial}{\partial X} \varepsilon \right) \left(\frac{\partial^2}{\partial r^2} - \frac{1}{r} \frac{\partial}{\partial r} + \frac{\partial^2}{\partial X^2} \varepsilon^2 \right) \varphi - a \frac{\partial \varphi}{\partial X} \varepsilon \\
&= Q \varepsilon^3 \left[\left(\frac{\partial^2}{\partial r^2} - \frac{1}{r} \frac{\partial}{\partial r} + \frac{\partial^2}{\partial X^2} \varepsilon^{2\alpha} \right) \left(\frac{\partial^2}{\partial r^2} - \frac{1}{r} \frac{\partial}{\partial r} + \frac{\partial^2}{\partial X^2} \varepsilon^2 \right) \varphi \right].
\end{aligned}
\tag{14}
$$

Then, we extend perturbed flow function about ε as follows:

$$
\varphi = \varepsilon^2 \varphi_0 + \varepsilon^3 \varphi_1 + \varepsilon^4 \varphi_2 + \cdots.
\tag{15}
$$

Due to the fact that the velocity of wave propagation in blood is much faster than that of blood flow on the axis of the blood vessel, we can obtain $\overline{u} \ll c$. Thus, substituting (15) into (14), we can yield all levels of approximation equations about ε:

$$
\varepsilon^3 : \Gamma \varphi_0 = 0,
$$

$$
\varepsilon^4 : \Gamma \varphi_1 = -\frac{\partial}{\partial T} \left(\frac{\partial^2}{\partial r^2} - \frac{1}{r} \frac{\partial}{\partial r} \right) \varphi_0,
$$

$$
\begin{aligned}
\varepsilon^5 : \Gamma \varphi_2 = &-\frac{\partial}{\partial T} \left(\frac{\partial^2}{\partial r^2} - \frac{1}{r} \frac{\partial}{\partial r} \right) \varphi_1 + c \frac{\partial^3}{\partial X^3} \varphi_0 \\
&- \left(\frac{1}{r} \frac{\partial \varphi_0}{\partial r} \frac{\partial}{\partial X} - \frac{1}{r} \frac{\partial \varphi_0}{\partial X} \frac{\partial}{\partial r} + \frac{2}{r^2} \frac{\partial \varphi_0}{\partial X} \right) \left(\frac{\partial^2}{\partial r^2} - \frac{1}{r} \frac{\partial}{\partial r} \right) \varphi_0 \\
&+ Q \left[\left(\frac{\partial^2}{\partial r^2} - \frac{1}{r} \frac{\partial}{\partial r} \right) \left(\frac{\partial^2}{\partial r^2} - \frac{1}{r} \frac{\partial}{\partial r} \right) \varphi_0 \right],
\end{aligned}
\tag{16}
$$

where $\Gamma \equiv -c(\partial/\partial X)((\partial^2/\partial r^2) - (1/r)(\partial/\partial r)) - a(\partial/\partial X)$.

For ε^3, it is easy to see that φ_0 has a solution, and the form is $\varphi_0 = A(X,T)\phi_0(r)$; then, we have

$$
-c\left(\frac{\partial^2}{\partial r^2} - \frac{1}{r} \frac{\partial}{\partial r} \right) \phi_0 - a\phi_0 = 0.
\tag{17}
$$

For ε^4, by analysis, we assume $(\partial \varphi_1/\partial X) = (\partial A/\partial T)\phi_1(r)$, where $\phi_1(r)$ satisfies the following equation:

$$
-c\left(\frac{\partial^2}{\partial r^2} - \frac{1}{r} \frac{\partial}{\partial r} \right) \phi_1 - a\phi_1 = \frac{a}{c} \phi_0.
\tag{18}
$$

Let us consider the equation of order ε^5. By substituting $\varphi_0 = A(X,T)\phi_0(r)$, $(\partial \varphi_1/\partial X) = (\partial A/\partial T)\phi_1(r)$, (17), and (18) into the equation and multiplying the both sides of the order ε^5 equation by $(\phi_0/r)(\partial/\partial X)$, we have

$$
\begin{aligned}
&\frac{\partial^2}{\partial X^2} \frac{\phi_0}{r} \left(\frac{\partial^2}{\partial r^2} - \frac{1}{r} \frac{\partial}{\partial r} \right) \varphi_2 + a \frac{\partial^2 \varphi_2}{\partial X^2} \frac{\phi_0}{r} \frac{1}{c} \\
&= -\frac{\partial^2 A}{\partial T^2} \frac{\phi_0}{r} \frac{a}{c^2} \left(\phi_1 + \frac{\phi_0}{c} \right) - \frac{\partial^4 A}{\partial X^4} \frac{\phi_0^2}{r} \\
&\quad - \frac{a}{c^2} \frac{\phi_0^2}{r^3} \frac{\partial^2 A^2}{\partial X^2} - Q \frac{\partial A}{\partial X} \frac{1}{c} \frac{\phi_0}{r} \left(\frac{\partial^2}{\partial r^2} - \frac{1}{r} \frac{\partial}{\partial r} \right)^2 \phi_0.
\end{aligned}
\tag{19}
$$

And then integrating it with respect to r from 0 to R, we can have the following equation:

$$
\frac{\partial^2 A}{\partial T^2} + a_1 \frac{\partial^2 A^2}{\partial X^2} + a_2 \frac{\partial^4 A}{\partial X^4} + a_3 \frac{\partial A}{\partial X} = 0,
\tag{20}
$$

where

$$
a_0 = \int_0^R \frac{\phi_0}{r} \frac{a}{c^2} \left(\phi_1 + \frac{\phi_0}{c} \right) dr,
$$

$$
a_1 = \int_0^R \frac{(a/c^2)(\phi_0^2/r^3) dr}{a_0},
$$

$$
a_2 = \int_0^R \frac{(\phi_0^2/r) dr}{a_0},
$$

$$
a_3 = Q \int_0^R \frac{((1/c)(\phi_0/r))((\partial^2/\partial r^2) - (1/r)(\partial/\partial r))^2 \phi_0 dr}{a_0}.
\tag{21}
$$

Equation (20) is a new Boussinesq equation with viscosity effect which can be used to describe the state of the disturbance flow of blood with viscous properties. Comparing with the previous KdV model, the above model has stronger nonlinear properties. Besides, it can be concluded that there is disturbance flow in the form of solitary waves in the arteries.

3. Derivation of the Time-Fractional Boussinesq Equation

In this section, we seek for the time-fractional Boussinesq equation by using the semi-inverse method and the fractional variational principle. Firstly, we use a potential function $V_X(X, T)$, where $A(X, T) = V_X(X, T)$ gives the potential equation of (20) in the following form:

$$V_{XTT} + a_1 (A^2)_{XX} + a_2 V_{XXXXX} + a_3 A_X = 0. \quad (22)$$

The functional of the potential equation (22) can be represented by

$$J(V_X) = \int_{\widetilde{X}} dX \int_{\widetilde{T}} dT \Big\{ V_X \Big[c_0 V_{XTT} + c_1 a_1 (A^2)_{XX} + c_2 a_2 V_{XXXXX} + c_3 a_3 A_X \Big] \Big\}, \quad (23)$$

where c_0, c_1, c_2, and c_3 are the Lagrangian multipliers which can be obtained later by taking the variation of (23). A_X and $(A^2)_{XX}$ are considered as the fixed functions.

Making use of integrating (23) by parts and assuming $V_T|_{\widetilde{T}} = V_X|_{\widetilde{X}} = V_{XX}|_{\widetilde{X}} = V_{XXX}|_{\widetilde{X}} = 0$, we can gain

$$J(V_X) = \int_{\widetilde{X}} dX \int_{\widetilde{T}} dT \Big\{ -c_0 V_{XT}^2 + c_1 a_1 V_X (A^2)_{XX} + c_2 a_2 V_{XXX}^2 + c_3 a_3 V_X A_X \Big\}. \quad (24)$$

Applying the variation optimum condition, we can derive the Euler equation as follows:

$$2c_0 V_{XTT} + c_1 a_1 (A^2)_{XX} + 2c_2 a_2 V_{XXXXX} + c_3 a_3 A_X = 0. \quad (25)$$

Comparing (25) with (22), we can obtain the following Lagrangian multipliers:

$$c_0 = \frac{1}{2},$$
$$c_1 = 1,$$
$$c_2 = \frac{1}{2}, \quad (26)$$
$$c_3 = 1.$$

Therefore, the Lagrangian form of (20) can be given by

$$L(V_{XT}, V_X, V_{XX}, V_{XXX}) = -\frac{1}{2} V_{XT}^2 + a_1 V_X (A^2)_{XX} + \frac{1}{2} a_2 V_{XXX}^2 + a_3 V_X A_X. \quad (27)$$

At this time, the Lagrangian form of the time-fractional Boussinesq equation can be represented as

$$F(_0 D_T^\beta V_X, V_X, V_{XX}, V_{XXX}) = -\frac{1}{2} (_0 D_T^\beta V_X)^2 + a_1 V_X (A^2)_{XX} + \frac{1}{2} a_2 V_{XXX}^2 + a_3 V_X A_X, \quad (28)$$

where based on the left Riemann–Liouville compression derivative, the fractional derivative $_0 D_T^\beta V_X$ is defined as

$$_0 D_T^\beta f(T) = \frac{1}{\Gamma(1-\beta)} \frac{d}{dT} \left[\int_a^T d\tau (T-\tau)^{-\beta} f(\tau) \right], \quad (29)$$
$$0 \le \beta \le 1, T \in [a, b].$$

Therefore, the time-fractional form of (20) can be expressed by

$$J(V_X) = \int_{\widetilde{X}} dX \int_{\widetilde{T}} dT F(_0 D_T^\beta V_X, V_X, V_{XX}, V_{XXX}). \quad (30)$$

Thus, the variation of functional (30) can be obtained:

$$\delta J(V_X) = \int_{\widetilde{X}} dX \int_{\widetilde{T}} dT \Big\{ \frac{\partial F}{\partial_0 D_T^\beta V_X} \delta(_0 D_T^\beta V_X) + \frac{\partial F}{\partial V_X} \delta V_X + \frac{\partial F}{\partial V_{XX}} \delta V_{XX} + \frac{\partial F}{\partial V_{XXX}} \delta V_{XXX} \Big\}. \quad (31)$$

As we all know, the fractional integration by parts is obtained by the following rule:

$$\int_b^a dT \{ f(T)_a D_T^\beta g(T) \} = \int_a^b dT \{ g(T)_T D_b^\beta f(T) \}, \quad (32)$$
$$f(T), g(T) \in [a, b],$$

based on the right Riemann–Liouville fractional derivative, $_0 D_T^\beta f(T)$ is obtained by

$$_T D_T^\beta f(T) = \frac{-1}{\Gamma(1-\beta)} \frac{d}{dT} \left[\int_T^b d\tau (\tau - T)^{-\beta} f(\tau) \right], \quad (33)$$
$$0 \le \beta \le 1, T \in [a, b].$$

Using (31) and (32), we get

$$\delta J(V_X) = \int_{\widetilde{X}} dX \int_{\widetilde{T}} dT \Big\{ _T D_b^\beta \Big(\frac{\partial F}{\partial_0 D_T^\beta V_X} \Big) + \frac{\partial F}{\partial V_X} - \frac{\partial}{\partial X} \Big(\frac{\partial F}{\partial V_{XX}} \Big) + \frac{\partial^2}{\partial X^2} \Big(\frac{\partial F}{\partial V_{XXX}} \Big) \Big\} \delta V_X. \quad (34)$$

By using variation principle, when $\delta J(V) = 0$, we obtain the optimization of the variation of functional. And then, we yield the Euler–Lagrange equation of (20) as the following equation:

$$-_0D_T^\beta\left(\frac{\partial F}{\partial_0D_T^\beta V_X}\right)+\frac{\partial F}{\partial V_X}-\frac{\partial}{\partial X}\left(\frac{\partial F}{\partial V_{XX}}\right)+\frac{\partial^2}{\partial X^2}\left(\frac{\partial F}{\partial V_{XXX}}\right)=0.$$

(35)

Substituting (28) into (35) and letting $_0D_T^\beta V_X = A(X,T)$, (35) is turned into the following form:

$$_0D_T^{2\beta}A(X,T)+a_1\left(A^2\right)_{XX}+a_2A_{XXXX}+a_3A_X=0.$$

(36)

Equation (36) is a new model, which is gained by the time-fractional method. Therefore, it is named as time-fractional Boussinesq equation.

4. Solution of the Time-Fractional Boussinesq Equation

In the previous section, a new time-fractional Boussinesq equation had been gained. It can be used to describe the flow characteristics of blood with viscous properties. Due to this reason, we decide to yield the solution of the time-fractional Boussinesq equation to further characterize the flow state of blood.

Let we define the fractional complex transform as follows:

$$\tau=\frac{T^\alpha}{\Gamma(1+\alpha)},$$

(37)

where α is the unknown constant. And then, we can yield the fractional derivatives into classical derivatives with (37):

$$\frac{\partial^\alpha A}{\partial T^\alpha}=\frac{\partial^2 A}{\partial\tau^2}.$$

(38)

It is obvious that (36) can be deduced to

$$\frac{\partial^2 A}{\partial\tau^2}+a_1\left(A^2\right)_{XX}+a_2A_{XXXX}+a_3A_X=0.$$

(39)

Next, we consider to gain the solution of (39). Due to the fact that a_3 describes viscous properties of blood, we set $\mu = a_3$ as a small parameter. Assuming that $A_0 = A_0(X,\mu^{(1/2)}\tau)$ and considering to get the properties of (39), two time scales are defined as follows:

$$\zeta=\tau,$$
$$\tilde{\eta}=\mu^{(1/2)}\tau,$$

(40)

and A is expanded as

$$A(X,\tau)=A_1(X,\zeta,\tilde{\eta})+\mu A_2(X,\zeta,\tilde{\eta}).$$

(41)

Thus, we obtain all levels of approximation equations about μ:

$$\mu^0:\frac{\partial^2 A_1}{\partial\zeta^2}+a_1\frac{\partial^2 A_1^2}{\partial X^2}+a_2\frac{\partial^4 A_1}{\partial X^4}=0,$$

$$\mu^1:\frac{\partial^2 A_2}{\partial\zeta^2}+a_1\frac{\partial^2(A_1A_2)}{\partial X^2}+a_2\frac{\partial^4 A_2}{\partial X^4}=-\frac{\partial^2 A_1}{\partial\tilde{\eta}^2}-\frac{\partial A_1}{\partial X}.$$

(42)

For μ^0, it is obvious that the solution of the equation can be expressed as

$$A_1(X,\zeta,\tilde{\eta})=A_0\sec h^2\left[\left(\frac{a_1A_0}{6a_2}\right)^{(1/2)}(X-\nu\zeta)+\tilde{c}\right],$$

(43)

where $\nu=(-(2a_1A_0/3))^{(1/2)}$ and A_0 represents the maximum amplitude at initial moment. Then, for μ^1, we use the equation to determine the form of A_0. Assuming that

$$A_2=B(I),$$
$$I=X+\zeta.$$

(44)

By substituting (44) into the order one of μ equation from (42), the following equation is obtained:

$$\frac{\partial^2 B}{\partial I^2}+a_1\frac{\partial^2}{\partial I^2}(A_1B)+a_2\frac{\partial^4 B}{\partial I^4}=M(A_1),$$

(45)

where $M(A_1)=-(\partial^2 A_1/\partial\tilde{\eta}^2)-(\partial A_1/\partial X)$. In order to describe the structure of A_2, we consider to choose proper function G which should be orthogonal to $M(A_1)$ as

$$\int_{-\infty}^{+\infty}G(I)M(A_1)dI=0.$$

(46)

Multiplying both sides of (45) by G, integrating them by parts and using $B|_{I=\pm\infty}=0$ and $(dB/dI)|_{I=\pm\infty}=0$, we can see that $G(I)$ satisfies

$$\frac{d^2 G}{dI^2}+a_1A_1\frac{d^2 G}{dI^2}+a_2\frac{d^4 G}{dI^4}=0.$$

(47)

By assuming $G(\pm\infty)=0$, the solution of (47) can be obtained as

$$G=A_0\sec h^2\left[\left(\frac{a_1A_0}{6a_2}\right)^{(1/2)}I+\tilde{c}\right].$$

(48)

Substituting (48) into (46) and using (45), we obtain

$$A_0=e^{-\sqrt{\mu}\tau-X}.$$

(49)

Therefore, we obtain the approximate solution of (39) as follows:

$$A(X,\zeta,\tilde{\eta})=A_0\sec h^2\left[\left(\frac{a_1A_0}{6a_2}\right)^{(1/2)}(X-\nu\zeta)+\tilde{c}\right],$$

(50)

where $A_0(X,\mu^{(1/2)}\tau)=e^{-\sqrt{\mu}\tau-X}$. The above equation is the solution of (39) and can be used to describe the flow state of blood more specifically.

Finally, the solution of the time-fractional Boussinesq equation is

$$A(X,T)=\exp\left(\frac{-\sqrt{\mu}T^\alpha}{\Gamma(1+\alpha)}-X\right)$$
$$\cdot\sec h^2\left[\left(\frac{a_1}{6a_2}\exp\left(\frac{-\sqrt{\mu}T^\alpha}{\Gamma(1+\alpha)}-X\right)\right)^{(1/2)}\right.$$
$$\left.\cdot\left(X-\nu\frac{T^\alpha}{\Gamma(1+\alpha)}\right)+\tilde{c}\right],$$

(51)

where $v = (-(2a_1/3)\exp((-\sqrt{\mu}\,T^\alpha/\Gamma(1+\alpha)) - X))^{(1/2)}$.

In order to study the influence of blood viscosity and fractional order on the evolution of blood flow, we change the value of μ, α, X, and T to get related results. From Figure 1, we can see that when viscosity parameter $\mu = 0$, the amplitude of solitary waves is largest; at the same time, the width of solitary waves is the smallest. With the decrease of the amplitude, the width increases gradually. Figure 2 depicts the evolution of solitary waves in blood under different viscosity coefficient μ. It is evident that amplitude of the solitary waves becomes smaller with time T from Figure 2(a), while the width of the solitary waves becomes larger with time T. And we can know that the viscosity effect leads to the amplitude of the solitary waves to decrease and the width of the solitary waves to increase. In addition, in contrast with Figure 2(b), we find with the increasing viscosity coefficient μ, the rate of amplitude reduction has been accelerated and the direction of the wave changes from the positive direction of X to the negative direction of it. Figure 3 shows the solitary waves under different fractional order α. We find the peak value of amplitude is not linear with α, and there is a minimum of the peak with the corresponding critical value of α. According to the critical value, the peak value of amplitude increases firstly and then decreases.

5. Analysis and Discussion

In this section, we consider to calculate the value which can represent the state of blood by using the results from the previous sections. First, we search for the solution of (17) and (18). Taking $\phi_0(r) = \phi_0((\sqrt{c/a}\,)z) = zw(z)$ and substituting them into (17) yield

$$z^2\frac{d^2 w}{dz^2} + z\frac{dw}{dz} + \left(z^2 - 1\right) = 0. \tag{52}$$

And the solution of (52) is expressed as

$$w(z) = C_1 J_1(z) + C_2 N_1(z), \tag{53}$$

where C_1 and C_2 are the constants and $J_1(z)$ and $N_1(z)$ are expressed as

$$J_1(z) = \sum_{m=1}^{\infty} \frac{(-1)^m}{m!\,\Gamma(m+2)}\left(\frac{z}{2}\right)^{2m+1},$$

$$N_1(z) = \frac{J_1(z)\cos(\pi) - J_{-1}(z)}{\sin(\pi)}. \tag{54}$$

Thus, the solution of (17) can be described as

$$\phi_0(r) = C_1 r\sqrt{\frac{a}{c}} J_1\left(r\sqrt{\frac{a}{c}}\right). \tag{55}$$

Similarly, by substituting (55) into (18), we obtain

$$\phi_1(r) = C_3 r\sqrt{\frac{a}{c}} J_1\left(r\sqrt{\frac{a}{c}}\right), \tag{56}$$

where C_3 is a constant. We take the physiological parameters of the human body as follows:
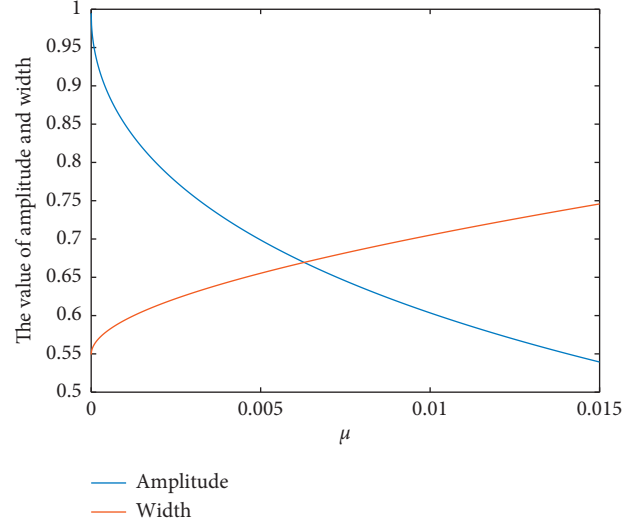

FIGURE 1: Variation of amplitude and width according to the viscosity coefficient μ ($\alpha = 1, T = 5, X = 0.005, a_2 = -1, a_1 = -20, \tilde{c} = 0$).

$$\begin{aligned}
R &= 1.25 \times 10^{-2}\,\text{m}, \\
u_{\max} &= 0.4\,\text{m/s}, \\
L &= 6.3 \times 10^{-2}\,\text{m}, \\
c &= 5.5\,\text{m/s}.
\end{aligned} \tag{57}$$

And set $Q = -0.01$, $C_1 = 0.1$, and $C_3 = -500$. Therefore, by using (21), we obtain the coefficients of (36) as follows:

$$\begin{aligned}
a_0 &= -8.52776 \times 10^{-1}, \\
a_1 &= -2.5917, \\
a_2 &= -5.9084 \times 10^{-7}, \\
a_3 &= 3.7 \times 10^{-3}.
\end{aligned} \tag{58}$$

Due to that the basic flow in a human artery can be assumed to be the Poiseuille flow, the stream function can be expressed as

$$\overline{\psi} = u_{\max}\left(\frac{r^2}{2} - \frac{r^4}{4R^2}\right). \tag{59}$$

So the stream function can be obtained as follows:

$$\begin{aligned}
\Psi = {} & u_{\max}\left(\frac{r^2}{2} - \frac{r^4}{4R^2}\right) + \varepsilon^2 \exp\left(\frac{-\sqrt{\mu}\,T^\alpha}{\Gamma(1+\alpha)} - X\right) \\
& \cdot \sec h^2\left[\left(\frac{a_1}{6a_2}\exp\left(\frac{-\sqrt{\mu}\,T^\alpha}{\Gamma(1+\alpha)} - X\right)\right)^{(1/2)} \right. \\
& \left. \cdot \left(X - v\frac{T^\alpha}{\Gamma(1+\alpha)}\right) + \tilde{c}\right]C_1 r\sqrt{\frac{a}{c}} J_1\left(r\sqrt{\frac{a}{c}}\right),
\end{aligned} \tag{60}$$

where $X = \varepsilon(x - ct)$ and $T = \varepsilon^2 t$ following (12).

Because in the cylindrical coordinate system, the difference of the flow function values of any two points in the
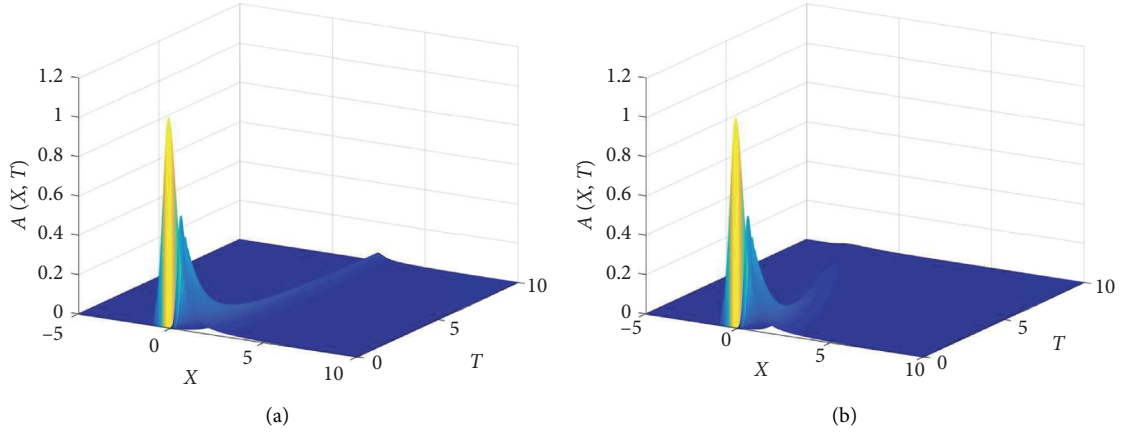
(a)

(b)

FIGURE 2: The evolution of solitary waves in blood with viscosity: (a) $\alpha = 1, a_2 = -1, a_1 = -20, \tilde{c} = 0, \mu = 0.005$; (b) $\alpha = 1, a_2 = -1, a_1 = -20, \tilde{c} = 0, \mu = 0.45$.
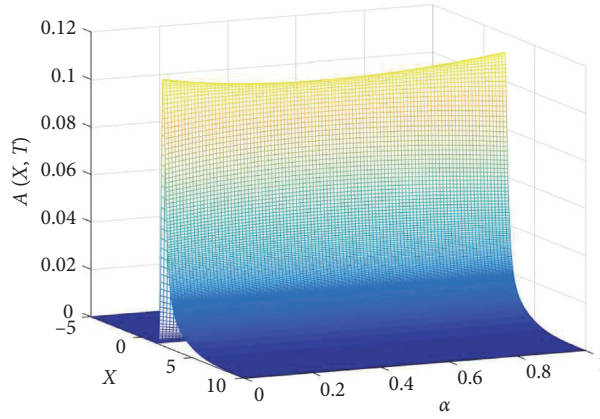

FIGURE 3: The evolution of solitary waves with different numbers of fractional order α ($T = 1, a_2 = -1, a_1 = -20, \tilde{c} = 0, \mu = 0.005$).

plane passing through the symmetry axis multiplied by 2π is equal to the value, which is the flow rate of the rotating surface formed by the rotation of any curve passing through these two points around the symmetric axis, we decide to calculate blood flow by using the values of the outlet and entrance of blood vessels. We take the flow function of the central position of the vessel at the entrance of the aorta as Ψ_1, where $X = 0$ and $r = 0$, and take the flow function at the junction of heart and aorta as Ψ_1, where $x = 0$ and $r = R$. Thus, we obtain

$$\Psi_1 = 0,$$

$$\Psi_2 = \frac{1}{4} u_{\max} R^2 + \varepsilon^2 \exp\left(\frac{-\sqrt{\mu} \left(\varepsilon^2 t\right)^\alpha}{\Gamma(1+\alpha)} + \varepsilon c t\right) C_1 r \sqrt{\frac{a}{c}} J_1\left(r\sqrt{\frac{a}{c}}\right)$$

$$\cdot \sec h^2 \left[\left(\frac{a_1}{6a_2} \exp\left(\frac{-\sqrt{\mu} \left(\varepsilon^2 t\right)^\alpha}{\Gamma(1+\alpha)} + \varepsilon c t\right)\right)^{(1/2)} \left(-\varepsilon c t - \left(-\frac{2a_1}{3} \exp\left(\frac{-\sqrt{\mu} \left(\varepsilon^2 t\right)^\alpha}{\Gamma(1+\alpha)} + \varepsilon c t\right)\right)^{(1/2)} \frac{\left(\varepsilon^2 t\right)^\alpha}{\Gamma(1+\alpha)}\right) + \tilde{c}\right].$$
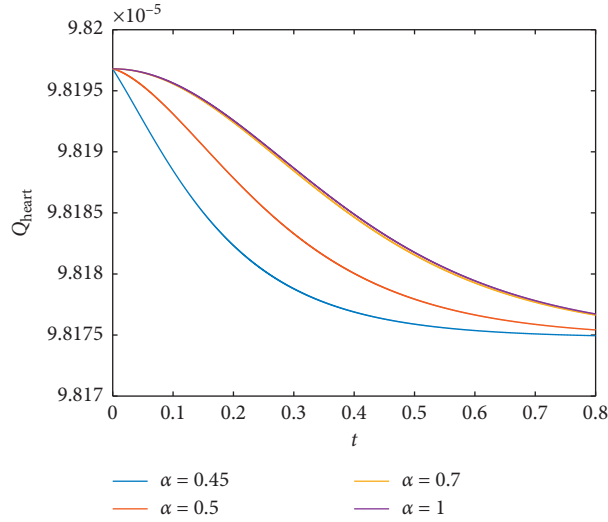
(61)

FIGURE 4: The blood flow volume of cardiac outlet at the different values of time and α ($\widetilde{c} = 0$).

Thus, the blood flow at the outlet of the heart can be expressed as

$$
\begin{aligned}
Q_{\text{heart}} = {} & \frac{1}{2}\pi u_{\max} R^2 + 2\pi\varepsilon^2 \exp\left(\frac{-\sqrt{\mu}\,(\varepsilon^2 t)^{\alpha}}{\Gamma(1+\alpha)} + \varepsilon c t\right) C_1 R \sqrt{\frac{a}{c}} J_1\left(R\sqrt{\frac{a}{c}}\right) \\
& \cdot \sec h^2\left[\left(\frac{a_1}{6a_2}\exp\left(\frac{-\sqrt{\mu}\,(\varepsilon^2 t)^{\alpha}}{\Gamma(1+\alpha)} + \varepsilon c t\right)\right)^{(1/2)}\left(-\varepsilon c t + \left(\frac{2a_1}{3}\exp\left(\frac{-\sqrt{\mu}\,(\varepsilon^2 t)^{\alpha}}{\Gamma(1+\alpha)} + \varepsilon c t\right)\right)^{(1/2)}\frac{(\varepsilon^2 t)^{\alpha}}{\Gamma(1+\alpha)}\right) + \widetilde{c}\right].
\end{aligned}
\tag{62}
$$

In a cardiac cycle, the time-dependent image of the blood flow volume of the cardiac outlet is shown in Figure 4.

From Figure 4, we can see that, when α is smaller, this model can be used to describe people with less blood flow or faster blood flow conduction. And when α is large, this model can be used to describe people with slow blood flow in the body, or blood output from the heart is not easy to circulate throughout the body. These people may have lesions in some parts of the blood vessels, causing obstruction to blood flow. Or they are in good physical condition, but they are at high risk of cardiovascular and cerebrovascular diseases. Furthermore, we can find the appropriate value of α to describe different populations by combining the actual monitoring data.

As we all know, stroke volume of healthy people is basically stable. When stroke volume is not stable for a long time, we can infer that there may be something wrong with that person's cardiovascular system. If the amount of stroke volume is smaller, it will lead to insufficient oxygen supply to other tissues and organs. On the contrary, when stroke volume is too large, it will increase the load of human blood vessels, thus causing some cardiovascular and cerebrovascular diseases. According to the above introduction, we can find that stroke volume in each cycle of the heart is an important index which can reflect the health status of human

cardiovascular system. Thus, we give the description of the stroke volume as follows:

$$
V = \int_0^{\widetilde{T}} Q_{\text{heart}} \mathrm{d}t,
\tag{63}
$$

where $\widetilde{T}$ represents the pulsatile cycle of the heart. By calculating, with $u_{\max} = 0.4$ and $R = 1.25 \times 10^{-2}$, we obtain the stroke volume in each cycle of the heart as 78.54 ml which is close to the theoretical calculation value 78.5 ml. Therefore, this model can well reflect the actual blood flow of the human body.

Considering that there is always a certain degree of difference in genetic characteristics of different people, it is easy to misjudge the disease condition if we use a unified health standard to measure the population with different characteristics. Thus, we consider to yield several different standards which can be used to measure the health of different groups of people by adjusting the value of fractional order α. Figure 5 shows that the stroke volume increases with the increase of α. V has a larger growth rate in the range of α value from 0.4 to 0.8, while it grows slowly in other value ranges. Thus, we can consider selecting the appropriate value of α from 0.4 to 0.8 with the actual test data.
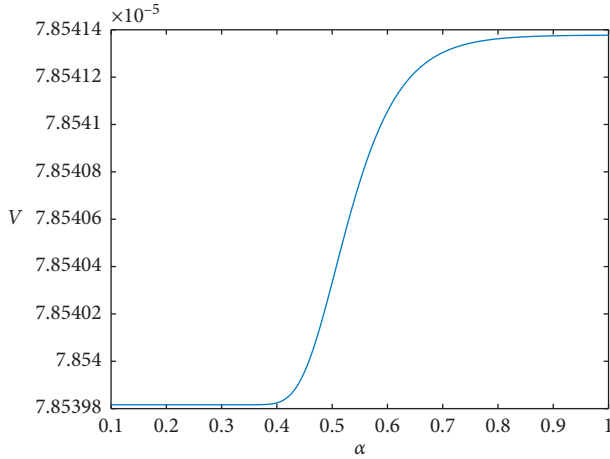
FIGURE 5: Relationship between fractional order and stroke volume ($R = 1.25 \times 10^{-2}, u_{\max} = 0.4, \widetilde{c} = 0$).
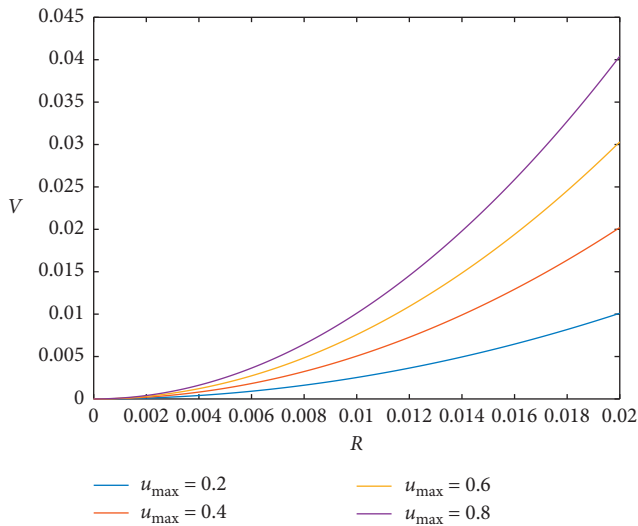

FIGURE 6: Relationship between blood vessel radius and stroke volume ($\alpha = 0.5, \widetilde{c} = 0$).

Because the radius of the blood vessel can influence stroke volume, we consider changing the value of R to get several results as shown in Figure 6.

In Figure 6, the values of α from bottom to top are 0.2, 0.4, 0.6, and 0.8. We can find that under the condition of the same vessel radius, stroke volume increases with the increase of the maximum velocity of blood vessel center. In addition, under the same $u_{\max}$, the value of V is also related to the size of the vascular radius. As the vessel radius increases, stroke volume increases as well.

6. Conclusion

In this paper, we derive time-fractional Boussinesq equation with viscous term to describe blood flow and discuss the effects of fractional order and viscosity on blood flow volume. This indicates that local hemodynamic factors play an important role in the occurrence and development of cardiovascular disease. Therefore, it is of great significance to study the changes of blood flow in blood vessels to reveal the pathogenesis of major vascular diseases.

Data Availability

No data were used to support the findings of the study.

Conflicts of Interest

The authors declare that there are no conflicts of interest regarding the publication of this paper.

Acknowledgments

References

[1] Q. Liu, R. Zhang, L. Yang, and J. Song, "A new model equation for nonlinear Rossby waves and some of its solutions," *Physics Letters A*, vol. 383, no. 6, pp. 514–525, 2019.

[2] R. Zhang, L. Yang, Q. Liu, and X. Yin, "Dynamics of nonlinear Rossby waves in zonally varying flow with spatial-temporal varying topography," *Applied Mathematics and Computation*, vol. 346, pp. 666–679, 2019.

[3] M. H. Gao, Y. F. Zhang, J. F. Wang, and H. W. Yang, "A new model for describing the gravity solitary wave in the atmosphere," *Mathematical Modeling and its Applications*, vol. 4, pp. 10–16, 2015.

[4] J. R. Womersley, "XXIV. Oscillatory motion of a viscous liquid in a thin-walled elastic tube-I: the linear approximation for long waves," *The London, Edinburgh, and Dublin Philosophical Magazine and Journal of Science*, vol. 46, no. 373, pp. 199–221, 1955.

[5] J. R. Womersley, "Oscillatory flow in arteries: the constrained elastic tube as a model of arterial flow and pulse transmission," *Physics in Medicine and Biology*, vol. 2, no. 2, pp. 178–187, 1957.

[6] D. A. McDonald, "The velocity of blood flow in the rabbit aorta studied with high-speed cinematography," *The Journal of Physiology*, vol. 118, no. 3, pp. 328–339, 1952.

[7] D. A. McDonald, "The relation of pulsatile pressure to flow in arteries," *The Journal of Physiology*, vol. 127, no. 3, pp. 533–552, 1955.

[8] R. Ravindran and P. Prasad, "A mathematical analysis of nonlinear waves in a fluid filled visco-elastic tube," *Acta Mechanica*, vol. 31, no. 3, pp. 253–280, 1979.

[9] Y. Sigeo, "Solitary waves in large blood vessels," *Journal of the Physical Society of Japan*, vol. 56, no. 2, pp. 506–520, 1987.

[10] Y. Hashizume, "Nonlinear pressure waves in a fluid-filled elastic tube," *Journal of the Physical Society of Japan*, vol. 54, no. 9, pp. 3305–3312, 1985.

[11] Z. R. Liu, G. Xu, Y. Chen, Z.-Z. Teng, and K.-R. Qin, "An analysis model of pulsatile blood flow in arteries," *Applied Mathematics and Mechanics*, vol. 24, no. 2, pp. 230–240, 2003.

[12] H. Demiray, "Wave propagation through a viscous fluid contained in a prestressed thin elastic tube," *International Journal of Engineering Science*, vol. 30, no. 11, pp. 1607–1620, 1992.

[13] H. Demiray, "Weakly nonlinear waves in a fluid with variable viscosity contained in a prestressed thin elastic tube," *Chaos, Solitons & Fractals*, vol. 36, no. 2, pp. 196–202, 2008.

[14] Y. Y. Choy, K. G. Tay, and C. T. Ong, "Modulation of nonlinear waves in an inviscid fluid (blood) contained in a stenosed artery," *Applied Mathematical Sciences*, vol. 7, pp. 5003–5012, 2013.

[15] S. A. El-Wakil, E. M. Abulwafa, M. A. Zahran, and A. A. Mahmoud, "Time-fractional KdV equation: formulation and solution using variational methods," *Nonlinear Dynamics*, vol. 65, no. 1-2, pp. 55–63, 2011.

[16] F. Riewe, "Mechanics with fractional derivatives," *Physical Review E*, vol. 55, no. 3, pp. 3582–3592, 1997.

[17] O. P. Agrawal, "Formulation of Euler-Lagrange equations for fractional variational problems," *Journal of Mathematical Analysis and Applications*, vol. 272, no. 1, pp. 368–379, 2002.

[18] O. P. Agrawal, "A general formulation and solution scheme for fractional optimal control problems," *Nonlinear Dynamics*, vol. 38, no. 1–4, pp. 323–337, 2004.

[19] J. C. Sun, Z. G. Zhang, H. H. Dong, and H. W. Yang, "Fractional order model and lump solution in dusty plasma," *Acta Physica Sinica*, vol. 68, no. 21, Article ID 210201, 2019.

[20] S. Y. Lukashchuk, "Conservation laws for time-fractional subdiffusion and diffusion-wave equations," *Nonlinear Dynamics*, vol. 80, no. 1-2, pp. 791–802, 2015.

[21] Q. S. Liu and L. G. Chen, "Time-Space fractional model for complex cylindrical ion-acoustic waves in ultrarelativistic plasmas," *Complexity*, vol. 2020, Article ID 9075823, 16 pages, 2020.

[22] Z. B. Bai, "The introduction to the fractional differential equation boundary value problems," *Mathematical Modeling and its Applications*, vol. 6, pp. 1–10, 2017.

[23] K. R. Raslan, K. K. Ali, and M. A. Shallal, "The modified extended tanh method with the Riccati equation for solving the space-time fractional EW and MEW equations," *Chaos, Solitons & Fractals*, vol. 103, pp. 404–409, 2017.

[24] O. Guner, A. Bekir, and H. Bilgil, "A note on exp-function method combined with complex transform method applied to fractional differential equations," *Advances in Nonlinear Analysis*, vol. 4, no. 3, pp. 201–208, 2015.

[25] S. Momani, Z. Odibat, and A. Alawneh, "Variational iteration method for solving the space-and time-fractional KdV equation," *Numerical Methods for Partial Differential Equations*, vol. 24, no. 1, pp. 262–271, 2008.

[26] N. Shang and B. Zheng, "Exact solutions for three fractional partial differential equations by the (G'/G) method," *International Journal of Applied Mathematics*, vol. 43, no. 3, pp. 1–6, 2013.

WILEY | Hindawi

Research Article

Dynamical Analyses on Beta Oscillations in a STN-GPE-GPI Model of Parkinson's Disease

Yuanhong Bi,[1,2] Quansheng Liu ,[3] Jingyi Zhao,[3] and Wuritu Yang[4]

[1]*School of Statistics and Mathematics, Inner Mongolia University of Finance and Economics, Hohhot 010070, China*
[2]*Inner Mongolia Key Laboratory for Economic Data Analysis and Mining, Hohhot 010070, China*
[3]*School of Mathematical Sciences, Inner Mongolia University, Hohhot 010021, China*
[4]*State Key Laboratory of Reproductive Regulation and Breeding of Grassland Livestock, College of Life Sciences, Inner Mongolia University, Hohhot 010021, China*

Correspondence should be addressed to Quansheng Liu; smslqs@imu.edu.cn

Exploring the behaviors of beta oscillations in the basal ganglia is helpful to understand the mechanism of Parkinson's disease. Studies have shown that the external and internal segments (GPe, GPi) of the globus pallidus receive different intensities of signals from the striatum in Parkinson's disease and play different roles in the production of beta oscillations, but the relevant mechanism still remains unclear. Based on a model of the subthalamic nucleus (STN) and globus pallidus (GP), we propose an extended STN-GPe-GPi model and analyze the dynamical behaviors of beta oscillations in this model. The stability condition is obtained through theoretical analyses, and the generation of beta oscillations by the inputs from the cortex and striatum is further considered. The influence of some parameters related to GPi on its firing rate oscillations is discussed. The results obtained in this paper are expected to play a guiding role in the medical treatment of Parkinson's disease.

1. Introduction

Parkinson's disease is a chronic neurodegenerative disease with the symptoms of involuntary tremor of the hand and head, muscle rigidity, slow movement, and imbalance of posture [1]. The main pathological causes of Parkinson's disease ascribe to the loss of dopamine neurons in the basal ganglia [2], which consists of the striatum, globus pallidus (GP), subthalamic nucleus (STN), compacta (SNc), and reticular (SNr) structure of the substantia nigra [3–5]. The loss of dopamine neurons causes beta oscillations with frequencies ranging from 13 Hz to 30 Hz in the basal ganglia [6, 7]. Therefore, it is necessary for understanding the mechanism of Parkinson's disease to analyze the conditions of beta oscillations in the basal ganglia [8].

Many researches explored the origin of beta oscillations in the basal ganglia [9–12]. Van Albada et al. believed that oscillations originated from the cortical-thalamic loop and then spread to the basal ganglia with the development of the

disease [13]. Holgado et al. found that the STN-GP loop in the basal ganglia plays an important role in generating oscillations, which are related to connection weight and synaptic transmission time between STN and GP [14]. Furthermore, a model with two STN and one GP populations are considered to get the stability boundary of oscillations [15, 16]. However, GP population has not been divided into the external and internal segment (GPe and GPi) in the above models, where GPi is the main output structure of the basal ganglia and also used to treat dystonia by deep brain electrical stimulation in medicine [5]. Actually, GPi and GPe are affected by different intensities from striatum to result in Parkinson's disease. Therefore, it is necessary to add both GPe and GPi into the basal ganglia network.

Based on the above considerations, we introduce both GPe and GPi in the above model proposed by Holgado et al. as a new STN-GPe-GPi model. The mechanism of generating beta oscillations for the new model is explored through

theoretical analyses and numerical simulation. The model of STN-GPe-GPi loop is given in Section 2. Section 3 shows the results. Stability analyses and bifurcation for this model are given through theory analyses. Also, the effect of inputs from the cortex and striatum and some parameters related to GPi on beta oscillations is discussed in Section 4. Finally, the conclusion is given in Section 5.

2. Model

The model of STN- GPe-GPi loop , which is an extended STN-GP model, is considered here in order to understand the mechanism of Parkinson's disease. Actually, GP can be divided into two parts, GPe and GPi. They can receive different excitatory inputs from the cortex in Parkinson's disease, and GPi as the output part of the basal ganglia mainly affects the activity of neurons in thalamic and cortical areas. GPe and GPi receive inhibitory and excitatory stimulations from striatum and STN, respectively, but GPe sends inhibitory signal to GPi and STN. Besides, STN also receives excitatory stimulation from the cortex (see Figure 1).

The following firing rate equations are used to describe the dynamical behavior of the model, as shown in Figure 1 [17–18] :

$$
\tau_G G_1'(t) = F_G\left(-W_{GG}G_2\left(t - T_{GG}\right) + W_{SGI}S\left(t - T_{SGI}\right) \\ -W_{XG}\mathrm{Str}\right) - G_1(t),
\tag{1}
$$

$$
\tau_G G_2'(t) = F_G\left(W_{SGE}S\left(t - T_{SGE}\right) - W_{XG}\mathrm{Str}\right) - G_2(t),
\tag{2}
$$

$$
\tau_S S'(t) = F_S\left(-W_{GS}G_2\left(t - T_{GS}\right) + W_{CS}\mathrm{Ctx}\right) - S(t),
\tag{3}
$$

where $G_1(t)$, $G_2(t)$, and $S(t)$ represent the firing rate of GPi , GPe, and STN; τ_G and τ_S are time constants of GP and STN; W and T are synaptic connection weight and the delay of signal transmission between neural populations, respectively, W_{ij} and T_{ij} are connection weight and time delay between the neural populations i and j, W_{SGE}, W_{SGI}, T_{SGE}, and T_{SGI} denote connection weights and the time delays from STN to GPe and GPi, respectively, Str and Ctx are input constants from the striatum and cortex. F_S and F_G are activation functions of STN and GP, which are given by the following formulas [14]:

$$
F_S(x) = \frac{M_S}{1 + (M_S - B_S/B_S)\exp\left(-4x/M_S\right)},
$$

$$
F_G(x) = \frac{M_G}{1 + (M_G - B_G/B_G)\exp\left(-4x/M_G\right)},
\tag{4}
$$

where M_i is the maximum firing rate of neuron population i and B_i is the firing rate of neuron population i with no input. The activation functions $F_S(x)$ and $F_G(x)$ with their derivatives are shown in Figures 2(a) and 2(b), respectively.
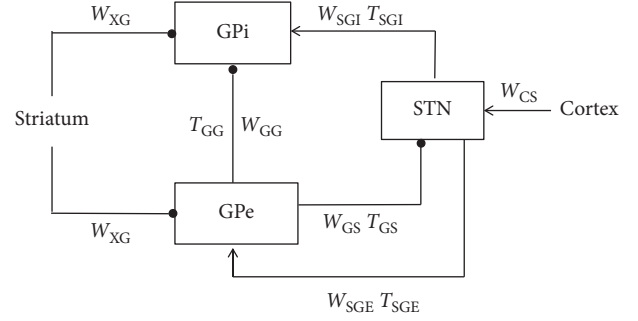

Figure 1: Schematic diagram of STN-GPe-GPi. Each rectangular represents neural population, arrows indicate excitatory inputs, lines ending with black dots mean inhibitory inputs, and the striatum and cortex represent their inputs, respectively.

The parameters and their source are given in Table 1, and the connection weights between neuron populations in healthy and disease states are given in Table 2. Figure 3 shows time series of the firing rate of healthy and disease states, which oscillates for Parkinson's disease and reaches the steady state in the healthy state.

3. Results and Discussion

3.1. Stability Analyses for the STN-GPE-GPI Model. In this section, we obtain the following equations (5)–(7) by simplifying equations (1)–(3) with $F(x) = x$ without inputs from the striatum and cortex and the identical τ and T:

$$
\tau G_1'(t) = -W_{GG}G_2(t - T) + W_{SGI}S(t - T) - G_1(t),
\tag{5}
$$

$$
\tau G_2'(t) = W_{SGE}S(t - T) - G_2(t),
\tag{6}
$$

$$
\tau S'(t) = -W_{GS}G_2(t - T) - S(t).
\tag{7}
$$

Equations (5)–(7) are given in matrix form as follows:

$$
\begin{pmatrix} G_1'(t) \\ G_2'(t) \\ S'(t) \end{pmatrix} + \begin{pmatrix} 0 & \dfrac{W_{GG}}{\tau} & -\dfrac{W_{SGI}}{\tau} \\ 0 & 0 & -\dfrac{W_{SGE}}{\tau} \\ 0 & \dfrac{W_{GS}}{\tau} & 0 \end{pmatrix} \begin{pmatrix} G_1(t - T) \\ G_2(t - T) \\ S(t - T) \end{pmatrix}
$$

$$
+ \begin{pmatrix} \dfrac{1}{\tau} & 0 & 0 \\ 0 & \dfrac{1}{\tau} & 0 \\ 0 & 0 & \dfrac{1}{\tau} \end{pmatrix} \begin{pmatrix} G_1(t) \\ G_2(t) \\ S(t) \end{pmatrix} = 0.
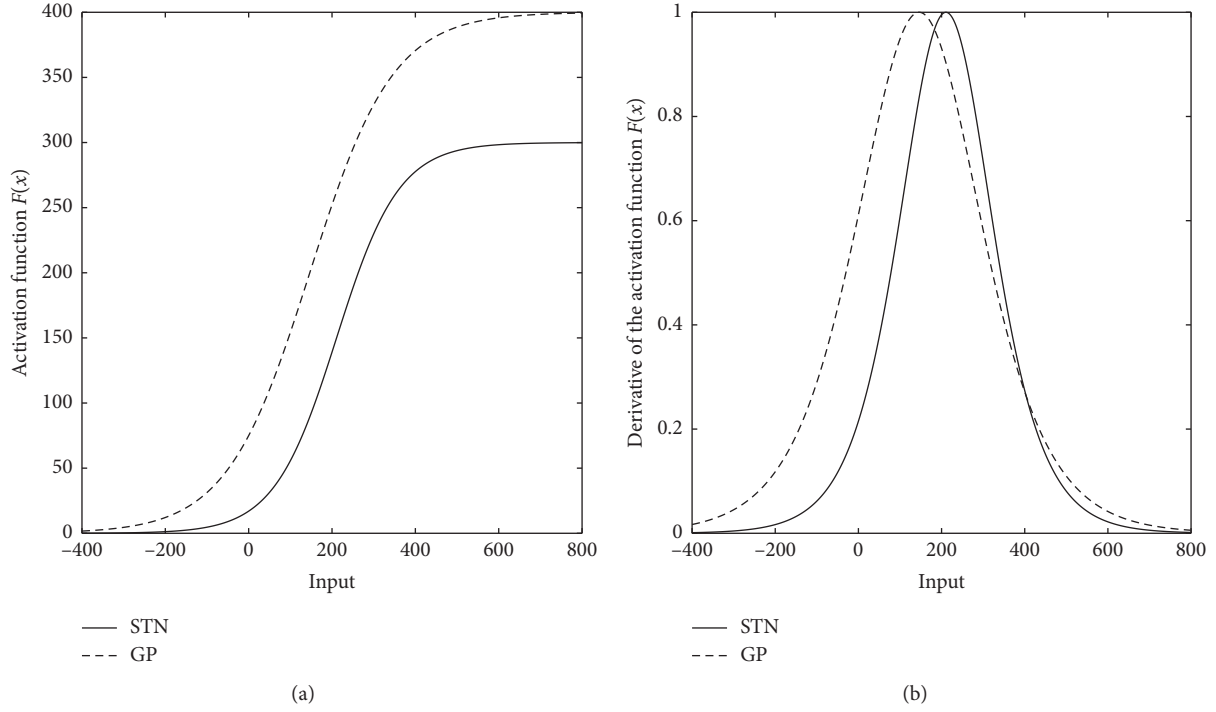\tag{8}
$$

FIGURE 2: (a) Curves of the activation functions $F_S(x)$ and $F_G(x)$. (b) Derivatives of activation functions $F_S(x)$ and $F_G(x)$.

TABLE 1: Parameter values in the model and their sources.

Parameter	Value	Reference
T	6 ms	[19, 20]
τ_S	6 ms	[21–23]
τ_G	14 ms	[24]
Ctx	27 spk/s	[25]
Str	2 spk/s	[26]
M_S	300 spk/s	[27]
B_S	17 spk/s	[27]
M_G	400 spk/s	[20, 28]
B_G	75 spk/s	[28, 29]

TABLE 2: Connection weights between neurons in different states.

Parameter	Healthy state	Parkinson's disease
W_{GS}	1.12	10.7
W_{SGE}	19.0	20.0
W_{SGI}	19.0	20.0
W_{GG}	6.60	12.3
W_{CS}	2.42	9.2
W_{GG}	15.1	139.4

Let

$$A = \begin{pmatrix} 0 & \dfrac{W_{GG}}{\tau} & -\dfrac{W_{SGI}}{\tau} \\ 0 & 0 & \dfrac{W_{SGE}}{\tau} \\ 0 & \dfrac{W_{GS}}{\tau} & 0 \end{pmatrix},$$

$$B = \begin{pmatrix} \dfrac{1}{\tau} & 0 & 0 \\ 0 & \dfrac{1}{\tau} & 0 \\ 0 & 0 & \dfrac{1}{\tau} \end{pmatrix}.$$
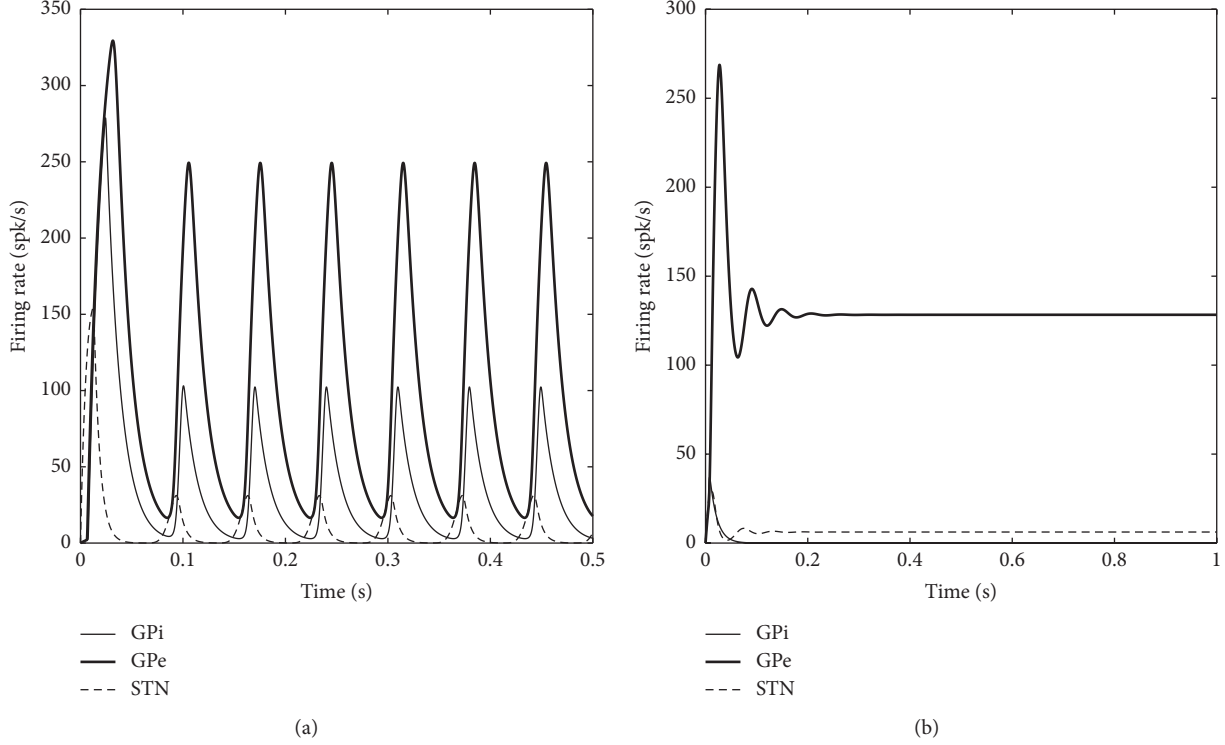
(9)

Using Laplace transform [30],

(a)

(b)

FIGURE 3: Time series of systems (1)–(3): (a) Parkinson's disease and (b) healthy state.

$$L[f(t - T)] = e^{-sT}F(s),$$
$$L[f(t)] = F(s), \tag{10}$$
$$L[f\prime(t)] = sF(s) - F(0).$$

Equation (8) can be given as follows:

$$s\begin{pmatrix} G_1(s) \\ G_2(s) \\ S(s) \end{pmatrix} - \begin{pmatrix} G_1(0) \\ G_2(0) \\ S(0) \end{pmatrix} + Ae^{-sT}\begin{pmatrix} G_1(s) \\ G_2(s) \\ S(s) \end{pmatrix} + B\begin{pmatrix} G_1(s) \\ G_2(s) \\ S(s) \end{pmatrix} = 0. \tag{11}$$

Without loss of generality, let

$$\begin{pmatrix} G_1(0) \\ G_2(0) \\ S(0) \end{pmatrix} = 0. \tag{12}$$

Then,

$$sI + Ae^{-sT} + B = 0, \tag{13}$$

where S is the eigenvalue of the characteristic equation and I is the unit matrix. Taking the determinant on both sides of matrix (13),

$$\det\left(sI + Ae^{-sT} + B\right) = 0, \tag{14}$$

then

$$\left(s + \frac{1}{\tau}\right)^3 + \frac{W_{GS}W_{SGE}}{\tau^2}\left(s + \frac{1}{\tau}\right)e^{-2sT}$$
$$= \left(s + \frac{1}{\tau}\right)\left[\left(s + \frac{1}{\tau}\right)^2 + \frac{W_{GS}W_{SGE}}{\tau^2}e^{-2sT}\right] = 0. \tag{15}$$

$s \neq (-1/\tau)$, so

$$\left(s + \frac{1}{\tau}\right)^2 + \frac{W_{GS}W_{SGE}}{\tau^2}e^{-2sT} = 0. \tag{16}$$

Let $s = i\lambda$ and e^{-2sT} be expanded by Euler transformation, and equation (16) is changed into

$$-\lambda^2 + \frac{1}{\tau^2} + \frac{2i\lambda}{\tau} + \frac{W_{GS}W_{SGE}}{\tau^2}(\cos 2\lambda T - i\sin 2\lambda T) = 0. \tag{17}$$

For simplification, let $\tau = 1$ and $\widehat{T} = T/\tau$, equation (17) can be written as follows:

$$-\lambda^2 + 1 + 2i\lambda + W_{GS}W_{SGE}(\cos 2\lambda\widehat{T} - i\sin 2\lambda\widehat{T}) = 0. \tag{18}$$

Let the real part and the imaginary part be zero, respectively:
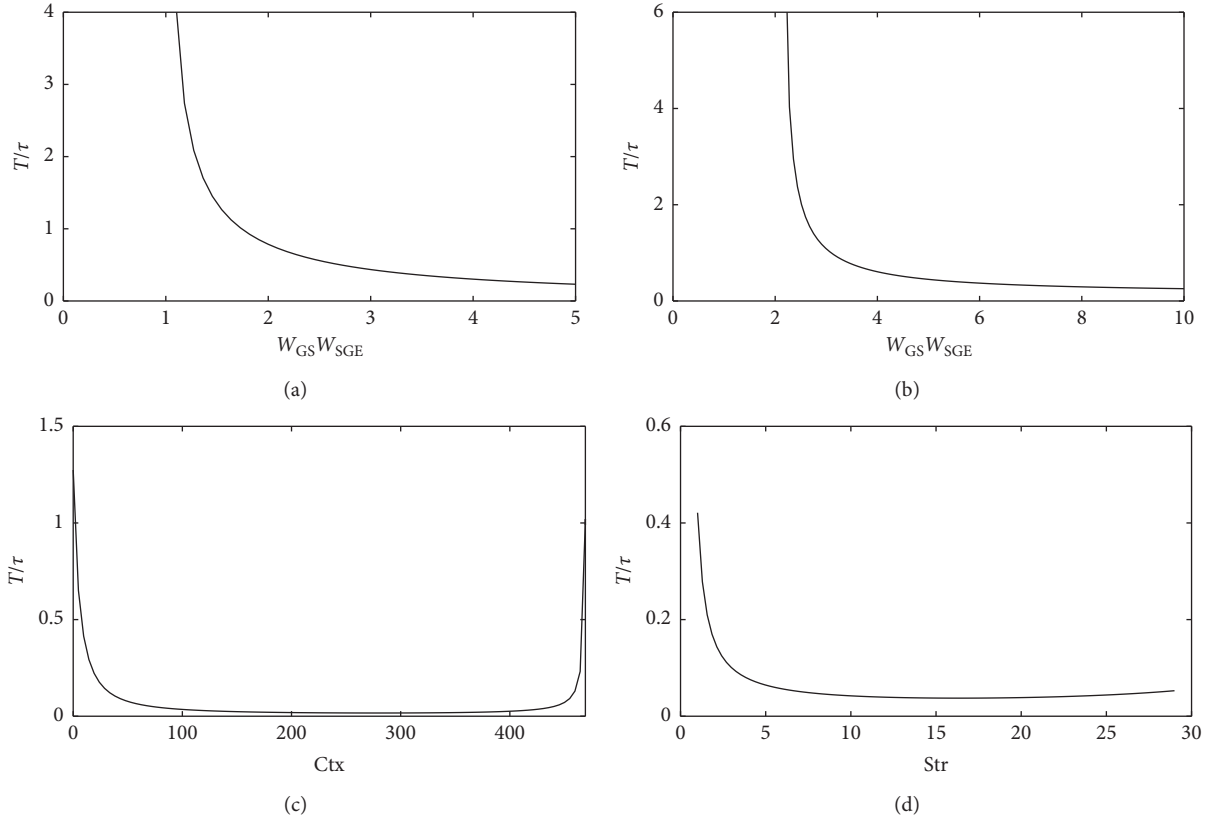
(a)

(b)

(c)

(d)

FIGURE 4: (a) Stability boundary curve for the linear system; (b) stability boundary for the nonlinear system; (c) the effect of cortical input on oscillation; (d) the effect of the striatum input on the oscillation. Ctx and Str denote the inputs from the cortex and striatum.

$$-\lambda^2 + 1 + W_{GS}W_{SGE} \cos 2\lambda\widehat{T} = 0, \tag{19}$$

$$2\lambda - W_{GS}W_{SGE} \sin 2\lambda\widehat{T} = 0. \tag{20}$$

Add the squares of (19) and (20) to get the following equation:

$$\lambda = \sqrt{W_{GS}W_{SGE} - 1}. \tag{21}$$

Bring equation (21) into equation (19), and we get stability boundary of the linear system:

$$\widehat{T} = \frac{1}{2\sqrt{W_{GS}W_{SGE} - 1}} \arccos\left(1 - \frac{2}{W_{GS}W_{SGE}}\right). \tag{22}$$

So, the linear model equations (5)–(7) oscillate at the following condition:

$$\frac{T}{\tau} > \frac{1}{2\sqrt{W_{GS}W_{SGE} - 1}} \arccos\left(1 - \frac{2}{W_{GS}W_{SGE}}\right). \tag{23}$$

3.2. Stability Analysis for the Nonlinear Model. For the nonlinear model with activation functions, we linearize the activation functions at the steady state (G_1^*, G_2^*, S^*) and get the characteristic equation (24) in a matrix form based on the steps in Section 3.1.

$$\det\left(sI + A_1 e^{-s\widehat{T}} + B\right) = 0, \tag{24}$$

where

$$A_1 = \begin{pmatrix} 0 & -F'_{G_1^*}\dfrac{W_{GG}}{\tau} & F'_{G_1^*}\dfrac{W_{SGI}}{\tau} \\[2mm] 0 & 0 & F'_{G_2^*}\dfrac{W_{SGE}}{\tau} \\[2mm] 0 & -F'_{S^*}\dfrac{W_{GS}}{\tau} & 0 \end{pmatrix},$$

$$B = \begin{pmatrix} \dfrac{1}{\tau} & 0 & 0 \\[2mm] 0 & \dfrac{1}{\tau} & 0 \\[2mm] 0 & 0 & \dfrac{1}{\tau} \end{pmatrix}, \tag{25}$$

$$F'_{G_1^*} = F'_{G_1}\left(-W_{GG}G_2^* + W_{SGI}S^* - W_{XG}Str\right),$$

$$F'_{G_2^*} = F'_{G_2}\left(W_{SGE}S^* - W_{XG}Str\right),$$

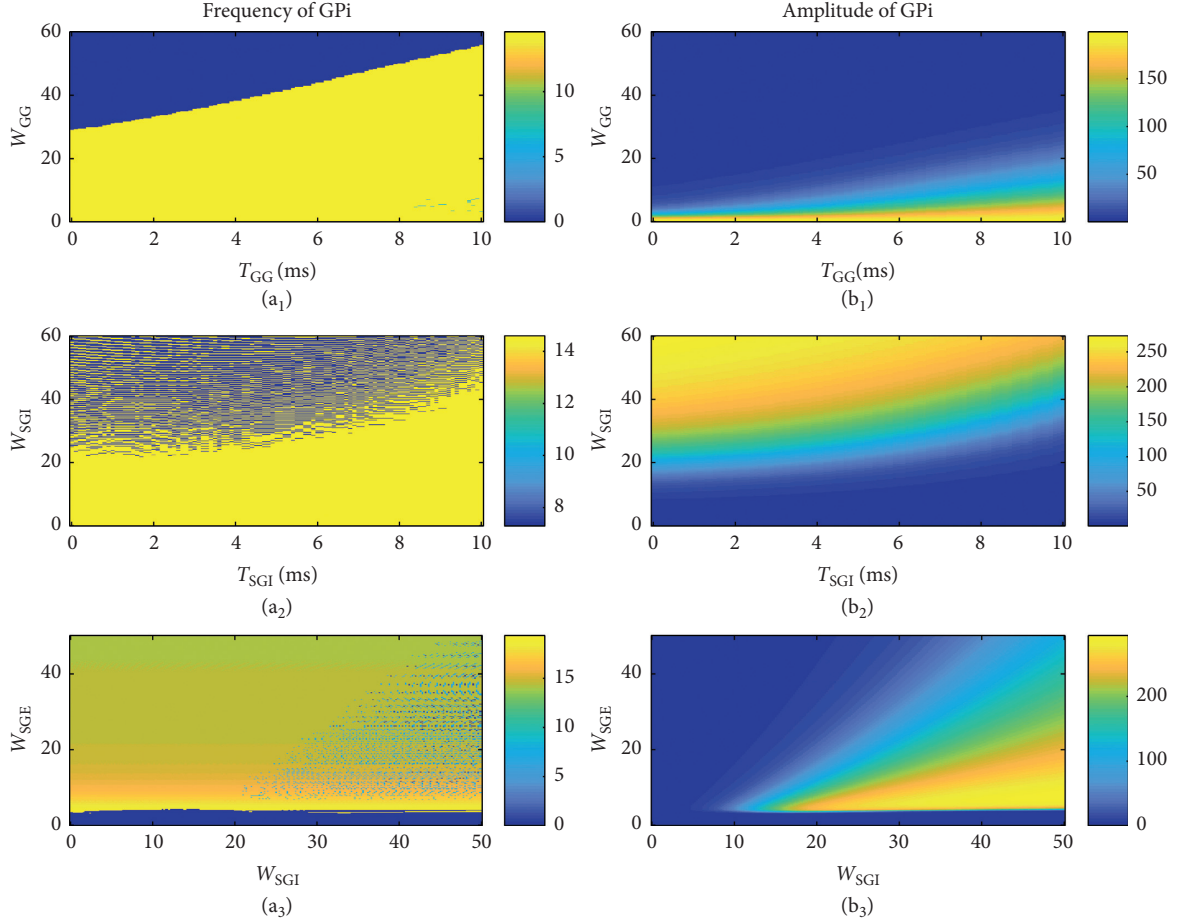$$F'_{S^*} = F_S^*\left(-W_{GS}G_2^* + W_{CS}Ctx\right).$$

FIGURE 5: The effect of $W_{GG} - T_{GG}$, $W_{SGI} - T_{SGI}$, and $W_{SGE} - W_{SGI}$ on the frequency of the GPi firing rate (a$_1$)–(a$_3$) and the amplitude of GPi (b$_1$)–(b$_3$). Other parameters are taken from Parkinson's state in Table 2.

Therefore, the stability boundary of the nonlinear model is as follows:

$$\widehat{T} = \frac{1}{2\sqrt{F'_{S^*}W_{GS}F'_{G_2^*}W_{SGE} - 1}} \arccos\left(1 - \frac{2}{F'_{S^*}W_{GS}F'_{G_2^*}W_{SGE}}\right).$$

(26)

The oscillation condition is

$$\frac{T}{\tau} > \frac{1}{2\sqrt{F'_{S^*}W_{GS}F'_{G_2^*}W_{SGE} - 1}} \arccos\left(1 - \frac{2}{F'_{S^*}W_{GS}F'_{G_2^*}W_{SGE}}\right).$$

(27)

We analyze the stability of the model shown in Figure 1 and get the stability conditions equations (22) and (26) for the linear and nonlinear model, respectively. Next, we draw the stability boundary curves of equations (22) and (26) and explore the effect of the inputs from the striatum and cortex on oscillation through numerical simulation.

3.3. Numerical Simulation of Stability Conditions. Figures 4(a) and 4(b) describe the stability boundary curves of linear and nonlinear models based on equations (22) and (26),

respectively. The decreasing boundary curve is infinitely close to x-axis with the increase of $W_{GS}W_{SGE} \longrightarrow \infty$. The system oscillates for parameter values above the curve while it is stable for ones below the curve. However, the nonlinear system oscillate for a larger weight $W_{GS}W_{SGE}$ than the one of linear system at the same T/τ.

Figures 4(c) and 4(d), respectively, show the influence of the inputs from the cortex and striatum on the stability of the nonlinear system. The boundary curve of the cortex is in the shape of "U," where the system will oscillate in the area of above "U" and it will reach a stable steady state in the area below "U." While the boundary curve of the striatum decreases to x-axis with the increase of the input of the striatum.

4. The Effect of Parameters Related to GPI on Frequency and Amplitude of Nonlinear Model Oscillation

In this section, the effect of three groups of parameters related to GPi, $W_{GG} - T_{GG}$, $W_{SGI} - T_{SGI}$, and $W_{SGE} - W_{SGI}$, on oscillation frequency (Figures 5 (a$_1$)–(a$_3$)) and amplitude (Figures 5 (b$_1$)–(b$_3$)) are also considered. Besides, time series of the GPI firing rate are given in Figure 6 for typical parameter values in each group of parameters in order to clearly see the
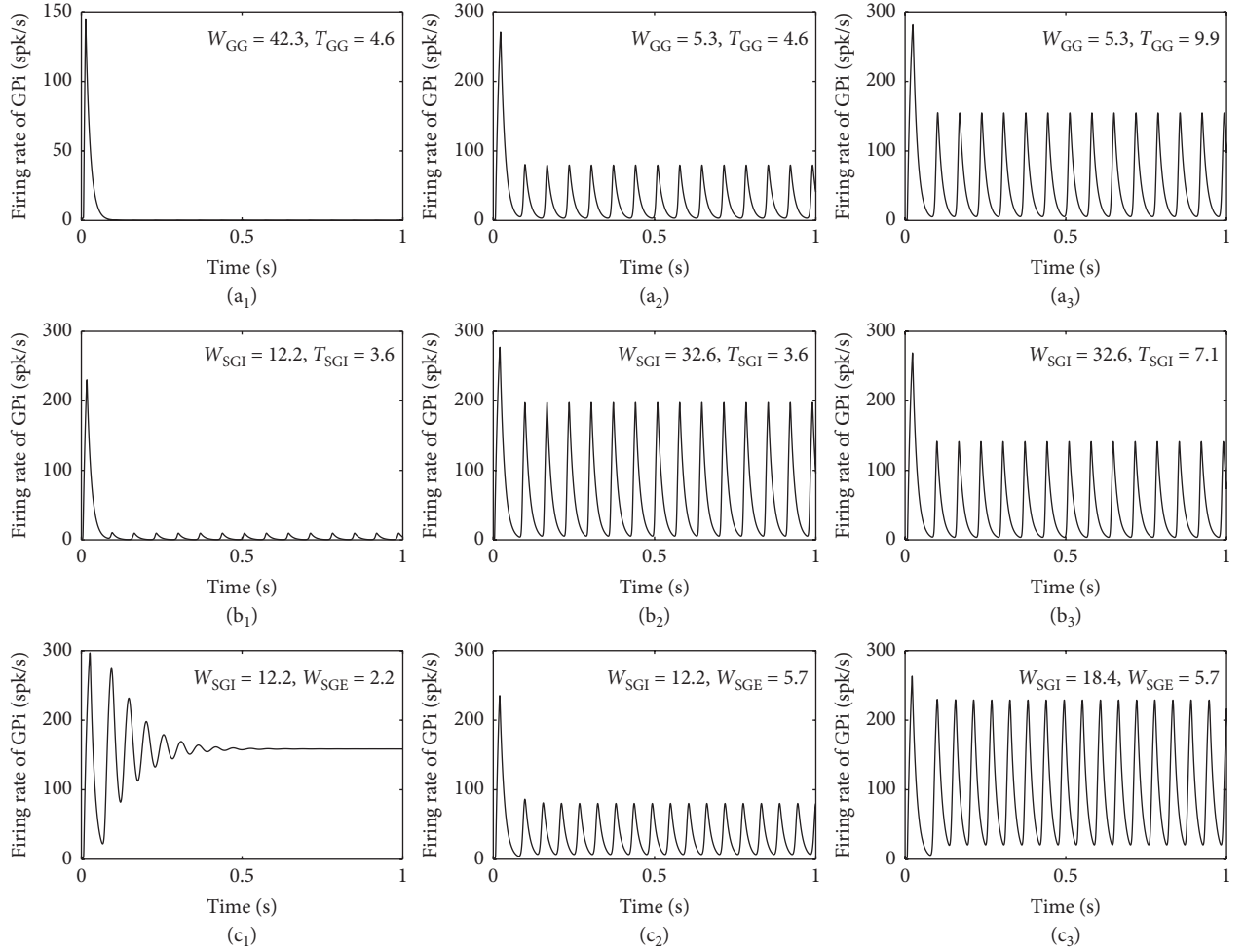
Figure 6: Typical time series of the firing rate of GPi for some parameters: (a$_1$)–(a$_3$) $W_{GG} - T_{GG}$, (b$_1$)–(b$_3$) $W_{SGI} - T_{SGI}$, and (c$_1$)–(c$_3$) $W_{SGE} - W_{SGI}$.

influence of these parameters on the frequency and amplitude of GPi oscillation. We set the frequency of the stable steady state to be 0. As can be seen from Figures 5 (a$_1$) and (b$_1$), the plane is divided into two parts, where the firing rate of GPi reaches a steady state for parameters taken in the blue area of the upper half while it will oscillate for parameters taken in the red area of the lower half. Frequency of oscillation with 14 Hz almost is not affected by W_{GG} and T_{GG}, while smaller W_{GG} and larger T_{GG} increase the amplitude of oscillation to 180. Figures 5 (a$_2$) and (b$_2$) shows that the firing rate of GPi always oscillates with beta frequency band of about 14 Hz and lower amplitudes for $W_{SGI} < 20$ otherwise alpha oscillations with frequency of 8 Hz–12 Hz and higher amplitude for $W_{SGI} > 20$. Besides, Figure 5 (a$_3$) shows that the firing rate of GPi reaches the steady state for smaller W_{SGE} ($W_{SGE} < 3.0$) while it oscillates for large W_{SGE} ($W_{SGE} > 3.0$), where the frequency and amplitude increase for smaller W_{SGE} and larger W_{SGI}.

Furthermore, time series of the GPi firing rate are given in Figure 6 for three pairs of parameters from each group of parameter plane in Figure 5 to clearly see the influence of these parameters on the frequency and amplitude of the GPi firing rate. It can be seen from Figures 6 (a$_1$)–(a$_3$) that the firing rate of GPi oscillates for smaller W_{GG} and larger T_{GG}.

According to Figures 6 (b$_1$)–(b$_3$), the firing rate of GPi always oscillates with smaller amplitude and larger frequency for smaller W_{SGI} and T_{SGI} while the case is opposite for larger W_{SGI} and T_{SGI}. Figures 6 (c$_1$)–(c$_3$) show that larger W_{SGE} makes the firing rate of GPi oscillate and larger W_{SGI} increases the amplitude of oscillation.

To sum up, the connection weights between neurons have a great influence on oscillation of the GPi firing rate, where smaller W_{GG} and larger W_{SGE}, W_{SGI} easily induce the oscillation of the GPi firing rate. However, transmission delays between neurons affect the amplitude of the GPi firing rate, where larger T_{GG} and smaller T_{SGI} will increase the amplitude.

5. Conclusions

Analyzing the conditions of beta oscillation in the basal ganglia is helpful to understand the mechanism of Parkinson's disease. In this paper, we analyze the conditions of beta oscillation in the STN-GPe-GPi model for different cases. First, stability analyses give stability boundary condition equations (22) and (26) for the linear system and nonlinear system, respectively, which are shown in

Figures 4(a) and 4(b). The nonlinear system oscillates for larger connection weight than the one of the linear system due to activation function. In addition, we consider the influence of the cortex and striatum as external input of the STN-GPe-GPi loop on the stability boundary of the nonlinear system. As can be seen from Figures 4(c) and 4(d), the nonlinear system is in the state of oscillation for $100 < \text{ctx} < 400$ or $5 < \text{str} < 25$. Comparing with the results in [15], the stability boundary system in this model moves to the right and other results almost are consistent with the ones in [15]. Furthermore, it can be seen from numerical simulation that the influence of the connection weights and delays is related to GPi on its oscillation. Smaller connection weight from GPe to GPi (W_{GG}) and larger one from STN to GPe (W_{SGE}) make the system oscillate easily, regardless of connection weight (W_{SGI}) and transmission delay (T_{SGI}) from STN to GPi. We hope that the results may provide guidance for the therapy of reducing pathological oscillations of PD, especially for the operation of the region related to GPi. However, it is necessary to consider a more complete neural network related to Parkinson's disease and explore the conditions of beta oscillation in response to different time delay, noise, and temperature [31]. Furthermore, we will investigate the pathogenesis of Parkinson's disease from the perspective of systems' biology in the future [32].

Data Availability

The data used to support the findings of the study can be obtained from the link https://pan.baidu.com/s/1HCTdFTukmkp29_kushR6Bg (password: hypg) and from the corresponding author upon request.

Conflicts of Interest

The authors declare that there are no conflicts of interest regarding the publication of this paper.

Acknowledgments

References

[1] R. J. Moran, N. Mallet, V. Litvak et al., "Alterations in brain connectivity underlying beta oscillations in parkinsonism," *PloS Computational Biology*, vol. 7, no. 8, Article ID e1002124, 2011.

[2] T. Boraud, P. Brown, J. A. Goldberg et al., *The Basal Ganglia VIII*, Springer, New York, NY, USA, 2005.

[3] G. Porenta, "A computer model of neuronal pathways in the basal ganglia," *Computer Methods and Programs in Biomedicine*, vol. 22, no. 3, pp. 325–331, 1986.

[4] B. Degos, J.-M. Deniau, B. Degos, and C. Bosch, "Evidence for a direct subthalamo-cortical loop circuit in the rat," *Journal of Neuroscience*, vol. 27, no. 10, pp. 2599–2610, 2008.

[5] F. Liu, J. Wang, C. Liu et al., "A neural mass model of basal ganglia nuclei simulates pathological beta rhythm in parkinson's disease," *Chaos: An Interdisciplinary Journal of Nonlinear Science*, vol. 26, no. 12, p. 123113, 2016.

[6] N. Mallet, A. Pogosyan, L. F. Marton et al., "Parkinsonian beta oscillations in the external globus pallidus and their relationship with subthalamic nucleus activity," *Journal of Neuroscience*, vol. 28, no. 52, pp. 14245–14258, 2008.

[7] P. J. Magill, A. Pogosyan, A. Sharott, J. Csicsvari, J. P. Bolam, and P. Brown, "Changes in functional connectivity within the rat striatopallida axis during global brain activation in vivo," *The Journal of Neuroscience*, vol. 26, no. 23, pp. 6318–6329, 2006.

[8] R. Bogacz, *Basal Ganglia: Beta Oscillations*, Springer, New York, NY, USA, 2015.

[9] A. J. Nevado-Holgado, N. Mallet, P. J. Magill et al., "Effective connectivity of the subthalamic nucleus –globus pallidus network during parkinsonian oscillations," *Journal of Physiology*, vol. 592, no. 7, pp. 1429–1455, 2014.

[10] H. Yan and J. Wang, "Quantification of motor network dynamics in parkinson's disease by means of landscape and flux theory," *PLoS One*, vol. 12, no. 3, pp. 1–21, 2017.

[11] J. E. Rubin, "Computational models of basal ganglia dysfunction: the dynamics is in the details," *Current Opinion in Neurobiology*, vol. 46, pp. 127–135, 2017.

[12] Y. Yu and Q. Y. Wang, "Oscillation dynamics in an extended model of thalamic-basal ganglia," *Nonlinear Dynamics*, vol. 98, no. 4, pp. 1065–1080, 2019.

[13] S. J. Van Albada, R. T. Gray, P. M. Drysdale, and P. A. Robinson, "Mean-field modeling of the basal ganglia-thalamocortical system. II," *Journal of Theoretical Biology*, vol. 257, no. 4, pp. 664–688, 2009.

[14] A. J. N. Holgado, J. R. Terry, and R. Bogacz, "Conditions for the generation of beta oscillations in the subthalamic nucleus-globus pallidus network," *Journal of Neuroscience*, vol. 30, no. 37, pp. 12340–12352, 2010.

[15] B. Hu and Q. Wang, "The conditions for onset of beta oscillations in an extended subthalamic nucleus-globus pallidus network," *Science China Technological Sciences*, vol. 57, no. 10, pp. 2020–2027, 2014.

[16] A. Pavlides, S. John Hogan, and R. Bogacz, "Improved conditions for the generation of beta oscillations in the subthalamic nucleus-globus pallidus network," *European Journal of Neuroscience*, vol. 36, no. 2, pp. 2229–2239, 2012.

[17] Y. H. Wang, *Stereotactic Neurosurgery*, People's Medical Publishing House, Beijing, China, 2005.

[18] P. Dayan and L. F. Abbott, *Theoretical Neuroscience*, pp. 7–16, MIT Press, Cambridge, MA, USA, 2001.

[19] T. P. Vogels, K. Rajan, and L. F. Abbott, "Neural network dynamics," *Annual Review of Neuroscience*, vol. 28, no. 1, pp. 357–376, 2005.

[20] K. Fujimoto and H. Kita, "Response characteristics of subthalamic neurons to the stimulation of the sensorimotor cortex in the rat," *Brain Research*, vol. 609, pp. 1-2, 1993.

[21] H. Kita, "Balance of monosynaptic excitatory and disynaptic inhibitory responses of the globus pallidus induced after stimulation of the subthalamic nucleus in the monkey," *Journal of Neuroscience*, vol. 25, no. 38, pp. 8611–8619, 2005.

[22] H. Kita, H. T. Chang, and S. T. Kitai, "Pallidal inputs to subthalamus: intracellular analysis," *Brain Research*, vol. 264, no. 2, pp. 255–265, 1983.

[23] H. Nakanishi, H. Kita, and S. T. Kitai, "Intracellular study of rat substantia nigra pars reticulata neurons in an in vitro slice preparation: electrical membrane properties and response

characteristics to subthalamic stimulation," *Brain Research*, vol. 437, no. 1, pp. 0–55, 1987.

[24] J. T. Paz and J. M. Deniau, "Rhythmic bursting in the cortico-subthalamo-pallidal network during spontaneous genetically determined spike and wave discharges," *Journal of Neuroscience*, vol. 25, no. 8, pp. 2092–2101, 2005.

[25] H. Kita and S. T. Kitai, "Intracellular study of rat globus pallidus neurons: membrane properties and responses to neostriatal, subthalamic and nigral stimulation," *Brain Research*, vol. 564, no. 2, pp. 296–305, 1991.

[26] M. A. Lebedev and S. P. Wise, "Oscillations in the premotor cortex: single-unit activity from awake, behaving monkeys," *Experimental Brain Research*, vol. 130, no. 2, pp. 195–215, 2000.

[27] W. Schultz and R. Romo, "Neuronal activity in the monkey striatum during the initiation of movements," *Experimental Brain Research*, vol. 71, no. 2, pp. 431–436, 1988.

[28] E. Nicholas, J. C. Wilson, and D. Mark, "Apamin-sensitive small conductance calcium-activated potassium channels, through their selective coupling to voltage-gated calcium channels, are critical determinants of the precision, pace, and pattern of action potential generation in rat subthalamic nucleus neurons in vitro," *Journal of Neuroscience*, vol. 23, no. 20, pp. 7525–7542, 2003.

[29] H. Kita, "Globus pallidus external segment," *Progress in Brain Research*, vol. 160, no. 1, pp. 111–133, 2007.

[30] H. Kita, A. Nambu, K. Kaneda, Y. Tachibana, and M. Takada, "Role of ionotropic glutamatergic and GABAergic inputs on the firing activity of neurons in the external pallidum in awake monkeys," *Journal of Neurophysiology*, vol. 92, no. 5, pp. 3069–3084, 2004.

[31] Y. Li and R. Y. Wei, "Dynamic analysis and synchronization control of the discrete coupled complex network model with delay and non-delay," *Mathematical Modeling and Its Applications*, vol. 6, no. 4, pp. 18–23, 2017.

[32] T. S. Zhou and Y. Tang, "Modeling and analysis of biomolecular systems," *Mathematical Modeling and Its Applications*, vol. 6, no. 1, pp. 1–12, 2017.

WILEY | Hindawi

Research Article

Dynamics Analysis of a Stochastic Hybrid Logistic Model with Delay and Two-Pulse Perturbations

Haokun Qi [ID] **and Hua Guo** [ID]

College of Mathematics and Systems Science, Shandong University of Science and Technology, Qingdao 266590, China

Correspondence should be addressed to Hua Guo; skd993121@sdust.edu.cn

In this paper, we propose and discuss a stochastic logistic model with delay, Markovian switching, Lévy jump, and two-pulse perturbations. First, sufficient criteria for extinction, nonpersistence in the mean, weak persistence, persistence in the mean, and stochastic permanence of the solution are gained. Then, we investigate the lower (upper) growth rate of the solutions. At last, we make use of Matlab to illustrate the main results and give an explanation of biological implications: the large stochastic disturbances are disadvantageous for the persistence of the population; excessive impulsive harvesting or toxin input can lead to extinction of the population.

1. Introduction

It is universally known that the logistic model is one of the most significant and classical models in mathematical biology. Many scholars have studied it and achieved fruitful results (see [1–8]). The classical logistic equation is expressed by

$$dX(t) = X(t)[r - a_1 X(t)]dt, \qquad (1)$$

where r and a_i $(i = 1, 2, 3)$ are non-negative constants. $\tau \geq 0$ is the time delay. $\varsigma(\theta)$ stands for a probability measure on $(-\infty, 0]$. $B(t)$ is the independent standard Brownian motion defined on a complete probability space $(\Omega, \mathcal{F}, \{\mathcal{F}_t\}_{t\geq 0}, \mathbb{P})$ and $\sigma \geq 0$ is the intensity of the white noise. $X(t^-)$ is the left limit of $X(t)$. $N(dt, dv)$ is a Poisson random measure with

where X denotes the population size and r and a_1 stand for the intrinsic growth rate and the intraspecific competition rate, respectively. With the improvement of the understanding of biological mathematical models, some factors have been considered, such as random interference, time delay, and so on. Compared with the classical original model, stochastic models (see [9–16]) can better reflect the actual situation. Based on model (1), we obtain the following stochastic model:

$$
\begin{aligned}
dX(t) = {}& X(t)\left(r - a_1 X(t) + a_2 X(t - \tau) + a_3 \int_{-\infty}^{0} X(t + \theta) d\varsigma(\theta) \right)dt \\
& + \sigma X(t)dB(t) + X(t^-) \int_{\mathbb{Y}} \gamma(v)\tilde{N}(dt, dv),
\end{aligned}
\qquad (2)
$$

characteristic measure λ on a measurable bounded below subset $\mathbb{Y}$ of $\mathbb{R}\backslash 0$ with $\lambda(\mathbb{Y}) < \infty$, γ is a Lévy measure such that $\tilde{N}(dt, dv) = N(dt, dv) - \lambda(dv)dt$.

In addition to the white noise and Lévy noise mentioned above, there are other noises in nature, such as telegraph noise, which can be expressed by continuous-time Markov

chain that mainly describes the random switching between two or more environment states [17] and which is different due to rainfall, nutrition, and other factors [18, 19]. Thus, a

series of articles about Markovian switching have been investigated (see [20–28]). We focus on the stochastic logistic model with Markovian switching:

$$
\begin{aligned}
dX(t) = X(t)&\left[r(\xi(t)) - a_1(\xi(t))X(t) + a_2(\xi(t))x(t-\tau) + a_3(\xi(t))\int_{-\infty}^{0} X(t+\theta)d\varsigma(\theta)\right]dt \\
&+ \sigma(\xi(t))X(t)dB(t) + X(t^-)\int_{\mathbb{Y}}\gamma((\xi(t)), v)\widetilde{N}(dt, dv),
\end{aligned}
\tag{3}
$$

where $\xi(t)$ is a continuous-time Markov chain with values in finite state space $\mathbb{M} = \{1, 2, \ldots, N\}$. We assume that $B(t)$ and $\xi(t)$ are independent.

As we all know human activities will have a significant impact on the population system, we must pay attention to the growing influence of human beings on population systems. The main manifestation of human activities is the regular harvesting of species or the regular stocking for the protection of endangered species, which cannot be considered continuously. Therefore, these phenomena can be described more accurately by the stochastic models with impulsive effects (see [29–34]).

On the other hand, human activities not only have a direct impact on the population but also have an indirect impact. The toxin produced by environmental pollution has

an indirect impact on the species. Environmental pollution caused by human activities has become an important issue that the world has to consider. Environmental pollution not only pollutes the atmosphere but also produces toxins that can enter into animals and plants, causing unimaginable harm to them; the light ones can make some populations die, and the heavy ones may cause species extinction. And these toxins will also accumulate in animals and plants. People transfer toxins in their bodies by eating the animals and plants, which can cause harm to human health. Therefore, it has become an inevitable trend to consider the influence of environmental toxins on the population (see [35–38]).

Based on the above discussion, we first consider the following stochastic hybrid logistic model with two-pulse perturbations:

$$
\left\{
\begin{aligned}
&dX(t) = X(t)\left[r(\xi(t)) - \alpha(\xi(t))C_0(t) - a_1(\xi(t))X(t) + a_2(\xi(t))X(t-\tau) + a_3(\xi(t))\int_{-\infty}^{0} X(t+\theta)d\varsigma(\theta)\right]dt \\
&\qquad\qquad + \sigma(\xi(t))X(t)dB(t) + X(t^-)\int_{\mathbb{Y}}\gamma((\xi(t)), v)\widetilde{N}(dt, dv), \\
&dC_0(t) = [kC_e(t) - (g+m)C_0(t)]dt, \\
&dC_e(t) = -hC_e(t)dt, \\
&\Delta X(t) = \delta_n X(t), \Delta C_0(t) = 0, \Delta C_e(t) = 0, \quad t = t_n, n \in \mathbb{Z}^+, \\
&\Delta X(t) = 0, \Delta C_0(t) = 0, \Delta C_e(t) = u, \quad t = nT, n \in \mathbb{Z}^+,
\end{aligned}
\right\}, \quad t \neq t_n, t \neq nT, n \in \mathbb{Z}^+,
\tag{4}
$$

where $C_0(t)$ and $C_e(t)$ represent the concentration of toxins in organism and in environment at time t, respectively. $\alpha \geq 0$ is the decreasing rate of the growth rate associated with the uptake of the toxins, $k > 0$ stands for the uptake rate of toxicant in the environment, $g > 0$ and $m > 0$ are the excretion rate and depuration rate, respectively, $h > 0$ is the loss rate of toxicant in the environment, and u stands for the toxin input amount at every time. Let $0 < t_1 < t_2 < \cdots$, $\lim_{n \to +\infty} t_n = +\infty$, $n \in \mathbb{Z}^+$, where $\mathbb{Z}^+$ is the set of positive integers. When $\delta_n > 0$, the impulsive effects imply releasing population, while if $\delta_n < 0$, the impulsive effects indicate harvesting for population. In this paper, we always suppose that $1 + \delta_n > 0$ for all $n \in \mathbb{Z}^+$.

The rest of the paper is organized as follows. In Section 2, we give some preliminaries. The existence and uniqueness of the global positive solution of the model are given in Section 3. The sufficient conditions for the

stochastic permanence and extinction are studied in Section 4. Some asymptotic properties of the solution are proved in Section 5. Finally, we give some numerical simulations to illustrate our results.

2. Preliminaries

Denote the generator $\Gamma = (\gamma_{kl})_{N \times N}$ of the Markov chain $\xi(t)$ given by

$$
\mathbb{P}(\xi(t+\Delta) = l \mid \xi(t) = k) = \begin{cases} \gamma_{kl}\Delta + o(\Delta), & \text{if } k \neq l, \\ 1 + \gamma_{kk}\Delta + o(\Delta), & \text{if } k = l, \end{cases}
\tag{5}
$$

where $\Delta > 0$, $\gamma_{kl} \geq 0$ if $k \neq l$ while $\sum_{l=1}^{N} \gamma_{kl} = 0$. When $\xi(t)$ is irreducible, then $\xi(t)$ has a unique stationary distribution $\pi = \{\pi_1, \pi_2, \ldots, \pi_N\}$ which is the solution of

$$\begin{cases} \pi\Gamma = 0, \\ \sum_{k=1}^{N} \pi_k = 1, \pi_k > 0, \quad \forall k \in \mathbb{M}. \end{cases} \tag{6}$$

Consider a stochastic differential delay equation (SDDE) with Markovian switching and Lévy noise (see [12]) as follows:

$$\begin{cases} dx(t) = f(x(t), x(t-\tau(t)), t, \xi(t))dt + g(x(t), x(t-\tau(t)), t, \xi(t))dB(t) + \int_{\mathbb{Y}} J(x(t^-), t, \xi(t), v)\widetilde{N}(dt, dv), \\ x(0) = x_0 \in L_{\mathscr{F}_0}([-\tau, 0]; \mathbb{R}^n), \\ \xi(0) = \xi_0 \in \mathbb{M}, \end{cases} \tag{7}$$

where $x(t) = (x_1(t), x_2(t), \ldots, x_n(t))^T \in \mathbb{R}^n$ is the state vector and $x(t-\tau(t)) = (x_1(t-\tau(t)), x_2(t-\tau(t)), \ldots, x_n(t-\tau(t)))^T \in \mathbb{R}^n$ is the delayed state vector. $x(t^-) = \lim_{s \to t} x(s)$. The time-varying delay $\tau(\cdot): \mathbb{R}_+ \longrightarrow [0, \tau]$ is a Borel measurable function. $f(\cdot, \cdot, \cdot, \cdot): \mathbb{R}^n \times \mathbb{R}^n \times \mathbb{R}_+ \times \mathbb{M} \longrightarrow \mathbb{R}^n$ is the drift coefficient vector, $g(\cdot, \cdot, \cdot, \cdot): \mathbb{R}^n \times \mathbb{R}^n \times$ $\mathbb{R}_+ \times \mathbb{M} \longrightarrow \mathbb{R}^{n \times n}$ is the diffusion coefficient matrix, and $J(\cdot, \cdot, \cdot, \cdot): \mathbb{R}^n \times \mathbb{R}^n \times \mathbb{M} \times \mathbb{Y} \longrightarrow \mathbb{R}^n$.

For each $k \in \mathbb{M}$, let $V(x, y, t, k) \in C^{1,2}(\mathbb{R}^n \times \mathbb{R}^n \times \mathbb{R}_+ \times \mathbb{M}; \mathbb{R}_+)$ be any twice continuously differentiable function; the operator $\mathscr{L}V(x, y, t, k): \mathbb{R}^n \times \mathbb{R}^n \times \mathbb{R}_+ \times \mathbb{M} \longrightarrow \mathbb{R}$ can be defined by

$$\mathscr{L}V(x, y, t, k) = V_t(x, t, k) + V_x(x, t, k)f(x, y, t, k)$$

$$+ \frac{1}{2}\text{trace}\left[g^T(x, y, t, k)V_{xx}(x, t, k)g(x, y, t, k)\right] \tag{8}$$

$$+ \int_{\mathbb{Y}}\left[V(x + J(x, t, k, v), t, k) - V(x, t, k) - J(x, t, k, v)V_x(x, t, k)\right]\lambda(dv) + \sum_{l=1}^{N}\gamma_{kl}V(x, t, k),$$

where

$$\begin{cases} V_t(x, t, k) = \dfrac{\partial V(x, t, k)}{\partial t}, \\ \\ V_x(x, t, k) = \left(\dfrac{\partial V(x, t, k)}{\partial x_1}, \dfrac{\partial V(x, t, k)}{\partial x_2}, \ldots, \dfrac{\partial V(x, t, k)}{\partial x_n}\right), \\ \\ V_{xx}(x, t, k) = \left(\dfrac{\partial^2 V(x, t, k)}{\partial x_i \partial x_j}\right)_{n \times n}. \end{cases} \tag{9}$$

Then, one has the generalized Itô's formula:

$$dV = \mathscr{L}V(x, y, t, k)dt + V_x(x, t, k)f(x, y, t, k)dB(t)$$

$$+ \int_{\mathbb{Y}}\ln(1 + J(x, t, k, v))\widetilde{N}(dt, dv). \tag{10}$$

Hypothesis 1 (locally Lipschitz condition). For any integer $h \geq 1$, there exists a constant $L_k > 0$ such that

$$|f(x, y, t, k) - f(\overline{x}, \overline{y}, \overline{t}, k)| \vee |g(x, y, t, k) - g(\overline{x}, \overline{t}, k)|$$

$$\leq L_k(|x - \overline{x}| + |y - \overline{y}|), \tag{11}$$

for those $x, y, \overline{x}, \overline{y} \in \mathbb{R}^n$ with $|x| \vee |y| \vee |\overline{x}| \vee |\overline{y}| \leq h$ and any $(t, k) \in [0, T] \times \mathbb{M}$.

Hypothesis 2 (linear growth condition). There is a constant $L > 0$ such that

$$|f(x, y, t, k)| \vee |g(x, y, t, k)| \leq L(1 + |x| + |y|), \tag{12}$$

for any $(x, y, t, k) \in \mathbb{R}^n \times \mathbb{R}^n \times \mathbb{R}_+ \times \mathbb{M}$.

Hypothesis 3. For each $\xi > 0$, there is a constant L_ξ that depends on ξ such that

$$\int_{\mathbb{Y}}|J(x, t, k, v) - J(y, t, k, v)|^2\lambda(dv) \leq L_\xi|x - y|^2, \tag{13}$$

with $|x| \vee |y| \leq \xi$.

Here, Hypotheses 1–3 are the conservative conditions to check the existence and uniqueness of the global solution of (7). In this paper, Hypotheses 1–3 are always satisfied.

For simplicity, denote some notations

$$
\begin{cases}
\langle f \rangle_t = \dfrac{1}{t} \displaystyle\int_0^t f(s)\mathrm{d}s, \quad t > 0, \\[2mm]
\widehat{g} = \min_{k \in \mathbb{M}}\{g(k)\}, \\[2mm]
\breve{g} = \max_{k \in \mathbb{M}}\{g(k)\}, \\[2mm]
f_* = \liminf_{t \longrightarrow +\infty} f(t), \\[2mm]
f^* = \limsup_{t \longrightarrow +\infty} f(t), \\[2mm]
b(k) = r(k) - \dfrac{\sigma^2(k)}{2} - \displaystyle\int_{\mathbb{Y}} [\gamma((k),v) - \ln(1+\gamma((k),v))]\lambda(\mathrm{d}v), \\[3mm]
\overline{b}(k) = 2r(k) - \sigma^2(k) - 2\displaystyle\int_{\mathbb{Y}}(\gamma((k),v))\lambda(\mathrm{d}v) - 2\alpha(k)C_0^*, \\[3mm]
\eta^* = \limsup_{t \longrightarrow +\infty} \dfrac{1}{t}\left[\displaystyle\sum_{0 < t_n < t} \ln(1+\delta_n)\right] + \displaystyle\sum_{k \in \mathbb{M}} \pi_k b(k), \eta_* = \liminf_{t \longrightarrow +\infty} \dfrac{1}{t}\left[\displaystyle\sum_{0 < t_n < t} \ln(1+\delta_n)\right] + \displaystyle\sum_{k \in \mathbb{M}} \pi_k b(k).
\end{cases}
\tag{14}
$$

In order to give the proof in this paper, we provide some assumptions.

A.1: there exists a constant $K_1 > 0$ such that

$$
\int_{\mathbb{Y}} \ln(1+\gamma((\xi(t)),v))^2 \lambda(\mathrm{d}v) \le K_1.
\tag{15}
$$

A.2: $1+\gamma((\xi(t)),v) > 0$, and there exists constant $K_2 > 0$ such that

$$
\int_{\mathbb{Y}} [\gamma((\xi(t)),v) - \ln(1+\gamma((\xi(t)),v))]\lambda(\mathrm{d}v) < K_2.
\tag{16}
$$

A.3: let the initial value $X = \beta$ be positive and $\beta \in C_g$ (see [31, 39]), which is defined by

$$
C_g = \left\{ \psi \in C((-\infty, 0]; \mathbb{R}_+): \|\psi\|_{C_g} = \sup_{-\infty < \theta \le 0} e^{r\theta}|\varphi(\theta)| < +\infty \right\}.
\tag{17}
$$

There exists a probability measure ρ and a constant $r > 0$ such that

$$
\rho_r = \int_{-\infty}^0 e^{-2r\theta}\mathrm{d}\varsigma(\theta) < +\infty.
\tag{18}
$$

A.4: $a = (\widehat{a}_1 - \breve{a}_2 - \breve{a}_3) > 0$.

A.5: there exist two positive constants m and M such that

$$
m \le \prod_{0 < t_n < t}(1+\delta_n) \le M.
\tag{19}
$$

A.6: $m\widehat{a}_1 > \max\{M(\breve{a}_2 + \breve{a}_3), M(\breve{a}_2 e^\tau + \breve{a}_3\rho_r)\}$.

We give some useful inequality in [40].

(1) (Exponential martingale inequality) Let T, α, β be any positive numbers. Then,

$$
\mathbb{P}\left\{ \sup_{0 \le t \le T}\left[\int_0^t g(s)\mathrm{d}B(s) - \frac{\alpha}{2}\int_0^t |g(s)|^2\mathrm{d}s \right] > \beta \right\} \le e^{-\alpha\beta}.
\tag{20}
$$

(2) (Chebyshev's inequality) If $c > 0$, $p > 0$, $X \in L^p$ $(\Omega, \mathbb{R}^d)$ which is the family of $\mathbb{R}^d$-valued random variables X with $\mathbb{E}|X|^p < \infty$. Then,

$$
\mathbb{P}\{\omega: |X(\omega)| \ge c\} \le c^{-p}\mathbb{E}|X|^p.
\tag{21}
$$

Next, we consider the following subsystem of system (4):

$$
\begin{cases}
\mathrm{d}C_0(t) = [kC_e(t) - (g+m)C_0(t)]\mathrm{d}t, \\
\mathrm{d}C_e(t) = -hC_e(t)\mathrm{d}t, \\
\Delta C_0(t) = 0, \Delta C_e(t) = u, t = nT,
\end{cases}
\begin{array}{l} t \ne nT, n \in \mathbb{Z}^+, \\[2mm] n \in \mathbb{Z}^+. \end{array}
\tag{22}
$$

From [38], we can get the following lemma.

Lemma 1 (see [38]). *System (22) has a unique globally asymptotical stable positive T-periodic solution $(\widetilde{C}_0(t), \widetilde{C}_e(t))^T$. If $C_0(0) > \widetilde{C}_0(0)$, $C_e(0) > \widetilde{C}_e(0)$, then $C_0(t) > \widetilde{C}_0(t)$, $C_e(t) > \widetilde{C}_e(t)$ for all $t \ge 0$, where*

$$\begin{cases} \widetilde{C}_0(t) = \widetilde{C}_0(0)e^{-(g+m)(t-nT)} + \dfrac{ku\left(e^{-(g+m)(t-nT)} - e^{-h(t-nT)}\right)}{(h-g-m)\left(1-e^{-hT}\right)}, \\[2ex] \widetilde{C}_0(0) = \dfrac{ku\left(e^{-(g+m)T} - e^{-hT}\right)}{(h-g-m)\left(1-e^{-(g+m)T}\right)\left(1-e^{-hT}\right)}, \\[2ex] \widetilde{C}_e(t) = \dfrac{ue^{-h(t-nT)}}{1-e^{-hT}}, \\[2ex] \widetilde{C}_e(0) = \dfrac{u}{1-e^{-hT}}, \end{cases} \tag{23}$$

for $t \in (nT, (n+1)T]$, $n \in \mathbb{Z}^+$. *In addition,*

$$\lim_{t \to +\infty} \langle C_0(t) \rangle = \frac{ku}{h(g+m)T} \triangleq \overline{C}_0. \tag{24}$$

From Lemma 1, system (4) can be replaced by the dynamical behaviors of the following limiting system:

$$\begin{cases} \mathrm{d}X(t) = X(t)\left[r(\xi(t)) - \alpha(\xi(t))C_0(t) - a_1(\xi(t))X(t) + a_2(\xi(t))X(t-\tau) + a_3(\xi(t))\displaystyle\int_{-\infty}^0 X(t+\theta)\mathrm{d}\varsigma(\theta)\right]\mathrm{d}t \\ \qquad + \sigma(\xi(t))X(t)\mathrm{d}B(t) + x(t^-)\displaystyle\int_{\mathbb{Y}} \gamma((\xi(t)),v)\widetilde{N}(\mathrm{d}t,\mathrm{d}v), \\ \Delta X(t) = \delta_n X(t), \quad t = t_n, \quad n \in \mathbb{Z}^+. \end{cases} \quad t \neq t_n, n \in \mathbb{Z}^+, \tag{25}$$

3. Positive and Global Solutions

Theorem 1. *For any initial data* $(X(0), \xi(0)) \in \mathbb{R} \times \mathbb{M}$, *system (25) has a unique positive solution* $(X(t), \xi(t)) \in \mathbb{R} \times \mathbb{M}$ *with probability one*

Proof. Consider the following SDDEs with Markovian switching and without impulses:

$$\begin{aligned} \mathrm{d}Y(t) = Y(t)\Bigg[& r(\xi(t)) - \alpha(\xi(t))C_0(t) - a_1(\xi(t))\prod_{0<t_n<t}(1+\delta_n)Y(t) \\ & + a_2(\xi(t))\prod_{0<t_n<t-\tau}(1+\delta_n)Y(t-\tau) \\ & + a_3(\xi(t))\int_{-\infty}^0 \prod_{0<t_n<t+\theta}(1+\delta_n)Y(t+\theta)\mathrm{d}\varsigma(\theta) \Bigg]\mathrm{d}t \\ & + \sigma(\xi(t))Y(t)\mathrm{d}B(t) + Y(t^-)\int_{\mathbb{Y}} \gamma((\xi(t)),v)\widetilde{N}(\mathrm{d}t,\mathrm{d}v), \end{aligned} \tag{26}$$

with initial value $(Y(0), \xi(0))$. By the theory of SDDEs with Markovian switching and Lévy jump, we refer the reader to [12]. System (26) has a unique global positive solution $(Y(t), \xi(t))$.

Let $X(t) = \prod_{0<t_n<t}(1+\delta_n)Y(t)$ with initial value $(X(0), \xi(0))$.

Since $X(t)$ is continuous on each interval $(t_n, t_{n+1}) \subset \mathbb{R}_+$, then

$$\begin{aligned} \mathrm{d}X(t) &= \prod_{0<t_n<t}(1+\delta_n)\mathrm{d}Y(t) \\ &= \prod_{0<t_n<t}(1+\delta_n)Y(t)\Bigg[r(\xi(t)) - \alpha(\xi(t))C_0(t) - a_1(\xi(t))\prod_{0<t_n<t}(1+\delta_n)Y(t) \\ &\qquad + a_2(\xi(t))\prod_{0<t_n<t-\tau}(1+\delta_n)Y(t-\tau) + a_3(\xi(t))\int_{-\infty}^0 \prod_{0<t_n<t+\theta}(1+\delta_n)Y(t+\theta)\mathrm{d}\varsigma(\theta) \Bigg]\mathrm{d}t \end{aligned}$$

$$+ \sigma(\xi(t)) \prod_{0 < t_n < t} (1 + \delta_n) Y(t) \mathrm{d}B(t) + \prod_{0 < t_n < t} (1 + \delta_n) Y(t^-) \int_{\mathbb{Y}} \gamma((\xi(t)), v) \tilde{N}(\mathrm{d}t, \mathrm{d}v)$$

$$= X(t) \Big[r(\xi(t)) - \alpha(\xi(t)) C_0(t) - a_1(\xi(t)) X(t) + a_2(\xi(t)) X(t - \tau)$$

$$+ a_3(\xi(t)) \int_{-\infty}^{0} X(t + \theta) \mathrm{d}\varsigma(\theta) \Big] \mathrm{d}t + \sigma(\xi(t)) X(t) \mathrm{d}B(t) + X(t^-) \int_{\mathbb{Y}} \gamma((\xi(t)), v) \tilde{N}(\mathrm{d}t, \mathrm{d}v),$$

$$(27)$$

for $t \neq t_n$, $n \in \mathbb{Z}^+$.

And for $\forall t_n \in \mathbb{R}_+$, we get

$$X(t_n^+) = \lim_{t \to t_n^+} X(t) = \prod_{0 < t_n < t} (1 + \delta_n) Y(t_n^+)$$

$$= (1 + \delta_n) \prod_{0 < t_n < t} (1 + \delta_n) Y(t_n) = (1 + \delta_n) X(t_n).$$

$$(28)$$

Moreover,

$$X(t_n^-) = \lim_{t \to t_n^-} X(t) = \prod_{0 < t_n < t} (1 + \delta_n) Y(t_n^-)$$

$$= \prod_{0 < t_n < t} (1 + \delta_n) Y(t_n) = X(t_n).$$

$$(29)$$

Thus, system (25) has the unique global positive solution $(X(t), \xi(t))$. □

4. Extinction and Persistence

Theorem 2. When A.1–A.4 hold, if $\eta^* < \hat{\alpha} \overline{C}_0$, then

$$\lim_{t \to +\infty} X(t) = 0, \quad \text{a.s.}$$

$$(30)$$

Namely, the population $X(t)$ of system (25) is extinct.

Proof. Applying Itô's formula to system (26), we have

$$\mathrm{d}\ln Y(t) = \Big[r(\xi(t)) - \frac{\sigma^2(\xi(t))}{2} - \int_{\mathbb{Y}} [\gamma((\xi(t)), v) - \ln(1 + \gamma((\xi(t)), v))] \lambda(\mathrm{d}v)$$

$$- \alpha(\xi(t)) C_0(t) - a_1(\xi(t)) \prod_{0 < t_n < t} (1 + \delta_n) Y(t)$$

$$+ a_2(\xi(t)) \prod_{0 < t_n < t - \tau} (1 + \delta_n) Y(t - \tau)$$

$$+ a_3(\xi(t)) \int_{-\infty}^{0} \prod_{0 < t_n < t + \theta} (1 + \delta_n) Y(t + \theta) \mathrm{d}\xi(\theta) \Big] \mathrm{d}t$$

$$+ \sigma(\xi(t)) \mathrm{d}B(t) + \int_{\mathbb{Y}} \ln(1 + \gamma((\xi(t)), v)) \tilde{N}(\mathrm{d}t, \mathrm{d}v).$$

$$(31)$$

Integrating both sides of (31) from 0 to t yields

$$\ln Y(t) - \ln Y(0) = \int_{0}^{t} \Big[b(\xi(s)) - \alpha(\xi(s)) C_0(s) - a_1(\xi(s)) \prod_{0 < t_n < s} (1 + \delta_n) Y(s)$$

$$+ a_2(\xi(s)) \prod_{0 < t_n < s - \tau} (1 + \delta_n) Y(s - \tau)$$

$$+ a_3(\xi(s)) \int_{-\infty}^{0} \prod_{0 < t_n < s + \theta} (1 + \delta_n) Y(s + \theta) \mathrm{d}\xi(\theta) \Big] \mathrm{d}s$$

$$+ \sigma(\xi(s)) \mathrm{d}B(s) + \int_{\mathbb{Y}} \ln(1 + \gamma((\xi(s)), v)) \tilde{N}(\mathrm{d}s, \mathrm{d}v)$$

$$
= \int_0^t \left[b(\xi(s)) - \alpha(\xi(s))C_0(s) - a_1(\xi(s))X(s) + a_2(\xi(s))X(s-\tau) \right.
$$

$$
\left. + a_3(\xi(s)) \int_{-\infty}^0 X(s+\theta)d\xi(\theta) \right] ds + \int_0^t \sigma(\xi(s))dB(s)
$$

$$
+ \int_0^t \int_{\mathbb{Y}} \ln(1 + \gamma((\xi(s)),v)) \widetilde{N}(ds,dv),
$$

(32)

owing to

$$
\int_0^t a_3(\xi(s)) \int_{-\infty}^0 X(s+\theta)d\xi(\theta)ds = \int_0^t a_3(\xi(s)) \left[\int_{-\infty}^{-s} X(s+\theta)d\xi(\theta) + \int_{-s}^0 X(s+\theta)d\xi(\theta) \right] ds
$$

$$
= \int_0^t a_3(\xi(s))ds \int_{-\infty}^{-s} e^{r(s+\theta)} X(s+\theta)e^{-r(s+\theta)}d\xi(\theta)
$$

$$
+ \int_{-t}^0 d\xi(\theta) \int_{-\theta}^t a_3(\xi(s))X(s+\theta)ds
$$

(33)

$$
\leq \check{a}_3 \|\varphi\|_{C_g} \int_0^t e^{-rs}ds \int_{-\infty}^0 e^{-2r\theta}d\xi(\theta) + \check{a}_3 \int_{-\infty}^0 d\xi(\theta) \int_0^t X(s)ds
$$

$$
\leq \frac{1}{r}\check{a}_3 \|\varphi\|_{C_g}\rho_r\left(1 - e^{-rt}\right) + \check{a}_3 \int_0^t X(s)ds.
$$

Then, we have

$$
\ln Y(t) - \ln Y(0) = \int_0^t \left[b(\xi(s)) - \alpha(\xi(s))C_0(s) - a_1(\xi(s))X(s) + a_2(\xi(s))X(s-\tau) \right.
$$

$$
\left. + a_3(\xi(s)) \int_{-\infty}^0 X(s+\theta)d\xi(\theta) \right] ds + \int_0^t \sigma(\xi(s))dB(s)
$$

$$
+ \int_0^t \int_{\mathbb{Y}} \ln(1 + \gamma((\xi(s)),v)) \widetilde{N}(ds,dv)
$$

$$
\leq \int_0^t \left[b(\xi(s)) - \alpha(\xi(s))C_0(s) - (\widehat{a}_1 - \check{a}_2 - \check{a}_3)X(s) \right] ds
$$

(34)

$$
+ \frac{1}{r}\check{a}_3 \|\varphi\|_{C_g}\rho_r\left(1 - e^{-rt}\right) + \int_{-\tau}^0 a_2(\xi(s+\tau))X(s)ds
$$

$$
+ \int_0^t \sigma(\xi(s))dB(s) + \int_0^t \int_{\mathbb{Y}} \ln(1 + \gamma((\xi(s)),v))\widetilde{N}(ds,dv)
$$

$$
\leq \int_0^t \left[b(\xi(s)) - \alpha(\xi(t))C_0(s) - aX(s) \right] ds + \frac{1}{r}\check{a}_3 \|\varphi\|_{C_g}\rho_r\left(1 - e^{-rt}\right)
$$

$$
+ \int_{-\tau}^0 a_2(\xi(s+\tau))X(s)ds + M_1(t) + M_2(t),
$$

where

$$M_1(t) = \int_0^t \sigma(\xi(s)) dB(s),$$

$$M_2(t) = \int_0^t \int_{\mathbb{Y}} \ln(1 + \gamma((\xi(s)), v)) \tilde{N}(ds, dv). \quad (35)$$

Since $M_1(t)$ and $M_2(t)$ are local martingales, the quadratic variations are

$$\langle M_1(t), M_1(t) \rangle = \int_0^t \sigma^2(\xi(s)) ds \le (\check{\sigma}_1)^2 t,$$

$$\langle M_2(t), M_2(t) \rangle = \int_0^t \int_{\mathbb{Y}} \ln(1 + \gamma((\xi(s)), v))^2 \lambda(dv) ds \le K_1 t. \quad (36)$$

Making use of the strong law of large numbers for local martingales (see [41]) yields

$$\lim_{t \to +\infty} \frac{M_1(t)}{t} = 0,$$

$$\lim_{t \to +\infty} \frac{M_2(t)}{t} = 0, \quad (37)$$

a.s.

From (34), we can get that

$$\sum_{0 < t_n < t} \ln(1 + \delta_n) + \ln Y(t) \le \sum_{0 < t_n < t} \ln(1 + \delta_n) + \int_0^t b(\xi(s)) ds - \int_0^t \alpha(\xi(t)) C_0(s) ds$$

$$- \int_0^t aX(s) ds + \frac{1}{r} \check{a}_3 \|\varphi\|_{C_g} \rho_r (1 - e^{-rt})$$

$$+ \int_{-\tau}^0 a_2(\xi(s + \tau)) X(s) ds + \ln Y(0) + M_1(t) + M_2(t). \quad (38)$$

Thus,

$$\ln X(t) \le \sum_{0 < t_n < t} \ln(1 + \delta_n) + \int_0^t b(\xi(s)) ds - \int_0^t \alpha(\xi(t)) C_0(s) ds$$

$$- \int_0^t aX(s) ds + \frac{1}{r} \check{a}_3 \|\varphi\|_{C_g} \rho_r (1 - e^{-rt})$$

$$+ \int_{-\tau}^0 a_2(\xi(s + \tau)) X(s) ds + \ln Y(0) + M_1(t) + M_2(t)$$

$$\le \sum_{0 < t_n < t} \ln(1 + \delta_n) + \int_0^t b(\xi(s)) ds - \hat{\alpha} \int_0^t C_0(s) ds$$

$$- a \int_0^t X(s) ds + \frac{1}{r} \check{a}_3 \|\varphi\|_{C_g} \rho_r (1 - e^{-rt})$$

$$+ \int_{-\tau}^0 a_2(\xi(s + \tau)) X(s) ds + \ln Y(0) + M_1(t) + M_2(t). \quad (39)$$

Taking superior limit on both sides of (39) and applying the ergodicity of $\xi(\cdot)$ and (37), we obtain

$$\limsup_{t \to +\infty} \frac{\ln X(t)}{t} \le \limsup_{t \to +\infty} \frac{1}{t} \left[\sum_{0 < t_n < t} \ln(1 + \delta_n) \right]$$

$$+ \sum_{k \in \mathbb{M}} \pi_k b(k) - \hat{\alpha} \overline{C}_0 := \eta^* - \hat{\alpha} \overline{C}_0 < 0, \quad \text{a.s.} \quad (40)$$

□

Theorem 3. *When A.1–A.4 hold, if $\eta^* \ge \hat{\alpha} \overline{C}_0$, then*

$$\limsup_{t \to +\infty} \frac{1}{t} \int_0^t X(s) ds \le \frac{\eta^* - \hat{\alpha} \overline{C}_0}{a} = \overline{X}^*. \quad (41)$$

Particularly, if $\eta^* = \hat{\alpha} \overline{C}_0$, then $\lim_{t \to +\infty} (1/t) \int_0^t X(s) ds = 0$, that is, the population $X(t)$ of system (25) is nonpersistent in the mean.

Proof. For $\forall \varepsilon > 0$, there exists a constant $T > 0$, for all $0 < T < n - 1 \le t \le n$, such that

$$\frac{1}{t}\left[\ln Y(0) + \frac{1}{r}\breve{a}_3\|\varphi\|_{C_g}\rho_r\left(1 - e^{-rt}\right) + \int_{-\tau}^0 a_2\left(\xi(s+\tau)\right)X(s)ds + M_1(t) + M_2(t)\right] \leq \frac{\varepsilon}{2},$$

$$(42)$$

$$\frac{1}{t}\left[\sum_{0<t_n<t}\ln\left(1+\delta_n\right) + \int_0^t b(\xi(s))ds - \widehat{\alpha}\int_0^t C_0(s)ds\right] \leq \eta^* - \widehat{\alpha}\overline{C}_0 + \frac{\varepsilon}{2}.$$

Substituting above inequalities into (39), we have

$$\ln X(t) \leq \sum_{0<t_n<t}\ln\left(1+\delta_n\right) + \int_0^t b(\xi(s))ds - \widehat{\alpha}\int_0^t C_0(s)ds$$

$$- a\int_0^t X(s)ds + \frac{1}{r}\breve{a}_3\|\varphi\|_{C_g}\rho_r\left(1 - e^{-rt}\right)$$

$$+ \int_{-\tau}^0 a_2\left(\xi(s+\tau)\right)X(s)ds + \ln Y(0) + M_1(t) + M_2(t)$$

$$\leq \left(\eta^* - \widehat{\alpha}\overline{C}_0 + \varepsilon\right)t - a\int_0^t X(s)ds, \quad \text{a.s.}$$

$$(43)$$

Denote $g(t) = \int_0^t X(s)ds$; then, we have $(dg(t)/dt) = X(t)$. Taking exponent on both sides of (43) yields

$$e^{ag(t)}\frac{dg(t)}{dt} \leq e^{(\eta^* - \widehat{\alpha}\overline{C}_0 + \varepsilon)t}.$$

$$(44)$$

Integrating (44) from T to t, we can show that

$$e^{ag(t)} \leq \frac{a}{\eta^* - \widehat{\alpha}\overline{C}_0 + \varepsilon}e^{(\eta^* - \widehat{\alpha}\overline{C}_0 + \varepsilon)t} + e^{ag(T_0)}$$

$$- \frac{a}{\eta^* - \widehat{\alpha}\overline{C}_0 + \varepsilon}e^{(\eta^* - \widehat{\alpha}\overline{C}_0 + \varepsilon)T}.$$

$$(45)$$

Taking logarithm of (45) yields

$$\int_0^t X(s)ds \leq \frac{1}{a}\ln\left[\frac{a}{\eta^* - \widehat{\alpha}\overline{C}_0 + \varepsilon}e^{(\eta^* - \widehat{\alpha}\overline{C}_0 + \varepsilon)t}\right.$$

$$\left. + e^{ag(T)} - \frac{a}{\eta^* - \widehat{\alpha}\overline{C}_0 + \varepsilon}e^{(\eta^* - \widehat{\alpha}\overline{C}_0 + \varepsilon)T}\right].$$

$$(46)$$

Taking superior limit on (46) elicits that

$$\limsup_{t\to+\infty}\frac{1}{t}\int_0^t X(s)ds \leq \limsup_{t\to+\infty}\frac{1}{at}\ln\left(\frac{a}{\eta^* - \widehat{\alpha}\overline{C}_0 + \varepsilon}e^{(\eta^* - \widehat{\alpha}\overline{C}_0 + \varepsilon)t}\right.$$

$$\left. + e^{ag(T)} - \frac{a}{\eta^* - \widehat{\alpha}\overline{C}_0 + \varepsilon}e^{(\eta^* - \widehat{\alpha}\overline{C}_0 + \varepsilon)T}\right).$$

$$(47)$$

Utilizing L'Hospital's rule results in

$$\limsup_{t\to+\infty}\frac{1}{t}\int_0^t X(s)ds \leq \limsup_{t\to+\infty}\frac{\eta^* - \widehat{\alpha}\overline{C}_0 + \varepsilon}{a} = \frac{\eta^* - \widehat{\alpha}\overline{C}_0}{a} = \overline{X}^*.$$

$$(48)$$

$$\square$$

Theorem 4. *When A.1–A.4 hold, if $\eta^* > \widehat{\alpha}\overline{C}_0$, then the population $X(t)$ of system (25) is weakly persistent a.s.*

Proof. Denote $L = \{\omega \mid \limsup_{t\to+\infty}X(t,\omega) = 0\}$; suppose that $\mathbb{P}(L) > 0$. Then, it follows from (39) that

$$\frac{\ln X(t) - \ln X(0)}{t} \leq \frac{1}{t}\left[\sum_{0<t_n<t}\ln\left(1+\delta_n\right) + \int_0^t b(\xi(s))ds - \widehat{\alpha}\int_0^t C_0(s)ds\right]$$

$$- \frac{a}{t}\int_0^t X(s)ds + \frac{1}{rt}\breve{a}_3\|\varphi\|_{C_g}\rho_r\left(1 - e^{-rt}\right)$$

$$+ \frac{1}{t}\int_{-\tau}^0 a_2\left(\xi(s+\tau)\right)X(s)ds + \frac{M_1(t)}{t} + \frac{M_2(t)}{t}.$$

$$(49)$$

For $\forall\omega \in L$, we have $\lim_{t\to+\infty}X(t,\omega) = 0$. As a result,

$$\limsup_{t\to+\infty}\frac{\ln X(t,\omega) - \ln X(0)}{t} \leq 0,$$

$$\limsup_{t\to+\infty}\frac{a}{t}\int_0^t X(s)ds = 0.$$

$$(50)$$

From (49), one has

$$0 \geq \limsup_{t\to+\infty}\ln X(t,w) = \eta^* - \widehat{\alpha}\overline{C}_0 > 0,$$

$$(51)$$

which is a contradiction. $\square$

Remark 1. Through Theorems 2–4, we find an interesting biological phenomenon: when $\eta^* > \widehat{\alpha}\overline{C}_0$, the population $X(t)$ is weakly persistent; when $\eta^* < \widehat{\alpha}\overline{C}_0$, the population $X(t)$ goes to extinction, which means that the persistence and extinction of $X(t)$ depend on η^* and the absorption intensity of toxins $\widehat{\alpha}\overline{C}_0$.

Theorem 5. *When A.1–A.3 hold, if $\eta_* > \breve{\alpha}\overline{C}_0$, then*

$$\liminf_{t \longrightarrow +\infty} \frac{1}{t} \int_0^t X(s)\mathrm{d}s \geq \frac{\eta_* - \check{\alpha}\overline{C}_0}{\check{a}_1} = \underset{-}{\overset{*}{X}}, \quad \text{a.s.} \qquad (52)$$

That is, the population $X(t)$ of system (25) is persistent in the mean a.s.

Proof. Applying Itô's formula to (26) yields

$$
\begin{aligned}
\mathrm{d}\ln Y(t) = & \left[r(\xi(t)) - \frac{\sigma^2(\xi(t))}{2} - \int_{\mathbb{Y}} [\gamma((\xi(t)),v) - \ln(1 + \gamma((\xi(t)),v))]\lambda(\mathrm{d}v) \right. \\
& - \alpha(\xi(t))C_0(t) - a_1(\xi(t)) \prod_{0<t_n<t}(1 + \delta_n)Y(t) \\
& + a_2(\xi(t)) \prod_{0<t_n<t-\tau}(1 + \delta_n)Y(t - \tau) \\
& + a_3(\xi(t)) \int_{-\infty}^0 \prod_{0<t_n<t+\theta}(1 + \delta_n)Y(t + \theta)\mathrm{d}\xi(\theta) \bigg] \mathrm{d}t \\
& + \sigma(\xi(t))\mathrm{d}B(t) + \int_{\mathbb{Y}} \ln(1 + \gamma((\xi(t)),v))\widetilde{N}(\mathrm{d}t,\mathrm{d}v) \\
\geq & \left[b(\xi(t)) - \check{\alpha}C_0(t) - \check{a}_1 X(t) \right]\mathrm{d}t + \sigma(\xi(t))\mathrm{d}B(t) \\
& + \int_{\mathbb{Y}} \ln(1 + \gamma((\xi(t)),v))\widetilde{N}(\mathrm{d}t,\mathrm{d}v).
\end{aligned}
\qquad (53)
$$

Calculating inequality (53), one has

$$
\begin{aligned}
\ln X(t) \geq & \sum_{0<t_n<t} \ln(1 + \delta_n) + \int_0^t b(\xi(s))\mathrm{d}s - \check{\alpha}\int_0^t C_0(s)\mathrm{d}s \\
& - \check{a}_1 \int_0^t X(s)\mathrm{d}s + \ln Y(0) + M_1(t) + M_2(t).
\end{aligned}
\qquad (54)
$$

According to the properties of the limit, there exists $T_1 > 0$ such that for $\forall \varepsilon_1 > 0$,

$$\sum_{0<t_n<t} \ln(1 + \delta_n) + \int_0^t b(\xi(s))\mathrm{d}s - \check{\alpha}\int_0^t C_0(s)\mathrm{d}s \geq \left(\eta_* - \check{\alpha}\overline{C}_0 - \frac{\varepsilon_1}{4} \right)t,$$

$$\ln y(0) \geq -\frac{\varepsilon_1}{4}t,$$

$$M_1(t) \geq -\frac{\varepsilon_1}{4}t,$$

$$M_2(t) \geq -\frac{\varepsilon_1}{4}t. \qquad (55)$$

Then, inequality (54) becomes

$$\ln X(t) \geq \left(\eta_* - \check{\alpha}\overline{C}_0 - \varepsilon_1 \right)t - \check{a}_1 \int_0^t X(s)\mathrm{d}s, \qquad (56)$$

for $t > T_1$. By using a method similar to Theorem 3, we can obtain that

$$\liminf_{t \longrightarrow +\infty} \frac{1}{t} \int_0^t X(s)\mathrm{d}s \geq \liminf_{t \longrightarrow +\infty} \frac{\eta_* - \check{\alpha}\overline{C}_0 - \varepsilon_1}{\check{a}_1} = \frac{\eta_* - \check{\alpha}\overline{C}_0}{\check{a}_1} = \underset{-}{\overset{*}{X}}. \qquad (57)$$

□

Theorem 6. *When A.1–A.3, A.5, and A.6 hold, if $\sum_{k=1}^N \pi_k \overline{b}(k) > 0$, then the population $X(t)$ of system (25) is stochastically permanent.*

Proof. First, we prove that for $\forall \varepsilon > 0$, there exists a constant $b_1 > 0$ such that

$$\liminf_{t \longrightarrow +\infty} \mathbb{P}\{X(t) \geq b_1\} \geq 1 - \varepsilon. \qquad (58)$$

Define

$$
\begin{aligned}
V_1(Y) &= \frac{1}{Y^2}, \\
V_2(Y) &= \vartheta_k (1 + V_1(Y))^\varrho, \\
V_3(Y) &= e^{\kappa t} V_2(Y),
\end{aligned}
\qquad (59)
$$

where ϱ and κ are sufficiently small positive constants and satisfy

$$
\begin{aligned}
\vartheta_k \left(\varrho\overline{b}(k) - 2\varrho^2\sigma^2(k) \right) - \sum_{l=1}^N \gamma_{kl}\vartheta_l > 0, \quad 1 \leq k \leq N, \\
\vartheta_k \left(\varrho\overline{b}(k) - 2\varrho^2\sigma^2(k) \right) - \sum_{l=1}^N \gamma_{kl}\vartheta_l - \kappa\vartheta_k > 0, \quad 1 \leq k \leq N,
\end{aligned}
\qquad (60)
$$

where $\vartheta = (\vartheta_1, \vartheta_2, \ldots, \vartheta_N)^T \gg 0$ such that $A(\varrho)\vartheta \gg 0$.

From (26), we can calculate that

$$dV_1(Y) = 2V_1(Y)\left[-r(\xi(t)) + \frac{3}{2}\sigma^2(\xi(t)) + \alpha(\xi(t))C_0(t) + a_1(\xi(t))\prod_{0<t_n<t}(1+\delta_n)Y(t)\right.$$

$$- a_2(\xi(t))\prod_{0<t_n<t-\tau}(1+\delta_n)Y(t-\tau) - a_3(\xi(t))\int_{-\infty}^0\prod_{0<t_n<t+\theta}(1+\delta_n)Y(t+\theta)d\varsigma(\theta)$$

$$+ \frac{1}{2}\int_{\mathbb{Y}}\left(\frac{1}{(1+\gamma((\xi(t)),v))^2} - 1 + 2\gamma((\xi(t)),v)\right)\lambda(dv)\Bigg]dt$$

$$- 2V_1(Y)\sigma(\xi(t))dB(t) + V_1(Y)\int_{\mathbb{Y}}\left(\frac{1}{(1+\gamma((\xi(t)),v))^2} - 1\right)\tilde{N}(dt,dv) \tag{61}$$

$$\leq 2V_1(Y)\left[-r(\xi(t)) + \frac{3}{2}\sigma^2(\xi(t)) + \alpha(\xi(t))C_0(t) + a_1(\xi(t))\prod_{0<t_n<t}(1+\delta_n)Y(t)\right.$$

$$+ \frac{1}{2}\int_{\mathbb{Y}}\left(\frac{1}{(1+\gamma((\xi(t)),v))^2} - 1 + 2\gamma((\xi(t)),v)\right)\lambda(dv)\Bigg]dt$$

$$- 2V_1(Y)\sigma(\xi(t))dB(t) + V_1(Y)\int_{\mathbb{Y}}\left(\frac{1}{(1+\gamma((\xi(t)),v))^2} - 1\right)\tilde{N}(dt,dv).$$

Applying the generalized Itô's formula yields

$$dV_2(Y) \leq (1+V_1(Y))^{\varrho-2}\left[\varrho\vartheta_k(1+V_1(Y))\left(-2V_1(Y)\left[r(k) - \frac{3}{2}\sigma^2(k) - \alpha(k)C_0(t)\right.\right.\right.$$

$$-\frac{1}{2}\int_{\mathbb{Y}}\left(\frac{1}{(1+\gamma((k),v))^2} - 1 + 2\gamma((k),v)\right)\lambda(dv)\bigg]$$

$$+ 2a_1(k)\prod_{0<t_n<t}(1+\delta_n)V_1^{1/2}(Y)\bigg)\bigg]dt + 2\varrho(\varrho-1)\vartheta_k\sigma^2(k)(1+V_1(Y))^{\varrho-2}V_1^2(Y)$$

$$+ \vartheta_k\int_{\mathbb{Y}}\left[\left(1+V_1(Y)+V_1(Y)\left(\frac{1}{(1+\gamma((k),v))^2}-1\right)\right)^{\varrho} - (1+V_1(Y))^{\varrho}\right.$$

$$-\varrho(1+V_1(Y))^{\varrho-1}V_1(Y)\left(\frac{1}{(1+\gamma((k),v))^2}-1\right)\bigg]\lambda(dv)dt$$

$$+ \sum_{l=1}^N\gamma_{kl}\vartheta_l(1+V_1(Y))^{\varrho}dt - 2\varrho\vartheta_k\sigma(k)(1+V_1(Y))^{\varrho-1}V_1(Y)dB(t)$$

$$+ \int_{\mathbb{Y}}\left[\left(1+V_1(Y)+V_1(Y)\left(\frac{1}{(1+\gamma((k),v))^2}-1\right)\right)^{\varrho} - (1+V_1(Y))^{\varrho}\right]\tilde{N}(dt,dv)$$

$$\leq (1+V_1(Y))^{\varrho-2}\left\{-\left[\vartheta_k\left(2r(k)\varrho - \sigma^2(k)\varrho - 2\varrho\int_{\mathbb{Y}}(\gamma((k),v))\lambda(dv) - 2\alpha(k)C_0^*\right.\right.\right.$$

$$-2\varrho^2\sigma^2(k)\bigg) - \sum_{l=1}^N\gamma_{kl}\vartheta_l\bigg]V_1^2(Y) + 2a_1(k)MV_1^{3/2}(Y)$$

$$-\left[\vartheta_k\left(2r(k)\varrho - 3\sigma^2(k)\varrho - 2\varrho\int_{\mathbb{Y}}(\gamma((k),v))\lambda(dv) - 2\alpha(k)C_0^*\right) - \sum_{l=1}^N\gamma_{kl}\vartheta_l\right]V_1(Y)$$

$$
\begin{aligned}
&+ 2a_1(k)MV_1^{1/2}(Y) + \sum_{l=1}^{N} \gamma_{kl}\vartheta_l \Bigg\} dt - 2\varrho\vartheta_k\sigma(k)\left(1 + V_1(Y)\right)^{\varrho-1}V_1(Y)dB(t) \\
&+ \int_{\mathbb{Y}} \vartheta_k\left[\left(1 + V_1(Y) + V_1(Y)\left(\frac{1}{\left(1 + \gamma((k),v)\right)^2} - 1\right)\right)^{\varrho} - \left(1 + V_1(Y)\right)^{\varrho}\right]\tilde{N}(dt,dv) \\
&= \left(1 + V_1(Y)\right)^{\varrho-2}\Bigg\{ -\left(\vartheta_k\left(\varrho\bar{b}(k) - 2\varrho^2\sigma^2(k)\right) - \sum_{l=1}^{N}\gamma_{kl}\vartheta_l\right)V_1^2(Y) \\
&+ 2a_1(k)MV_1^{3/2}(Y) - \left(\vartheta_k\left(\varrho\bar{b}(k) - 2\varrho\sigma^2(k)\right) - \sum_{l=1}^{N}\gamma_{kl}\vartheta_l\right)V_1(Y) \\
&+ 2a_1(k)MV_1^{1/2}(Y) + \sum_{l=1}^{N}\gamma_{kl}\vartheta_l\Bigg\}dt - 2\varrho\vartheta_k\sigma(k)\left(1 + V_1(Y)\right)^{\varrho-1}V_1(Y)dB(t) \\
&+ \int_{\mathbb{Y}}\vartheta_k\left[\left(1 + V_1(Y) + V_1(Y)\left(\frac{1}{\left(1 + \gamma((k),v)\right)^2} - 1\right)\right)^{\varrho} - \left(1 + V_1(Y)\right)^{\varrho}\right]\tilde{N}(dt,dv),
\end{aligned}
\tag{62}
$$

and we use the following equation:

$$
\int_{\mathbb{Y}}\left[\left(1 + V_1(Y) + V_1(Y)\left(\frac{1}{\left(1 + \gamma((k),v)\right)^2} - 1\right)\right)^{\varrho}\right.
$$
$$
\left. - \left(1 + V_1(Y)\right)^{\varrho}\right]\lambda(dv) < 0.
\tag{63}
$$

Therefore, we obtain that

$$
\begin{aligned}
dV_3(Y) &= \kappa e^{\kappa t}V_2(Y)dt + e^{\kappa t}dV_2(Y) \le e^{\kappa t}\left(1 + V_1(Y)\right)^{\varrho-2}\Bigg\{ -\left(\vartheta_k\left(\varrho\bar{b}(k) - 2\varrho^2\sigma^2(k)\right) - \sum_{l=1}^{N}\gamma_{kl}\vartheta_l - \kappa\vartheta_k\right)V_1^2(Y) \\
&+ 2a_1(k)MV_1^{3/2}(Y) - \left(\vartheta_k\left(\varrho\bar{b}(k) - 2\varrho\sigma^2(k)\right) - \sum_{l=1}^{N}\gamma_{kl}\vartheta_l - 2\kappa\vartheta_k\right)V_1(Y) \\
&+ 2a_1(k)MV_1^{1/2}(Y) + \sum_{l=1}^{N}\gamma_{kl}\vartheta_l + \kappa\vartheta_k\Bigg\}dt - 2\varrho\vartheta_k e^{\kappa t}\sigma(k)\left(1 + V_1(Y)\right)^{\varrho-1}V_1(Y)dB(t) \\
&+ \vartheta_k e^{\kappa t}\int_{\mathbb{Y}}\left[\left(1 + V_1(Y) + V_1(Y)\left(\frac{1}{\left(1 + \gamma(k),v\right)^2} - 1\right)\right)^{\varrho} - \left(1 + V_1(Y)\right)^{\varrho}\right]\tilde{N}(dt,dv) \\
&= e^{\kappa t}H(Y)dt - 2\varrho\vartheta_k e^{\kappa t}\sigma(k)\left(1 + V_1(Y)\right)^{\varrho-1}V_1(Y)dB(t) \\
&+ \vartheta_k e^{\kappa t}\int_{\mathbb{Y}}\left[\left(1 + V_1(Y) + V_1(Y)\left(\frac{1}{\left(1 + \gamma(k),v\right)^2} - 1\right)\right)^{\varrho} - \left(1 + V_1(Y)\right)^{\varrho}\right]\tilde{N}(dt,dv),
\end{aligned}
\tag{64}
$$

where

$$
\begin{aligned}
H(Y) &= \left(1 + V_1(Y)\right)^{\varrho-2}\Bigg\{ -\left(\vartheta_k\left(\varrho\bar{b}(k) - 2\varrho^2\sigma^2(k)\right) - \sum_{l=1}^{N}\gamma_{kl}\vartheta_l - \kappa\vartheta_k\right)V_1^2(Y) + 2a_1(k)MV_1^{3/2}(Y) \\
&- \left(\vartheta_k\left(\varrho\bar{b}(k) - 2\varrho\sigma^2(k)\right) - \sum_{l=1}^{N}\gamma_{kl}\vartheta_l - 2\kappa\vartheta_k\right)V_1(Y) + 2a_1(k)MV_1^{1/2}(Y) + \sum_{l=1}^{N}\gamma_{kl}\vartheta_l + \kappa\vartheta_k\Bigg\}.
\end{aligned}
\tag{65}
$$

Since $H = \sup_{Y \in \mathbb{R}^+} H(Y) < +\infty$,

$$
\begin{aligned}
dV_3(Y) \leq{} & e^{\kappa t} H dt - 2\varrho \vartheta_k e^{\kappa t} \sigma(k) \left(1 + V_1(Y)\right)^{\varrho - 1} V_1(Y) dB(t) \\
& + \vartheta_k e^{\kappa t} \int_{\mathbb{Y}} \left[\left(1 + V_1(Y) + V_1(Y)\left(\frac{1}{(1 + \gamma(k), v)^2} - 1\right)\right)^{\varrho} - \left(1 + V_1(Y)\right)^{\varrho} \right] \tilde{N}(dt, dv).
\end{aligned}
\tag{66}
$$

Calculating (66), it is not difficult to show that

$$
\mathbb{E}\left[\vartheta_k \left(1 + V_1(Y)\right)^{\varrho}\right] \leq \vartheta_k V_2(Y_0)\mathbb{E}\left[e^{-\kappa t}\right] + \frac{H}{\kappa}\mathbb{E}\left[1 - e^{-\kappa t}\right].
\tag{67}
$$

Thus,

$$
\begin{aligned}
\limsup_{t \to +\infty} \mathbb{E}\left[Y(t)^{-2\varrho}\right] &\leq \limsup_{t \to +\infty} \mathbb{E}\left[\left(1 + V_1(Y(t))\right)^{\varrho}\right] \\
&\leq \limsup_{t \to +\infty} \left[\frac{V_2(Y_0)}{e^{\kappa t}} + \frac{H\left(1 - e^{-\kappa t}\right)}{\kappa \min_{k \in \mathbb{M}}\{\vartheta_k\}}\right] = \overline{H}.
\end{aligned}
\tag{68}
$$

Consequently,

$$
\begin{aligned}
&\limsup_{t \to +\infty} \mathbb{E}\left[X(t)^{-2\varrho}\right] \\
&= \limsup_{t \to +\infty} \mathbb{E}\left[\left(\prod_{0 < t_n < t}\left(1 + \delta_n\right)\right)^{-2\varrho} Y(t)^{-2\varrho}\right] \leq M^{-2\varrho}\overline{H}.
\end{aligned}
\tag{69}
$$

Then, for $\forall \varepsilon > 0$, let $b_1 = M(\varepsilon/\overline{H})^{1/2\varrho}$; using Chebyshev's inequality, we have

$$
\begin{aligned}
\limsup_{t \to +\infty} \mathbb{P}\{|X(t)| < b_1\} &= \limsup_{t \to +\infty} \mathbb{P}\left\{|X(t)|^{-2\varrho} > b_1^{-2\varrho}\right\} \\
&\leq \lim_{t \to +\infty} \frac{\mathbb{E}\left[|X(t)|^{-2\varrho}\right]}{b_1^{-2\varrho}} \leq \varepsilon.
\end{aligned}
\tag{70}
$$

In other words,

$$
\liminf_{t \to +\infty} \mathbb{P}\{|X(t)| \geq b_1\} \geq 1 - \varepsilon.
\tag{71}
$$

Next, we prove that for $\forall \varepsilon > 0$, there exists $b_2 > 0$ such that

$$
\liminf_{t \to +\infty} \mathbb{P}\{X(t) \leq b_2\} \geq 1 - \varepsilon.
\tag{72}
$$

Applying generalized Itô's formula to (26):

$$
\begin{aligned}
d(Y(t)) ={} & Y(t)\Bigg[r(\xi(t)) - \alpha(\xi(t))C_0(t) - a_1(\xi(t)) \prod_{0 < t_n < t}\left(1 + \delta_n\right)Y(t) \\
& + a_2(\xi(t)) \prod_{0 < t_n < t - \tau}\left(1 + \delta_n\right)Y(t - \tau) \\
& + a_3(\xi(t)) \int_{-\infty}^{0} \prod_{0 < t_n < t + \theta}\left(1 + \delta_n\right)Y(t + \theta)d\varsigma(\theta)\Bigg]dt \\
& + \sigma(\xi(t))Y(t)dB(t) + Y(t^-)\int_{\mathbb{Y}} \gamma((\xi(t)), v)\tilde{N}(dt, dv) \\
\leq{} & \Big[\left(r(\xi(t)) - \hat{\alpha}C_0(t)\right)Y(t) - m\hat{a}_1 Y^2(t) + M\check{a}_2 Y(t)Y(t - \tau) \\
& + M\check{a}_3 Y(t) \int_{-\infty}^{0} Y(t + \theta)d\varsigma(\theta)\Big]dt + \sigma(\xi(t))Y(t)dB(t) \\
& + e^t Y(t^-)\int_{\mathbb{Y}} \gamma((\xi(t)), v)\tilde{N}(dt, dv) \\
\leq{} & \Big[\left(r(\xi(t)) - \hat{\alpha}C_0(t)\right)Y(t) - m\hat{a}_1 Y^2(t) + \frac{M\check{a}_2}{2}Y^2(t) \\
& + \frac{M\check{a}_2}{2}Y^2(t - \tau) + \frac{M\check{a}_3}{2}Y^2(t) + \frac{M\check{a}_3}{2}\int_{-\infty}^{0} Y^2(t + \theta)d\varsigma(\theta)\Big]dt \\
& + \sigma(\xi(t))Y(t)dB(t) + Y(t^-)\int_{\mathbb{Y}} \gamma((\xi(t)), v)\tilde{N}(dt, dv).
\end{aligned}
\tag{73}
$$

Thus,

$$d\left(e^t Y(t)\right) \le e^t \left[(1 + r(\xi(t)) - \widehat{\alpha} C_0(t))Y(t) - m\widehat{a}_1 Y^2(t) + \frac{M\breve{a}_2}{2} Y^2(t) \right.$$

$$\left. + \frac{M\breve{a}_2}{2} Y^2(t - \tau) + \frac{M\breve{a}_3}{2} Y^2(t) + \frac{M\breve{a}_3}{2} \int_{-\infty}^{0} Y^2(t + \theta) d\varsigma(\theta) \right] dt$$

$$+ e^t \sigma(\xi(t)) Y(t) dB(t) + e^t Y(t^-) \int_{\mathbb{Y}} \gamma((\xi(t)), v) \widetilde{N}(dt, dv) \tag{74}$$

$$= e^t \left[G(Y(t)) - \frac{m\widehat{a}_1}{2} Y^2(t) + \frac{M\breve{a}_2}{2} Y^2(t - \tau) + \frac{M\breve{a}_3}{2} \int_{-\infty}^{0} Y^2(t + \theta) d\varsigma(\theta) \right] dt$$

$$+ e^t \sigma(\xi(t)) Y(t) dB(t) + e^t Y(t^-) \int_{\mathbb{Y}} \gamma((\xi(t)), v) \widetilde{N}(dt, dv),$$

where

$$G(Y(t)) = (1 + r(\xi(t)) - \widehat{\alpha} C_0(t))Y(t)$$

$$- \frac{m\widehat{a}_1}{2} Y^2(t) + \frac{M\breve{a}_2}{2} Y^2(t) + \frac{M\breve{a}_3}{2} Y^2(t). \tag{75}$$

According to $m\widehat{a}_1 > M(\breve{a}_2 + \breve{a}_3)$, we get

$$G = \sup_{Y \in \mathbb{R}_+} G(Y) < +\infty. \tag{76}$$

Then,

$$e^t Y(t) - Y(0) \le G\left(e^t - 1\right) - \frac{m\widehat{a}_1}{2} \int_0^t e^s Y^2(s) ds + \frac{M\breve{a}_2}{2} \int_0^t e^s Y^2(s - \tau) ds$$

$$+ \frac{M\breve{a}_3}{2} \int_0^t e^s \int_{-\infty}^{0} Y^2(s + \theta) d\varsigma(\theta) ds + \int_0^t e^s \sigma(\xi(s)) Y(s) dB(s) \tag{77}$$

$$+ \int_0^t e^s \int_{\mathbb{Y}} \gamma((\xi(s)), v) Y(t^-) \widetilde{N}(ds, dv).$$

On the one hand,

$$\frac{M\breve{a}_2}{2} \int_0^t e^s Y^2(s - \tau) ds = \frac{M\breve{a}_2}{2} \int_{-\tau}^{t-\tau} e^{s+\tau} Y^2(s) ds$$

$$\le \frac{M\breve{a}_2}{2} \int_{-\tau}^{0} e^{s+\tau} Y^2(s) ds + \frac{M\breve{a}_2 e^{\tau}}{2} \int_0^t e^s Y^2(s) ds,$$

$$\cdot \frac{M\breve{a}_3}{2} \int_0^t e^s \int_{-\infty}^{0} Y^2(s + \theta) d\varsigma(\theta) ds$$

$$= \frac{M\breve{a}_3}{2} \int_0^t e^s \left[\int_{-\infty}^{-s} Y^2(s + \theta) d\varsigma(\theta) + \int_{-s}^{0} Y^2(s + \theta) d\varsigma(\theta) \right] ds$$

$$= \frac{M\breve{a}_3}{2} \int_0^t e^s ds \int_{-\infty}^{-s} e^{2r(s+\theta)} Y^2(s + \theta) e^{-2r(s+\theta)} d\varsigma(\theta)$$

$$+ \frac{M\breve{a}_3}{2} \int_{-t}^{0} d\varsigma(\theta) \int_{-\theta}^{t} e^s Y^2(s + \theta) ds$$

$$= \frac{M\check{a}_3}{2} \int_0^t e^s \mathrm{d}s \int_{-\infty}^{-s} e^{2r(s+\theta)} Y^2(s+\theta) e^{-2r(s+\theta)} \mathrm{d}\varsigma(\theta)$$

$$+ \frac{M\check{a}_3}{2} \int_{-t}^0 \mathrm{d}\varsigma(\theta) \int_0^{t+\theta} e^{(s-\theta)} Y^2(s) \mathrm{d}s$$

$$\leq \frac{M\check{a}_3}{2} \|\xi\|_{C_g}^2 \int_0^t e^{(1-2r)s} \mathrm{d}s \int_{-\infty}^0 e^{-2r\theta} \mathrm{d}\varsigma(\theta)$$

$$+ \frac{M\check{a}_3}{2} \int_{-\infty}^0 e^{-\theta} \mathrm{d}\varsigma(\theta) \int_0^t e^s Y^2(s) \mathrm{d}s$$

$$\leq \frac{M\check{a}_3}{2} \|\xi\|_{C_g}^2 \rho_r t + \frac{M\check{a}_3 \rho_r}{2} \int_0^t e^s Y^2(s) \mathrm{d}s. \tag{78}$$

Therefore,

$$e^t Y(t) \leq Y(0) + G\left(e^t - 1\right) - \frac{m\hat{a}_1 - M\left(\check{a}_2 e^\tau + \check{a}_3 \rho_r\right)}{2} \int_0^t e^s Y^2(s) \mathrm{d}s$$

$$+ \frac{M\check{a}_2}{2} \int_{-\tau}^0 e^{s+\tau} Y^2(s) \mathrm{d}s + \frac{M\check{a}_3}{2} \|\xi\|_{C_g}^2 h_r t \tag{79}$$

$$+ \int_0^t e^s \sigma(\xi(s)) Y(s) \mathrm{d}B(s) + \int_0^t e^s \int_{\mathbb{Y}} \gamma((\xi(s)), v) Y(t^-) \widetilde{N}(\mathrm{d}s, \mathrm{d}v).$$

Taking expectations on both sides of (79) yields

$$\limsup_{t \longrightarrow +\infty} \mathbb{E}[Y(t)] \leq G. \tag{80}$$

This leads to

$$\limsup_{t \longrightarrow +\infty} \mathbb{E}[X(t)] \leq \limsup_{t \longrightarrow +\infty} \mathbb{E}\left[\prod_{0 < t_n < t} (1 + \delta_n) Y(t)\right] \leq MG. \tag{81}$$

Then, for $\forall \varepsilon > 0$, let $b_2 = (MG/\varepsilon)$, and we have

$$\limsup_{t \longrightarrow +\infty} \mathbb{P}\{|X(t)| > b_2\} \leq \lim_{t \longrightarrow +\infty} \frac{\mathbb{E}[|X(t)|]}{b_2} = \varepsilon. \tag{82}$$

That is,

$$\limsup_{t \longrightarrow +\infty} \mathbb{P}\{|X(t)| \leq b_2\} \geq 1 - \varepsilon. \tag{83}$$

From (71) and (83), $X(t)$ of system (25) is stochastically permanent. □

5. Asymptotic Properties

Theorem 7. *When A.1–A.3, A.5, and A.6 hold and any solution $X(t)$ of system (25) have the property that*

$$\limsup_{t \longrightarrow +\infty} \frac{\ln|X(t)|}{\ln t} \leq 1, \quad \text{a.s.}, \tag{84}$$

and if $\sum_{k=1}^N \pi_k \overline{b}(k) > 0$,

$$\liminf_{t \longrightarrow +\infty} \frac{\ln|X(t)|}{\ln t} \geq -\frac{1}{2\varrho}, \quad \text{a.s.} \tag{85}$$

Proof. From (73), we have

$$\mathrm{d}Y(t) = Y(t)\left[r(\xi(t)) - \alpha(\xi(t))C_0(t) - a_1(\xi(t)) \prod_{0<t_n<t} (1 + \delta_n) Y(t)\right.$$

$$+ a_2(\xi(t)) \prod_{0<t_n<t-\tau} (1 + \delta_n) Y(t - \tau)$$

$$\left. + a_3(\xi(t)) \int_{-\infty}^0 \prod_{0<t_n<t+\theta} (1 + \delta_n) Y(t + \theta) \mathrm{d}\varsigma(\theta) \right] \mathrm{d}t \tag{86}$$

$$+ \sigma(\xi(t)) Y(t) \mathrm{d}B(t) + Y(t^-) \int_{\mathbb{Y}} \gamma((\xi(t)), v) \widetilde{N}(\mathrm{d}t, \mathrm{d}v).$$

Then,

$$\mathbb{E}\left[\limsup_{t\leq v\leq t+1} Y(v)\right] \leq \mathbb{E}[Y(t)] + \mathbb{E}\left[\sup_{t\leq v\leq t+1}\left|\int_t^{t+1} Y(s)\mathrm{d}s\right|\right]$$
$$+ \mathbb{E}\left[\limsup_{t\leq v\leq t+1}\int_t^v \sigma(\xi(s))Y(s)\mathrm{d}B(s)\right]$$
$$+ \mathbb{E}\left[\limsup_{t\leq v\leq t+1}\int_t^v\int_{\mathbb{Y}}\gamma((\xi(s)),v)y(s)\tilde{N}(\mathrm{d}s,\mathrm{d}v)\right].$$
$$(87)$$

By the Burkholder–Davis–Gundy inequality (see [40]), one has

$$\mathbb{E}\left[\sup_{t\leq v\leq t+1}\int_t^v \sigma(\xi(s))Y(s)\mathrm{d}B(s)\right]$$
$$\leq \sqrt{32}\,\mathbb{E}\left[\left(\int_t^{t+1}\sigma^2(\xi(s))Y^2(s)\mathrm{d}s\right)^{1/2}\right] \qquad (88)$$
$$\leq 4\sqrt{2}\check{\sigma}\,\mathbb{E}\left[\sup_{t\leq v\leq t+1} Y(s)\right],$$

$$\mathbb{E}\left[\limsup_{t\leq v\leq t+1}\int_t^v\int_{\mathbb{Y}}\gamma((\xi(s)),v)Y(s)\tilde{N}(\mathrm{d}s,\mathrm{d}v)\right]$$
$$\leq \sqrt{32}\,\mathbb{E}\left[\int_t^v\int_{\mathbb{Y}}\gamma^2((\xi(s)),v)Y^2(s)N(\mathrm{d}s,\mathrm{d}v)\right]^{1/2} \qquad (89)$$
$$\leq 4\sqrt{2}\left(\int_{\mathbb{Y}}\check{\gamma}^2\lambda(\mathrm{d}v)\right)^{1/2}\mathbb{E}\left[\sup_{t\leq v\leq t+1} Y(v)\right].$$

Substituting (80), (88), and (89) into (87) yields

$$\mathbb{E}\left[\limsup_{t\leq v\leq t+1} Y(v)\right] \leq \mathbb{E}[Y(t)] + B\mathbb{E}\left[\sup_{t\leq v\leq t+1} [Y(v)]\right], \qquad (90)$$

where $B = G + 4\sqrt{2}\check{\sigma} + 4\sqrt{2}\left(\int_{\mathbb{Y}}\check{\gamma}\lambda(\mathrm{d}v)\right)^{1/2}$.

In view of (90), we have

$$\mathbb{E}\left[\limsup_{t\leq\theta\leq t+1} Y(v)\right] \leq \overline{B}. \qquad (91)$$

By Chebyshev's inequality, for $\forall\varepsilon>0$, we can obtain

$$\mathbb{P}\left\{\omega\mid \sup_{\zeta\leq t\leq\zeta+1} Y(t) > \zeta^{1+\varepsilon}\right\} \leq \frac{\overline{B}}{\zeta^{1+\varepsilon}}, \quad \zeta=1,2,\ldots. \qquad (92)$$

By using the Borel–Cantelli lemma [27], we get

$$\sup_{\zeta\leq t\leq\zeta+1} [Y(t)] \leq \zeta^{1+\varepsilon}. \qquad (93)$$

Therefore, for $\zeta\leq t\leq\zeta+1$ and $\zeta\geq\zeta_0(\omega)$, if $t\longrightarrow\infty$, then $\zeta\longrightarrow\infty$.

$$\limsup_{t\longrightarrow+\infty}\frac{\ln|Y(t)|}{\ln t} \leq \frac{\ln\left(\sup_{\zeta\leq t\leq\zeta+1}[Y(t)]\right)}{\ln t} \leq \frac{\ln\zeta^{1+\varepsilon}}{\ln t} \leq 1+\varepsilon. \qquad (94)$$

Let $\varepsilon\longrightarrow 0$; then, $\limsup_{t\longrightarrow+\infty}(\ln Y(t)/\ln t)\leq 1$, that is,

$$\limsup_{t\longrightarrow+\infty}\frac{\ln|X(t)|}{\ln t} = \limsup_{t\longrightarrow+\infty}\frac{\sum_{0<t_n<t}\ln(1+\delta_n)+\ln|Y(t)|}{\ln t} \leq 1. \qquad (95)$$

Now, we prove the lower growth rate of the solution. From (68), we obtain

$$\limsup_{t\longrightarrow+\infty}\mathbb{E}\left[(1+V_1(Y))^\varrho\right] \leq \overline{H}, \qquad (96)$$

where $\overline{H}$ is a positive constant.

Similarly,

$$\mathrm{d}\left[(1+V_1(Y))^\varrho\right] \leq \varrho(1+V_1(Y))^{\varrho-2}\left[-2\left[r(\xi(t))-\frac{1}{2}\sigma^2(\xi(t))-\varrho\sigma^2(\xi(t))-\alpha(\xi(t))C_0(t)\right.\right.$$
$$-\int_{\mathbb{Y}}(\gamma((\xi(t)),v))\lambda(\mathrm{d}v)\right]V_1^2(Y) + 2a_1(\xi(t))\prod_{0<t_n<t}(1+\delta_n)V_1^{3/2}(Y)$$
$$-2\left[r(\xi(t))-\frac{3}{2}\sigma^2(\xi(t))-\alpha(\xi(t))C_0(t)-\int_{\mathbb{Y}}(\gamma((\xi(t)),v))\lambda(\mathrm{d}v)\right]V_1(Y)$$
$$\left.+2a_1(\xi(t))\prod_{0<t_n<t}(1+\delta_n)V_1^{1/2}(Y)\right]\mathrm{d}t - 2\varrho\sigma(\xi(t))(1+V_1(Y))^{\varrho-1}V_1(Y)\mathrm{d}B(t) \qquad (97)$$
$$+\int_{\mathbb{Y}}\left[\left(1+V_1(Y)+V_1(Y)\left(\frac{1}{(1+\gamma((\xi(t)),v))^2}-1\right)\right)^\varrho-(1+V_1(Y))^\varrho\right]\tilde{N}(\mathrm{d}t,\mathrm{d}v)$$
$$\leq \varrho(1+V_1(Y))^{\varrho-2}\left[D_1V_1^2(Y)+D_2V_1^{3/2}(Y)+D_3V_1(Y)+D_2V_1^{1/2}(Y)\right]\mathrm{d}t$$
$$-2\varrho\sigma(\xi(t))(1+V_1(Y))^{\varrho-1}V_1(Y)\mathrm{d}B(t)$$
$$+\int_{\mathbb{Y}}\left[\left(1+V_1(Y)+V_1(Y)\left(\frac{1}{(1+\gamma((\xi(t)),v))^2}-1\right)\right)^\varrho-(1+V_1(Y))^\varrho\right]\tilde{N}(\mathrm{d}t,\mathrm{d}v),$$

where

$$D_1 = -2\left[r\left(\xi(t)\right) - \frac{1}{2}\sigma^2\left(\xi(t)\right) - \varrho\sigma^2\left(\xi(t)\right) - \alpha\left(\xi(t)\right)C_0(t) - \int_{\mathbb{Y}}\left(\gamma\left(\left(\xi(t)\right), v\right)\right)\lambda(dv)\right],$$

$$D_2 = 2Ma_1\left(\xi(t)\right),$$

$$D_3 = -2\left[r\left(\xi(t)\right) - \frac{3}{2}\sigma^2\left(\xi(t)\right) - \alpha\left(\xi(t)\right)C_0(t) - \int_{\mathbb{Y}}\left(\gamma\left(\left(\xi(t)\right), v\right)\right)\lambda(dv)\right].$$

(98)

Let $D > 0$ be sufficiently large for

$$\varrho\left(D_1 V_1^2(Y) + D_2 V_1^{3/2}(Y) + D_3 V_1(Y) + D_2 V_1^{1/2}(Y)\right)$$
$$\leq D\left(1 + V_1(Y)\right)^2.$$

(99)

Then,

$$d\left[\left(1 + V_1(Y)\right)^\varrho\right] \leq D\left(1 + V_1(Y)\right)^\varrho + 2\varrho\sigma\left(\xi(t)\right)\left(1 + V_1(Y)\right)^{\varrho-1}V_1(Y)dB(t)$$

$$+ \int_{\mathbb{Y}}\left[\left(1 + V_1(Y) + V_1(Y)\left(\frac{1}{\left(1 + \gamma\left(\left(\xi(t)\right), v\right)\right)^2} - 1\right)\right)^\varrho - \left(1 + V_1(Y)\right)^\varrho\right]\widetilde{N}(dt, dv).$$

(100)

Let $\zeta = 1, 2, \ldots$, and making use of (100) gives

$$\mathbb{E}\left[\limsup_{(k-1)\zeta \leq t \leq k\zeta}\left(1 + V_1(Y(t))\right)^\varrho\right]$$

$$\leq \mathbb{E}\left[\left(1 + V_1\left(Y\left((k-1)\zeta\right)\right)\right)^\varrho\right] + D\mathbb{E}\left[\limsup_{(k-1)\zeta \leq t \leq k\zeta}\int_{(k-1)\zeta}^t\left(1 + V_1(Y(t))\right)^\varrho ds\right]$$

$$+ \mathbb{E}\left[\limsup_{(k-1)\zeta \leq t \leq k\zeta}\left|\int_{(k-1)\zeta}^t 2\varrho\sigma\left(\xi(t)\right)\left(1 + V_1(Y)\right)^{\varrho-1}V_1(Y)dB(t)\right|\right]$$

$$+ \mathbb{E}\left[\limsup_{(k-1)\zeta \leq t \leq k\zeta}\left|\int_{(k-1)\zeta}^t \varrho\left(1 + V_1(Y)\right)^{\varrho-1}V_1(Y)\int_{\mathbb{Y}}\left(\frac{1}{\left(1 + \gamma\left(\left(\xi(t)\right), v\right)\right)^2} - 1\right)\widetilde{N}(dt, dv)\right|\right].$$

(101)

We compute that

$$D\mathbb{E}\left[\limsup_{(k-1)\zeta \leq t \leq k\zeta}\left|\int_{(k-1)\zeta}^t\left(1 + V_1(Y(s))\right)^\varrho ds\right|\right] \leq D\mathbb{E}\left[\int_{(k-1)\zeta}^t\left|\left(1 + V_1(Y(s))\right)^\varrho\right|ds\right]$$

$$\leq D\zeta\mathbb{E}\left[\limsup_{(k-1)\zeta \leq t \leq k\zeta}\left(1 + V_1(Y(t))\right)^\varrho\right],$$

(102)

$$\mathbb{E}\left[\limsup_{(k-1)\zeta \leq t \leq k\zeta}\left|\int_{(k-1)\zeta}^{t} 2\varrho\sigma(\xi(t))(1+V_1(Y))^{\varrho-1}V_1(Y)dB(s)\right|\right]$$

$$\leq \sqrt{32}\mathbb{E}\left[\left(\int_{(k-1)\zeta}^{k\zeta} 4\varrho^2\sigma^2(\xi(t))(1+V_1(Y))^{2\varrho-2}V_1^2(Y)ds\right)^{1/2}\right]$$

$$\leq 8\sqrt{2}\varrho\check{\sigma}\mathbb{E}\left[\left(\int_{(k-1)\zeta}^{k\zeta}(1+V_1(Y))^{2\varrho}ds\right)^{1/2}\right] \tag{103}$$

$$\leq 8\sqrt{2\zeta}\varrho\check{\sigma}\mathbb{E}\left[\limsup_{(k-1)\zeta \leq t \leq k\zeta}(1+V_1(Y(t)))^{\varrho}\right],$$

$$\mathbb{E}\left[\limsup_{(k-1)\zeta \leq t \leq k\zeta}\left|\int_{(k-1)\zeta}^{t}\varrho(1+V_1(Y))^{\varrho-1}V_1(Y)\int_{\mathbb{Y}}\left(\frac{1}{(1+\gamma((\xi(t)),\nu))^2}-1\right)\widetilde{N}(dt,d\nu)\right|\right]$$

$$\leq \sqrt{32}\mathbb{E}\left[\int_{(k-1)\zeta}^{t}\int_{\mathbb{Y}}\varrho^2(1+V_1(Y))^{2\varrho-2}V_1^2(Y)\int_{\mathbb{Y}}\left(\frac{1}{(1+\gamma((\xi(t)),\nu))^2}-1\right)^2 N(ds,d\nu)\right]^{1/2}$$

$$\leq \sqrt{32}\varrho\left(\int_{\mathbb{Y}}\left(\frac{1}{(1+\widehat{\gamma})^2}-1\right)^2\lambda(d\nu)\right)^{1/2}\mathbb{E}\left[\int_{(k-1)\zeta}^{t}\int_{\mathbb{Y}}(1+V_1(Y))^{2\varrho}N(ds,d\nu)\right]^{1/2} \tag{104}$$

$$\leq 4\sqrt{2\zeta}\varrho\left(\int_{\mathbb{Y}}\left(\frac{1}{(1+\widehat{\gamma})^2}-1\right)^2\lambda(d\nu)\right)^{1/2}\mathbb{E}\left[\sup_{(k-1)\zeta \leq t \leq k\zeta}(1+V_1(Y))^{\varrho}\right].$$

Substituting (102)–(104) into (101) results in

$$\mathbb{E}\left[\limsup_{(k-1)\zeta \leq t \leq k\zeta}(1+V_1(Y(t)))^{\varrho}\right]$$

$$\leq \mathbb{E}\left[(1+V_1(Y((k-1)\zeta)))^{\varrho}\right] \tag{105}$$

$$+ C\mathbb{E}\left[\limsup_{(k-1)\zeta \leq t \leq k\zeta}(1+V_1(Y(t)))^{\varrho}\right],$$

where
$C = D\zeta + 8\sqrt{2\zeta}\varrho\check{\sigma} + 4\sqrt{2\zeta}\varrho(\int_{\mathbb{Y}}((1/(1+\widehat{\gamma})^2)-1)^2\lambda(d\nu))^{1/2}$.
Then, from (96) and the above inequality, we get

$$\mathbb{E}\left[\limsup_{(k-1)\zeta \leq t \leq k\zeta}(1+V_1(Y(t)))^{\varrho}\right] \leq \overline{C}. \tag{106}$$

Then, for $\forall \varepsilon > 0$, we have

$$\mathbb{P}\left\{\omega \mid \sup_{(k-1)\zeta \leq t \leq k\zeta}(1+V_1(Y(t)))^{\varrho} > (k\zeta)^{1+\varepsilon}\right\}$$

$$\leq \frac{\overline{C}}{(k\zeta)^{1+\varepsilon}}, \quad k = 1, 2, \ldots. \tag{107}$$

Thus,

$$\frac{\ln(1+V_1(Y(t)))^{\varrho}}{\ln t} \leq \frac{(1+\varepsilon)\ln(k\zeta)}{\ln((k-1)\zeta)}. \tag{108}$$

That is,

$$\limsup_{t \longrightarrow +\infty} \frac{\ln(1+V_1(Y(t)))^{\varrho}}{\ln t} \leq 1+\varepsilon. \tag{109}$$

Letting $\varepsilon \longrightarrow 0$ gives

$$\limsup_{t \longrightarrow +\infty} \frac{\ln(|Y(t)|^{-2\varrho})}{\ln t} \leq 1. \tag{110}$$

Consequently,

$$\liminf_{t \longrightarrow +\infty} \frac{\ln(|Y(t)|)}{\ln t} \geq -\frac{1}{2\varrho}. \tag{111}$$

That is,

$$\liminf_{t \longrightarrow +\infty} \frac{\ln(|X(t)|)}{\ln t} \geq \liminf_{t \longrightarrow +\infty} \frac{\ln(m|Y(t)|)}{\ln t} \geq -\frac{1}{2\varrho}. \tag{112}$$
□

6. Numerical Simulations

Now, we use Matlab to analyze our results. We choose the same initial value $(X(0), C_0(0), C_e(0)) = (1, 0.3, 0.6)$ and the same parameter value as follows:

$$r(1) = 1,$$
$$\alpha(1) = 0.2,$$
$$(a_1(1), a_2(1), a_3(1)) = (0.25, 0.1, 0.02),$$
$$r(2) = 0.8,$$
$$\alpha(2) = 0.3,$$
$$(a_1(2), a_2(2), a_3(2)) = (0.3, 0.03, 0.05),$$
$$k = 0.6, \tag{113}$$
$$g = 0.26,$$
$$m = 0.05,$$
$$h = 0.23,$$
$$T = 4,$$
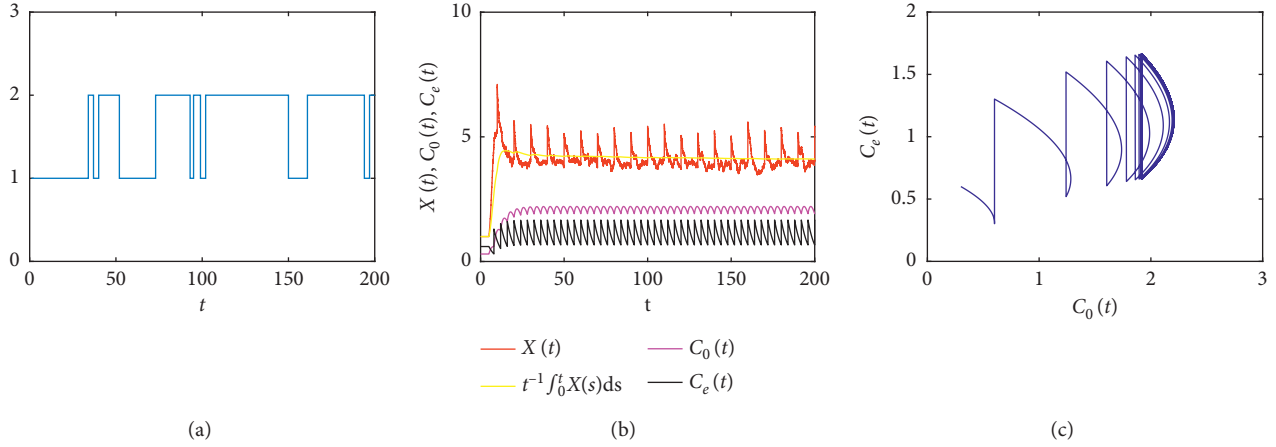$$\tau_1 = 2,$$
$$\lambda(\mathbb{Y}) = 1.$$

FIGURE 1: (a) Markov chains, (b) the time sequence diagram, and (c) the phase portrait of $C_0(t)$ and $C_e(t)$.
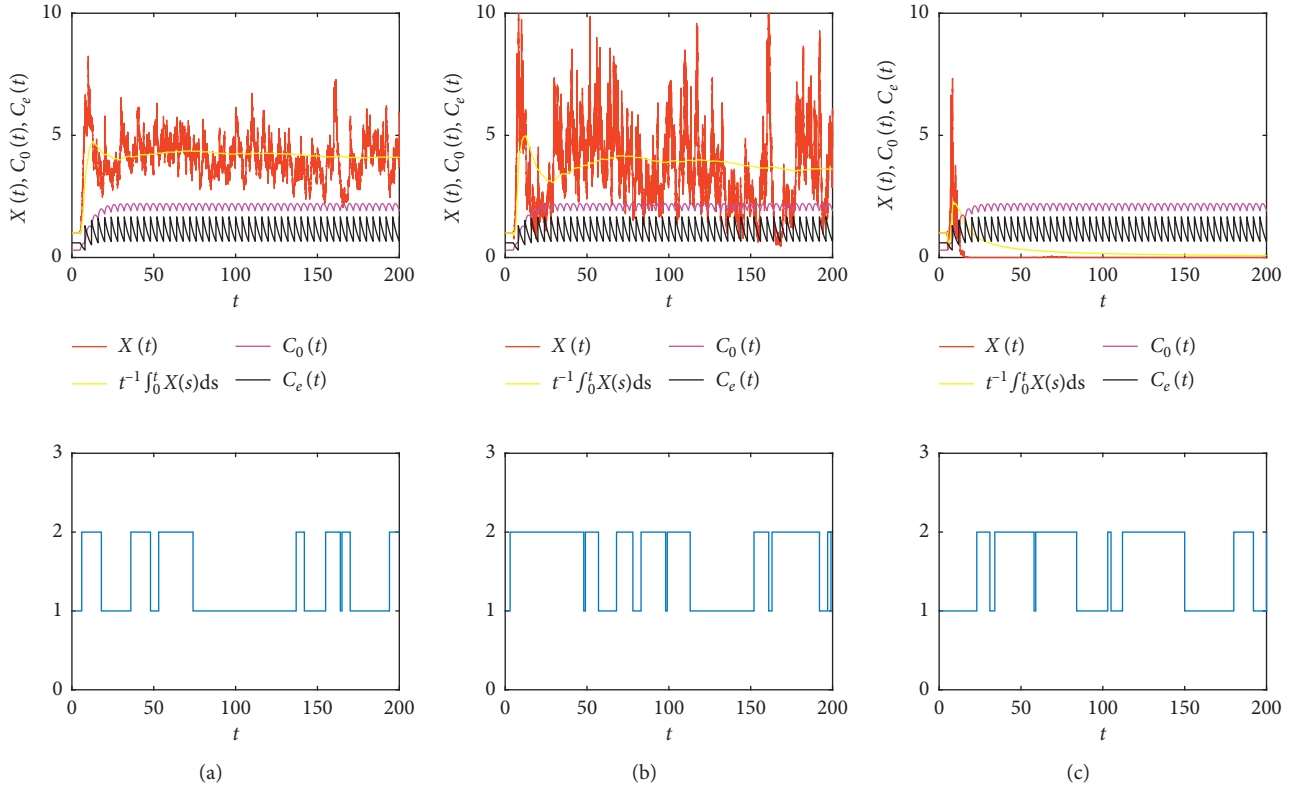

FIGURE 2: Effect of the white noise: (a) $\sigma(1) = 0.2, \sigma(2) = 0.2$; (b) $\sigma(1) = 0.5, \sigma(2) = 0.5$; (c) $\sigma(1) = 1, \sigma(2) = 1$.

In system (4), let $\xi(t) \in S = \{1, 2\}$ and the generator

$$\Gamma = \begin{pmatrix} -7 & 7 \\ 3 & -3 \end{pmatrix}. \tag{114}$$

By solving (6), we get a stationary distribution $\pi = (\pi_1, \pi_2) = (0.3, 0.7)$.

Now, we discuss the effects of different parameters on the population.

Example 1. Let $\gamma(1) = 0.5, \gamma(2) = 1.1, \sigma(1) = 0.04, \sigma(2) = 0.1, u = 1, \delta_n = e^{0.3} - 1$. Then, we obtain $\eta^* = 0.8771 >$

$0.4208 = \widehat{\alpha}\overline{C}_0$. According to Theorem 4, we know that $X(t)$ is weakly persistent (see Figure 1(a)). It can be seen from Figures 1(b) and 1(c) that the toxins in the organism $C_0(t)$ and the toxins in the environment $C_e(t)$ have a periodic solution.

6.1. Effect of the White Noise σ. Choosing the same parameters as in Example 1 but σ: by comparing Figure 1(a) and Figures 2(a) and 2(b), we found that the disturbance of population in the stochastic model is positively correlated
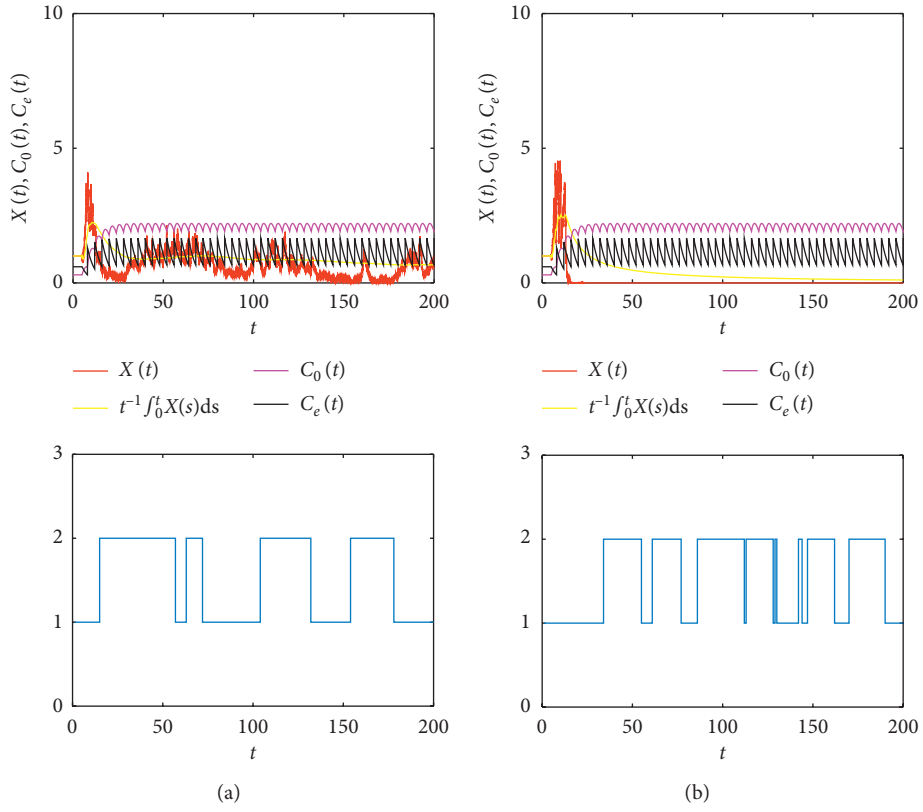
Figure 3: Effect of the Lévy noise: (a) $\gamma(1) = 3, \gamma(2) = 3$; (b) $\gamma(1) = 10, \gamma(2) = 10$.
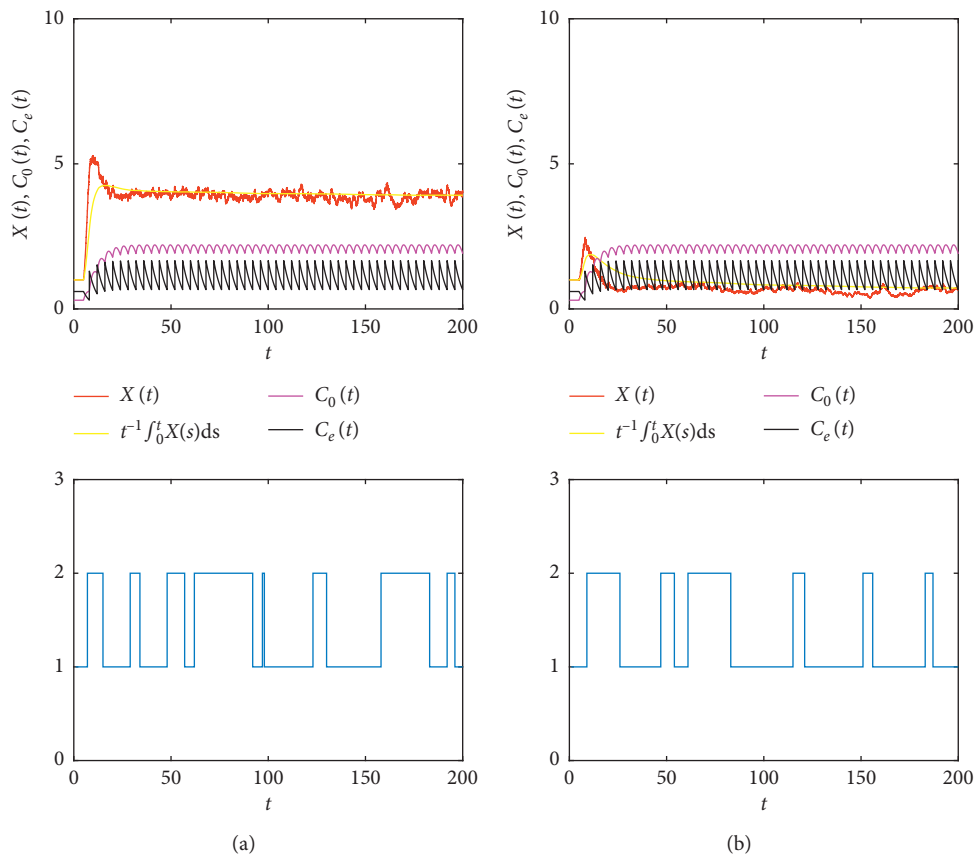

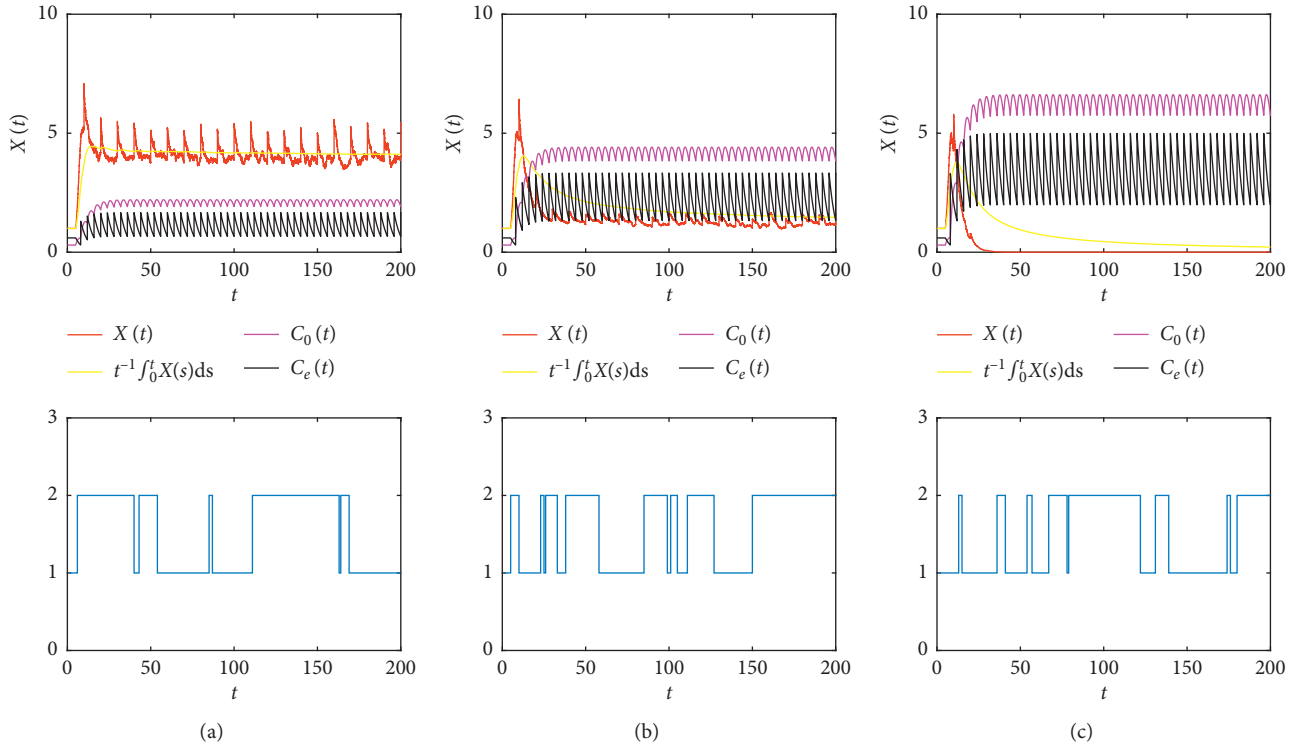Figure 4: Effect of telegraph noise.

Figure 5: Effect of the exogenous total toxicant input: (a) $u = 1$; (b) $u = 2$; (c) $u = 3$.
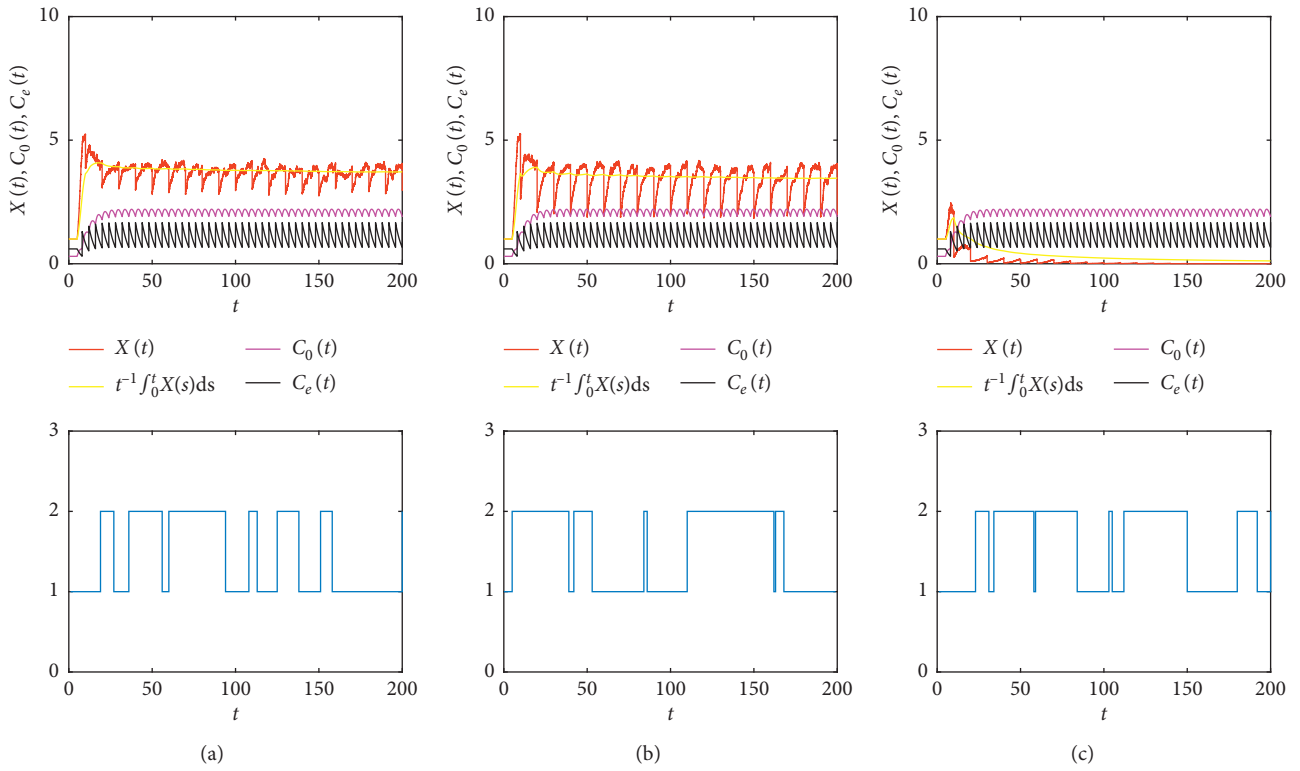

Figure 6: Effect of impulse: (a) $\delta_n = e^{-0.3} - 1$; (b) $\delta_n = e^{-0.7} - 1$; (c) $\delta_n = e^{-2} - 1$.

with the intensity of white noise. By comparing Figures 2(a)–2(c), the population will go extinct with increasing intensity of white noise. When the intensity of white noise is less than a certain level, the population still be persistent, while the white noise with large intensity may cause population extinction.

6.2. Effect of the Lévy Noise γ. Choosing the same parameters as in Example 1 but $\sigma(1) = 0.4, \sigma(2) = 0.4$, and γ: from Figure 3, it is concluded that the Lévy noise has a large impact on the persistence of population. It is shown that the number of the population will decrease when the intensity of the Lévy noise increases. When the intensity of the Lévy noise became larger, the population became extinct. Therefore, Lévy noise will not only reduce the number of species but also lead to population extinction.

6.3. Effect of Telegraph Noise. Choosing the same parameters as in Example 1 but $\delta_n = 0$: from Figure 4, we find that all parameter values are the same except the Markov chain. Since telegraph noise is described by a Markov chain, choosing a different Markov chain will produce different results.

6.4. Effect of the Exogenous Total Toxicant Input u. Choosing the same parameters as in Example 1 but u: from Figure 5, we find that the population can still be persistent when the total input of exogenous toxicant is small (see Figures 5(a) and 5(b)), while the population will go extinct when the total input of exogenous toxicant is strong (see Figure 5(c)).

6.5. Effect of Impulse δ_n. Choosing the same parameters as in Example 1 but δ_n: in Figure 6, we describe the impact of pulse harvest on the population. By comparing Figures 6(a)–6(c), we find that with the increase of the harvest, the population will gradually decrease until it becomes completely extinct.

7. Conclusion

In this paper, we explore the dynamics of a stochastic delay hybrid logistic model with two-pulse perturbations. First, by using Itô's formula, exponential martingale inequality, Chebyshev's inequality, and other mathematical skills, we establish some sufficient conditions for extinction, nonpersistence in the mean, weak persistence, persistence in the mean, and stochastic permanence. Then, the asymptotic properties of the lower growth rate and the upper growth rate of the solution are estimated.

Now, we give the key results as follows:

(I) (1) If $\eta^* < \widecheck{\alpha}\overline{C}_0$, then the population $X(t)$ is extinct.

(2) If $\eta^* = \widehat{\alpha}\overline{C}_0$, then the population $X(t)$ is nonpersistent in the mean.

(3) If $\eta^* > \widehat{\alpha}\overline{C}_0$, then the population $X(t)$ is weakly persistent.

(4) If $\eta_* > \widecheck{\alpha}\overline{C}_0$, then the population $X(t)$ is persistent in the mean.

(5) If $\sum_{k=1}^{N} \pi_k \overline{b}(k) > 0$, then the population $X(t)$ is stochastically permanent.

(II) The solution $X(t)$ obeys

$$\underline{\overset{*}{X}} = \frac{\eta_* - \widecheck{\alpha}\overline{C}_0}{\widecheck{a}_1} \leq \liminf_{t \to +\infty} \frac{1}{t} \int_0^t X(s)\mathrm{d}s$$

$$\leq \limsup_{t \to +\infty} \frac{1}{t} \int_0^t X(s)\mathrm{d}s \leq \frac{\eta^* - \widehat{\alpha}\overline{C}_0}{a} = \overline{X}^*, \quad \text{a.s.}$$

(115)

(III) The solution satisfies

$$\limsup_{t \to +\infty} \frac{\ln|X(t)|}{\ln t} \leq 1,$$

$$\liminf_{t \to +\infty} \frac{\ln|X(t)|}{\ln t} \geq -\frac{1}{2\varrho}, \quad \text{a.s.}$$

(116)

From our results and analysis, we can obtain the following conclusions. (1) Both white noise and Lévy noise tend to have negative effects on the persistence of population. However, the Lévy jump may have a greater influence than white noise on the persistence of population. (2) If the choice of telegraph noise is different, the persistence of the population will produce different results. (3) The total input of exogenous toxicant has a great disadvantaged influence on persistence of the population. With the increase of the total input of exogenous toxicant, the number of population will decrease, which enlightens us to reduce pollutant emissions to protect the ecological system. (4) The pulse release of the population is beneficial to the growth of the population; the pulse harvest of the population is beneficial to the growth of the population under reasonable conditions, but once overharvested, it will cause the population to become extinct.

These give us significant enlightenment: (1) when fishermen are fishing, they must maintain reasonable fishing to avoid overfishing that can lead to population extinction; (2) the discharge of factory sewage, exhaust gas, domestic sewage, etc., should be strictly controlled, and we should do our best to reduce the discharge of polluted toxins; and (3) humans should reduce interference with populations.

Data Availability

No data were used to support this study.

Conflicts of Interest

The authors declare that they have no conflicts of interest.

Acknowledgments

References

[1] Q. Liu, D. Jiang, T. Hayat, and A. Alsaedi, "Long-time behavior of a stochastic logistic equation with distributed delay and nonlinear perturbation," *Physica A: Statistical Mechanics and Its Applications*, vol. 508, pp. 289–304, 2018.

[2] D. Li, J. a. Cui, and G. Song, "Permanence and extinction for a single-species system with jump-diffusion," *Journal of Mathematical Analysis and Applications*, vol. 430, no. 1, pp. 438–464, 2015.

[3] B. Yang, Y. Cai, K. Wang, and W. Wang, "Optimal harvesting policy of logistic population model in a randomly fluctuating environment," *Physica A: Statistical Mechanics and Its Applications*, vol. 526, Article ID 120817, 2019.

[4] Y. Xu, S. Gao, and D. Chen, "Persistence and extinction of a nonautonomous switching single-species population model," *Applied Mathematics Letters*, vol. 103, Article ID 106187, 2019.

[5] Y. Lv, L. Chen, and F. Chen, "Stability and bifurcation in a single species logistic model with additive Allee effect and feedback control," *Advances in Difference Equations*, vol. 2020, no. 1, p. 129, 2020.

[6] C. Xu, "Phenomenological bifurcation in a stochastic logistic model with correlated colored noises," *Applied Mathematics Letters*, vol. 101, Article ID 106064, 2020.

[7] M. Liu and K. Wang, "Persistence and extinction in stochastic non-autonomous logistic systems," *Journal of Mathematical Analysis and Applications*, vol. 375, no. 2, pp. 443–457, 2011.

[8] E. Beretta and Y. Takeuchi, "Global stability of single-species diffusion Volterra models with continuous time delays," *Bulletin of Mathematical Biology*, vol. 49, no. 4, pp. 431–448, 1987.

[9] M. Liu and K. Wang, "On a stochastic logistic equation with impulsive perturbations," *Computers & Mathematics with Applications*, vol. 63, no. 5, pp. 871–886, 2012.

[10] S. Zhao, S. Yuan, and H. Wang, "Threshold behavior in a stochastic algal growth model with stoichiometric constraints and seasonal variation," *Journal of Differential Equations*, vol. 268, no. 9, pp. 5113–5139, 2020.

[11] X. Yu and S. Yuan, "Asymptotic properties of a stochastic chemostat model with two distributed delays and nonlinear perturbation," *Discrete & Continuous Dynamical Systems—B*, vol. 25, no. 7, pp. 2373–2390, 2020.

[12] W. Zhou, J. Yang, X. Yang, A. Dai, H. Liu, and J. a. Fang, "*p*th moment exponential stability of stochastic delayed hybrid systems with Lévy noise," *Applied Mathematical Modelling*, vol. 39, no. 18, pp. 5650–5658, 2015.

[13] X. Yu, S. Yuan, and T. Zhang, "Asymptotic properties of stochastic nutrient-plankton food chain models with nutrient recycling," *Nonlinear Analysis: Hybrid Systems*, vol. 34, pp. 209–225, 2019.

[14] S. Yuan, D. Wu, G. Lan, and H. Wang, "Noise-induced transitions in a nonsmooth producer-Grazer model with stoichiometric constraints," *Bulletin of Mathematical Biology*, vol. 82, no. 5, p. 55, 2020.

[15] X. Sun, W. Zuo, D. Jiang, and T. Hayat, "Unique stationary distribution and ergodicity of a stochastic logistic model with distributed delay," *Physica A: Statistical Mechanics and Its Applications*, vol. 512, pp. 864–881, 2018.

[16] S. Ma and D. Dong, "The asymptotic stability analysis in stochastic logistic model with Poisson growth coefficient," *Theoretical and Applied Mechanics Letters*, vol. 4, no. 1, Article ID 013004, 2014.

[17] N. Kaplan, "A continuous time Markov branching model with random environments," *Advances in Applied Probability*, vol. 5, no. 1, pp. 37–54, 1973.

[18] N. H. Du, R. Kon, K. Sato, and Y. Takeuchi, "Dynamical behavior of Lotka-Volterra competition systems: non-autonomous bistable case and the effect of telegraph noise," *Journal of Computational and Applied Mathematics*, vol. 170, no. 2, pp. 399–422, 2004.

[19] M. Slatkin, "The dynamics of a population in a Markovian environment," *Ecology*, vol. 59, no. 2, pp. 249–256, 1978.

[20] A. Settati and A. Lahrouz, "Stationary distribution of stochastic population systems under regime switching," *Applied Mathematics and Computation*, vol. 244, pp. 235–243, 2014.

[21] X. Li, A. Gray, D. Jiang, and X. Mao, "Sufficient and necessary conditions of stochastic permanence and extinction for stochastic logistic populations under regime switching," *Journal of Mathematical Analysis and Applications*, vol. 376, no. 1, pp. 11–28, 2011.

[22] T. Zhang and H. Chen, "The stability with a general decay of stochastic delay differential equations with Markovian switching," *Applied Mathematics and Computation*, vol. 359, no. 9, pp. 294–307, 2019.

[23] Y. Cai, S. Cai, and X. Mao, "Stochastic delay foraging arena predator-prey system with Markov switching," *Stochastic Analysis and Applications*, vol. 38, no. 2, pp. 191–212, 2020.

[24] X. Li, D. Jiang, and X. Mao, "Population dynamical behavior of Lotka-Volterra system under regime switching," *Journal of Computational and Applied Mathematics*, vol. 232, no. 2, pp. 427–448, 2009.

[25] X. Yu, S. Yuan, and T. Zhang, "Persistence and ergodicity of a stochastic single species model with Allee effect under regime switching," *Communications in Nonlinear Science and Numerical Simulation*, vol. 59, pp. 359–374, 2018.

[26] M. Gao, D. Jiang, and T. Hayat, "The threshold of a chemostat model with single-species growth on two nutrients under telegraph noise," *Communications in Nonlinear Science and Numerical Simulation*, vol. 75, pp. 160–173, 2019.

[27] X. Mao and C. Yuan, *Stochastic Differential Equations with Markovian Switching*, Imperial College Press, London, UK, 2006.

[28] X. Li and G. Yin, "Logistic models with regime switching: permanence and ergodicity," *Journal of Mathematical Analysis and Applications*, vol. 441, no. 2, pp. 593–611, 2016.

[29] M. Liu and K. Wang, "Dynamics and simulations of a logistic model with impulsive perturbations in a random environment," *Mathematics and Computers in Simulation*, vol. 92, pp. 53–75, 2013.

[30] Y. Deng and M. Liu, "Analysis of a stochastic tumor-immune model with regime switching and impulsive perturbations," *Applied Mathematical Modelling*, vol. 78, pp. 482–504, 2020.

[31] H. Lv, Z. Liu, Z. Li, L. Wang, and D. Xu, "Two impulsive stochastic delay single-species models incorporating Lévy noise," *Journal of Applied Mathematics and Computing*, vol. 58, no. 1-2, pp. 721–753, 2018.

[32] C. Lu and X. Ding, "Persistence and extinction of a stochastic logistic model with delays and impulsive perturbation," *Acta Mathematica Scientia*, vol. 34, no. 5, pp. 1551–1570, 2014.

[33] C. Lu, B. Li, L. Zhou, and L. Zhang, "Survival analysis of an impulsive stochastic delay logistic model with Lévy jumps," *Mathematical Biosciences and Engineering*, vol. 16, no. 5, pp. 3251–3271, 2019.

[34] C. Lu, Q. Ma, and X. Ding, "Persistence and extinction for stochastic logistic model with Lévy noise and impulsive perturbation," *Electronic Journal of Differential Equations*, vol. 2015, no. 247, pp. 1–14, 2015.

[35] D. Li, T. Guo, and Y. Xu, "The effects of impulsive toxicant input on a single-species population in a small polluted environment," *Mathematical Biosciences and Engineering*, vol. 16, no. 6, pp. 8179–8194, 2019.

[36] M. Liu and K. Wang, "Persistence and extinction of a single-species population system in a polluted environment with random perturbations and impulsive toxicant input," *Chaos, Solitons & Fractals*, vol. 45, no. 12, pp. 1541–1550, 2012.

[37] Y. Liu, Q. Liu, and Z. Liu, "Dynamical behaviors of a stochastic delay logistic system with impulsive toxicant input in a polluted environment," *Journal of Theoretical Biology*, vol. 329, pp. 1–5, 2013.

[38] B. Liu, L. Chen, and Y. Zhang, "The effects of impulsive toxicant input on a population in a polluted environment," *Journal of Biological Systems*, vol. 11, no. 3, pp. 265–274, 2003.

[39] J. K. Hale and J. Kato, "Phase space for retarded equations with infinite delay," *Funkcialaj Ekvacioj-Serio Internacia*, vol. 21, pp. 11–41, 1978.

[40] X. Mao, *Stochastic Differential Equations and Applications*, Horwood Publishing, Chichester, UK, 1997.

[41] R. Lipster, "A strong law of large numbers for local martingales," *Stochastics*, vol. 3, pp. 217–228, 1980.

WILEY | Hindawi

Research Article

Mathematical Modelling of the Inhibitory Role of Regulatory T Cells in Tumor Immune Response

Zhongtao Yang,[1,2] Cuihong Yang,[1] Yueping Dong [ID],[1] and Yasuhiro Takeuchi[3]

[1]*School of Mathematics and Statistics, Central China Normal University, Wuhan 430079, China*
[2]*School of Finance and Mathematics, Huainan Normal University, Huainan 232038, China*
[3]*College of Science and Engineering, Aoyama Gakuin University, Sagamihara 252-5258, Japan*

Correspondence should be addressed to Yueping Dong; dongyueping0531@gmail.com

The immune system against tumors acts through a complex dynamical process showing a dual role. On the one hand, the immune system can activate some immune cells to kill tumor cells (TCs), such as cytotoxic T lymphocytes (CTLs) and natural killer cells (NKs), but on the other hand, more evidence shows that some immune cells can help tumor escape, such as regulatory T cells (Tregs). In this paper, we propose a tumor immune interaction model based on Tregs-mediated tumor immune escape mechanism. When helper T cells' (HTCs) stimulation rate by the presence of identified tumor antigens is below critical value, the coexistence (tumor and immune) equilibrium is always stable in its existence region. When HTCs stimulation rate is higher than the critical value, the inhibition rate of effector cells (ECs) by Tregs can destabilize the coexistence equilibrium and cause Hopf bifurcations and produce a limit cycle. This model shows that Tregs might play a crucial role in triggering the tumor immune escape. Furthermore, we introduce the adoptive cellular immunotherapy (ACI) and monoclonal antibody immunotherapy (MAI) as the treatment to boost the immune system to fight against tumors. The numerical results show that ACI can control TCs more, while MAI can delay the inhibitory effect of Tregs on ECs. The result also shows that the combination of both immunotherapies can control TCs and reduce the inhibitory effect of Tregs better than a single immunotherapy can control.

1. Introduction

Tumors can be benignant (not cancerous), premalignant (precancerous), and malignant (cancerous). Every year millions of people suffer with cancer and die from this disease throughout the world [1]. It is important to understand tumor's mechanisms of establishment and destruction, cell-mediate immunity with cytotoxic T lymphocytes (CTLs), and natural killer cells (NKs), generally called effector cells (ECs) that are cytotoxic to tumor cells (TCs), and play a basic role in immune response against tumors [2, 3]. Moreover, efficient antitumor immunity requires the action of helper T cells (HTCs), which can directly activate naive CD8^{+} T cells to differentiate into CTLs [4–6]. Recently, it has been reported that regulatory T cells (Tregs) can inhibit CTLs and promote the escape of TCs [7]. Tregs suppress immune cells, and when the war

between T cells and infection is over, the Tregs signal to stop [8]. Cancer immunotherapy fights against cancer by strengthening the body's immune system, but the involvement of Tregs inhibits the immune response and turns off the anticancer effect. Tregs inhibition is important in the dynamics of the tumor immune system, which is one motivation of this work.

Adoptive T cell immunotherapy (ACI) as a common immunotherapy involves injecting adoptive T cells directly into tumor patients [9–11]. Its advantages are good destruction of tumor and persistence, while its disadvantages are serious toxic and side effects. The monoclonal antibody immunotherapy (MAI) is the immune checkpoint inhibitor [12, 13], which has the advantage of removing the suppression state of the immune system and restoring the immune function of the body to TCs and the disadvantage of having serious immune-related adverse reactions.

Tregs have become an important target in tumor immunotherapy because of their contribution to tumor immune escape. Cytotoxic T lymphocyte antigen 4 (CTLA-4) is a marker that is expressed on the surface of activated T cells and transmits inhibitory signals in the immune response [14–16]. Blocking CTLA-4 can reduce the inhibitory activity of Tregs, and the anti-CTLA-4 humanized monoclonal antibody Ipilimumab and Tremelimumab are used to treat advanced melanoma and malignant mesothelioma, respectively [17]. Similar to CTLA-4, programmed death receptor 1 (PD-1) can also promote the activation and development of Tregs [18–21]. Blocking PD-1 can prevent the development of Tregs and prevent the conversion of HTCs into Tregs [22]. Currently, OPDIVO (Nivolumab), an anti-PD-1 monoclonal antibody, has been approved by the US FDA for the treatment of melanoma, renal cell carcinoma, and non-small cell lung cancer [23–25]. Establishment of a mathematical model to study the immunotherapy on the reduction of Tregs inhibition has both theoretical and practical significance.

In order to describe the mechanisms of host's own immune response to against TCs, various types of mathematical models have been proposed [26–43]. The modelling of the tumor immune system described by ordinary differential equations (ODEs) has a long history, which can be traced back to the classic research of Stepanova in 1980 [26]. In 1994, Kuznetsov et al. established the famous two-dimensional ODEs model, postulating that tumor growth follows the Logistic growth pattern. They evaluated the parameters of the model by fitting experimental data from mice [27]. In 2003, Stolongo-Costa et al. assumed that TCs follows the exponential growth pattern and constructed a two-dimensional ODEs model. They analyzed the basic properties of the model and provided conditions for stability of the tumor-free equilibrium, explaining its epidemiological significance [28]. In 2004, Galach simplified Kuznetsov's system to account for the effect of immune delay on the tumor immune system [29]. In 2014, Dong et al. constructed a three-dimensional ODEs model focusing on the effects of HTCs on the tumor immune system [4].

In 1998, Kirschner and Panetta generalized Kuznetsov–Taylor model and illustrated the dynamics between TCs, ECs, and IL-2. They firstly introduced ACI into their model which can explain both short-term tumor oscillations in tumor sizes as well as long-term tumor relapse [11]. In 2003, in order to study the role of cytokine therapy in the activation of the immune system, Stolongo-Costa et al. introduced cycle therapy term $F\cos^2\omega t$ and established a cycle immunotherapy model. They obtained some thresholds of the frequency and intensity of immunotherapy [28]. In 2006, de Pillis et al. constructed the six-dimensional ODEs model to investigate the effects of combined chemotherapy and immunotherapy on tumor control. They briefly analyzed the nature of the model and discussed the optimal treatment using optimal control theory [30]. In 2008, Bunimovich-Mendrazitsky et al. established a pulsed differential equation model with Bacillus Calmette-Guerin tumor immunotherapy. They obtained the critical threshold and pulse frequency of BCG injection dose that could

successfully treat superficial bladder cancer [31]. In 2012, Wilson and Levy established a mathematical model containing Tregs. They studied the absence of treatment, vaccine treatment, anti-TGF treatment, and combination vaccine and anti-TGF treatment, as well as sensitivity analysis of some important parameters [8]. In 2018, Radunskaya et al. established a mathematical model with blood, spleen, and tumor compartments to study PD-L1 inhibitors in the role of tumor immunotherapy. The model was used to fit parameters with the experimental data. The results showed that increasing the resistance of PD-L1 doses can greatly improve the clearance rate of tumor [32].

This paper investigates the role of Tregs in the tumor immune system. Therefore, we incorporate the fourth population of Tregs into the previous system in [8]. For the mathematical simplicity, a bilinear term also has been used to describe the interactions between immune response and tumor. To our knowledge, HTCs can recognize TCs and promote the growth of ECs. And ECs can provide direct protective immunity by attacking TCs. When there are more HTCs and ECs, in order to maintain immune homeostasis, the body will produce corresponding Tregs to suppress ECs, and Tregs originating from both HTCs and ECs. Then, we establish a four-dimensional ODEs model described as below:

$$
\begin{cases}
\dfrac{dT(t)}{dt} = aT(t)(1 - bT(t)) - nE(t)T(t), \\[2mm]
\dfrac{dE(t)}{dt} = pE(t)H(t) - qR(t)E(t) - d_1E(t), \\[2mm]
\dfrac{dH(t)}{dt} = s_2 + k_2T(t)H(t) - d_2H(t), \\[2mm]
\dfrac{dR(t)}{dt} = r_1E(t) + r_2H(t) - d_3R(t),
\end{cases}
\tag{1}
$$

where $T(t)$, $E(t)$, $H(t)$, and $R(t)$ represent the populations of TCs, ECs, HTCs, and Tregs, respectively. The first equation describes the rate change of TCs population. The tumor follows logistic growth dynamics with growth rate a, and the maximum capacity is $1/b$. n represents the loss rate of TCs by ECs interaction. The second equation describes the rate change of the ECs population. d_1 is the mortality rate of ECs. p is the activation rate of ECs by HTCs, and q is the inhibition rate of Tregs on ECs. The third equation describes the rate change of the HTCs population, s_2 is birth rate of HTCs produced in the bone marrow, and HTCs have a natural lifespan of an average $1/d_2$ days. k_2 is HTCs stimulation rate by the presence of identified tumor antigens. The fourth equation gives the rate change of the Tregs population, r_1 and r_2 are the activation rates of Tregs by ECs and HTCs, respectively. d_3 represents per capita decay rate of Tregs. A diagram of the various interactions between these cell populations is shown in Figure 1.

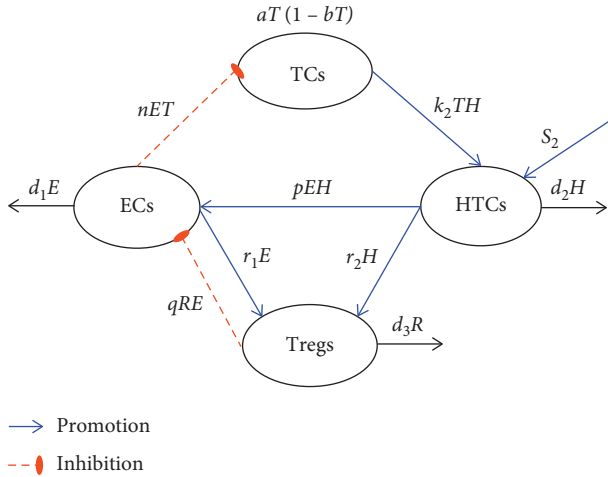We nondimensionalize model (1) by taking the following scaling:

FIGURE 1: A diagram of interactions among the different cell populations in model (1).

$$t = \frac{\tau}{nT_0}, \; T(t) = T_0 x(\tau), \; E(t) = E_0 y(\tau), \; H(t)$$

$$= H_0 z(\tau), \; R(t) = R_0 u(\tau), \; \alpha = \frac{a}{nT_0}, \; \beta = bT_0,$$

$$\rho = \frac{p}{n}, \; \omega_2 = \frac{k_2}{n}, \; \theta = \frac{qR_0}{nT_0}, \; \delta_1 = \frac{d_1}{nT_0}, \; \delta_2 \tag{2}$$

$$= \frac{d_2}{nT_0}, \; \delta_3 = \frac{d_3}{nT_0}, \; \sigma_2 = \frac{s_2}{nT_0 H_0}, \; \gamma_1 = \frac{r_1}{nR_0}, \; \gamma_2 = \frac{r_2}{nR_0},$$

and we choose the scaling $T_0 = E_0 = H_0 = R_0 = 10^6$. By replacing τ by t, we obtain the following scaled model:

$$\begin{cases} \dfrac{dx(t)}{dt} = \alpha x(t)(1 - \beta x(t)) - x(t)y(t), \\[2mm] \dfrac{dy(t)}{dt} = \rho y(t)z(t) - \theta y(t)u(t) - \delta_1 y(t), \\[2mm] \dfrac{dz(t)}{dt} = \sigma_2 + \omega_2 x(t)z(t) - \delta_2 z(t), \\[2mm] \dfrac{du(t)}{dt} = \gamma_1 y(t) + \gamma_2 z(t) - \delta_3 u(t), \end{cases} \tag{3}$$

with initial conditions

$$\begin{aligned} x(0) &= x_0 \geq 0, \\ y(0) &= y_0 \geq 0, \\ z(0) &= z_0 \geq 0, \\ u(0) &= u_0 \geq 0. \end{aligned} \tag{4}$$

Here, $x, y, z,$ and u denote the dimensionless densities of TCs, ECs, HTCs, and Tregs populations, respectively.

2. Model Analysis

2.1. Well Posedness of Model (3). The following proposition establishes the well posedness of model (3) with initial conditions (4).

Proposition 1. *The solutions* $(x(t), y(t), z(t), u(t))$ *of model (3) with initial conditions (4) are existent, unique, and nonnegative on the interval* $[0, +\infty)$.

Proof. Since the right-hand side of model (3) is completely continuous and locally Lipschitz on the interval $[0, +\infty)$, there exists a constant $\delta > 0$ such that the solutions $(x(t), y(t), z(t), u(t))$ of model (3) with initial conditions (4) are existent and unique on the interval $[0, \delta)$, where $0 < \delta \leq +\infty$ [44].

From model (3) with initial conditions (4), we obtain

$$x(t) = x_0 e^{\int_0^t (\alpha(1 - \beta(s)) - y(s))ds} \geq 0,$$

$$y(t) = y_0 e^{\int_0^t (\rho z(s) - \theta u(s) - \delta_1)ds} \geq 0,$$

$$z(t) = z_0 e^{\int_0^t (\omega_2 x(\tau) - \delta_2)d\tau} + \sigma_2 \int_0^t e^{\int_s^t (\omega_2 x(\tau) - \delta_2)d\tau} ds \geq 0,$$

$$u(t) = u_0 e^{-\delta_3 t} + \int_0^t (\gamma_1 y(s) + \gamma_2 z(s))e^{-\delta_3(t-s)} ds \geq 0. \tag{5}$$

It is obvious to see that the solutions $(x(t), y(t), z(t), u(t))$ of model (3) with initial conditions (4) are nonnegative for all $t \geq 0$. The proof is complete. □

2.2. Existence of Equilibria. In this section, we will study the existence of various equilibria for system (3). We set $(dx/dt) = 0, \; (dy/dt) = 0, \; (dz/dt) = 0,$ and $(du/dt) = 0$ in system (3), and we have

$$\begin{cases} \alpha x(1 - \beta x) - xy = 0, \\ \rho yz - \theta yu - \delta_1 y = 0, \\ \sigma_2 + \omega_2 xz - \delta_2 z = 0, \\ \gamma_1 y + \gamma_2 z - \delta_3 u = 0. \end{cases} \tag{6}$$

Putting $x = 0$ and $y = 0$ yields the tumor-free and ECs-free equilibrium, namely,

$$P_0 = (x_0, y_0, z_0, u_0) = \left(0, 0, \frac{\sigma_2}{\delta_2}, \frac{\gamma_2 \sigma_2}{\delta_2 \delta_3}\right), \tag{7}$$

which always exists.

Putting $x = 0$ and $y \neq 0$ yields the tumor-free equilibrium, namely,

$$P_1 = (x_1, y_1, z_1, u_1) = \left(0, \frac{\delta_3(\rho\sigma_2 - \delta_1\delta_2) - \gamma_2\theta\sigma_2}{\theta\gamma_1\delta_2}, \frac{\sigma_2}{\delta_2}, \frac{\rho\sigma_2 - \delta_1\delta_2}{\delta_2\theta}\right), \tag{8}$$

which exists when $\rho > \delta_1 \delta_2 / \sigma_2$ and $\theta < \delta_3 (\rho \sigma_2 - \delta_1 \delta_2)/\gamma_2 \sigma_2 \triangleq \theta_1$.

Putting $x = 1/\beta$ yields the tumor-dominant equilibrium, namely,

$$P_2 = (x_2, y_2, z_2, u_2) = \left(\frac{1}{\beta}, 0, \frac{\beta \sigma_2}{\beta \delta_2 - \omega_2}, \frac{\beta \gamma_2 \sigma_2}{\delta_3 (\beta \delta_2 - \omega_2)} \right),$$
(9)

which exists when $\omega_2 < \beta \delta_2 \triangleq \omega_2^*$.

Putting $x \neq 0$ and $x \neq 1/\beta$ and eliminating y, z, and u in (6), we have

$$F(x) = Ax^2 + Bx + C = 0,$$
(10)

where $A = -\alpha \beta \theta \gamma_1 \omega_2 < 0, B = \theta \alpha \gamma_1 (\omega_2^* + \omega_2) + \delta_1 \delta_3 \omega_2 > 0$, and $C = \delta_3 (\rho \sigma_2 - \delta_1 \delta_2) - \theta (\alpha \gamma_1 \delta_2 + \gamma_2 \sigma_2)$.

Then, we have the coexistence equilibrium

$$P^* = (x^*, y^*, z^*, u^*) = \left(x^*, \alpha(1 - \beta x^*), \frac{\sigma_2}{\delta_2 - \omega_2 x^*}, \right.$$

$$\left. \cdot \frac{\alpha \gamma_1 (1 - \beta x^*)(\delta_2 - \omega_2 x^*) + \gamma_2 \sigma_2}{\delta_3 (\delta_2 - \omega_2 x^*)} \right),$$
(11)

which exists when $x^* < \mu \triangleq \min\{(1/\beta), (\delta_2/\omega_2)\}$, where x^* is the positive root of (10).

Below, we consider the existence condition of P^*:

Case (1): $C \geq 0$, i.e., $\theta \leq \delta_3 (\rho \sigma_2 - \delta_1 \delta_2)/\alpha \gamma_1 \delta_2 + \gamma_2 \sigma_2 \triangleq \theta_0$. Since $F(1/\beta) = \theta \alpha \beta \gamma_1 \delta_2 + \delta_1 \delta_3 \omega_2 + C \beta/\beta > 0$ and $F(\delta_2/\omega_2) = \theta \alpha \gamma_1 \delta_2 + \delta_1 \delta_2 \delta_3 + C > 0$, we have $1/\beta < x^*$ and $\delta_2/\omega_2 < x^*$, which contradicts with $x^* < \mu$. Hence, P^* does not exist in this case.

Case (2): $C < 0$, i.e., $\theta > \theta_0$.

Let $\Delta = B^2 - 4AC = 4\alpha \beta \gamma_1 \theta \omega_2 (\delta_3 (\rho \sigma_2 - \delta_1 \delta_2) - \theta (\alpha \gamma_1 \delta_2 + \gamma_2 \sigma_2)) + (\theta \alpha \gamma_1 (\omega_2^* + \omega_2) + \delta_1 \delta_3 \omega_2)^2 = [\theta \alpha \gamma_1 (\omega_2 - \omega_2^*) + \delta_1 \delta_3 \omega_2]^2 + 4\alpha \beta \theta \gamma_1 \omega_2 \sigma_2 (\rho \delta_3 - \theta \gamma_2)$.

If $\Delta < 0$, then (10) does not have a positive root. Hence, P^* does not exist in this case.

If $\Delta = 0$, then (10) has one positive root x^*, where $x^* = \theta \alpha \gamma_1 (\omega_2^* + \omega_2) + \delta_1 \delta_3 \omega_2/2\alpha \beta \theta \gamma_1 \omega_2 > \omega_2^* + \omega_2/2\beta \omega_2 = 1/2 ((\delta_2/\omega_2) + (1/\beta)) \geq \mu$, which contradicts with $x^* < \mu$. Hence, P^* does not exist in this case.

If $\Delta > 0$, then (10) has two positive roots, where $x_+^* = \theta \alpha \gamma_1 (\omega_2^* + \omega_2) + \delta_1 \delta_3 \omega_2 + \sqrt{\Delta}/2\alpha \beta \theta \gamma_1 \omega_2$ and $x_-^* = \theta \alpha \gamma_1 (\omega_2^* + \omega_2) + \delta_1 \delta_3 \omega_2 - \sqrt{\Delta}/2\alpha \beta \theta \gamma_1 \omega_2$. Since $x_+^* > \theta \alpha \gamma_1 (\omega_2^* + \omega_2) + \delta_1 \delta_3 \omega_2/2\alpha \beta \theta \gamma_1 \omega_2 > \omega_2^* + \omega_2/2\beta \omega_2 = (1/2) ((\delta_2/\omega_2) + (1/\beta)) \geq \mu$, which contradicts with $x^* < \mu$. If $x_-^* < \mu$, i.e., $F(1/\beta) = (\delta_1 \delta_3 \omega_2 + \beta \delta_2 (\rho \sigma_2 - \delta_1 \delta_2) - \theta \beta \gamma_2 \sigma_2/\beta) > 0 \Rightarrow \theta < (\delta_1 \delta_3 \omega_2 + \beta \delta_3 (\rho \sigma_2 - \delta_1 \delta_2)/\beta \gamma_2 \sigma_2 \triangleq \theta_2$ and $F(\delta_2/\omega_2) = \sigma_2 (\rho \delta_3 - \theta \gamma_2) > 0 \Rightarrow \theta < \rho \delta_3/\gamma_2 \triangleq \theta_3$, there exists a unique coexistence equilibrium $P^* = (x^*, y^*, z^*, u^*) = (x^*, \alpha(1 - \beta x^*), \sigma_2/\delta_2 - \omega_2 x^*, \alpha \gamma_1 (1 - \beta x^*)(\delta_2 - \omega_2 x^*) + \gamma_2 \sigma_2/\delta_3 (\delta_2 - \omega_2 x^*))$, where $x^* = x_-^*$.

The existence conditions for each equilibrium are given in Table 1.

2.3. Stability of Equilibria.
In order to investigate the local stability of the above equilibria P_0, P_1, P_2, and P^* of system (3), we linearize the system and obtain Jacobian matrix at each equilibrium $\overline{P}(\overline{x}, \overline{y}, \overline{z}, \overline{u})$:

$$\mathbf{J}(\overline{P}) = \begin{pmatrix} \alpha - 2\alpha \beta \overline{x} - \overline{y} & -\overline{x} & 0 & 0 \\ 0 & \rho \overline{z} - \theta \overline{u} - \delta_1 & \rho \overline{y} & -\theta \overline{y} \\ \omega_2 \overline{z} & 0 & \omega_2 \overline{x} - \delta_2 & 0 \\ 0 & \gamma_1 & \gamma_2 & -\delta_3 \end{pmatrix}.$$
(12)

The corresponding characteristic equation is

$$\det (\mathbf{J}(\overline{P}) - \lambda \mathbf{I}) = \begin{vmatrix} \alpha - 2\alpha \beta \overline{x} - \overline{y} - \lambda & -\overline{x} & 0 & 0 \\ 0 & \rho \overline{z} - \theta \overline{u} - \delta_1 - \lambda & \rho \overline{y} & -\theta \overline{y} \\ \omega_2 \overline{z} & 0 & \omega_2 \overline{x} - \delta_2 - \lambda & 0 \\ 0 & \gamma_1 & \gamma_2 & -\delta_3 - \lambda \end{vmatrix} = 0.$$
(13)

Theorem 1. *System (3) always has one tumor-free and ECs-free equilibrium P_0, which is unstable.*

Proof. At P_0, characteristic (13) becomes

$$(\lambda - \alpha)(\lambda + \delta_2)(\lambda + \delta_3)\left(\lambda + \frac{\theta \gamma_2 \sigma_2 + \delta_1 \delta_2 \delta_3 - \rho \sigma_2 \delta_3}{\delta_2 \delta_3} \right) = 0.$$
(14)

It can be seen that one eigenvalue α is positive. Hence, P_0 is unstable. □

Theorem 2. *System (3) has one tumor-free equilibrium P_1, when $\rho > \delta_1 \delta_2 / \sigma_2$ and $\theta < \theta_1$, which is locally asymptotically stable (LAS) if the inequality $\theta < \theta_0$ holds.*

Proof. At P_1, characteristic (13) becomes

$$\left(\lambda - \frac{\theta (\alpha \gamma_1 \delta_2 + \gamma_2 \sigma_2) - \delta_3 (\rho \sigma_2 - \delta_1 \delta_2)}{\theta \gamma_1 \delta_2} \right)$$

$$(\lambda + \delta_2)(\lambda^2 + \delta_3 \lambda + \theta \gamma_1 y_1) = 0.$$
(15)

TABLE 1: The existence and stability conditions of each equilibrium.

	Existence conditions	Stability conditions
P_0	Always	Unstable
P_1	$\theta < \theta_1$	$\theta < \theta_0$
P_2	$\omega_2 < \omega_2^*$	$\theta > \theta_2$
P^*	$\theta > \theta_0 \begin{cases} (i):\ \omega_2 \leq \omega_2^*,\ \theta < \theta_2 < \theta_3 \\ (ii):\ \omega_2 > \omega_2^*,\ \theta < \theta_3 < \theta_2 \end{cases}$	(20)

Then, one root of characteristic equation is $-\delta_2 < 0$. It is easily noted that as $\delta_3 > 0$, $\theta\gamma_1 y_1 > 0$, so $\lambda^2 + \delta_3\lambda + \theta\gamma_1 y_1 = 0$ has solutions with negative real parts. Therefore, P_1 is LAS when $\theta(\alpha\gamma_1\delta_2 + \gamma_2\sigma_2) - \delta_3(\rho\sigma_2 - \delta_1\delta_2)/\theta\gamma_1\delta_2 < 0$, that is, $\theta < \theta_0$. □

Theorem 3. *System (3) has one tumor-dominant equilibrium P_2, when $\omega_2 < \omega_2^*$, which is LAS if the inequality $\theta > \beta\delta_3(\rho\sigma_2 - \delta_1\delta_2) + \delta_1\delta_3\omega_2/\beta\gamma_2\sigma_2 \equiv \theta_2$ holds.*

Proof. At P_2, characteristic (13) becomes

$$(\lambda + \alpha)(\lambda + \delta_3)\left(\lambda - \frac{\omega_2 - \omega_2^*}{\beta}\right)[\lambda - (\rho z_2 - \theta u_2 - \delta_1)] = 0. \tag{16}$$

The three roots of characteristic equation are $\lambda_1 = -\alpha < 0$, $\lambda_2 = -\delta_3 < 0$, and $\lambda_3 = \omega_2 - \omega_2^*/\beta < 0$, if $\omega_2 < \omega_2^*$. So, P_2 is LAS when $\lambda_4 = \rho z_2 - \theta u_2 - \delta_1 = \rho\beta\sigma_2\delta_3 - \delta_1\delta_3(\omega_2^* - \omega_2) - \theta\beta\gamma_2\sigma_2/\delta_3(\omega_2^* - \omega_2) < 0$, which is equivalent to $\theta > \theta_2$.

At P^*, characteristic (13) becomes

$$\lambda^4 + A_1\lambda^3 + A_2\lambda^2 + A_3\lambda + A_4 = 0, \tag{17}$$

where

$$A_1 = \alpha\beta x^* + \delta_3 + \delta_2 - \omega_2 x^* > 0,$$
$$A_2 = \theta\gamma_1 y^* + \alpha\beta(\delta_2 - \omega_2 x^*)x^* + (\alpha\beta x^* + \delta_2 - \omega_2 x^*)\delta_3 > 0,$$
$$A_3 = \theta\gamma_1(\alpha\beta x^* + \delta_2 - \omega_2 x^*)y^* + \alpha\beta\delta_3(\delta_2 - \omega_2 x^*)x^*$$
$$\qquad + \rho\omega_2 x^* y^* z^* > 0,$$
$$A_4 = \theta\alpha\beta\gamma_1(\delta_2 - \omega_2 x^*)x^* y^* + (\rho\delta_3 - \theta\gamma_2)\omega_2 x^* y^* z^*. \tag{18}$$

Note that $\delta_2 > \omega_2 x^*$ and $\theta < \min\{\theta_2, \theta_3\}$ are necessary for the existence of P^*, then we have $A_4 > 0$. By the Routh–Hurwitz criterion, the roots of (17) have only negative real parts if and only if

$$A_1 > 0, A_2 > 0, A_3 > 0, A_4 > 0, A_1 A_2$$
$$\quad - A_3 > 0, A_1(A_2 A_3 - A_1 A_4) - A_3^2 > 0. \tag{19}$$

Hence, we obtain the sufficient conditions for stability of P^*:

$$(H1):\ \delta_2 > \omega_2 x^*,\ \theta < \min\{\theta_2, \theta_3\},$$
$$(H2):\ A_1 A_2 - A_3 = \theta\gamma_1(\alpha\beta x^* + \delta_2 - \omega_2 x^*)y^*$$
$$\qquad\qquad + \alpha\beta\delta_3(\delta_2 - \omega_2 x^*)x^*$$
$$\qquad\qquad - \rho x^* y^* z^* > 0,$$
$$(H3):\ A_1(A_2 A_3 - A_1 A_4) - A_3^2 = B_1\theta + B_2 > 0, \tag{20}$$

where

$$B_1 = \Big(\big(\alpha\beta x^* + \delta_2 - \omega_2 x^*\big)^2\delta_3 + \alpha\beta x^* + \delta_2 - \omega_2 x^*\big)\delta_3^2$$
$$\quad - \rho\omega_2 x^* y^* z^*(\alpha\beta x^* + \delta_2 - \omega_2 x^*)\gamma_1 y^*$$
$$\quad - (\alpha\beta x^* + \delta_2 - \omega_2 x^* + \delta_3)^2(\alpha\beta\gamma_1(\delta_2 - \omega_2 x^*)x^* y^*$$
$$\quad - \omega_2\gamma_2 x^* y^* z^*),$$
$$B_2 = \Big[\big(\big(\alpha\beta x^* + \delta_2 - \omega_2 x^*\big)^2\delta_3 + \alpha\beta x^* + \delta_2 - \omega_2 x^*\big)\delta_3^2$$
$$\quad - \rho\omega_2 x^* y^* z^*(\alpha\beta\delta_3(\delta_2 - \omega_2 x^*)x^* + \rho\omega_2 x^* y^* z^*)\Big]$$
$$\quad - (\alpha\beta x^* + \delta_2 - \omega_2 x^* + \delta_3)^2\rho\omega_2\delta_3 x^* y^* z^*. \tag{21}$$

□

Theorem 4. *System (3) has a unique coexistence equilibrium P^*, when $\omega_2 \leq \omega_2^*, \theta_0 < \theta < \theta_2$ or $\omega_2 > \omega_2^*, \theta_0 < \theta < \theta_3$ hold, and P^* is LAS, when conditions (20) are satisfied.*

We summarize the above results in Table 1, where $\omega_2^* = \beta\delta_2, \theta_0 = \delta_3(\rho\sigma_2 - \delta_1\delta_2)/\alpha\gamma_1\delta_2 + \gamma_2\sigma_2$, $\theta_1 = \delta_3(\rho\sigma_2 - \delta_1\delta_2)/\gamma_2\sigma_2$, $\theta_2 = \beta\delta_3(\rho\sigma_2 - \delta_1\delta_2) + \delta_1\delta_3\omega_2/\beta\gamma_2\sigma_2$, and $\theta_3 = \rho\delta_3/\gamma_2$.

2.4. Numerical Simulations. In this section, we choose some suitable parameters in (3) to simulate numerically the theoretical conclusions obtained in the previous sections by using the Matlab software package MATCONT [45]. We select the following parameters' set [4]:

$$\alpha = 1.636,\ \beta = 0.002,\ \delta_1 = 0.3743,\ \sigma_2 = 0.38,$$
$$\delta_2 = 0.055,\ \rho = 0.48,\ \gamma_1 = 0.15,\ \gamma_2 = 0.2,\ \delta_3 = 0.25. \tag{22}$$

Note that $\omega_2^* = \beta\delta_2 = 0.00011$. By calculations, we have

$$\theta_0 = \frac{\delta_3 \left(\rho\sigma_2 - \delta_1\delta_2 \right)}{\alpha\gamma_1\delta_2 + \gamma_2\sigma_2} = 0.452,$$

$$\theta_1 = \frac{\delta_3 \left(\rho\sigma_2 - \delta_1\delta_2 \right)}{\gamma_2\sigma_2} = 0.5323,$$

$$\theta_3 = \frac{\rho\delta_3}{\gamma_2} = 0.6,$$

$$\theta_2 = \frac{\beta\delta_3 \left(\rho\sigma_2 - \delta_1\delta_3 \right) + \delta_1\delta_3\omega_2}{\beta\gamma_2\sigma_2} = 615.625\omega_2 + 0.5323. \tag{23}$$

And we find the stability region of $P^* = (x^*, y^*, z^*, u^*)$ (see Figure 2). P^* is LAS in regions **I** and **II**. P^* is unstable in region **III**.

Let us denote the point in $\theta - \omega_2$ plane as $Q_i = (\theta, \omega_2)$.

Case (a): we choose a point $Q_1 = (0.48, 0.0001)$ in the region **I**; then, system (3) has one interior equilibrium:

$$P_1^* = (77.6449, 1.38195, 8.0448, 7.265). \tag{24}$$

The eigenvalues of Jacobian matrix of (12) are

$$\begin{aligned} &-0.4623, \ -0.049151, \ -0.01991 - 0.378i \text{ and} \\ &-0.01991 + 0.378i, \end{aligned} \tag{25}$$

so P_1^* is stable, as shown in Figure 3(a).

Case (b): we choose a point $Q_2 = (0.455, 0.0004)$ in the region **II**; then, system (3) has one interior equilibrium:

$$P_2^* = (2.84485, 1.62669, 7.05506, 6.62006). \tag{26}$$

The eigenvalues of Jacobian matrix of (12) are

$$\begin{aligned} &-0.0931 + 0.301i, \ -0.0931 - 0.301i, \ -0.0633 \\ &+ 0.0188i \text{ and} -0.0633 - 0.0188i, \end{aligned} \tag{27}$$

so P_2^* is stable, as shown in Figure 3(b).

Case (c): we choose a point $Q_3 = (0.48, 0.000111)$ in the region **II**, then system (3) has one interior equilibrium:

$$P_3^* = (72.569, 1.39855, 8.094, 7.314). \tag{28}$$

The eigenvalues of Jacobian matrix of (12) are

$$-0.458, \ -0.0491, \ -0.0132 + 0.383i \text{ and } -0.0132 - 0.383i, \tag{29}$$

so P_3^* is stable, as shown in Figure 3(c).

Case (d): we choose a point $Q_4 = (0.48, 0.0004)$ in the region **III**; then, system (3) has one interior equilibrium:

$$P_4^* = (26.365, 1.54973, 8.54816, 7.76837). \tag{30}$$

The eigenvalues of Jacobian matrix of (12) are

$$-0.4328, \ -0.0497, \ 0.0509 + 0.416i \text{ and } 0.0509 - 0.416i, \tag{31}$$

so P_4^* is unstable, as shown in Figure 3(d).

Below, we perform numerically bifurcation analysis of x against θ for different values of ω_2.

Case (1): we choose $\omega_2 = 0.0001 < \omega_2^* = 0.00011$ (see Figure 4(a)).

We obtain the following result.

Proposition 2. *When $0 < \theta < \theta_0$, P_0 exists and is unstable, P_1 exists and is LAS, P_2 exists and is unstable, and P^* does not exist. When $\theta_0 < \theta < \theta_1$, P_0 exists and is unstable, P_1 exists and is unstable, P_2 exists and is unstable, and P^* exists and is LAS. When $\theta_1 < \theta < \theta_2$, P_0 exists and is unstable, P_1 does not exist, P_2 exists and is unstable, and P^* exists and is LAS. When $\theta > \theta_2$, P_0 exists and is unstable, P_1 does not exist, P_2 exists and is LAS, and P^* does not exist.*

Case (2): we choose $\omega_2 = 0.0004 > \omega_2^* = 0.00011$ (see Figure 4(b)).

We obtain the following result.

Proposition 3. *When $0 < \theta < \theta_0$, P_0 exists and is unstable, P_1 exists and is LAS, and P^* does not exist. When $\theta_0 < \theta < \theta_4$, where $\theta_4 = 0.4657$ is a Hopf bifurcation, P_0 exists and is unstable, P_1 exists and is LAS, and P^* exists and is LAS. When $\theta_4 < \theta < \theta_1$, P_0 exists and is unstable, P_1 exists and is unstable, and P^* exists and is unstable. When $\theta_1 < \theta < \theta_3$, P_0 exists and is unstable, P_1 does not exist, and P^* exists and is unstable. When $\theta > \theta_3$, P_0 exists and is unstable, P_1 does not exist, and P^* does not exist.*

Consider the case where HTCs stimulation rate (ω_2) is low by the presence of identified tumor antigens ($\omega_2 < \omega_2^*$). When the inhibition rate of Tregs to ECs θ is lower than θ_0, the solution of system (3) approaches P_1 implying that ECs can still effectively remove TCs. When $\theta_0 < \theta < \theta_2$, the solution of system (3) approaches P^* showing the coexistence of TCs and immune cells, which means that the patient can survive with tumors. When $\theta > \theta_2$, TCs escape the control of the immune system and develop into malignant tumors.

Next consider the case where HTCs stimulation rate (ω_2) is high by the presence of identified tumor antigens ($\omega_2 > \omega_2^*$). When $\theta < \theta_0$, the solution of system (3) approaches P_1 implying that TCs can be effectively removed by ECs. When $\theta_0 < \theta < \theta_4$, the solution of system (3) approaches P^* implying that TCs can still be controlled by the immune system. When $\theta > \theta_4$, the system has a Hopf bifurcation point and induces a limit cycle (see Figure 3(e)). In the biological sense, it can be understood that the number of TCs presents a periodic change.
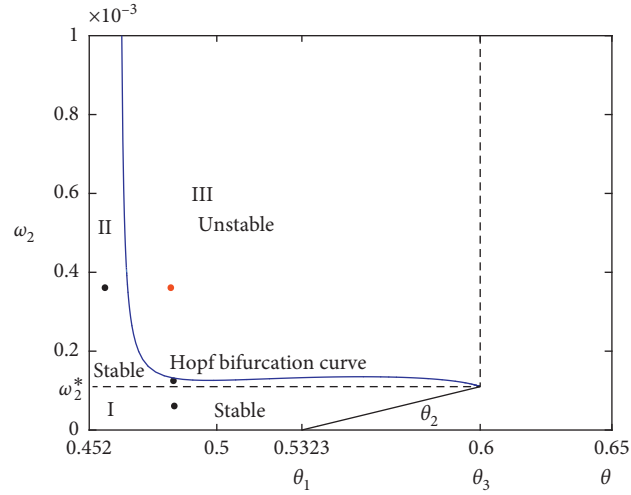
FIGURE 2: Stability region of P^* and Hopf bifurcation curve in $\theta - \omega_2$ parameter plane.

(a)

(b)

(c)

(d)

(e)
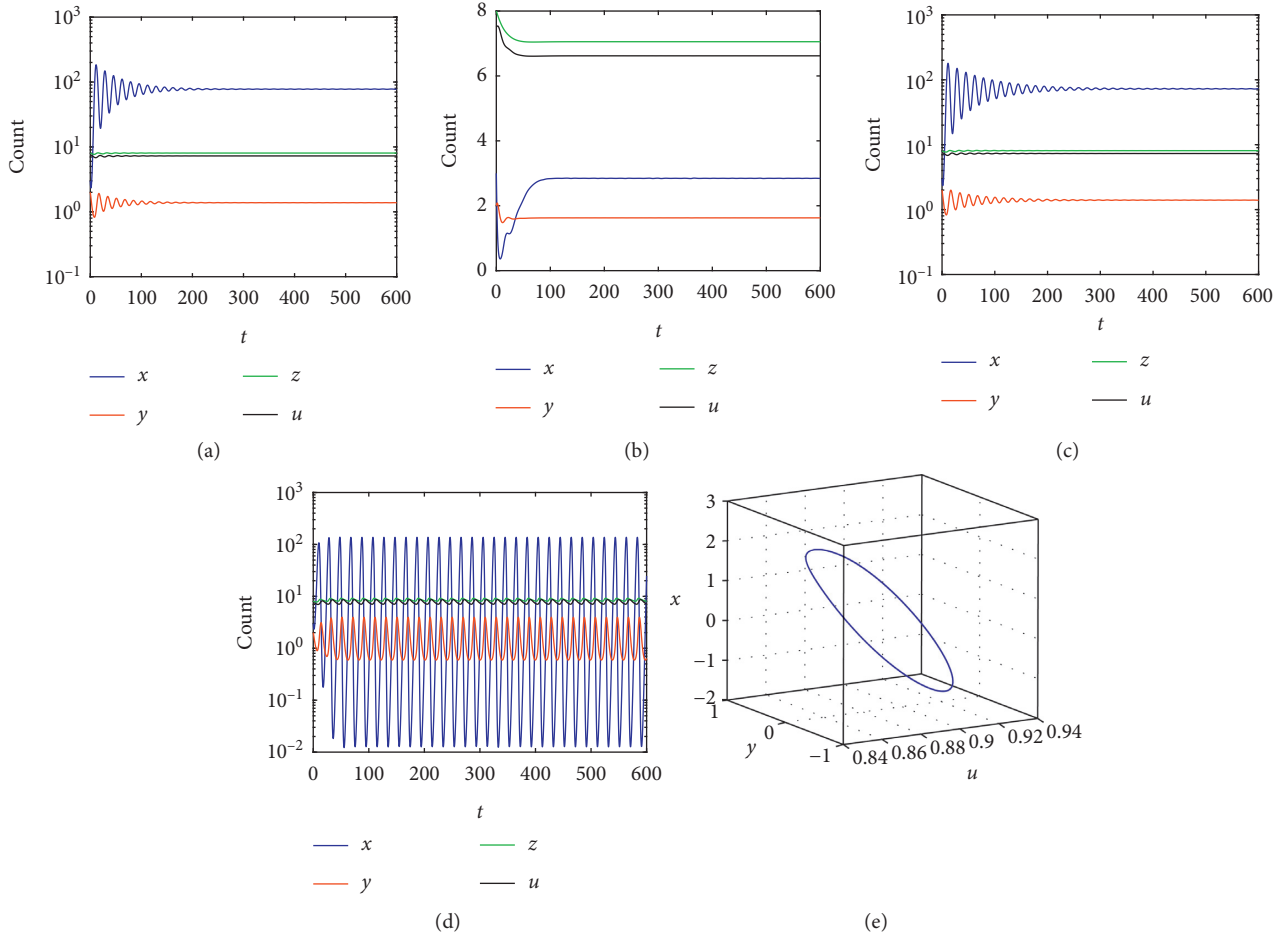
FIGURE 3: The other parameter values are given in (22). (a) P_1^* (77.644, 1.381, 8.044, 7.265) is LAS, $\theta = 0.48$ and $\omega_2 = 0.0001$. (b) P_2^* (2.844, 1.626, 7.055, 6.62) is LAS, $\theta = 0.455$ and $\omega_2 = 0.0004$. (c) P_3^* (72.569, 1.398, 8.094, 7.314) is LAS, $\theta = 0.48$ and $\omega_2 = 0.000111$. (d) P_4^* (26.365, 1.549, 8.548, 7.768) is unstable, $\theta = 0.48$ and $\omega_2 = 0.0004$. (e) The 3D phase portrait depicts tumor cell, ECs, and Tregs, $\theta = 0.48$ and $\omega_2 = 0.0004$.

(a)

(b)

FIGURE 4: The bifurcation diagrams of x with respect to θ for different $\omega_2 = 0.0001$ and 0.0004, respec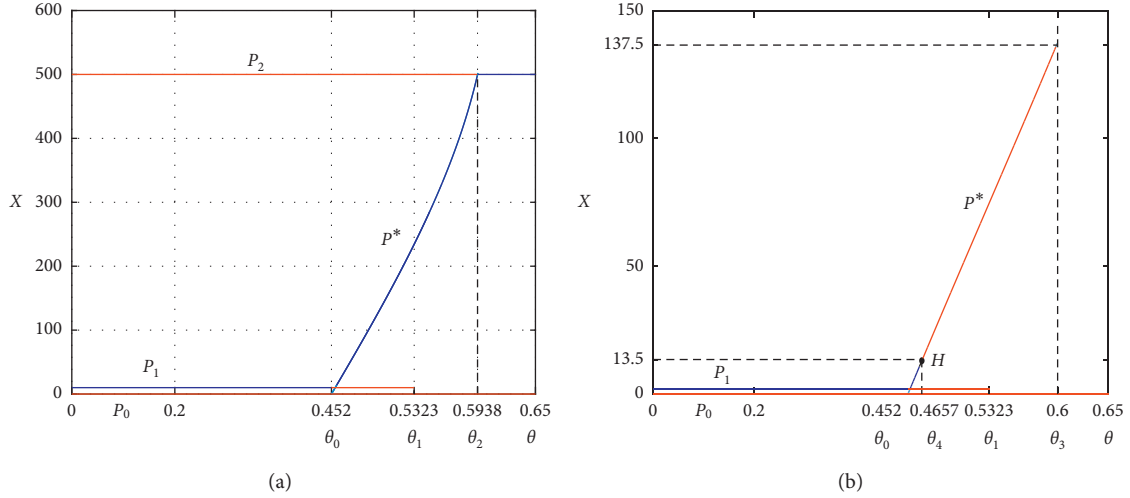tively. The stable state is represented by the blue curve, and the unstable one corresponds to the red curve. The equilibria are $P_0(0, 0, z_0, u_0)$, $P_1(0, y_1, z_1, u_1)$, $P_2(500, 0, z_2, u_2)$, and $P^*(x^*, y^*, z^*, u^*)$ of system (3) (in order to distinguish P_0 from P_1, we move P_1 up a little bit). (a) $\omega_2 = 0.0001$. (b) $\omega_2 = 0.0004$.

3. Treatment Model

In order to investigate well the effect of Tregs in tumor immune response under the treatment, we follow the way in [11] to introduce the constant treatment term s_1 into the second equation of (1). Since CTLA-4 and PD-1 can inhibit the development of Tregs and prevent the transformation of HTCs into Tregs [12], the effect of CTLA4 or PD-1 on Tregs can be considered. Then, we shall establish a five-dimensional ODEs model described as below:

$$\begin{cases} \dfrac{dT(t)}{dt} = aT(t)(1 - bT(t)) - nE(t)T(t), \\[2mm] \dfrac{dE(t)}{dt} = s_1 + pE(t)H(t) - qR(t)E(t) - d_1E(t), \\[2mm] \dfrac{dH(t)}{dt} = s_2 + k_2T(t)H(t) - d_2H(t), \\[2mm] \dfrac{dR(t)}{dt} = r_1E(t) + r_2H(t) - d_3R - mR(t)W(t), \\[2mm] \dfrac{dW(t)}{dt} = s_3 - d_4W(t), \end{cases} \tag{32}$$

where $W(t)$ represents the concentration of monoclonal antibody in human body at time t, s_1 represents the treatment term of introducing LAK and TIL into the region of tumor localization, m represents the inhibition rate of monoclonal antibody on Tregs, s_3 represents the amount of monoclonal antibody entering human body at time t, and d_4 represents the attenuation coefficient of monoclonal antibody.

We scale those new parameters in model (32) as follows:

$$W(t) = W_0\nu(\tau), \sigma_1 = \frac{s_1}{nE_0T_0}, \xi = \frac{mW_0}{nT_0}, \sigma_3 = \frac{s_3}{nW_0T_0}, \delta_4 = \frac{d_4}{nT_0}, \tag{33}$$

and we choose the scaling $W_0 = 10^6$. By replacing τ by t, we obtain the following scaled model with treatment:

$$\begin{cases} \dfrac{dx(t)}{dt} = \alpha x(t)(1 - \beta x(t)) - x(t)y(t), \\[2mm] \dfrac{dy(t)}{dt} = \sigma_1 + \rho y(t)z(t) - \theta y(t)u(t) - \delta_1 y(t), \\[2mm] \dfrac{dz(t)}{dt} = \sigma_2 + \omega_2 x(t)z(t) - \delta_2 z(t), \\[2mm] \dfrac{du(t)}{dt} = \gamma_1 y(t) + \gamma_2 z(t) - \delta_3 u(t) - \xi u(t)\nu(t), \\[2mm] \dfrac{d\nu(t)}{dt} = \sigma_3 - \delta_4\nu(t), \end{cases} \tag{34}$$

with initial conditions

$$x(0) = x_0 \geq 0, \ y(0) = y_0 \geq 0, \ z(0) = z_0 \geq 0, \ u(0) \\ = u_0 \geq 0, \ \nu(0) = \nu_0 \geq 0. \tag{35}$$

Here, ν denotes the dimensionless concentration of monoclonal antibody.

3.1. Model Analysis. By a similar proof of Proposition 1, we can obtain the well posedness of model (34) with initial conditions (35) as follows.

Proposition 4. *The solutions* $(x(t), y(t), z(t), u(t))$ *of model (34) with initial conditions (35) are existent, unique, and nonnegative on the interval* $[0, +\infty)$.

Next, we discuss the effect of three types of immunotherapy on tumors such as

Case I: ACI model ($\sigma_1 > 0$, $\sigma_3 = 0$)

Case II: MAI model ($\sigma_1 = 0$, $\sigma_3 > 0$)

Case III: combined immunotherapy model ($\sigma_1 > 0$, $\sigma_3 > 0$)

We set $dx/dt = 0$, $dy/dt = 0$, $dz/dt = 0$, $du/dt = 0$, and $dv/dt = 0$ in (34), and we have

$$
\begin{cases}
\alpha x (1 - \beta x) - xy = 0, \\
\rho yz - \theta yu - \delta_1 y + \sigma_1 = 0, \\
\sigma_2 + \omega_2 xz - \delta_2 z = 0, \\
\gamma_1 y + \gamma_2 z - \delta_3 u - \xi uv = 0, \\
\sigma_3 - \delta_4 v = 0.
\end{cases}
\tag{36}
$$

3.1.1. ACI Model. When $\sigma_1 > 0$ and $\sigma_3 = 0$, we put $v = 0$ and (36) becomes

$$
\begin{cases}
\alpha x (1 - \beta x) - xy = 0, \\
\rho yz - \theta yu - \delta_1 y + \sigma_1 = 0, \\
\sigma_2 + \omega_2 xz - \delta_2 z = 0, \\
\gamma_1 y + \gamma_2 z - \delta_3 u = 0.
\end{cases}
\tag{37}
$$

Putting $x = 0$ yields the tumor-free equilibrium, namely,

$$
E_0 = (x_0, y_0, z_0, u_0) = \left(0, y_0, \frac{\sigma_2}{\delta_2}, \frac{\gamma_1 \delta_2 y_0 + \gamma_2 \sigma_2}{\delta_2 \delta_3} \right),
\tag{38}
$$

where $y_0 = -B + \sqrt{B^2 - 4AC}/2A$, $A = \theta \gamma_1 \delta_2 > 0$, $B = \delta_1 \delta_2 \delta_3 + \theta \gamma_2 \sigma_2 - \rho \sigma_2 \delta_3$, and $C = -\sigma_1 \delta_2 \delta_3 < 0$. E_0 always exists.

Putting $x \neq 0$ and eliminating y, z, and u in (37), we have

$$
\begin{aligned}
F(x) &= C_3 x^3 + C_2 x^2 + C_1 x + C_0 \\
C_3 &= \theta \alpha^2 \beta^2 \gamma_1 \omega_2 > 0, \\
C_2 &= -\theta \alpha^2 \beta \gamma_1 \omega_2 - \alpha \beta [\theta \alpha \gamma_1 (\beta \delta_2 + \omega_2) + \delta_1 \delta_3 \omega_2] < 0, \\
C_1 &= \theta \alpha (2 \alpha \beta \gamma_1 \delta_2 + \alpha \gamma_1 \omega_2 + \beta \gamma_2 \sigma_2) \\
&\quad + \alpha \delta_3 [\delta_1 \omega_2 - \beta (\rho \sigma_2 - \delta_1 \delta_2)] - \sigma_1 \omega_2 \delta_3, \\
C_0 &= \sigma_1 \delta_2 \delta_3 + \alpha \delta_3 (\rho \sigma_2 - \delta_1 \delta_2) - \theta \alpha (\alpha \gamma_1 \delta_2 + \gamma_2 \sigma_2).
\end{aligned}
\tag{39}
$$

Case (a): if $F(0)F(\mu) = C_0 F(\mu) < 0$ (where $\mu = \min\{(1/\beta), (\delta_2/\omega_2)\}$, due to $F(+\infty) > 0$ and $F(-\infty) < 0$, then (39) has one positive root x^* in the interval $[0, \mu]$. Therefore, system (34) has a unique coexistence equilibrium:

$$
E^* = (x^*, y^*, z^*, u^*) = \left(x^*, \alpha (1 - \beta x^*), \frac{\sigma_2}{\delta_2 - \omega_2 x^*}, \right.
$$
$$
\left. \frac{\alpha \gamma_1 (1 - \beta x^*)(\delta_2 - \omega_2 x^*) + \gamma_2 \sigma_2}{\delta_3 (\delta_2 - \omega_2 x^*)} \right).
\tag{40}
$$

We show the existence conditions of E^* in the following:

Case (1): $C_0 > 0$, $F(\mu) < 0$.
Since $C_0 > 0$, we have $\theta < \sigma_1 \delta_2 \delta_3 + \alpha \delta_3 (\rho \sigma_2 - \delta_1 \delta_2)/\alpha (\alpha \gamma_1 \delta_2 + \gamma_2 \sigma_2) \triangleq \theta_5$. Since $F(\mu) < 0$, we have the following two cases:
Case where $1/\beta < \delta_2/\omega_2$, i.e., $\omega_2 < \beta \delta_2$. Since $\mu = 1/\beta$, we have $F(\mu) = \delta_3 \sigma_1 (\beta \delta_2 - \omega_2)/\beta > 0$. That is a contradiction.
Case where $1/\beta > \delta_2/\omega_2$, i.e., $\omega_2 > \beta \delta_2$. Since $\mu = \delta_2/\omega_2$, we have $F(\mu) = \alpha \sigma_2 (\beta \delta_2 - \omega_2)(\gamma_2 \theta - \delta_3 \rho)/\omega_2 < 0$ implying $\theta > \rho \delta_3/\gamma_2 = \theta_3$. If $\theta_5 \geq \theta_3$, i.e., $\sigma_1 \delta_2 \delta_3 + \alpha \delta_3 (\rho \sigma_2 - \delta_1 \delta_2)/\alpha (\alpha \gamma_1 \delta_2 + \gamma_2 \sigma_2) \geq \rho \delta_3/\gamma_2$, we have $\sigma_1 \geq \alpha (\alpha \rho \gamma_1 + \delta_1 \gamma_2)/\gamma_2$, there exists E^*.
Case (2): $C_0 < 0$, $F(\mu) > 0$.
Since $C_0 < 0$, we have $\theta > \theta_5$. Since $F(\mu) > 0$, we have the following two cases:
Case where $1/\beta < \delta_2/\omega_2$, i.e., $\omega_2 < \beta \delta_2$. Since $\mu = 1/\beta$, we have $F(\mu) = \delta_3 \sigma_1 (\beta \delta_2 - \omega_2)/\beta > 0$, there exists E^*.
Case where $1/\beta > \delta_2/\omega_2$, i.e., $\omega_2 > \beta \delta_2$. Since $\mu = \delta_2/\omega_2$, we have $F(\mu) = \alpha \sigma_2 (\beta \delta_2 - \omega_2)(\gamma_2 \theta - \delta_3 \rho)/\omega_2 > 0$ implying $\theta < \theta_3$. If $\theta_3 \geq \theta_5$, i.e., $\rho \delta_3/\gamma_2 \geq \sigma_1 \delta_2 \delta_3 + \alpha \delta_3 (\rho \sigma_2 - \delta_1 \delta_2)/\alpha (\alpha \gamma_1 \delta_2 + \gamma_2 \sigma_2)$, we have $\sigma_1 \leq \alpha (\alpha \rho \gamma_1 + \delta_1 \gamma_2)/\gamma_2$, there exists E^*.

Case (b): If $F(0)F(\mu) = C_0 F(\mu) > 0$, then (39) can have two positive roots x_1^* and x_2^* in the interval $[0, \mu]$, where x_1^* and x_2^* are the roots of (39). Therefore, system (34) can have two coexistence equilibria:

$$
E_1^* = (x_1^*, y_1^*, z_1^*, u_1^*) = \left(x_1^*, \alpha (1 - \beta x_1^*), \frac{\sigma_2}{\delta_2 - \omega_2 x_1^*}, \right.
$$
$$
\left. \frac{\alpha \gamma_1 (1 - \beta x_1^*)(\delta_2 - \omega_2 x_1^*) + \gamma_2 \sigma_2}{\delta_3 (\delta_2 - \omega_2 x_1^*)} \right),
\tag{41}
$$

$$
E_2^* = (x_2^*, y_2^*, z_2^*, u_2^*) = \left(x_2^*, \alpha (1 - \beta x_2^*), \frac{\sigma_2}{\delta_2 - \omega_2 x_2^*}, \right.
$$
$$
\left. \frac{\alpha \gamma_1 (1 - \beta x_2^*)(\delta_2 - \omega_2 x_2^*) + \gamma_2 \sigma_2}{\delta_3 (\delta_2 - \omega_2 x_2^*)} \right).
\tag{42}
$$

In the following, we show the existence condition of E_1^* and E_2^*.

Differentiating (39), we have

$$F'(x) = 3C_3 x^2 + 2C_2 x + C_1 = 0, \tag{43}$$

where $C_3 > 0$ and $C_2 < 0$. If $C_1 > 0$ and $\Delta \triangleq C_2^2 - 3C_1 C_3 > 0$, then (43) has two positive roots $x_1^+ = -C_2 - \sqrt{\Delta}/3C_3$ and $x_2^+ = -C_2 + \sqrt{\Delta}/3C_3$. And if $C_1 < 0$, then (43) has one positive root $x_2^+ = -C_2 + \sqrt{\Delta}/3C_3$.

  Case (1): $C_0 > 0$, $F(\mu) > 0$.

  Since $C_0 > 0$, we have $\theta < \theta_5$. Since $F(\mu) > 0$, we have the following two cases:

  Case where $1/\beta < \delta_2/\omega_2$, i.e., $\omega_2 < \beta\delta_2$. Since $\mu = 1/\beta$, we have $F(\mu) = \delta_3\sigma_1(\beta\delta_2 - \omega_2)/\beta > 0$. If $F(x_2^+) < 0$, then there exist E_1^* and E_2^*.

  Case where $1/\beta > \delta_2/\omega_2$, i.e., $\omega_2 > \beta\delta_2$. Since $\mu = \delta_2/\omega_2$, we have $F(\mu) = \alpha\sigma_2(\beta\delta_2 - \omega_2)(\gamma_2\theta - \delta_3\rho)/\omega_2 > 0$ implying $\theta < \theta_3$. Then, we have $\theta < \min\{\theta_3, \theta_5\}$. If $F(x_2^+) < 0$, then there exist E_1^* and E_2^*.

  Case (2): $C_0 < 0$, $F(\mu) < 0$.

  Since $C_0 < 0$, we have $\theta > \theta_5$. Since $F(\mu) > 0$, we have the following two cases:

  Case where $1/\beta < \delta_2/\omega_2$, i.e., $\omega_2 < \beta\delta_2$. Since $\mu = 1/\beta$, we have $F(\mu) = \delta_3\sigma_1(\beta\delta_2 - \omega_2)/\beta > 0$. That is a contradiction.

  Case where $1/\beta > \delta_2/\omega_2$, i.e., $\omega_2 > \beta\delta_2$. Since $\mu = \delta_2/\omega_2$, we have $F(\mu) = \alpha\sigma_2(\beta\delta_2 - \omega_2)(\gamma_2\theta - \delta_3\rho)/\omega_2 < 0$ implying $\theta > \theta_3$. Then, we have $\theta > \max\{\theta_3, \theta_5\}$. If $F(x_1^+) > 0$, then there exist E_1^* and E_2^*.

  Next, we show the stability of the above two equilibria E_0 and E^* of system (34) with $\nu = 0$. We linearize the system and obtain the characteristic equation whose expression is the same as (13).

Theorem 5. *System (34) with $\nu = 0$ always has one tumor-free equilibrium E_0, which is LAS if the inequality $\theta < \theta_5$ holds.*

Proof. At $E_0 = (x_0, y_0, z_0, u_0) = (0, y_0, \sigma_2/\delta_2, \gamma_1\delta_2 y_0 + \gamma_2\sigma_2/\delta_2\delta_3)$, the characteristic equation becomes

$$(\lambda - \alpha + y_0)(\lambda + \delta_2)\left(\lambda^2 + \left(\frac{\sigma_1}{y_0} + \delta_3\right)\lambda + \theta\gamma_1 y_0 + \frac{\sigma_1\delta_3}{y_0}\right) = 0, \tag{44}$$

and one root of characteristic equation is $-\delta_2 < 0$. It is easily noted that as $\sigma_1/y_0 + \delta_3 > 0$, $\theta\gamma_1 y_1 + \sigma_1\delta_3/y_0 > 0$, so the solutions of $\lambda^2 + ((\sigma_1/y_0) + \delta_3)\lambda + \theta\gamma_1 y_1 + (\sigma_1\delta_3/y_0) = 0$ have always negative real parts. Therefore, E_0 is LAS if and only if $\alpha - y_0 = 2\alpha A + B - \sqrt{B^2 - 4AC}/2A < 0$, that is, if and only if $\theta < \theta_5$.

  At $E^* = (x^*, y^*, z^*, u^*)$, characteristic (13) becomes

$$\lambda^4 + B_1\lambda^3 + B_2\lambda^2 + B_3\lambda + B_4 = 0, \tag{45}$$

where

$$B_1 = \alpha\beta x^* + \delta_3 + \frac{\sigma_1}{y^*} + \frac{\sigma_2}{z^*} > 0,$$

$$B_2 = \left(\alpha\beta x^* + \frac{\sigma_2}{z^*}\right)\left(\frac{\sigma_1}{y^*} + \delta_3\right) + \alpha\beta x^*\frac{\sigma_2}{z^*} + \delta_3\frac{\sigma_1}{y^*} + \theta\gamma_1 y^* > 0,$$

$$B_3 = \left(\theta\gamma_1 y^* + \delta_3\frac{\sigma_1}{y^*}\right)\left(\alpha\beta x^* + \frac{\sigma_2}{z^*}\right) + \alpha\beta x^*\frac{\sigma_2}{z^*}\left(\delta_3 + \frac{\sigma_1}{y^*}\right)$$
$$\quad + \rho\omega_2 x^* y^* z^* > 0,$$

$$B_4 = \alpha\beta x^*\frac{\sigma_2}{z^*}\left(\theta\gamma_1 y^* + \delta_3\frac{\sigma_1}{y^*}\right) + (\rho\delta_3 - \theta\gamma_2)\omega_2 x^* y^* z^*. \tag{46}$$

  By the Routh–Hurwitz criterion, the roots of (45) have negative real parts if and only if $B_1 > 0$, $B_2 > 0$, $B_3 > 0$, $B_4 > 0$, $B_1 B_2 - B_3 > 0$, and $B_1(B_2 B_3 - B_1 B_4) - B_3^2 > 0$.

  Hence, we obtain the sufficient condition for the stability of P^*:

$$(H4):\ B_4 = \alpha\beta x^*\frac{\sigma_2}{z^*}\left(\theta\gamma_1 y^* + \delta_3\frac{\sigma_1}{y^*}\right)$$
$$\quad\quad + (\rho\delta_3 - \theta\gamma_2)\omega_2 x^* y^* z^* > 0,$$

$$(H5):\ B_1 B_2 - B_3 = K_1\theta + K_2 > 0,$$

$$(H6):\ B_1(B_2 B_3 - B_1 B_4) - B_3^2 = B_3(K_1\theta + K_2) - B_1^2 B_4 \tag{47}$$

where

$$K_1 = (\sigma_1 + \delta_3 y^*)\gamma_1,$$

$$K_2 = \left(\delta_3 + \frac{\sigma_1}{y^*} + \frac{\sigma_2}{z^*}\right)\left[\alpha^2\beta^2 x^{*2} + \left(\alpha\beta x^* + \frac{\sigma_2}{z^*}\right)\left(\frac{\sigma_1}{y^*} + \delta_3\right)\right.$$
$$\left. + \alpha\beta x^*\frac{\sigma_2}{z^*}\right] + \delta_3\frac{\sigma_1}{y^*}\left(\frac{\sigma_1}{y^*} + \delta_3\right) - \rho\omega_2 x^* y^* z^*,$$

$$K_3 = K_1\left(\alpha\beta x^* + \frac{\sigma_2}{z^*}\right)\gamma_1 y^*,$$

$$K_4 = \left[\left(K_2\gamma_1 y^* + K_1\frac{\sigma_1\delta_3}{y^*}\right)\left(\alpha\beta x^* + \frac{\sigma_2}{z^*}\right)\right]$$
$$\quad + K_1\left[\alpha\beta x^*\frac{\sigma_2}{z^*}\left(\delta_3 + \frac{\sigma_1}{y^*} - \left(\alpha\beta x^* + \delta_3 + \frac{\sigma_1}{y^*} + \frac{\sigma_2}{z^*}\right)^2\gamma_1 y^*\right)\right]$$
$$\quad + (\rho + \gamma_2)\omega_2 x^* y^* z^*\Big],$$

$$K_5 = K_2\left(\alpha\beta x^* + \frac{\sigma_2}{z^*}\right)\frac{\sigma_1\delta_3}{y^*} - \alpha\beta x^*\frac{\sigma_2}{z^*}\left[K_2\left(\delta_3 + \frac{\sigma_1}{y^*}\right)\right.$$
$$\left. - \left(\alpha\beta x^* + \delta_3 + \frac{\sigma_1}{y^*} + \frac{\sigma_2}{z^*}\right)^2\frac{\sigma_1\delta_3}{y^*}\right] + (K_2 - \delta_3)\rho\omega_2 x^* y^* z^*. \tag{48}$$

$\square$

Theorem 6. *System (34) with $v = 0$ has a coexistence equilibrium E^* when $\omega_2 > \beta\delta_2$, $\sigma_1 \geq \alpha(\alpha\rho\gamma_1 + \delta_1\gamma_2)/\gamma_2$, $\theta_3 < \theta < \theta_5$ or $\omega_2 > \beta\delta_2$, $\sigma_1 \leq \alpha(\alpha\rho\gamma_1 + \delta_1\gamma_2)/\gamma_2$, $\theta_5 < \theta < \theta_3$ or $\omega_2 < \beta\delta_2$, $\theta > \theta_5$ hold. Further E^* is LAS when condition (47) is satisfied.*

3.1.2. MAI Model.

When $\sigma_1 = 0$, $\sigma_3 > 0$, (36) becomes

$$\begin{cases} \alpha x(1 - \beta x) - xy = 0, \\ \rho yz - \theta yu - \delta_1 y = 0, \\ \sigma_2 + \omega_2 xz - \delta_2 z = 0, \\ \gamma_1 y + \gamma_2 z - \delta_3 u - \xi uv = 0, \\ \sigma_3 - \delta_4 v = 0. \end{cases} \tag{49}$$

Equation (49) can be simplified as follows:

$$\begin{cases} \alpha x(1 - \beta x) - xy = 0, \\ \rho yz - \theta yu - \delta_1 y = 0, \\ \sigma_2 + \omega_2 xz - \delta_2 z = 0, \\ \gamma_1 y + \gamma_2 z - \delta_{31} u = 0, \end{cases} \tag{50}$$

where $\delta_{31} = \delta_3\delta_4 + \xi\sigma_3/\delta_4$.

The analysis of (50) is similar to that of (12), and the equilibria of (34) can be obtained as follows:

$$\begin{aligned} F_0 &= \left(0, 0, \frac{\sigma_2}{\delta_2}, \frac{\gamma_2\sigma_2}{\delta_2\delta_{31}}, \frac{\sigma_3}{\delta_4}\right) \\ &= \left(0, \frac{\delta_{31}(\rho\sigma_2 - \delta_1\delta_2) - \theta\gamma_2\sigma_2}{\theta\gamma_1\delta_2}, \frac{\sigma_2}{\delta_2}, \frac{\rho\sigma_2 - \delta_1\delta_2}{\theta\delta_2}, \frac{\sigma_3}{\delta_4}\right), \end{aligned}$$

$$F_2 = \left(\frac{1}{\beta}, 0, \frac{\beta\sigma_2}{\beta\delta_2 - \omega_2}, \frac{\beta\gamma_2\sigma_2}{\delta_{31}(\beta\delta_2 - \omega_2)}, \frac{\sigma_3}{\delta_4}\right),$$

$$\begin{aligned} F^* &= \left(x^*, \alpha(1 - \beta x^*), \frac{\sigma_2}{\delta_2 - \omega_2 x^*}, \right. \\ &\quad \left. \frac{\alpha\gamma_1(1 - \beta x^*)(\delta_2 - \omega_2 x^*) + \gamma_2\sigma_2}{\delta_{31}(\delta_2 - \omega_2 x^*)}, \frac{\sigma_3}{\delta_4}\right). \end{aligned}$$

$$\tag{51}$$

Here, $x^* \in (0, \mu)$ and satisfies the equation $a_2 x^2 + a_1 x + a_0 = 0$, where coefficients are defined as $a_2 = -\theta\alpha\beta\gamma_1\omega_2 < 0$, $a_1 = \theta\alpha\gamma_1(\beta\delta_2 + \omega_2) + \delta_1\delta_{31}\omega_2 > 0$, and $a_0 = \delta_{31}(\rho\sigma_2 - \delta_1\delta_2) - \theta(\alpha\gamma_1\delta_2 + \gamma_2\sigma_2)$.

The Jacobian matrix of system (34) at any equilibrium $\overline{F}(\overline{x}, \overline{y}, \overline{z}, \overline{u}, \overline{v})$ is as follows:

$$\mathbf{J}(\overline{F}) = \begin{pmatrix} \alpha - 2\alpha\beta\overline{x} - \overline{y} & -\overline{x} & 0 & 0 & 0 \\ 0 & \rho\overline{z} - \theta\overline{u} - \delta_1 & \rho\overline{y} & -\theta\overline{y} & 0 \\ \omega_2\overline{z} & 0 & \omega_2\overline{x} - \delta_2 & 0 & 0 \\ 0 & \gamma_1 & \gamma_2 & -\delta_3 - \xi\overline{v} & \xi\overline{u} \\ 0 & 0 & 0 & 0 & -\delta_4 \end{pmatrix} = \begin{pmatrix} \alpha - 2\alpha\beta\overline{x} - \overline{y} & -\overline{x} & 0 & 0 & 0 \\ 0 & \rho\overline{z} - \theta\overline{u} - \delta_1 & \rho\overline{y} & -\theta\overline{y} & 0 \\ \omega_2\overline{z} & 0 & \omega_2\overline{x} - \delta_2 & 0 & 0 \\ 0 & \gamma_1 & \gamma_2 & -\delta_{31} & \xi\overline{u} \\ 0 & 0 & 0 & 0 & -\delta_4 \end{pmatrix}. \tag{52}$$

The corresponding characteristic equation is

$$|\mathbf{J}(\overline{F}) - \lambda\mathbf{I}| = 0. \tag{53}$$

Substituting δ_{31} for δ_3 in (12), we have

$$|\mathbf{J}(\overline{F}) - \lambda\mathbf{I}| = (\lambda + \delta_4)|\mathbf{J}(\overline{P}) - \lambda\mathbf{I}| = 0. \tag{54}$$

Thus, the stability analysis of $\overline{F}$ is similar to that of $\overline{P}$.

Substituting δ_{31} for δ_3 in (20) to get new conditions for the stability of F^*:

$$\begin{aligned} (h1): A_4 &= \theta\alpha\beta\gamma_1(\delta_2 - \omega_2 x^*)x^* y^* \\ &\quad + (\rho\delta_{31} - \theta\gamma_2)\omega_2 x^* y^* z^* > 0, \\ (h2): A_1 A_2 - A_3 &= \theta\gamma_1(\alpha\beta x^* + \delta_2 - \omega_2 x^*)y^* \\ &\quad + \alpha\beta\delta_{31}(\delta_2 - \omega_2 x^*)x^* \\ &\quad - \rho x^* y^* z^* > 0, \\ (h3): A_1(A_2 A_3 - A_1 A_4) - A_3^2 &= B_1\theta + B_2 > 0, \end{aligned}$$

$$\tag{55}$$

where

$$\begin{aligned} B_1 &= \left((\alpha\beta x^* + \delta_2 - \omega_2 x^*)^2\delta_{31} + (\alpha\beta x^* + \delta_2 - \omega_2 x^*)\delta_{31}^2 \right. \\ &\quad - \rho\omega_2 x^* y^* z^*)(\alpha\beta x^* + \delta_2 - \omega_2 x^*)\gamma_1 y^* \\ &\quad - (\alpha\beta x^* + \delta_2 - \omega_2 x^* + \delta_{31})^2(\alpha\beta\gamma_1(\delta_2 - \omega_2 x^*)x^* y^* \\ &\quad \left. - \omega_2\gamma_2 x^* y^* z^*\right), \end{aligned}$$

$$\begin{aligned} B_2 &= \left((\alpha\beta x^* + \delta_2 - \omega_2 x^*)^2\delta_{31} + (\alpha\beta x^* + \delta_2 - \omega_2 x^*)\delta_{31}^2 \right. \\ &\quad - \rho\omega_2 x^* y^* z^*)(\alpha\beta\delta_{31}(\delta_2 - \omega_2 x^*)x^* + \rho\omega_2 x^* y^* z^*) \\ &\quad \left. - (\alpha\beta x^* + \delta_2 - \omega_2 x^* + \delta_{31})^2\rho\omega_2\delta_{31} x^* y^* z^*\right). \end{aligned}$$

$$\tag{56}$$

We set

$$\theta_{70} = \frac{\delta_{31}(\rho\sigma_2 - \delta_1\delta_2)}{\alpha\gamma_1\delta_2 + \gamma_2\sigma_2},$$

$$\theta_{71} = \frac{\delta_{31}(\rho\sigma_2 - \delta_1\delta_2)}{\gamma_2\sigma_2},$$

$$\theta_{72} = \frac{\beta\delta_{31}(\rho\sigma_2 - \delta_1\delta_2) + \delta_1\delta_{31}\omega_2}{\beta\gamma_2\sigma_2}, \tag{57}$$

$$\theta_{73} = \frac{\rho\delta_{31}}{\gamma_2},$$

and we obtain the following results.

Theorem 7. *System (34) always has one tumor-free and ECs-free equilibrium F_0, which is unstable.*

Theorem 8. *System (34) has one tumor-free equilibrium F_1 when $\rho > \delta_1\delta_2/\sigma_2$ and $\theta < \theta_{71}$, which is LAS if the inequality $\theta < \theta_{70}$ holds.*

Theorem 9. *System (34) has one tumor-dominant equilibrium F_2 when $\omega_2 < \omega_2^*$, which is LAS if the inequality $\theta > \theta_{72}$ holds.*

Theorem 10. *System (34) has a unique coexistence equilibrium F^* when $\omega_2 < \omega_2^*$, $\theta_0 < \theta < \theta_2$ or $\omega_2 > \omega_2^*$, $\theta_0 < \theta < \theta_3$ hold. Further F^* is LAS, when condition (55) is satisfied.*

3.1.3. Combined Immunotherapy Model. When $\sigma_1 > 0$ and $\sigma_3 > 0$, (36) can be simplified as follows:

$$\begin{cases} \alpha x(1 - \beta x) - xy = 0, \\ \rho yz - \theta yu - \delta_1 y + \sigma_1 = 0, \\ \sigma_2 + \omega_2 xz - \delta_2 z = 0, \\ \gamma_1 y + \gamma_2 z - \delta_{31} u = 0, \end{cases} \tag{58}$$

where $\delta_{31} = \delta_3\delta_4 + \xi\sigma_3/\delta_4$.

The analysis of (58) is similar to that of (37), and the equilibria of (34) can be obtained as follows:

$$N_0 = (x_0, y_0, z_0, u_0, v_0) = \left(0, y_0, \frac{\sigma_2}{\delta_2}, \frac{\gamma_1\delta_2 y_0 + \gamma_2\sigma_2}{\delta_2\delta_{31}}, \frac{\sigma_3}{\delta_4}\right), \tag{59}$$

where $y_0 = -B + \sqrt{B^2 - 4AC}/2A$ with $A = \theta\gamma_1\delta_2 > 0$, $B = \delta_{31}(\delta_1\delta_2 - \rho\sigma_2) + \theta\gamma_2\sigma_2$, and $C = -\sigma_1\delta_2\delta_{31} < 0$.

$$N^* = (x^*, y^*, z^*, u^*, v^*) = \left(x^*, \alpha(1 - \beta x^*), \frac{\sigma_2}{\delta_2 - \omega_2 x^*},\right.$$

$$\left.\frac{\alpha\gamma_1(1 - \beta x^*)(\delta_2 - \omega_2 x^*) + \gamma_2\sigma_2}{\delta_{31}(\delta_2 - \omega_2 x^*)}, \frac{\sigma_3}{\delta_4}\right), \tag{60}$$

where $x^* \in (0, \mu)$ and satisfies the equation $c_3 x^3 + c_2 x^2 + c_1 x + c_0 = 0$ with coefficients

$$c_3 = \theta\alpha^2\beta^2\gamma_1\omega_2 > 0,$$

$$c_2 = -\theta\alpha^2\beta\gamma_1\omega_2 - \alpha\beta[\theta\alpha\gamma_1(\beta\delta_2 + \omega_2) + \delta_1\delta_{31}\omega_2] < 0,$$

$$c_1 = \theta\alpha(2\alpha\beta\gamma_1\delta_2 + \alpha\gamma_1\omega_2 + \beta\gamma_2\sigma_2) + \alpha\delta_{31}[\delta_1\omega_2 - \beta(\rho\sigma_2 - \delta_1\delta_2)] - \sigma_1\omega_2\delta_{31},$$

$$c_0 = \sigma_1\delta_2\delta_{31} + \alpha\delta_{31}(\rho\sigma_2 - \delta_1\delta_2) - \theta\alpha(\alpha\gamma_1\delta_2 + \gamma_2\sigma_2). \tag{61}$$

For system (34) at $N_0 = (x_0, y_0, z_0, u_0, v_0)$, Jacobian matrix is expressed as follows:

$$\mathbf{J}(N_0) = \begin{pmatrix} \alpha - y_0 & 0 & 0 & 0 & 0 \\ 0 & -\dfrac{\sigma_1}{y_0} & \rho y_0 & -\theta y_0 & 0 \\ \omega_2 z_0 & 0 & -\delta_2 & 0 & 0 \\ 0 & \gamma_1 & \gamma_2 & -\delta_{31} & \xi u_0 \\ 0 & 0 & 0 & 0 & -\delta_4 \end{pmatrix}. \tag{62}$$

The corresponding characteristic equation is

$$|\mathbf{J}(N_0) - \lambda\mathbf{I}| = (\lambda + \delta_4)|\mathbf{J}(E_0) - \lambda\mathbf{I}| = 0. \tag{63}$$

Thus, the stability analysis of N_0 is similar to that of E_0. Set $\theta_8 = \alpha\delta_{31}(\rho\sigma_2 - \delta_1\delta_2) + \sigma_1\delta_2\delta_{31}/\alpha(\alpha\gamma_1\delta_2 + \sigma_2\gamma_2)$, and we can get the following result.

Theorem 11. *System (34) always has one tumor-free equilibrium N_0, which is LAS if the inequality $\theta < \theta_8$ holds.*
For system (34) at $N^* = (x^*, y^*, z^*, u^*, v^*)$, Jacobian matrix is given as follows:

$$\mathbf{J}(N^*) = \begin{pmatrix} -\alpha\beta x^* & -x^* & 0 & 0 & 0 \\ 0 & -\dfrac{\sigma_1}{y^*} & \rho y^* & -\theta y^* & 0 \\ \omega_2 z^* & 0 & \omega_2 x^* - \delta_2 & 0 & 0 \\ 0 & \gamma_1 & \gamma_2 & -\delta_{31} & \xi u^* \\ 0 & 0 & 0 & 0 & -\delta_4 \end{pmatrix}. \tag{64}$$

The corresponding characteristic equation is

$$|\mathbf{J}(N^*) - \lambda\mathbf{I}| = (\lambda + \delta_4)|\mathbf{J}(E^*) - \lambda\mathbf{I}| = 0. \tag{65}$$

Thus, the stability analysis of N^* is similar to that of E^*. Set $\theta_9 = \rho\delta_{31}/\gamma_2$ and substitute δ_{31} for δ_3 in (47) to get new conditions:

$$(h4): \quad B_4 = \alpha\beta x^* \frac{\sigma_2}{z^*}\left(\theta\gamma_1 y^* + \delta_{31}\frac{\sigma_1}{y^*}\right)$$

$$+ (\rho\delta_{31} - \theta\gamma_2)\omega_2 x^* y^* z^* > 0,$$

$$(h5): \quad B_1 B_2 - B_3 = k_1\theta + k_2 > 0,$$

$$(h6): \quad B_1(B_2 B_3 - B_1 B_4) - B_3^2 = B_3(k_1\theta + k_2) - B_1^2 B_4$$

$$= k_3\theta^2 + k_4\theta + k_5 > 0,$$

$$(66)$$

where

$$k_1 = (\sigma_1 + \delta_{31} y^*)\gamma_1,$$

$$k_2 = \left(\delta_{31} + \frac{\sigma_1}{y^*} + \frac{\sigma_2}{z^*}\right)\left[\alpha^2\beta^2 x^{*2} + \left(\alpha\beta x^* + \frac{\sigma_2}{z^*}\right)\left(\frac{\sigma_1}{y^*} + \delta_{31}\right)\right.$$

$$\left. + \alpha\beta x^* \frac{\sigma_2}{z^*}\right] + \delta_{31}\frac{\sigma_1}{y^*}\left(\frac{\sigma_1}{y^*} + \delta_{31}\right) - \rho\omega_2 x^* y^* z^*,$$

$$k_3 = k_1\left(\alpha\beta x^* + \frac{\sigma_2}{z^*}\right)\gamma_1 y^*,$$

$$k_4 = \left[\left(k_2\gamma_1 y^* + k_1\frac{\sigma_1\delta_{31}}{y^*}\right)\left(\alpha\beta x^* + \frac{\sigma_2}{z^*}\right)\right]$$

$$+ k_1\left[\alpha\beta x^* \frac{\sigma_2}{z^*}\left(\delta_{31} + \frac{\sigma_1}{y^*} - \left(\alpha\beta x^* + \delta_{31} + \frac{\sigma_1}{y^*} + \frac{\sigma_2}{z^*}\right)^2\gamma_1 y^*\right)\right.$$

$$\left. + (\rho + \gamma_2)\omega_2 x^* y^* z^*\right], k_5 = k_2\left(\alpha\beta x^* + \frac{\sigma_2}{z^*}\right)\frac{\sigma_1\delta_{31}}{y^*}$$

$$- \alpha\beta x^* \frac{\sigma_2}{z^*}\left[k_2\left(\delta_{31} + \frac{\sigma_1}{y^*}\right) - \left(\alpha\beta x^* + \delta_{31} + \frac{\sigma_1}{y^*} + \frac{\sigma_2}{z^*}\right)^2\frac{\sigma_1\delta_{31}}{y^*}\right]$$

$$+ (k_2 - \delta_{31})\rho\omega_2 x^* y^* z^*.$$

$$(67)$$

Therefore, we can obtain the following result.

Theorem 12. *System (34) has a coexistence equilibrium N^* when $\omega_2 > \beta\delta_2, \sigma_1 \geq \alpha(\alpha\rho\gamma_1 + \delta_1\gamma_2)/\gamma_2, \theta_9 < \theta < \theta_8$ or $\omega_2 > \beta\delta_2$, $\sigma_1 \leq \alpha(\alpha\rho\gamma_1 + \delta_1\gamma_2)/\gamma_2, \theta_8 < \theta < \theta_9$ or $\omega_2 < \beta\delta_2, \theta > \theta_8$ hold. Further N^* is LAS when condition (66) is satisfied.*

3.2. Numerical Simulations

3.2.1. ACI Model ($\sigma_1 > 0, \sigma_3 = 0$).
We conduct numerical simulations of the ACI model. We choose $\omega_2 = 0.0004$ and the other parameter values are given in (22). We find the stability region of $E^* = (x^*, y^*, z^*, u^*)$, as shown in Figure 5(a). E^* is stable in region **I** and unstable in region **II**.

Case (a): we choose a point $G_1 = (\sigma_1, \theta) = (0.4, 0.5)$ in the region **I**, then system (34) has one coexistence equilibrium:

$$E^* = (11.560, 1.598, 7.543, 6.993). \quad (68)$$

The eigenvalues of characteristic equation of (47) are

$$-0.269, \; -0.041, \; -0.1388 + 0.334i \text{ and } -0.1388 - 0.334i, \quad (69)$$

so E^* is stable, as shown in Figure 6(b).

Case (b): we choose a point $G_2 = (\sigma_1, \theta) = (0.4, 0.55)$ in the region **II**; then, system (34) has one coexistence equilibrium:

$$E^* = (69.131, 1.409, 13.895, 11.962). \quad (70)$$

The eigenvalues of characteristic equation of (47) are

$$-0.830, \; -0.021, \; 0.0326 + 0.6039i \text{ and } 0.0326 - 0.6039i, \quad (71)$$

so E^* is unstable, as shown in Figures 6(c) and 6(d).

According to the stability condition of tumor-free equilibrium E_0 in Theorem 5, ACI curve can be obtained as

$$\theta = \frac{\alpha\delta_3(\rho\sigma_2 - \delta_1\delta_2) + \sigma_1\delta_2\delta_3}{\alpha(\alpha\gamma_1\delta_2 + \gamma_2\sigma_2)} = 0.09391\sigma_1 + 0.452. \quad (72)$$

We find the stability region of $E_0 = (0, y_0, z_0, u_0)$ shown in Figure 5(b). E_0 is stable in the region **III** and unstable in the region **IV.** With the increase of σ_1, region **III** gradually increases, while region **IV** gradually decreases.

Case (c): we choose a point $G_3 = (\sigma_1, \theta) = (0.4, 0.48)$ in the region **III**; then, system (34) has a tumor-free equilibrium:

$$E_0 = (0, 1.782, 6.909, 6.596). \quad (73)$$

The eigenvalues of Jacobian matrix of E_0 are

$$-0.055, \; -0.146, \; -0.237 + 0.358i \text{ and } -0.237 - 0.358i, \quad (74)$$

so E_0 is stable, as shown in Figure 6(a).

Case (d): we choose a point $G_4 = (\sigma_1, \theta) = (0.4, 0.53)$ in the region **IV**; then, system (34) has a tumor-free equilibrium:

$$E_0 = (0, 1.141, 6.909, 6.212). \quad (75)$$

The eigenvalues of Jacobian matrix of E_0 are

$$0.494, \; -0.055, \; -0.3 + 0.297i \text{ and } -0.3 - 0.297i, \quad (76)$$

so E_0 is unstable.

We choose ACI parameter $\sigma_1 = 0.4$ to study the relationship between the number of TCs x and the parameter θ (see Figure 5(c)). By some calculations, we have $\theta_3 = \rho\delta_3/\gamma_2 =$
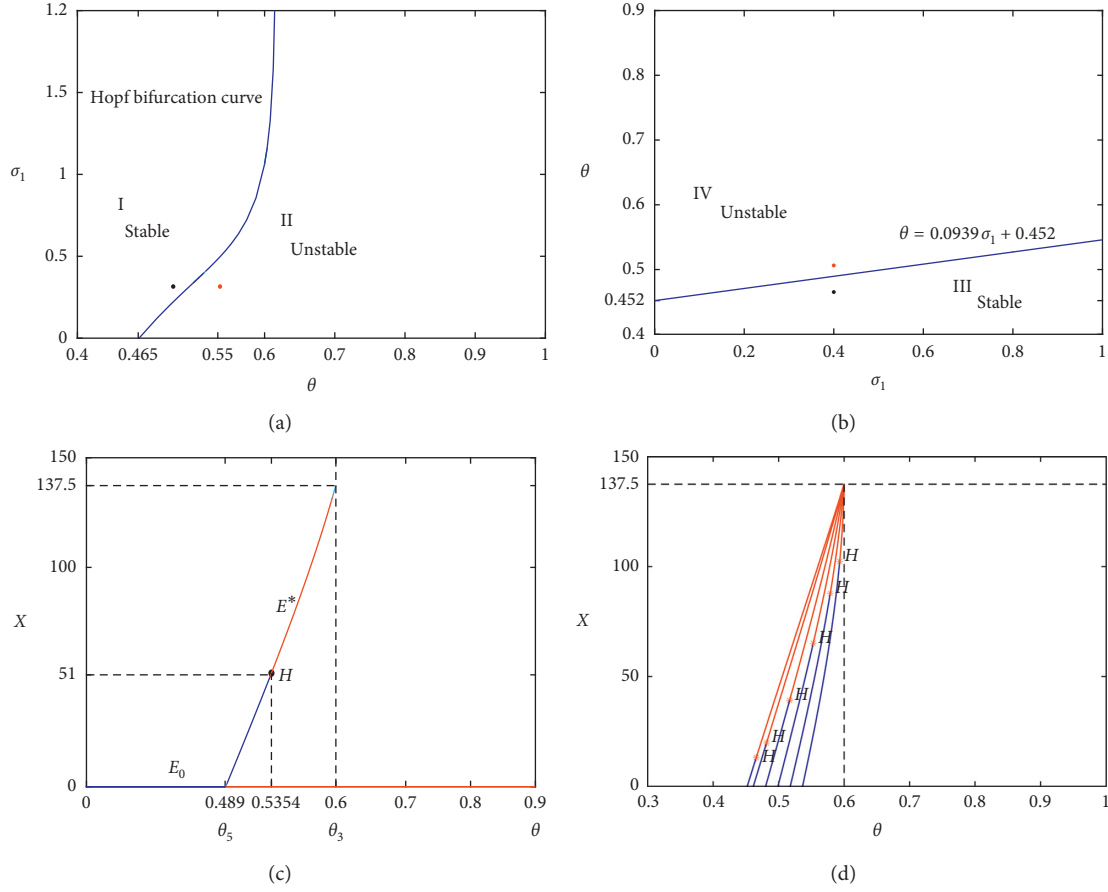
Figure 5: (a) Stability region of E^* and Hopf bifurcation curve in $\theta - \sigma_1$ parameter plane. E^* is stable in region **I** and unstable in region **II**. (b) ACI curve. E_0 is stable in region **III** and unstable in region **IV**. (c) The bifurcation diagram of x with respect to θ for fixed $\sigma_1 = 0.4$. Hopf bifurcation point appears at $\theta_{ACI}^* = 0.5354$. (d) The bifurcation diagram of x with respect to θ for different $\sigma_1 = 0, 0.1, 0.3, 0.5, 0.7, 0.9$ (the blue curves represent the stable steady states of system (34), while the red curves represent the unstable steady states).

0.6, $\theta_5 = \alpha\delta_3(\rho\sigma_2 - \delta_1\delta_2) + \sigma_1\delta_2\delta_3/\alpha(\alpha\gamma_1 \; \delta_2 + \gamma_2\sigma_2) = 0.489$. And Hopf bifurcation point appears at $\theta_{ACI}^* = 0.5354$. We can obtain the following result.

Proposition 5. When $0 < \theta < \theta_5$, E_0 exists and is LAS, and E^* is nonexistent. When $\theta_5 < \theta < \theta_{ACI}^*$, E_0 exists and is unstable, and E^* exists and is LAS. When $\theta_{ACI}^* < \theta < \theta_3$, E_0 exists and is unstable, and E^* exists and is unstable. When $\theta > \theta_3$, E_0 exists and is unstable, and E^* is nonexistent.

Next, we choose different ACI parameters $\sigma_1 = 0, 0.1, 0.3, 0.5, 0.7, 0.9$, to study the relationship between the number of TCs x and the parameter θ (see Figure 5(d)).

By comparing the curves in Figure 5(d), we see that, as σ_1 increases gradually, the stable region of tumor-free equilibrium E_0 of system (34) gradually increases (the intersection point of the curve and the x-coordinate gradually moves to the right) and the stability region of equilibrium E^* in system (34) gradually increases (the blue curve gradually moves upward). This indicates that increasing the injection volume of adoptive T cells can not only delay the inhibitory effect of Tregs on tumor immune response but also help the immune system to

remove more TCs. It also helps the immune system to control more TCs, keeping them at a stable state.

3.2.2. MAI Model ($\sigma_1 = 0$, $\sigma_3 > 0$). We conduct numerical simulations of the MAI model. We choose $\omega_2 = 0.0004$, $\xi = 0.05$, and $\delta_4 = 0.25$ and the other parameter values are given in (22). We find the stability region of $F^* = (x^*, y^*, z^*, u^*)$, as shown in Figure 7(a). F^* is stable in region **I** and unstable in region **II**.

Case (a): we choose a point $M_1 = (\sigma_3, \theta) = (0.4, 0.6)$ in region **I**; then, system (34) has one coexistence equilibrium:

$$F^* = (2.413, 1.628, 7.032, 5.002, 1.6). \tag{77}$$

The eigenvalues of Jacobian matrix of F^* are

$$-0.25, \; -0.146 + 0.336i, \; -0.146 - 0.336i, \; -0.0499 + 0.033i \text{ and } -0.0499 - 0.033i, \tag{78}$$
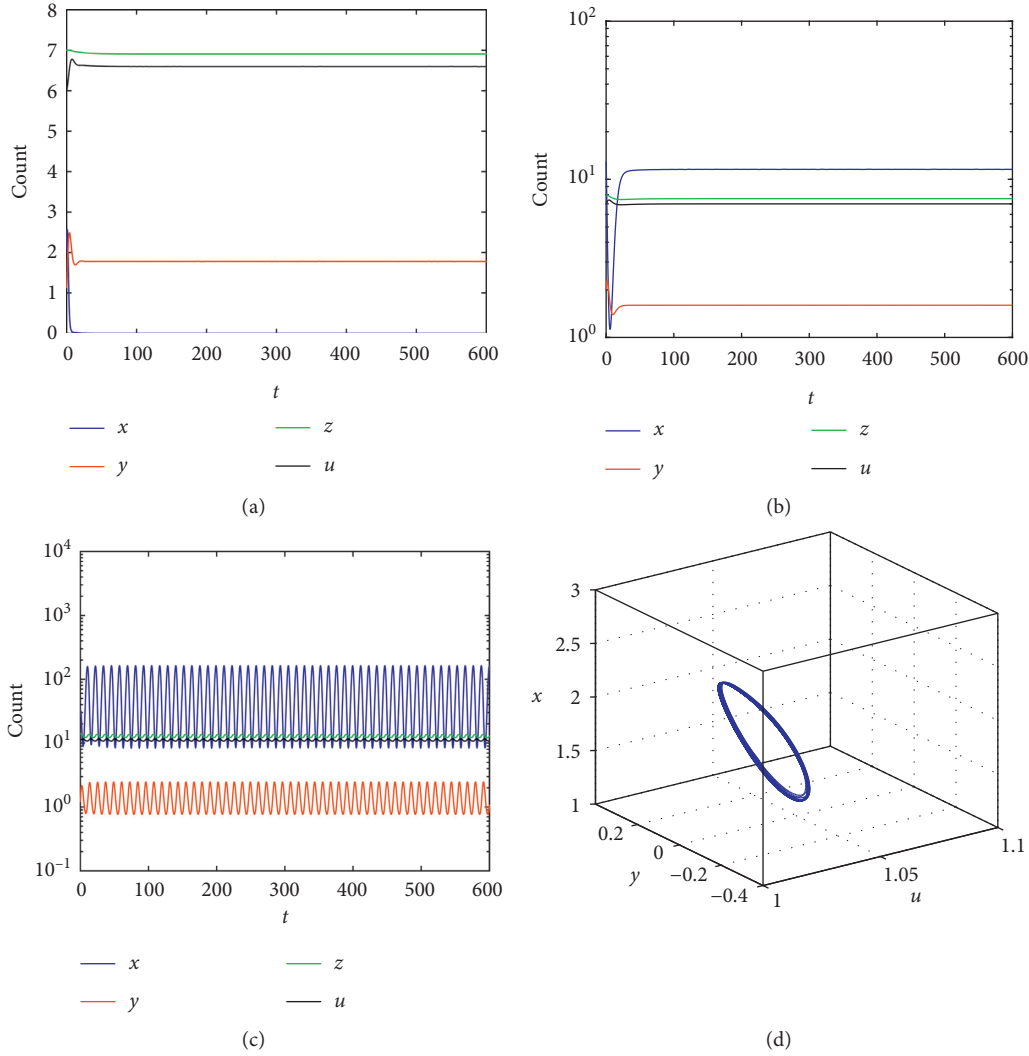
(a)

(b)

(c)

(d)

Figure 6: Choose $\sigma_1 = 0.4$, and the other parameter values are given in (22). (a) When $\theta = 0.48$, E_0 (0, 1.782, 6.909, 6.596) is LAS. (b) When $\theta = 0.50$, E^* (11.560, 1.598, 7.543, 6.993) is LAS. (c) When $\theta = 0.55$, E^* (69.131, 1.409, 13.895, 11.962) is unstable. (d) When $\theta = 0.55$, the 3D phase portrait depicts TCs, ECs, and Tregs.

so F^* is stable, as shown in Figure 8(b).

Case (b): we choose a point $M_2 = (\sigma_3, \theta) = (0.4, 0.635)$ in region **II**; then, system (34) has one coexistence equilibrium:

$$F^* = (27.345, 1.546, 8.624, 5.93, 1.6). \quad (79)$$

The eigenvalues of Jacobian matrix of F^* are

$$-0.4334, \ -0.25, \ -0.0644, \ 0.0172 \\ + 0.429i \text{ and } 0.0172 - 0.429i, \quad (80)$$

so F^* is unstable, as shown in Figures 8(c) and 8(d).

According to the stability condition of tumor-free equilibrium F_1 in Theorem 7, MAI curve can be obtained as

$$\theta = \left(\delta_3\delta_4 + \xi\sigma_3\right)\left(\rho\sigma_2 - \delta_1\delta_2\right)/\left(\alpha\gamma_1\delta_2 + \sigma_2\gamma_2\right) \quad (81)$$
$$\delta_4 = 0.3616\,\sigma_3 + 0.452.$$

We find the stability region of F_1, as shown in Figure 7(b). F_0 is stable in region **III** and unstable in region **IV**. With the increase of σ_3, region **III** gradually increases, while region **IV** gradually decreases.

Case (c): we choose a point $M_3 = (\sigma_3, \theta) = (0.4, 0.5)$ in region **III**; then, system (34) has a tumor-free equilibrium:

$$F_1 = (0, 2.556, 6.909, 5.349, 1.6). \quad (82)$$

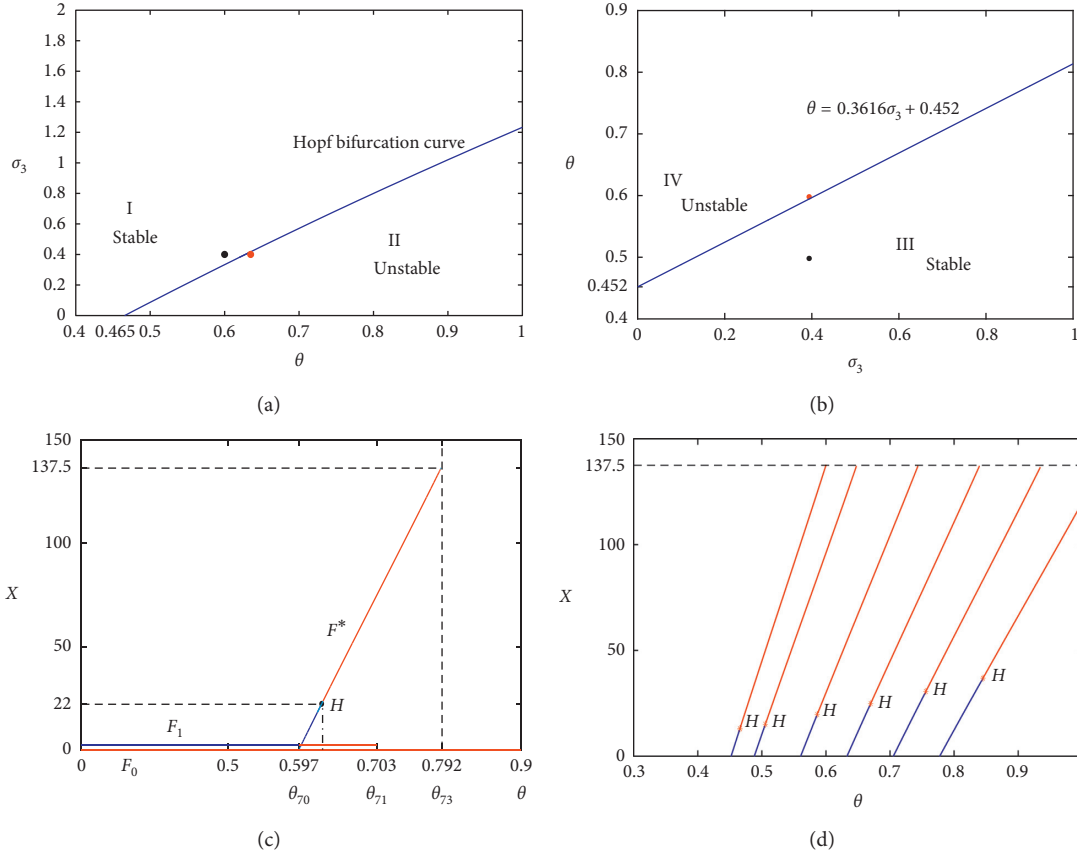The eigenvalues of Jacobian matrix of F_1 are

(a)

(b)

(c)

(d)

FIGURE 7: (a) Stability region of F^* and Hopf bifurcation curve in $\theta - \sigma_3$ parameter plane. F^* is stable in region **I** and unstable in region **II**. (b) MAI curve. F_1 is stable in region **III** and unstable in region **IV**. (c) The bifurcation diagram of x with respect to θ for fixed $\sigma_3 = 0.4$. Hopf bifurcation point appears at $\theta^*_{MAI} = 0.627$. (d) The bifurcation diagrams of x with respect to θ for different $\sigma_3 = 0, 0.1, 0.3, 0.5, 0.7, 0.9$ (the blue curves represent the stable steady states of system (34), while the red curves represent the unstable steady states).

$$-0.92, \ -0.25, \ -0.055, \ -0.164 + 0.428i \ \text{and} \ -0.164 - 0.428i, \tag{83}$$

so F_1 is stable, as shown in Figure 8(a).

Case (d): we choose a point $M_4 = (\sigma_3, \theta) = (0.4, 0.6)$ in region **IV**; then, system (34) has a tumor-free equilibrium:

$$F_1 = (0, 1.575, 6.909, 4.903, 1.6). \tag{84}$$

The eigenvalues of Jacobian matrix of F_1 are

$$0.061, \ -0.25, \ -0.055, \ -0.164 + 0.338i \ \text{and} \ -0.164 - 0.338i, \tag{85}$$

so F_1 is unstable.

We choose MAI parameter $\sigma_3 = 0.4$ to study the relationship between the number of TCs x and the parameter θ (see Figure 7(c)). By some calculations, we have $\theta_{70} = \delta_{31}(\rho\sigma_2 - \delta_1\delta_2)/\alpha\gamma_1\delta_2 + \gamma_2\sigma_2 = 0.597$, $\theta_{71} = \delta_{31}(\rho\sigma_2 - \delta_1\delta_2)/\gamma_2\sigma_2 = 0.703$, and $\theta_{73} = \rho\delta_{31}/\gamma_2 = 0.792$. And Hopf bifurcation point appears at $\theta^*_{MAI} = 0.627$. We can obtain the following result.

Proposition 6. When $0 < \theta < \theta_{70}$, F_0 exists and is unstable, F_1 exists and is LAS, and F^* exists and is LAS. When

$\theta_{70} < \theta < \theta^*_{MAI}$, F_0 exists and is unstable, F_1 exists and is unstable, and F^* exists and is unstable. When $\theta^*_{MAI} < \theta < \theta_{71}$, F_0 exists and is unstable, F_1 exists and is unstable, and F^* exists and is unstable. When $\theta_{71} < \theta < \theta_{73}$, F_0 exists and is unstable, F_1 is nonexistent, and F^* exists and is unstable. When $\theta > \theta_3$, F_0 exists and is unstable, F_1 is nonexistent, and F^* is nonexistent.

Next, we choose different MAI parameters $\sigma_3 = 0, 0.1, 0.3, 0.5, 0.7, 0.9$, to study the relationship between the number of TCs x and the parameter θ (see Figure 7(d)).

By comparing the curves in Figure 7(d), we can find that, with the gradual increase of σ_3, the stability region of the tumour-free equilibrium F_1 of system (34) gradually increases (the intersection point of curves and x-coordinate gradually moves to the right). This shows that the increase of antibody injection quantity can help to slow down Tregs inhibition of tumor immune responses. The stability region of equilibrium F^* of system (34) gradually increases (the blue curve gradually moves upward), which means that increasing the amount of antibody injected can help the immune system to control more TCs. By comparing Figures 5 and 7, we find that the effect of MAI is better than that of AIC in delaying the inhibitory effect of Tregs on tumor immune response (at the same injection dose, the intersection point of curves and x-coordinate in Figure 7 moves to the right more widely than that in Figure 5). AIC is more effective than MAI in controlling TCs (the blue
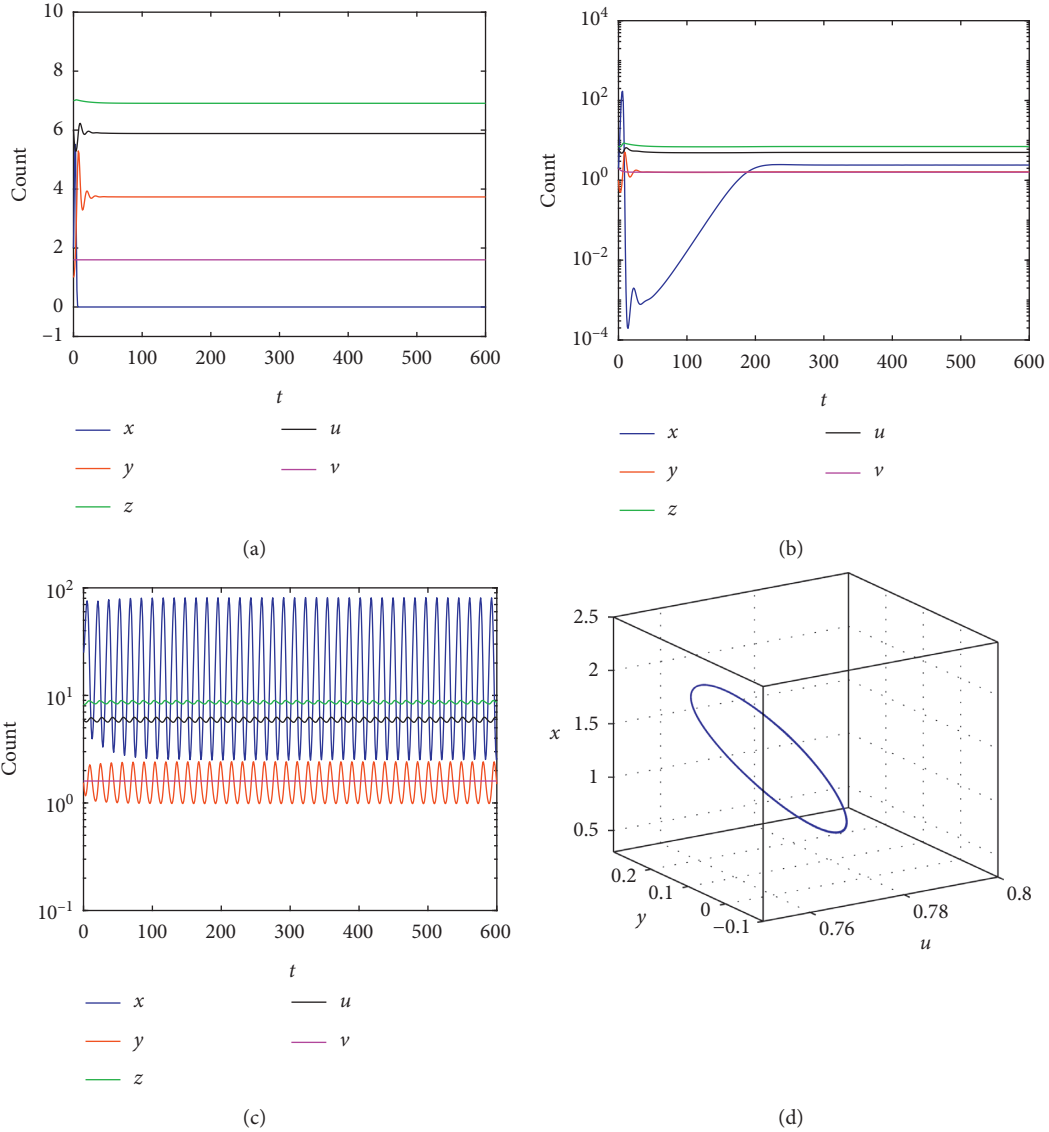
(a)

(b)

(c)

(d)

FIGURE 8: Choose $\sigma_3 = 0.4$, and the other parameter values are given in (22). (a) When $\theta = 0.5$, $F_1 (0, 2.556, 6.909, 5.349, 1.6)$ is LAS. (b) When $\theta = 0.6$, $F^* (2.413, 1.628, 7.032, 5.002, 1.6)$ is LAS. (c) When $\theta = 0.635$, $F^* (27.345, 1.546, 8.624, 5.93, 1.6)$ is unstable. (d) When $\theta = 0.635$, the 3D phase portrait depicts TCs, ECs, and Treg.

curve in Figure 7 moves up more than the blue curves in Figure 5 at the same injection dose).

3.2.3. Combined Immunotherapy Model $(\sigma_1 > 0, \sigma_3 > 0)$.

We conduct numerical simulations of the combined immunotherapy model. We choose $\omega_2 = 0.0004$, $\xi = 0.05$, and $\delta_4 = 0.25$, and the other parameter values are given in (22). We find the stability region of $N^* = (x^*, y^*, z^*, u^*, v^*)$, as shown in Figure 9(a). When σ_3 increases gradually, the stability region of N^* also increases gradually.

Case (a): we choose a point $L_1 = (\theta, \sigma_1) = (0.7, 0.4)$ on the left of the curve $\sigma_3 = 0.5$; then, system (34) has one coexistence equilibrium:

$$N^* = (11.56, 1.59, 7.54, 4.99, 2). \tag{86}$$

The eigenvalues of Jacobian matrix of (64) are

$$-0.06, \ -0.176, \ -0.25, \ -0.22 - 0.37i \text{ and } -0.22 + 0.37i, \tag{87}$$

so N^* is stable, as shown in Figure 10(b).

Case (b): we choose a point $L_2 = (\theta, \sigma_1) = (0.78, 0.4)$ on the right of the curve $\sigma_3 = 0.5$; then, system (34) has one coexistence equilibrium:
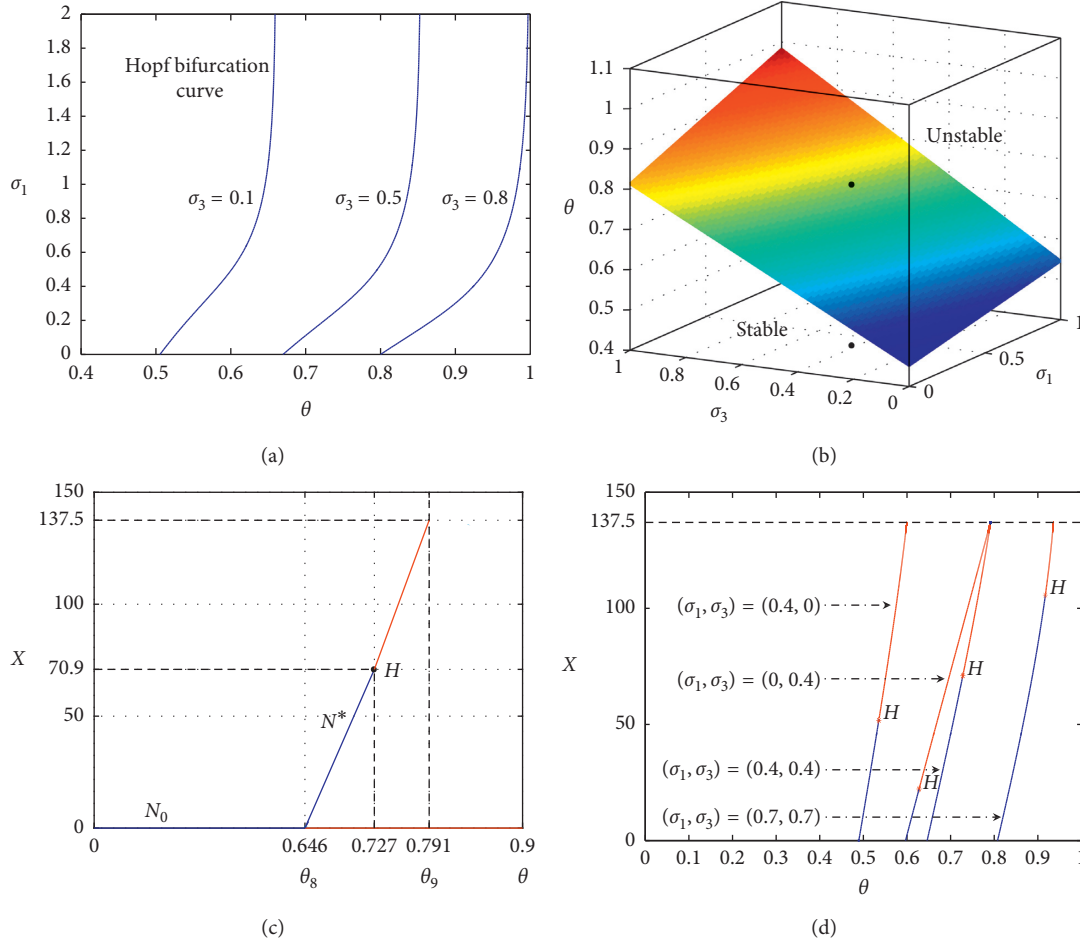
$$N^* = (77.887, 1.381, 15.936, 9.698, 2). \tag{88}$$

(a)

(b)

(c)

(d)

FIGURE 9: (a) Choose different $\sigma_3 = 0.1$, 0.5, 0.8. Stability region of N^* and Hopf bifurcation curve in $\theta - \sigma_1$ parameter plane. N^* is stable to the left of the curve and unstable to the right of the curve. (b) Combined immunotherapy surface. N_0 is stable below the surface and unstable above the surface. (c) When $\sigma_1 = 0.4$ and $\sigma_3 = 0.4$, the bifurcation diagram of x with respect to θ for system (34). Hopf bifurcation point appears at $\theta_{CI}^* = 0.727$. (d) Choose different $(\sigma_1, \sigma_3) = (0.4, 0)$, $(0, 0.4)$, $(0.4, 0.4)$, $(0.7, 0.7)$. The bifurcation diagram of x with respect to θ (the stable steady state is represented by the blue curve, and the unstable one corresponds to the red curve).

The eigenvalues of Jacobian matrix of (64) are

$$-0.906238, \ -0.0248, \ -0.25, \ 0.00641$$
$$-0.66i \text{ and } 0.00641 + 0.66i, \tag{89}$$

so N^* is unstable, as shown in Figures 10(c) and 10(d).

According to the stability condition of tumor-free equilibrium N_0 in Theorem 11, combined immunotherapy surface can be obtained as

$$\theta = \frac{\alpha\delta_{31}\left(\rho\sigma_2 - \delta_1\delta_2\right) + \sigma_1\delta_2\delta_{31}}{\alpha\left(\alpha\gamma_1\delta_2 + \sigma_2\gamma_2\right)} \tag{90}$$
$$= \left(0.055\sigma_1 + 0.2647\right)\left(1.366\sigma_3 + 1.707\right).$$

Therefore, the stability region of tumor-free equilibrium N_0 of system (34) is obtained (see Figure 9(b)).

Case (c): we choose a point $L_3 = (\sigma_1, \sigma_2, \theta) = (0.5, 0.5, 0.4)$ below surface (90); then, system (34) has a tumor-free equilibrium:

$$N_0 = (0, 8.3, 6.909, 7.505, 2). \tag{91}$$

The eigenvalues of Jacobian matrix of (64) are

$$-6.664, \ -0.055, \ -0.25, \ -0.204 + 0.69i \text{ and } -0.204 - 0.69i, \tag{92}$$

so N_0 is stable, as shown in Figure 10(a).

Case (d): we choose a point $L_4 = (\sigma_1, \sigma_2, \theta) = (0.5, 0.5, 0.8)$ above surface (90); then, system (34) has a tumor-free equilibrium:

$$N_0 = (0, 0.886, 6.909, 4.32, 2). \tag{93}$$

The eigenvalues of Jacobian matrix of (64) are

$$0.75, \ -0.055, \ -0.25, \ -0.453 + 0.311i \text{ and}$$
$$-0.453 - 0.311i, \tag{94}$$

so N_0 is unstable.

We choose combined immunotherapy parameter $\sigma_1 = 0.4$ and $\sigma_3 = 0.4$ to study the relationship between the number of TCs x and the parameter θ (see Figure 9(c)). By some calculations, we have $\theta_8 = \alpha\delta_{31}\left(\rho\sigma_2 - \delta_1\delta_2\right) +$
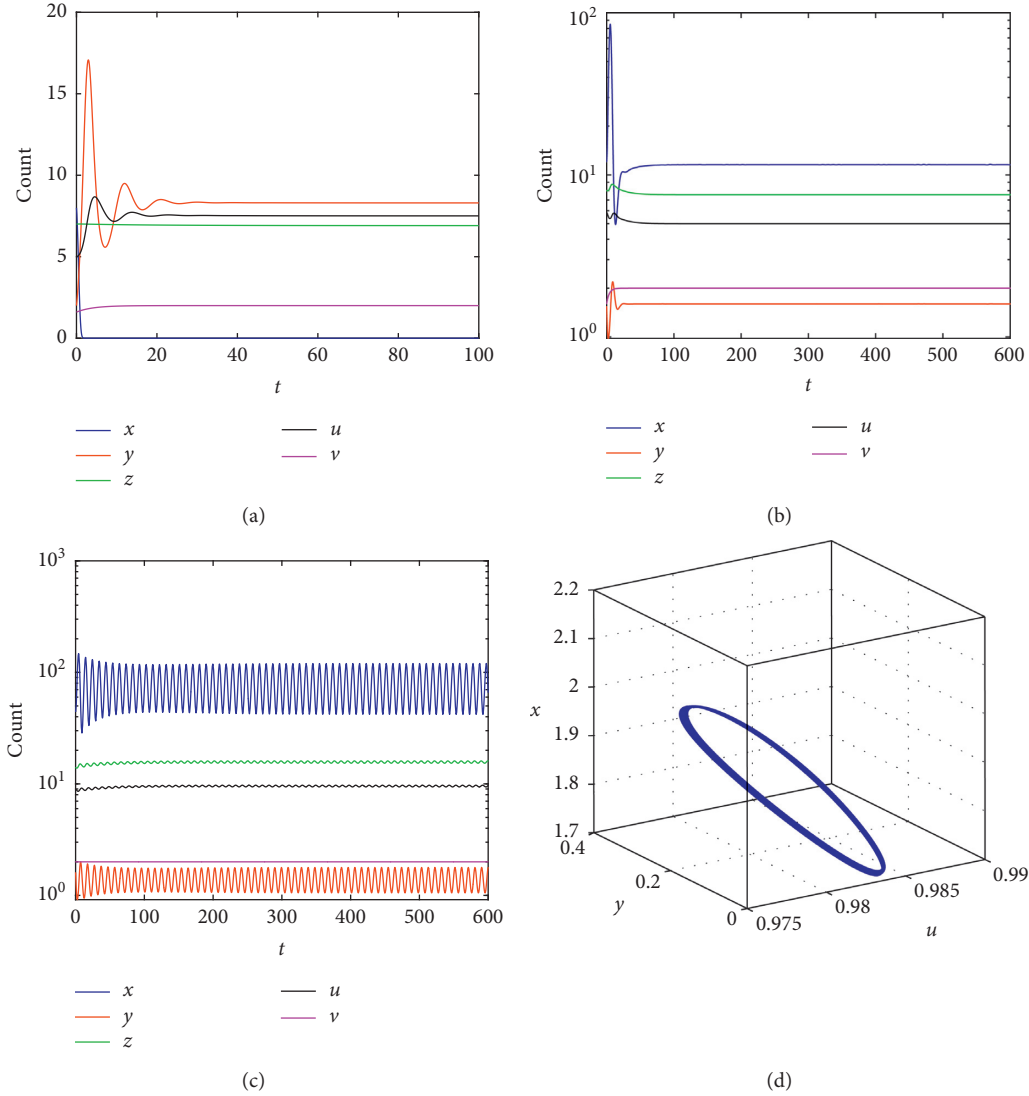
(a)

(b)

(c)

(d)

FIGURE 10: (a) When $\sigma_1 = \sigma_3 = 0.5$, $\theta = 0.4$, $N_0(0, 8.3, 6.909, 7.505, 2)$ is LAS. (b) When $\sigma_1 = 0.4$, $\sigma_3 = 0.5$, $\theta = 0.7$, $N^*(11.56, 1.59, 7.54, 4.99, 2)$ is LAS. (c) When $\sigma_1 = 0.4$, $\sigma_3 = 0.5$, $\theta = 0.78$, $N^*(77.887, 1.381, 15.936, 9.698, 2)$ is unstable. (d) When $\sigma_1 = 0.4$, $\sigma_3 = 0.5$, $\theta = 0.78$, the 3D phase portrait depicts TCs, ECs, and Tregs.

$\sigma_1 \delta_2 \delta_{31} / \alpha(\alpha \gamma_1 \delta_2 + \sigma_2 \gamma_2) = 0.646$, and $\theta_9 = \rho \delta_{31} / \gamma_2 = 0.791$. And Hopf bifurcation point appears at $\theta_{CI}^* = 0.727$. We can obtain the following result.

Proposition 7. *When $0 < \theta < \theta_8$, N_0 exists and is LAS, and N^* is nonexistent. When $\theta_8 < \theta < \theta_{CI}^*$, N_0 exists and is unstable, and N^* exists and is LAS. When $\theta_{CI}^* < \theta < \theta_9$, N_0 exists and is unstable, and N^* exists and is unstable. When $\theta > \theta_9$, N_0 exists and is unstable, and N^* is nonexistent.*

For combined immunotherapy, by comparing the curves in Figure 9(d), we know that, with the increase of σ_1 and σ_3, the stability region of the tumour-free equilibrium of N_0 of system (34) gradually increases (the intersection point of curves and x-coordinate gradually moves to the right), and the stability region of equilibrium N^* of system (34) gradually increases (the blue curve gradually moves upward). By comparing Figure 9 with Figures 5 and 7, it can be

seen that combined immunotherapy has better effects on delaying the inhibitory effect of Tregs on tumor immune response and helps the immune system to control more TCs than ACI or MAI.

4. Discussion and Conclusion

Tregs-mediated tumor immune escape is one of the core mechanisms of tumor immune regulation. And Tregs have been found to mediate tumor evasion and immune escape in many different solid tumors [46]. The study on Tregs has a very high research value and application prospect in the immunotherapy of tumors. If the activity of Tregs is controlled or blocked during the tumor immune response, or a barrier is set to prevent Tregs from migrating into the tumor microenvironment, then the effect of tumor immunotherapy can be improved [47].

First, we developed a mathematical model to study the inhibitory role of Tregs in the tumor immune system. For the lower recognition of tumor antigens by the immune system, the stronger the inhibition effect of Tregs on ECs, TCs can easily escape the control of the immune system (see Figure 4(a)). When the immune system is highly sensitive to tumor antigens, the immune system activates ECs; the stronger the inhibition effect of Tregs on ECs, the more complicated interactions between TCs and immune cells (see Figure 4(b)).

Second, we incorporated the previous mathematical model with three types of immunotherapy to obtain ACI model, MAI model, and combined both ACI and MAI model. Through the theoretical analysis and numerical simulations, we found that ACI can control more TCs, but have no obvious effects on reducing the inhibitory effect of Tregs on ECs (see Figure 5). MAI can effectively reduce the inhibitory effect of Tregs on ECs, but cannot control more TCs (see Figure 7). However, combination immunotherapy with ACI and MAI is more effective than single immunotherapy. It can not only significantly reduce the inhibitory effect of Tregs on ECs but also help the immune system to kill TCs to the maximum extent (see Figure 9). Therefore, we recommend the use of combined immunotherapy in the treatment of tumors. Besides, clinical trials are needed to further evaluate the safety and efficacy of combined immunotherapy.

This paper focused on the general process of tumor immune response with negative feedback. Using the mathematical model, it is possible to simulate the state of tumors in the immune system at different inhibition states. The results of the study can contribute to the understanding of tumor immunity; at the same time, it also provides new ideas for the treatment of tumors. However, due to the complexity and heterogeneity of tumor microenvironment, there is still a certain gap between the mathematical model and the description of the real interactions between the tumor and immune system. Therefore, specific tumor microenvironment and heterogeneous tumoral populations should be considered in practical application to make the model more realistic [34]. In addition to the bilinear incidence model considered in this paper, non-bilinear model with saturation incidence should be employed in the further study [35]. Besides, other important factors such as immune activation delays [36–38, 48], stochastic effects [39, 40, 49], and impulsive perturbations [41, 42, 50] can be considered in the modelling of the tumor immune system. The tumor immune response dynamics in vivo is very complex and not well understood primarily because the measurements of the necessary parameters are difficult in vivo [43].

Data Availability

No data were used to support this study.

Conflicts of Interest

The authors declare that there are no conflicts of interest regarding the publication of this paper.

Acknowledgments

References

[1] P. Boyle, "Measuring progress against cancer in Europe: has the 15% decline targeted for 2000 come about?" *Annals of Oncology*, vol. 14, pp. 1312–1325, 2003.

[2] T. Boon and P. Van der Bruggen, "Human tumor antigens recognized by T lymphocytes," *The Journal of Experimental Medicine*, vol. 183, no. 3, pp. 725–729, 1996.

[3] K. E. De Visser, A. Eichten, and L. M. Coussens, "Paradoxical roles of the immune system during cancer development," *Nature Reviews Cancer*, vol. 6, no. 1, pp. 24–37, 2006.

[4] Y. Dong, R. Miyazaki, R. Miyazaki, and Y. Takeuchi, "Mathematical modeling on helper T cells in a tumor immune system," *Discrete & Continuous Dynamical Systems-B*, vol. 19, no. 1, pp. 55–72, 2014.

[5] A. Talkington, C. Dantoin, and R. Durrett, "Ordinary differential equation models for adoptive immunotherapy," *Bulletin of Mathematical Biology*, vol. 9, pp. 1–25, 2017.

[6] Y.-P. Lai, C.-J. Jeng, and S.-C. Chen, "The roles of CD4+T cells in tumor immunity," *ISRN Immunology*, vol. 2011, pp. 1–6, 2011.

[7] T. Maj, W. Wang, J. Crespo et al., "Oxidative stress controls regulatory T cell apoptosis and suppressor activity and PD-L1-blockade resistance in tumor," *Nature Immunology*, vol. 18, no. 12, pp. 1332–1341, 2017.

[8] S. Wilson and D. Levy, "A mathematical model of the enhancement of tumor vaccine efficacy by immunotherapy," *Bulletin of Mathematical Biology*, vol. 74, no. 7, pp. 1485–1500, 2012.

[9] A. Albert, M. Freedman, and A. S. Perelson, "Tumors and the immune system: the effects of a tumor growth modulator," *Mathematical Biosciences*, vol. 50, no. 1-2, pp. 25–58, 1980.

[10] A. d'Onofrio, "A general framework for modeling tumor-immune system competition and immunotherapy: mathematical analysis and biomedical inferences," *Physica D*, vol. 208, pp. 220–235, 2005.

[11] D. Kirschner and J. C. Panetta, "Modeling immunotherapy of the tumor - immune interaction," *Journal of Mathematical Biology*, vol. 37, no. 3, pp. 235–252, 1998.

[12] S. Amarnath, C. W. Mangus, J. C. M. Wang et al., "The PDL1-PD1 Axis converts human TH1 cells into regulatory T cells," *Science Translational Medicine*, vol. 3, no. 111, pp. 111–120, 2011.

[13] L. Spain, S. Diem, and J. Larkin, "Management of toxicities of immune checkpoint inhibitors," *Cancer Treatment Reviews*, vol. 44, pp. 51–60, 2016.

[14] K. S. Peggs, S. A. Quezada, A. J. Korman, and J. P. Allison, "Principles and use of anti-CTLA4 antibody in human cancer immunotherapy," *Current Opinion in Immunology*, vol. 18, no. 2, pp. 206–213, 2006.

[15] A. A. Hurwitz, B. A. Foster, E. D. Kwon et al., "Combination immunotherapy of primary prostate cancer in a transgenic mouse model using CTLA-4 blockade," *Cancer Research*, vol. 60, no. 9, pp. 2444–2448, 2000.

[16] J. G. Egen, M. S. Kuhns, and J. P. Allison, "CTLA-4: new insights into its biological function and use in tumor immunotherapy," *Nature Immunology*, vol. 3, no. 7, pp. 611–618, 2002.

[17] T. Takahashi, T. Tagami, S. Yamazaki et al., "Immunologic self-tolerance maintained by Cd25+Cd4+Regulatory T cells constitutively expressing cytotoxic T lymphocyte-associated antigen 4," *The Journal of Experimental Medicine*, vol. 192, no. 2, pp. 303–310, 2000.

[18] Y.-F. Ma, C. Chen, D. Li et al., "Targeting of interleukin (IL)-17A inhibits PDL1 expression in tumor cells and induces anticancer immunity in an estrogen receptor-negative murine model of breast cancer," *Oncotarget*, vol. 8, no. 5, pp. 7614–7624, 2016.

[19] K. R. Jordan, V. Borges, and M. D. Mccarter, "Abstract 1671: immunosuppressive myeloid-derived suppressor cells expressing PDL1 are increased in human melanoma tumor tissue," *Cancer Research*, vol. 74, p. 1671, 2014.

[20] E. Baldelli, V. Calvert, and K. A. Hodge, "Abstract 5656: quantitative measurement of PDL1 expression across tumor types using laser capture microdissection and reverse phase protein microarray," *Cancer Research*, vol. 77, p. 5656, 2017.

[21] E. E. West, H.-T. Jin, A.-U. Rasheed et al., "PD-L1 blockade synergizes with IL-2 therapy in reinvigorating exhausted T cells," *Journal of Clinical Investigation*, vol. 123, no. 6, pp. 2604–2615, 2013.

[22] L. M. Francisco, P. T. Sage, and A. H. Sharpe, "The PD-1 pathway in tolerance and autoimmunity," *Immunological Reviews*, vol. 236, no. 1, pp. 219–242, 2010.

[23] B. Brady, "Dramatic survival benefit with nivolumab in melanoma," *Cancer Research*, vol. 6, p. OF7, 2016.

[24] D. Kazandjian, D. L. Suzman, G. Blumenthal et al., "FDA approval summary: nivolumab for the treatment of metastatic non-small cell lung cancer with progression on or after platinum-based chemotherapy," *The Oncologist*, vol. 21, no. 5, pp. 634–642, 2016.

[25] C. Voena and R. Chiarle, "Advances in cancer immunology and caner immunotherapy," *Cancer Research*, vol. 21, pp. 125–133, 2016.

[26] N. V. Stepanova, "Course of the immune reaction during the development of a malignant tumour," *Cancer Research*, vol. 24, pp. 917–923, 1979.

[27] V. A. Kuznetsov, I. A. Makalkin, M. A. Taylor, and A. S. Perelson, "Nonlinear dynamics of immunogenic tumors: parameter estimation and global bifurcation analysis," *Bulletin of Mathematical Biology*, vol. 56, no. 2, pp. 295–321, 1994.

[28] O. Sotolongo-Costa, L. Morales Molina, D. Rodríguez Perez, J. C. Antoranz, and M. Chacón Reyes, "Behavior of tumors under nonstationary therapy," *Physica D: Nonlinear Phenomena*, vol. 178, no. 3-4, pp. 242–253, 2003.

[29] M. Galach, "Dynamics of the tumor-immune system competition-the effect of time delay," *International Journal of Applied Mathematics and Computer Science*, vol. 13, pp. 395–406, 2003.

[30] L. G. de Pillis, W. Gu, and A. E. Radunskaya, "Mixed immunotherapy and chemotherapy of tumors: modeling, applications and biological interpretations," *Journal of Theoretical Biology*, vol. 238, no. 4, pp. 841–862, 2006.

[31] S. Bunimovich-Mendrazitsky, H. Byrne, and L. Stone, "Mathematical model of pulsed immunotherapy for superficial bladder cancer," *Bulletin of Mathematical Biology*, vol. 70, no. 7, pp. 2055–2076, 2008.

[32] A. Radunskaya, R. Kim, and T. Woods, "Mathematical modeling of tumor immune interactions: a closer look at the role of a PD-L1 inhibitor in cancer immunotherapy," *Spora: A Journal of Biomathematics*, vol. 4, pp. 25–41, 2018.

[33] Y. Shu, J. Huang, Y. Dong, and Y. Takeuchi, "Mathematical modeling and bifurcation analysis of pro- and anti-tumor macrophages," *Applied Mathematical Modelling*, vol. 88, pp. 758–773, 2020.

[34] E. Piretto, M. Delitala, and M. Ferraro, "How combination therapies shape drug resistance in heterogeneous tumoral populations," *Letters in Biomathematics*, vol. 5, no. 2, pp. S160–S177, 2018.

[35] H. Dritschel, S. Waters, A. Roller, and H. Byrne, "A mathematical model of cytotoxic and helper T cell interactions in a tumour microenvironment," *Letters in Biomathematics*, vol. 5, no. 2, pp. S36–S68, 2018.

[36] Y. Dong, G. Huang, R. Miyazaki, and Y. Takeuchi, "Dynamics in a tumor immune system with time delays," *Applied Mathematics and Computation*, vol. 252, pp. 99–113, 2015.

[37] M. Yu, Y. Dong, and Y. Takeuchi, "Dual role of delay effects in a tumour-immune system," *Journal of Biological Dynamics*, vol. 11, no. 2, pp. 334–347, 2017.

[38] M. Yu, G. Huang, Y. Dong, and Y. Takeuchi, "Complicated dynamics of tumor-immune system interaction model with distributed time delay," *Discrete & Continuous Dynamical Systems-B*, vol. 25, no. 7, pp. 2391–2406, 2020.

[39] G. Caravagna, A. d'Onofrio, P. Milazzo, and R. Barbuti, "Tumour suppression by immune system through stochastic oscillations," *Journal of Theoretical Biology*, vol. 265, no. 3, pp. 336–345, 2010.

[40] J. T. George and H. Levine, "Stochastic modeling of tumor progression and immune evasion," *Journal of Theoretical Biology*, vol. 458, pp. 148–155, 2018.

[41] H.-P. Ren, Y. Yang, M. S. Baptista, and C. Grebogi, "Tumour chemotherapy strategy based on impulse control theory," *Philosophical Transactions of the Royal Society A: Mathematical, Physical and Engineering Sciences*, vol. 375, no. 2088, p. 20160221, 2017.

[42] Y. Deng and M. Liu, "Analysis of a stochastic tumor-immune model with regime switching and impulsive perturbations," *Applied Mathematical Modelling*, vol. 78, pp. 482–504, 2020.

[43] G. E. Mahlbacher, K. C. Reihmer, and H. B. Frieboes, "Mathematical modeling of tumor-immune cell interactions," *Journal of Theoretical Biology*, vol. 469, pp. 47–60, 2019.

[44] J. K. Hale, *Theory of Functional Differential Equations*, Springer, New York, NY, USA, 1977.

[45] A. Dhooge, W. Govaerts, and Y. A. Kuznetsov, "Matcont," *ACM SIGSAM Bulletin*, vol. 38, no. 1, pp. 21-22, 2004.

[46] A. Facciabene, G. T. Motz, and G. Coukos, "T-regulatory cells: key players in tumor immune escape and angiogenesis," *Cancer Research*, vol. 72, no. 9, pp. 2162–2171, 2012.

[47] K. Shitara and H. Nishikawa, "Regulatory T cells: a potential target in cancer immunotherapy," *Annals of the New York Academy of Sciences*, vol. 1417, no. 1, pp. 104–115, 2018.

[48] T. Zhang, J. Wang, Y. Li, Z. Jiang, and X. Han, "Dynamics analysis of a delayed virus model with two different transmission methods and treatments," *Advances in Difference Equations*, vol. 1, p. 2020, 2020.

[49] H. Zhang and T. Zhang, "The stationary distribution of a microorganism flocculation model with stochastic perturbation," *Applied Mathematics Letters*, vol. 103, p. 106217, 2020.

[50] T. Zhang, N. Gao, N. Gao, T. Wang, H. Liu, and Z. Jiang, "Global dynamics of a model for treating microorganisms in sewage by periodically adding microbial flocculants," *Mathematical Biosciences and Engineering*, vol. 17, no. 1, pp. 179–201, 2020.

WILEY | Hindawi

Research Article

A Stage-Structured Predator-Prey Model in a Patchy Environment

Xuejuan Lu,[1] **Yuming Chen** **,**[2] **and Shengqiang Liu** [3]

[1]*College of Science, Qiqihar University, Qiqihar, Heilongjiang 161006, China*
[2]*Department of Mathematics, Wilfrid Laurier University, Waterloo, Ontario N2L 3C5, Canada*
[3]*School of Mathematical Sciences, Tiangong University, Tianjin 300387, China*

Correspondence should be addressed to Shengqiang Liu; sqliu@tiangong.edu.cn

In this paper, we propose a stage-structured predator-prey model with migrations among patches in an n-patch environment. The net reproduction number for each patch in isolation is obtained along with the net reproduction number of the system of patches, $\mathcal{R}_0$. Inequalities describing the relationship among these numbers are also given. Furthermore, threshold dynamics determined by $\mathcal{R}_0$ is established: the predator dies out if $\mathcal{R}_0 < 1$ while the predator persists if $\mathcal{R}_0 > 1$. Focusing on the case with two patches, we obtain that the dispersal decreases the net reproduction number $\mathcal{R}_0$. By numerical simulations, we find that the dispersal may be a good thing or a bad thing because the dispersal could make the predator population thrive or extinct, and hence we might seek steady state in the ecological environment by controlling parameters related to the prey and the predator.

1. Introduction

The effect of dispersal of organisms on population dynamics is one of the central topics in ecology and evolutionary biology [1–5]. Each species has a characteristic pattern of variation in abundance over space. Understanding the factors responsible for manifest diversity in distributional patterns is an important prerequisite for studying survival and extinction of species. For example, many types of birds and mammals migrate from cold regions to warm regions in search of a better habitat or a breeding site [6], and for ecological communities of insects, dispersal of a predator is usually driven by its nonrandom foraging behavior which can often respond to prey-contact stimuli [7, 8].

During the past couple of decades, due to the prevalence of the predator-prey relationship in the nature, predator-prey models with diffusion in patchy environment have attracted significant attention from ecologists, biologists, and bio-mathematicians. Levin [9] proposed two-species competition and prey-predator models with population dispersal among patches. Takeuchi [10] and Kuang and Takeuchi [11] found that stabilizing and destabilizing effects could be induced by prey dispersal. Gramlich et al. [12] considered a 2-patch 2-species system and found that dispersal between different

habitats influences the dynamics and stability of populations considerably. Moreover, these effects depend on the local interactions of a population with others. Kang et al. [8] formulated a two-patch Rosenzweig–MacArthur prey-predator model with mobility only in the predator, and they found that dispersal may stabilize or destabilize the coupled system; dispersal may generate multiple interior equilibria or may destroy interior equilibria. In a few patch models, the common findings for most studies on interactions of prey and predator are that dispersal makes the dynamics very complicated. This means that dispersals of prey and predator play an important role in regulating, stabilizing, or destabilizing population dynamics of both prey and predator. In an n-patch environment, due to the intricacies that arise from dispersal, not much has been done yet. Qiu and Mitsui [13] considered a predator-prey system with diffusion and time delay in an n-patch environment, where prey disperses between n patches of a heterogeneous environment with barriers between patches where a predator cannot cross. Al-Darabsah et al. [14] proposed a prey-predator model in multiple patches through the stage-structured maturation time delay with migrations among patches. However, they only discussed the existence of equilibrium points and the uniform persistence for the special case of two patches.

To our best acknowledgment, little attention has been paid to the relation between the long-term dynamics and dispersal rate of the multipatch predator-prey model. In two recent references [15, 16], net reproduction number $\mathscr{R}_0$ was introduced into the nondiffusion predator-prey models; it was shown that the net reproduction number determines its threshold dynamics; here $\mathscr{R}_0$ has the similar definition to the basic reproduction number of general compartmental epidemic model, as discussed in [17]. Since there are many excellent results on investigating the effects of mobility rate on basic reproduction number and the threshold dynamics of multipatch epidemic model, for reference, we refer to Hsieh et al. [18], Wang et al. [19], and Wang et al. [20]. This motivates us to study an n-patch predator-prey model with prey and predator diffusing simultaneously.

In this paper, we focus on a model with prey and predator dispersal in an n-patch environment. In addition, the predator is structured as juvenile and adult. We assume that juvenile predators may diffuse as they can follow adult one. We also need to pay attention to acquisition probability of the juvenile predator, which can be zero and less than unity. Moreover, the dispersal among patches may occur only in a single species. The main focus of our study of such prey-predator interactions in an n-patch heterogeneous environment is to explore the following ecological questions:

(1) What is the net reproduction number $\mathscr{R}_0$? And whether there is a limit on $\mathscr{R}_0$?

(2) In a two-patch model, what is the relationship between the constant dispersal rates of prey and predator and $\mathscr{R}_0$?

(3) How does dispersal of prey and predator affect the extinction and persistence of predator in all patches?

(4) How may dispersal promote the coexistence of prey and predator when predator goes extinct in a single patch?

The paper is organized as follows. In the next section, we propose the model and show the positiveness and ultimate boundedness of solution under some conditions. In Section 3, we derive a general formula for the net reproduction number and give a bound for $\mathscr{R}_0$, show the local asymptotical stability of the predator-free equilibrium when $\mathscr{R}_0 < 1$, and also obtain the global attractivity of the predator-free equilibrium under some conditions. Moreover, we consider the special case with the linear predation function in a two-patch environment. In Section 4, we prove the uniform persistence when $\mathscr{R}_0 > 1$, and hence the system has at least one positive equilibrium. Numerical simulations are provided in Section 5 to demonstrate our results. The paper concludes with a brief discussion.

2. The Model

In this section, we formulate a predator-prey model in n patches by taking into consideration diffusion among patches and a stage structure in the predator. In each patch i, there are prey individuals, juvenile predator individuals, and adult predator individuals, denoted by N_i, P_i^J, and P_i^A, respectively.

For patch i, let r_i be the intrinsic growth rate in the absence of predation and K_i be the carrying capacity of the

prey; d_i^N, d_i^J, and d_i^A denote the death rates of prey, juvenile predators, and adult predators, respectively; we always assume $r_i > d_i^N$; σ_i stands for the acquisition probability of juvenile predators and $\sigma_i \in [0, 1)$; we always assume e_i to be the probability of the captured prey being converted into juvenile predators; α_i is the progression rate of juvenile predators. All parameters are assumed to be positive except that σ_i can be zero.

We assume that the predation function $f_i(N_i)$ satisfies the following basic assumptions for $N_i \in (0, \infty)$.

(1) $f_i(N_i) > 0$, $i \in \mathbb{N}_n = \{1, 2, \ldots, n\}$.

(2) $f_i(N_i) = N_i g_i(N_i)$, $g_i(N_i)$ is a continuous function about N_i and $g_i(N_i) > 0$, $i \in \mathbb{N}_n$.

(3) $f_i'(N_i) \geq 0$, $i \in \mathbb{N}_n$.

The following three types of predation functions $f(N)$ in [21] satisfy the above assumptions.

(1) $f(N) = bN$, $b > 0$.

(2) $f(N) = (bN/1 + cN)$, $b, c > 0$.

(3) $f(N) = (bN^2/1 + cN^2)$, $b, c > 0$.

We assume that there is no capture and captured behavior in the diffusion process, and m_{ij}^K for $K = N, J, A$ are the constant dispersal rates from patch j to patch i for $i \neq j$ of prey, juvenile predators, and adult predators, respectively, with $m_{ii}^K = 0$. It is assumed that the matrices $\mathbf{M}^K = (m_{ij}^K)$, $i, j \in \mathbb{N}_n$ for $K = N, J, A$ are irreducible. The flowchart of diffusion is shown in Figure 1.

Based on the above assumptions, our model is as follows:

$$
\begin{cases}
\dot{N}_i = r_i N_i \left(1 - \dfrac{N_i}{K_i}\right) - f_i(N_i)\left(P_i^A + \sigma_i P_i^J\right) - d_i^N N_i \\
\qquad + \displaystyle\sum_{j \in \mathbb{N}_n} m_{ij}^N N_j - \sum_{j \in \mathbb{N}_n} m_{ji}^N N_i, \\[2mm]
\dot{P}_i^J = e_i f_i(N_i)\left(P_i^A + \sigma_i P_i^J\right) - \left(d_i^J + \alpha_i\right) P_i^J \\
\qquad + \displaystyle\sum_{j \in \mathbb{N}_n} m_{ij}^J P_j^J - \sum_{j \in \mathbb{N}_n} m_{ji}^J P_i^J, \\[2mm]
\dot{P}_i^A = \alpha_i P_i^J - d_i^A P_i^A + \displaystyle\sum_{j \in \mathbb{N}_n} m_{ij}^A P_j^A - \sum_{j \in \mathbb{N}_n} m_{ji}^A P_i^A.
\end{cases}
\tag{1}
$$

Similar to [19], for a vector $\mathbf{x} \in \mathbb{R}^n$, we use $\operatorname{diag}(\mathbf{x})$ to denote the $n \times n$ diagonal matrix, whose diagonal elements are the components of $\mathbf{x}$. We use the ordering in $\mathbb{R}^n$ generated by the cone $\mathbb{R}_+^n$, that is, $\mathbf{x} \leq \mathbf{y}$ if $\mathbf{y} - \mathbf{x} \in \mathbb{R}_+^n$, $\mathbf{x} < \mathbf{y}$ if $\mathbf{x} \leq \mathbf{y}$ and $\mathbf{x} \neq \mathbf{y}$, and finally $\mathbf{x} \ll \mathbf{y}$ means $x_i < y_i$ for any index i.

Denote the vector

$$
\begin{aligned}
\left(\mathbf{N}(t), \mathbf{P^J}(t), \mathbf{P^A}(t)\right) &= \left(N_1(t), \ldots, N_n(t), P_1^J(t), \ldots,\right. \\
&\quad \left. P_n^J(t), P_1^A(t), \ldots, P_n^A(t)\right)^{\mathrm{T}} \in \mathbb{R}_+^{3n},
\end{aligned}
\tag{2}
$$

$$
\mathbf{A}_0 = \left(\mathbf{N}(0), \mathbf{P^J}(0), \mathbf{P^A}(0)\right).
\tag{3}
$$
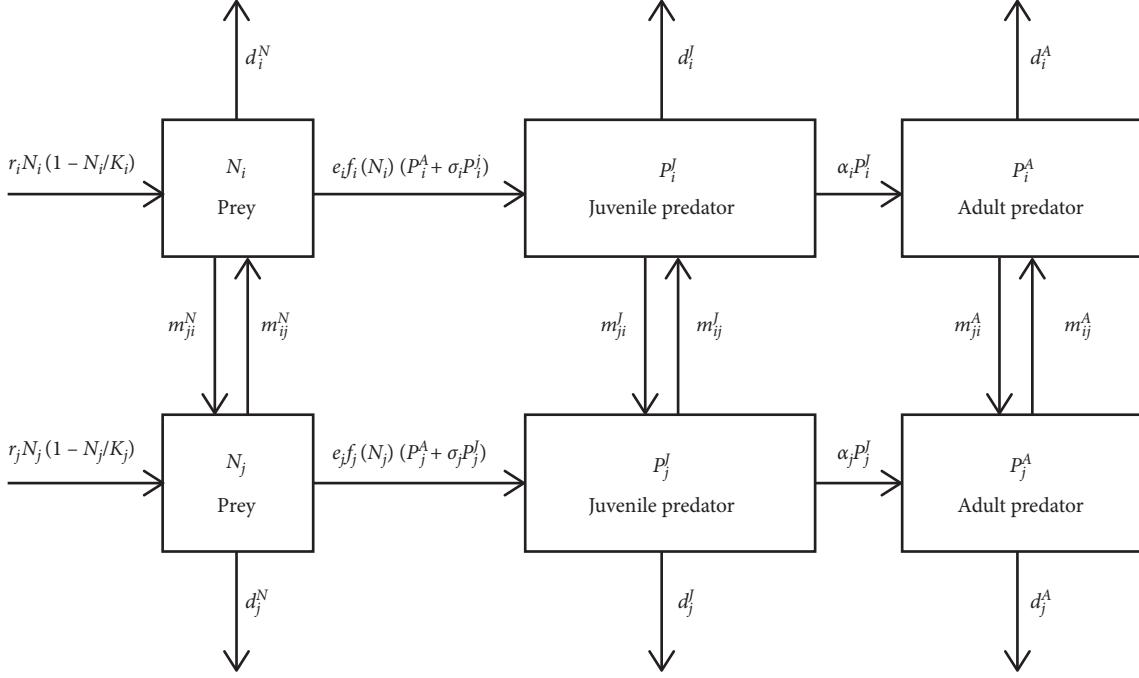
Figure 1: Flowchart of the dispersal process between patch i and j.

Moreover, we assume that each component of $\mathbf{A}_0$ is nonnegative with the following initial conditions:

$$\sum_{i \in \mathbb{N}_n} N_i(0) > 0,$$
$$\sum_{i \in \mathbb{N}_n} \left(P_i^A(0) + \sigma_i P_i^J(0) \right) > 0. \tag{4}$$

Then, it follows from the standard existence and uniqueness theorem for ordinary differential equations that there is a unique solution to system (1).

Theorem 1. *Consider system (1) with nonnegative initial conditions (4). Then, for each $i \in \mathbb{N}_n$ and $t > 0$, $\mathbf{N}(t)$, $\mathbf{P}^J(t)$, and $\mathbf{P}^A(t)$ are all positive and ultimately bounded.*

Proof of Theorem 1. Firstly, we prove that for $i \in \mathbb{N}_n$, $N_i(t) > 0$ for $t > 0$. For convenience, we rewrite the first equation of (1) as

$$\dot{N}_i(t) = P_i(t)N_i(t) + Q_i(t), \quad i \in \mathbb{N}_n, \tag{5}$$

where

$$P_i(t) = r_i - \frac{r_i}{K_i}N_i(t) - g_i\left(N_i(t)\right)$$
$$\cdot \left(P_i^A(t) + \sigma_i P_i^J(t) - d_i^N - \sum_{j \in \mathbb{N}_n} m_{ji}^N \right), \tag{6}$$

$$Q_i(t) = \sum_{j \in \mathbb{N}_n} m_{ij}^N N_j(t).$$

Let $I_1 = \{i \in \mathbb{N}_n \mid N_i(0) > 0\}$ and $I_2 = \mathbb{N}_n \backslash I_1$. Since $\sum_{i \in \mathbb{N}_n} N_i(0) > 0$, we know that $I_1 \neq \varnothing$. If $i_0 \in I_1$, then from (5)

with $i = i_0$, we easily see that $N_{i_0}(t) > 0$ for $t > 0$. If $I_2 = \varnothing$, then we are done. Now suppose that $I_2 \neq \varnothing$. Since (m_{ij}^N) is irreducible, there exists $i_1 \in I_2$ such that $m_{i_1 j}^N \neq 0$ for some $j \in I_1$. Then, $Q_{i_1}(t) > 0$ for $t > 0$. This and (5) with $i = i_1$ imply that $N_{i_1}(t) > 0$ for $t > 0$. Denote $J_1 = I_1 \cup \{i_1\}$ and $J_2 = I_2 \backslash \{i_1\}$. If $J_2 = \varnothing$, then we are done. Otherwise, continuing this way, after a finite number of steps, we have $N_i(t) > 0$ for $t > 0$ and $i \in \mathbb{N}$.

Next, we prove that for $i \in \mathbb{N}_n$, $P_i^J(t) > 0$ and $P_i^A(t) > 0$ for $t > 0$. Since $\sum_{i \in \mathbb{N}_n} (P_i^A(0) + \sigma_i P_i^J(0)) > 0$, there exists $i_2 \in \mathbb{N}_n$ such that $P_{i_2}^A(0) + \sigma_{i_2} P_{i_2}^J(0) > 0$. First, we assume that $P_{i_2}^A(0) > 0$. By noting

$$\dot{P}_i^A(t) = \left[-d_i^A - \sum_{j \in \mathbb{N}_n} m_{ji}^A \right] P_i^A(t) + \left[\alpha_i P_i^J(t) + \sum_{j \in \mathbb{N}_n} m_{ij}^A P_j^A(t) \right], \tag{7}$$

which is similar to (5), we can use similar arguments as those of showing $N_i(t) > 0$ for $t > 0$ and $i \in \mathbb{N}_n$ to obtain $P_i^A(t) > 0$ for $t > 0$ and $i \in \mathbb{N}_n$. Then, from

$$\dot{P}_i^J(t) \geq -\left[d_i^J + \alpha_i + \sum_{j \in \mathbb{N}_n} m_{ji}^J \right] P_i^J(t) + e_i f_i\left(N_i(t)\right) P_i^A(t), \tag{8}$$

we see that $P_i^J(t) > 0$ for $t > 0$ and $i \in \mathbb{N}_n$. Now, assume that $\sigma_{i_2} P_{i_2}^J(0) > 0$, which implies that $P_{i_2}^J(0) > 0$. Then, from the second equation of (1), we get $P_{i_2}^J(t) > 0$ for $t > 0$. This, combined with the third equation of (1), yields $P_{i_2}^A(t) > 0$ for $t > 0$. Then as before, we can show that $P_i^A(t) > 0$ and $P_i^J(t) > 0$ for $t > 0$ and $i \in \mathbb{N}_n$.

Finally, we show the boundedness of solutions. On the one hand, let $N(t) = \sum_{i \in \mathbb{N}_n} N_i(t)$. Then, by the Cauchy–Schwartz inequality, we have

$$
\begin{aligned}
\dot{\mathbf{N}}(t) &\leq \sum_{i \in \mathbb{N}_n} \left(r_i - d_i^N \right) N_i(t) - \sum_{i \in \mathbb{N}_n} \frac{r_i}{K_i} N_i^2(t) \\
&\leq \max_{i \in \mathbb{N}_n} \{ r_i - d_i^N \} \mathbf{N}(t) - \min_{i \in \mathbb{N}_n} \left\{ \frac{r_i}{K_i} \right\} \sum_{i \in \mathbb{N}_n} N_i^2(t) \qquad (9) \\
&\leq \max_{i \in \mathbb{N}_n} \{ r_i - d_i^N \} \mathbf{N}(t) - \min_{i \in \mathbb{N}_n} \left\{ \frac{r_i}{K_i} \right\} \frac{\mathbf{N}^2(t)}{n}.
\end{aligned}
$$

It follows that $\limsup_{t \to \infty} \mathbf{N}(t) \leq n \max_{i \in \mathbb{N}_n} \{ r_i - d_i^N \} / \min_{i \in \mathbb{N}_n} \{ r_i / K_i \}$. On the other hand, let $\mathbf{G}(t) = \sum_{i \in \mathbb{N}_n} (e_i N_i(t) + P_i^J(t) + P_i^A(t))$. Then,

$$
\begin{aligned}
\dot{G}(t) &= \sum_{i \in \mathbb{N}_n} \left[e_i r_i N_i(t) \left(1 - \frac{N_i(t)}{K_i} \right) - e_i d_i^N N_i(t) + e_i \sum_{j \in \mathbb{N}_n} m_{ij}^N N_j(t) - e_i \sum_{j \in \mathbb{N}_n} m_{ji}^N N_i(t) - d_i^J P_i^J(t) - d_i^A P_i^A(t) \right] \\
&\leq \sum_{i \in \mathbb{N}_n} \left[2 e_i r_i N_i(t) + e_i \max_{j \in \mathbb{N}_n} \{ m_{ij}^N \} N(t) \right] - \sum_{i \in \mathbb{N}_n} \left[e_i r_i N_i(t) + d_i^J P_i^J(t) + d_i^A P_i^A(t) \right] \qquad (10) \\
&\leq \left(\max_{i \in \mathbb{N}_n} \{ 2 e_i r_i \} + \sum_{i \in \mathbb{N}_n} \left(e_i \max_{j \in \mathbb{N}_n} \{ m_{ij}^N \} \right) \right) \mathbf{N}(t) - \min_{i \in \mathbb{N}_n} \{ e_i, d_i^J, d_i^A \} \mathbf{G}(t).
\end{aligned}
$$

It is easy to see from this and $\limsup_{t \to \infty} \mathbf{N}(t) \leq n \max_{i \in \mathbb{N}_n} \{ r_i - d_i^N \} / \min_{i \in \mathbb{N}_n} \{ r_i / K_i \}$ that

$$
\begin{aligned}
\limsup_{t \to \infty} \mathbf{G}(t) &\leq \frac{\max_{i \in \mathbb{N}_n} \{ 2 e_i r_i \} + \sum_{i \in \mathbb{N}_n} \left(e_i \max_{j \in \mathbb{N}_n} \{ m_{ij}^N \} \right)}{\min_{i \in \mathbb{N}_n} \{ e_i, d_i^J, d_i^A \}} \\
&\quad \times \frac{n \max_{i \in \mathbb{N}_n} \{ r_i - d_i^N \}}{\min_{i \in \mathbb{N}_n} \{ r_i / K_i \}}.
\end{aligned}
$$

(11)

This completes the proof.

To show the existence of predator-free equilibria (PFE), we let $P_i^J = P_i^A = 0, i \in \mathbb{N}_n$ in equation (1) to get

$$
\begin{aligned}
\dot{N}_i &= r_i N_i \left(1 - \frac{N_i}{K_i} \right) - d_i^N N_i + \sum_{j \in \mathbb{N}_n} m_{ij}^N N_j \\
&\quad - \sum_{j \in \mathbb{N}_n} m_{ji}^N N_i, \quad \sum_{i \in \mathbb{N}_n} N_i(0) > 0.
\end{aligned}
$$

(12)

In order to obtain a positive equilibrium for system (12), we assume that

$$
s \left(\mathrm{diag} \left(r_i - d_i^N \right) + \mathbf{M}^N \right) > 0, \qquad (13)
$$

where $s(\cdot)$ represents the stability modulus of an $n \times n$ matrix and is defined by $s(\mathbf{H}) := \max \{ \mathrm{Re} \lambda \mid \lambda$ is an eigenvalue of $\mathbf{H} \}$ for an $n \times n$ matrix $\mathbf{H}$. From [19, 20, 22], we have the following two lemmas. $\qquad \square$

Lemma 1. *Under assumption (13), system (12) admits a unique equilibrium* $\mathbf{N}^0 = (N_1^0, N_2^0, \ldots, N_n^0)^T$, *which is positive and globally asymptotically stable in* $\mathbb{R}_+^n \backslash \{0\}$.

Lemma 2. *Under assumption (13), system (1) admits a unique PFE* $P^0 = (N^0, 0, 0)^T$, *where* $\mathbf{N}^0 = (N_1^0, N_2^0, \ldots, N_n^0)^T \in \mathbb{R}_+^n$ *is the unique equilibrium of (12) and* $\mathbf{0} = \underbrace{(0, \ldots, 0)^T}_{n} \in \mathbb{R}_+^n$.

3. Threshold Dynamics

3.1. The Net Reproduction Number. In this section, we first give definition of the net reproduction number $\mathcal{R}_0$ for the general predator-prey dispersal model (1), which is similar to the basic reproduction number for epidemic system; for reference, we refer to [17, 23].

Let $\mathbf{P}^0$ be the PFE of (1). From [17], we have

$$
\mathbf{F} = \begin{pmatrix} \mathbf{F}_{11} & \mathbf{F}_{12} \\ \mathbf{0} & \mathbf{0} \end{pmatrix} = \begin{pmatrix} \mathrm{diag} \left(e_i \sigma_i f_i \left(N_i^0 \right) \right) & \mathrm{diag} \left(e_i f_i \left(N_i^0 \right) \right) \\ \mathbf{0} & \mathbf{0} \end{pmatrix},
$$

(14)

$$
\mathbf{V} = \begin{pmatrix} \mathbf{V}_{11} & \mathbf{0} \\ -\mathbf{V}_{21} & \mathbf{V}_{22} \end{pmatrix},
$$

(15)

where

$$
\begin{aligned}
\mathbf{V}_{11} &= \mathrm{diag} \left(d_i^J + \alpha_i + \sum_{j \in \mathbb{N}_n} m_{ji}^J \right) - \mathbf{M}^J, \\
\mathbf{V}_{21} &= \mathrm{diag} (\alpha_i), \\
\mathbf{V}_{22} &= \mathrm{diag} \left(d_i^A + \sum_{j \in \mathbb{N}_n} m_{ji}^A \right) - \mathbf{M}^A.
\end{aligned}
$$

(16)

Note that $\mathbf{V}_{11}$ and $\mathbf{V}_{22}$ are both irreducible nonsingular M-matrices with positive column sums and hence $\mathbf{V}_{11}^{-1} > 0$ and $\mathbf{V}_{22}^{-1} > 0$. Following the procedure introduced in [17], the

net reproduction number $\mathscr{R}_0$ of equation (1) is given by $\mathscr{R}_0 = \rho(\mathbf{F}\mathbf{V}^{-1})$, where ρ represents the spectral radius of the matrix. Let $\mathbf{M}_1 = \mathbf{F} - \mathbf{V}$. Then, by [17], there hold two equivalences:

$$\mathscr{R}_0 > 1 \Longleftrightarrow s(\mathbf{M}_1) > 0,$$
$$\mathscr{R}_0 < 1 \Longleftrightarrow s(\mathbf{M}_1) < 0. \tag{17}$$

As

$$\mathbf{F}\mathbf{V}^{-1} = \begin{pmatrix} \mathbf{F}_{11} & \mathbf{F}_{12} \\ \mathbf{0} & \mathbf{0} \end{pmatrix} \begin{pmatrix} \mathbf{V}_{11}^{-1} & \mathbf{0} \\ \mathbf{V}_{22}^{-1}\mathbf{V}_{21}\mathbf{V}_{11}^{-1} & \mathbf{V}_{22}^{-1} \end{pmatrix}, \tag{18}$$

we have

$$\mathscr{R}_0 = \rho\left(\mathbf{F}_{11}\mathbf{V}_{11}^{-1} + \mathbf{F}_{12}\mathbf{V}_{22}^{-1}\mathbf{V}_{21}\mathbf{V}_{11}^{-1}\right). \tag{19}$$

In equation (19), $\mathbf{F}_{11}\mathbf{V}_{11}^{-1}$ accounts for the contribution of juvenile predators to the adult predators, while $\mathbf{F}_{12}\mathbf{V}_{22}^{-1}\mathbf{V}_{21}\mathbf{V}_{11}^{-1}$ accounts for the contribution by adult predators themselves. Diffusion rates of preys influence the

predator population capture rate, and diffusion rates of predators affect their consumption.

The net reproduction number gives an important threshold of the n-patch diffusion predator-prey system.

Theorem 2. *Consider model (1). Suppose (13) holds. If $\mathscr{R}_0 < 1$, then the PFE is locally asymptotically stable, and if $\mathscr{R}_0 > 1$, then the PFE is unstable. Moreover, if $\mathscr{R}_0 < 1$, then the PFE is globally attractive for solutions with initial conditions (2).*

Proof of Theorem 2. It follows from ([10], Theorem 2) that the PFE is locally asymptotically stable if $\mathscr{R}_0 < 1$ and unstable if $\mathscr{R}_0 > 1$.

Now, we prove the global attractivity of the PFE as follows.

Let $(\mathbf{N}(t), \mathbf{P}^J(t), P^A(t))$ be an arbitrary solution of (1). We first show that $\lim_{t\to\infty} P^J(t) = \lim_{t\to\infty} P^A(t) = 0$.

Since $s(\mathbf{M}_1) < 0$, there exists an $\varepsilon > 0$ such that $s(\mathbf{M}_1 + \mathbf{M}_2(\varepsilon)) < 0$, where

$$\mathbf{M}_2(\varepsilon) = \begin{pmatrix} \operatorname{diag}\left(e_i\sigma_i\left[f_i\left(N_i^0 + \varepsilon\right) - f_i\left(N_i^0\right)\right]\right) & \operatorname{diag}\left(e_i\left[f_i\left(N_i^0 + \varepsilon\right) - f_i\left(N_i^0\right)\right]\right) \\ \mathbf{0} & \mathbf{0} \end{pmatrix}. \tag{20}$$

Note that $\mathbf{N}(t)$ satisfies

$$\dot{N}_i(t) \le r_i N_i(t)\left(1 - \frac{N_i(t)}{K_i}\right) - d_i^N N_i(t) + \sum_{j\in\mathbb{N}_n} m_{ij}^N N_j(t) - \sum_{j\in\mathbb{N}_n} m_{ji}^N N(t), \tag{21}$$

where $i \in \mathbb{N}_n$. By Lemma 1 and Comparison Theorem [24, 25], we have $\limsup_{t\to\infty}\mathbf{N}(t) \le \mathbf{N}^0$. It follows that there exists $t_0 \ge 0$ such that $\mathbf{N}(t) \le \mathbf{N}^0 + \underbrace{(\varepsilon, \ldots, \varepsilon_n)}$ for $t \ge t_0$. Then, for $t \ge t_0$, $(\mathbf{P}^J(t), \mathbf{P}^A(t))$ satisfies

$$\begin{pmatrix} \dot{\mathbf{P}}^J(t) \\ \dot{\mathbf{P}}^A(t) \end{pmatrix} \le (\mathbf{M}_1 + \mathbf{M}_2(\varepsilon))\begin{pmatrix} \mathbf{P}^J(t) \\ \mathbf{P}^A(t) \end{pmatrix}. \tag{22}$$

Since $s(\mathbf{M}_1 + \mathbf{M}_2(\varepsilon)) < 0$, we obtain $\lim_{t\to\infty}\mathbf{P}^J(t) = \lim_{t\to\infty}\mathbf{P}^A(t) = 0$ by applying Comparison Theorem [24, 25].

Next, we prove that $\lim_{t\to\infty}\mathbf{N}(t) = \mathbf{N}^0$. It suffices to show $\liminf_{t\to\infty}\mathbf{N}(t) \ge \mathbf{N}^0$ as $\limsup_{t\to\infty}\mathbf{N}(t) \le \mathbf{N}^0$. Since g_i is continuous and N_i is bounded, $i \in \mathbb{N}_n$, there exists $\kappa > 0$ such that $g_i(N_i(t)) \le \kappa$ for $t \ge 0$. By equation (13), there exists $\eta_0 > 0$ such that $s(\operatorname{diag}(r_i - d_i^N - (1 + \sigma_i)\kappa\eta) + \mathbf{M}^N) > 0$ for $\eta \in (0, \eta_0)$. For any $\eta \in (0, \eta_0)$, there exists $t_1 \ge 0$ such that $0 \le P_i^J(t), P_i^A(t) \le \eta$ for $t \ge t_1$. Then,

$$\dot{N}_i(t) \ge r_i N_i(t)\left(1 - \frac{N_i(t)}{K_i}\right) - \left(d_i^N + (1 + \sigma_i)\eta\kappa\right)N_i(t) + \sum_{j\in\mathbb{N}_n} m_{ij}^N N_j(t) - \sum_{j\in\mathbb{N}_n} m_{ji}^N N_i(t) \tag{23}$$

for $t \ge t_1$ and $i \in \mathbb{N}_n$. By Lemma 1 and Comparison Theorem [24, 25], we know that $\liminf_{t\to\infty}\mathbf{N}(t) \ge \mathbf{N}^0(\eta)$, where $\mathbf{N}^0(\eta)$ is the positive equilibrium of (12) with d_i being replaced by $d_i^N + (1 + \sigma_i)\eta\kappa$, $i \in \mathbb{N}_n$. It is easy to see that $\lim_{\eta\to0}\mathbf{N}^0(\eta) = \mathbf{N}^0$. Therefore, we have $\liminf_{t\to\infty}\mathbf{N}(t) \ge \mathbf{N}^0$ as required.

To summarize, we have shown that $\lim_{t\to\infty}(N(t), \mathbf{P}^J(t), \mathbf{P}^A(t)) = (N^0, 0, 0)$. This completes the proof.

Next, we consider the effect of dispersal on $\mathscr{R}_0$ and provide lower and upper bounds of $\mathscr{R}_0$. In the rest of this paper, we let $a_i = d_i^J + \alpha_i$ for $i \in \mathbb{N}_n$. When there is no diffusion of prey, that is, $\mathbf{M}^N = [\mathbf{0}]_{n\times n}$, we have $\mathbf{N}^0 = (N_1^0, N_2^0, \ldots, N_n^0)^{\mathrm{T}}$ with $N_i^0 = K(r_i - d_i^N)/r_i$ for $i \in \mathbb{N}_n$ and the net reproduction number in patch i in isolation is given by

$$\mathscr{R}_0^{(i)} = \frac{e_i\sigma_i f_i\left(K_i(r_i - d_i^N)/r_i\right)}{a_i} + \frac{e_i\alpha_i f_i\left(K_i(r_i - d_i^N)/r_i\right)}{d_i^A a_i}. \tag{24}$$

We define a modified reproduction number in patch i:

$$\widetilde{\mathscr{R}}_0^{(i)} = \frac{e_i\sigma_i f_i\left(K_i(r_i - d_i^N)/r_i\right)}{a_i + \sum_{j=1}^n m_{ji}^J} + \frac{e_i\alpha_i f_i\left(K_i(r_i - d_i^N)/r_i\right)}{\left(d_i^A + \sum_{j=1}^n m_{ji}^A\right)\left(a_i + \sum_{j=1}^n m_{ji}^J\right)}. \tag{25}$$

Clearly, $\widetilde{\mathscr{R}}_0^{(i)} < \mathscr{R}_0^{(i)}$. Then, we can obtain the following result on the bounds for the net reproduction number for system (1), in terms of the numbers defined in equations (24) and (25) for each patch. □

Theorem 3. *For system (1), if* $\mathbf{M}^N = [\mathbf{0}]_{n \times n}$, *then*

$$\mathscr{R}_0 \geq \max_{1 \leq i \leq n} \widetilde{\mathscr{R}}_0^{(i)}. \tag{26}$$

Moreover, if $a_i = a$, $e_i = e$, $\alpha_i = \alpha$, $\sigma_i = \sigma$, $f_i = f$, $d_i^N = d_1$, $d_i^A = d_2$, *and* $r_i = r$ *for* $i \in \mathbb{N}_n$, *then*

$$\max\left(\max_{1 \leq i \leq n} \widetilde{\mathscr{R}}_0^{(i)}, \min_{1 \leq i \leq n} \mathscr{R}_0^{(i)}\right) \leq \mathscr{R}_0 \leq \max_{1 \leq i \leq n} \mathscr{R}_0^{(i)}. \tag{27}$$

Proof of Theorem 3. From [18, 26], let $\mathbf{V}_{jj}[1']$ denote the matrix obtained by deleting the first row and the first column of $\mathbf{V}_{jj}$ ($j = 1, 2$); $\mathbf{Y} = [y_{ij}]$ and $\mathbf{Z} = [z_{ij}]$ denote $\mathbf{V}_{11}^{-1}$ and $\mathbf{V}_{22}^{-1}$, respectively.   Let $\mathbf{W} = [w_{ij}] = \mathbf{G} + \mathbf{H}$,   where $\mathbf{G} = [g_{ij}] = \mathbf{F}_{11}\mathbf{Y}$ and $\mathbf{H} = [h_{ij}] = \mathbf{F}_{12}\mathbf{Z}\mathbf{V}_{21}\mathbf{Y}$. It follows that $y_{ij} > 0$ and $z_{ij} > 0$ for $i, j \in \mathbb{N}_n$. By [26], we have

$$\mathscr{R}_0 = \rho(\mathbf{W}) \geq w_{ii} = g_{ii} + h_{ii}, \quad i \in \mathbb{N}_n. \tag{28}$$

Here,

$$g_{11} = e_1 \sigma_1 f_1 \left(\frac{K_1 (r_1 - d_1^N)}{r_1}\right)$$

$$y_{11} = e_1 \sigma_1 f_1 \left(\frac{K_1 (r_1 - d_1^N)}{r_1}\right) \frac{\det \mathbf{V}_{11}[1']}{\det \mathbf{V}_{11}}. \tag{29}$$

By virtue of Fisher's inequality [27],

$$\det \mathbf{V}_{11} \leq \left(a_1 + \sum_{j=1}^{n} m_{j1}^J\right) \det \mathbf{V}_{11}[1']. \tag{30}$$

Then,

$$g_{11} \geq \frac{e_1 \sigma_1 f_1 ((K_1 (r_1 - d_1^N)/r_1))}{a_1 + \sum_{j=1}^{n} m_{j1}^J}. \tag{31}$$

Similarly,

$$h_{11} = e_1 \alpha_1 f_1 \left(\frac{K_1 (r_1 - d_1^N)}{r_1}\right) z_{11} y_{11}$$

$$+ \sum_{k=2}^{n} e_1 f_1 \left(\frac{K_1 (r_1 - d_1^N)}{r_1}\right) \alpha_k z_{1k} y_{k1}. \tag{32}$$

Thus, we have

$$h_{11} \geq e_1 \alpha_1 f_1 \left(\frac{K_1 (r_1 - d_1^N)}{r_1}\right) z_{11} y_{11}$$

$$= e_1 \alpha_1 f_1 \left(\frac{K_1 (r_1 - d_1^N)}{r_1}\right) \frac{\det \mathbf{V}_{22}[1']}{\det \mathbf{V}_{22}} \frac{\det \mathbf{V}_{11}[1']}{\det \mathbf{V}_{11}}. \tag{33}$$

Again, by Fisher's inequality,

$$h_{11} \geq \left(\frac{e_1 \alpha_1 f_1 (K_1 (r_1 - d_1^N)/r_1)}{\left(d_1^A + \sum_{j=1}^{n} m_{j1}^A\right)\left(a_1 + \sum_{j=1}^{n} m_{j1}^J\right)}\right). \tag{34}$$

Then, from these conclusions, we know

$$\mathscr{R}_0 \geq \widetilde{\mathscr{R}}_0^{(1)}. \tag{35}$$

Similarly, it can be shown that

$$\mathscr{R}_0 \geq \widetilde{\mathscr{R}}_0^{(i)}, \quad i = 2, 3, \ldots, n, \tag{36}$$

and (26) is proved.

If we let $a_i = a$, $e_i = e$, $\alpha_i = \alpha$, $\sigma_i = \sigma$, $f_i = f$, $d_i^N = d_1$, $d_i^A = d_2$, and $r_i = r$ for $i \in \mathbb{N}_n$, then $w_{ij} = e\sigma f (K_i (r - d_1)/r) y_{ij} + e\alpha f (K_i (r - d_1)/r) \sum_{k=1}^{n} z_{ik} y_{ik}$ for $i, j \in \mathbb{N}_n$. Without loss of generality, assume that $0 < K_1 \leq K_2 \leq \ldots \leq K_n$. From the fact that the sum of each column of the matrix $\mathbf{V}_{11}$ is equal to $a > 0$ and the sum of each column of the matrix $\mathbf{V}_{22}$ is $d_2 > 0$, we see that $\sum_{i=1}^{n} y_{ij} = (1/a)$ and $\sum_{i=1}^{n} z_{ij} = (1/d_2)$ for $j \in \mathbb{N}_n$. Thus, for the matrix $\mathbf{W}$, the sum of column j is

$$\sum_{i=1}^{n} w_{ij} = \sum_{i=1}^{n} e\sigma f\left(\frac{K_i (r - d_1)}{r}\right) y_{ij} + \sum_{i=1}^{n} e\alpha f\left(\frac{K_i (r - d_1)}{r}\right) \sum_{k=1}^{n} z_{ik} y_{ik}$$

$$\leq e\sigma f\left(\frac{K_n (r - d_1)}{r}\right) \sum_{i=1}^{n} y_{ij} + e\alpha f\left(\frac{K_n (r - d_1)}{r}\right) \sum_{i=1}^{n} \sum_{k=1}^{n} z_{ik} y_{ik}$$

$$= e\sigma f\left(\frac{K_n (r - d_1)}{r}\right) \sum_{i=1}^{n} y_{ij} + e\alpha f\left(\frac{K_n (r - d_1)}{r}\right) \sum_{k=1}^{n} \left(\sum_{i=1}^{n} z_{ik}\right) y_{ik} = \frac{e\sigma f (K_n (r - d_1)/r)}{a} + \frac{e\alpha f (K_n (r - d_1)/r)}{d_2 a}$$

$$= \mathscr{R}_0^{(n)}. \tag{37}$$

Similarly, we can prove $\sum_{i=1}^{n} w_{ij} \geq (e\sigma f (K_1 (r - d_1)/r)/a) + (e \; \alpha f (K_1 (r - d_1)/r)/d_2 a) = \mathscr{R}_0^{(1)}$. From [26], we obtain the following inequalities:

$$\min_{1 \leq i \leq n} \mathscr{R}_0^{(i)} \leq \mathscr{R}_0 \leq \max_{1 \leq i \leq n} \mathscr{R}_0^{(i)}. \tag{38}$$

Combining this with (26), we get (27). This completes the proof. $\qquad\square$

3.2. The Model with Two Patches.

In this section, we consider a special case of equation (1) with $n = 2$ and assume that $f_i (N_i) = b_i N_i$, $b_i > 0$ for $i = 1, 2$, namely,

$$
\begin{cases}
\dot{N}_1 = r_1 N_1 \left(1 - \dfrac{N_1}{K_1}\right) - b_1 N_1 \left(P_1^A + \sigma_1 P_1^J\right) - d_1^N N_1 + m_{12}^N N_2 - m_{21}^N N_1, \\[4mm]
\dot{P}_1^J = e_1 b_1 N_1 P_1^A + e_1 b_1 \sigma_1 N_1 P_1^J - \left(d_1^J + \alpha_1\right) P_1^J + m_{12}^J P_2^J - m_{21}^J P_1^J, \\[4mm]
\dot{P}_1^A = \alpha_1 P_1^J - d_1^A P_1^A + m_{12}^A P_2^A - m_{21}^A P_1^A, \\[4mm]
\dot{N}_2 = r_2 N_2 \left(1 - \dfrac{N_2}{K_2}\right) - b_2 N_2 \left(P_2^A + \sigma_2 P_2^J\right) - d_2^N N_2 + m_{21}^N N_1 - m_{12}^N N_2, \\[4mm]
\dot{P}_2^J = e_2 b_2 N_2 P_2^A + e_2 b_2 \sigma_2 N_2 P_2^J - \left(d_2^J + \alpha_2\right) P_2^J + m_{21}^J P_1^J - m_{12}^J P_2^J, \\[4mm]
\dot{P}_2^A = \alpha_2 P_2^J - d_2^A P_2^A + m_{21}^A P_1^A - m_{12}^A P_2^A.
\end{cases}
\tag{39}
$$

The PFE of equation (39) is $(N_1^0, N_2^0, 0, 0, 0, 0)^{\mathrm{T}}$, where $(N_1^0, N_2^0)^{\mathrm{T}}$ satisfies

$$
\begin{cases}
r_1 N_1 \left(1 - \dfrac{N_1}{K_1}\right) - d_1^N N_1 + m_{12}^N N_2 - m_{21}^N N_1 = 0, \\[4mm]
r_2 N_2 \left(1 - \dfrac{N_2}{K_2}\right) - d_2^N N_2 + m_{21}^N N_1 - m_{12}^N N_2 = 0.
\end{cases}
\tag{40}
$$

Let

$$
\mathbf{N}^0 = \left(N_1^0, N_2^0\right)^{\mathrm{T}}.
\tag{41}
$$

Note that

$$
\begin{aligned}
\mathbf{F}_{11} &= \operatorname{diag}\left(e_1 \sigma_1 b_1 N_1^0, e_2 \sigma_2 b_2 N_2^0\right), \\
\mathbf{F}_{12} &= \operatorname{diag}\left(e_1 b_1 N_1^0, e_2 b_2 N_2^0\right),
\end{aligned}
\tag{42}
$$

$$
\mathbf{V}_{21} = \operatorname{diag}\left(\alpha_1, \alpha_2\right),
\tag{43}
$$

$$
\begin{aligned}
\mathbf{V}_{11} &= \begin{pmatrix} a_1 + m_{21}^J & -m_{12}^J \\ -m_{21}^J & a_2 + m_{12}^J \end{pmatrix}, \\
\mathbf{V}_{22} &= \begin{pmatrix} d_1^A + m_{21}^A & -m_{12}^A \\ -m_{21}^A & d_2^A + m_{12}^A \end{pmatrix}.
\end{aligned}
\tag{44}
$$

Recall that $a_i = d_i^J + \alpha_i$ for $i = 1, 2$. Hence, we have

$$
\mathscr{R}_0 = \rho\left(\mathbf{F}_{11} \mathbf{V}_{11}^{-1} + \mathbf{F}_{12} \mathbf{V}_{22}^{-1} \mathbf{V}_{21} \mathbf{V}_{11}^{-1}\right) = \rho\left(\mathbf{W}\right),
\tag{45}
$$

where

$$
\mathbf{W} = \begin{pmatrix} w_{11} & w_{12} \\ w_{21} & w_{22} \end{pmatrix},
\tag{46}
$$

with

$$
\begin{aligned}
w_{11} &= \frac{e_1 \sigma_1 b_1 N_1^0 \left(a_2 + m_{12}^J\right)}{a_1 a_2 + a_1 m_{12}^J + a_2 m_{21}^J} + \frac{e_1 b_1 \alpha_1 N_1^0 \left(a_2 + m_{12}^J\right)\left(d_2^A + m_{12}^A\right) + e_1 b_1 \alpha_2 N_1^0 m_{21}^J m_{12}^A}{\left(a_1 a_2 + a_1 m_{12}^J + a_2 m_{21}^J\right)\left(d_1^A d_2^A + d_1^A m_{12}^A + d_2^A m_{21}^A\right)}, \\[3mm]
w_{12} &= \frac{e_1 \sigma_1 b_1 N_1^0 m_{12}^J}{a_1 a_2 + a_1 m_{12}^J + a_2 m_{21}^J} + \frac{e_1 b_1 \alpha_1 N_1^0 m_{12}^J \left(d_2^A + m_{12}^A\right) + e_1 b_1 \alpha_2 N_1^0 m_{12}^A \left(a_1 + m_{21}^J\right)}{\left(a_1 a_2 + a_1 m_{12}^J + a_2 m_{21}^J\right)\left(d_1^A d_2^A + d_1^A m_{12}^A + d_2^A m_{21}^A\right)}, \\[3mm]
w_{21} &= \frac{e_2 \sigma_2 b_2 N_2^0 m_{21}^J}{a_1 a_2 + a_1 m_{12}^J + a_2 m_{21}^J} + \frac{e_2 b_2 \alpha_1 N_2^0 m_{21}^A \left(a_2 + m_{12}^J\right) + e_2 b_2 \alpha_2 N_2^0 m_{21}^J \left(d_1^A + m_{21}^A\right)}{\left(a_1 a_2 + a_1 m_{12}^J + a_2 m_{21}^J\right)\left(d_1^A d_2^A + d_1^A m_{12}^A + d_2^A m_{21}^A\right)}, \\[3mm]
w_{22} &= \frac{e_2 \sigma_2 b_2 N_2^0 \left(a_1 + m_{21}^J\right)}{a_1 a_2 + a_1 m_{12}^J + a_2 m_{21}^J} + \frac{e_2 b_2 \alpha_1 N_2^0 m_{12}^J m_{21}^A + e_2 b_2 \alpha_2 N_2^0 \left(a_1 + m_{21}^J\right)\left(d_1^A + m_{21}^A\right)}{\left(a_1 a_2 + a_1 m_{12}^J + a_2 m_{21}^J\right)\left(d_1^A d_2^A + d_1^A m_{12}^A + d_2^A m_{21}^A\right)}.
\end{aligned}
\tag{47}
$$

It follows from equation (45) that

$$\mathscr{R}_0 = \frac{1}{2}\left(w_{11} + w_{22} + \sqrt{(w_{11} - w_{22})^2 + 4w_{12}w_{21}}\right). \quad (48)$$

Theorem 4. *If* $e_1 = e_2 = e$, $\sigma_1 = \sigma_2 = \sigma$, $a_1 = a_2 = a$, $b_1 = b_2 = b$, $\alpha_1 = \alpha_2 = \alpha$, $d_1^A = d_2^A = d$, $m_{ij}^I = m$, *and* $m_{ij}^A = km$, $i, j = 1, 2$, *where* k *is a positive constant, then* $\mathscr{R}_0$ *decreases as* m *increases.*

Proof of Theorem 4. From equation (46) and under the assumptions on parameters, we get

$$\mathbf{W} = \begin{pmatrix} w_{11} & w_{12} \\ w_{21} & w_{22} \end{pmatrix} = \begin{pmatrix} b_1 N_1^0 u & b_1 N_1^0 v \\ b_2 N_2^0 v & b_2 N_2^0 u \end{pmatrix}, \quad (49)$$

where

$$u = \frac{e\sigma(a+m)}{a(a+2m)} + \frac{e\alpha[2km^2 + (d+ka)m + ad]}{ad(a+2m)(d+2km)},$$

$$v = \frac{e\sigma m}{a(a+2m)} + \frac{e\alpha m(2km+d+ak)}{ad(a+2m)(d+2km)}. \quad (50)$$

By equation (48), $\mathscr{R}_0$ is the larger root of the following quadratic equation:

$$\lambda^2 - (b_1 N_1^0 + b_2 N_2^0)u\lambda + b_1 b_2 N_1^0 N_2^0(u^2 - v^2) = 0. \quad (51)$$

Note that

$$u + v = \frac{e(\sigma d + \alpha)}{ad},$$

$$u - v = \frac{e[\alpha + \sigma(d + 2km)]}{(a+2m)(d+2km)}, \quad (52)$$

$$u^2 - v^2 = \frac{e(\sigma d + \alpha)}{ad} \cdot \frac{e[\alpha + \sigma(d + 2km)]}{(a+2m)(d+2km)}. \quad (53)$$

It follows from $u + v = e(\sigma d + \alpha)/ad$ that $\partial u/\partial m = -\partial v/\partial m$. Taking partial derivatives with respect to m for equation (51) gives

$$\left(2\lambda - (b_1 N_1^0 + b_2 N_2^0)u\right)\frac{\partial\lambda}{\partial m} = \lambda(b_1 N_1^0 + b_2 N_2^0)\frac{\partial u}{\partial m} - b_1 b_2 N_1^0 N_2^0\frac{\partial(u^2 - v^2)}{\partial m} =$$

$$\left(\lambda(b_1 N_1^0 + b_2 N_2^0) - 2b_1 b_2 N_1^0 N_2^0\frac{e(\alpha + \sigma d)}{ad}\right)\frac{\partial u}{\partial m}. \quad (54)$$

Moreover, from the definition of u, we have

$$\frac{\partial u}{\partial m} = -\frac{e\sigma a}{a(a+2m)^2} - \frac{e\alpha}{ad} \cdot \frac{6kmad + 8k^2m^3 + ad^2 + 4km^2d + ka^2d + 4k^2m^2a}{(a+2m)^2(d+2km)^2} < 0. \quad (55)$$

Note that $2\lambda|_{\lambda=\mathscr{R}_0} > (b_1 N_1^0 + b_2 N_2^0)u$. Thus, to show $\partial\mathscr{R}_0/\partial m < 0$, that is to say, $\partial\lambda/\partial m|_{\lambda=\mathscr{R}_0} < 0$, it is sufficient to show for $\lambda = \mathscr{R}_0$,

$$(b_1 N_1^0 + b_2 N_2^0)\lambda - 2b_1 b_2 N_1^0 N_2^0 \cdot \frac{e(\sigma d + \alpha)}{ad} > 0. \quad (56)$$

We claim that $\lambda > (1/2)(b_1 N_1^0 + b_2 N_2^0)(u + v)$. Since

$$\lambda = \frac{1}{2}\left[(b_1 N_1^0 + b_2 N_2^0)u + \sqrt{(b_1 N_1^0 + b_2 N_2^0)^2 u^2 - 4b_1 b_2 N_1^0 N_2^0(u^2 - v^2)}\right], \quad (57)$$

it is equivalent to show that

$$(b_1 N_1^0 + b_2 N_2^0)^2 u^2 - 4b_1 b_2 N_1^0 N_2^0(u^2 - v^2) > (b_1 N_1^0 + b_2 N_2^0)^2 v^2, \quad (58)$$

or

$$(b_1 N_1^0 - b_2 N_2^0)^2(u^2 - v^2) > 0. \quad (59)$$

This is automatically true since $u > v > 0$. It follows from $\lambda > (1/2)(b_1 N_1^0 + b_2 N_2^0)(u + v)$ that

$$(b_1 N_1^0 + b_2 N_2^0)\lambda > \frac{1}{2}(b_1 N_1^0 + b_2 N_2^0)^2(u + v)$$

$$= \frac{1}{2}\frac{e(\sigma d + \alpha)}{ad}(b_1 N_1^0 + b_2 N_2^0)^2. \quad (60)$$

Thus, as required,

$$(b_1 N_1^0 + b_2 N_2^0)\lambda - 2b_1 b_2 N_1^0 N_2^0\frac{e(\sigma d + \alpha)}{ad}$$

$$> \frac{1}{2}\frac{e(\sigma d + \alpha)}{ad}(b_1 N_1^0 - b_2 N_2^0)^2 > 0. \quad (61)$$

This completes the proof. □

Remark 1. Under the condition of Theorem 4, the following result can be proved similarly; each entry of the matrix $\mathbf{W}$ decreases in terms of a or d, and it increases in terms of e, σ,

and α. Hence, the net reproduction number decreases in terms of a or d, and it increases in terms of e, σ, and α.

4. Persistence and Existence of Positive Equilibria

Under certain conditions, we use the techniques of persistence theory [28, 29] to show the uniform persistence of the predator population and the existence of at least one positive equilibrium (or coexistence equilibrium) when $\mathscr{R}_0 > 1$.

Theorem 5. *If equation (13) holds and $\mathscr{R}_0 > 1$, then system (1) is uniformly persistent, that is, there exists a positive constant ϵ such that every solution $\Phi_t(\mathbf{A}_0) \equiv (\mathbf{N}(t), \mathbf{P}^J(t), \mathbf{P}^A(t))$ with $\mathbf{A}_0 \in \mathbb{R}_+^n \times Int\mathbb{R}_+^{2n}$ satisfies*

$$\liminf_{t \longrightarrow \infty} \left(P_i^J(t), P_i^A(t) \right) \geq (\varepsilon, \varepsilon), \quad i \in \mathbb{N}_n. \tag{62}$$

Hence, it has at least one positive equilibrium.

Proof of Theorem 5. Let

$$\begin{aligned} \widetilde{X} &= \left\{ \mathbf{A}_0 \in \mathbb{R}_+^{3n} \,\middle|\, N_i(0) > 0, \quad i \in \mathbb{N}_n \right\}, \\ \widetilde{X}_0 &= \left\{ \mathbf{A}_0 \in \widetilde{X} \,\middle|\, P_i^J(0) > 0, \quad P_i^A(0) > 0, i \in \mathbb{N}_n \right\}, \end{aligned} \tag{63}$$

$$\partial \widetilde{X}_0 = \widetilde{X} \smallsetminus \widetilde{X}_0. \tag{64}$$

It then suffices to prove that (1) is uniformly persistent with respect to $(\widetilde{X}_0, \partial \widetilde{X}_0)$.

It is easy to see from Theorem 1 that $\widetilde{X}_0$ is positively invariant and system (1) is dissipative. Define

$$M_\partial := \left\{ \mathbf{A}_0 \in \partial \widetilde{X}_0 \,\middle|\, \Phi_t(\mathbf{A}_0) \in \partial \widetilde{X}_0, \quad t \geq 0 \right\}. \tag{65}$$

We claim that

$$M_\partial = \left\{ \mathbf{A}_0 \in \widetilde{X} \,\middle|\, P_i^J(0) = P_i^A(0) = 0, \quad i \in \mathbb{N}_n \right\}. \tag{66}$$

Suppose on the contrary that there exists $i_0 \in \mathbb{N}_n$ such that either $P_{i_0}^J(0) > 0$ or $P_{i_0}^A(0) > 0$, then similar arguments as those in the proof of Theorem 1 gives $P_i^J(t) > 0$ and $P_i^A(t) > 0$ for $t > 0$ and $i \in \mathbb{N}_n$. This contradicts with the definition of M_∂, and hence the claim has been proved.

Next, choose $\varepsilon > 0$ such that $s(\mathbf{M}_1 + \mathbf{M}_2(-\varepsilon)) > 0$. Then, choose $\eta > 0$ such that $\mathbf{N}^0(\eta) \geq \mathbf{N}^0 - \underbrace{(\varepsilon/2, \ldots, \varepsilon/2}_{n})$ and $s(\mathrm{diag}(r_i - d_i^N - (1 + \sigma_i)\kappa\eta) + \mathbf{M}^N) < 0$. Here, $\mathbf{M}_2(\varepsilon)$, $\mathbf{N}^0(\eta)$, and κ are those defined in the proof of Theorem 2. We claim that

$$\limsup_{t \longrightarrow \infty} \max_{i \in \mathbb{N}_n} \left\{ P_i^J(t), P_i^A(t) \right\} > \frac{\eta}{2}. \tag{67}$$

It is similar to the proof of Theorem 2. By way of contradiction, suppose there exists $\mathbf{A}_0$ such that $\limsup_{t \longrightarrow \infty} \max_{i \in \mathbb{N}_n} \left\{ P_i^J(t), P_i^A(t) \right\} \leq \eta/2$. Then, there exists $t_0 \geq 0$ such that

$$\max_{i \in \mathbb{N}_n} \left\{ P_i^J(t), P_i^A(t) \right\} \leq \eta, \quad \text{for } t \geq t_0. \tag{68}$$

Then, $\mathbf{N}(t)$ satisfies (23) for $t \geq t_0$. As $s(\mathrm{diag}(r_i - d_i^N - (1 + \sigma_i)\kappa\eta) + \mathbf{M}^N) < 0$, we have $\liminf_{t \longrightarrow \infty} \mathbf{N}(t) \geq \mathbf{N}^0(\eta)$ by Lemma 1 and Comparison Theorem. Thus,

there exists $t_1 \geq t_0$ such that $\mathbf{N}(t) \geq \mathbf{N}^0 - \underbrace{(\varepsilon, \ldots, \varepsilon_n)}$ for $t \geq t_1$. It follows that $(\mathbf{P}^J(t), \mathbf{P}^A(t))$ satisfies

$$\begin{pmatrix} \dot{\mathbf{P}}^J(t) \\ \dot{\mathbf{P}}^A(t) \end{pmatrix} \geq (\mathbf{M}_1 + \mathbf{M}_2(-\varepsilon)) \begin{pmatrix} \mathbf{P}^J(t) \\ \mathbf{P}^A(t) \end{pmatrix}, \tag{69}$$

for $t \geq t_1$. Consider the following auxiliary system:

$$\begin{pmatrix} \dot{\overline{\mathbf{P}}}^J(t) \\ \dot{\overline{\mathbf{P}}}^A(t) \end{pmatrix} = (\mathbf{M}_1 + \mathbf{M}_2(-\varepsilon)) \left(\overline{\mathbf{P}}^J(t) \overline{\mathbf{P}}^A(t) \right). \tag{70}$$

Since $s(\mathbf{M}_1 + \mathbf{M}_2(-\varepsilon)) > 0$, we know $\lambda := s(\mathbf{M}_1 + \mathbf{M}_2(-\varepsilon))$ is an eigenvalue of $\mathbf{M}_1 + \mathbf{M}_2(-\varepsilon)$ with a positive eigenvector, say $\overline{v}$. As $(\mathbf{P}^J(t_1), \mathbf{P}^A(t_1)) \gg (\mathbf{0}, \mathbf{0})$, there exists $\xi > 0$ such that $(\mathbf{P}^J(t_1), \mathbf{P}^A(t_1)) \geq \xi \overline{v}$. Again, by Comparison Theorem, we have $(\mathbf{P}^J(t), \mathbf{P}^A(t)) \geq \xi e^{\lambda(t-t_1)} \overline{v}$ for $t \geq t_1$. It follows that none of $P_i^J(t)$ and $P_i^A(t)$, $i \in \mathbb{N}_n$, is bounded, a contradiction to the boundedness of solutions (see Theorem 1).

Note that $\mathbf{N}^0$ is globally asymptotically stable in $\mathbb{R}_+^n \smallsetminus \{\mathbf{0}\}$ for equation (17). By the above claim, we know that both $\{\mathbf{0}, \mathbf{0}, \mathbf{0}\}$ and $\{\mathbf{P}^0\}$ are isolated invariant subsets in X, $W^s((\mathbf{0}, \mathbf{0}, \mathbf{0})) \cap \mathbf{A}_0 = \varnothing$, where $W^s((\mathbf{0}, \mathbf{0}, \mathbf{0}))$ is stable manifold of $((\mathbf{0}, \mathbf{0}, \mathbf{0}))$. Clearly, every orbit in M_∂ converges to either $(\mathbf{0}, \mathbf{0}, \mathbf{0})$ or $\mathbf{P}^0$, and $\{(\mathbf{0}, \mathbf{0}, \mathbf{0})$ and $\{\mathbf{P}^0\}$ are acyclic in M_∂. By ([30], Theorem 5 and Remark 1), we conclude that system (1) is uniformly persistent with respect to $(\widetilde{X}_0, \partial \widetilde{X}_0)$. By [31], system (1) has at least one equilibrium $(\mathbf{N}^*, \mathbf{P}^{J*}, \mathbf{P}^{A*}) \in \mathbf{A}_0$ with $\mathbf{P}^{J*} \gg 0$ and $\mathbf{P}^{A*} \gg 0$. We further claim that $N^* \neq 0$. Otherwise, if $\mathbf{N}^* = 0$, by summing up the equilibrium equations for $\mathbf{P}^J$, we get $\sum_{i \in \mathbb{N}_n} (d_i^J + \alpha_i) P_i^{J*} = 0$. Thus, $\mathbf{P}^{J*} = 0$, a contradiction. This completes the proof. $\qquad\square$

5. Simulations

In this section, numerical simulations are used to analyse the effects of the diffusion rates m_{ij}^N, m_{ij}^J, and m_{ij}^A on the net reproduction number $\mathscr{R}_0$ in a two-patch environment. Here, for having concrete observation, we let $m_{ij}^J = m_{ij}^A = m$ and $m_{ij}^N = m^N$, $i, j = 1, 2$.

First, we fix the parameters as follows:

$$\begin{aligned} r_1 &= 0.45, \\ b_1 &= 1, \\ \sigma_1 &= 0.01, \\ e_1 &= 0.3, \\ \alpha_1 &= 0.4, \\ d_1^J &= d_1^A = 0.3, \\ r_2 &= 0.5, \\ b_2 &= 1, \\ \sigma_2 &= 0.01, \\ e_2 &= 0.3, \\ \alpha_2 &= 0.4, \\ d_2^J &= d_2^A = 0.3. \end{aligned} \tag{71}$$

TABLE 1: The relationship of $\mathscr{R}_{01}$ with $\mathscr{R}_{02}$.

	$\mathscr{R}_{01} < 1$	$\mathscr{R}_{01} > 1$
$\mathscr{R}_{02} < 1$	Figure 2, $\mathscr{R}_{01} < 1$, $\mathscr{R}_{02} < 1$, $K_1 < K_2$ Figure 3, $\mathscr{R}_{01} < 1$, $\mathscr{R}_{02} < 1$, $K_1 > K_2$	Figure 4, $\mathscr{R}_{01} > 1$, $\mathscr{R}_{02} < 1$, $K_1 < K_2$ Figure 5, $\mathscr{R}_{01} > 1$, $\mathscr{R}_{02} < 1$, $K_1 > K_2$
$\mathscr{R}_{02} > 1$	Figure 6, $\mathscr{R}_{01} < 1$, $\mathscr{R}_{02} > 1$, $K_1 < K_2$ Figure 7, $\mathscr{R}_{01} < 1$, $\mathscr{R}_{02} > 1$, $K_1 > K_2$	Figure 8, $\mathscr{R}_{01} > 1$, $\mathscr{R}_{02} > 1$, $K_1 < K_2$ Figure 9, $\mathscr{R}_{01} > 1$, $\mathscr{R}_{02} > 1$, $K_1 > K_2$

We change the reproduction number of each isolated patch by changing the carrying capacity and the death rate of prey. Table 1 summarizes all the possibilities of the reproduction numbers in both patches.

When $m^N \longrightarrow 0$, from Figure 2, we find that the net reproduction number $\mathscr{R}_0$ increases and then decreases as m increases, and the final value of the threshold is greater than unity, but it is not difficult to observe that $\mathscr{R}_0$ is almost unchanged if the predator population hardly diffuses ($m \longrightarrow 0$). When the prey population and the predator population simultaneously diffuse, $\mathscr{R}_0$ increases and then decreases, and the final value of the threshold is less than unity. In Figure 3, if we reduce the carrying capacity and the death rate of the second isolated patch in Figure 2, that is, K_2 decreases from 3 to 2.45 and d_2^N decreases from 0.23 to 0.15, we draw the conclusion that $\mathscr{R}_0$ increases and the final value is greater than unity as m increases no matter how m^N changes, and $\mathscr{R}_0$ does not change if $m \longrightarrow 0$.

When we increase the production number of the first isolated patch and have $\mathscr{R}_{01} > 1$, $\mathscr{R}_{02} < 1$ in Figure 4, it is easy to find that the threshold $\mathscr{R}_0$ always decreases and is close to unity as m increases and $m^N \longrightarrow 0$. On the contrary, $\mathscr{R}_0$ first decreases and then increases and is greater than unity as m^N increases when $m \longrightarrow 0$. However, $\mathscr{R}_0$ always decreases and is less than unity as the prey population and the predator population simultaneously diffuse. In Figure 5, we increase the parameters including the carrying capacity and the death rate in the first isolated patch in Figure 4, that is, K_1 increases from 2.8 to 3.2 and d_1^N increases from 0.15 to 0.18. Under these circumstances, we find that the curve of $\mathscr{R}_0$ changes a lot. The curve of $\mathscr{R}_0$ is waved as m increases when $m^N \longrightarrow 0$ and is greater than unity when $m \longrightarrow 1$. $\mathscr{R}_0$ always decreases and tends to stabilize as m^N increases when $m \longrightarrow 0$. When the dispersal of the prey and the predator happens simultaneously, the curve of $\mathscr{R}_0$ is waved and is finally less than unity.

The situations of Figures 6 and 7 are similar to Figures 4 and 5 owing to the differences of the carrying capacities and the death rates of the preys. Contrary to circumstances of Figures 4 and 5, we know that the final values of $\mathscr{R}_0$ in Figures 6 and 7 are greater than unity as $m^N, m^J, m^A \longrightarrow 1$.

The situations of Figures 8 and 9 are very interesting; $\mathscr{R}_0$ increases and is greater than unity if $m^N \longrightarrow 0$ or $m^J, m^A \longrightarrow 0$, but $\mathscr{R}_0$ gradually decrease and is even less than unity when $m^N, m \longrightarrow 1$.

6. Discussion

In this paper, we studied a predator-prey model to describe the dynamics of predation with stage structure in the predator and dispersal in an n-patch environment. The
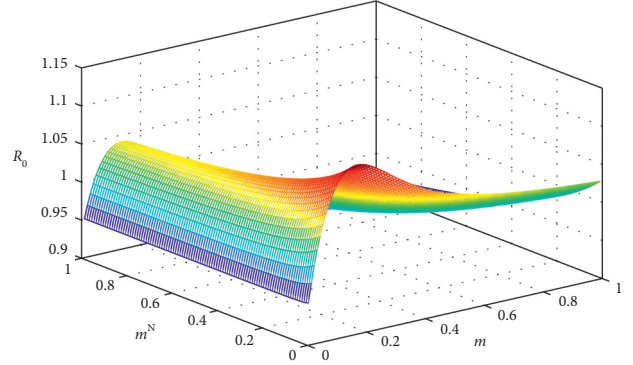

FIGURE 2: The effects of the diffusion rates on the net reproduction number $\mathscr{R}_0$ where $\mathscr{R}_{01} = 0.96$, $\mathscr{R}_{02} = 0.9257$, $K_1 = 2.8$, $K_2 = 3$, $d_1^N = 0.18$, $d_2^N = 0.23$, and m^N, $m^J = m^A = m$ vary from 0.01 to 1; all other parameters are given in equation (71).
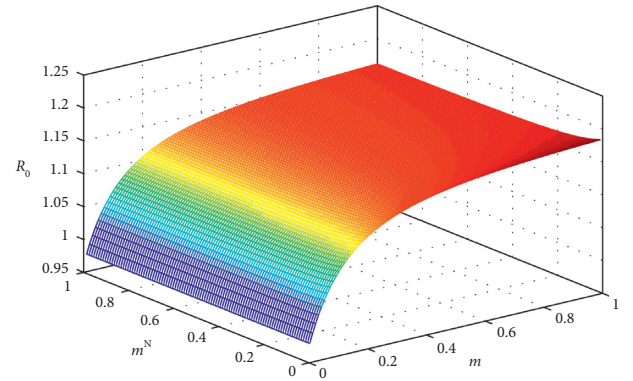

FIGURE 3: The effects of the diffusion rates on the net reproduction number $\mathscr{R}_0$ where $\mathscr{R}_{01} = 0.96$, $\mathscr{R}_{02} = 0.98$, $K_1 = 2.8$, $K_2 = 2.45$, $d_1^N = 0.18$, $d_2^N = 0.15$, and m^N, $m^J = m^A = m$ vary from 0.01 to 1; all other parameters are given in equation (71).

population dispersal among patches can be interpreted as migration or predation in which the predator has to seek prey by virtue of food reduction. In addition, predation function $f(N)$ includes three typical types having biological significance.

In Section 2, we first proposed the predator-prey model with diffusion in an n-patch environment. And we proved that the solutions of system (1) are all positive and ultimately bounded with nonnegative initial conditions (Theorem 1). In Section 3, we derived the net reproduction number and obtained the stability of the PFE through the relationship between $\rho(\mathbf{FV}^{-1})$ and 1 (Theorem 2). Moreover, we provided the upper bound and the lower bound of $\mathscr{R}_0$ (Theorem
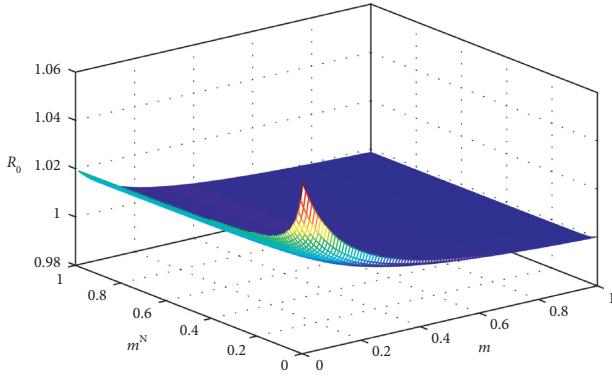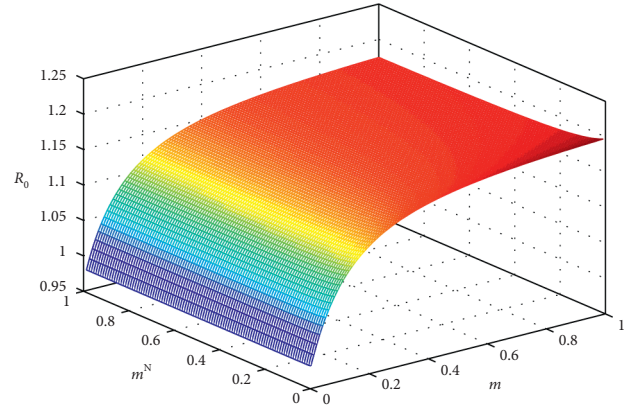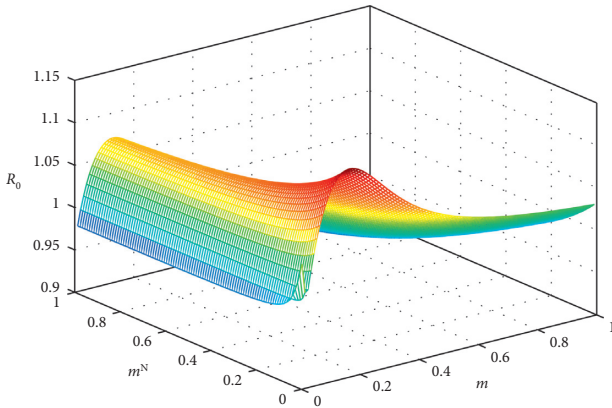
FIGURE 4: The effects of the diffusion rates on the net reproduction number $\mathcal{R}_0$ where $\mathcal{R}_{01} = 1.0667$, $\mathcal{R}_{02} = 0.9257$, $K_1 = 2.8$, $K_2 = 3$, $d_1^N = 0.15$, $d_2^N = 0.23$, and m^N, $m^J = m^A = m$ vary from 0.01 to 1; all other parameters are given in equation (71).
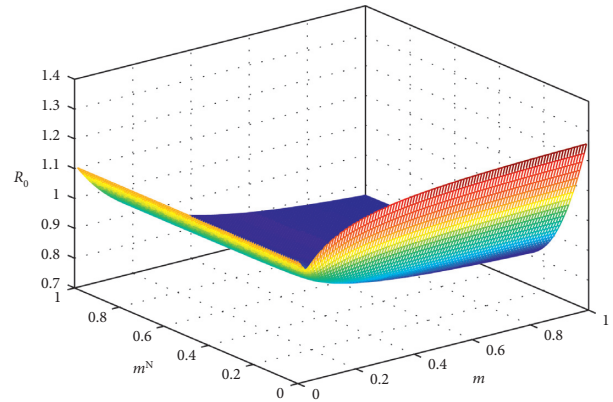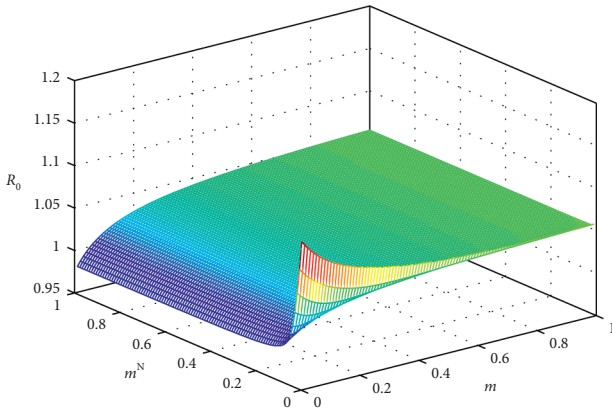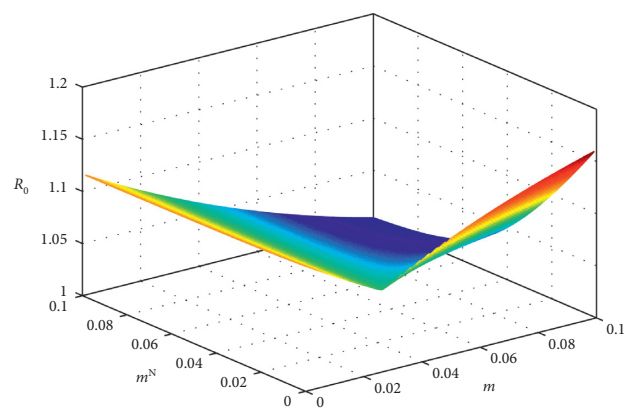

FIGURE 7: The effects of the diffusion rates on the net reproduction number $\mathcal{R}_0$ where $\mathcal{R}_{01} = 0.96$, $\mathcal{R}_{02} = 1.008$, $K_1 = 2.8$, $K_2 = 2.45$, $d_1^N = 0.18$, $d_2^N = 0.14$, and m^N, $m^J = m^A = m$ vary from 0.01 to 1; all other parameters are given in equation (71).

FIGURE 5: The effects of the diffusion rates on the net reproduction number $\mathcal{R}_0$ where $\mathcal{R}_{01} = 1.0971$, $\mathcal{R}_{02} = 0.9257$, $K_1 = 3.2$, $K_2 = 3$, $d_1^N = 0.18$, $d_2^N = 0.23$, and m^N, $m^J = m^A = m$ vary from 0.01 to 1; all other parameters are given in equation (71).

FIGURE 8: The effects of the diffusion rates on the net reproduction number $\mathcal{R}_0$ where $\mathcal{R}_{01} = 1.0286$, $\mathcal{R}_{02} = 1.12$, $K_1 = 3$, $K_2 = 3.5$, $d_1^N = 0.18$, $d_2^N = 0.22$, and m^N, $m^J = m^A = m$ vary from 0.01 to 1; all other parameters are given in equation (71).

FIGURE 6: The effects of the diffusion rates on the net reproduction number $\mathcal{R}_0$ where $\mathcal{R}_{01} = 0.96$, $\mathcal{R}_{02} = 1.1657$, $K_1 = 2.8$, $K_2 = 3$, $d_1^N = 0.18$, $d_2^N = 0.16$, and m^N, $m^J = m^A = m$ vary from 0.01 to 1; all other parameters are given in equation (71).

FIGURE 9: The effects of the diffusion rates on the net reproduction number $\mathcal{R}_0$ where $\mathcal{R}_{01} = 1.0286$, $\mathcal{R}_{02} = 1.12$, $K_1 = 3$, $K_2 = 2.8$, $d_1^N = 0.18$, $d_2^N = 0.15$, and m^N, $m^J = m^A = m$ vary from 0.01 to 1; all other parameters are given in equation (71).

3). For a two-patch model (39), the constant dispersal rate of prey and predator decreases $\mathcal{R}_0$ (Theorem 4). If $\rho(\mathbf{FV}^{-1}) > 1$ and the dispersal rate matrices of prey and predator are assumed to be irreducible, system (1) persists globally (i.e., in all patches) under some conditions in Section 4 (Theorem 5).

By numerical simulations, we found some interesting phenomena. From Figures 2 and 3, we first know that the net reproduction number $\mathcal{R}_0$ may be greater than unity even if $\mathcal{R}_{01} < 1$, $\mathcal{R}_{02} < 1$, and it may also be less than unity. This phenomenon is related with the carrying capacities K_1, K_2 and the death rates of prey d_1^N, d_2^N. In Figures 4–7, if one of the isolated patch thresholds is greater than unity and the other is less than unity, when the diffusion happens, the curve of $\mathcal{R}_0$ changes in a complex way. Here, we still obtain all kinds of figures through changing parameters K_1, K_2, d_1^N, d_2^N. It is not hard to think that the curve of $\mathcal{R}_0$ becomes complicated when we change the other parameters. In addition, because dispersal leads to extinction of predators, we believe that dispersal may be a bad thing, but sometimes dispersal may be a good thing if we want to eliminate some pests.

There are some interesting questions worthy of further study; for instance, the corresponding conclusions for the above two functional response types still remain open due to the analytical challenge, which remain as future questions.

Data Availability

The data used to support the findings of this study are available from the corresponding author upon request.

Conflicts of Interest

The authors declare that there are no conflicts of interest regarding the publication of this paper.

Acknowledgments

References

[1] D. E. Bowler and T. G. Benton, "Causes and consequences of animal dispersal strategies: relating individual behaviour to spatial dynamics," *Biological Reviews*, vol. 80, no. 2, pp. 205–225, 2005.

[2] R. S. Cantrell and C. Cosner, *Spatial Ecology via Reaction-Diffusion Equations*, John Wiley & Sons, Chichester, UK, 2003.

[3] M. L. Johnson and M. S. Gaines, "Evolution of dispersal: theoretical models and empirical tests using birds and mammals," *Annual Review of Ecology and Systematics*, vol. 21, no. 1, pp. 449–480, 1990.

[4] S. A. Levin, H. C. Muller-Landau, R. Nathan, and J. Chave, "The ecology and evolution of seed dispersal: a theoretical perspective," *Annual Review of Ecology, Evolution, and Systematics*, vol. 34, no. 1, pp. 575–604, 2003.

[5] Y. Lou and C.-H. Wu, "Global dynamics of a tritrophic model for two patches with cost of dispersal," *SIAM Journal on Applied Mathematics*, vol. 71, no. 5, pp. 1801–1820, 2011.

[6] L. Zhang and Z. Teng, "Permanence in a periodic predator-prey system with prey dispersal and predator density-independent," *Journal of Biological Systems*, vol. 14, no. 4, pp. 491–507, 2006.

[7] M. P. Hassell and R. M. May, "Aggregation of predators and insect parasites and its effect on stability," *The Journal of Animal Ecology*, vol. 43, no. 2, pp. 567–594, 1974.

[8] Y. Kang, S. K. Sasmal, S. Kumar Sasmal, and K. Messan, "A two-patch prey-predator model with predator dispersal driven by the predation strength," *Mathematical Biosciences and Engineering*, vol. 14, no. 4, pp. 843–880, 2017.

[9] S. A. Levin, "Dispersion and population interactions," *The American Naturalist*, vol. 108, no. 960, pp. 207–228, 1974.

[10] Y. Takeuchi, "Diffusion effect on stability of lotka-volterra model," *Bulletin of Mathematical Biology*, vol. 48, no. 5-6, pp. 585–601, 1986.

[11] Y. Kuang and Y. Takeuchi, "Predator-prey dynamics in models of prey dispersal in two-patch environments," *Mathematical Biosciences*, vol. 120, no. 1, pp. 77–98, 1994.

[12] P. Gramlich, S. J. Plitzko, L. Rudolf, B. Drossel, and T. Gross, "The influence of dispersal on a predator-prey system with two habitats," *Journal of Theoretical Biology*, vol. 398, pp. 150–161, 2016.

[13] L. Qiu and T. Mitsui, "Predator-prey dynamics with delay when prey dispersing inn-patch environment," *Japan Journal of Industrial and Applied Mathematics*, vol. 20, no. 1, pp. 37–49, 2003.

[14] I. Al-Darabsah, X. Tang, and Y. Yuan, "A prey-predator model with migrations and delays," *Discrete and Continuous Dynamical Systems - Series B*, vol. 21, no. 3, pp. 737–761, 2016.

[15] Y. Lu, D. Li, and S. Liu, "Modeling of hunting strategies of the predators in susceptible and infected prey," *Applied Mathematics and Computation*, vol. 284, pp. 268–285, 2016.

[16] Y. Lu, K. A. Pawelek, and S. Liu, "A stage-structured predator-prey model with predation over juvenile prey," *Applied Mathematics and Computation*, vol. 297, pp. 115–130, 2017.

[17] P. van den Driessche and J. Watmough, "Reproduction numbers and sub-threshold endemic equilibria for compartmental models of disease transmission," *Mathematical Biosciences*, vol. 180, no. 1-2, pp. 29–48, 2002.

[18] Y.-H. Hsieh, P. van den Driessche, and L. Wang, "Impact of travel between patches for spatial spread of disease," *Bulletin of Mathematical Biology*, vol. 69, no. 4, pp. 1355–1375, 2007.

[19] X. Wang, S. Liu, L. Wang, and W. Zhang, "An epidemic patchy model with entry-exit screening," *Bulletin of Mathematical Biology*, vol. 77, no. 7, pp. 1237–1255, 2015.

[20] W. Wang and X.-Q. Zhao, "An epidemic model in a patchy environment," *Mathematical Biosciences*, vol. 190, no. 1, pp. 97–112, 2004.

[21] C. S. Holling, "The functional response of predator to prey density and its role in mimicry and population regulation," *Mem. Ent. Sec. Can.* vol. 97, no. 45, pp. 1–60, 1965.

[22] X. Zhao and Z. Jing, "Global asymptotic behavior in some cooperative systems of functional differential equations," *Canadian Applied Math Quarterly*, vol. 4, no. 4, pp. 421–444, 1996.

[23] W. Wang and G. Mulone, "Threshold of disease transmission in a patch environment," *Journal of Mathematical Analysis and Applications*, vol. 285, no. 1, pp. 321–335, 2003.

[24] M. Y. Li and Z. Shuai, "Global stability of an epidemic model in a patchy environment," *Canadian Applied Mathematics Quarterly*, vol. 17, no. 1, pp. 175–187, 2009.

[25] L. Perko, *Differential Equations and Dynamical Systems*, Springer, New York, NY, USA, 2001.

[26] R. A. Horn and C. R. Johnson, *Matrix Analysis*, Cambridge University Press, New York, NY, USA, 1985.

[27] R. A. Horn and C. R. Johnson, *Topics in Matrix Analysis*, Cambridge University Press, New York, NY, USA, 1991.

[28] H. L. Smith and H. R. Thieme, *Dynamical Systems and Population Persistence*, American Mathematical Society, Providence, RI, USA, 2010.

[29] H. R. Thieme, "Persistence under relaxed point-dissipativity (with application to an endemic model)," *SIAM Journal on Mathematical Analysis*, vol. 24, no. 2, pp. 407–435, 1993.

[30] M. W. Hirsch, H. L. Smith, and X.-Q. Zhao, "Chain transitivity attractivity and strong repellors for semidynamical systems," *Journal of Dynamics and Differential Equations*, vol. 13, no. 1, pp. 107–131, 2001.

[31] L. Wang and X. Wang, "Influence of temporary migration on the transmission of infectious diseases in a migrants' home village," *Journal of Theoretical Biology*, vol. 300, pp. 100–109, 2012.

WILEY | Hindawi

Research Article

Rich Dynamics of a Brucellosis Model with Transport

Juan Liang [iD],[1,2] Zhirong Zhao,[1] and Can Li[1]

[1]*Department of Science, Taiyuan Institute of Technology, Taiyuan, Shanxi 030008, China*
[2]*Data Science and Technology, North University of China, Taiyuan, Shanxi 030051, China*

Correspondence should be addressed to Juan Liang; liangjuan76@126.com

Brucellosis is one of the major infectious diseases in China. In this study, we consider an SI model of animal brucellosis with transport. The basic reproduction number $\mathscr{R}_0$ is obtained, and the stable state of the equilibria is analyzed. Numerical simulation shows that different initial values have a great influence on results of the model. In addition, the sensitivity analysis of $\mathscr{R}_0$ with respect to different parameters is analyzed. The results reveal that the transport has dual effects. Specifically, transport can lead to increase in the number of infected animals; besides, transport can also reduce the number of infected animals in a certain range. The analysis shows that the number of infected animals can be controlled if animals are transported reasonably.

1. Introduction

Brucellosis is a zoonosis. It is one of the animal diseases, especially domesticated livestock. Brucellosis mainly attacks sheep, cattle, horses, dogs, pigs, humans, and so on. This epidemic is highly infectious and can be transmitted directly or indirectly through brucella carriers. Humans and animals have certain immunity after suffering from the disease, but they can be infected again. Its incidence is higher in spring and summer. Humans are generally susceptible to the disease and can acquire certain immunity. There is cross immunity among different Brucella species, and the reinfection rate is 2–7. Some scholars have studied the infectious diseases and obtained some results [1–8].

Many articles have studied brucellosis through dynamic models [9–12]. Hou et al. [9] proposed a model with general incidences and analyzed the dynamics of this model. Sun and Zhang [11] gave a brucellosis model which incorporated proportional birth and studied the global stability. Yang et al. [13] proposed to combine age structured brucellosis disease model with spatial diffusion infection firstly (R_0 was obtained by mathematical analysis), analyzed the sensitivity to parameters, and gave the prevention and control measures of the disease. Yang et al. [14] studied a nonlinear model including spatial and seasonal variations to study the

transmission dynamics of brucellosis and proved the importance of spatial and seasonal heterogeneity in disease control. The mathematical model of sheep brucellosis and the effect of slaughtering policy have also been studied [15].

The Chinese government has taken many measures to prevent diseases: vaccination, disinfection and elimination, and so on. If the disease is found, culling measure is taken immediately. However, in fact, some breeders do not take these measures in order to reduce economic losses, which can cause the spread of disease; besides, because the disease has a latent period, breeders do not discover brucellosis in time. In these cases, they transport animals which include the infected.

There has been some studies on the impact of transport on disease transmission [16–18]. A delay periodic patch model with transmission related infection was studied and the authors discussed the difference between the periodic model and the corresponding autonomous model [19]. Liu and Stechlinski [20] proposed a periodic SIS epidemic model with time delay and transport related infection in patchy environment. They discussed the dependence of R_0 on transport related infection parameters and fluctuation amplitude. This paper studies the disease transmission of the remaining animals after the animals are transported away, which will be helpful for disease prevention and control.

In this paper, we study an SI model of animal brucellosis with transport. We show that transport has dual effects. In Section 2, we study the existence of the equilibrium. In Section 3, we study the dynamic behavior of the equilibrium. In Section 4, the numerical simulation is given. Finally, some conclusion are summarized and discussed.

2. Equilibria

We study a two-dimensional model: densities of the susceptible (S) and densities of the infected (I), in this paper. It is assumed that the transport rate B is a nonzero constant when the number of infected is less than a certain value; when the number of infected is greater than a certain value, B equals 0. The detailed relation between susceptible and infected is given in Figure 1. Then, the model is expressed in the following form:

$$\begin{cases} \dot{S} = A - BC - \beta SI - dS, \\ \dot{I} = -B(1 - C) + \beta SI - dI - uI, \end{cases} \quad (1)$$

where

$$\begin{cases} B \neq 0, & if \; I \leq I_0, \\ B = 0, & if \; I > I_0. \end{cases} \quad (2)$$

We assume that all parameters are nonnegative in this model.

A is the recruitment rate of the animal populations, β is the infection coefficient, B is transport proportion, $0 < C < 1$ is the rate of susceptible in this transport, d is the natural death rate of the animal populations, and μ is the disease-related death rate.

When $I \leq I_0$, the steady state of (1) can be written as follows:

$$\begin{cases} A - BC - \beta SI - dS = 0, \\ -B(1 - C) + \beta SI - dI - uI = 0. \end{cases} \quad (3)$$

When $I > I_0$, the steady state of (1) can be written as follows:

$$\begin{cases} A - \beta SI - dS = 0, \\ \beta SI - dI - uI = 0. \end{cases} \quad (4)$$

(1) has no disease-free equilibrium.

Based on Ref. [21], we can obtain the basic reproduction number $\mathscr{R}_0$:

$$\mathscr{F} = [\beta SI],$$

$$\nu = [(d + u)I],$$

$$F = \beta S = \frac{\beta A}{d}, \quad (5)$$

$$V = d + u,$$

$$\mathscr{R}_0 = \rho\left(FV^{-1}\right) = \frac{\beta A}{d(d + u)}.$$

System (4) has a positive equilibrium $E^* = (S^*, I^*) = ((d + u)/\beta, (d(\mathscr{R}_0 - 1))/\beta)$.
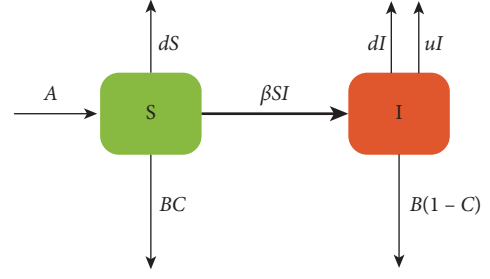

FIGURE 1: Flow diagram of disease transmission. Here, S denotes susceptible, I denotes infected, B is transport proportion, and C is the proportion of susceptible in the transport.

Evidently, we have

$$\mathscr{R}_0 > \frac{\beta I_0}{d} + 1. \quad (6)$$

Next, we calculate the positive solution of system (3). Through the first equation of system (3), we obtain $S = (A - BC)/\beta I + d$. Then, we substitute it into the other equation of (3), so we have

$$\beta(d + \mu)I^2 + \left(\mu d + d^2 + B\beta - A\beta\right)I + Bd(1 - C) = 0. \quad (7)$$

Assume $b = \mu d + d^2 + B\beta - A\beta$. Note that $A - BC > 0$.

If $b \geq 0$, it is easy to know that there is no positive equilibrium; then, we consider $b < 0$, where

$$b = \mu d + d^2 + B\beta - A\beta = \left(-\mathscr{R}d(d + u) + ud + d^2 + B\beta\right). \quad (8)$$

Consequently, we have the following expression:

$$\Delta = \left(-\left(-\mathscr{R}d(d + u) + ud + d^2 + B\beta\right)d(d + u) + ud + d^2 + B\beta\right)^2 - 4\beta(d + \mu)(1 - C)Bd. \quad (9)$$

$\Delta \geq 0$ is equivalent to

$$\mathscr{R}_0 \leq 1 + \frac{B\beta}{d(d + u)} - \frac{2\sqrt{\beta(d + \mu)(1 - C)Bd}}{d(d + \mu)}, \quad (10)$$

$$\mathscr{R}_0 \geq 1 + \frac{B\beta}{d(d + u)} + \frac{2\sqrt{\beta(d + \mu)(1 - C)Bd}}{d(d + \mu)} \overset{\Delta}{=} p_0.$$

$b < 0$ is equivalent to

$$\mathscr{R}_0 \geq 1 + \frac{B\beta}{d(d + u)}. \quad (11)$$

$b < 0$ and $\Delta \geq 0$ if and only if (10) holds. If (10) holds, there are two solutions of (3):

$$I_1 = \frac{-b - \sqrt{\Delta}}{2\beta(d + \mu)}, \quad (12)$$

$$I_2 = \frac{-b + \sqrt{\Delta}}{2\beta(d + \mu)}.$$

If the condition $I_1 \leq I_0$ holds, then we have

$$-b - \sqrt{\Delta} < 2\beta(d + \mu)I_0. \tag{13}$$

This is equivalent to

$$\begin{cases} b + 2\beta(d + \mu)I_0 \leq 0, \\ \left(b + 2\beta(d + \mu)I_0\right)^2 \leq \Delta, \end{cases} \tag{14}$$

or

$$b + 2\beta(d + \mu)I_0 \geq 0. \tag{15}$$

By calculating, (14) is equivalent to

$$\begin{cases} \mathcal{R}_0 \geq 1 + \dfrac{B\beta}{d(d + u)} + \dfrac{2\beta I_0}{d} \overset{\Delta}{=} p_1, \\[4mm] \mathcal{R}_0 \geq 1 + \dfrac{B\beta}{d(d + u)} + \dfrac{\beta I_0}{d} + \dfrac{(1 - C)B}{(d + u)I_0} \overset{\Delta}{=} p_2. \end{cases} \tag{16}$$

(15) is equivalent to

$$\mathcal{R}_0 \leq p_1. \tag{17}$$

As a conclusion, when $\mathcal{R}_0 \geq \max(p_1, p_2)$ or $\mathcal{R}_0 \leq p_1$, $I_1 < I_0$ holds.

If $I_2 < I_0$ holds, we have

$$-b + \sqrt{\Delta} \leq 2\beta(d + \mu)I_0. \tag{18}$$

It is equivalent to an inequality as follows:

$$\begin{cases} b + 2\beta(d + \mu)I_0 \geq 0, \\ \left(b + 2\beta(d + \mu)I_0\right)^2 \geq \Delta, \end{cases} \tag{19}$$

We have that (19) is equivalent to

$$\mathcal{R}_0 \leq \min(p_1, p_2). \tag{20}$$

According to the discussions above, we can obtain two theorems as follows.

Theorem 1. E^* *is the unique endemic equilibrium of (1) if and only if* $(\beta I_0/d) + 1 < \mathcal{R}_0 < p_0$.

Note that $p_1 < p_2$ *is equivalent to* $\beta(d + \mu)I_0^2 < (1 - C)Bd$. *Besides, if* E_i *exist, they must satisfy* $\mathcal{R}_0 \geq p_0$ *which is equivalent to* $\beta(d + \mu)I_0^2 > (1 - C)Bd$. *Therefore, we can obtain that* $p_1 < p_2$ *is impossible. Note that* $p_1 > p_2$ *is equivalent to* $\beta(d + \mu)I_0^2 > (1 - C)Bd$. *So, we have the following.*

Theorem 2. *(1) If* $\mathcal{R}_0 < p_0$, *endemic equilibria* E_1 *and* E_2 *do not exist.*

(2) If $p_0 < \mathcal{R}_0 < p_2$ *and* $\beta(d + \mu)I_0^2 > (1 - C)Bd$, *then* $E_1(S_1, I_1)$ *and* $E_2(S_2, I_2)$ *exist.*

(3) If $p_2 < \mathcal{R}_0 < p_1$ *and* $\beta(d + \mu)I_0^2 > (1 - C)Bd$, *then* $E_1(S_1, I_1)$ *exists.*

According to Theorems 1 and 2, the changes in the number of equilibrium with the basic reproduction number are shown in Figure 2. When $p_0 < \mathcal{R}_0 < p_2$, there are three endemic equilibria; when $p_2 < \mathcal{R}_0 < p_1$, two endemic equilibria exist. We can see that the number of infected is proportional to $\mathcal{R}_0$ if there is no transport. On the contrary,

the number of infected does not always increase with $\mathcal{R}_0$ when there is transport. Consequently, the proper transport might reduce the chance of infection in this area.

Next, we give the relationship between the transport rate B and I in Figure 3. As seen from the Figure 3, model (1) has two endemic equilibria when there is transport. When $B < B^*$ or $B > B^*$ and $I < I^*$, the number of the infected always increases with the increase of B; when $B > B^*$ and $I > I^*$, transport is good for disease control. So, the transport has dual effects on the number of I; it can not only promote the growth of brucellosis but also inhibit the growth of the disease. Consequently, the transport rate B plays a very important role.

3. Stability Analysis

J is the Jacobian matrix of (1) with respect to E^*:

$$J = \begin{pmatrix} -d\mathcal{R}_0 & -(d + u) \\ d(\mathcal{R}_0 - 1) & 0 \end{pmatrix}, \tag{21}$$

with $\quad \operatorname{tr} J = -d\mathcal{R}_0 < 0, \quad \det J = d(d + u)(\mathcal{R}_0 - 1)$. Then, $\lambda_1 < 0, \lambda_2 < 0$, and we have the following result [22–24].

Theorem 3. E^* *is locally asymptotically when* $\mathcal{R}_0 > (\beta/d)I_0 + 1$.

This conclusion can be easily obtained. The dynamic behavior of the stable node indicates that susceptible and infected animal populations can coexist for a long time.

The Jacobian matrix of system (1) with respect to E_i is

$$J = \begin{pmatrix} -d\mathcal{R}_0 & -(d + u) \\[3mm] \beta I & \beta\dfrac{A - BC}{\beta I + d} - d - \mu \end{pmatrix}, \tag{22}$$

with

$$\det J = -\beta(A - BC) + (d + \mu)(\beta I + d) + \dfrac{\beta^2 I(A - BC)}{\beta I + d} \tag{23}$$

$$= (d + u)(\beta I + d)^2 < d\beta(A - BC).$$

If $\det J < 0$, then E_1 is a saddle. Note that $I < I_0$, and we have the following results [25–27].

Theorem 4. *(1)* E_1 *is a saddle if* $(\beta I_0 + d)^2(d + \mu) < d\beta(A - BC)$.

(2) E_2 *is stable if*

$$\begin{cases} \beta A < \beta BC + \beta^2 I_0^2 + 3d\beta I_0 + 2d^2 + \mu\beta I_0 + \mu d, \\[3mm] (d + \mu)(\beta I_0 + d)^2 + d\beta BC > \max\{d(d + \mu) + 2\beta I_0(d + \mu) + B\beta, \\[3mm] d^2 + d\mu + \beta dI_0 + \beta\mu I_0 + B\beta + \dfrac{(1 - C)Bd}{I_0}\}. \end{cases} \tag{24}$$
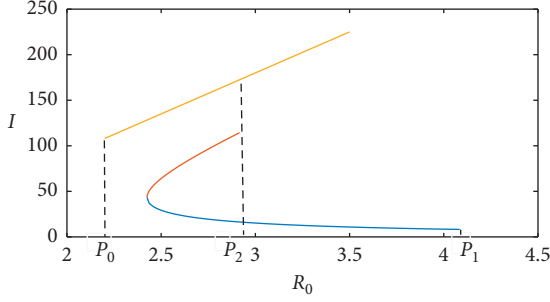
Figure 2: The density of the infected animal populations as a function of basic reproduction number $\mathscr{R}_0$. P_0 indicates that the equilibrium will appear when there is no transport, P_1 indicates that the equilibrium will disappear in the case of transport, and P_2 indicates that there are three equilibria in two cases. Parameter values: $B = 50, I_0 = 110, d = 0.9, \mu = 0.3, \beta = 0.01,$ and $C = 0.5$.
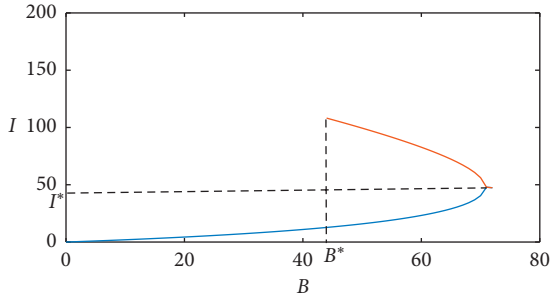

Figure 3: The relationship between the transport rate B and the infected animal populations I. B^* indicates that there are two equilibria. Parameter values: $I_0 = 110, d = 0.9, \mu = 0.3, \beta = 0.01, C = 0.5,$ and $A = 300$.

(3) E_2 is unstable if either

$$
\begin{cases}
\beta A > \beta BC + \beta^2 I_0^2 + 3\,d\beta\,I_0 + 2d^2 + \mu\beta I_0 + \mu d, \\[2mm]
(d + \mu)(\beta I_0 + d)^2 + d\beta BC > \max\{d(d + \mu) + 2\beta I_0(d + \mu) + B\beta, \\[2mm]
\quad d^2 + d\mu + \beta d I_0 + \beta \mu I_0 + B\beta + \dfrac{(1 - C)Bd}{I_0}\},
\end{cases}
\tag{25}
$$

or

$$
\begin{cases}
(d + \mu)(\beta I_0 + d)^2 + d\beta\, BC > \max\{d(d + \mu) + 2\beta I_0(d + \mu) + B\beta, \\[2mm]
\quad d^2 + d\mu + \beta d I_0 + \beta \mu I_0 + B\beta + \dfrac{(1 - C)Bd}{I_0}\}.
\end{cases}
\tag{26}
$$

Theorem 5. *The unique endemic equilibrium $E^*(S^*, I^*)$ of system (1) is globally asymptotically stable when $\mathscr{R}_0 > 1 + (\beta/d)I_0$.*

Proof. Define the Lyapunov function [28, 29]:

$$
V(S, I) = S - S^* - S^* \ln \frac{S}{S_0} + I - I^* - I^* \ln \frac{I}{I_0}.
\tag{27}
$$

The derivative of $V(S, I)$ along solutions of system (1) is

$$
\begin{aligned}
\frac{dV}{dt} &= \dot{S}\left(1 - \frac{S^*}{S}\right) + \dot{i}\left(1 - \frac{I^*}{I}\right) \\[2mm]
&= (A - \beta SI - dS)\left(1 - \frac{S^*}{S}\right) + (\beta SI - (d + \mu)I)\left(1 - \frac{I^*}{I}\right) \\[2mm]
&= dS^*\left\{2 - \frac{S}{S^*} - \frac{S^*}{S}\right\} + \beta S^* I^*\left\{2 - \frac{S}{S^*} - \frac{S^*}{S}\right\}.
\end{aligned}
\tag{28}
$$

Since $(S/S^*) - (S^*/S) < 2$, $(dV/dt) = (dS^* + \beta S^* I^*)(2 - (S/S^*) - (S^*/S)) \leq 0$.

When $\mathscr{R}_0 > 1 + (\beta/d)I_0$, we have $(dV/dt) < 0$. $(dV/dt) = 0$ holds if and only if $S = S^*, I = I^*$. By Lyapunov–Lasalle theorem [30–32], the endemic equilibrium $E^*(S^*, I^*)$ is globally asymptotically stable when $\mathscr{R}_0 > 1 + (\beta/d)I_0$. $\qquad\square$

4. Numerical Results

In an epidemic model, the basic reproduction number $\mathscr{R}_0$ is an important parameter which can predict the dynamics of the disease. If $\mathscr{R}_0 < 1$, it indicates that the disease can be controlled and can even disappear. Otherwise, the disease will outbreak when the basic reproduction number $\mathscr{R}_0 > 1$. In this paper, when the endemic equilibrium exists, the basic reproduction number $\mathscr{R}_0 > 1$. Next, we analyze the spread of the disease over time.

Figure 4 represents time series of the infected animal populations with different initial values. We take $B = 50, I_0 = 110, d = 0.9, \mu = 0.3, \beta = 0.01, c = 0.5,$ and $A = 441.99$ with different initial values: (a) $S_0 = 200, I_0 = 130$; (b) $S_0 = 100, I_0 = 80$; (c) $S_0 = 300, I_0 = 180$; (d) $S_0 = 300, I_0 = 100$. One can conclude from this figure that there is great distinction between different initial values. As seen from Figure 4(b), the number of infected decreases over time. On the contrary, in the other three figures, the number of infected increases in the beginning. Therefore, initial values play an important role in the control of the disease.

Next, we give sensitivity analysis of $\mathscr{R}_0$ in order to find better control strategies. Different parameters are substituted into the expression $\mathscr{R}_0 = \beta A/(d(d + u))$. We use the normalized forward sensitivity index and derive an analytical expression [33]:

$$
\gamma_p^{\mathscr{R}_0} = \frac{\partial \mathscr{R}_0}{\partial p} \times \frac{\partial p}{\partial \mathscr{R}_0}.
\tag{29}
$$

Table 1 shows the sensitivity index of $\mathscr{R}_0$ with respect to different parameters. We can conclude from Table 1 that $\mathscr{R}_0$ is more sensitive to the recruitment rate A and the infection coefficient β, which means that the main influencing factors of $\mathscr{R}_0$ are A and β. Since A and β are proportional to $\mathscr{R}_0$, the most effective way to reduce $\mathscr{R}_0$ is to reduce the recruitment rate and the infection coefficient.
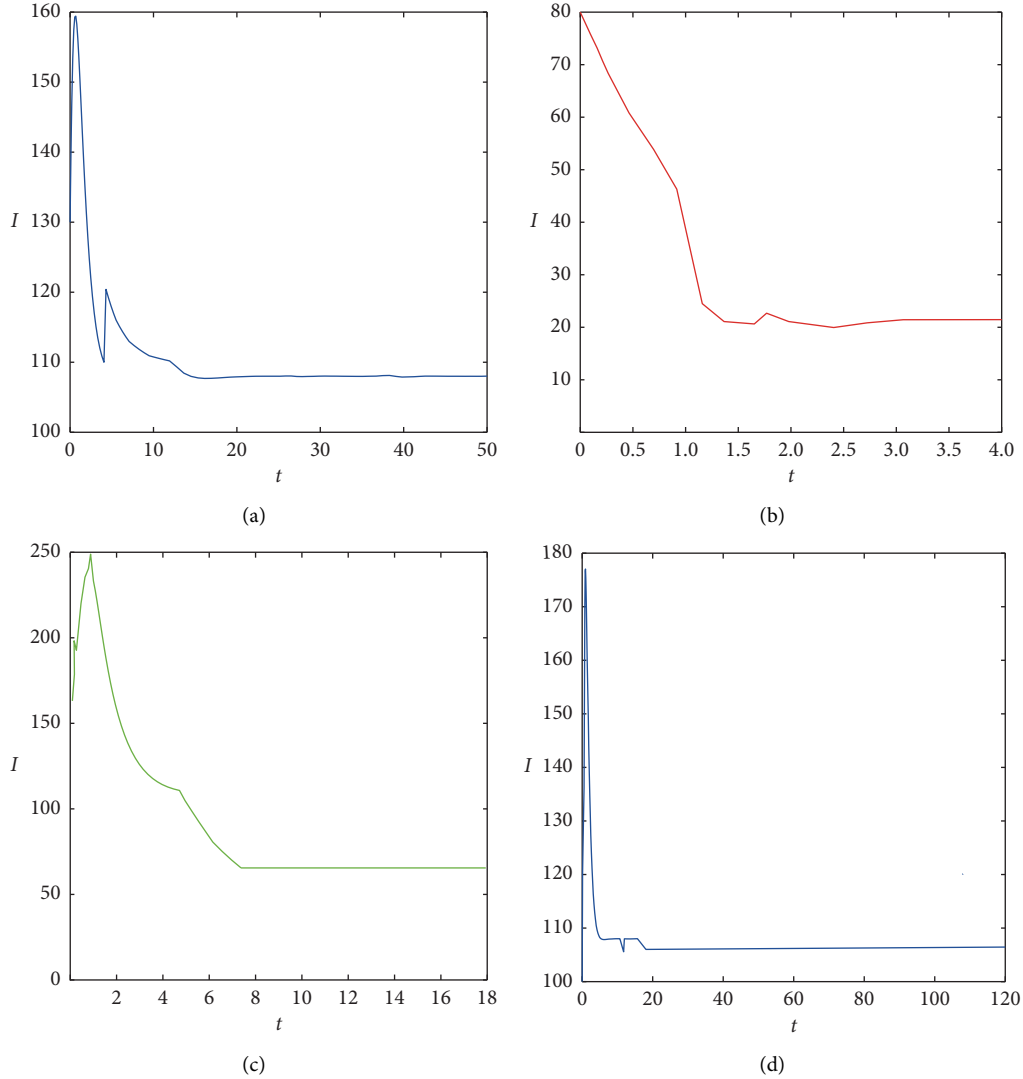
(a)

(b)

(c)

(d)

FIGURE 4: Time series of the infected animal populations with different initial values. Parameter values: $B = 50, I_0 = 110, d = 0.9, \mu = 0.3, \beta = 0.01, c = 0.5$, and $A = 441.99$. Initial values: (a) $S_0 = 200, I_0 = 130$; (b) $S_0 = 100, I_0 = 80$; (c) $S_0 = 300, I_0 = 180$; (d) $S_0 = 300, I_0 = 100$.

TABLE 1: The sensitivity index of $\mathscr{R}_0$ with respect to different parameters.

Parameter	Sensitivity index
β	1
A	1
μ	−1.836
d	−4.282

5. Conclusion and Discussion

Brucellosis has always been a research focus in infectious diseases. Measures to control the spread of brucellosis are vaccinating susceptible and culling infected animal populations. However, in fact, due to some practical factors, such as the incubation period of the disease and economic factor, the breeders will transport the animals containing the infected and fail to take effective measures in time. This case is tremendously overlooked despite its real existence in China. In order to study the influence of transport on the spread of brucellosis, we present an SI model with transport. Through mathematical analysis, we obtain the basic reproduction number $\mathscr{R}_0$ and the positive equilibria. The existence and global stability of these equilibria are analyzed. Our results reveal that initial values have important effects on the spread of disease.

Our work demonstrates that the transport has dual effects. Specifically, transport can lead to increase in the number of the infected; besides, transport can also reduce the number of the infected animals in a certain range. This is an interesting result. This indicates that transport can help control the disease for a time. Besides, sensitivity of the basic reproduction number $\mathscr{R}_0$ is calculated. The results show that the main influencing factors are the recruitment rate and the infection coefficient. Some measures should be taken, such as vaccination and disinfection. We suggest that breeders

can increase animal vaccination coverage rate and enhance the awareness of disease prevention.

The analysis shows that the number of infected animals can be controlled if animals are transported reasonably. However, we do not analyze how the disease spreads in the transported animals; this may not be good at disease control. Consequently, we will analyze the dynamic behavior of the animals which have been transported and give a better strategy to control brucellosis. Besides, infectious diseases spread in space, and spatial infectious disease models can describe the dynamics of disease transmission. Therefore, we will integrate the diffusion term into the disease model in the future study [34–36].

Data Availability

No data were used to support this study.

Conflicts of Interest

The authors declare that they have no conflicts of interest.

Acknowledgments

References

[1] J. Zinsstag, F. Roth, D. Orkhon et al., "A model of animal-human brucellosis transmission in Mongolia," *Preventive Veterinary Medicine*, vol. 69, no. 1-2, pp. 77–95, 2005.

[2] J. Gonzalez-Guzman and R. Naulin, "Analysis of a model of bovine brucellosis using singular perturbations," *Journal of Mathematical Biology*, vol. 33, no. 2, pp. 211–223, 1994.

[3] G. Pappas, N. Akritidis, M. Bosilkovski, and E. Tsianos, "Brucellosis and the respiratory system," *Clinical Infectious Diseases*, vol. 37, no. 7, pp. 95–99, 2003.

[4] M. Doganay and B. Aygen, "Human brucellosis: an overview," *International Journal of Infectious Diseases*, vol. 7, no. 3, pp. 173–182, 2003.

[5] R. S. Cantrell, C. Cosner, and W. F. Faganantrell, "Brucellosis, botflies, and brainworms: the impact of edge habitats on pathogen transmission and species extinction," *Journal of Mathematical Biology*, vol. 42, no. 2, pp. 95–119, 2001.

[6] M.-T. Li, G.-Q. Sun, Y.-F. Wu, J. Zhang, and Z. Jin, "Transmission dynamics of a multi-group brucellosis model with mixed cross infection in public farm," *Applied Mathematics and Computation*, vol. 237, pp. 582–594, 2014.

[7] B. Ruben, J. D. Band, P. Wong, and J. Colville, "Person-to-person transmission of Brucella melitensis," *Lancet*, vol. 337, no. 8732, pp. 14-15, 1982.

[8] G.-Q. Sun, C.-H. Wang, and Z.-Y. Wu, "Pattern dynamics of a Gierer-Meinhardt model with spatial effects," *Nonlinear Dynamics*, vol. 88, no. 2, pp. 1385–1396, 2017.

[9] Q. Hou, X. Sun, Y. Wang, B. Huang, and Z. Jin, "Global properties of a general dynamic model for animal diseases: a case study of brucellosis and tuberculosis transmission,"

[10] Q. Hou, X. Sun, J. Zhang, Y. Liu, Y. Wang, and Z. Jin, "Modeling the transmission dynamics of sheep brucellosis in inner Mongolia autonomous region, China," *Mathematical Biosciences*, vol. 242, no. 1, pp. 51–58, 2013.

[11] G.-Q. Sun and Z.-K. Zhang, "Global stability for a sheep brucellosis model with immigration," *Applied Mathematics and Computation*, vol. 246, pp. 336–345, 2014.

[12] N. Jing and G. Q. Sun, "Modeling the transmission dynamics of dairy cattle brucellosis in Jilin province, China," *Journal of Biological System*, vol. 22, no. 04, pp. 533–554, 2014.

[13] J. Yang, R. Xu, and J. Li, "Threshold dynamics of an age-space structured brucellosis disease model with Neumann boundary condition," *Nonlinear Analysis: Real World Applications*, vol. 50, pp. 192–217, 2019.

[14] C. Y. Yang, P. O. Lolika, S. Mushayabasa, and J. Wang, "Modeling the spatiotemporal variations in brucellosis transmission," *Nonlinear Analysis: Real World Applications*, vol. 38, pp. 49–67, 2017.

[15] B. Aïnseba, C. Benosman, and P. Magal, "A model for ovine brucellosis incorporating direct and indirect transmission," *Journal of Biological Dynamics*, vol. 4, no. 1, pp. 2–11, 2010.

[16] J. Liu, J. Wu, and Y. Zhou, "Modeling disease spread via transport-related infection by a delay differential equation," *Rocky Mountain Journal of Mathematics*, vol. 38, no. 5, pp. 1525–1540, 2008.

[17] X. Liu and Y. Takeuchi, "Spread of disease with transport-related infection and entry screening," *Journal of Theoretical Biology*, vol. 242, no. 2, pp. 517–528, 2006.

[18] Y. Takeuchi, X. Liu, and J. Cui, "Global dynamics of SIS models with transport-related infection," *Journal of Mathematical Analysis and Applications*, vol. 329, no. 2, pp. 1460–1471, 2007.

[19] J. Liu, Z. Bai, and T. Zhang, "A periodic two-patch SIS model with time delay and transport-related infection," *Journal of Theoretical Biology*, vol. 437, pp. 36–44, 2018.

[20] X. Liu and P. Stechlinski, "Transmission dynamics of a switched multi-city model with transport-related infections," *Nonlinear Analysis: Real World Applications*, vol. 14, no. 1, pp. 264–279, 2013.

[21] O. Diekmann, J. A. P. Heesterbeek, and J. A. J. Metz, "On the definition and the computation of the basic reproduction ratio $\mathcal{R}_0$ in models for infectious diseases in heterogeneous populations," *Journal of Mathematical Biology*, vol. 28, no. 4, pp. 365–382, 1990.

[22] A. Q. Khan, "Stability and Neimark-Sacker bifurcation of a ratio-dependence predator-prey model," *Mathematical Methods in the Applied Sciences*, vol. 40, pp. 404109–404117, 2017.

[23] G.-Q. Sun, C.-H. Wang, L.-L. Chang, Y.-P. Wu, L. Li, and Z. Jin, "Effects of feedback regulation on vegetation patterns in semi-arid environments," *Applied Mathematical Modelling*, vol. 61, pp. 200–215, 2018.

[24] L. Li, J. Zhen, and S. Gui-Quan, "Spatial pattern of an epidemic model with cross-diffusion," *Chinese Physics Letters*, vol. 25, no. 9, pp. 3500–3503, 2008.

[25] G.-Q. Sun, J.-H. Xie, S.-H. Huang, Z. Jin, M.-T. Li, and L. Liu, "Transmission dynamics of cholera: mathematical modeling and control strategies," *Communications in Nonlinear Science and Numerical Simulation*, vol. 45, pp. 235–244, 2017.

[26] L. Li, G.-Q. Sun, and Z. Jin, "Bifurcation and chaos in an epidemic model with nonlinear incidence rates," *Applied*

Mathematics and Computation, vol. 216, no. 4, pp. 1226–1234, 2010.

[27] G.-Q. Sun, "Pattern formation of an epidemic model with diffusion," *Nonlinear Dynamics*, vol. 69, no. 3, pp. 1097–1104, 2012.

[28] X. Zhang and X. Liu, "Backward bifurcation of an epidemic model with saturated treatment function," *Journal of Mathematical Analysis and Applications*, vol. 348, no. 1, pp. 433–443, 2008.

[29] W. D. Wang, "Backward bifurcation of an epidemic model with treatment," *Mathematical Biosciences*, vol. 201, no. 1-2, pp. 58–71, 2006.

[30] J. Hespanha, "Uniform stability of switched linear systems: extensions of LaSalle's invariance principle," *IEEE Transactions on Automatic Control*, vol. 49, no. 4, pp. 470–482, 2004.

[31] J. P. LaSalle, "Stability theory for ordinary differential equations," *Journal of Differential Equations*, vol. 4, no. 1, pp. 57–65, 1968.

[32] J. P. LaSalle, "Stability theory and invariance principles," *Dynamical Systems*, vol. 1, pp. 211–222, 1976.

[33] N. Chitnis, J. M. Hyman, and J. M. Cushing, "Determining important parameters in the spread of malaria through the sensitivity analysis of a mathematical model," *Bulletin of Mathematical Biology*, vol. 70, no. 5, pp. 1272–1296, 2008.

[34] G.-Q. Sun, M. Jusup, Z. Jin, Y. Wang, and Z. Wang, "Pattern transitions in spatial epidemics: mechanisms and emergent properties," *Physics of Life Reviews*, vol. 19, pp. 43–73, 2016.

[35] Z. G. Guo, G. Q. Sun, Z. Wang et al., "Spatial dynamics of an epidemic model with nonlocal infection," *Applied Mathematics and Computation*, vol. 377, Article ID 125158, 2020.

[36] Z. G. Guo, L. P. Song, G. Q. Sun, C. Li, and Z. Jin, "Pattern dynamics of an SIS epidemic model with nonlocal delay," *International Journal of Bifurcation and Chaos*, vol. 29, no. 2, Article ID 1950027, 2019.

WILEY | Hindawi

Research Article

Global Stability for Fractional Diffusion Equations in Biological Systems

Khalid Hattaf [ID]^{1,2} **and Noura Yousfi** [ID]^{2}

^{1}*Centre Régional des Métiers de L'Education et de La Formation (CRMEF), 20340 Derb Ghalef, Casablanca, Morocco*
^{2}*Laboratory of Analysis, Modeling and Simulation (LAMS), Faculty of Sciences Ben M'sik, Hassan II University of Casablanca, P.O. Box 7955 Sidi Othman, Casablanca, Morocco*

Correspondence should be addressed to Khalid Hattaf; k.hattaf@yahoo.fr

This paper proposes a new method of construction of Lyapunov functionals for the dynamical systems described by fractional differential equations and fractional partial differential equations. The proposed method is rigorously presented. Furthermore, the method is applied to establish the global stability of some fractional biological models with and without diffusion.

1. Introduction

In recent years, fractional differential equations (FDEs) are used to describe the temporal dynamics of various systems in many fields. These equations are the generalization of the classical ordinary differential equations (ODEs). However, fractional partial differential equations (FPDEs) are the generalization of the partial differential equations (PDEs) which can be an effective tool to describe the spatiotemporal dynamics of several phenomena with memory or have hereditary properties.

The construction of Lyapunov functionals to prove the global stability of fractional dynamic systems has attracted the attention of some authors. Aguila-Camacho et al. [1] established a new lemma for fractional derivative in Caputo sense with order $\alpha \in (0, 1)$. They used this lemma to demonstrate the stability of some fractional-order systems by mean of quadratic Lyapunov functionals. Duarte-Mermoud et al. [2] extended the lemma of [1] to a vector of differentiable functions, and they used Lyapunov functionals containing general quadratic forms in order to analyze the stability of fractional-order model reference adaptive control (FOMRAC) schemes. Vargas-De-León [3] extended the Volterra-type Lyapunov function to fractional-order epidemic systems via an inequality to estimate the Caputo

fractional derivative of this function. On the other hand, a study in [4] has been devoted to establish the global stability for some diffusion equations in biology by means of Lyapunov functionals.

The methods mentioned above are applied for particular Lyapunov functionals such as quadratic or Volterra-type. Likewise, the work in [4] is especially applicable for the models formulated by PDEs. Therefore, the main goal of this study is to develop a new mathematical method to construct the Lyapunov functionals for FDEs and FPDEs based on those of ODEs. To do this, the next section deals with the description of the method and the last section is devoted to the application of our method to investigate the global stability of some mathematical models in epidemiology as well as in virology.

2. Description of the Method

Consider the following FDE:

$$D_t^\alpha u = f(u), \qquad (1)$$

where D_t^α is the fractional derivative in the Caputo sense of order $\alpha \in (0, 1]$, the state variable u is a non-negative vector of concentrations $u_1, \ldots, u_m$, and $f: \mathrm{IR}^m \longrightarrow \mathrm{IR}^m$ is a C^1

function. It is obvious that if $\alpha = 1$, then (1) becomes the following ordinary differential equation:

$$\dot{u} = f(u). \tag{2}$$

Let Ω be a bounded domain in IR^n with smooth boundary $\partial\Omega$ and $\mathscr{D} = (d_1, \ldots, d_m)$ with $d_i \geq 0$. Assume that u^* is a steady state of (1). Then, u^* is also the steady state of the following fractional diffusion system with homogeneous Neumann boundary condition:

$$\begin{cases} \partial_t^\alpha u = \mathscr{D}\Delta u + f(u) \text{ in } \Omega \times (0, +\infty), \\[2mm] \dfrac{\partial u}{\partial \nu} = 0 \text{ on } \partial\Omega \times (0, +\infty), \\[2mm] u(x, 0) = u_0(x) \text{ in } \overline{\Omega}, \end{cases} \tag{3}$$

where $\triangle = \sum_{i=1}^n \partial^2/\partial x_i^2$ represents the Laplacian operator and $\partial u/\partial \nu$ denotes the outward normal derivative on the boundary $\partial\Omega$.

Let $V(u)$ be a C^1 function defined on some domain in R_+^m and $u(t)$ is a solution of (1). Further, we suppose that the range of $u(t)$ is contained in the domain of $V(u)$ and

$$D_t^\alpha V(u(t)) \leq \nabla V(u) \cdot f(u), \tag{4}$$

whose equality holds if $\alpha = 1$.

We observe that the right-hand side of the above inequality is given by the scalar product of the gradient of the function $V(u)$ and the vector field $f(u)$. Hence, the right-hand side is defined without the fact that $u(t)$ is a solution of (1), which is very important for the construction of Lyapunov functionals.

Let $u(t, x)$ be a solution of (3). Denote

$$W = \int_\Omega V(u(t, x)) \mathrm{d}x. \tag{5}$$

The fractional time derivative of W along the positive solution of (3) satisfies

$$D_t^\alpha W \leq \int_\Omega \nabla V(u) \cdot (\mathscr{D}\Delta u + f(u)) \mathrm{d}x$$

$$= \int_\Omega \nabla V(u) \cdot f(u) \mathrm{d}x + \int_\Omega \nabla V(u) . \mathscr{D}\Delta u \mathrm{d}x \tag{6}$$

$$= \int_\Omega \nabla V(u) \cdot f(u) \mathrm{d}x + \sum_{i=1}^m d_i \int_\Omega \frac{\partial V}{\partial u_i} \Delta u_i \mathrm{d}x.$$

By applying Green's formula, we find

$$\int_\Omega \frac{\partial V}{\partial u_i} \Delta u_i \mathrm{d}x = \int_{\partial\Omega} \frac{\partial V}{\partial u_i} \frac{\partial u_i}{\partial \nu} \mathrm{d}\sigma - \int_\Omega \nabla u_i \cdot \nabla\left(\frac{\partial V}{\partial u_i}\right) \mathrm{d}x. \tag{7}$$

According to $(\partial u/\partial \nu) = 0$ on $\partial\Omega$, we have

$$\int_\Omega \frac{\partial V}{\partial u_i} \Delta u_i \mathrm{d}x = -\int_\Omega \nabla u_i \cdot \nabla\left(\frac{\partial V}{\partial u_i}\right) \mathrm{d}x. \tag{8}$$

Therefore,

$$\frac{\mathrm{d}W}{\mathrm{d}t} \leq \int_\Omega \nabla V(u) \cdot f(u) \mathrm{d}x - \sum_{i=1}^m d_i \int_\Omega \nabla u_i \cdot \nabla\left(\frac{\partial V}{\partial u_i}\right) \mathrm{d}x. \tag{9}$$

Additionally, we assume that the function V satisfies the following condition:

$$d_i \int_\Omega \nabla u_i \cdot \nabla\left(\frac{\partial V}{\partial u_i}\right) \mathrm{d}x \geq 0, \quad \text{for all } i = 1, \ldots, m. \tag{10}$$

From the above, it is not difficult to obtain the following result.

Theorem 1. *Let V be a Lyapunov functional for the ordinary differential equation (2).*

    (i) If V satisfies the condition (4), then V is also a Lyapunov functional for fractional differential equation (1).

    (ii) If V satisfies the conditions (4) and (10), then the function W defined by (5) is a Lyapunov functional for fractional diffusion system (3).

In the literature, several researchers constructed the Lyapunov functional in the following form:

$$V = \sum_{i=1}^m a_i\left(u_i - u_i^* - u_i^* \ln \frac{u_i}{u_i^*}\right). \tag{11}$$

Corollary 2. *If V is a Lyapunov functional for ordinary differential equation (2) of the form given in (11), then V is a Lyapunov functional for fractional differential equation (1). Moreover, the function W defined by (5) is a Lyapunov functional for fractional diffusion system (3).*

Proof. We have

$$D_t^\alpha V = \sum_{i=1}^m a_i D_t^\alpha\left(u_i - u_i^* - u_i^* \ln \frac{u_i}{u_i^*}\right). \tag{12}$$

By applying Lemma 3.1 in [3], we get

$$D_t^\alpha V \leq \sum_{i=1}^m a_i\left(1 - \frac{u_i^*}{u_i}\right) D_t^\alpha u_i$$

$$= \nabla V(u) \cdot f(u). \tag{13}$$

Then, V satisfies the condition (4). It follows from Theorem 1 (i) that V is also a Lyapunov functional for fractional differential equation (1).

On the other hand, we have

$$\int_\Omega \nabla u_i \cdot \nabla\left(\frac{\partial V}{\partial u_i}\right) \mathrm{d}x = a_i u_i^* \int_\Omega \frac{|\nabla u_i|^2}{u_i^2} \mathrm{d}x \geq 0, \tag{14}$$

which implies that V satisfies the condition (10). According to Theorem 1 (ii), we deduce that the function W given by (4) is also a Lyapunov functional for fractional diffusion system (3). This completes the proof. $\qquad\square$

Remark 3. The method described above can be used to prove the stability of many fractional systems with and without diffusion. It is very important to recall that the steady state u^* is stable if there exists a Lyapunov functional satisfying $D_t^\alpha V(u) \le 0$. Moreover, if $D_t^\alpha V(u) < 0$ for all $u \ne u^*$, then u^* is asymptotically stable. Additionally, according to [5], if $D_t^\alpha V(u) \le 0$ and the largest invariant set in $\{u \mid D_t^\alpha V(u) = 0\}$ is the singleton $\{u^*\}$, then u^* is asymptotically stable. This means that the solution of the system starting from any initial conditions converges to u^*.

3. Applications

This section focuses on the application of the method described in the above section in order to establish the global stability of some fractional diffusion biological models by constructing Lyapunov functionals from those of the corresponding systems which are formulated by ODEs.Example 1. Consider the SIR epidemic model described by the following nonlinear system of FDEs:

$$\begin{cases} D_t^\alpha S = A - \mu S - \dfrac{\beta SI}{\alpha_0 + \alpha_1 S + \alpha_2 I + \alpha_3 SI}, \\ D_t^\alpha I = \dfrac{\beta SI}{\alpha_0 + \alpha_1 S + \alpha_2 I + \alpha_3 SI} - (\mu + d + r)I, \\ D_t^\alpha R = rI - \mu R, \end{cases} \quad (15)$$

where S, I, and R are the populations of susceptible, infected, and recovered individuals, respectively. The parameters A, μ, d, and r are, respectively, the recruitment rate, the natural death rate, the death rate due to disease, and the recovery rate. The incidence function of system (15) is described by Hattaf–Yousfi functional response [6] of the form $\beta SI/1 + \alpha_1 S + \alpha_2 I + \alpha_3 SI$, where the non-negative constants α_i, $i = 0, 1, 2, 3$, measure the saturation, inhibitory, or psychological effects, and the positive constant β is the infection rate. This functional response covers the most famous forms existing in the literature such as the classical bilinear incidence, the saturated incidence, the Beddington–DeAngelis functional response [7], the Crowley–Martin functional response [8], and the specific functional response introduced in [9]. Further, the fractional models proposed in [10, 11] are particular cases of model (15); it suffices to take $\alpha_0 = 1$ and $\alpha_1 = \alpha_2 = \alpha_3 = 0$ for [10] and $\alpha_0 = 1$ for [11].

Since the state variable R does not appear in the two first equations of fractional model (15), we can reduce (15) to the following system:

$$\begin{cases} D_t^\alpha S = A - \mu S - \dfrac{\beta SI}{\alpha_0 + \alpha_1 S + \alpha_2 I + \alpha_3 SI}, \\ D_t^\alpha I = \dfrac{\beta SI}{\alpha_0 + \alpha_1 S + \alpha_2 I + \alpha_3 SI} - (\mu + d + r)I. \end{cases} \quad (16)$$

Due to the great mobility of individuals inside or outside a country or region, we consider the following fractional model:

$$\begin{cases} \partial_t^\alpha S = d_S \Delta S + A - \psi(S(x,t), I(x,t))I(x,t), \\ \partial_t^\alpha I = d_I \Delta I + \psi(S(x,t), I(x,t))I(x,t) - \eta I(x,t), \end{cases} \quad (17)$$

where $\psi(S, I) = (\beta S/\alpha_0 + \alpha_1 S + \alpha_2 I + \alpha_3 SI)$ and $\eta = \mu + d + r$. The parameters d_S and d_I are the diffusion coefficients for the susceptible and infected populations, respectively. Also, we consider model (17) with homogeneous Neumann boundary conditions:

$$\frac{\partial S}{\partial \nu} = \frac{\partial I}{\partial \nu} = 0, \text{ on } \partial\Omega \times (0 + \infty), \quad (18)$$

and initial conditions:

$$\begin{aligned} S(x, 0) &= S_0(x) \ge 0, \\ I(x, 0) &= I_0(x) \ge 0, \\ x &\in \overline{\Omega}. \end{aligned} \quad (19)$$

For $\alpha = 1$, model (16) becomes the following nonlinear system of ODEs:

$$\begin{cases} \dot{S} = A - \mu S - \psi(S, I)I, \\ \dot{I} = \psi(S, I)I - \eta I. \end{cases} \quad (20)$$

Obviously, model (20) has always one disease-free equilibrium $E_f((A/\mu), 0)$. By a simple computation, the basic reproduction number is given by

$$\mathscr{R}_0 = \frac{\beta A}{(\alpha_0 \mu + \alpha_1 A)(\mu + d + r)}. \quad (21)$$

When $\mathscr{R}_0 > 1$, model (20) has another equilibrium named endemic equilibrium $E^*(S^*, I^*)$, where

$$\begin{aligned} S^* &= \frac{2(\eta\alpha_0 + \alpha_2 A)}{\beta - \alpha_1\eta + \alpha_2\mu - \alpha_3 A + \sqrt{\delta}}, \\ I^* &= \frac{\Lambda - \mu S^*}{\eta}, \end{aligned} \quad (22)$$

with $\delta = (\beta - \alpha_1\eta + \alpha_2\mu - \alpha_3\Lambda)^2 + 4\alpha_3\mu(\eta\alpha_0 + \alpha_2 A)$.

System (20) is a special case of the mathematical model presented in [12]. Thus, the disease-free equilibrium E_f is globally asymptotically stable when $\mathscr{R}_0 \le 1$. However, E_f becomes unstable and the endemic equilibrium E^* is globally asymptotically stable if $\mathscr{R}_0 > 1$.

Let $S^0 = A/\mu$ and $\Phi(z) = z - 1 - \ln(z)$ for $z > 0$. From [12], the function

$$V_1(u) = \frac{\alpha_0 S^0}{\alpha_0 + \alpha_1 S^0} \Phi\left(\frac{S}{S^0}\right) + I \quad (23)$$

is a Lyapunov functional for ODE model (20) at E_f. Moreover, we have

$$\begin{aligned} \nabla V_1(u) \cdot f(u) &= \frac{\alpha_0}{\alpha_0 + \alpha_1 S^0}\left(1 - \frac{S^0}{S}\right)(A - \mu S - \psi(S, I)I) \\ &\quad + \psi(S, I)I - \eta I \\ &= \frac{-\alpha_0\mu(S - S^0)^2}{(\alpha_0 + \alpha_1 S^0)S} + \eta I\left(\frac{\psi(S, I)}{\psi(S, 0)}\mathscr{R}_0 - 1\right) \\ &\le \frac{-\alpha_0\mu(S - S^0)^2}{(\alpha_0 + \alpha_1 S^0)S} + \eta I(\mathscr{R}_0 - 1). \end{aligned} \quad (24)$$

Additionally, we have

$$D_t^\alpha V_1(u) \leq \nabla V_1(u) \cdot f(u). \tag{25}$$

Then, V_1 satisfies the condition (4). By applying Theorem 1 (i), we deduce that V_1 is also a Lyapunov functional for FDE model (16) at E_f.

Now, we construct the Lyapunov functional for fractional diffusion model (17) at E_f as follows:

$$W_1 = \int_\Omega V_1(u(x,t))dx. \tag{26}$$

In this case, we have

$$d_i \int_\Omega \nabla u_i \cdot \nabla\left(\frac{\partial V_1}{\partial u_i}\right)dx \geq 0, \quad \text{for all } i = 1, 2. \tag{27}$$

In fact,

$$d_S \int_\Omega \nabla S \cdot \nabla\left(\frac{\partial V_1}{\partial S}\right)dx = \frac{\alpha_0 d_S S^0}{\alpha_0 + \alpha_1 S^0} \int_\Omega \frac{|\nabla S|^2}{S^2}dx \geq 0,$$

$$d_I \int_\Omega \nabla I \cdot \nabla\left(\frac{\partial V_1}{\partial I}\right)dx = 0. \tag{28}$$

This implies that V_1 satisfies the condition (10). It follows from Theorem 1 (ii) that W_1 is a Lyapunov functional for fractional diffusion systems (17)–(19) at E_f when $\mathscr{R}_0 \leq 1$.

For the global stability of the endemic equilibrium E^*, we consider the following function:

$$V_2(u) = S - S^* - \int_{S^*}^S \frac{\psi(S^*, I^*)}{\psi(X, I^*)}dX + I^*\Phi\left(\frac{I}{I^*}\right), \tag{29}$$

which is a Lyapunov functional for ODE model (20) at E^*. On the other hand, we have

$$\nabla V_2(u) \cdot f(u) = \left(1 - \frac{\psi(S^*, I^*)}{\psi(S, I^*)}\right)(A - \mu S - \psi(S, I)I)$$

$$+ \left(1 - \frac{I^*}{I}\right)(\psi(S, I)I - \eta I),$$

$$D_t^\alpha V_1(u) \leq \nabla V_1(u) \cdot f(u). \tag{30}$$

Thus, V_2 obeys the condition (4) and then V_2 is a Lyapunov functional for FDE model (8) at E^*.

Denote

$$W_2 = \int_\Omega V_2(u(x,t))dx. \tag{31}$$

It is not hard to show that

$$d_S \int_\Omega \nabla S \cdot \nabla\left(\frac{\partial V_2}{\partial S}\right)dx = \frac{(\alpha_0 + \alpha_2 I^*)d_S S^*}{\alpha_0 + \alpha_1 S^* + \alpha_2 I^* + \alpha_3 S^* I^*} \int_\Omega \frac{|\nabla S|^2}{S^2}dx \geq 0,$$

$$d_I \int_\Omega \nabla I \cdot \nabla\left(\frac{\partial V_2}{\partial I}\right)dx = d_I I^* \int_\Omega \frac{|\nabla I|^2}{I^2}dx \geq 0. \tag{32}$$

Then, condition (10) holds. Therefore, W_2 is a Lyapunov functional for fractional diffusion systems (17)–(19) at E^* when $\mathscr{R}_0 > 1$.

Consequently, we have the following:

(i) When $\mathscr{R}_0 \leq 1$, the disease-free equilibrium E_f of (17)–(19) is globally asymptotically stable.

(ii) When $\mathscr{R}_0 > 1$, the endemic equilibrium E^* of (17)–(19) is globally asymptotically stable.

Example 2. Consider the following fractional viral infection model:

$$\begin{cases} D_t^\alpha H = \lambda - \mu H - \beta_1 HV - \beta_2 HI, \\ D_t^\alpha I = \beta_1 HV + \beta_2 HI - \delta I, \\ D_t^\alpha V = pI - cV, \end{cases} \tag{33}$$

where healthy cells (H) are produced at rate λ, die at rate μH, and become infected by contact with virus at rate $\beta_1 HV$ and by contact with infected cells at rate $\beta_2 HI$. Infected cells (I) die at rate δI. Free viral particles (V) are released from infected cells at rate pI and decay at rate cV. Note that when $\alpha = 1$ and $\beta_1 = 0$, we obtain the basic model which was used to study some viral infections such as HIV, HBV, and HCV [13–16].

Now, we extend the above fractional model (33) by taking into account the mobility of the virus as well as the cells. Then, model (33) becomes

$$\begin{cases} \partial_t^\alpha H = d_H \Delta H + \mu - \mu H(x,t) - \beta_1 H(x,t)V(x,t) \\ \quad - \beta_2 H(x,t)I(x,t), \\ \partial_t^\alpha I = d_I \Delta I + \beta_1 H(x,t)V(x,t) + \beta_2 H(x,t)I(x,t) \\ \quad - \delta I(x,t), \\ \partial_t^\alpha V = d_V \Delta V + pI(x,t) - cV(x,t), \end{cases}$$

$$\tag{34}$$

where $H(x,t)$, $I(x,t)$, and $V(x,t)$ denote the concentrations of healthy cells, infected cells, and free viral particles at position x and at time t, respectively. The parameters d_H, d_I, and d_V represent, respectively, the diffusion coefficients of healthy cells, infected cells, and free viral particles.

The cells and virus are biological quantities which should be non-negative, and they also should not cross the boundary of the domain. Then, we consider system (34) with the homogeneous Neumann boundary conditions:

$$\frac{\partial H}{\partial \nu} = \frac{\partial I}{\partial \nu} = \frac{\partial V}{\partial \nu} = 0, \text{ on } \partial\Omega \times (0, +\infty), \tag{35}$$

and initial conditions:

$$H(x, 0) = H_0(x) \geq 0,$$
$$I(x, 0) = I_0(x) \geq 0,$$
$$V(x, 0) = V_0(x) \geq 0,$$
$$\forall x \in \overline{\Omega}. \tag{36}$$

The corresponding ordinary system of the above models is given by

$$\begin{cases} \dot{H} = \lambda - \mu H - \beta_1 HV - \beta_2 HI, \\ \dot{I} = \beta_1 HV + \beta_2 HI - \delta I, \\ \dot{V} = pI - cV. \end{cases} \tag{37}$$

This system admits a unique infection-free equilibrium $Q_f(H^0, 0, 0)$, where $H^0 = (\lambda/\mu)$. Further, the basic reproduction number is given by

$$\mathscr{R}_0 = \frac{\lambda(p\beta_1 + c\beta_2)}{c\delta\mu}. \tag{38}$$

This basic reproduction number is the sum of two basic reproduction numbers due to virus-to-cell and cell-to-cell transmissions. If $\mathscr{R}_0 > 1$, ODE model (37) has another biological steady state called the infection chronic which is labeled by $Q^*(H^*, I^*, V^*)$, where

$$H^* = \frac{\lambda}{d\mathscr{R}_0},$$

$$I^* = \frac{c\mu(R_0 - 1)}{p\beta_1 + c\beta_2}, \tag{39}$$

$$V^* = \frac{pc\mu(R_0 - 1)}{c(p\beta_1 + c\beta_2)}.$$

These two equilibria are also steady states of both models (33) and (34). First, we consider a Lyapunov functional for ODE model (37) at Q_f as follows:

$$L_1(u) = H^0 \Phi\left(\frac{H}{H^0}\right) + I + \frac{\beta_1 H^0}{c} V. \tag{40}$$

Calculating the time derivative of L_1 along the solution of (37), we get

$$\begin{aligned} \frac{dL_1}{dt} &= \nabla L_1(u) \cdot f(u) \\ &= \left(1 - \frac{H^0}{H}\right)(\lambda - \mu H - \beta_1 HV - \beta_2 HI) \\ &\quad + \beta_1 HV + \beta_2 HI - \delta I \\ &\quad + \frac{\beta_1 H^0}{c}(pI - cV) \\ &= \frac{-\mu}{H}(H - H^0)^2 + \delta I(\mathscr{R}_0 - 1). \end{aligned} \tag{41}$$

If $\mathscr{R}_0 \leq 1$, then $(dL_1/dt) \leq 0$ with equality if and only if $H = H^0$, $I = 0$ and $V = 0$. Therefore, the infection-free equilibrium Q_f is globally asymptotically stable when $\mathscr{R}_0 \leq 1$. Since

$$D_t^\alpha L_1(u) \leq \nabla L_1(u) \cdot f(u), \tag{42}$$

it follows from Theorem 1 (i) that L_1 is also a Lyapunov functional for FDE model (33) at Q_f.

Next, we construct a Lyapunov functional for fractional diffusion model (34) at Q_f as follows:

$$\mathscr{L}_1 = \int_\Omega L_1(u(x,t))dx. \tag{43}$$

We have

$$d_H \int_\Omega \nabla H \cdot \nabla\left(\frac{\partial L_1}{\partial H}\right)dx = d_H H^0 \int_\Omega \frac{|\nabla H|^2}{H^2}dx \geq 0,$$

$$d_I \int_\Omega \nabla I \cdot \nabla\left(\frac{\partial L_1}{\partial I}\right)dx = 0, \tag{44}$$

$$d_V \int_\Omega \nabla V \cdot \nabla\left(\frac{\partial L_1}{\partial V}\right)dx = 0.$$

Then, L_1 satisfies the condition (10). Using Theorem 1 (ii), we deduce that $\mathscr{L}_1$ is a Lyapunov functional for fractional diffusion systems (34)–(36) at Q_f if $\mathscr{R}_0 \leq 1$.

Based on the results in [17], the function

$$\begin{aligned} L_2(u) &= H - H^* - H^* \ln\frac{T}{T^*} + I - I^* - I^* \ln\frac{I}{I^*} \\ &\quad + \frac{\beta_1 H^* V^*}{pV^*}\left(V - V^* - V^* \ln\frac{V}{V^*}\right) \end{aligned} \tag{45}$$

is a Lyapunov functional for ODE model (37) at Q^* when $\mathscr{R}_0 > 1$. Let

$$\mathscr{L}_2 = \int_\Omega L_2(u(x,t))dx. \tag{46}$$

Since L_2 has the form given in (11), we conclude, by applying Corollary 2, that L_2 is a Lyapunov functional for FDE model (33) and $\mathscr{L}_2$ is a Lyapunov functional for fractional diffusion systems (34)–(36) at Q^* when $\mathscr{R}_0 > 1$.

Data Availability

The data used to support the findings of this study are available from the corresponding author upon request.

Conflicts of Interest

The authors declare that they have no conflicts of interest.

References

[1] N. Aguila-Camacho, M. A. Duarte-Mermoud, and J. A. Gallegos, "Lyapunov functions for fractional order systems," *Communications in Nonlinear Science and Numerical Simulation*, vol. 19, no. 9, pp. 2951–2957, 2014.

[2] M. A. Duarte-Mermoud, N. Aguila-Camacho, J. A. Gallegos, and R. Castro-Linares, "Using general quadratic Lyapunov functions to prove Lyapunov uniform stability for fractional order systems," *Communications in Nonlinear Science and Numerical Simulation*, vol. 22, no. 1-3, pp. 650–659, 2015.

[3] C. Vargas-De-León, "Volterra-type Lyapunov functions for fractional-order epidemic systems," *Communications in Nonlinear Science and Numerical Simulation*, vol. 24, no. 1-3, pp. 75–85, 2015.

[4] K. Hattaf and N. Yousfi, "Global stability for reaction-diffusion equations in biology," *Computers & Mathematics with Applications*, vol. 66, no. 8, pp. 1488–1497, 2013.

[5] J. Huo, H. Zhao, and L. Zhu, "The effect of vaccines on backward bifurcation in a fractional order HIV model,"

Nonlinear Analysis: Real World Applications, vol. 26, pp. 289–305, 2015.

[6] K. Hattaf and N. Yousfi, "A class of delayed viral infection models with general incidence rate and adaptive immune response," *International Journal of Dynamics and Control*, vol. 4, no. 3, pp. 254–265, 2016.

[7] D. L. DeAngelis, R. A. Goldstein, and R. V. O'Neill, "A model for tropic interaction," *Ecology*, vol. 56, no. 4, pp. 881–892, 1975.

[8] P. H. Crowley and E. K. Martin, "Functional responses and interference within and between year classes of a dragonfly population," *Journal of the North American Benthological Society*, vol. 8, no. 3, pp. 211–221, 1989.

[9] K. Hattaf, N. Yousfi, and A. Tridane, "Stability analysis of a virus dynamics model with general incidence rate and two delays," *Applied Mathematics and Computation*, vol. 221, pp. 514–521, 2013.

[10] H. A. A. El-Saka, "The fractional-order SIR and SIRS epidemic models with variable population," *Mathematical Sciences Letters*, vol. 2, no. 3, pp. 195–200, 2013.

[11] A. Mouaouine, A. Boukhouima, K. Hattaf, and N. Yousfi, "A fractional order SIR epidemic model with nonlinear incidence rate," *Advances in Difference Equations*, vol. 2018, no. 1, p. 160, 2018.

[12] K. Hattaf, A. Lashari, Y. Louartassi, and N. Yousfi, "A delayed SIR epidemic model with a general incidence rate," *Electronic Journal of Qualitative Theory of Differential Equations*, vol. 3, no. 3, pp. 1–9, 2013.

[13] M. A. Nowak and C. R. M. Bangham, "Population dynamics of immune responses to persistent viruses," *Science*, vol. 272, no. 5258, pp. 74–79, 1996.

[14] M. A. Nowak, S. Bonhoeffer, A. M. Hill, R. Boehme, H. C. Thomas, and H. McDade, "Viral dynamics in hepatitis B virus infection," *Proceedings of the National Academy of Sciences*, vol. 93, no. 9, pp. 4398–4402, 1996.

[15] S. M. Ciupe, R. M. Ribeiro, P. W. Nelson, and A. S. Perelson, "Modeling the mechanisms of acute hepatitis B virus infection," *Journal of Theoretical Biology*, vol. 247, no. 1, pp. 23–35, 2007.

[16] A. U. Neumann, N. P. Lam, H. Dahari et al., "Hepatitis C viral dynamics in vivo and the antiviral efficacy of interferon-therapy," *Science*, vol. 282, no. 5386, pp. 103–107, 1998.

[17] K. Hattaf and N. Yousfi, "Qualitative analysis of a generalized virus dynamics model with both modes of transmission and distributed delays," *International Journal of Differential Equations*, vol. 2018, Article ID 9818372, 7 pages, 2018.

WILEY | Hindawi

Research Article

Dual-Source Optimization of the "Diverting Water from the Yangtze River to Tai Lake (DWYRTL)" Project Based on the Euler Method

Ruichen Xu [1,2] **Yong Pang** [1,2] **Zhibing Hu,** [1,2] **and John Paul Kaisam** [1,2,3]

^{1}*Key Laboratory of Integrated Regulation and Resource Development on Shallow Lakes, Ministry of Education, Hohai University, Nanjing 210098, China*
^{2}*College of Environment, Hohai University, Nanjing 210098, China*
^{3}*Department of Chemistry, School of Environmental Sciences, Njala University, Freetown, Sierra Leone*

Correspondence should be addressed to Ruichen Xu; 1349439798@qq.com and Yong Pang; ypang@hhu.edu.cn

Appropriate water body diversion can improve the water quality of Tai Lake. Excessive diversion of water would, however, dramatically alter the local flow fields, which are not conducive to the growth of aquatic plants and the stability of ecosystems. The current "Diverting Water from the Yangtze River to Tai Lake (DWYRTL)" project uses a single water source, the Wangyu River, for diversion, a model that may significantly affect the nearby flow rate or uniformity of the lake and is not conducive to the long-term stability of the aquatic ecosystem in the Tai Lake district of the eastern part of the lake. In order to simulate the different situations of single- and dual-source water diversions (Wangyu-Xinmeng Rivers) in Tai Lake, we based this study on a three-dimensional hydrodynamic model coupled with the Euler method, which can accurately calculate the water exchange rates in the different districts of Tai Lake. The results show that (1) it is recommended that the total annual diversion of water should not exceed $20 \times 10^{8} \, m^{3}$; (2) the wind field is the most important factor determining the distribution of spatial water exchange; (3) under wind-free conditions, the flow rate of a single-source diversion of water is approximately 50% higher than that of dual-source diversion; and (4) water diversion under the prevailing conditions of the northwest wind in winter will reduce the semiexchange period of the eastern part of the lake area from 50 to 30 days, significantly changing the nearby district's uniformity, leading to ecological risks. Therefore, it is recommended that the dual-source water diversion mode be used in winter and windless season, and single-source water diversion mode be used in other seasons.

1. Introduction

Diverting water from the Yangtze River to Tai Lake (DWYRTL) is one of the major water conservation projects in the Tai Lake Basin. This diversion supplies a large amount of water resources to downstream areas including the city of Shanghai and Zhejiang Province while serving as one of the essential basic projects for social and economic development in the Yangtze River Delta [1]. However, the continuous increase in downstream water demand, the overflow rate, and the water exchange uniformity (WEU) index [2] will have a certain adverse effect on the stability of the aquatic

ecosystem. In particular, the East Lake District forms the region with the most complete aquatic ecosystem that can only be sustained by relying on diversion of the Wangyu River alone. The Wangyu River is very close to the district that is most sensitive to changes in hydrology, and an excessive diversion of water from the Wangyu River will have a significant impact on the East Lake District [3]. An uneven mixing of water bodies will also change the original aquatic environment, thereby reducing the survival rate of aquatic vegetation [4, 5]. Many scholars have found that cyanobacterial blooms will be directly affected by hydrodynamic forces and pollutant fluxes caused by water diversion [6, 7].

Therefore, further research and discussion are needed to determine whether this risk can be mitigated by the Wangyu-Xinmeng River dual-source diversion method.

At present, researchers have mainly used on-site monitoring and hydrodynamic models to study the flow velocity of water bodies. On-site monitoring may provide measured field data and basic boundary conditions for a hydrodynamic model. A hydrodynamic model can predict and compare different future scenarios quantitatively [8]. The exchange of water in a water body is mainly reflected by the water exchange rate and the semiexchange cycle [9]. Currently, water body exchange studies have mainly been conducted using the Lagrange method and the Euler method [10]. Based on a three-dimensional unsteady state model, Luff and Pohlmann [11] used the Lagrange method to study the exchange of water between water bodies (e.g., flushing-time, turn-over time, and half-life time) in the North Sea. However, the Lagrange method ignores the convective diffusion of water [12, 13]. By contrast, Euler's Method uses a conservative method, namely, a coupled convective diffusion model, to simulate the water body exchange in a local area [14].

Based on a current tidal model, Xie et al. [15] simulated the exchange of water in water bodies on an impounded lake in Taipingwan Port of Dalian, Liaoning Province, China. The simulation suggested that the construction of a submerged dike would hinder the exchange of water between water bodies, i.e., the elevation of the underwater soil would have a significant impact on the exchange capacity of regional water. Dai et al. [16] used an unstable state model to analyze the exchange of water bodies between Dongting Lake and Yangtze River before and after the implementation of the Three Gorges Project. Dai and colleagues have identified a significant change in the amount of water entering and exiting the lake and documented an extended period of water body exchange during the postconstruction phase. Based on the three-dimensional Euler algorithm of the Environmental Fluid Dynamics Code, Xu et al. [17] examined the exchange of water between water bodies in urban man-made lakes and obtained good results for some recently completed projects through optimizations. Water body exchange research based on the Euler method can, therefore, more intuitively and accurately reflect the unique influence of water diversion on the exchange of water between water body in a large scale and local areas of Tai Lake.

Most of the studies on the DWYRTL project only considered a single-source water diversion model, which may lose another viable solution if the demand for water resources is met, but a dual-source diversion may be able to resolve the related problems [18]. Among them, Li et al. [19] analyzed the relationship between the diversion of the Wangyu River and the hydrodynamic conditions of Tai Lake, determined the basic hydrodynamic parameters of Tai Lake, and optimized the economic applicability of the water diversion project. During the implementation of WDYRTL in the Wangyu River basin, Yang et al. [20] revealed that short-term water diversion would cause a deterioration in the quality of water in the Gong Bay area. Qing [21] adopted a two-dimensional unsteady state model to assess the hydrodynamic conditions and water quality of the Taihu River after the diversion of water from the Xinmeng River to Tai Lake. The study suggested that the diversion of the Xingeng River would improve the aquatic environment of Tai Lake, but comprehensive control would be needed to prevent the most negative effects of single-channel drainage on the quality of water in the Yangtze River. Yong [22] studied the environmental changes of Tai Lake after the diversion of the Xingeng River. The study not only found that the aquatic environment improved in the Northwest Lake District but also documented the relatively poor water diversion efficiency from the Yangtze River and the associated water diversion management conditions. In general, there are still some drawbacks with regard to the optimization of dual-source water diversion in different situations.

This study involved the construction of a three-dimensional hydrodynamic mathematical model based on the measured data acquired from 2017 to 2018. The changes in nearby flow velocity were studied and analyzed using different diversion models and scales. The calculation of the water exchange rate and the semiexchange period for eight wind field conditions prevailing at different time periods was coupled with the Euler algorithm during the analysis. The calculation of the water exchange rate and semiexchange period of the eight main districts of Tai Lake were expected to be obtained, and a more in-depth study of the difference and linkages between single-source diversion and dual source diversion should continue in order to provide a scientific reference for future diversion strategies. The paper mainly discusses (1) the research area, (2) the research method, (3) results and discussion, and (4) conclusions.

2. Study Area

Tai Lake, located at the lower reaches of the Yangtze River Basin ($119°08'$–$122°55'$E, $30°05'$–$32°08'$N), covers an area of $2,338\,km^2$ to a maximum water depth of up to 3 m. This typical large shallow lake [23] has been previously divided into three lake bay districts and five major water areas in order to accurately analyze the water exchange characteristics of the various areas of the lake [24]. Using data downloaded from the China Meteorological Data Network (http://data.cma.cn/), in the last decade, Tai Lake was mainly affected by the easterly winds in autumn and mainly affected by the southeastern and northwestern monsoons in spring-summer and winter, respectively (Figure 1). According to the Tai Lake Basin Authority, Ministry of Water Resources (http://www.tba.gov.cn/), the DWYRTL project consists mainly of the Xinmeng River Extension Project, the Xingou River Extension Project, and the Wangyu River Project, where the first and last of these projects directly divert water from the Yangtze River into Tai Lake. In the last decade, the average annual water intake was 7.5 billion m^3, with the main water diversion periods occurring between January-March, July-August, and October-December and the longest continuous water diversion period being 90 days [16].
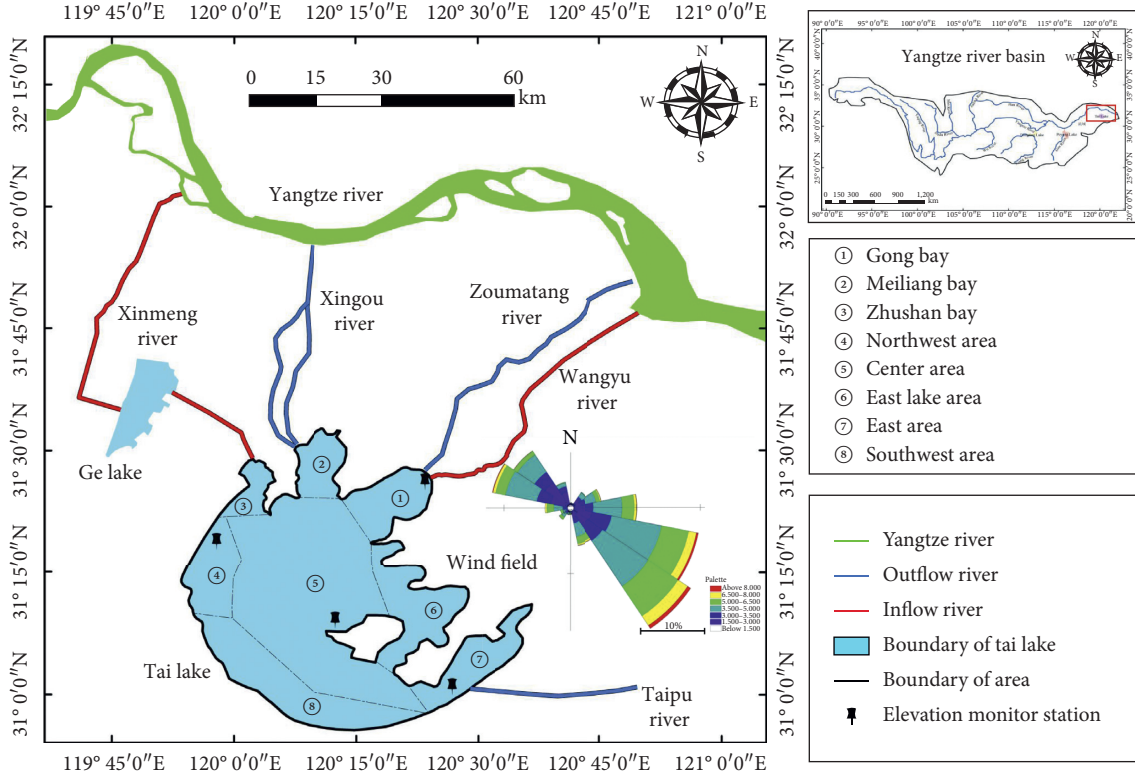
FIGURE 1: Map showing the location of water diversion from the Yangtze River to Tai Lake project. An inset map shows the location of the study area within China.

From 1990 to 2017, the amount of water diverted from the Yangtze River to the west of the Wangyu River increased annually [25], with the annual amount of water diversion increasing from 1.6 billion m³ to 5.2 billion m³ during this period—an increase of 225% (Figure 2). Over the same period, the total amount of water entering the lake also increased, while the number of days of water exchange in Tai Lake decreased correspondingly year-on-year, from 266 days to 160 days, by 39.8%.

3. Methodology

3.1. 3D Hydrodynamic Model. To accurately calculate the volume of water body exchange, this study employed a hydrodynamic model used in this study that is based on the Navier–Stokes equations of three-way incompressible flow and Reynolds values and was subject to the assumption of Boussinesq and hydrostatic pressure. The finite volume method was applied to calculate the spatial discretization. Its mathematic expression is shown in the equations below [26].

The water flow continuity equation is given by the following equation:

$$\frac{\partial u}{\partial x} + \frac{\partial v}{\partial y} + \frac{\partial w}{\partial z} = S. \tag{1}$$

The Navier–Stokes equations for horizontal momentum in the *X* and *Y* directions are shown in equations (2) and (3), respectively:

$$\frac{\partial u}{\partial t} + \frac{\partial u^2}{\partial x} + \frac{\partial vu}{\partial y} + \frac{\partial wu}{\partial z} = fv - g\frac{\partial \eta}{\partial x} - \frac{1}{\rho_0}\frac{\partial P_a}{\partial x} -$$
$$\frac{g}{\rho_0}\int_z^\eta \frac{\partial p}{\partial x}dz - \frac{1}{\rho_0 h}\left(\frac{\partial s_{xx}}{\partial x} + \frac{\partial s_{xy}}{\partial y}\right) + F_u + \frac{\partial}{\partial z}\left(v_t\frac{\partial u}{\partial z}\right) + u_s S, \tag{2}$$

$$\frac{\partial v}{\partial t} + \frac{\partial v^2}{\partial x} + \frac{\partial vu}{\partial y} + \frac{\partial wv}{\partial z} = fv - g\frac{\partial \eta}{\partial x} - \frac{1}{\rho_0}\frac{\partial P_a}{\partial x} -$$
$$\frac{g}{\rho_0}\int_z^\eta \frac{\partial p}{\partial x}dz - \frac{1}{\rho_0 h}\left(\frac{\partial s_{yx}}{\partial x} + \frac{\partial s_{yy}}{\partial y}\right) + Fv + \frac{\partial}{\partial z}\left(v_t\frac{\partial v}{\partial z}\right) + v_s S, \tag{3}$$

where *t* represents time; *x*, *y*, and *z* are the Cartesian coordinates; *u*, *v*, and *w* are the components of velocity along the *x*, *y*, and *z* coordinate directions, respectively; f_u and f_v are the Coriolis accelerations along the *X* and *Y* coordinate directions; $f = 2\Omega \sin \varphi$ represents the Coriolis factor (Ω is the angular velocity of the Earth's rotation, and φ is the geographic latitude); *g* is the acceleration of gravity; η represents the water level; ρ_0 and ρ represent the density of air and water, respectively; P_a is the atmospheric pressure; *h* represents the total water depth; S_{xx}, S_{xy}, and S_{yy} are the radiation stress tensors; v_t is the vertical vortex viscosity coefficient; *S* is the source-sink term; and F_u and F_v are the horizontal stresses along the *X* and *Y* coordinate directions, respectively. The flow velocity gradient-stress relationships can be expressed by
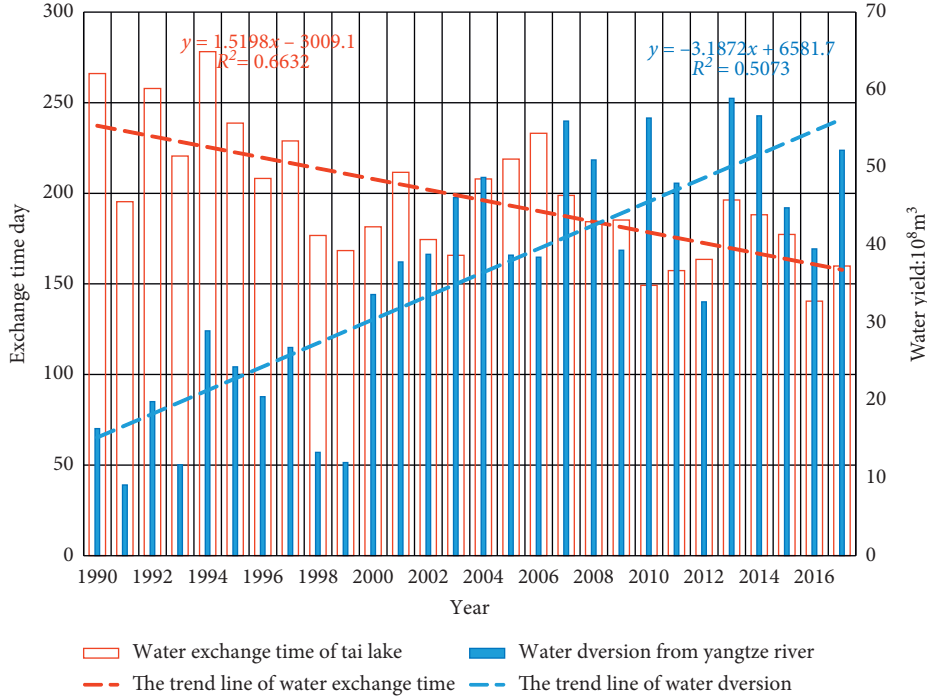
FIGURE 2: Trends in the amount of water entering Tai Lake from 1990 to 2017 and its water body exchange time.

$$F_u = \frac{\partial}{\partial x}\left(2A\frac{\partial u}{\partial x}\right) + \frac{\partial}{\partial x}\left(A\left(\frac{\partial u}{\partial y} + \frac{\partial v}{\partial x}\right)\right),$$

$$F_v = \frac{\partial}{\partial y}\left(2A\frac{\partial v}{\partial y}\right) + \frac{\partial}{\partial x}\left(A\left(\frac{\partial u}{\partial y} + \frac{\partial v}{\partial x}\right)\right),$$

$$(4)$$

where A is the horizontal eddy viscosity coefficient.

3.2. Convective Diffusion Model.
To simulate the water exchange more intuitively and accurately, we use a convective diffusion model based on the Euler method, given by [27], as seen in equation (5):

$$\frac{\partial(hC)}{\partial t} + \frac{\partial(uhC)}{\partial x} + \frac{\partial(vhC)}{\partial y} = \frac{\partial}{\partial x}\left(E_x h\frac{\partial C}{\partial x}\right) + \frac{\partial}{\partial y}\left(E_y h\frac{\partial C}{\partial y}\right) + S,$$

$$(5)$$

where C is the contaminant concentration; E_x, and E_y are the diffusion coefficients in the X and Y directions, respectively. According to the Elder empirical formula, it can be known that

$$E_x = \frac{5.93\sqrt{g}n|hu|}{h^{1/6}},$$

$$E_y = \frac{5.93\sqrt{g}n|hv|}{h^{1/6}},$$

$$(6)$$

where n is the Manning coefficient.

3.3. Water Body Exchange Research Methods.
A dissolved conservation substance with an initial concentration of 100 mg/L was placed in the lake body (note that the initial

concentration in the lake water was zero). After a certain period of convective diffusion, the ratio of the total amount of the remaining substance in the various areas of Tai Lake to the total amount of the initial substance is the water exchange rate of the region at that moment as shown in equation (7). An exchange rate that reaches 50% of the time is the semiexchange period [28].

$$\text{EX}(t_j) = 1 - \left[\frac{\sum_{i=1}^{M} C_i(t_j)H_i(t_j)}{\sum_{i=1}^{M} C_i(t_0)H_i(t_0)}\right] \times 100\%,$$

$$(7)$$

where EX is the water exchange rate; H is the water depth; i is the grid number in the calculated area; and j is the specific time number.

Based on the constructed model, we will extract the nodes and grids of different districts (taking Gong Bay as an example), calculate the local water exchange rate, and then, determine the semiexchange period of different districts under this scenario through the water exchange method (Figure 3).

4. Results and Discussions

4.1. Determining the Model Parameter Rates.
In order to ensure that the constructed hydrodynamic model can meet the research needs of water body exchange studies, the water body was divided into 9422 nonstructural grids with a spatial resolution of 300 m; data acquired from 2017 to 2018 were employed. After calibration and verification of the depth of the lake, measurements of the coefficient of turbulence, the height of the bottom friction, and the wind drag coefficient were estimated at 0.28, 0.02 m, and 0.003 m, respectively. The simulation results were well aligned with the measured water
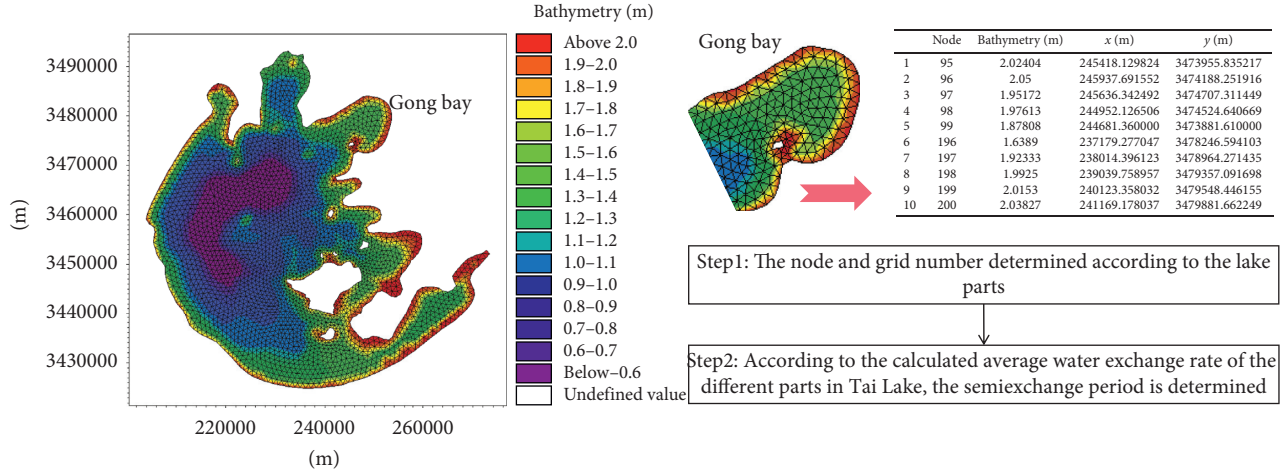
Bathymetry (m)
Above 2.0
1.9–2.0
1.8–1.9
1.7–1.8
1.6–1.7
1.5–1.6
1.4–1.5
1.3–1.4
1.2–1.3
1.1–1.2
1.0–1.1
0.9–1.0
0.8–0.9
0.7–0.8
0.6–0.7
Below–0.6
Undefined value

Node	Bathymetry (m)	x (m)	y (m)
1	95	2.02404	245418.129824	3473955.835217
2	96	2.05	245937.691552	3474188.251916
3	97	1.95172	245636.342492	3474707.311449
4	98	1.97613	244952.126506	3474524.640669
5	99	1.87808	244681.360000	3473881.610000
6	196	1.6389	237179.277047	3478246.594103
7	197	1.92333	238014.396123	3478964.271435
8	198	1.9925	239039.758957	3479357.091698
9	199	2.0153	240123.358032	3479548.446155
10	200	2.03827	241169.178037	3479881.662249

Step1: The node and grid number determined according to the lake parts

Step2: According to the calculated average water exchange rate of the different parts in Tai Lake, the semiexchange period is determined

FIGURE 3: Two-step approach used to calculate the semiexchange period of Tai Lake using bathymetry data.

level at each monitoring station (Figure 4). The flow field structure simulated by the southeast and northwest monsoons at a speed of 5 m/s had exactly the same circulation shape as the measured results (Figure 5). The results in direction and velocity of circulation flow were also consistent with the results reported in previous studies [29].

In order to further compare the simulated water levels with the measured values, this study uses three model evaluation methods, namely, average relative error (MRE), root mean square error (RMSE), and correlation coefficient analysis (R^2). The evaluation process involves an error and correlation analysis of the measured values (M) and simulated values (S) with the following formulations [30]:

$$
\begin{aligned}
\text{RMSE} &= \sqrt{\frac{1}{N} \sum_{i=1}^{N} (S_i - M_i)^2}, \\
\text{MRE} &= \frac{1}{N} \sum_{i=1}^{N} |S_i - M_i|, \\
R^2 &= \frac{\sum_{i=1}^{N} (S_i - \overline{S})(M_i - \overline{M})}{\sqrt{\sum_{i=1}^{N} (S_i - \overline{S})^2 \sum_{i=1}^{N} (M_i - \overline{M})^2}},
\end{aligned}
\tag{8}
$$

where N is the number of times of total simulation; i is the number of times of simulation; S_i is the value of the ith simulation; M_i is the value of the ith measurement; $\overline{S}$ is the simulated average value; and $\overline{M}$ is the measured average value.

The assessment results of the four stations (Table 1) show that the simulated water levels fit well with the measured water levels (the highest water level error <0.09 m). Simulation results can account for more than 90% of the actual situation. As a result, the constructed hydrodynamic model met the requirements for subsequent water body exchange research.

4.2. Optimizing the DWYRTL Project. Wind field conditions (i.e., windless and 5 m/s in either easterly, southeasterly, or northwesterly directions) were determined in accordance

with the climatic conditions of Tai Lake [31]. Following the relationship between the level of flood control at Tai Lake and the ecologically accepted water level, the initial water level was set at 3.25 m in the model [32], while the total calculation time was set at 60 days; this depended on the average time between 2007 and 2017, with the time step at 86,400 s. Based on these settings (Table 2), the exchange characteristics of Tai Lake under the conditions of single-source diversion of the Wangyu River and dual-source diversion of the Wangyu and Xinmeng rivers were simulated. Also, because this simulation was primarily a comparative study, it was assumed that other external conditions remained unchanged; that is, the effects of rainfall, runoff, and evaporation were not considered separately.

Ignoring wind conditions, the simulation outputs show that Gong Bay, Center District, and East Lake District were the main areas of the water exchange operating mode (a), but the water quality of the Yangtze River was poor compared to that of the exchange area (Figure 6). In addition, dependence on a single source of water diversion from the Wangyu River would increase the concentration of water with poor quality in this region while reducing the water capacity of Tai Lake. In addition, the flow field would be subjected to frequent changes that would not be appropriate for the growth of aquatic plants and the restoration of aquatic ecosystems. The operation mode (b) would significantly reduce the effects on the flow field in the East Lake District, ensuring the stability of the ecosystem as long as the volume of water and the hydrological conditions are constant. This is true because the dual-source common diversion areas would include the water body exchange areas of Zhushan Bay and the Northwest Lake District. As an auxiliary measure, the diversion of water bodies should not be used to meet the unconditional needs of the society or the economy. Operating modes (c) and (d) indicate that when water diversion is extended to 400 m³/s, approximately 45% of Tai Lake water would be exchanged within 60 days, while the Tai Lake water body exchange period under natural conditions is approximately 300 days. This suggests that this level of water body diversion has caused significant disturbances to the aquatic
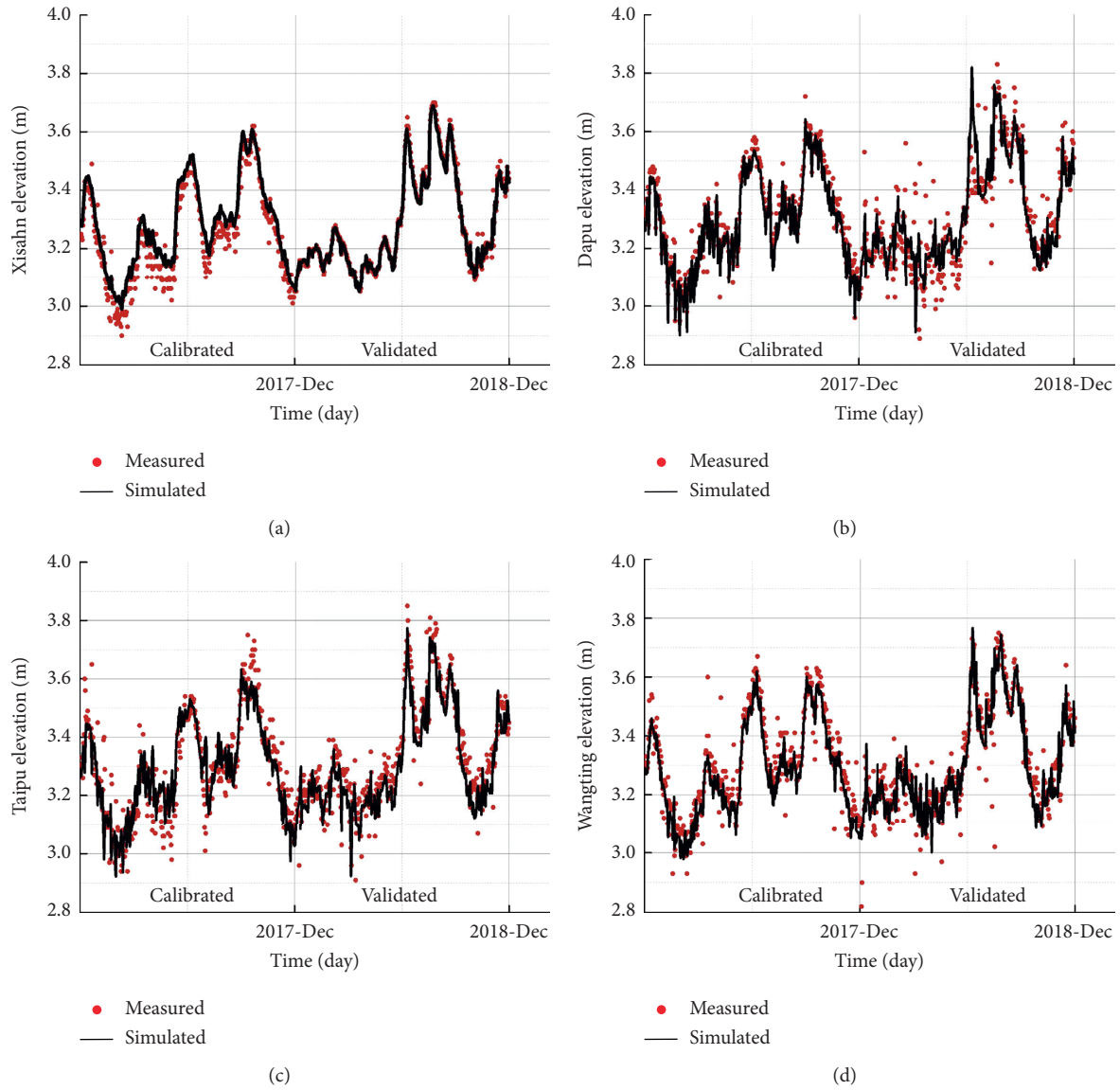
(a)

(b)

(c)

(d)

Figure 4: Calibration and verification of surface elevation: (a) Xishan, (b) Dapu, (c) Taipu, and (d) Wangting monitoring station elevations.
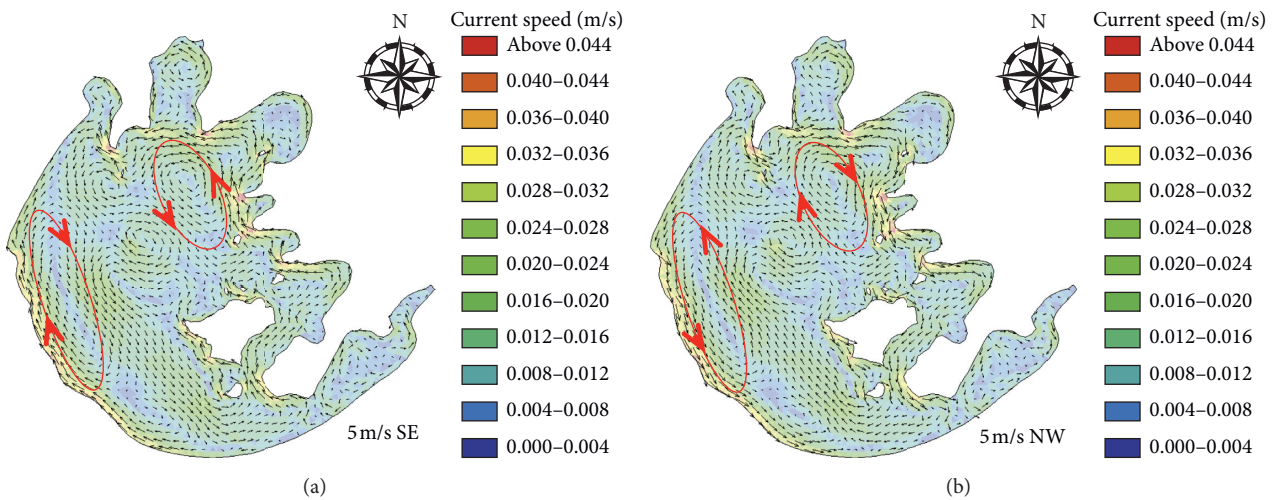

(a)

(b)

Figure 5: Verification of flow fields with winds at 5 m/s from the (a) southeast and (b) northwest.

TABLE 1: Model calculation evaluation.

Monitor	Year	RMSE	MRE (%)	R^2
Xishan	2017	0.056	4.66	0.971
	2018	0.018	1.30	0.995
Dapu	2017	0.039	3.06	0.976
	2018	0.100	6.64	0.839
Taipu	2017	0.049	3.51	0.968
	2018	0.075	6.12	0.923
Wangting	2017	0.059	4.37	0.934
	2018	0.087	6.02	0.876

TABLE 2: Simulated operating mode under different water diversion and hydrological conditions.

Scene	Time	Wind speed/(m/s)	Wind direction	Wangyu River/(m³/s)	Xinmeng River/(m³/s)	Taipu River/(m³/s)
a	All year	0	—	200	0	−200
b	All year	0	—	100	100	−200
c	All year	0	—	400	0	−400
d	All year	0	—	200	200	−400
e	Spring-Summer	5	SE	200	0	−200
f		5	SE	100	100	−200
g	Autumn	5	E	200	0	−200
h		5	E	100	100	−200
i	Winter	5	NW	200	0	−200
j		5	NW	100	100	−200
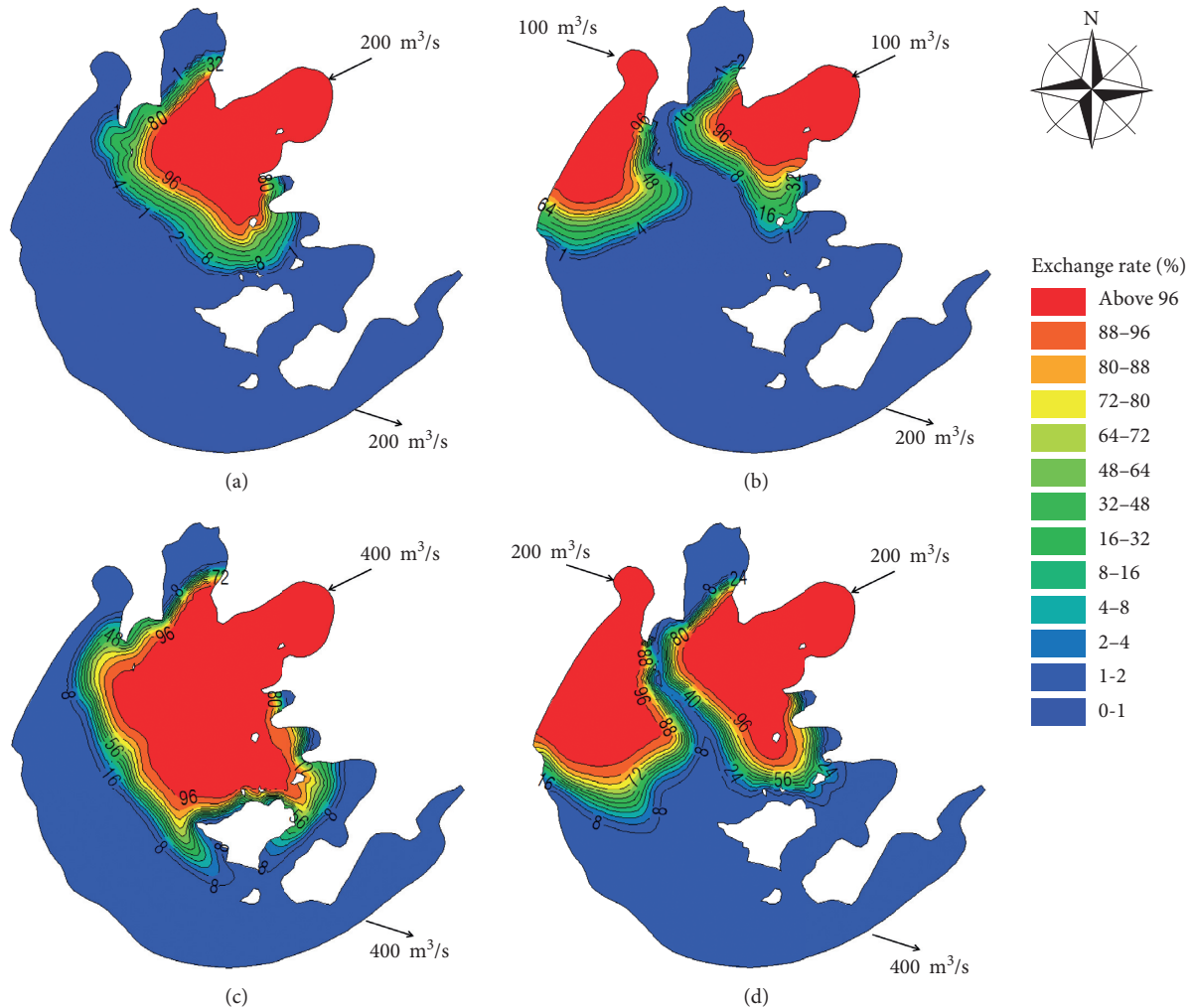
FIGURE 6: Simulated water body exchange rates under operating modes (a)–(d) as described in the main text.

(a)

(b)
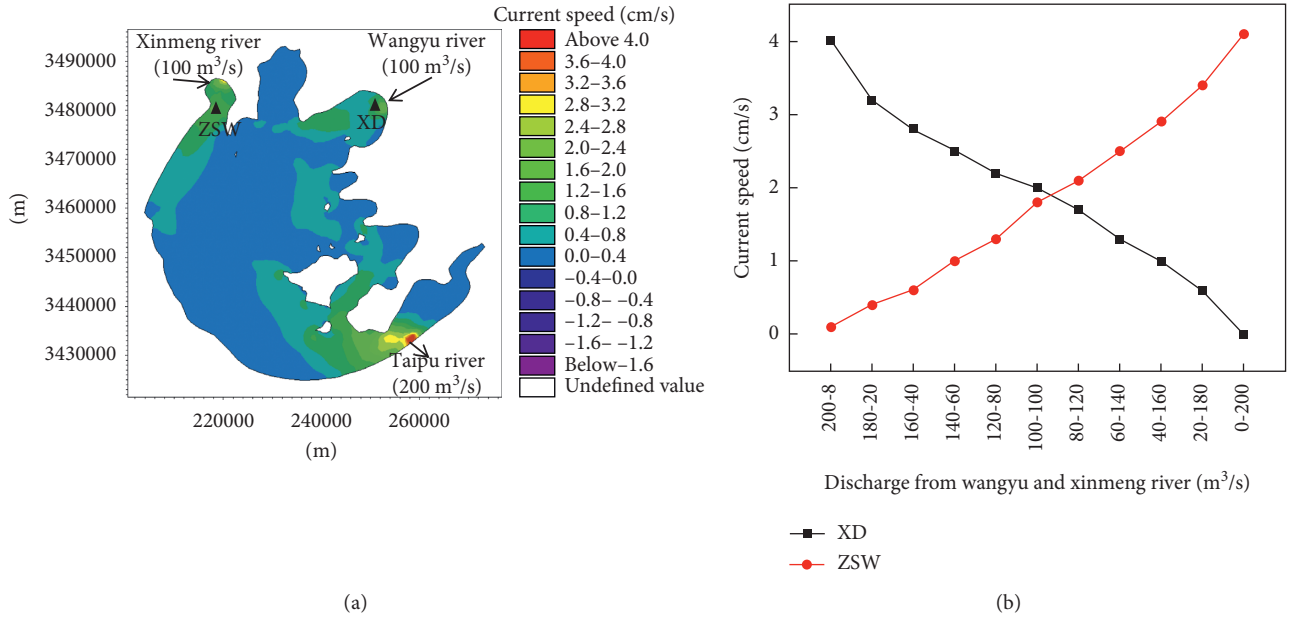
Figure 7: (a) Map of Tai Lake showing the speed of water flow, and (b) flow rates in different levels of water diversion from the Yangtze River to Tai Lake scales from the Wangyu and Xingmeng rivers.

environment of Tai Lake, which would have a serious impact on the storage capacity of Tai Lake and the stability of the aquatic ecosystem [28]. It is recommended that the total water intake in the future should not exceed 20% of the total annual lake water intake, i.e., $20 \times 10^8 \, \text{m}^3/\text{a}$.

The rate at which water flows through Tai Lake is mainly affected by the wind field and the exchange rate of water; an excessive flow rate will have a certain adverse effect on the stability of the ecosystem [33–35]. The flow field of the surrounding area will be controlled by the inflow-outflow discharge under windless conditions. Under the different diversion scales of the Wangyu and Xingeng rivers, the changes in velocity at two monitoring points, XD and ZSW, can be seen in Figure 7. From the calculation results and the change in flow rate, the flow rate of a single-source water diversion ($200 \, \text{m}^3/\text{s}$) is predicted to be approximately 50% higher than that of a dual-source water diversion ($100 \, \text{m}^3/\text{s}$ average), i.e., the best strategy under wind-free conditions is to divert water from the Wangyu and Xingeng rivers by $100 \, \text{m}^3/\text{s}$. At this time, water diversion has the lowest impact on the different districts and contributes to the stability of the ecosystem [36].

The simulation results show that when the total amount of water is $200 \, \text{m}^3/\text{s}$, the Tai Lake water exchange rate is approximately 20% over the four seasons, regardless of whether the water diversion method is a single- or a dual-source (Figure 8). This indicates that the water exchange rate is not mainly related to the amount of water entering/leaving the lake but related to the spatiotemporal distribution of the exchange of the water body, which depends primarily on the wind field [37]. This occurs because the wind field mainly determines the flow field of large shallow lakes. Single-source water diversion is prone to creating an imbalance in hydrodynamics, which makes it difficult to replace the water

in Zhushan Bay and the western lake areas where pollution is serious and algae easily accumulate. The water exchange areas created by dual-source flow were predicted to be 18.84%, 16.24%, and 15.02% higher than when single-source water diversion occurs in the same areas during the spring-summer, autumn, and winter seasons. These changes may enhance the hydrodynamics of the western lake region under the influence of the southeastern monsoon in spring and summer; meanwhile, the hydrodynamics of Zhushan and Meiliang bays are under the influence of the north-western monsoon in winter. Consequently, taking into account both economic benefits of a dual-source system and local meteorological conditions, it is vital that appropriate methods of water diversion be chosen in accordance with the needs of different periods.

By conducting a statistical analysis of the eight major sublake areas of Tai Lake, we found that the water exchange rate and the semiexchange period of the eight districts under ten operating modes would change significantly. The results of the present study show the wind field has a significant impact on the spatiotemporal water exchange rate and the semiexchange period (Table 3, e, g, and i and f, h, and j), which is consistent with the conclusion of Safak [38]. The most significant change for the East Lake District would occur when single-source water diversion is carried out in the Wangyu River during winter. Its semiexchange period would be 29–30 days, i.e., 60 days of water diversion can completely replace the water volume of the East Lake District, which is unfavorable to the stability of the eco-system of the East Lake District [39]. However, if dual-source water diversion is adopted in winter for optimization purposes, the water exchange period would increase to 102 days, which would significantly reduce the negative impact on the eastern lake region. The joint-source diversion
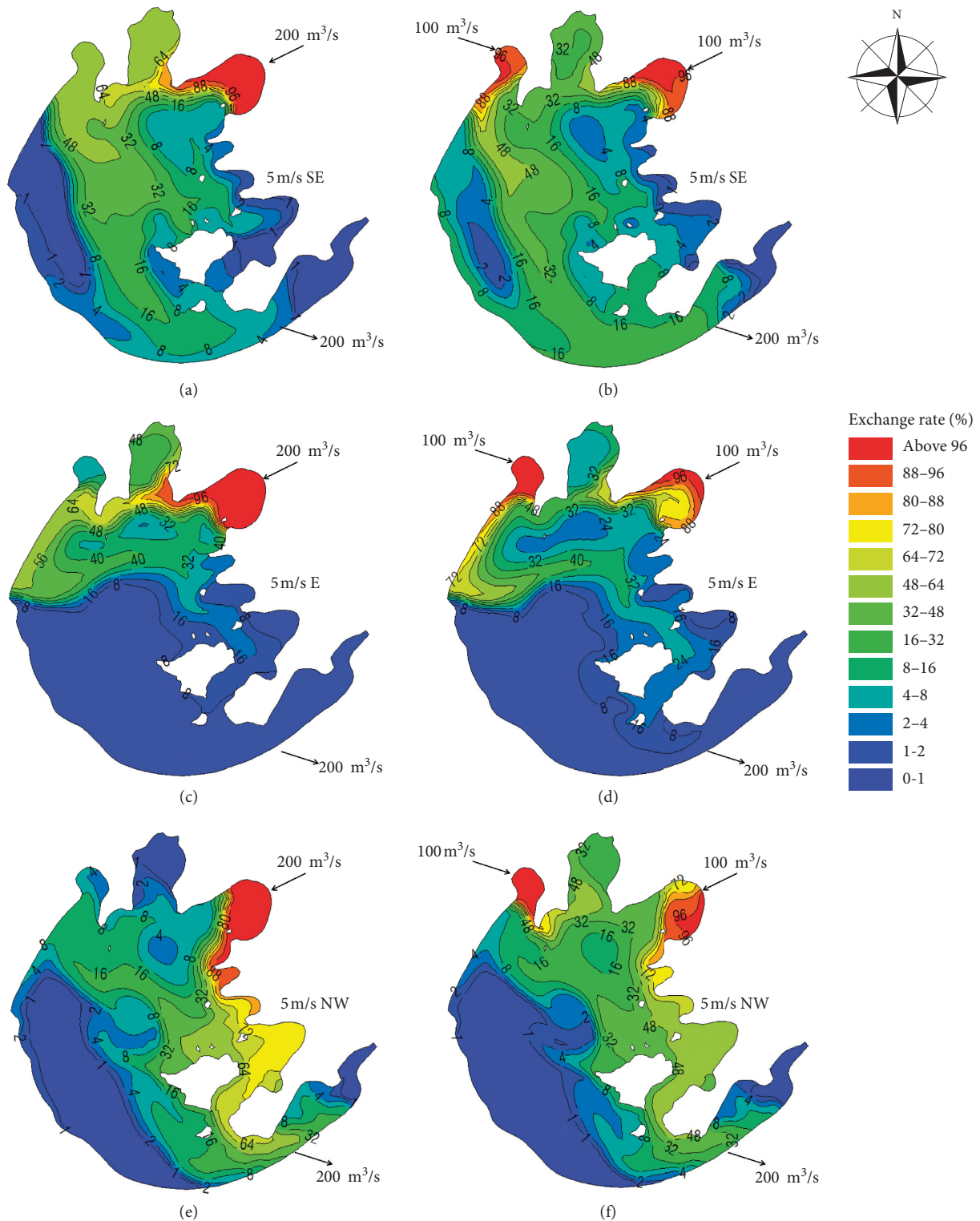
FIGURE 8: Water exchange rate simulation results for operating modes (e)–(j).

method for the Wangyu-Xingeng rivers should, therefore, be adopted in winter, with each river water volume accounting for half of the total amount of diverted water. During spring and summer, different methods of diversion of water should be applied in accordance with the actual need to replace the water body in particular areas. Specifically, when an

exchange of water is required in the Meiliang Bay area, a single-source diversion method is recommended for the Wangyu River; when an exchange of water is required in the western lake area, the Wangyu River-Xingeng River joint-source diversion method should be adopted with 50% of the water contributed by the Wangyu River. In autumn, sewage

TABLE 3: Water exchange rate and the semiexchange period of eight lake districts under ten operating modes.

Scene	Indicator	Gong Bay	Meiliang Bay	Zhushan Bay	Center area	Northwest area	Southwest area	East Lake	East area
a	EX (%)	100	21.07	0.32	29.51	0	0	5.58	0
	SEP (day)	7–8	—	—	—	—	—	—	—
b	EX (%)	99.72	8.69	99.99	15.25	53.99	0	0.54	0
	SEP (day)	16–17	—	5~6	—	54~55	—	—	—
c	EX (%)	100	32.32	9.27	62.27	3.72	0.01	45.68	0
	SEP (day)	3–4	—	—	48~49	—	—	—	—
d	EX (%)	100	20.43	100	43.32	89.76	2.69	16.58	0
	SEP (day)	8–9	—	3~4	—	37~38	—	—	—
e	EX (%)	65.60	59.08	55.19	9.64	9.33	1.52	3.35	1.57
	SEP (day)	8–9	47~48	53~54	—	—	—	—	—
f	EX (%)	51.60	35.93	77.97	9.91	19.46	11.68	4.74	7.63
	SEP (day)	53–54	—	9~10	—	—	—	—	—
g	EX (%)	83.07	55.15	50.43	17.73	40.28	0.32	12.73	0
	SEP (day)	8–9	52~53	59~60	—	—	—	—	—
h	EX (%)	64.43	36.78	83.15	18.62	47.08	1.24	19.01	2.47
	SEP (day)	34–35	—	8~9	—	—	—	—	—
i	EX (%)	72.74	7.81	30.57	18.55	3.82	1.66	70.49	20.19
	SEP (day)	7–8	—	—	—	—	—	29~30	—
j	EX (%)	68.68	36.19	80.09	19.18	2.22	0.77	54.93	12.91
	SEP (day)	18–19	—	6~7	—	—	—	50~51	—

"/" means that the semiexchange period (SEP) has not been reached within the calculation time and no value is assigned.

TABLE 4: Three optimal water diversion strategies.

Strategy	Wangyu River (m³/s)	Xinmeng River (m³/s)	Wind field	Index optimization
1	100	100	Windless	Flow rate
2	200	0	E, SE (4 m/s)	Evenness for the east part of Tai Lake
3	100	100	NW (4 m/s)	Evenness for the east part of Tai Lake

from the western part of the lake would flow rapidly to the East Lake District under the influence of the easterly wind flow. In this case, a single-source water diversion of the Wangyu River should be undertaken so that pollutants in the heart of the lake can be neutralized and the impact on the ecosystem of the East Lake District can be reduced.

Using the modeled results above, all strategies were analyzed according to the flow rate and uniformity index [40]. It was found that more attention should be paid to the effects of the flow rate, which will change the stability of the ecosystem. When the wind field dominates the flow field, more attention should be paid to the water exchange uniformity index, which will have a significant impact on the large forms of wetland vegetation [2]. Finally, this study sets out the scientifically sound management strategies (Table 4) for the "DWYRTL" project based on the specific conditions of the wind field.

5. Conclusions

First, an appropriate type of water body diversion can improve the water quality of Tai Lake. Excessive diversion of water would, however, dramatically alter the local flow fields, which would not be conducive to the growth of aquatic plants and the stability of various parts of the Tai Lake ecosystem. Excessive diversion would also have serious effects on the original storage capacity and the natural ability of the lake to adjust to various types of changing conditions.

Therefore, the WDYRTL project should not unintentionally expand the scale of water diversion in the future. It is recommended that the total annual diversion of water should not exceed 20% of the total intake of water, i.e., $20 \times 10^8 \, \text{m}^3/\text{a}$. The optimization of water management can be carried out by combining weather forecast information with the dual-source water diversion mode.

Second, the exchange rate of water depends mainly on the amount of water entering/exiting the lake. Ignoring wind conditions, the flow rate of a single-source water diversion is approximately 50% higher than that of dual-source water diversion. In southeastern monsoon conditions, the exchange of water occurs mainly in three lake bay areas and in the center of the lakes. Under the conditions of the east monsoon, water exchange rates will be the highest in three lake bay areas and the Northwest Lake area. Meanwhile, during the northwest monsoon, water exchange will primarily occur in the Center and East Lake districts. In a sense, the wind field is predicted to be the key factor determining the spatiotemporal distribution of the water exchange area.

Third, under normal conditions, the dual-source water diversion method has many more advantages than the single-source water diversion method; however, some differences would recommend use of the single-source method at times. In spring and summer, single- and double-source water diversion methods should be selected based on the needs of the actual water replacement areas. In autumn, a single-source water diversion method is preferable to ensure

both an adequate water supply in the West Lake area and the stability of the aquatic ecosystem in the East Lake area. In winter, the Wangyu-Xinmeng River dual-source water diversion method is recommended, with each river accounting for 50% of the total amount diverted water.

Data Availability

The other data used to support the findings of this study are included within the article.

Conflicts of Interest

The authors declare that they have no conflicts of interest.

Acknowledgments

References

[1] Y. Qin, Q. Wen, Y. Ma, C. Yang, and Z. Liu, "Antibiotics pollution in gonghu bay in the period of water diversion from Yangtze River to Taihu lake," *Environmental Earth Sciences*, vol. 77, pp. 1–11, 2018.

[2] Y. Pan, L. Jin, Z.-H. Wei et al., "Experimental evidence that water-exchange unevenness affects individual characteristics of two wetland macrophytes Phalaris arundinacea and Polygonum hydropiper," *Ecological Indicators*, vol. 107, p. 105617, 2019.

[3] A. B. G. Janssen, V. C. L. de Jager, J. H. Janse et al., "Spatial identification of critical nutrient loads of large shallow lakes: implications for Lake Taihu (China)," *Water Research*, vol. 119, pp. 276–287, 2017.

[4] Q. Zhang, Y.-S. Xu, L. Huang et al., "Does mechanical disturbance affect the performance and species composition of submerged macrophyte communities?" *Scientific Reports*, vol. 4, no. 1, p. 4888, 2015.

[5] H. Gao, X. Qian, H. Wu, H. Li, H. Pan, and C. Han, "Combined effects of submerged macrophytes and aquatic animals on the restoration of a eutrophic water body-A case study of Gonghu Bay, Lake Taihu," *Ecological Engineering*, vol. 102, pp. 15–23, 2017.

[6] P. Zhang, R.-F. Liang, P.-X. Zhao et al., "The hydraulic driving mechanisms of cyanobacteria accumulation and the effects of flow pattern on ecological restoration in lake dianchi caohai," *International Journal of Environmental Research and Public Health*, vol. 16, no. 3, p. 361, 2019.

[7] T. Wu, B. Qin, J. D. Brookes et al., "The influence of changes in wind patterns on the areal extension of surface cyanobacterial blooms in a large shallow lake in China," *Science of The Total Environment*, vol. 518-519, pp. 24–30, 2015.

[8] X. Zhang, R. Zou, Y. Wang et al., "Is water age a reliable indicator for evaluating water quality effectiveness of water diversion projects in eutrophic lakes?" *Journal of Hydrology*, vol. 542, pp. 281–291, 2016.

[9] Y. Li, J. Šimůnek, S. Wang, W. Zhang, and J. Yuan, "Simulating the effects of lake wind waves on water and solute exchange across the lakeshore using hydrus-2D," *Water*, vol. 9, no. 8, p. 566, 2017.

[10] F. Christian, R. Arturas, G. Saulius, U. Georg, and B. Lina, "Hydraulic regime-based zonation scheme of the Curonian Lagoon," *Hydrobiologia*, vol. 611, no. 1, pp. 133–146, 2008.

[11] R. Luff and T. Pohlmann, "Calculation of water exchange times in the ICES-boxes with a eulerian dispersion model using a half-life time approach," *Deutsche Hydrographische Zeitschrift*, vol. 47, no. 4, pp. 287–299, 1995.

[12] K. Cui-ping, D. Zhi-chao, G. Jie, Z. Hua-ming, and Z. Wei, "Impact of dredging project on water exchange of Qilihai Lagoon wetland," *China Environmental Science*, vol. 39, pp. 343–350, 2019.

[13] P. A. Lozovik, M. B. Zobkov, G. S. Borodulina, and I. V. Tokarev, "Effects of external water exchange between bays of lakes on chemical indicators of water," *Vodnye Resursy*, vol. 46, pp. 91–101, 2019.

[14] A. Cucco, G. Umgiesser, C. Ferrarin, A. Perilli, D. M. Canu, and C. Solidoro, "Eulerian and Lagrangian transport time scales of a tidal active coastal basin," *Ecological Modelling*, vol. 220, no. 7, pp. 913–922, 2009.

[15] M. X. Xie, M. G. Li, M. Y. Mai, and W. D. Li, "Numerical modeling of the water exchange ability of the artificial lake at Taiping Bay Harbor, Dalian," *Journal of Waterway and Harbor*, vol. 39, pp. 17–24, 2018.

[16] J. Dai, S. Wu, X. Wu et al., "Effects of water diversion from Yangtze River to lake Taihu on the phytoplankton habitat of the Wangyu River channel," *Water*, vol. 10, no. 6, p. 759, 2018.

[17] L. Xu, X. Gao, C. Zhang, and C. Wang, "Numerical simulation-based study on exchange of water in urban artificial lake," *Water Resources and Hydropower Engineering*, vol. 49, pp. 94–100, 2018.

[18] Y. Li, C. Tang, J. Zhu et al., "Parametric uncertainty and sensitivity analysis of hydrodynamic processes for a large shallow freshwater lake," *Hydrological Sciences Journal*, vol. 60, no. 6, pp. 1078–1095, 2015.

[19] Y. Li, C. Tang, C. Wang et al., "Assessing and modeling impacts of different inter-basin water transfer routes on Lake Taihu and the Yangtze River, China," *Ecological Engineering*, vol. 60, pp. 399–413, 2013.

[20] Q. Yang, S. Wu, J. Dai, X. Wu, W. Xue, and F. Liu, "Effects of short-term water diversion in summer on water quality and algae in Gonghu Bay, Lake Taihu." *Journal of Lake Sciences*, vol. 30, pp. 34–43, 2018.

[21] G. Qing, "Research on influence of Xinmeng River dredging and extending project on water environment of Yangtze River," *Yangtze River*, vol. 47, p. 20, 2016.

[22] Z. Yong, "Research on effects of water diversion and drainage engineering on water environment improvement in Taihu lake—a case of Xinmeng river," *Pearl River*, vol. 4, pp. 37–40, 2014.

[23] A. Jalil, Y. Li, K. Zhang et al., "Wind-induced hydrodynamic changes impact on sediment resuspension for large, shallow Lake Taihu, China," *International Journal of Sediment Research*, vol. 34, no. 3, pp. 205–215, 2019.

[24] L. Jiang, Y. Li, X. Zhao et al., "Parameter uncertainty and sensitivity analysis of water quality model in Lake Taihu, China," *Ecological Modelling*, vol. 375, pp. 1–12, 2018.

[25] Z. Yan, H. Yang, H. Dong et al., "Occurrence and ecological risk assessment of organic micropollutants in the lower reaches of the Yangtze River, China: a case study of water diversion," *Environmental Pollution*, vol. 239, pp. 223–232, 2018.

[26] L. Zhu, R. Hu, H. Zhu, S. Jiang, Y. Xu, and N. Wang, "Modeling studies of tidal dynamics and the associated responses to coastline changes in the Bohai Sea, China," *Ocean Dynamics*, vol. 68, no. 12, pp. 1625–1648, 2018.

[27] H. Wang, M. Wu, Y. Deng, C. Tang, and R. Yang, "Surface water quality monitoring site optimization for Poyang Lake, the largest freshwater lake in China," *International Journal of Environmental Research and Public Health*, vol. 11, no. 11, pp. 11833–11845, 2014.

[28] R. Xu, Y. Pang, Z. Hu, T. Zhu, and J. P. Kaisam, "Influence of water diversion on spatial and temporal distribution of flow field and total phosphorus (TP) concentration field in Taihu Lake," *Water Supply*, vol. 20, no. 3, pp. 1059–1071, 2020.

[29] J. Huang, Q. Xu, B. Xi et al., "Impacts of hydrodynamic disturbance on sediment resuspension, phosphorus and phosphatase release, and cyanobacterial growth in Lake Tai," *Environmental Earth Sciences*, vol. 74, no. 5, pp. 3945–3954, 2015.

[30] Y. Li, S. Zhou, Z. Jia et al., "Influence of industrialization and environmental protection on environmental pollution: a case study of Taihu lake, China," *International Journal of Environmental Research and Public Health*, vol. 15, no. 12, p. 2628, 2018.

[31] J. Wang, Q. Zhao, Y. Pang, Y. Li, Z. Yu, and Y. Wang, "Dynamic simulation of sediment resuspension and its effect on water quality in Lake Taihu, China," *Water Supply*, vol. 17, no. 5, pp. 1335–1346, 2017.

[32] M. Kong, J. Chao, W. Zhuang et al., "Spatial and temporal distribution of particulate phosphorus and their correlation with environmental factors in a shallow eutrophic Chinese lake (lake Taihu)," *International Journal of Environmental Research and Public Health*, vol. 15, no. 11, p. 2355, 2018.

[33] J. Yao, Y. Li, D. Zhang, Q. Zhang, and J. Tao, "Wind effects on hydrodynamics and implications for ecology in a hydraulically dominated river-lake floodplain system: poyang Lake," *Journal of Hydrology*, vol. 571, pp. 103–113, 2019.

[34] A. Jalil, Y. Li, W. Du et al., "Wind-induced flow velocity effects on nutrient concentrations at Eastern Bay of Lake Taihu, China," *Environmental Science and Pollution Research*, vol. 24, no. 21, pp. 17900–17911, 2017.

[35] D.-y. Yuan, X. Meng, C.-q. Duan et al., "Effects of water exchange rate on morphological and physiological characteristics of two submerged macrophytes from Erhai Lake," *Ecology and Evolution*, vol. 8, no. 24, pp. 12750–12760, 2018.

[36] J.-P. Descy, F. Leprieur, S. Pirlot et al., "Identifying the factors determining blooms of cyanobacteria in a set of shallow lakes," *Ecological Informatics*, vol. 34, pp. 129–138, 2016.

[37] A. Jalil, Y. Li, W. Du et al., "The role of wind field induced flow velocities in destratification and hypoxia reduction at Meiling Bay of large shallow Lake Taihu, China," *Environmental Pollution*, vol. 232, pp. 591–602, 2018.

[38] I. Safak, P. L. Wiberg, D. L. Richardson, and M. O. Kurum, "Controls on residence time and exchange in a system of shallow coastal bays," *Continental Shelf Research*, vol. 97, pp. 7–20, 2015.

[39] F. Li, Y. Pan, Y. Xie et al., "Different roles of three emergent macrophytes in promoting sedimentation in Dongting Lake, China," *Aquatic Sciences*, vol. 78, no. 1, pp. 159–169, 2015.

[40] C. Tang, Y. Yi, Z. Yang, S. Zhang, and H. Liu, "Effects of ecological flow release patterns on water quality and ecological restoration of a large shallow lake," *Journal of Cleaner Production*, vol. 174, pp. 577–590, 2018.

Research Article

Pattern Dynamics of Nonlocal Delay SI Epidemic Model with the Growth of the Susceptible following Logistic Mode

Zun-Guang Guo,[1,2] Jing Li [ID],[3] Can Li,[1] Juan Liang [ID],[1] and Yiwei Yan[1]

[1]*Department of Science, Taiyuan Institute of Technology, Taiyuan, Shanxi 030008, China*
[2]*Department of Computer Science and Technology, North University of China, Taiyuan, Shanxi 030051, China*
[3]*College of Applied Mathematics, Shanxi University of Finance and Economics, Taiyuan, Shanxi 030006, China*

Correspondence should be addressed to Jing Li; jingli_2016@126.com

In this paper, we investigate pattern dynamics of a nonlocal delay SI epidemic model with the growth of susceptible population following logistic mode. Applying the linear stability theory, the condition that the model generates Turing instability at the endemic steady state is analyzed; then, the exact Turing domain is found in the parameter space. Additionally, numerical results show that the time delay has key effect on the spatial distribution of the infected, that is, time delay induces the system to generate stripe patterns with different spatial structures and affects the average density of the infected. The numerical simulation is consistent with the theoretical results, which provides a reference for disease prevention and control.

1. Introduction

Research on infectious disease models can be traced back to the pioneering work of Kermack and Mckendrick [1, 2], and the traditional model is usually described by ordinary differential equations as a result of the spatially homogeneous assumption [3–10]. Considering the instantaneous change, researchers have established epidemic models via impulsive differential equations [11–15]. However, besides the change of time, the spatial distribution of populations has an significant effect on diseases transmission. As a matter of fact, spatial distribution of the population is not homogeneous, but depend on the spatial location and the surrounding environment factors, such as the amount of food, the number of natural enemies, and the number of the infected [16, 17]. Therefore, considering the space in epidemic models is more suitable for the spread process of infectious diseases. Recently, many reaction-diffusion models have been proposed to study their dynamical behaviors and study the corresponding control measures [18–29].

Since they can reach the current position from any other positions in the whole space when humans or animals are

moving in space, which is more reflective for the actual situation, therefore, the nonlocal delay of infectious disease has become a research focus in epidemiology. Wang and Wu [30] studied the Kermack–Mckendrick SIR model with nonlocal delay and discussed the dynamic properties of disease spatial diffusion. Pan [31] studied the existence of wave front solutions for a class of infectious disease models with nonlocal diffusion and time delay by constructing upper and lower solutions. Zhen et al. [32] also obtained the traveling wave solutions for a class of SIR epidemic models with spatiotemporal delays. Using the upper and lower solutions and its related monotone iterative techniques, Tang et al. [33] studied the sufficient conditions for the global asymptotic stability of the disease-free equilibrium of the bird system.

Most of the abovementioned studies focus on the traveling wave solutions and global stability of the nonlocal epidemic model. However, few literatures study the pattern formation of infectious disease models based on reaction-diffusion equation with nonlocal delay. Pattern dynamics can effectively characterize the spatial distribution of the infected, so as to provide decision-making guidance for the

government. In fact, in the natural environments with limited resources, the assumption of logistic growth is more consistent with the actual situation [34–37]; then, we assume the susceptible possess the logistic growth in the absence of

$$
\begin{cases}
\dfrac{\partial S}{\partial t} = D_S \Delta S + rS\left(\left(1 - \dfrac{S}{K}\right)\right) - \beta S \dfrac{\int_{-\infty}^{t}\int_{\Omega} Q(x - y, t - s)I(y,s)\mathrm{d}y\mathrm{d}s}{S + I} - dS - AS, \\[4mm]
\dfrac{\partial I}{\partial t} = D_I \Delta I + \beta S \dfrac{\int_{-\infty}^{t}\int_{\Omega} Q(x - y, t - s)I(y,s)\mathrm{d}y\mathrm{d}s}{S + I} - \mu I - dI,
\end{cases}
\tag{1}
$$

with initial boundary value condition

$$
(\overrightarrow{n} \cdot \nabla)\begin{pmatrix} S \\ I \end{pmatrix} = 0, S(x,0), I(x,0) \text{ are given}, \tag{2}
$$

and the descriptions of the symbols in model (1) are shown in Table 1. The kernel function $Q(x, t) = (1/4\pi t)\exp(-|x|^2/4t)(1/\tau)\exp(-(t/\tau))$ represents the weight from the other possible positions to the position (HTML translation failed) before time t. The nonlocal item.depicts the cumulative number of the infected reaching x position at t time who starts from any y position in the entire space at s time.

$$
\int_{-\infty}^{t}\int_{R^2} Q(x - y, t - s)I(y,s)\mathrm{d}s\,\mathrm{d}y. \tag{3}
$$

In order to study the spatiotemporal dynamics of model (1), in Section 2, we first obtain the steady states of model (1), linearize the model at the endemic steady state, and then analyze the conditions of system generating Turing instability and parameter space of Turing pattern generated. In Section 3, different stripe patterns are shown for different time delays, which indicates that time delay affects the structures of Turing patterns. In Section 4, the summary and discussion are given.

2. Linear Analysis and Turing Patterns

In this section, we define a new variable $V(x, t)$ to replace the nonlocal term $\int_{-\infty}^{t}\int_{R^2} Q(x - y, t - s)I(y,s)\mathrm{d}y\mathrm{d}s$; then, system (1) can be transformed into 3-variable reaction-diffusion system:

$$
\frac{\partial \mathbf{c}}{\partial t} = \mathbf{F}(\mathbf{c}) + D\Delta\mathbf{c}, \tag{4}
$$

where

$$
\mathbf{c} = \begin{pmatrix} S \\ I \\ V \end{pmatrix},
$$

the infected. In addition, we take the standard incidence ratio to describe the infection between the susceptible and the infected. To this end, we propose the following model:

$$
\mathbf{F}(\mathbf{c}) = \begin{pmatrix} rS\left(1 - \dfrac{S}{K}\right) - \dfrac{\beta SV}{S + I} - (d + A)S \\[4mm] \dfrac{\beta SV}{S + I} - (\mu + d)I \\[4mm] \dfrac{1}{\tau}(I - V) \end{pmatrix},
$$

$$
D = \begin{pmatrix} D_S & & \\ & D_I & \\ & & 1 \end{pmatrix}. \tag{5}
$$

By studying system (4) without diffusion, so the ordinary differential equation is given:

$$
\frac{\mathrm{d}S(t)}{\mathrm{d}t} = rS(t)\left(1 - \frac{S(t)}{K}\right) - \frac{\beta S(t)V(t)}{S(t) + I(t)} - (d + A)S(t),
$$

$$
\frac{\mathrm{d}I(t)}{\mathrm{d}t} = \frac{\beta S(t)V(t)}{S(t) + I(t)} - (\mu + d)I(t),
$$

$$
\frac{\mathrm{d}V(t)}{\mathrm{d}t} = \frac{1}{\tau}(I(t) - V(t)),
\tag{6}
$$

system (6) has two constant steady states $E_0 = (S_0, I_0, V_0) = (K(r - A - d)/r, 0, 0)$ and $E_1^* = (S_1^*, I_1^*, V_1^*)$, where

$$
S_1^* = \frac{K(r + \mu - A - \beta)}{r},
$$

$$
I_1^* = \frac{K(r + \mu - A - \beta)(\beta - d - \mu)}{r(d + \mu)}, \tag{7}
$$

$$
V_1^* = \frac{K(r + \mu - A - \beta)(\beta - d - \mu)}{r(d + \mu)}.
$$

According to the actually biological situation, the population number should be nonnegative. So, if $r > A + d$ holds, then $S_0 > 0$, that is, E_0 is disease-free steady states. In addition, if the condition

$$
\text{(H1)} \quad r > A + \beta - \mu, \quad \beta > \mu + d, \tag{8}
$$

TABLE 1: Symbol descriptions of model (1).

Symbol	Interpretations
$S(x,t)$	The density of the susceptible at position $x(x \in R^2)$ at time t
$I(x,t)$	The density of the infected at position $x(x \in R^2)$ at time t
A	The emigration rate of the susceptible
Ω	The diffusion domain
$\overrightarrow{n}$	Unit outward normal to $\partial\Omega$
$\partial\Omega$	The closed boundary of the diffusion domain Ω
Δ	Laplace operator $(\partial^2/\partial X^2) + (\partial^2/\partial Y^2)$
D_S	The diffusion rate of the susceptible
D_I	The diffusion rate of the infected
β	The infection rate
μ	The mortality rate due to infectious disease caused
d	The natural mortality
r	The intrinsic growth rate
K	The carrying capacity

is satisfied, then $S_1^* > 0$, $I_1^* > 0$, and $V_1^* > 0$, which shows that E_1^* is the endemic steady state.

The main focus of infectious diseases is to study the outbreak and prevalence, so as to provide theoretical guidance for the prevention and control of infectious diseases. Then, the following contents only study endemic steady state E_1^*.

Through setting

$$\mathbf{w} = \begin{pmatrix} S - S_1^* \\ I - I_1^* \\ V - V_1^* \end{pmatrix}, \tag{9}$$

we substitute (9) into (4), expand $\mathbf{F}(\mathbf{c})$ at the endemic steady state E_1^* based on Talyor expansion, and then obtain the following linear equation:

$$\frac{\partial \mathbf{w}}{\partial t} = D\Delta\mathbf{w} + \mathbf{J}\mathbf{w}, \mathbf{J} = \begin{pmatrix} a_{11} & a_{12} & a_{13} \\ a_{21} & a_{22} & a_{23} \\ a_{31} & a_{32} & a_{33} \end{pmatrix}, \tag{10}$$

where

$$
\begin{aligned}
a_{11} &= \frac{A\beta + \beta^2 + \beta d - \beta r - d^2 - 2d\mu - \mu^2}{\beta}, \\
a_{12} &= \frac{(\beta - d - \mu)(d + \mu)}{\beta}, \\
a_{13} &= -d - \mu, \\
a_{21} &= \frac{(\beta - d - \mu)^2}{\beta}, \\
a_{22} &= -\frac{2\beta d + 2\beta\mu - d^2 - 2d\mu - \mu^2}{\beta}, \\
a_{23} &= d + \mu, \\
a_{31} &= 0, \\
a_{32} &= \frac{1}{\tau}, \\
a_{33} &= -\frac{1}{\tau}.
\end{aligned} \tag{11}
$$

In order to solve the solution of system (10) satisfying the boundary condition (2), we first define $\mathbf{W}(x)$ as the time-independent spatial eigenvalue problem, which satisfies the following system:

$$\Delta\mathbf{W} + k^2\mathbf{W} = 0, (\overrightarrow{n} \cdot \nabla)\mathbf{W} = 0, \quad \text{for } x \text{ on } \partial\Omega, \tag{12}$$

where k is the eigenvalue (i.e., wavenumber).

We now look for solutions $\mathbf{w}(x,t)$ of (10) in the form

$$\mathbf{w}(x,t) = \begin{pmatrix} C_1 \\ C_2 \\ C_3 \end{pmatrix} e^{\lambda t + i\overrightarrow{k} \cdot x}, \tag{13}$$

where $\overrightarrow{k}$ is the wave vector with magnitude $k = |\overrightarrow{k}|$. By inserting (13) into (10), the characteristic equation matrix is obtained:

$$|J - \lambda E - D| = 0, \tag{14}$$

which is equivalent as follows:

$$\lambda^3 + a_2(k)\lambda^2 + a_1(k)\lambda + a_0(k) = 0, \tag{15}$$

with

$$a_2(k) = (D_S + D_I + 1)k^2 - A - \beta + d + 2\mu + r + \frac{1}{\tau},$$

$$
\begin{aligned}
a_1(k) = &(D_S + D_I + D_S D_I)k^4 \\
&- \frac{1}{\beta\tau}\big((A\beta D_I\tau + \beta^2 D_I\tau - 2\beta d D_S\tau + \beta d D_I\tau - 2\beta D_S\mu\tau - \beta D_I r\tau \\
&+ d^2 D_S\tau - d^2 D_I\tau + 2d D_S\mu\tau - 2d D_I\mu\tau + D_S\mu^2\tau - D_I\mu^2\tau + A\beta\tau \\
&+ \beta^2\tau - \beta d\tau - 2\beta\mu\tau - \beta r\tau - \beta D_S - \beta D_I)k^2\big) - \frac{1}{\beta\tau}(2A\beta d\tau
\end{aligned}
$$

$$+ 2A\beta\mu\tau - Ad^2\tau - 2A\,d\mu\,\tau - A\mu^2\tau + 3\beta^2 d\tau + 3\beta^2\mu\tau - 2\beta d^2\tau$$

$$- 6\beta\,d\mu\,\tau - 2\beta\,dr\,\tau - 4\beta\mu^2\tau - 2\beta\mu r\tau + d^2\mu\tau + d^2 r\tau + 2\,d\mu^2\tau$$

$$+ 2\,d\mu\,r\tau + \mu^3\tau + \mu^2 r\tau + A\beta + \beta^2 - \beta\mu - \beta r\big),$$

$$a_0(k) = D_S D_I k^6 - \frac{1}{\beta\tau}\Big(\big(A\beta D_I\tau + \beta^2 D_I\tau - 2\beta\,dD_S\tau + \beta\,dD_I\tau - 2\beta D_S\mu\tau$$

$$- \beta D_I r\tau + d^2 D_S\tau - d^2 D_I\tau + 2\,dD_S\mu\tau - 2\,dD_I\mu\tau + D_S\mu^2\tau - D_I\mu^2\tau$$

$$-\beta D_S D_I\big)k^4\Big) - \frac{1}{\beta\tau}\Big(\big(2A\beta\,d\tau + 2A\beta\mu\tau - Ad^2\tau - 2A\,d\mu\,\tau$$

$$- A\mu^2\tau + 3\beta^2 d\tau + 3\beta^2\mu\tau - 2\beta d^2\tau - 6\beta\,d\mu\,\tau - 2\beta\,dr\,\tau - 4\beta\mu^2\tau$$

$$- 2\beta\mu r\tau + d^2\mu\tau + d^2 r\tau + 2\,d\mu^2\tau + 2\,d\mu\,r\tau + \mu^3\tau + \mu^2 r\tau$$

$$+ A\beta D_I + \beta^2 D_I - \beta\,dD_S + \beta\,dD_I - \beta D_S\mu - \beta D_I r + d^2 D_S$$

$$-d^2 D_I + 2\,dD_S\mu - 2\,dD_I\mu + D_S\mu^2 - D_I\mu^2\big)k^2\Big)$$

$$- \frac{(d + \mu)(-d + \beta - \mu)(A + \beta - \mu - r)}{\beta\tau},$$

$$(16)$$

where $a_2(k) > 0$ for any k because of condition (H1) satisfied.

Moreover, one can obtain the corresponding characteristic equation for system (6) as follows:

$$\lambda^3 + a_2(0)\lambda^2 + a_1(0)\lambda + a_0(0) = 0, \qquad (17)$$

where

$$a_2(0) = -A - \beta + d + 2\mu + r + \frac{1}{\tau},$$

$$a_1(0) = -\frac{1}{\beta\tau}\big(2A\beta\,d\tau + 2\,d\mu\,r\tau + \mu^3\tau$$

$$+ \mu^2 r\tau + A\beta + \beta^2 - \beta\mu - \beta r$$

$$+ 2A\beta\mu\tau - Ad^2\tau - 2A\,d\mu\,\tau - A\mu^2\tau$$

$$+ 3\beta^2 d\tau + 3\beta^2\mu\tau - 2\beta d^2\tau \qquad (18)$$

$$-6\beta\,d\mu\,\tau - 2\beta\,dr\,\tau - 4\beta\mu^2\tau - 2\beta\mu r\tau$$

$$+ d^2\mu\tau + d^2 r\tau + 2\,d\mu^2\tau\big),$$

$$a_0(0) = -\frac{(d + \mu)(\beta - d - \mu)(A + \beta - \mu - r)}{\beta\tau}.$$

On the basis of condition (H1), one can derive $a_2(0) > 0$ and $a_0(0) > 0$. According to Hurwitz criterion, the condition for the local asymptotic stability of E_1^* of system (6) is

$$(H2)\, a_2(0)a_1(0) - a_0(0) > 0. \qquad (19)$$

Theorem 1. *The nonspatial system (6) gives rise to a Hopf bifurcation at endemic steady state E_1^* if only and if the condition*

$$(H3)\, a_2(0)a_1(0) - a_0(0) = 0, \qquad (20)$$

is established.

Proof. It is obvious that $a_2(0) > 0$ and $a_0(0) > 0$ due to the existence of endemic equilibrium E_1^* (i.e., (H1)). According to the theorem of [38], when conditions $a_2(0) > 0$, $a_0(0) > 0$, and $a_2(0)a_1(0) - a_0(0) = 0$ hold, a Hopf bifurcation occurs for nonspatial system (6).

Next, we find the conditions under which system (4) generates Turing instability near endemic steady state E_1^*: E_1^* is locally asymptotic stability for system (6), but E_1^* loses stability for system (6) with diffusion (i.e., system (4)). Furthermore, we already know $a_2(k) > 0$ for any k, while the signs of $a_0(k)$ and $a_2(k)a_1(k) - a_0(k)$ are uncertain. Now, we need to look for the condition that E_1^* of system (4) becomes unstable. Obviously, Hurwitz criterion is not satisfied, that is, $a_0(k) < 0$ or $a_2(k)a_1(k) - a_0(k) < 0$; then, the corresponding instability conditions are given. Based on such two cases, we derive the following theorems with respect to Turing instability. □

Theorem 2. *For system (4), if condition (H1) holds, and one of the following conditions*

(C1) $h_1 < 0$ and $H_2(z_1) < 0$

(C2) $h_1 > 0$, $h_2 < 0$, $(h_2)^2 - 3h_3 h_1 > 0$ and $H_2(z_1) < 0$

is satisfied, then endemic steady state E_1^* is unstable for some k, where

$$z_1 = \frac{-h_2 + \sqrt{(h_2)^2 - 3h_3h_1}}{3h_3}. \tag{21}$$

Proof. Let $z = k^2 > 0$ and $H_2(k^2) = a_0(k)$, then $H_2(z) = h_3z^3 + h_2z^2 + h_1z + h_0$, where

$h_3 = D_S D_I > 0,$

$h_2 = -\frac{1}{\beta\tau}\big(A\beta D_I\tau + \beta^2 D_I\tau - 2\beta dD_S\tau + \beta dD_I\tau$

$\quad - 2\beta D_S\mu\tau - \beta D_S D_I$

$\quad -\beta D_I r\tau + d^2 D_S\tau - d^2 D_I\tau + 2 dD_S\mu\tau$

$\quad - 2 dD_I\mu\tau + D_S\mu^2\tau - D_I\mu^2\tau\big),$

$h_1 = -\frac{1}{\beta\tau}\big(2A\beta d\tau + 2A\beta\mu\tau - Ad^2\tau - 2A d\mu\,\tau$

$\quad - A\mu^2\tau + 3\beta^2 d\tau + 3\beta^2\mu\tau - 2\beta d^2\tau - 6\beta d\mu\,\tau$

$\quad - 2\beta dr\,\tau - 4\beta\mu^2\tau$

$\quad - 2\beta\mu r\tau + d^2\mu\tau + d^2 r\tau + 2 d\mu^2\tau + 2 d\mu\,r\tau + \mu^3\tau + \mu^2 r\tau$

$\quad + A\beta D_I + \beta^2 D_I - \beta dD_S + \beta dD_I - \beta D_S\mu - \beta D_I r + d^2 D_S$

$\quad -d^2 D_I + 2 dD_S\mu - 2 dD_I\mu + D_S\mu^2 - D_I\mu^2\big),$

$h_0 = -\dfrac{(d + \mu)(-d + \beta - \mu)(A + \beta - \mu - r)}{\beta\tau} > 0.$

$$\tag{22}$$

Considering the properties of cubic polynomials, the coefficient of the third order of $H_2(z)$ is greater than zero and $H_2(0) = h_0 > 0$. By solving the first-order derivative $H_2(z)$ about z, namely, $H_2'(z) = 3h_3z^2 + 2h_2z + h_1 = 0$, we can deduce

$$z_2 = \frac{-h_2 - \sqrt{(h_2)^2 - 3h_3h_1}}{3h_3} \le z_1 = \frac{-h_2 + \sqrt{(h_2)^2 - 3h_3h_1}}{3h_3}. \tag{23}$$

(i) If condition $h_1 < 0$ holds, then one can obtain $z_2 < 0 < z_1$, which further shows that z_1 is the minimum point. Then, we can get $a_2(k) < 0$ for some k when $H_2(z_{2,\min}) < 0$ combining with $H_2(0) = h_0 > 0$ (see Figure 1(a)).

(ii) If conditions $h_1 > 0$, $h_2 < 0$, and $(h_2)^2 - 3h_3h_1 > 0$ hold, then we can get $0 < z_2 < z_1$, and z_2 and z_1 are maximum and minimum points, respectively. Furthermore, according to $H_2(z_1) < 0$, one can derive that $a_2(k) < 0$ for some k (see Figure 1(b)).

Obviously, Hurwitz criterion does not hold for Case (i) or Case (ii), and then the endemic steady state E_1^* is unstable for system (4).

Thus, the conditions of system (4) generating Turing instability is given:

$$\begin{cases} \text{(H1),} & \text{(H2),} \\ \text{(C1) or,} & \text{(C2).} \end{cases} \tag{24}$$

In addition, we set $H_3(z) = a_2(k)a_1(k) - a_0(k)$ and $z = k^2 > 0$, that is,

$$H_3(z) = h_{q_3}z^3 + h_{q_2}z^2 + h_{q_1}z + h_{q_0}, \tag{25}$$

where

$h_{q_3} = (D_I + 1)(D_S + 1)(D_S + D_I) > 0,$

$h_{q_2} = -\dfrac{1}{\tau\beta}\big(2A\beta D_S D_I\tau + A\beta D_I^2\tau + 2\beta^2 D_S D_I\tau + \beta^2 D_I^2\tau - 2\beta dD_S^2\tau$

$\quad - 2\beta dD_S D_I\tau + \beta dD_I^2\tau - 2\beta D_S^2\mu\tau - 4\beta D_S D_I\mu\tau - 2\beta D_S D_I r\tau$

$\quad - \beta D_I^2 r\tau + d^2 D_S^2\tau - d^2 D_I^2\tau + 2 dD_S^2\mu\tau - 2 dD_I^2\mu\tau + D_S^2\mu^2\tau$

$\quad - D_I^2\mu^2\tau + 2A\beta D_S\tau + 2A\beta D_I\tau + 2\beta^2 D_S\tau + 2\beta^2 D_I\tau - 2\beta dD_S\tau$

$\quad - 2\beta dD_I\tau - 4\beta D_S\mu\tau - 2\beta D_S r\tau - 4\beta D_I\mu\tau - 2\beta D_I r\tau + A\beta\tau$

$\quad +\beta^2\tau - \beta d\tau - \beta D_S^2 - 2\beta D_S D_I - \beta D_I^2 - 2\beta\mu\tau - \beta r\tau - 2\beta D_S - 2\beta D_I\big),$

$h_{q_1} = \dfrac{1}{\tau^2\beta}\big(A^2\beta D_I\tau^2 + 2A\beta^2 D_I\tau^2 - 4A\beta dD_S\tau^2 - 2A\beta dD_I\tau^2 - 4A\beta D_S\mu\tau^2$

$\quad - 4A\beta D_I\mu\tau^2 - 2A\beta D_I r\tau^2 + 2Ad^2 D_S\tau^2 + 4A dD_S\mu\tau^2 + 2AD_S\mu^2\tau^2$

$\quad + \beta^3 D_I\tau^2 - 5\beta^2 dD_S\tau^2 - 3\beta^2 dD_I\tau^2 - 5\beta^2 D_S\mu\tau^2 - 5\beta^2 D_I\mu\tau^2$

$\quad - 2\beta^2 D_I r\tau^2 + 5\beta d^2 D_S\tau^2 + 14\beta dD_S\mu\tau^2 + 4\beta dD_S r\tau^2 + 2\beta dD_I\mu\tau^2$

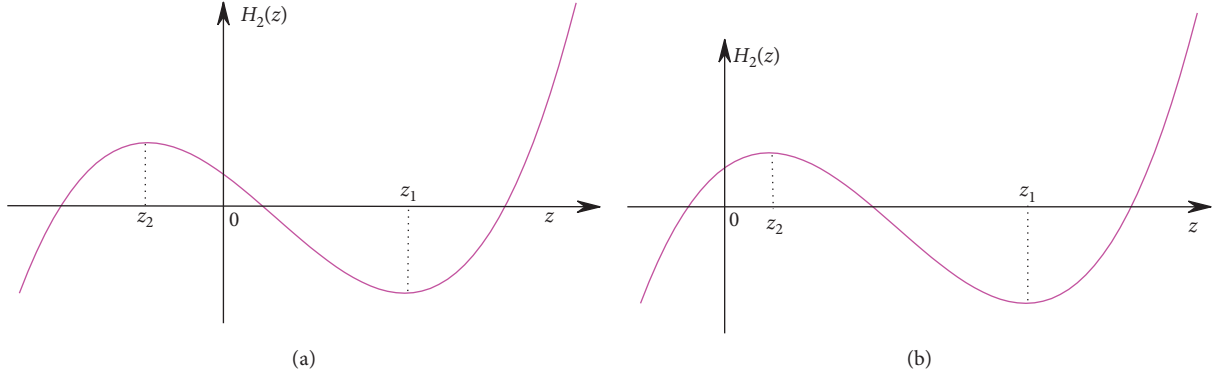FIGURE 1: The diagrams of the cubic function $H_2(z)$ in Theorem 1: (a) case (i) and (b) case (ii).

$$+ 2\beta \, dD_I r\tau^2 + 9\beta D_S \mu^2 \tau^2 + 4\beta D_S \mu r\tau^2 + 3\beta D_I \mu^2 \tau^2 + 4\beta D_I \mu r\tau^2$$

$$+ \beta D_I r^2 \tau^2 - d^3 D_S \tau^2 + d^3 D_I \tau^2 - 5d^2 D_S \mu\tau^2 - 2d^2 D_S r\tau^2$$

$$+ 3d^2 D_I \mu\tau^2 - 7 \, dD_S \mu^2 \tau^2 - 4 \, dD_S \mu r\tau^2 + 3 \, dD_I \mu^2 \tau^2 - 3D_S \mu^3 \tau^2$$

$$- 2D_S \mu^2 r\tau^2 + D_I \mu^3 \tau^2 + A^2 \beta \tau^2 + 2A\beta^2 \tau^2 - 2A\beta \, d\tau^2 - 4A\beta\mu\tau^2$$

$$- 2A\beta r\tau^2 + \beta^3 \tau^2 - 2\beta^2 d\tau^2 - 4\beta^2 \mu\tau^2 - 2\beta^2 r\tau^2 + \beta d^2 \tau^2$$

$$+ 4\beta \, d\mu \, \tau^2 + 2\beta \, dr \, \tau^2 + 4\beta\mu^2 \tau^2 + 4\beta\mu r\tau^2 + \beta r^2 \tau^2 - 2A\beta D_S \tau$$

$$- 2A\beta D_I \tau - 2\beta^2 D_S \tau - 2\beta^2 D_I \tau + 2\beta \, dD_S \tau + \beta \, dD_I \tau + 4\beta D_S \mu\tau$$

$$+ 2\beta D_S r\tau + 3\beta D_I \mu\tau + 2\beta D_I r\tau - 2A\beta\tau - 2\beta^2 \tau + \beta \, d\tau$$

$$+3\beta\mu\tau + 2\beta r\tau + \beta D_S + \beta D_I),$$

$$h_{q_0} = \frac{1}{\tau^2 \beta} \Big(2A^2 \beta \, d\tau^2 + 2A^2 \beta\mu\tau^2 - A^2 d^2 \tau^2 - 2A^2 \, d\mu \, \tau^2 - A^2 \mu^2 \tau^2$$

$$+ 5A\beta^2 d\tau^2 + 5A\beta^2 \mu\tau^2 - 5A\beta d^2 \tau^2 - 14A\beta \, d\mu \, \tau^2 - 4A\beta \, dr \, \tau^2$$

$$- 9A\beta\mu^2 \tau^2 - 4A\beta\mu r\tau^2 + Ad^3 \tau^2 + 5Ad^2 \mu\tau^2 + 2Ad^2 r\tau^2$$

$$+ 7A \, d\mu^2 \tau^2 + 4A \, d\mu \, r\tau^2 + 3A\mu^3 \tau^2 + 2A\mu^2 r\tau^2 + 3\beta^3 d\tau^2$$

$$+ 3\beta^3 \mu\tau^2 - 5\beta^2 d^2 \tau^2 - 15\beta^2 d\mu \, \tau^2 - 5\beta^2 dr \, \tau^2 - 10\beta^2 \mu^2 \tau^2$$

$$- 5\beta^2 \mu r\tau^2 + 2\beta d^3 \tau^2 + 11\beta d^2 \mu\tau^2 + 5\beta d^2 r\tau^2 + 18\beta \, d\mu^2 \tau^2$$

$$+ 14\beta \, d\mu \, r\tau^2 + 2\beta \, dr^2 \tau^2 + 9\beta\mu^3 \tau^2 + 9\beta\mu^2 r\tau^2 + 2\beta\mu r^2 \tau^2$$

$$- d^3 \mu\tau^2 - d^3 r\tau^2 - 4d^2 \mu^2 \tau^2 - 5d^2 \mu r\tau^2 - d^2 r^2 \tau^2 - 5 \, d\mu^3 \tau^2$$

$$- 7 \, d\mu^2 r\tau^2 - 2 \, d\mu \, r^2 \tau^2 - 2\mu^4 \tau^2 - 3\mu^3 r\tau^2 - \mu^2 r^2 \tau^2 + A^2 \beta\tau$$

$$+ 2A\beta^2 \tau - 2A\beta \, d\tau - 4A\beta\mu\tau - 2A\beta r\tau + \beta^3 \tau - 3\beta^2 d\tau$$

$$- 5\beta^2 \mu\tau - 2\beta^2 r\tau + \beta d^2 \tau + 4\beta \, d\mu \, \tau + 2\beta \, dr \, \tau + 4\beta\mu^2 \tau$$

$$+ 4\beta\mu r\tau + \beta r^2 \tau - A\beta - \beta^2 + \beta\mu + \beta r \Big). \tag{26}$$

Through some analyses, we can give the following conclusion. □

Theorem 3. *For system (4), suppose that the following holds*

(C3) $h_{q_1} < 0$, $h_{q_0} > 0$, and $H_3(z_3) < 0$

(C4) $h_{q_1} > 0$, $h_{q_0} > 0$, $h_{q_2} < 0$, $(h_{q_2})^2 - 3h_{q_3}h_{q_1} > 0$, and $H_3(z_3) < 0$

Then, endemic steady state E_1^* becomes unstable for some k, where

$$z_3 = \frac{-h_{q_2} + \sqrt{(h_{q_2})^2 - 3h_{q_3}h_{q_1}}}{3h_{q_3}}. \tag{27}$$

Given that the cubic polynomial functions $H_2(z)$ and $H_3(z)$ have similar structures and conditions, thus the proof process of Theorem 3 is similar to that of Theorem 2; then, one can easily obtain the above result.

Therefore, we derive another condition for system (4) to give rise to Turing instability:

$$\begin{cases} \text{(H1)}, & \text{(H2)}, \\ \text{(C3)or}, & \text{(C4).} \end{cases} \tag{28}$$

3. Numerical Results

In this section, we will carry out numerical simulations for system (4) with Neumann boundary conditions, which will be used to illustrate our theoretical analysis. For the convenience of numerical simulation, we select two-dimensional space area $\Omega = [0, a] \times [0, a]$ and set the same space step h in X and Y directions of the space area. Simultaneously, time step is fixed as Δt. Then, the mesh generation is given:

$$x_i = ih, \quad i = 0, 1, 2, \ldots, J,$$
$$y_j = jh, \quad j = 0, 1, 2, \ldots, J, \ Jh = a, \tag{29}$$
$$t_n = n\Delta t, \quad n = 0, 1, 2, \ldots.$$

$\mathbf{F}(\mathbf{c})$ in system (4) is relabeled as $\mathbf{F}(\mathbf{c}) = \begin{pmatrix} f_1(S, I, V) \\ f_2(S, I, V) \\ f_3(S, I, V) \end{pmatrix}$, and the following finite difference scheme is adopted for system (4):

$$\begin{cases} \dfrac{S_{i,j}^{n+1} - S_{i,j}^n}{\Delta t} = D_S\left(\dfrac{S_{i+1,j}^n - 2S_{i,j}^n + S_{i-1,j}^n}{h^2} + \dfrac{S_{i,j+1}^n - 2S_{i,j}^n + S_{i,j-1}^n}{h^2}\right) + f_1\left(S_{i,j}^n, I_{i,j}^n, V_{i,j}^n\right), \\[3mm] \dfrac{I_{i,j}^{n+1} - I_{i,j}^n}{\Delta t} = D_I\left(\dfrac{I_{i+1,j}^n - 2I_{i,j}^n + I_{i-1,j}^n}{h^2} + \dfrac{I_{i,j+1}^n - 2I_{i,j}^n + I_{i,j-1}^n}{h^2}\right) + f_2\left(S_{i,j}^n, I_{i,j}^n, V_{i,j}^n\right), \\[3mm] \dfrac{V_{i,j}^{n+1} - V_{i,j}^n}{\Delta t} = \dfrac{V_{i+1,j}^n - 2V_{i,j}^n + V_{i-1,j}^n}{h^2} + \dfrac{V_{i,j+1}^n - 2V_{i,j}^n + V_{i,j-1}^n}{h^2} + f_3\left(S_{i,j}^n, I_{i,j}^n, V_{i,j}^n\right), \end{cases} \tag{30}$$

where $S_{i,j}^n$, $I_{i,j}^n$, and $V_{i,j}^n$ represent the approximate value of $S(x_i, y_j, t_n)$, $I(x_i, y_j, t_n)$, and $V(x_i, y_j, t_n)$, respectively. In the simulation process, the initial value is a small random disturbance at endemic steady state E_1^*, and the area range of individuals' activity is $\Omega = [0, 100] \times [0, 100]$. The space region is evenly divided into 100×100 grids, and the corresponding space step is $h = 1$. The time interval is $[0, 5000]$, and the time step is set to $\Delta t = 0.005$. The first-order difference is used for the first-order derivative of the time, and the second-order derivative of the space is discretized by the center difference method in process of numerical simulation. For infectious diseases, the spatial distribution of infected individuals is a key issue for the control of infectious disease. Turing pattern can visually describe the spatial distribution of infected individuals. The focus of our simulation is how nonlocal delay affects spatial distribution of infected individuals. We thus take parameter value as $K = 1000$, $d = 0.3$, $\mu = 0.2$, $r = 0.8$, $D_S = 1$, $D_I = 10$, $A = 0.4$, and $\beta = 0.58$; time

delay τ is selected as the control parameter. Figures 2 and 3 are the time sequence diagram of spatial distribution of the density of the infected for time delays $\tau = 0.1$ and $\tau = 0.6$, respectively. It can be seen from these two figures that spatial distribution of the density of the infected evolves with time, which finally presents a regular nonuniform macroscopic structure in limited time, namely, stripe patterns, which indicates the number of infected individuals gradually increases over time and eventually gathers together. Under different time delay parameters, the infected finally forms different spatial distribution structures in the first row of Figure 4, which are called strip patterns. These patterns are further presented in three-dimensional space in the second row of Figure 4, which directly reflects the change of the density of the infected with space. Figure 5 shows the relationship between the average density of the infected and time delay τ, that is, the average density of the infected decreases with the increase of time delay τ (τ is less than the
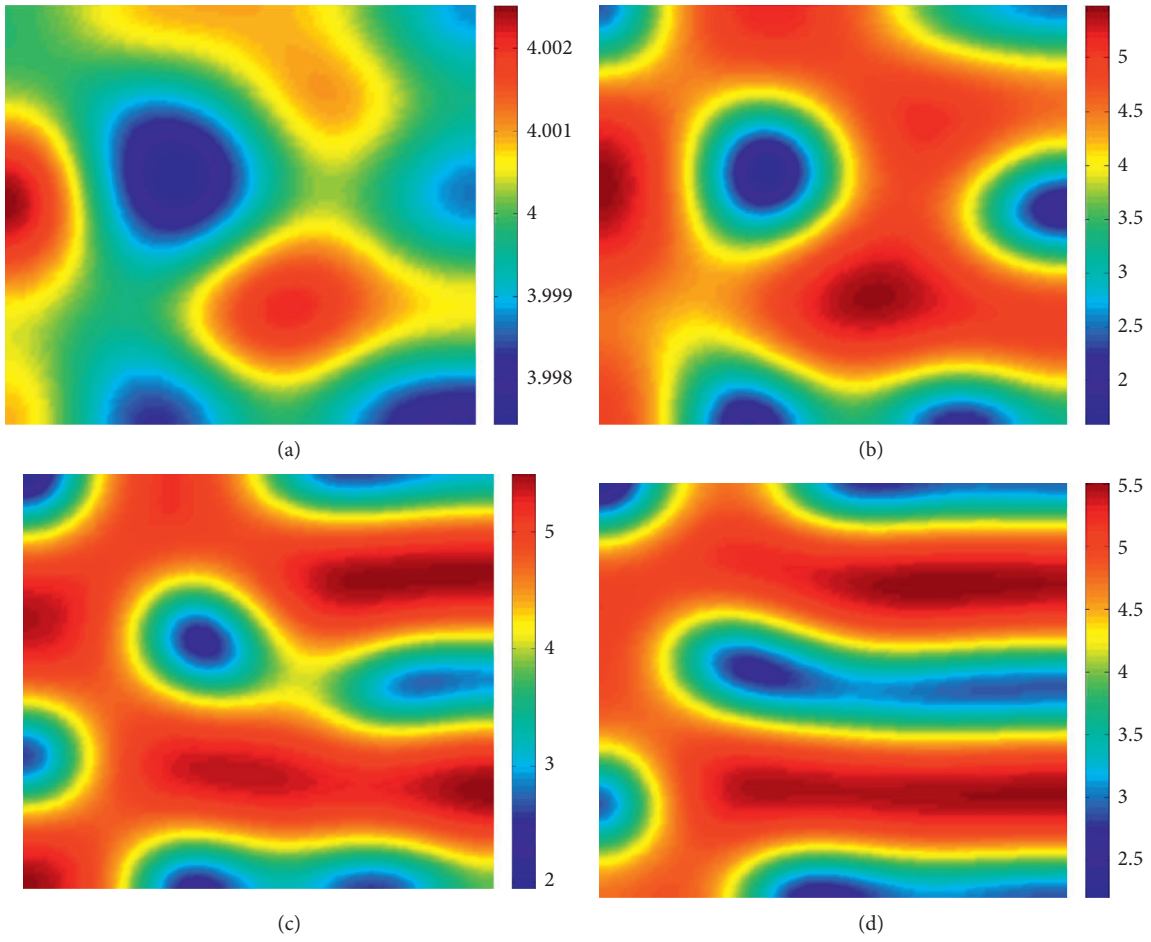
(a)

(b)

(c)

(d)

FIGURE 2: The spatial evolution of the density of the infected with time for time delay $\tau = 0.1$: (a) $t = 90000$; (b) $t = 200000$; (c) $t = 300000$; (d) $t = 1000000$.
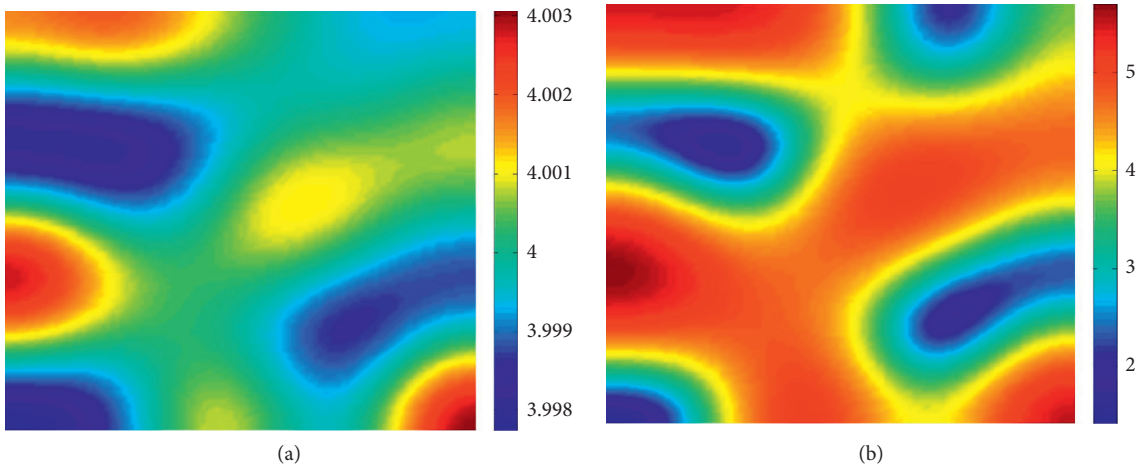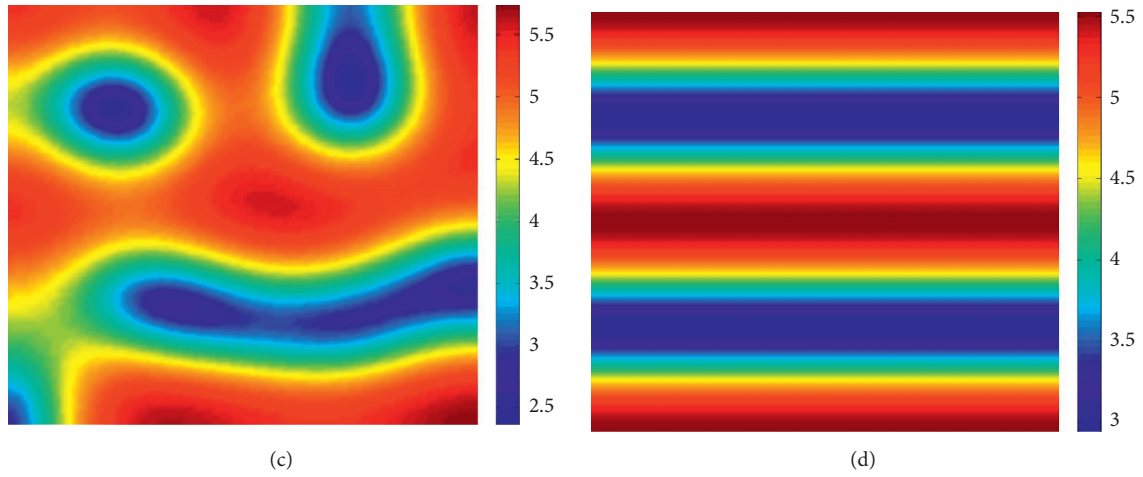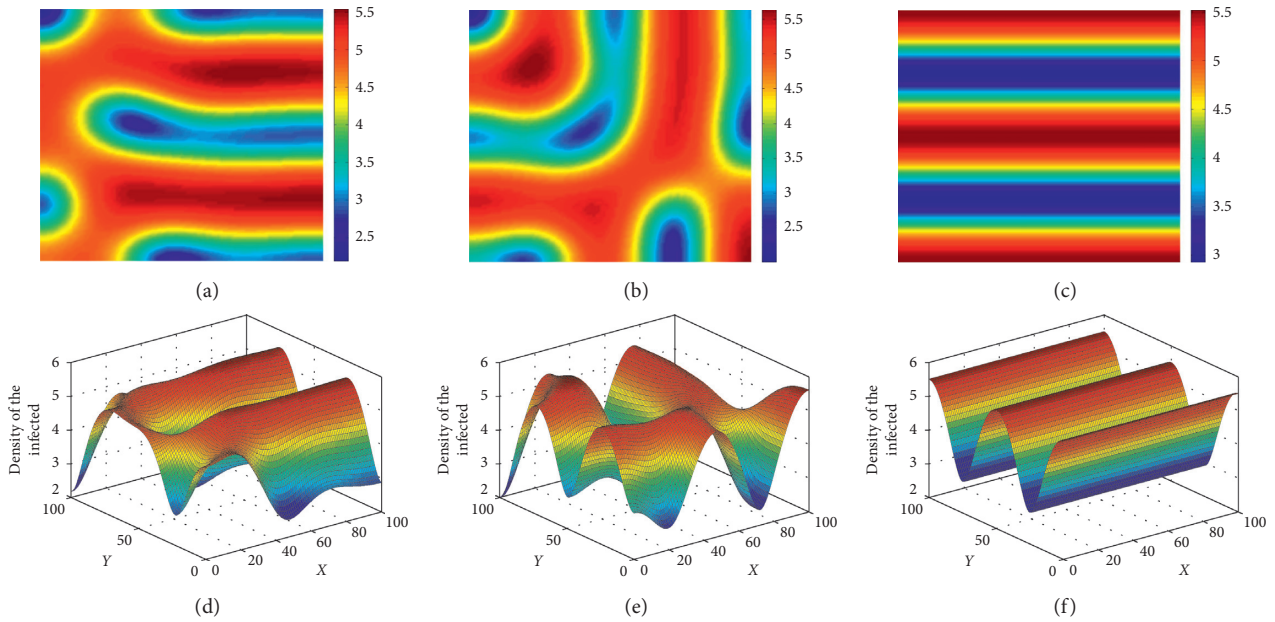

(a)

(b)

FIGURE 3: Continued.

(c)

(d)

FIGURE 3: The spatial evolution of the density of the infected with time for time delay $\tau = 0.6$: (a) $t = 80000$; (b) $t = 180000$; (c) $t = 400000$; (d) $t = 1000000$.

(a)

(b)

(c)

(d)

(e)

(f)

FIGURE 4: The first row shows stripe patterns with three different spatial structures in two-dimensional space for different time delay parameters: (a and d) $\tau = 0.1$; (b and e) $\tau = 0.2$; (c and f) $\tau = 0.3$. These patterns are further presented in a three-dimensional space in the second row.
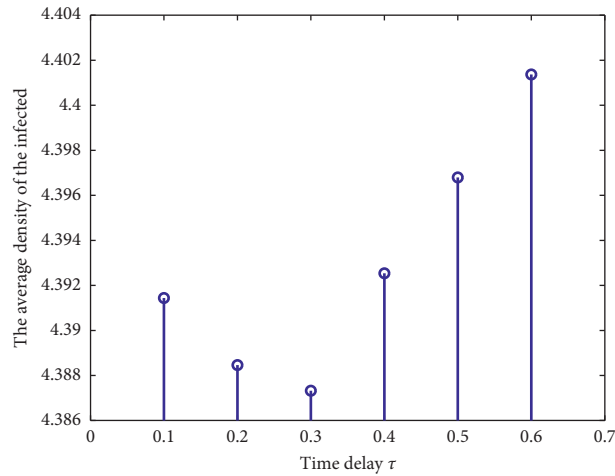
FIGURE 5: The relationship between the average density of the infected and time delay τ.

critical value), while the opposite case appears when τ is greater than the critical value.

4. Conclusions and Discussion

This paper investigates spatiotemporal dynamics of the SI epidemic model with nonlocal effect and the growth of the susceptible population following logistic mode, and we obtain two spatially homogeneous steady states including disease-free steady state and endemic steady state. We mainly analyze the dynamical behavior near endemic steady state-Turing instability. In general, the condition of system generating Turing instability is that the endemic steady state is stable in the system without diffusion (i.e., ordinary equation system), but becomes instability in the system with diffusion (i.e., reaction-diffusion system); then, the system finally gives rise to stable spatial structure, which is called Turing pattern. The conditions of system (4) generating Turing instability are (24) or (28) based on Hurwitz criterion, and the parameter space of the existence of Turing pattern is given by condition (24). While the corresponding parameter space is difficult to obtain because of the complexity condition (28), which will be carried out in the following work. Time delay widely exists in the process of disease transmission, such as incubation period and immune period. We thus study the influence of time delay on infectious diseases in numerical simulations, find that the average density of the infected firstly decreases, and then increase with the increase of time delay, which provides a theoretical support for disease control. At the same time, we simulate the evolution of spatial distribution of the density of the infected under different time delays, and the spatial distribution of the density of the infected finally forms stripe pattern with different spatial structure, which does not change with time. The high incidence area of infectious diseases is found, which also provides data information for prevention and control of infectious disease.

In the research process of pattern dynamics of system (4), we consider a special form of kernel function so that the nonlocal delay system could be transformed into general reaction-diffusion system; then, pattern dynamics can be followed. In fact, there are some other forms of kernel functions in the biological system, but different forms shall induce nonlocal delay system to convert into different differential system; thus, this is a very meaningful work to study the effects of different kernel functions on the pattern dynamics in the future.

Data Availability

No data were used to support this study.

Conflicts of Interest

The authors declare that they have no conflicts of interest.

Acknowledgments

References

[1] W. O. Kermack and A. G. McKendrick, "A contribution to the mathematical theory of epidemics," *Proceedings of the Royal Society of London. Series A, Containing Papers of a Mathematical and Physical Character*, vol. 115, no. 772, pp. 700–721, 1927.

[2] W. O. Kermack and A. G. McKendrick, "Contributions to the mathematical theory of epidemics—I," *Bulletin of Mathematical Biology*, vol. 53, no. 1-2, pp. 33–55, 1991.

[3] L. Li, G.-Q. Sun, and Z. Jin, "Bifurcation and chaos in an epidemic model with nonlinear incidence rates," *Applied Mathematics and Computation*, vol. 216, no. 4, pp. 1226–1234, 2010.

[4] Y. Kang and C. Castillo-Chavez, "Dynamics of SI models with both horizontal and vertical transmissions as well as Allee effects," *Mathematical Biosciences*, vol. 248, pp. 97–116, 2014.

[5] G.-Q. Sun and Z.-K. Zhang, "Global stability for a sheep brucellosis model with immigration," *Applied Mathematics and Computation*, vol. 246, no. 1, pp. 336–345, 2014.

[6] S. Usaini, R. Anguelov, and S. M. Garba, "Dynamics of SI epidemic with a demographic Allee effect," *Theoretical Population Biology*, vol. 106, pp. 1–13, 2015.

[7] J. P. Tripathi and S. Abbas, "Global dynamics of autonomous and nonautonomous SI epidemic models with nonlinear incidence rate and feedback controls," *Nonlinear Dynamics*, vol. 86, no. 1, pp. 337–351, 2016.

[8] G.-Q. Sun, J.-H. Xie, S.-H. Huang, Z. Jin, M.-T. Li, and L. Liu, "Transmission dynamics of cholera: mathematical modeling and control strategies," *Communications in Nonlinear Science and Numerical Simulation*, vol. 45, pp. 235–244, 2017.

[9] L. Li, J. Zhang, C. Liu, H.-T. Zhang, Y. Wang, and Z. Wang, "Analysis of transmission dynamics for Zika virus on networks," *Applied Mathematics and Computation*, vol. 347, pp. 566–577, 2019.

[10] L. Chen and J. Sun, "Global stability of an SI epidemic model with feedback controls," *Applied Mathematics Letters*, vol. 28, pp. 53–55, 2014.

[11] J. Jiao, L. Chen, and G. Luo, "An appropriate pest management SI model with biological and chemical control concern," *Applied Mathematics and Computation*, vol. 196, no. 1, pp. 285–293, 2008.

[12] K. M. Fuhrman, I. G. Lauko, and G. A. Pinter, "Asymptotic behavior of an SI epidemicmodel with pulse removal," *Mathematical and Computer Modelling*, vol. 40, no. 3-4, pp. 371–386, 2004.

[13] K. Y. Liu, T. Q. Zhang, and L. S. Chen, "State-dependent pulse vaccination and therapeutic strategy in an SI epidemic model with nonlinear incidence rate," *Computational and Mathematical Methods in Medicine*, vol. 2019, Article ID 3859815, 10 pages, 2019.

[14] B. Liu, Y. Duan, and S. Luan, "Dynamics of an SI epidemic model with external effects in a polluted environment," *Nonlinear Analysis: Real World Applications*, vol. 13, no. 1, pp. 27–38, 2012.

[15] Y. Pei, S. Liu, C. Li, and L. Chen, "The dynamics of an impulsive delay SI model with variable coefficients," *Applied Mathematical Modelling*, vol. 33, no. 6, pp. 2766–2776, 2009.

[16] L. Li, J. Zhen, and S. Gui-Quan, "Spatial pattern of an epidemic model with cross-diffusion," *Chinese Physics Letters*, vol. 25, no. 9, pp. 3500–3503, 2008.

[17] Y. Song, H. Jiang, H. Jiang, and Y. Yuan, "Turing-hopf bifurcation in the reaction-diffusion system with delay and application to a diffusive predator-prey model," *Journal of Applied Analysis & Computation*, vol. 9, no. 3, pp. 1132–1164, 2019.

[18] Y. Wang, J. Wang, and L. Zhang, "Cross diffusion-induced pattern in an SI model," *Applied Mathematics and Computation*, vol. 217, no. 5, pp. 1965–1970, 2010.

[19] G.-Q. Sun, "Pattern formation of an epidemic model with diffusion," *Nonlinear Dynamics*, vol. 69, no. 3, pp. 1097–1104, 2012.

[20] X. Tang and Y. Song, "Cross-diffusion induced spatiotemporal patterns in a predator-prey model with herd behavior," *Nonlinear Analysis: Real World Applications*, vol. 24, pp. 36–49, 2015.

[21] W. Ding, W. Z. Huang, W. Huang, and S. Kansakar, "Traveling wave solutions for a diffusive SIS epidemic model," *Discrete & Continuous Dynamical Systems—B*, vol. 18, no. 5, pp. 1291–1304, 2013.

[22] J. Li, G.-Q. Sun, and Z. Jin, "Pattern formation of an epidemic model with time delay," *Physica A: Statistical Mechanics and Its Applications*, vol. 403, pp. 100–109, 2014.

[23] G. Q. Sun, S. L. Wang, Q. Ren, Z. Jin, and Y. P. Wu, "Effects of time delay and space on herbivore dynamics: linking inducible defenses of plants to herbivore outbreak," *Scientific Reports*, vol. 5, no. 1, Article ID 11246, 2015.

[24] T. Zhang, W. Wang, and K. Wang, "Minimal wave speed for a class of non-cooperative diffusion-reaction system," *Journal of Differential Equations*, vol. 260, no. 3, pp. 2763–2791, 2016.

[25] G.-Q. Sun, C.-H. Wang, and Z.-Y. Wu, "Pattern dynamics of a Gierer-Meinhardt model with spatial effects," *Nonlinear Dynamics*, vol. 88, no. 2, pp. 1385–1396, 2017.

[26] Z. Lin and H. Zhu, "Spatial spreading model and dynamics of West Nile virus in birds and mosquitoes with free boundary," *Journal of Mathematical Biology*, vol. 75, no. 6-7, pp. 1381–1409, 2017.

[27] G.-Q. Sun, C.-H. Wang, L.-L. Chang, Y.-P. Wu, L. Li, and Z. Jin, "Effects of feedback regulation on vegetation patterns in semi-arid environments," *Applied Mathematical Modelling*, vol. 61, pp. 200–215, 2018.

[28] P. Magal, G. F. Webb, and Y. Wu, "On the basic reproduction number of reaction-diffusion epidemic models," *SIAM Journal on Applied Mathematics*, vol. 79, no. 1, pp. 284–304, 2019.

[29] J. Ge, C. Lei, and Z. Lin, "Reproduction numbers and the expanding fronts for a diffusion-advection SIS model in heterogeneous time-periodic environment," *Nonlinear Analysis: Real World Applications*, vol. 33, pp. 100–120, 2017.

[30] Z.-C. Wang and J. Wu, "Travelling waves of a diffusive Kermack-McKendrick epidemic model with non-local delayed transmission," *Proceedings of the Royal Society A: Mathematical, Physical and Engineering Sciences*, vol. 466, no. 2113, pp. 237–261, 2009.

[31] S. X. Pan, "Traveling wave fronts in an epidemic model with nonlocal diffusion and time delay," *International Journal of Mathematical Analysis*, vol. 2, no. 21–24, pp. 1083–1088, 2008.

[32] Z. Zhen, J. Wei, L. Tian, J. Zhou, and W. Chen, "Wave propagation in a diffusive SIR epidemic model with spatiotemporal delay," *Mathematical Methods in the Applied Sciences*, vol. 41, no. 16, pp. 7074–7098, 2018.

[33] Q. Tang, J. Ge, and Z. Lin, "An SEI-SI avian-human influenza model with diffusion and nonlocal delay," *Applied Mathematics and Computation*, vol. 247, pp. 753–761, 2014.

[34] F. M. Hilker, M. Langlais, and H. Malchow, "The allee effect and infectious diseases: extinction, multistability, and the (Dis-) appearance of oscillations," *The American Naturalist*, vol. 173, no. 1, pp. 72–88, 2009.

[35] L. Cai, G. Chen, and D. Xiao, "Multiparametric bifurcations of an epidemiological model with strong Allee effect," *Journal of Mathematical Biology*, vol. 67, no. 2, pp. 185–215, 2013.

[36] L. Q. Gao and H. W. Hethcote, "Disease transmission models with density-dependent demographics," *Journal of Mathematical Biology*, vol. 30, no. 7, pp. 717–731, 1992.

[37] J. Li, Z. Jin, Z. Jin, G.-Q. Sun, and L.-P. Song, "Pattern dynamics of a delayed eco-epidemiological model with disease in the predator," *Discrete & Continuous Dynamical Systems—S*, vol. 10, no. 5, pp. 1025–1042, 2017.

[38] P. Yu, "Closed-form conditions of bifurcation points for general differential equations," *International Journal of Bifurcation and Chaos*, vol. 15, no. 4, pp. 1467–1483, 2005.

Research Article

A General Model of Population Dynamics Accounting for Multiple Kinds of Interaction

Luciano Stucchi,[1,2] Juan Manuel Pastor,[2] Javier García-Algarra ⓘ,[3] and Javier Galeano ⓘ[2]

[1]*Universidad Del Pacífico, Lima, Peru*
[2]*Complex Systems Group, E. T. S. I. A. A. B, Universidad Politécnica de Madrid, Madrid, Spain*
[3]*Department of Engineering, Centro Universitario U-TAD, Las Rozas, Spain*

Correspondence should be addressed to Javier Galeano; javier.galeano@upm.es

Population dynamics has been modelled using differential equations almost since Malthus times, more than two centuries ago. Basic ingredients of population dynamics models are typically a growth rate, a saturation term in the form of Verhulst's logistic brake, and a functional response accounting for interspecific interactions. However, intraspecific interactions are not usually included in the equations. The simplest models use linear terms to represent a simple picture of the nature; meanwhile, to represent more complex landscapes, it is necessary to include more terms with a higher order or that are analytically more complex. The problem to use a simpler or more complex model depends on many factors: mathematical, ecological, or computational. To address it, here we discuss a new model based on a previous logistic-mutualistic model. We have generalized the interspecific terms (for antagonistic and competitive relationships), and we have also included new polynomial terms to explain any intraspecific interaction. We show that, by adding simple intraspecific terms, new free-equilibrium solutions appear driving a much richer dynamics. These new solutions could represent more realistic ecological landscapes by including a new higher order term.

1. Introduction

In the times of the coronavirus, many news on television and magazines try to explain how the size of the infected population evolves, showing exponential plots of the infected populations over time. These communications try to predict the time evolution of the size of this population in the future. Behind these predictions, there is always a differential equation model. These polynomial models have linear terms, but to account for more complex interactions, they can add higher order terms, as quadratic, cubic, or even, analytically more complex functions, such as decreasing hyperbolic terms. The problem of choosing a complex or a simple model depends on the balance between properly representing nature and being able to understand the model response. In many cases, the simplest model may be enough to understand the benchmarks in the big picture, but sometimes, we

need more complexity to represent significant aspects of our problem, and therefore, we need more complex and more difficult models. Finding the balance between simple and complex is a tricky problem, but how simple or complex should the model be? Let us try to answer this question in a population dynamics problem.

In the study of population dynamics, Lotka [1] and Volterra [2] were the first ones to model trophic interactions in order to study predator-prey relationships within two (or more) populations:

$$
\begin{aligned}
\dot{X}_1 &= (r_1 - b_{12} X_2) X_1, \\
\dot{X}_2 &= (-r_2 + b_{21} X_1) X_2,
\end{aligned}
\tag{1}
$$

where b_{ij} terms represent the rate of the interactions between populations X_i and X_j and the r_i represents their effective growth rates. In these equations, signs are

incorporated to give a clear meaning to each term, considering all parameters as positive real numbers. This simple model uses a linear term to represent the interaction with the environment and a pairwise second-order term to show the antagonistic interaction between the populations of two different species. It was necessary to introduce a higher order term, to represent this interaction.

Although most population dynamics models first dealt with antagonistic relations, mutualistic interactions are widely spread, e.g., [3, 4]. Garcia-Algarra et al. [5] proposed a logistic-mutualistic model. Their formulation was based on writing an *effective* growth rate as the sum of the *intrinsic* growth rate (r_i) plus the mutualistic benefit ($b_{ij}X_j$) and, associated with them, to include a saturation term for the whole *effective* growth term. The model was depicted as

$$\dot{X}_1 = (r_1 + b_{12}X_2)X_1 - (a_1 + c_1b_{12}X_2)X_1^2,$$
$$\dot{X}_2 = (r_2 + b_{21}X_1)X_2 - (a_2 + c_2b_{21}X_1)X_2^2. \quad (2)$$

The term $a_iX_i^2$ represents the intraspecific competition for resources, and the term $c_ib_{ij}X_jX_i^2$ plays the role of saturation for the mutualistic benefit. This model needs to reach a third-order term to prevent the unbounded growth and depicts a well behaved system, with enough richness to model large ensembles of mutualistic networks and their behaviour.

Other authors have addressed different strategies to introduce the mutualistic interaction. For example, Dean [6] introduced an exponential dependency on the carrying capacity, K, which consequently yields nonlinear terms into the equations. To avoid the unbounded growth, the authors in [7, 8] proposed restrictions using a type II Holling functional response. This functional leaves the path of introducing a polynomial term with a hyperbolic function.

Nowadays, several studies have focused on adding higher order terms to explain more complex ecological interactions. Letten and Stouffer [9] studied the influence of interspecific interactions as nonadditive density-dependent terms only for competitive communities. Bairey et al. [10] studied the new solutions that a third species adds in pairwise interactions, adding third degree terms with the three different populations, $b_{ijk}X_iX_jX_k$. It is well known that an increase in the order of a polynomial term introduces new solutions to the equations, but as AlAdwani and Saavedra [11] showed these new terms do not always produce viable solutions, furthermore, they must be free-equilibrium points, and of course, the solutions must have an ecological meaning.

Here, we propose a new general model in which any ecological interaction can be included in a simple way. In a first step, we generalise the model proposed by Garcia-Algarra et al. [5] overcoming the restrictions of the sign of the parameters; in a second step, we reorganize the intraspecific interactions allowing for both positive and negative interactions, and finally, we introduce a third-order term to brake any unbounded pairwise interactions.

2. Methods and Materials

We define a new general model. Equation (3) represents the population dynamics of the species X_i driven by an effective growth rate (first parenthesis in equation (3)) and limited by a logistic brake (second parenthesis in equation (3)). The view of the model is simple and similar to the original Verhulst idea [12], where the low-order terms represent the increase in the population and the high-order terms the brake. The differences with other models are in the terms included in the effective growth rate and logistic brake. The effective growth rate includes the vegetative growth rate, r_i, and all density-dependent pairwise interactions, interspecific interactions, $b_{ij}X_j$ ($\forall j \neq i$), and intraspecific ones, $b_{ii}X_i$; the logistic brake includes the logistic term due to intraspecific competition, a_i, the interspecific intraspecific brake, $b_{ij}X_jX_i$, and the intraspecific ones, $b_{ii}X_i^2$.

2.1. A New General Model including Intraspecific Interaction Terms.
Regarding the mutualistic model (equation (2)) we introduce two differences: first, the parameters of the equation, r_i and b_{ij}, can be positive or negative, representing the different ecological interactions, and second, we include the effect of the population in its own effective growth rate just adding the index $j = i$ in the sum of the interactions terms, so the model can be represented as

$$\dot{X}_i = X_i\left[\left(r_i + \sum_{j=1}^{n}b_{ij}X_j\right) - \left(a_i + c_i\sum_{j=1}^{n}b_{ij}X_j\right)X_i\right], \quad (3)$$

where the subscript i runs from 1 to n, including the intraspecific interaction ($j = i$). With this term, we are taking into account the interaction between individuals of the same populations. The new terms yield new solutions and a different phase space. In particular, the inclusion of the term $-c_ib_{ii}X_i^3$ is key for the emergence of new solutions although there was already a term with the same order in the mutualistic logistic model (equation (2)), $c_ib_{ij}X_jX_i^2$. It can be observed in Figure 13 in Supplementary Materials (available here). We explain all details about the number of solutions in Appendix in Supplementary Materials (available here).

Generally, in the literature of populations dynamics, the intraspecific interactions have been introduced only as a logistic brake, $-a_iX_i$, representing a growth limit due to resource sharing. In our model, the term, b_{ii}, can represent any kind of intraspecific interaction from beneficial, namely, *cooperation* to harmful interactions, such as *competition* or even *cannibalism*. Even though the logistic term $-a_iX_i$ can be seen as the result of intraspecific interactions that limit the growth by resource sharing and it can be included in the interaction term $b_{ii}X_i$, we maintain the separated formulation for the sake of comparison with the equation without this new term.

In fact, there are abundant examples of different intraspecific behaviours in the literature, such as those mentioned above. Cooperation is well known among social and eusocial species [13], and benefits of cooperative behaviour have been consistently reported, especially for eusocial animals [14]. On the other way, in nature, we can find different types of competition among members of the same population. For example, Stucchi and Figueroa [15] reported the aggressive intraspecific behaviour of the

Peruvian booby, which attacks their peers not by means of taking their food but for the sake of being around their nest. In the same way, adult boobies show little tolerance for pigeons that are not from them, pecking them to death. This behaviour is well known for other territorial animals, and it conceptually differs from the conventional intraspecific competition for resources.

2.2. Solutions with One Population.

In general, the equation system (3) cannot be solved analytically. However, the study of only one population can be solved and illustrates the possibilities of the model.

Consider equation (3) for only one population. The equation can be written as

$$\dot{X} = X[(r + b \cdot X) - (a + cb \cdot X)X], \tag{4}$$

where we have removed the subscripts for simplicity. Stationary points where $\dot{X} = 0$ give us the keys to understand the behaviour of the time evolution of the population sizes. The trivial solution, which corresponds to extinction, is $X^\star = 0$. Now, the nontrivial stationary solutions can be obtained from the following condition:

$$r + (b - a)X^\star - c \cdot bX^{\star 2} = 0. \tag{5}$$

Then, the stationary solutions of equation (4) are the extinction and the solutions of equation (5):

$$X_\pm^\star = \frac{(b - a) \pm \sqrt{(b - a)^2 + 4rbc}}{2bc}. \tag{6}$$

In ecology, we are only interested in the positive real solutions, generally called feasible solutions. To obtain these feasible solutions in equation (6), we need to study several cases:

(i) r and b have the same sign. In addition to the trivial solution, $X^\star = 0$, in both cases, there is one positive stationary point, which corresponds to the carrying capacity of the population, and the other is negative, which is not a feasible solution.

  (a) In the case that both parameters are negatives, $r < 0$ and $b < 0$, the positive solution is unstable and the trivial solution is the unique stable solution.

  (b) In the opposite case, $r > 0$ and $b > 0$, the carrying capacity is the stable solution.

(ii) r and b have different signs. The interesting point of having a high-order term comes from the possibility of different signs of the parameters. When r and b have different signs, there are two solutions as long as the condition $c \le (b - a)^2/4|rb|$ is fulfilled.

  (a) If $b > 0$, it is a necessary another condition to obtain a feasible solution that $b > a$. Ecologically speaking, this means that the term of intraspecific interaction overcomes the intrinsic growth deficiency and increases the population. In Figure 1(b), we plot a case with these conditions. We obtain three fixed points: initial and end

points are stable, and the intermediate point is unstable. This point marks the threshold population; above this value, intraspecific cooperation moves the population to reach the carrying capacity, and below this value, the population goes to extinction.

  (b) If $b < 0$. In this scenario, the intermediate point is stable, and the other solutions are unstable. Consequently, the intraspecific competitions produce a new stationary solution, lower than the carrying capacity. This behaviour has been called as Allee effect [16]. See the example in Figure 1(b).

In Figure 1, we depict on the top $\dot{X}$ vs. X and on the bottom, the temporal evolution of the population size $X(t)$ vs. t. On the left, the growth rate r is negative, and the intraspecific interaction coefficient b is positive. The intermediate stationary solution plays the role of a population threshold because smaller communities will go extinct (population in orange in Figure 1(c)), while larger communities will grow to its carrying capacity (population in green in Figure 1(c)). On the right, the growth rate r is positive, and the interaction coefficient b is negative. In this case, the carrying capacity becomes unstable, and the system evolves to the new stable intermediate solution because of the detrimental intraspecific interaction (both populations in Figure 1(d)). Two examples of population evolution are plotted in each scenario, where the orange and green dots in the upper plot depict the initial condition of each evolution in the lower plot.

2.3. Solutions with Two Populations.

In the case of two populations, the general model is written as

$$\dot{X}_1 = X_1[(r_1 + b_{11}X_1 + b_{12}X_2) - (a_1 + c_1b_{11}X_1 + c_1b_{12}X_2)X_1],$$
$$\dot{X}_2 = X_2[(r_2 + b_{22}X_2 + b_{21}X_1) - (a_2 + c_2b_{22}X_2 + c_2b_{21}X_1)X_2]. \tag{7}$$

For two populations, we also find the expected trivial solution, i.e., the total extinction ($X_1^\star = 0$ and $X_2^\star = 0$) and the partial extinctions ($X_1^\star, 0$) and ($0, X_2^\star$), from the following equations:

$$r_1 + (b_{11} - a_1)X_1^\star - c_1b_{11}X_1^{\star 2} = 0,$$
$$r_2 + (b_{22} - a_2)X_2^\star - c_2b_{22}X_2^{\star 2} = 0. \tag{8}$$

However, as they are second-order equations, there are two solutions of feasible partial extinctions for each population. The coexistence solutions can be obtained from equation (7); these equations can exhibit up to 6 new stationary solutions. Concerning the finite stationary solutions, the intraspecific term makes it more difficult to obtain an analytic expression from the following equations:

$$(r_1 + b_{11}X_1^\star + b_{12}X_2^\star) - (a_1 + c_1b_{11}X_1^\star + c_1b_{12}X_2^\star)X_1^\star = 0,$$
$$(r_2 + b_{22}X_2^\star + b_{21}X_1^\star) - (a_2 + c_2b_{22}X_2^\star + c_2b_{21}X_1^\star)X_2^\star = 0. \tag{9}$$
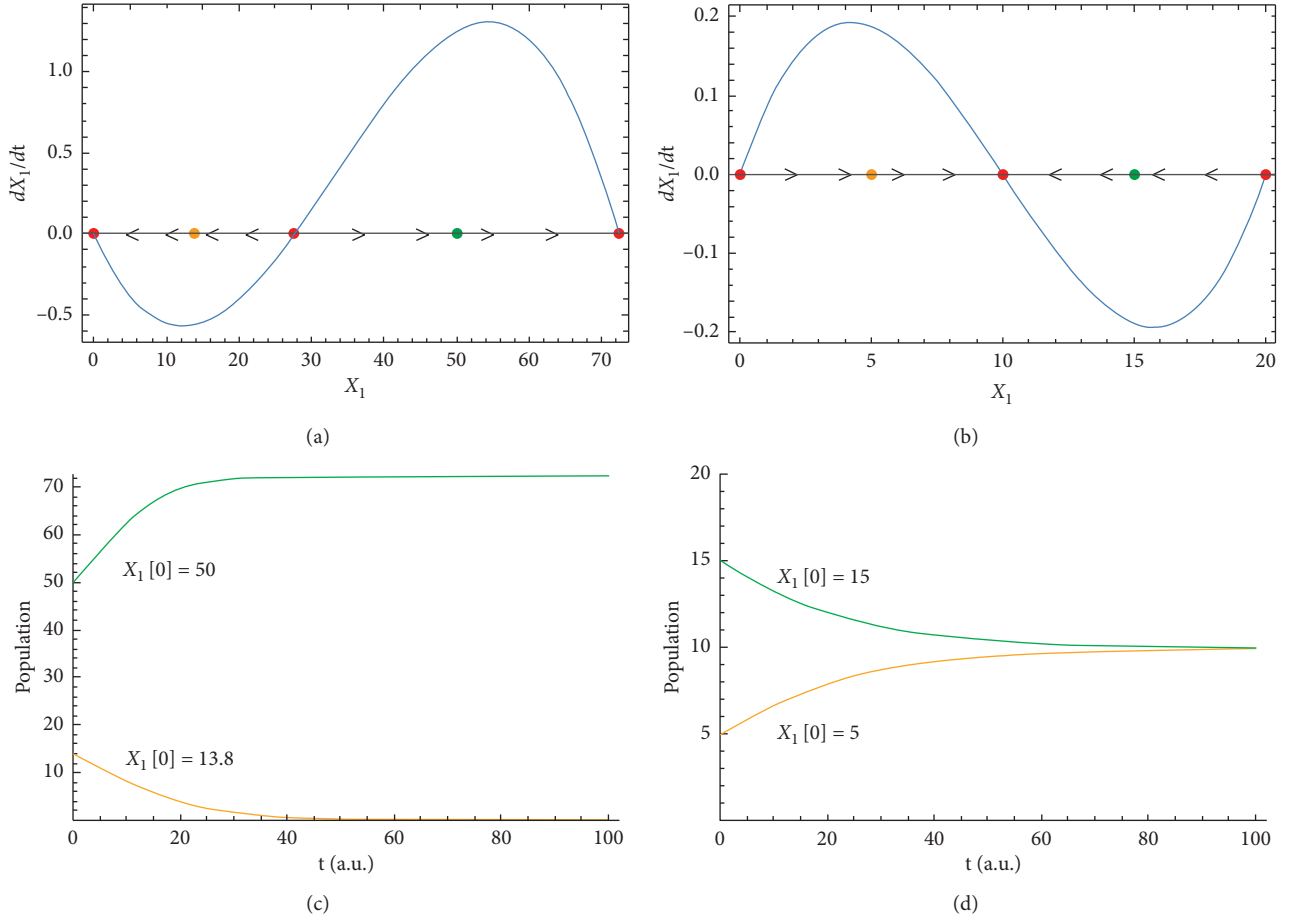
(a)

(b)

(c)

(d)

FIGURE 1: Temporal derivative (up) and population evolution (down) for one population with intraspecific interaction. Negative growth rate (left), $r = -0.1$, with positive intraspecific interaction $b = 0.005$ and $c = 0.005$. Positive growth rate (right), $r = 0.1$, with negative intraspecific interaction $b = -0.015$ and $c = 0.05$.

Two out of these six solutions are new free-equilibrium points, due to the new intraspecific terms (details in Supplementary Material). Even though we cannot obtain analytic expressions for all solutions, we explored different scenarios by performing numerical simulations with different parameter values. In the next section, we show how the intraspecific interaction changes the phase space of the standard biological interactions.

2.4. Linear Stability Analysis. In the next section, we explore the linear stability analysis of our system solutions.

2.4.1. One Population Model. To perform the linear stability analysis of the stationary solutions, we derive equation (4) at the fixed points:

$$\left.\frac{d\dot{X}}{dX}\right|_{X=0} = r, \tag{10}$$

$$\left.\frac{d\dot{X}}{dX}\right|_{X=X_{\pm}^{\star}} = r + \left[2\left(b-a\right)-3cbX^{\star}\right]X^{\star} = -r - cbX^{\star 2}. \tag{11}$$

In the trivial solution, the eigenvalue is $\lambda = r$ and the unique stable solution is $r < 0$.

According to equation (11), the derivative at the (positive) stationary solution $X^{\star}$ will be negative when

$$\left(b-a\right) - 2cbX_{\pm}^{\star} = \mp\delta < 0. \tag{12}$$

Then, $X_{+}^{\star}$ is always stable and $X_{-}^{\star}$ is unstable.

When $r > 0$ and $b > 0$, extinction is an unstable solution and population rises to the carrying capacity at $X_{+}^{\star}$, the only positive nontrivial solution. However, for $r > 0$ and $b < 0$, i.e., with intraspecific competition, a new stationary solution emerges, $X_{-}^{\star} > X_{+}^{\star}$. Now, the higher solution is unstable, and the population only reaches a lower value at the stable point $X_{+}^{\star}$. In this case, the negative intraspecific interaction results in a lower carrying capacity.

When $r < 0$, extinction is stable. If $b < 0$, the only positive finite solution is $X_{-}^{\star}$, which is unstable. However, when $b > a > 0$, a new stable solution, $X_{+}^{\star}$, emerges at higher values than $X_{-}^{\star}$. In this scenario, $X_{-}^{\star}$ marks the threshold population; above this value, intraspecific cooperation moves the population to reach the carrying capacity, and below this value, the population goes to extinction (see Figure 1(c)).

2.4.2. Two Populations Model. The linear stability for the general model (equation (3)) can be analyzed from the Jacobian matrix at the stationary solutions. Its entries are obtained from

$$\frac{\partial f_i}{\partial X_i}\bigg|_{X^\star} = g_i(X^\star) + (b_{ii} - a_i)X_i^\star - 2c_ib_{ii}X_i^{\star 2} - c_i\sum_{j\neq i}b_{ij}X_i^\star X_j^\star,$$

$$\frac{\partial f_i}{\partial X_j}\bigg|_{X^\star} = b_{ij}X_i^\star(1 - c_iX_i^\star),$$

(13)

where $X^\star = (X_1^\star, \ldots, X_i^\star, \ldots, X_j^\star, \ldots)$ is the vector of the stationary solution.

For two populations, the Jacobian matrix for the total extinction is

$$J_{\{0,0\}} = \begin{pmatrix} r_1 & 0 \\ 0 & r_2 \end{pmatrix}, \qquad (14)$$

whose eigenvalues $\lambda_1 = r_1$ and $\lambda_2 = r_2$ are negative when both growth rates are negative. For the partial extinctions, the Jacobian matrix reads

$$J_{\{X_1^\star,0\}} = \begin{pmatrix} -r_1 - c_1b_{11}X_1^{\star 2} & b_{12}X_1^\star[1 - c_1X_1^\star] \\ 0 & r_2 + b_{21}X_1^\star \end{pmatrix}. \qquad (15)$$

As expected, this Jacobian matrix is almost the same as the matrix for the logistic-mutualistic model (see Appendix A in [5]), but the first entry includes the intraspecific interaction term $-c_1b_{11}X_1^{\star 2}$. This new term makes the partial extinction to be stable when the intraspecific interaction is positive $b_{11} > 0$. The same is stated for the symmetric solution $(0, X_2^\star)$.

And for the nontrivial solution $(X_1^\star, X_2^\star)$, the Jacobian matrix is written as follows:

$$J_{\{X_1^\star,X_2^\star\}} = \begin{pmatrix} -r_1 - b_{12}X_2^\star - c_1b_{11}X_1^{\star 2} & b_{12}X_1^\star[1 - c_1X_1^\star] \\ b_{21}X_2^\star[1 - c_2X_2^\star] & -r_2 - b_{21}X_1^\star - c_2b_{22}X_2^{\star 2} \end{pmatrix}. \qquad (16)$$

In this case, both diagonal entries include the intraspecific term with a negative sign. This means that a positive intraspecific direct interaction enhances the stability of this stationary solution, while a negative intraspecific direct interaction contributes to destabilize it.

A qualitative study of the linear stability can also be made by analyzing the nullclines. Solving the nullclines, $f_1(X_1, X_2) = 0$, we obtain two solutions $X_1 = 0$, as follows:

$$g_1(X_1 \neq 0) = r_1 + (b_{11} - a_1)X_1 - c_1b_{11}X_1^2 - (c_1X_1 - 1)b_{12}X_2 = 0, \qquad (17)$$

or writing X_2 in terms of X_1:

$$X_2(g_1 = 0) = \frac{r_1 + (b_{11} - a_1)X_1 - c_1b_{11}X_1^2}{b_{12}(c_1X_1 - 1)}. \qquad (18)$$

This expression presents a discontinuity at $X_1 = 1/c_1$ and at $X_2 = 1/c_2$ for the f_2 nullcline. At this discontinuity, the growth rate of species 1 takes the value,

$g_1(X_1 = 1/c_1) = r_1 - a_1/c_1$, independently of X_2 (and the same for $g_2(X_2 = 1/c_2)$). The condition for a bounded growth leads to $c_1 \leq a_1/r_1$, and as in Verhulst's equation, this parameter, $1/c_1$, plays the role of the carrying capacity. With the same condition for species 2, i.e., $c_2 \leq a_2/r_2$, we may define a rectangle limited by $X_1 = 0$, $X_1 = 1/c_1$, $X_2 = 0$, and $X_2 = 1/c_2$ in whose boundary the flux vectors never point out of the rectangle, and therefore, the growth is bounded.

Figure 2 depicts the bounding rectangle limited by the axis and the dashed lines $1/c_1$ and $1/c_2$. In Figure 2(a), the conditions $c_1 \leq a_1/r_1$ and $c_2 \leq a_2/r_2$ are fulfilled, and the flux lines are pointing inside the rectangle. In Figure 2(b), the conditions are no longer satisfied, but one stable solution is located outside the rectangle, allowing some flux lines to go out. The asymptotic behaviour of the nullcline at $X_1 = 1/c_1$ has changed and now it rises to infinity.

The intersection of both nullclines defines the stationary solutions. As the expression equation (18) is nonlinear, there can be several solutions inside the rectangle. This allows more than one stable solution inside this area, separated by saddle points. As an example, Figure 2 shows the intersections of nullclines (black lines for X_1 and orange lines for X_2) as red points; two of them are stable stationary solutions, separated by a saddle point. In this example for a predator-prey system, the phase space shows the typical solution of a stable spiral (at $X_1 = 42$ and $X_2 = 79$) and a new stable node at a higher population of predator and prey (at $X_1 = 200$ and $X_2 = 164$). Note that even though a_1 does not fulfil the condition $a_1 \leq c_1 \cdot r_1$, in this example, the system is also bounded and stable outside the rectangle. Finally, the same study can be done for N species. For every species, the value $X_i = 1/c_i$ can define a threshold for the initial population for which the flux trajectories never go outside the N-dimensional rectangle. In this case, free-equilibrium solutions will be harder to obtain; however, the Jacobian at these points will have a similar expression (see Supplementary Material).

2.5. Solutions with Three Populations. Ecological complexity increases with species number. Just as a little example, we show in this section how the intraspecific interaction can change the outcomes in a 3-species predator-prey system. We show how a positive coefficient in the intraspecific term of the prey-1 avoids the extinction. Figure 3(a) shows the time evolution of three populations: two preys and one predator; the cooperation coefficient in prey-1 $(b_{11} = 0.001)$, even smaller than the interspecific coefficient $(b_{13} = -0.004)$, changes the initial outcome resulting in a stationary population for prey-1 and predator and the extinction of prey-2.

For the case of negative intraspecific interaction, we show another predator-prey system, with two preys and one predator. In this example, the intraspecific coefficient of the predator $(b_{33} = -0.0005)$ allows both preys to survive at higher populations (Figure 3(b)); the three populations exhibit initial oscillations until they reach a stationary population; however, the difference in the interspecific coefficient $(b_{13} = -0.004$ and $b_{23} = -00045)$ makes the
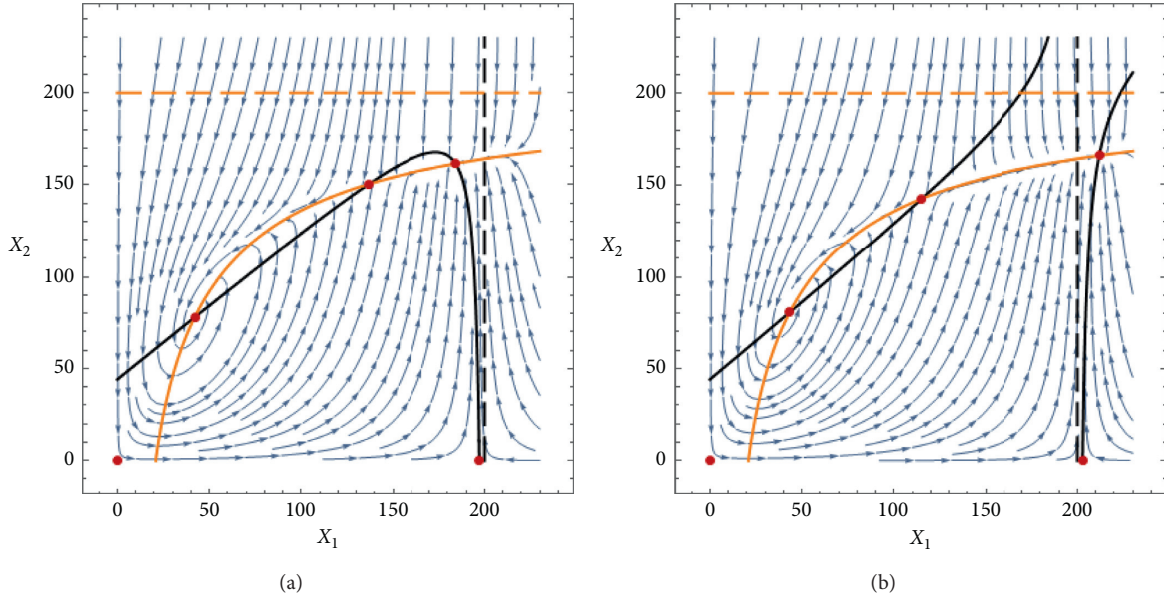
(a)

(b)

FIGURE 2: Nullclines and phase space for an antagonistic system where both populations cooperate intraspecifically. Dashed lines represent $X_i = 1/c_i$, and while solid lines are the nullclines (orange for X_2 and black for X_1). (a)$a_1 = 0.0008$ fulfils the condition $a_1 > c_1 \cdot r_1$, and flux lines inside the rectangle do not point out of this region. (b)$a_1 = 0.0007 < c_1 \cdot r_1$, and some flux lines go out of the rectangle. Parameters: $r_1 = 0.15$, $r_2 = -0.15$, $b_{11} = 0.0028$, $b_{12} = -0.0034$, $b_{21} = 0.0072$, $b_{22} = 0.0005$, $a_2 = 0.00075$, and $c_1 = c_2 = 0.005$.

prey-1 stationary population to be higher than that of prey-2.

3. Results

Here, we show the great variety of scenarios of ecological interactions that this general model is capable of producing. The aim of this section is to show the great richness of the model, but it is not an exhaustive study of the parameters. We show some examples of the solutions that the intraspecific interaction provides to the populations model with two populations. Since exploring all the possible combinations of signs and ratios among the parameters would be unmanageable and redundant, we only show some interesting cases. For all the figures shown in this section, we have varied the parameters in the effective growth rate, r_i, b_{ii}, and b_{ij}, and we have set the limiting parameters $a_1 = a_2 = 0.00075$ and $c_1 = c_2 = 0.005$.

3.1. Antagonism. The solutions of the classical predator-prey model are modified when intraspecific interactions come into play. In our following examples, we have X_1 as the prey and X_2 as the predators. We only show obligate predation since the facultative case only offers a minor change.

3.1.1. The Effect of Cooperation among Prey. The predator-prey system without any intraspecific interaction has only two free-equilibrium solutions: one convergent spiral and one unstable solution, located at the carrying capacity of the prey. The addition of cooperation among the population of preys can generate a new stable solution. Besides

the well known oscillatory solution, we may find a new stable node at high population values, separated by a saddle point. Figure 4(a) shows the phase space and trajectories (with the stationary solutions as red points) for a predator-prey system when preys (X_1) exhibit positive intraspecific interaction (*cooperation*). Phase trajectories keep around the stable spiral for low populations; however, the saddle point defines a new basin towards the new stable solution for high population values (note that the intraspecific parameter, $b_{11} = 0.0028$, is lower than the absolute value of the interspecific parameter, $b_{12} = -0.0036$).

If the detrimental interspecific interaction becomes less harmful, the original stable spiral may disappear and the only stable solution is the coexistence at the carrying capacity (Figure 4(b), with $b_{12} = -0.0036$).

When the intraspecific interaction is greater than the interspecific interactions, in our example, $|b_{12}| = b_{21} < b_{11}$, a new dynamic appears. The spiral becomes unstable, and the trajectories go outwards; as this stationary solution is in the repulsion basin of the saddle point, the trajectories cannot go out, and they will remain in a closed orbit, i.e., in a limit cycle. In Figure 5(a) (with $b_{11} = 0.0036$ and $b_{12} = -0.0072$, in addition to representing the trajectories and the stationary solutions), we depict 3 initial points (in green, yellow, and orange) corresponding to the time evolution picture shown below. The intermediate solution that appeared due to the cooperation term acts as a threshold between the spiral and the coexistence located at the carrying capacity of the prey, which remains as a stable solution. Now, if we decrease the intraspecific parameter, the saddle point moves towards the carrying capacity, all the stationary solutions become unstable, and all the trajectories fall into the limit cycle
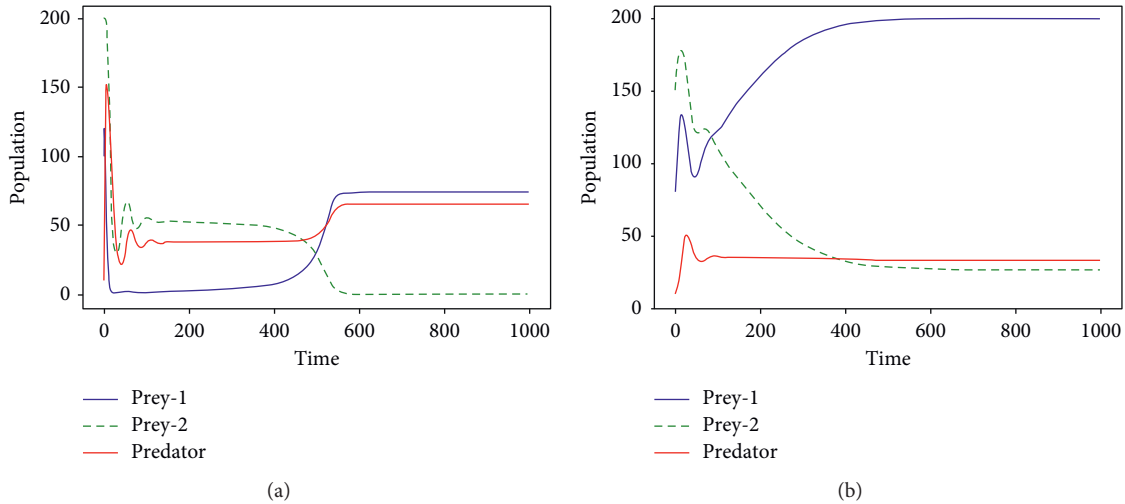
(a)

(b)

FIGURE 3: Population evolution in a predator-prey system with two preys: (a) prey-1 with cooperation $b_{11} = 0.001$ ($r_1 = r_2 = 0.15$, $r_3 = -0.15$, $b_{13} = b_{23} = -0.004$, and $b_{31} = b_{32} = 0.004$); (b) predator with competition $b_{33} = -0.0005$ ($r_1 = r_2 = 0.15$, $r_3 = -0.15$; $b_{13} = -0.004$, $b_{23} = -0.0045$, and $b_{31} = b_{32} = 0.001$).
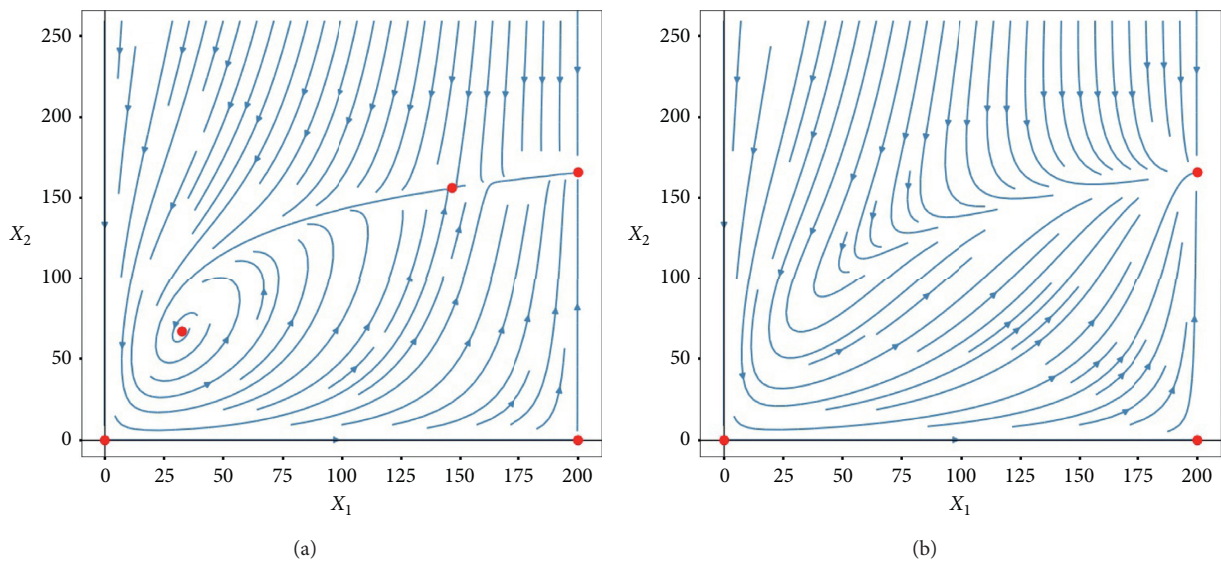

(a)

(b)

FIGURE 4: Phase space and trajectories for two populations involved in a predator-prey interaction. To the left, we have a case with a lower $b_{11} = 0.0028$ than to the right, $b_{11} = 0.0035$. Cooperation among prey allows a new intermediate solution, which is unstable and acts in the same way as in Figure 1. Also, as greater cooperation decreases the predatory term, and the relation may become commensalistic at some points. Here, $r_1 = 0.15$, $r_2 = -0.15$, $b_{12} = -0.0036$, and $b_{21} = 0.0072$.

(Figure 5(b)). The corresponding time evolution (Figure 5(b)) shows fluctuating population for all initial points.

3.1.2. *The Effect of Cooperation among Predators.* In Figure 6, we show the effect of the intraspecific interactions only on predators. As in the previous case, without any intraspecific interaction, the system has only two free-equilibrium points: one convergent spiral and one unstable solution, located at the carrying capacity of the prey. The addition of cooperation among predators can generate a

pair of new solutions, both of them corresponding to partial extinctions of prey. The effect is the same that we showed for one population in Figure 1 but acting on the predator axis. Thus, cooperation among predators introduces a similar effect of facultative predation. We tested two different values of predators cooperation parameter b_{22} to see its direct influence. Although, in both cases, the cooperative term is greater than predation, i.e., $b_{21} < b_{22}$, we can see that, at lower values of cooperation, almost no effect is notable, but at greater values, two partial extinctions of prey appear, one stable and one unstable, a saddle-node bifurcation. This allows predators to survive without preys when cooperation
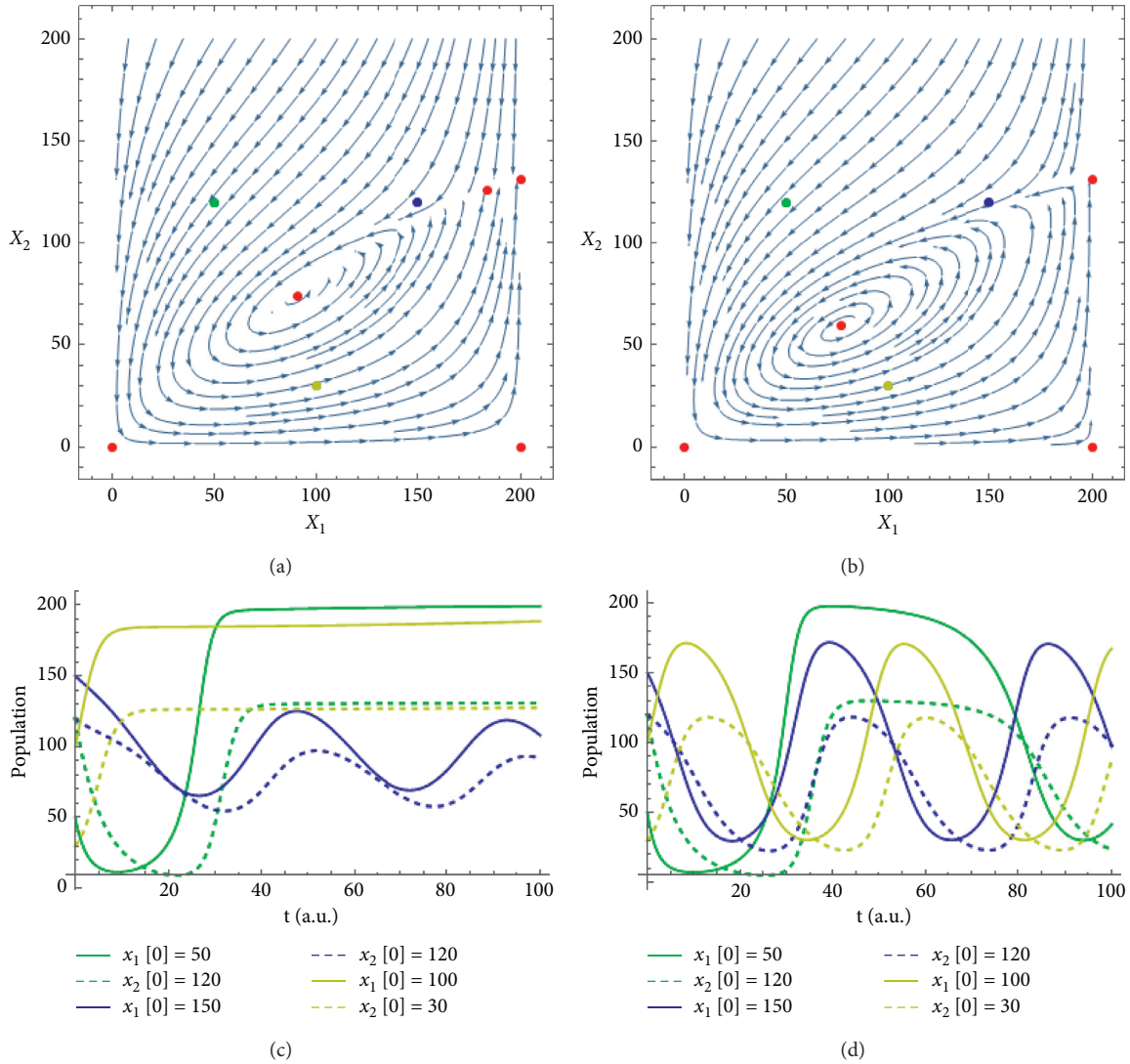
(a)

(b)

(c)

(d)

FIGURE 5: Phase space and trajectories for two populations involved in a predator-prey interaction. We show here a special case where the coexistence spiral solution diverges and become unstable. When that happens, a limit cycle appears. To the left, we have a case with a smaller predation, i.e., $b_{12} = -0.006435$ than to the right, where $b_{12} = -0.0072$. In both cases, $b_{11} = b_{21} = 0.0036$, which means that both populations benefit the same from population X_1, but the predatory effects of X_2 on X_1 are stronger on the right. For greater cooperation values, the intermediate solution might even disappear, as it is shown on the right. The green, blue, and yellow dots in the phase space mark the initial conditions of the simulations located below. Here, $r_1 = 0.15$ and $r_2 = -0.15$.

reaches a certain limit. In Figure 6(a), we have the case in which cooperation is weaker, and in Figure 6(b), the case in which is mildly stronger. The coexistence located at the carrying capacity of the prey remains unstable.

3.2. Competition.

In the case of competition, the principle of competitive exclusion stands that the stable solution is the partial extinction but, if interaction parameters are weak, another feasible stable solution is a coexistence point [17]. However, by including intraspecific interactions, the coexistence could become stable for higher or lower values of the interspecific interaction parameters. For a range of positive intraspecific parameters, partial extinctions and the total carrying capacity could be stable at the same time. Adding a positive intraspecific interaction term (*cooperation*) in one

species may induce a new saddle point, defining two basins, one towards partial extinction of this species and the other one to the system carrying capacity. When cooperation occurs in both species, these two saddle points and the origin define a central attraction basin towards the system carrying capacity; meanwhile, outside this basin, the system evolves towards one species extinction, as per the principle of competitive exclusion (see Figure 7(a)). When we have negative intraspecific parameters, the carrying capacity becomes unstable, and the only stable solutions are the partial extinctions; however, due to the intraspecific interaction, these points occur at a population below its carrying capacity. Both effects can be seen as consequences of intraspecific cooperation and competition in the same way as for one population in Figure 1. Cooperation induces new
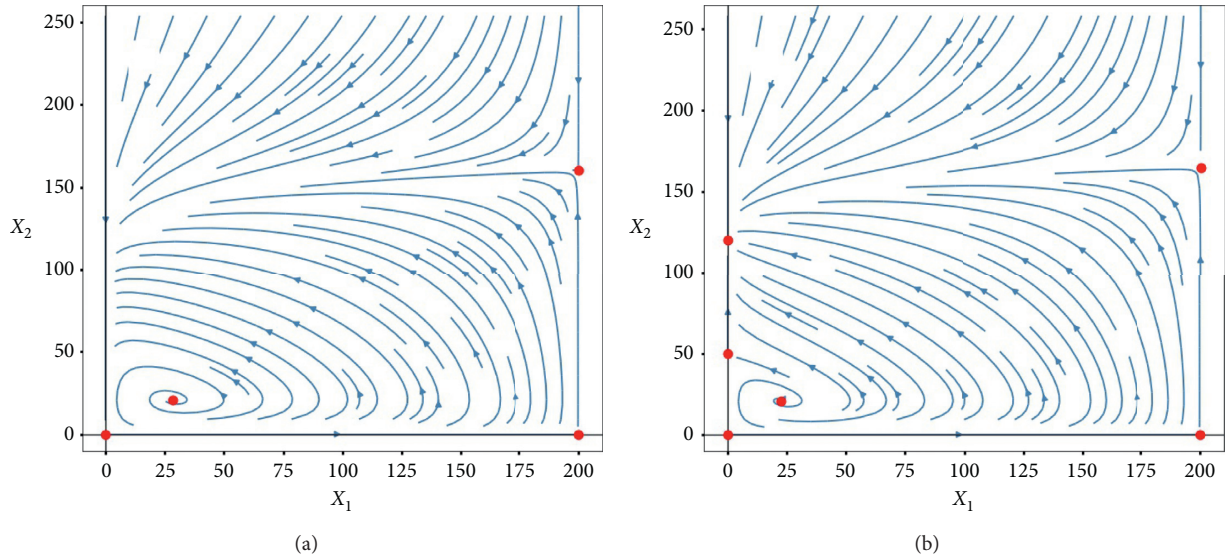
(a)

(b)

FIGURE 6: Phase space and trajectories for two populations involved in an antagonist interaction. To the left, we have a case with a lower $b_{22} = 0.004$ than to the right, $b_{22} = 0.005$. Cooperation among predators allows two new partial extinctions of prey, one stable and one unstable, in the same way in Figure 1 but on the predators axis. The coexistence located at the carrying capacity of the prey remains unstable. Here, $r_1 = 0.15, r_2 = -0.15, b_{11} = 0, b_{12} = -0.0072$, and $b_{21} = 0.0036$.

(a)

(b)
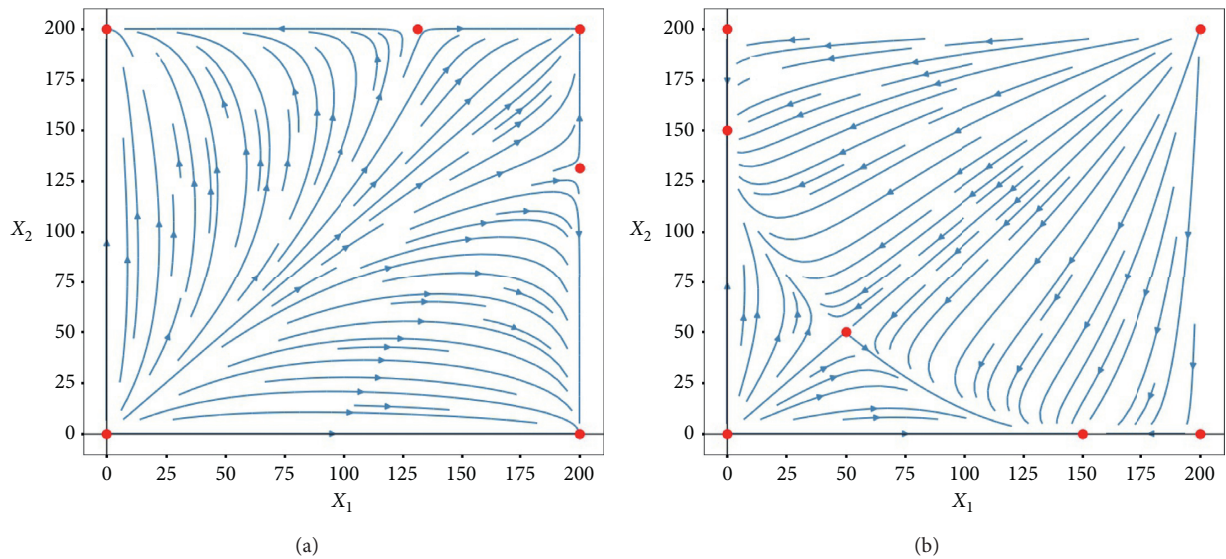
FIGURE 7: Phase space and trajectories for two populations involved in competition with positive intraspecific interaction. We used two different combinations of $b_{11} = b_{22}$ to see the influence of intraspecific cooperation and competition. (a) $b_{11} = b_{22} = 0.0019$, and we have the case in which both populations are cooperative and two new solutions appear together with a basin towards the carrying capacity of the system. (b) $b_{11} = b_{22} = -0.001$, and we have the case in which both are competitive. Noting that when both populations are cooperative, partial carrying capacities appear and they are both unstable. And when both populations are competitive, partial extinctions appear instead although stable and below the carrying capacities. Here, $r_1 = r_2 = 0.15$ and $b_{12} = b_{21} = -0.002$.

solutions as partial carrying capacities and intraspecific competition as partial extinctions.

3.3. Mutualism.
The logistic-mutualistic model exhibits, in addition to the total and partial extinctions, two feasible finite solutions (5): the larger one corresponds to the case where both populations reach their carrying capacities, and the lower one is a saddle point that allows us to define a

survival watershed. By adding intraspecific interactions, new partial extinctions and carrying capacities could appear.

3.3.1. Obligate-Obligate Mutualism.
For the sake of simplicity, we only expose the case of equal sign in the parameters for both species, i.e., $r_1, r_2 < 0$ and $b_{12}, b_{21} > 0$. In Figure 8, we show the phase space for two populations involved in a mutual obligatory mutualism with two
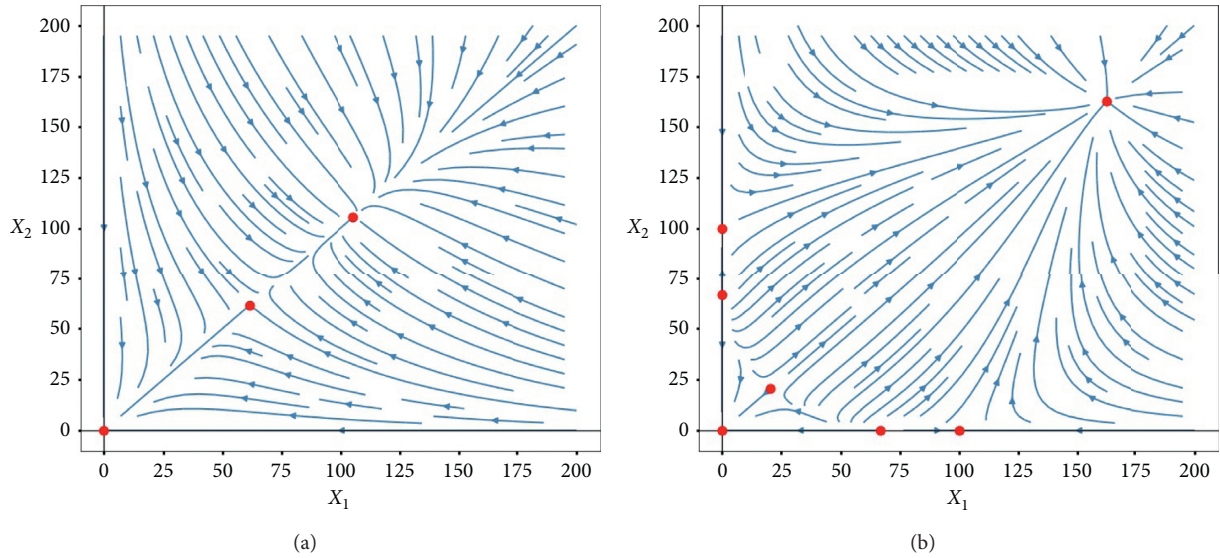
(a)

(b)

FIGURE 8: Obligate-obligate mutualism with cooperation in two populations: (a) we have the case where $b_{11} = b_{22} = 0.0001$, which means that intraspecific cooperation is lower than mutualism; (b) we have $b_{11} = b_{22} = 0.0045$, which means that both intraspecific cooperation and mutualism weight the same. Here, $r_1 = r_2 = -0.15$ and $b_{12} = b_{21} = 0.0045$.
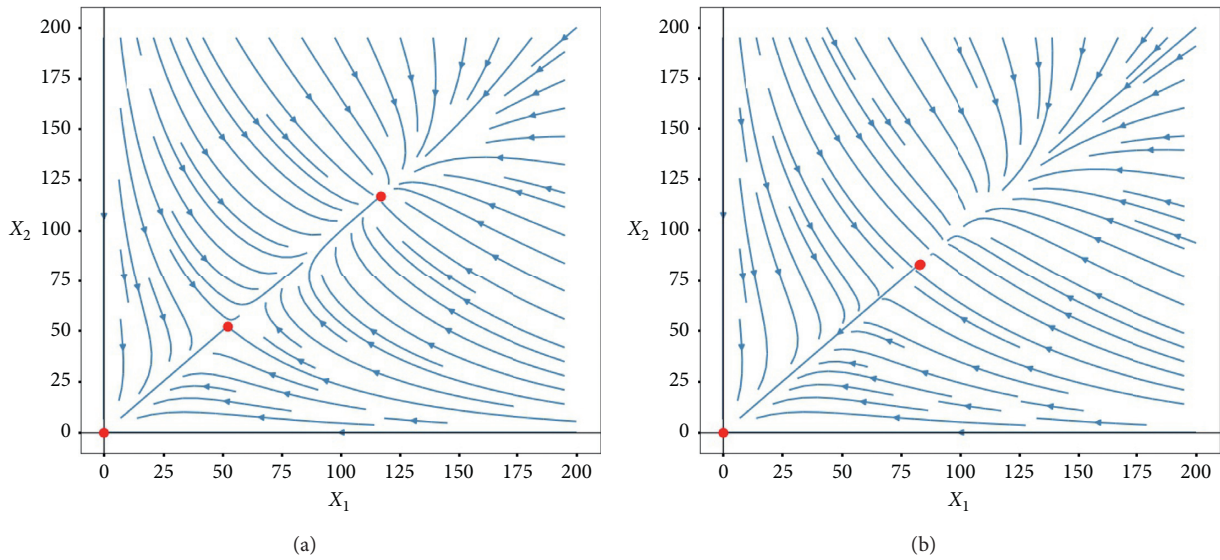

(a)

(b)

FIGURE 9: Obligate-obligate mutualism with competition in two populations: (a) we have the case where $b_{11} = b_{22} = -0.0001$, which means that intraspecific competition is lower than mutualism; (b) we have $b_{11} = b_{22} = -0.00062868$, which means that intraspecific competition has stronger effects than mutualism. Here, $r_1 = r_2 = -0.15$ and $b_{12} = b_{21} = 0.005$.

different values of the cooperation coefficients, b_{ii}. In Figure 8(a), with weak cooperation, the phase space exhibits two free-equilibrium points: the stable carrying capacity and a saddle point defining a *survival watershed*, as in [5]. However, with strong intraspecific interaction (Figure 8(b)), four new unstable solutions can appear: two saddle points and two unstable fixed nodes, corresponding to partial extinctions. As in the case of one population (see Figure 1), the new saddle points are the thresholds. Whenever a population is higher than this threshold, it will never go extinct. The total extinction basin is limited by the curve

passing through the nontrivial saddle point and these new unstable fixed nodes.

On the contrary, when mutualistic species exhibits negative intraspecific interactions, as in Figure 9, the stable carrying capacity moves towards the saddle point (Figure 9(a)). And eventually, when this negative term is high enough, these two solutions collide and total extinction remains as the exclusive stable stationary solution (Figure 9(b)).

In the case of one cooperative population and one competitive population, the system exhibits this asymmetry; again, a new saddle point in the cooperative population axis sets a survival threshold. Above it, the system always evolves
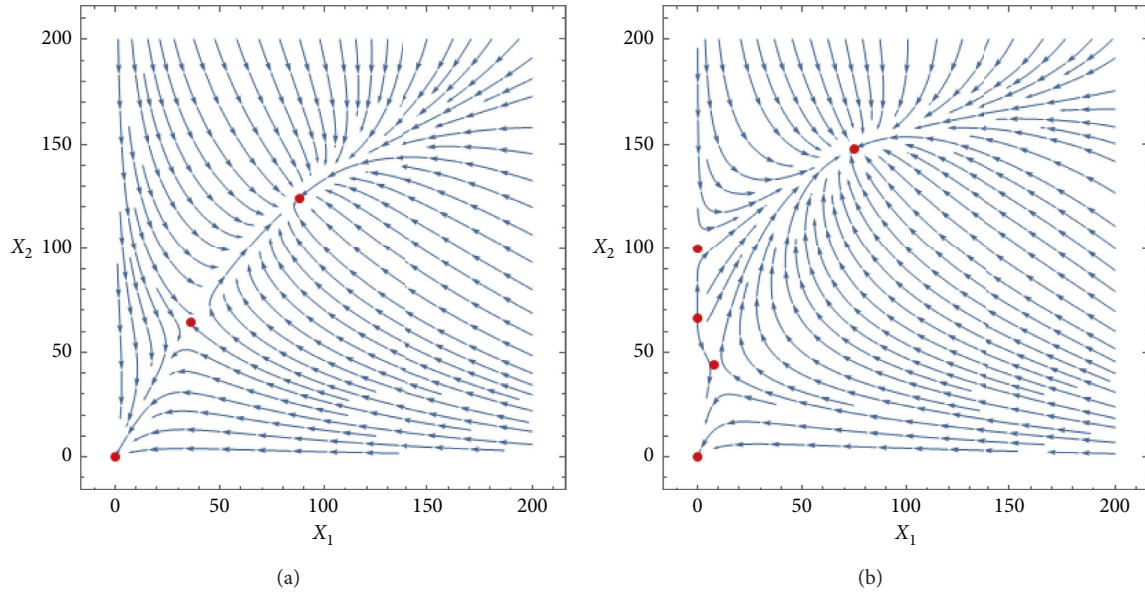
(a)

(b)

FIGURE 10: Obligate-obligate mutualism with positive and negative intraspecific interaction: (a) we have the case where $b_{11} = -0.002$ and $b_{22} = 0.002$, which means that intraspecific competition of X_1 is the same that intraspecific cooperation of X_2 and both interactions weight lower than mutualism; (b) we have $b_{11} = -0.0045$ and $b_{22} = 0.0045$, which means that intraspecific competition of X_1 weights the same than mutualism and intraspecific cooperation of X_2. Here, $r_1 = r_2 = -0.15$ and $b_{12} = b_{21} = 0.0045$.
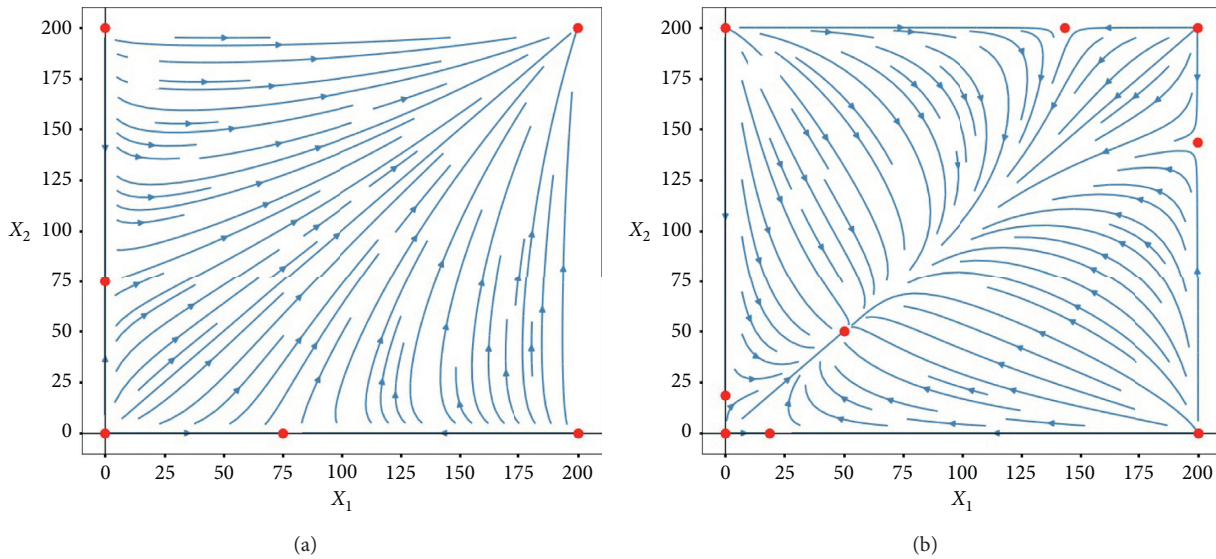

(a)

(b)

FIGURE 11: Facultative-facultative mutualism with negative intraspecific interaction: (a) we have the case where $b_{11} = b_{22} = -0.002$, which means that intraspecific competition is weaker than mutualism; (b) we have $b_{11} = b_{22} = -0.008$, which means that intraspecific competition is stronger than mutualism. Here, $r_1 = r_2 = 0.15$ and $b_{12} = b_{21} = 0.005$.

towards the coexistence solution and will never go extinct, and it is shown in Figure 10.

3.3.2. Facultative-Facultative Mutualism.

When both growth rates, r_1 and r_2, are positive, total extinction is an unstable solution and the carrying capacity is stable (Figure 11(a)). However, when both populations exhibit negative intraspecific interactions, the maximum system carrying capacity may become unstable and a new stable

finite solution emerges at lower populations (Figure 11(b)), as one expects following the one population solution with intraspecific competition (see Figure 1). In Figure 11(a), the intraspecific interaction generates four partial extinctions as unstable stationary solutions (two saddle points and two unstable nodes). In Figure 11(b), with higher negative intraspecific interaction, two extra solutions appear as partial carrying capacities, and the total carrying becomes unstable. In this case, the system exhibits 9 positive stationary
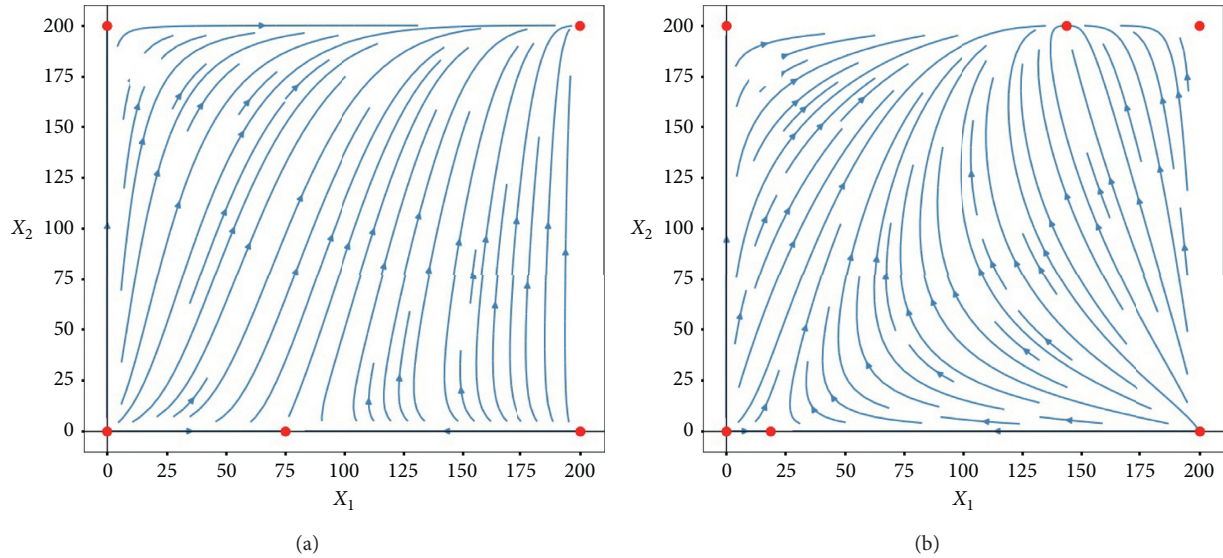
(a)

(b)

FIGURE 12: Facultative-facultative mutualism with intraspecific competition and cooperation: (a) we have the case where $b_{11} = -0.002$ and $b_{22} = 0.008$; (b) we have $b_{11} = -0.008$ and $b_{22} = 0.002$. Here, $r_1 = r_2 = 0.15$ and $b_{12} = b_{21} = 0.005$.

solutions: four saddle points, four unstable points, and only one stable solution.

In the case of facultative mutualism with different intraspecific interactions, one of them is beneficial and the other one is harmful; the carrying capacity could be reduced for populations with negative intraspecific interaction, while its partner, with positive intraspecific interaction, will grow until reaching its own saturation. Figure 12 depicts this scenario. In Figure 12(a), competition is weaker than cooperation, and the total carrying capacity is the stable stationary solution. In Figure 12(b), competition is stronger than cooperation, and the total carrying capacity becomes unstable. As before, competition only generates unstable a partial extinction, while cooperation pushes the coexistence solution into a transcritical bifurcation.

4. Conclusions

In the title of the paper, we ask how simple a population dynamics model should be. To address the discussion, we have introduced the intraspecific interactions in the [5] model using their same philosophy to include new terms. These appear in the first term of the interaction, representing the effective growth rate, and in the logistic brake to balance the first term. With respect to the previous model, this modification introduces two new terms: $b_{ii}X_i^2$ and $-c_ib_{ii}X_i^3$, regarding the intraspecific interactions. Furthermore, we have generalized the model allowing the parameters that define the interactions, b_{ij}, to be positive or negative.

In our opinion, the ecological reason to introduce different intraspecific interactions is supported by observations; cooperative and competitive intraspecific interactions are widely known in a wide variety of ecological systems, from social insects to microbial communities. They have been overseen by population dynamics modelling, which mainly focused on interactions with the environment or interspecific interactions (see, for example, the historical sequence developed in [18]).

Furthermore, the cubic term offers an interesting behaviour from the mathematical point of view. As AlAdwani and Saavedra [11] explain that new high-order terms can introduce new free-equilibrium solutions, but it is necessary that these solutions will be feasible, and of course, with a clear ecological meaning. In this way, several authors have used high-order interactions to improve the stability or diversity of ecological models. For example, Letten and Stouffer [9] show the advantages of the high-order terms, introducing nonadditive density-dependent effects; the authors study the influence of the high-order interactions in the competitive communities. Or Grilli et al. [19] show how the high-order interactions increase the stability of the systems. In our model, the term $-c_ib_{ii}X_i^3$ introduces 2 new free-equilibrium solutions (see Supplementary Material (available here)) that in our opinion can explain ecological situations that were not well explained before with the population dynamics equations.

Delving into the idea of high-order interactions, Bairey et al. [10] introduce 3-way or 4-way terms, overcoming the pairwise interactions. These terms are intended to simulate the effect that interactions between species are modulated by one or more species. This idea is inspiring, but we believe that simpler models like ours that use polynomial terms and pairwise interaction can still explain many ecological landscapes. Every time that we increase the order of a new term, it is more difficult to define it and their corresponding parameters in the field.

We would like to highlight that the inclusion of the intraspecific terms shows new solutions that could represent more complex ecological landscapes. For example, the case of predator-prey system with positive intraspecific term in the preys exhibits a new solution with a steady state at large populations. This solution could represent the way herds act as a defensive mechanism for preys [20, 21]. Also, large herds

of zebras or wildebeest seem to be stable in time; in [22], the authors presented data of the Kruger National Park, in South Africa, that showed a stable and increasing population of zebras and wildebeest (more than 10,000 individuals) over a period of twenty years, with more or less stable population of lions (around 400 individuals). Or the effects of intraspecific competition can act as a regulatory mechanism. Polis [23] showed that intraspecific predation acts in a reinforced way: higher populations decrease the resources available for individuals, reducing their growing rates and promoting smaller and weaker individuals, those are more easily killed or eaten, which increases the per capita food level, both by reducing the population and by satiating the cannibalists.

The main advantage of this general model (equation (3)) is that it can be used to describe any ecological regime and that it carries its own saturation mechanism that avoids the "*orgy of mutual benefaction*" of [24]. Stucchi [25] showed using a simplified generalized model, studying a nursery pollination system, and modelling all the interspecific interactions with the same functional. This allowed a clear interpretation of the parameters of the whole system and an unambiguous way to compare them. Furthermore, Stucchi t al. [26] showed that intraspecific interactions in a predator-prey system might lead to diffusion-driven instabilities.

Finally, we would like to venture to discuss some more speculative ideas. Nowadays, there are some attempts to model transitions from antagonistic to mutualistic interspecific relationships, limited by the fact that they deal with different mathematical functionals for mutualism and antagonism [27–29]. These models include changes that arise continually from one regime to another, but treating the transition only in a descriptive way. In addition, adaptive changes are modelled through parameter changing systems, where parameters have their own dynamic equations, but these models are still limited to specific ecological regimes, either antagonistic or mutualistic [30–32]. However, if one may adequately define the dynamics of the parameters in a general model of ecological interactions, it may reflect a deeper view of nature, where ecology meets evolution. Thus, by including evolutionary changes in our model, one may be capable of modelling transitions due to mutations and natural selection, which is surely the way how transitions on ecological regimes occur in nature.

Data Availability

This is a theoretical study, and we do not have experimental data.

Conflicts of Interest

The authors declare that they have no conflicts of interest.

Authors' Contributions

All authors contributed equally to the study.

Acknowledgments

Supplementary Materials

Quantifying the effect of the intraspecific term. The Jacobian matrix for N species. (*Supplementary Materials*)

References

[1] A. J. Lotka, *Elements of Physical Biology*, Williams and Wilkins Company, Baltimore, MD, USA, 1925.

[2] V. Volterra, "Fluctuations in the abundance of a species considered mathematically," *Nature*, vol. 118, no. 2972, pp. 558–560, 1926.

[3] J. Bascompte, "Disentangling the web of life," *Science*, vol. 325, no. 5939, pp. 416–419, 2009.

[4] J. Bascompte, "Mutualistic networks," *Frontiers in Ecology and the Environment*, vol. 7, no. 8, pp. 429–436, 2009.

[5] J. García-Algarra, J. Galeano, J. M. Pastor, J. M. Iriondo, and J. J. Ramasco, "Rethinking the logistic approach for population dynamics of mutualistic interactions," *Journal of Theoretical Biology*, vol. 363, pp. 332–343, 2014.

[6] A. M. Dean, "A simple model of mutualism," *The American Naturalist*, vol. 121, no. 3, pp. 409–417, 1983.

[7] D. H. Wright, "A simple, stable model of mutualism incorporating handling time," *The American Naturalist*, vol. 134, no. 4, pp. 664–667, 1989.

[8] U. Bastolla, M. A. Fortuna, A. Pascual-García, A. Ferrera, B. Luque, and J. Bascompte, "The architecture of mutualistic networks minimizes competition and increases biodiversity," *Nature*, vol. 458, no. 7241, pp. 1018–1020, 2009.

[9] A. D. Letten and D. B. Stouffer, "The mechanistic basis for higher-order interactions and non-additivity in competitive communities," *Ecology Letters*, vol. 22, no. 3, pp. 423–436, 2019.

[10] E. Bairey, E. D. Kelsic, and R. Kishony, "High-order species interactions shape ecosystem diversity," *Nature Communications*, vol. 7, no. 1, pp. 1–37, 2016.

[11] M. AlAdwani and S. Saavedra, "Is the addition of higher-order interactions in ecological models increasing the understanding of ecological dynamics?" *Mathematical Biosciences*, vol. 315, Article ID 108222, 2019.

[12] P. F. Verhulst, "Notice sur la loi que la population suit dans son accroissement," *Correspondance Mathematique et Physique*, vol. 10, pp. 113–117, 1838.

[13] E. O. Wilson, *The Insect Societies*, Belknap Press, Cambridge, MA, USA, 1971.

[14] B. Stadler and A. F. G. Dixon, "Ecology and evolution of aphid-ant interactions," *Annual Review of Ecology, Evolution, and Systematics*, vol. 36, no. 1, pp. 345–372, 2005.

[15] M. Stucchi and J. Figueroa, "La avifauna de las islas Lobos de Afuera y algunos alcances sobre su biodiversidad," Asociacion Ucumari. Lima, Perú, Reporte de Investigacion N 2, 2006.

[16] W. C. Allee, *Animal Aggregations: A Study in General Sociology*, University of Chicago Press, Chicago, IL, USA, 1931.

[17] J. D. Murray, *Mathematical Biology I. An Introduction*, Springer, Berlin, Germany, 1993.

[18] P. Turchin, *Complex Population Dynamics: A Theoretical/empirical Synthesis (MPB-35)*, Princeton University Press, Princeton, NJ, USA, 2003.

[19] J. Grilli, G. Barabás, M. J. Michalska-Smith, and S. Allesina, "Higher-order interactions stabilize dynamics in competitive network models," *Nature*, vol. 548, no. 7666, pp. 210–213, 2017.

[20] D. I. Rubenstein, *On Predation, Competition, and the Advantages of Group Living, 205–231*, Springer US, Boston, MA, USA, 1978.

[21] J. Berger, ""Predator harassment" as a defensive strategy in ungulates," *American Midland Naturalist*, vol. 102, no. 1, pp. 197–199, 1979.

[22] T. H. Fay and C. Greeff, "Lion, wildebeest and zebra: a predator-prey model," *Ecological Modelling*, vol. 196, no. 1-2, pp. 237–244, 2006.

[23] G. A. Polis, "The evolution and dynamics of intraspecific predation," *Annual Review of Ecology and Systematics*, vol. 12, no. 1, pp. 225–251, 1981.

[24] R. M. May, "Models for two interacting populations," in *Theoretical Ecology: Principles and Applications*, pp. 78–104, Oxford University Press, Oxford, UK, 1981.

[25] L. Stucchi, L. Giménez-Benavides, and J. Galeano, "The role of parasitoids in a nursery-pollinator system: a population dynamics model," *Ecological Modelling*, vol. 396, pp. 50–58, 2019.

[26] L. Stucchi, J. Galeano, and D. A. Vasquez, "Pattern formation induced by intraspecific interactions in a predator-prey system," *Physical Review E*, vol. 100, no. 8, 2019.

[27] V. I. Yukalov, E. P. Yukalova, and D. Sornette, "Modeling symbiosis by interactions through species carrying capacities," *Physica D: Nonlinear Phenomena*, vol. 241, no. 15, pp. 1270–1289, 2012.

[28] C. Neuhauser and J. E. Fargione, "A mutualism-parasitism continuum model and its application to plant-mycorrhizae interactions," *Ecological Modelling*, vol. 177, no. 3-4, pp. 337–352, 2004.

[29] S. Kéfi, V. Miele, E. A. Wieters, S. A. Navarrete, and E. L. Berlow, "How structured is the entangled bank? The surprisingly simple organization of multiplex ecological networks leads to increased persistence and resilience," *PLoS Biology*, vol. 14, no. 8, Article ID e1002527, 2016.

[30] U. Dieckmann and R. Law, "The dynamical theory of coevolution: a derivation from stochastic ecological processes," *Journal of Mathematical Biology*, vol. 34, no. 5-6, pp. 579–612, 1996.

[31] A. White and R. G. Bowers, "Adaptive dynamics of Lotka-Volterra systems with trade-offs: the role of interspecific parameter dependence in branching," *Mathematical Biosciences*, vol. 193, no. 1, pp. 101–117, 2005.

[32] J. N. Holland, D. L. DeAngelis, and S. T. Schultz, "Evolutionary stability of mutualism: interspecific population regulation as an evolutionarily stable strategy," *Proceedings of the Royal Society B: Biological Sciences*, vol. 271, pp. 1807–1814, 2004.